



International Journal of  
**Molecular Sciences**

# Therapeutic Strategies to Spinal Cord Injury

---

Edited by  
**Pavla Jendelova**

Printed Edition of the Special Issue Published in  
*International Journal of Molecular Sciences*

# **Therapeutic Strategies to Spinal Cord Injury**



# **Therapeutic Strategies to Spinal Cord Injury**

Special Issue Editor

**Pavla Jendelova**

MDPI • Basel • Beijing • Wuhan • Barcelona • Belgrade



*Special Issue Editor*

Pavla Jendelova

Institute of Experimental Medicine,  
Academy of Sciences of the Czech,  
Czech Republic

*Editorial Office*

MDPI

St. Alban-Anlage 66  
4052 Basel, Switzerland

This is a reprint of articles from the Special Issue published online in the open access journal *International Journal of Molecular Sciences* (ISSN 1422-0067) in 2018 (available at: [https://www.mdpi.com/journal/ijms/special\\_issues/Cord\\_Injury](https://www.mdpi.com/journal/ijms/special_issues/Cord_Injury))

For citation purposes, cite each article independently as indicated on the article page online and as indicated below:

LastName, A.A.; LastName, B.B.; LastName, C.C. Article Title. *Journal Name* **Year**, Article Number, Page Range.

**ISBN 978-3-03897-406-2 (Pbk)**

**ISBN 978-3-03897-407-9 (PDF)**

Cover image courtesy of Pavla Jendelova.

© 2018 by the authors. Articles in this book are Open Access and distributed under the Creative Commons Attribution (CC BY) license, which allows users to download, copy and build upon published articles, as long as the author and publisher are properly credited, which ensures maximum dissemination and a wider impact of our publications.

The book as a whole is distributed by MDPI under the terms and conditions of the Creative Commons license CC BY-NC-ND.

# Contents

<b>About the Special Issue Editor . . . . .</b>	vii
<b>Preface to "Therapeutic Strategies to Spinal Cord Injury" . . . . .</b>	ix
<b>Pavla Jendelova</b>	
Therapeutic Strategies for Spinal Cord Injury	
Reprinted from: <i>Int. J. Mol. Sci.</i> 2018, 19, 3200, doi:10.3390/ijms19103200 . . . . .	1
<b>Jure Tica, Elizabeth J. Bradbury and Athanasios Didangelos</b>	
Combined Transcriptomics, Proteomics and Bioinformatics Identify Drug Targets in Spinal Cord Injury	
Reprinted from: <i>Int. J. Mol. Sci.</i> 2018, 19, 1461, doi:10.3390/ijms19051461 . . . . .	4
<b>James Hong, Alex Chang, Mohammad-Masoud Zavvarian, Jian Wang, Yang Liu and Michael G. Fehlings</b>	
Level-Specific Differences in Systemic Expression of Pro- and Anti-Inflammatory Cytokines and Chemokines after Spinal Cord Injury	
Reprinted from: <i>Int. J. Mol. Sci.</i> 2018, 19, 2167, doi:10.3390/ijms19082167 . . . . .	23
<b>Katarina Bimbova, Maria Bacova, Alexandra Kisucka, Jaroslav Pavel, Jan Galik, Peter Zavacky, Martin Marsala, Andrea Stropkovska, Jana Fedorova, Stefania Papcunova, Jana Jachova and Nadezda Lukacova</b>	
A Single Dose of Atorvastatin Applied Acutely after Spinal Cord Injury Suppresses Inflammation, Apoptosis, and Promotes Axon Outgrowth, Which Might Be Essential for Favorable Functional Outcome	
Reprinted from: <i>Int. J. Mol. Sci.</i> 2018, 19, 1106, doi:10.3390/ijms19041106 . . . . .	36
<b>Ana Alastrue-Agudo, Francisco Javier Rodriguez-Jimenez, Eric López Mocholi, Francesca De Giorgio, Slaven Erceg and Victoria Moreno-Manzano</b>	
FM19G11 and Ependymal Progenitor/Stem Cell Combinatory Treatment Enhances Neuronal Preservation and Oligodendrogenesis after Severe Spinal Cord Injury	
Reprinted from: <i>Int. J. Mol. Sci.</i> 2018, 19, 200, doi:10.3390/ijms19010200 . . . . .	53
<b>Petr Krupa, Irena Vackova, Jiri Ruzicka, Kristyna Zaviskova, Jana Dubisova, Zuzana Koci, Karolina Turnovcova, Lucia Machova Urdzikova, Sarka Kubinova, Svatopluk Rehak and Pavla Jendelova</b>	
The Effect of Human Mesenchymal Stem Cells Derived from Wharton's Jelly in Spinal Cord Injury Treatment Is Dose-Dependent and Can Be Facilitated by Repeated Application	
Reprinted from: <i>Int. J. Mol. Sci.</i> 2018, 19, 1503, doi:10.3390/ijms19051503 . . . . .	69
<b>Dasa Cizkova, Veronika Cubinkova, Tomas Smolek, Adriana-Natalia Murgoci, Jan Danko, Katarina Vdoviakova, Filip Humenik, Milan Cizek, Jusal Quanico, Isabelle Fournier and Michel Salzet</b>	
Localized Intrathecal Delivery of Mesenchymal Stromal Cells Conditioned Medium Improves Functional Recovery in a Rat Model of Spinal Cord Injury	
Reprinted from: <i>Int. J. Mol. Sci.</i> 2018, 19, 870, doi:10.3390/ijms19030870 . . . . .	87
<b>Aleš Hejčl, Jiří Růžička, Kristýna Kekulová, Barbora Svobodová, Vladimír Proks, Hana Macková, Kateřina Jiránková, Kristýna Kárová, Lucia Machová Urdziková, Šárka Kubinová, Jiří Cihlář, Daniel Horák and Pavla Jendelová</b>	
Modified Methacrylate Hydrogels Improve Tissue Repair after Spinal Cord Injury	
Reprinted from: <i>Int. J. Mol. Sci.</i> 2018, 19, 2481, doi:10.3390/ijms19092481 . . . . .	100

<b>Sian F. Irvine and Jessica C. F. Kwok</b> Perineuronal Nets in Spinal Motoneurons: Chondroitin Sulphate Proteoglycan around Alpha Motoneurons Reprinted from: <i>Int. J. Mol. Sci.</i> <b>2018</b> , <i>19</i> , 1172, doi:10.3390/ijms19041172 . . . . .	<b>116</b>
<b>Kiyoshi Kikuchi, Kentaro Setoyama, Takuto Terashi, Megumi Sumizono, Salunya Tancharoen, Shotaro Otsuka, Seiya Takada, Kazuki Nakanishi, Koki Ueda, Harutoshi Sakakima, Ko-ichi Kawahara, Ikuro Maruyama, Gohsuke Hattori, Motohiro Morioka, Eiichiro Tanaka and Hisaaki Uchikado</b> Application of a Novel Anti-Adhesive Membrane, E8002, in a Rat Laminectomy Model Reprinted from: <i>Int. J. Mol. Sci.</i> <b>2018</b> , <i>19</i> , 1513, doi:10.3390/ijms19051513 . . . . .	<b>135</b>
<b>Yoshitoshi Kasuya, Hiroki Umezawa and Masahiko Hatano</b> Stress-Activated Protein Kinases in Spinal Cord Injury: Focus on Roles of p38 Reprinted from: <i>Int. J. Mol. Sci.</i> <b>2018</b> , <i>19</i> , 867, doi:10.3390/ijms19030867 . . . . .	<b>144</b>
<b>Marina Gazdic, Vladislav Volarevic, C. Randall Harrell, Crissy Fellabaum, Nemanja Jovicic, Nebojsa Arsenijevic and Miodrag Stojkovic</b> Stem Cells Therapy for Spinal Cord Injury Reprinted from: <i>Int. J. Mol. Sci.</i> <b>2018</b> , <i>19</i> , 1039, doi:10.3390/ijms19041039 . . . . .	<b>159</b>
<b>Dana M. Otzel, Jimmy Lee, Fan Ye, Stephen E. Borst and Joshua F. Yarrow</b> Activity-Based Physical Rehabilitation with Adjuvant Testosterone to Promote Neuromuscular Recovery after Spinal Cord Injury Reprinted from: <i>Int. J. Mol. Sci.</i> <b>2018</b> , <i>19</i> , 1701, doi:10.3390/ijms19061701 . . . . .	<b>173</b>
<b>Kyriakos Dalamagkas, Magdalini Tsintou, Amelia Seifalian and Alexander M. Seifalian</b> Translational Regenerative Therapies for Chronic Spinal Cord Injury Reprinted from: <i>Int. J. Mol. Sci.</i> <b>2018</b> , <i>19</i> , 1776, doi:10.3390/ijms19061776 . . . . .	<b>209</b>

## About the Special Issue Editor

**Pavla Jendelova, PhD**, is the Head of the Department of tissue cultures and stem cells at the Institute of Experimental Medicine, Czech Academy of Sciences. She has focused her research on the regeneration and repair of brain and spinal cord injury using different stem cells and anti-inflammatory compounds. Her group also works in collaboration with the Institute of Macromolecular Chemistry on developing biomaterials for CNS injury for combined therapies. For the success of cell therapy, it is important to monitor the fate of transplanted cells *in vivo*. Therefore, another research focus is to develop theranostic magnetic nanoparticles as labels for cell tracking and drug delivery.



## Preface to "Therapeutic Strategies to Spinal Cord Injury"

The first description of spinal cord injury comes from the Edwin Smith papyrus, dating from the seventeenth century BC. In this unique treatise, spinal cord injury (SCI) was considered as an ailment that could not be treated. To date, we still do not have the tools needed to regenerate nervous tissue. However, different approaches and strategies continue to emerge, putting pieces of knowledge together and trying to challenge SCI and improve patients' quality of life. Modern techniques have been employed to analyze the changes after SCI, and some of the new approaches and strategies are described or summarized in this Special Issue. We have put together eight research articles covering a broad range of strategies on how to combat spinal cord injuries, from searching for therapeutic target molecules, tackling the inflammatory reaction, and utilizing cell therapy or cell-based products, combining strategies (pharmacological treatment or polymer bridges) with cell therapy, to axonal plasticity assessment and the prevention of post-surgical epidural adhesions. Moreover, four reviews cover recent findings about the role of stress-activated protein kinases in SCI; progress in stem cell therapies; the mechanisms and benefits of activity-based physical rehabilitation therapies with adjuvant testosterone; and, finally, translational regenerative therapies for chronic spinal cord injury. I believe that this book will be inspiring for numerous readers, not only those from the field of spinal cord injury.

**Pavla Jendelova**

*Special Issue Editor*





Editorial

## Therapeutic Strategies for Spinal Cord Injury

Pavla Jendelova <sup>1,2</sup>

<sup>1</sup> Institute of Experimental Medicine, Czech Academy of Sciences, Vidéňská 1083, 142 20 Prague, Czech Republic; pavla.jendelova@iem.cas.cz; Tel.: +420-241-062-828; Fax: +420-241-062-782

<sup>2</sup> Department of Neuroscience, 2nd Faculty of Medicine, Charles University, V Úvalu 84, 150 06 Prague, Czech Republic

Received: 10 October 2018; Accepted: 12 October 2018; Published: 16 October 2018

The first description of spinal cord injury (SCI) comes from the Edwin Smith papyrus, dating from seventeenth century “B.C”. In this unique treatise, SCI was considered as an ailment that could not be treated [1]. To date, we still do not have the tools needed to regenerate nervous tissue. However, different approaches and strategies continue to emerge, putting pieces of knowledge together and trying to challenge SCI and improve patients’ quality of life. Modern techniques have been employed to analyze the changes after SCI. Some of the new approaches and strategies are described or summarized in this Special Issue. The combination of transcriptomics, proteomics, and bioinformatics provides a comprehensive overview of proteins with persistent differential expression at the mRNA and protein level, and from the subacute (7 days) to the chronic (8 weeks) phase of SCI lesion development. A combined analysis identified 40 significantly upregulated versus 48 significantly downregulated molecules. This screening revealed several possible therapeutic candidates, which were so far not considered as potential targets, but they possess important bioactivity, such as the upregulated purine nucleoside phosphorylase (PNP), cathepsins A, H, Z (CTSA, CTSH, CTSZ), and proteasome protease PSMB10, as well as the downregulated ATP citrate lyase (ACLY), malic enzyme (ME1), and sodium-potassium ATPase (ATP1A3) [2].

The first assessment of pro- and anti-inflammatory cytokines, depending on the site of injury, revealed differences in Vascular Endothelial Growth Factor (VEGF), leptin, Interferon gamma-induced protein 10 (IP10), Interleukin 8 (IL18), Granulocyte-colony stimulating factor (GCSF), and fractalkine in thoracic and cervical lesions. Overall, cervical SCI had reduced expression of both pro- and anti-inflammatory proteins relative to thoracic SCI [3]. In response to the release of inflammatory cytokines, stress-activated protein kinases (SAPKs)—c-Jun N-terminal kinase (JNK) and p38 mitogen-activated protein kinase (p38 MAPK)—are activated in various types of cells. In animal models of SCI, the inhibition of either JNK or p38 has been shown to promote neuroprotection-associated functional recovery. Therefore, p38 could serve as a promising target for therapeutic intervention in SCI [4]. Among the drugs used for other pathologies, atorvastatin (ATR)—a potent inhibitor of cholesterol biosynthesis—can modulate secondary injury, reducing Interleukin 1 (IL1), M1 macrophage infiltration, and decreasing the activity of caspase 3. These changes lead to increased sprouting and improved locomotor activity [5]. Pharmacological treatment can be combined with stem cells, but these therapies do not always have to synergize, as in the case of ependymal stem/progenitor cells combined with a pharmacological compound FM19G11, which reduced glial scar and increased the expression of Olig1 in vivo, but did not lead to greater behavioral improvement when compared with the individual treatments [6]. Stem cells have promising therapeutic potential to rescue or repair damaged spinal cord tissue. Particularly, endogenous stem cell populations have been considered as a promising therapeutic approach to enhance repair mechanisms in SCI. Their potential is reviewed in [7]. However, further investigations are necessary to confirm the neurological benefits by adjusting the doses and time points for the administrations of stem cells. It has been confirmed that the efficacy of cell therapy is dose-dependent and can be enhanced by repeated applications, as was shown in

a study of Wharton Jelly mesenchymal stem cells (WJMSCs) grafted into acute spinal cord balloon compression lesions. Histochemical analyses revealed a gradually increasing effect of grafted cells, resulting in a significant increase in the number of sprouting fibers, a higher amount of spared gray matter, and reduced astrogliosis. mRNA expression of macrophage markers and apoptosis was downregulated after the repeated application of 1.5 million cells [8]. An attractive option as an alternative to cell therapy is the use of stem cell secretomes, since the immunomodulatory and neurotrophic properties of stem cells rely on released secretomes, comprising a soluble fraction of proteins, growth factors, cytokines, miRNA, and other bioactive molecules. Indeed, an effect similar to cell grafting was obtained after the repeated intrathecal delivery of conditioned media obtained from bone marrow mesenchymal stem cells [9]. It is important to highlight that stem cell-based therapy alone is not sufficient to bridge a spinal cord lesion. Therefore, a repair strategy based on a combination of well-established therapeutic modalities, including surgery and medications, and/or bridging the lesion with biocompatible scaffolds, is another approach for the treatment of SCI. Methacrylate hydrogels are biocompatible polymers used for bridging large cavities. They can be coated or modified with extracellular matrix (ECM) components such as laminin and fibronectin, which can improve cell adhesion and survival by generating a permissive microenvironment within the biomaterial. Hydrogels based on hydroxypropylmethacrylamid (HPMA) and 2-hydroxyethylmethacrylate (HEMA) coated with fibronectin support the ingrowth of axons and blood vessels when grafted into rat hemisection [10].

Perineuronal nets (PNNs) are extracellular matrix structures surrounding neuronal sub-populations throughout the central nervous system, regulating plasticity. Enzymatically removing PNNs successfully enhances plasticity and thus functional recovery, particularly in models of spinal cord injury. While PNNs within various brain regions are well-studied, much of the composition and associated populations in the spinal cord is as yet unknown. Kwok's lab investigated the populations of PNN neurons involved in functional motor recovery. Insights into the role of PNNs and their molecular heterogeneity in the spinal motor pools could aid in designing targeted strategies to enhance functional recovery post-injury [11].

Neuropathic pain after spinal surgery—the so-called failed back surgery syndrome—is a frequently observed common complication. One cause of the pain is scar tissue formation, observed as post-surgical epidural adhesions. These adhesions may compress the surrounding spinal nerves, resulting in pain, even after successful spinal surgery. An anti-adhesive membrane can reduce adhesions and scar formation and lower the numbers of fibroblasts and inflammatory cells [12]. Neuromuscular impairment and reduced musculoskeletal integrity are hallmarks of SCI that hinder locomotor recovery. Activity-based physical rehabilitation therapies (ABTs) can promote neuromuscular plasticity after SCI. However, ABT efficacy declines as SCI severity increases. Additionally, many men with SCI exhibit low testosterone, which may exacerbate neuromusculoskeletal impairment. Incorporating testosterone adjuvant to ABTs may improve musculoskeletal recovery and neuroplasticity, as androgens attenuate muscle loss and promote motoneuron survival. In a review [13], the mechanisms and benefits of a multimodal strategy involving ABT with adjuvant testosterone are discussed.

Despite all the promising results in preclinical research, translation into the clinic is progressing slowly. The most promising clinical trials and biomaterials with high translational potential are presented in a review [14]. To date, the majority of patients remain in a chronic state for the rest of their lives. To solve this so-far incurable condition, we need to include more clinically relevant chronic SCI models, which would allow a reliable assessment of the therapeutic strategies for future treatments of SCI patients.

## References

1. Hughes, J.T. The Edwin Smith Surgical Papyrus: an analysis of the first case reports of spinal cord injuries. *Paraplegia* **1988**, *26*, 71–82. [[CrossRef](#)] [[PubMed](#)]
2. Tica, J.; Bradbury, E.J.; Didangelos, A. Combined Transcriptomics, Proteomics and Bioinformatics Identify Drug Targets in Spinal Cord Injury. *Int. J. Mol. Sci.* **2018**, *19*, 1461. [[CrossRef](#)] [[PubMed](#)]
3. Hong, J.; Chang, A.; Zavvarian, M.M.; Wang, J.; Liu, Y.; Fehlings, M.G. Level-Specific Differences in Systemic Expression of Pro- and Anti-Inflammatory Cytokines and Chemokines after Spinal Cord Injury. *Int. J. Mol. Sci.* **2018**, *19*, 2167. [[CrossRef](#)] [[PubMed](#)]
4. Kasuya, Y.; Umezawa, H.; Hatano, M. Stress-Activated Protein Kinases in Spinal Cord Injury: Focus on Roles of p38. *Int. J. Mol. Sci.* **2018**, *19*, 867. [[CrossRef](#)] [[PubMed](#)]
5. Bimbova, K.; Bacova, M.; Kisucka, A.; Pavel, J.; Galik, J.; Zavacky, P.; Marsala, M.; Stropkovska, A.; Fedorova, J.; Papcunova, S.; et al. A Single Dose of Atorvastatin Applied Acutely after Spinal Cord Injury Suppresses Inflammation, Apoptosis, and Promotes Axon Outgrowth, Which Might Be Essential for Favorable Functional Outcome. *Int. J. Mol. Sci.* **2018**, *19*, 1106. [[CrossRef](#)] [[PubMed](#)]
6. Alastrue-Agudo, A.; Rodriguez-Jimenez, F.J.; Mocholi, E.L.; De Giorgio, F.; Erceg, S.; Moreno-Manzano, V. FM19G11 and Ependymal Progenitor/Stem Cell Combinatory Treatment Enhances Neuronal Preservation and Oligodendrogenesis after Severe Spinal Cord Injury. *Int. J. Mol. Sci.* **2018**, *19*, 200. [[CrossRef](#)] [[PubMed](#)]
7. Gazdic, M.; Volarevic, V.; Harrell, C.R.; Fellabaum, C.; Jovicic, N.; Arsenijevic, N.; Stojkovic, M. Stem Cells Therapy for Spinal Cord Injury. *Int. J. Mol. Sci.* **2018**, *19*, 1039. [[CrossRef](#)] [[PubMed](#)]
8. Krupa, P.; Vackova, I.; Ruzicka, J.; Zaviskova, K.; Dubisova, J.; Koci, Z.; Turnovcova, K.; Urdzikova, L.M.; Kubinova, S.; Rehak, S.; et al. The Effect of Human Mesenchymal Stem Cells Derived from Wharton's Jelly in Spinal Cord Injury Treatment Is Dose-Dependent and Can Be Facilitated by Repeated Application. *Int. J. Mol. Sci.* **2018**, *19*, 1503. [[CrossRef](#)] [[PubMed](#)]
9. Cizkova, D.; Cubinkova, V.; Smolek, T.; Murgoci, A.N.; Danko, J.; Vdoviakova, K.; Humenik, F.; Cizek, M.; Quanico, J.; Fournier, I.; et al. Localized Intrathecal Delivery of Mesenchymal Stromal Cells Conditioned Medium Improves Functional Recovery in a Rat Model of Spinal Cord Injury. *Int. J. Mol. Sci.* **2018**, *19*, 870. [[CrossRef](#)] [[PubMed](#)]
10. Hejcl, A.; Ruzicka, J.; Kekulova, K.; Svobodova, B.; Proks, V.; Mackova, H.; Jirankova, K.; Karova, K.; Machova Urdzikova, L.; Kubinova, S.; et al. Modified Methacrylate Hydrogels Improve Tissue Repair after Spinal Cord Injury. *Int. J. Mol. Sci.* **2018**, *19*, 2481. [[CrossRef](#)] [[PubMed](#)]
11. Irvine, S.F.; Kwok, J.C.F. Perineuronal Nets in Spinal Motoneurons: Chondroitin Sulphate Proteoglycan around Alpha Motoneurons. *Int. J. Mol. Sci.* **2018**, *19*, 1172. [[CrossRef](#)] [[PubMed](#)]
12. Kikuchi, K.; Setoyama, K.; Terashi, T.; Sumizono, M.; Tancharoen, S.; Otsuka, S.; Takada, S.; Nakanishi, K.; Ueda, K.; Sakakima, H.; et al. Application of a Novel Anti-Adhesive Membrane, E8002, in a Rat Laminectomy Model. *Int. J. Mol. Sci.* **2018**, *19*, 1513. [[CrossRef](#)] [[PubMed](#)]
13. Otzel, D.M.; Lee, J.; Ye, F.; Borst, S.E.; Yarrow, J.F. Activity-Based Physical Rehabilitation with Adjuvant Testosterone to Promote Neuromuscular Recovery after Spinal Cord Injury. *Int. J. Mol. Sci.* **2018**, *19*, 1701. [[CrossRef](#)] [[PubMed](#)]
14. Dalamagkas, K.; Tsintou, M.; Seifalian, A.; Seifalian, A.M. Translational Regenerative Therapies for Chronic Spinal Cord Injury. *Int. J. Mol. Sci.* **2018**, *19*, 1776. [[CrossRef](#)] [[PubMed](#)]



© 2018 by the author. Licensee MDPI, Basel, Switzerland. This article is an open access article distributed under the terms and conditions of the Creative Commons Attribution (CC BY) license (<http://creativecommons.org/licenses/by/4.0/>).



Article

# Combined Transcriptomics, Proteomics and Bioinformatics Identify Drug Targets in Spinal Cord Injury

Jure Tica <sup>1</sup>, Elizabeth J. Bradbury <sup>2</sup> and Athanasios Didangelos <sup>3,\*</sup>

<sup>1</sup> Imperial College London, Alexander Fleming Building, London SW7 2AZ, UK; j.tica16@imperial.ac.uk

<sup>2</sup> King's College London, Wolfson CARD, Institute of Psychiatry, Psychology & Neuroscience, London SE1 1UL, UK; elizabeth.bradbury@kcl.ac.uk

<sup>3</sup> Department of Infection, Immunity and Inflammation, University of Leicester, Leicester LE1 7RH, UK

\* Correspondence: ad482@leicester.ac.uk; Tel.: +44-(0)116-3736-272

Received: 31 January 2018; Accepted: 9 April 2018; Published: 14 May 2018

**Abstract:** Spinal cord injury (SCI) causes irreversible tissue damage and severe loss of neurological function. Currently, there are no approved treatments and very few therapeutic targets are under investigation. Here, we combined 4 high-throughput transcriptomics and proteomics datasets, 7 days and 8 weeks following clinically-relevant rat SCI to identify proteins with persistent differential expression post-injury. Out of thousands of differentially regulated entities our combined analysis identified 40 significantly upregulated versus 48 significantly downregulated molecules, which were persistently altered at the mRNA and protein level, 7 days and 8 weeks post-SCI. Bioinformatics analysis was then utilized to identify currently available drugs with activity against the filtered molecules and to isolate proteins with known or unknown function in SCI. Our findings revealed multiple overlooked therapeutic candidates with important bioactivity and established druggability but with unknown expression and function in SCI including the upregulated purine nucleoside phosphorylase (PNP), cathepsins A, H, Z (CTSA, CTSH, CTSZ) and proteasome protease PSMB10, as well as the downregulated ATP citrate lyase (ACLY), malic enzyme (ME1) and sodium-potassium ATPase (ATP1A3), amongst others. This work reveals previously unappreciated therapeutic candidates for SCI and available drugs, thus providing a valuable resource for further studies and potential repurposing of existing therapeutics for SCI.

**Keywords:** spinal cord injury; transcriptomics; proteomics; bioinformatics

## 1. Introduction

Severe injury to the mammalian spinal cord causes irreversible tissue damage and in most cases, results in permanent loss of sensorimotor function below the affected site. At the molecular level SCI is characterized by neuronal death and loss of axons, aggressive inflammation, maladaptive tissue remodelling, excessive accumulation of extracellular matrix and scarring [1,2]. These events cause permanent pathological changes at the injury site and prevent neuronal regeneration and axonal growth. With the exception of reducing acute inflammation using corticosteroids, a therapeutic approach which remains controversial [3], followed by chronic rehabilitation physiotherapy, there are no approved therapies for SCI and to date, no drugs can reverse tissue damage or facilitate regrowth of surviving axons through the lesion site. There are few experimental therapies currently under investigation, including antibodies against highly neurotoxic myelin debris proteins (i.e., anti-Nogo antibodies [4]), stabilization of axonal microtubules using paclitaxel/taxol and epothilone B to facilitate the regrowth of damaged axons [5,6] and chondroitinase ABC, an enzyme that digests the growth inhibitory glycosaminoglycan moieties in proteoglycans, which accumulate abundantly in the fibrotic

scar that develops after severe SCI and prevent neuronal growth through the injury site [7–9]. The complexity of the spinal tissue and the very severe inflammatory, fibrotic and neurodegenerative pathology together with the fact that the SCI patient population is relatively small in comparison to other neurological disorders, make the process of drug discovery difficult.

One possible approach to facilitate the discovery of novel pathological mechanisms and therapeutic targets is to utilize high-throughput -omics such as transcriptomics and proteomics. Contemporary high-throughput methods allow the interrogation of thousands of differentially regulated transcripts or proteins in multiple biological replicates in single quantitative experiments [10]. When combined with rigorous computational analysis of the large data that they return, -omics experiments can provide systems-wide insight into the pathological changes taking place in disease and allow the screening of multi-molecular changes instead of limited focusing towards single genes or proteins.

In this article, we sought to identify previously unappreciated and potentially promising therapeutic candidates for SCI by combining high-throughput transcriptomics and proteomics to profile gene and protein expression changes following clinically-relevant models of rat SCI. To ensure careful filtering of potential therapeutic candidates, we only retrieved molecules that were significantly regulated at the mRNA and protein level in tandem and showed consistent differential expression at 7 days (subacute) and 8 weeks (chronic) post-injury. We subsequently isolated druggable proteins and mined their potential function in SCI. This work could provide the basis for future mechanistic and preclinical studies investigating bioactive molecules with disease-modifying potential in SCI. Importantly, all transcriptomics and proteomics data, as well as the source code for the computational analysis that we developed, are available and freely accessible online via the *Mendeley Data* repository (Elsevier; <https://data.mendeley.com>) and our analysis is based on highly-cited freely accessible bioinformatics tools.

## 2. Results

### 2.1. Transcriptomics and Proteomics Analysis 7 Days and 8 Weeks after Rat SCI

SCI is a complex disorder which involves multiple different cell types and tissue substrates (neurons and axons, microglia and infiltrating immune cells, astrocytes, vascular cells, meningeal cells and others). It is also affected by the immune privilege of the central nervous system and the vascular limitations of the blood-brain-barrier. Multiparametric high-throughput approaches that examine large-scale transcript and protein changes in tandem can offer a broad understanding of molecular changes in SCI. To this end, we combined high-throughput transcriptomics and proteomics and at two different time-points (7 days and 8 weeks) after SCI to capture consistent and persistent molecular changes post-SCI and to identify proteins with important bioactivity and drug-targeting potential.

First, we performed an intersection of differentially regulated genes identified in a publicly available rat SCI microarray performed recently by Chamankhah and colleagues [11], to identify molecules that were significantly up or downregulated at the mRNA level, both at 7 days and 8 weeks post-SCI. Injury was performed by clip-compression using a 35 g aneurysm clip for 60 s, producing moderate to severe SCI [11]. We chose to use this transcriptomics study because it was performed by an experienced group, it had identical time-points to our proteomics analysis (see below) and importantly, compression SCI shares pathological similarities to contusion injury. This transcriptomics analysis compared uninjured (control) T7 spinal cord segments ( $n = 4$ ) versus injured spinal cord, either at 7 days ( $n = 4$ ) or 8 weeks ( $n = 4$ ) post-injury. All microarray data was made freely accessible online from the authors [11] via the gene expression omnibus (GEO-NCBI: <https://www.ncbi.nlm.nih.gov/geo/query/acc.cgi?acc=GSE45006>). Moreover, all differentially regulated transcripts from 7 days and 8 weeks post-SCI were downloaded from GEO-NCBI and have been publicly deposited as easily accessible excel files in Mendeley Data: control versus 7 days post-SCI microarray: <https://goo.gl/XqbbgN>; control versus 8 weeks post-SCI microarray: <https://goo.gl/BXYEeT>. Only genes that had adjusted  $p$ -value  $\leq 0.05$  were accepted in the analysis. 902 were significantly upregulated at both 7 days and 8 weeks versus 835 genes significantly downregulated at both time-points.

Second, to expand the transcriptomics findings to protein expression post-SCI, we used high-throughput proteomics datasets obtained from spinal tissue LC-MS/MS (liquid chromatography-tandem mass spectrometry) performed in our lab. High-throughput analysis at the protein level is biologically important given that transcripts tend to be short-lived in comparison to proteins and mRNA expression does not necessarily reflect protein expression or accumulation at tissue sites, especially given the substantial tissue remodelling that takes place in injured tissues.

To improve the relative enrichment of different protein species and the depth of protein identifications, we used a solubility-based tissue protein subfractionation method previously developed by us, which allows separate analysis of cellular and extracellular proteins by LC-MS/MS and is based on using 0.08% SDS to isolate cellular proteins followed by 4 M guanidine for extracellular matrix and insoluble proteins [10,12,13]. Control ( uninjured) versus injured rat spinal cord proteomics comparisons were made again at 7 days and 8 weeks post-SCI, matching the transcriptomics data. Relative estimation of protein abundance in tissue samples by LC-MS/MS was performed using spectral counting [14]. This comparison returned 115 proteins that were significantly upregulated and 149 proteins that were significantly downregulated in tandem, at both 7 days and 8 weeks post-SCI. All protein identification datasets, differentially regulated proteins and statistically analysed spectral counts from 7 days and 8 weeks post-SCI are publicly deposited as easily accessible excel files in Mendeley Data: 7 days proteomics: <https://goo.gl/k93LwN>; 8 weeks proteomics: <https://goo.gl/qYoTJz>.

## 2.2. Integration of Transcriptomics and Proteomics Datasets to Identify Persistently Differentially Regulated Molecules

To filter entities with consistent and persistent differential regulation at the mRNA and protein level and at 7 days and 8 weeks post-SCI, we integrated the transcriptomics and proteomics datasets described above. To ensure stringent selection, we accepted only molecules that were significantly differentially regulated (control vs. injured; *t*-test  $p \leq 0.05$ ) in all 4 high-throughput datasets (transcriptomics and proteomics, 7 days and 8 weeks post-SCI). This combined analysis returned a filtered signature of only 40 upregulated (Figure 1a–c) and 48 downregulated (Figure 1d–f) molecules, at the transcript and protein level and both at 7 days and 8 weeks post-SCI. These consistent signatures are summarised as heatmaps, which display differential expression from shotgun proteomics (upregulated; Figure 1a and downregulated; Figure 1d) as well as protein-protein interaction networks, which highlight the interconnectivity of the differentially regulated proteins (upregulated; Figure 1b and downregulated; Figure 1e). Figure 1c,f depict 10 upregulated and downregulated proteins respectively, with the highest network betweenness centrality, a measure of how associated and central a protein is in comparison to other network proteins and offers an unbiased assessment of its relative biological importance [15]. Conceivably, proteins with high betweenness centrality and therefore extensive biological association with other proteins, might be considered as good drug targets given that they likely have an important function in the system either in isolation or as part of a functional pathway.

### 2.2.1. 40 Persistently Upregulated Proteins

The network of the 40 upregulated entities (Figure 1a,b) contains multiple proteins involved in extracellular matrix metabolism, including minor glycoproteins galectin 3 (LGALS3), lumican (LUM) and decorin (DCN) together with annexin A2 (ANXA2) and both alpha chains of collagen-1 (COL1A1 and COL1A2). The upregulated network (Figure 1a,b) also contains cytoskeletal proteins such as LIMA1 (actin-binding), CALD1 (actin-binding caldesmon), AIF1 (microglia/macrophage cytoskeletal protein commonly known as IBA1), LCP1 (plastin-2, T cell actin-binding protein), filamin A (FLNA) and vimentin (VIM) an abundant non-epithelial cytoskeletal protein with key collagen-1 mRNA-stabilising function.

Consistently upregulated proteins also include 5 cathepsins (lysosomal proteases); A (CTSA), B (CTSB), D (CTSD), H (CTSH) and Z (CTSZ) (Figure 1a,b) covering a large spectrum of cellular

and extracellular proteolytic substrates. Cathepsin upregulation, proteolytic activity and lysosomal involvement are often associated with inflammatory tissue remodelling and loss of normal tissue function as well as activation of cell death pathways. Cathepsins are typically associated with activated macrophages and other immune cells [16]. The multicatalytic proteinase PSMB10 and dipeptidase PEPD, the latter with an important function in collagen-1 metabolism, are also present (Figure 1a,b). VIM, CTSD and ANX A2 have high betweenness centrality (Figure 1c), followed by FLNA and COL1A1 (Figure 1c), indicating relative biological importance in the system. The persistent upregulation of these proteins highlights the dominance of inflammation and scarring after SCI, driving pathological matrix remodelling and extensive proteolysis.

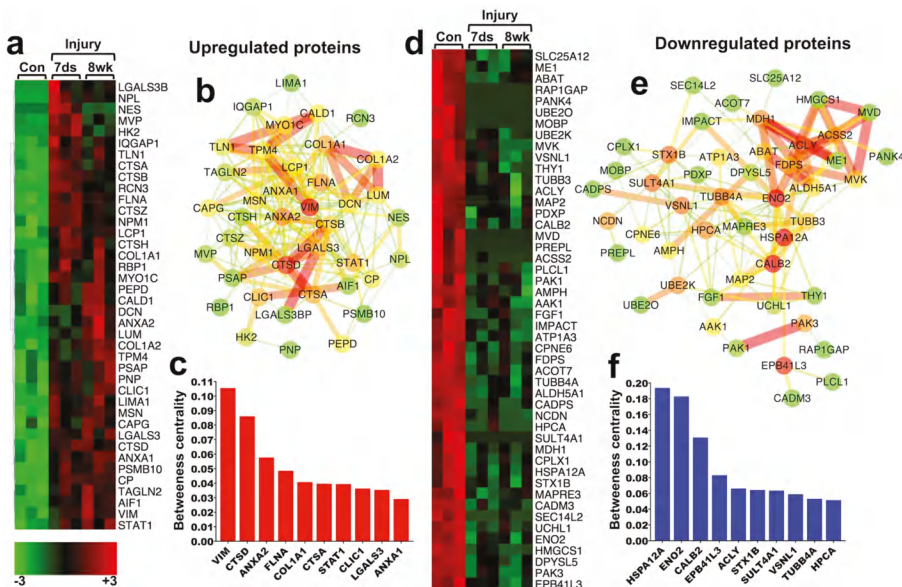


**Figure 1.** Persistently differentially regulated molecules at the mRNA and protein level 7 days and 8 weeks post-spinal cord injury (SCI): (a) 40 molecules that were consistently and significantly upregulated ( $t$ -test  $p \leq 0.05$ , Con vs. 7 ds and Con vs. 8 weeks) in all transcriptomics and proteomics datasets, at both 7 days and 8 weeks post-SCI. Heat-map displays differential protein expression quantified by spectral counting using shotgun proteomics. Heat-map values were normalised from -3 (green; low spectral counts) to +3 (red; high spectral counts). (b) The 40 persistently upregulated molecules were collected into a protein-protein interaction network using StringDB and Cytoscape. Node colours indicate protein betweenness centrality (how connected a protein is with others in the network); green nodes: low score; red nodes: high score. The width and colour of edges indicates protein-protein interaction score obtained from StringDB (green and slim: low interaction; red and broad: high interaction). Betweenness centrality and interaction scores were calculated and visualised in Cytoscape. (c) Ten upregulated proteins with the highest betweenness centrality score from network (b) are depicted. (d) 48 molecules that were consistently and significantly downregulated ( $t$ -test  $p \leq 0.05$ , Con vs. 7 ds and Con vs. 8 weeks) in all transcriptomics and proteomics datasets, at both 7 days and 8 weeks post-SCI. Heat-map displays differential protein expression quantified by spectral counting. (e) The 48 persistently downregulated molecules were collected into a protein-protein interaction network using StringDB and Cytoscape as above. (f) Ten downregulated proteins with the highest betweenness centrality from network (e) are depicted.

## 2.2.2. 48 Persistently Downregulated Proteins

Unsurprisingly, the network of the 48 persistently downregulated proteins (Figure 1d,e) contains multiple neuronal proteins with direct involvement in synaptic transmission including CPLX1 (complexin-1) and STX1B (syntaxin-1B) involved in synaptic vesicle function, ABAT (mitochondrial aminobutyrate aminotransferase) and ALDH5A1 (mitochondrial aldehyde dehydrogenase), both involved in the degradation of the neurotransmitter GABA, CPNE6 (copine-6; dendrite formation), HPCA (neuron-specific calcium-binding hippocalcin; regulates calcium channels), ME1 (malic enzyme) and AMPH (amphiphysin; involved in synaptic exocytosis). The persistent downregulation of synaptic-associated proteins is likely the result of neurodegeneration following SCI.

The downregulated network also contains 7 proteins involved in cholesterol and lipid synthesis and metabolism including MVD and MVK (mevalonate decarboxylase and kinase respectively), FDPS (farnesyl diphosphate/pyrophosphate kinase), HMGCS1 (catalyses synthesis of mevalonate from acetyl-CoA), ACSS2 (acetyl-CoA synthetase), ACLY (ATP citrate lyase) involved in acetyl-CoA metabolism and SEC14L2 (supernatant protein factor). The central nervous system-specific heat-shock protein 70, 12A (HSPA12A) has the highest betweenness centrality (Figure 1f) reflecting the role of chaperone heat-shock proteins in multiple biological functions. Neuron-specific gamma-enolase (ENO2 or NSE) with a catalytic role in the synthesis of pyruvate and CALB2 (calretinin; a neuron-specific calcium-binding protein) follow HSPA12A in betweenness centrality (Figure 1f). The consistent downregulation of proteins involved in cholesterol metabolism is very interesting and such mechanisms in SCI are not well understood. One likely hypothesis is their involvement in myelin synthesis [17] and as such, their restoration might promote myelination after SCI. In contrast, downregulation of cholesterol synthesis has been associated with the highly effective regenerative capacity that is observed in peripheral nerves [18].

## 2.3. Identification of Druggable Proteins in SCI

To examine further the tight list of 40 upregulated and 48 downregulated molecules, we first looked for proteins that could be targeted using currently available, clinically-approved or experimental drugs/bioactive chemicals and second, we asked whether these druggable proteins have been cited in studies related to SCI. Druggable proteins were predicted using DGIdb v3 [19] and further validated with StitchDB v5 [20]. The relevance of druggable proteins to SCI was then examined using an automated PubMed text-mining tool that we developed for this study (source code deposited online: <https://goo.gl/vRScJ3>). Druggable proteins were searched in PubMed in conjunction to the terms “spinal cord injury” and “spinal injury” as well as with the words “trauma,” “contusion” or “transection” replacing “injury” in the query.

DGIdb and StitchDB identified 15 upregulated druggable proteins, 10 of which returned at least one citation in SCI and 19 downregulated druggable proteins, 7 with at least one citation in SCI. These are summarised in Figure 2a. Druggable proteins are plotted against the number of drugs predicted to act against them (*x* axis) versus their betweenness centrality (*y* axis), to visualise druggability versus relative biological importance Figure 2a. Next, StitchDB-validated druggable proteins and their protein-protein as well as protein-drug interactions are illustrated in 4 networks. Figure 2b: 10 upregulated proteins with SCI citations plus 60 associated drugs; Figure 2c: 5 upregulated proteins with no SCI references plus 22 associated drugs; Figure 2d: 7 downregulated proteins with SCI citations plus 33 associated drugs; Figure 2e: 12 downregulated druggable proteins with no SCI citations plus 34 linked drugs. The predicted drugs from networks in Figure 2b–e were also text-mined in PubMed for potential reference to SCI (as described above) and the number of retrieved articles is shown in Figure 2f–i. All identified drugs from each network (Figure 2b–e) are listed here (<https://goo.gl/zwbuql>) together with the number of citations retrieved from text-mining using SCI terms (as explained above) and compared to terms “brain,” “spinal cord” and “central nervous system” for comparison. Links to the drug database PubChem is also provided for fast screening of essential drug information.

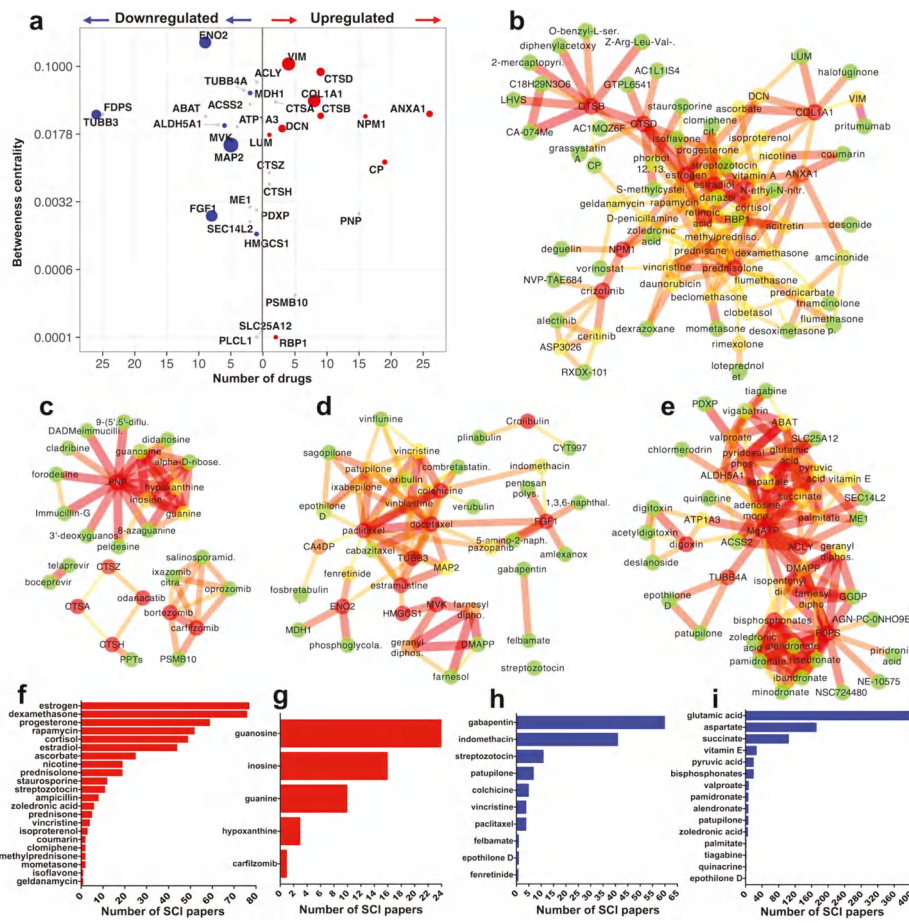


**Figure 2.** Mining druggable proteins using DGIdb and StitchDB: **(a)** DGIdb analysis followed by StitchDB identified 15 upregulated druggable proteins 10 of which returned at least one citation in SCI and 19 downregulated druggable proteins 7 of which with at least one citation in SCI. Proteins are summarised in 3 dimensions. Druggable proteins are plotted against the number of drugs predicted to act against them (*x* axis) versus their network betweenness centrality (*y* axis) to visualise druggability versus relative biological importance. The size of nodes (3rd dimension) indicates the number of PubMed articles citing these proteins in SCI. Grey nodes are proteins with no SCI citations in PubMed. **(b)** Protein-protein-drug interaction network of the 10 upregulated druggable proteins with at least one citation in SCI. The network was made using StitchDB and visualised in Cytoscape. Nodes and edges are colour-coded according to their betweenness centrality while the width and colour of edges indicates the strength of interaction between molecules (proteins and drugs) as predicted by StitchDB. **(c)** Protein-protein-drug interaction network of the 5 upregulated druggable proteins with no citations in SCI. **(d)** Protein-protein-drug interaction network of the 7 downregulated druggable proteins with at least one citation in SCI. **(e)** Protein-protein-drug interaction network of the 12 upregulated druggable proteins with no citations in SCI. **(f-i)** Predicted drugs from networks were text-mined in PubMed for potential reference to SCI and the number of articles is presented; **(f)** drugs interacting with proteins in network **(b)**; **(g)** drugs interacting with proteins in network **(c)**; **(h)** drugs interacting with proteins in network **(d)**; **(i)** drugs interacting with proteins in network **(e)**.

### 2.3.1. Upregulated Druggable Proteins with SCI Citations (Figure 2b,f)

In the group of upregulated proteins with SCI citations (Figure 2b), the association of annexin A1 (ANXA1) with classic corticosteroids (cortisone, dexamethasone, prednisone, amcinonide and associated steroids and hormones, i.e. estradiol and progesterone) dominates the network (Figure 2b). The potent anti-inflammatory effect of corticosteroids in tissues is thought to be exerted, at least in part, by regulating the synthesis and function of ANXA1 [21]. Interestingly, while ANXA1 has received limited attention in SCI, corticosteroids have been extensively used to reduce acute SCI inflammation (Figure 2f) but their efficacy in alleviating long-term pathology is debatable and their use is controversial [22,23]. Steroid hormones estradiol and progesterone are also well studied (Figure 2f) and are considered neuroprotective in SCI [24].

Another notable cluster in Figure 2b includes the well-studied cathepsins B and D (CTSB, CTSD) and the numerous mostly experimental inhibitors that block their proteolytic activity. Both CTSB and CTSD are likely involved in the degradation of axonal components after SCI [25] but notably anti-cathepsin drugs have not been used in SCI thus far in either preclinical or clinical studies. NPM1 (nucleophosmin; Figure 2b) is associated with anti-neoplastic drugs crizotinib and deguelin (plus associated compounds). While inhibition of NPM1 was recently noted to block neuronal apoptosis after SCI in one study [26], neither deguelin nor crizotinib have been tested in SCI (Figure 2f).

Although vimentin (VIM; Figure 2b) has been cited extensively in SCI, mainly as a non-specific marker of proliferating (astrocytes, ependymal cells, fibroblasts) or invading (macrophages, endothelial cells, progenitors) mesenchymal cells in the injury site, it has not been tested as a putative drug target thus far. The cytoskeletal protein, which has very high betweenness centrality (Figure 2a), is recently gaining attention as a potential target in glioma and other cancers using antibodies against its ectodomain (pritumumab [27]). In SCI, anti-vimentin antibodies could be conceivably used for the removal of vimentin-positive cells but the selectivity of such an approach against a protein that is highly abundant in multiple cell types, some with potentially neuroprotective roles [28], is questionable.

The archetypal matrix and fibrosis protein collagen-1 (chain COL1A1; Figure 2b) is persistently upregulated after SCI, it has high betweenness centrality (Figure 2f) and is associated with the anti-fibrosis collagen expression blocker halofuginone [29], as well as with the beta-adrenergic receptor agonist isoproterenol (Figure 2b), known to increase its expression [30]. Notably, this is one of the very few cases of an agonist present in our analysis. The potential involvement of collagen-1 in matrix remodelling, fibrosis and scarring after SCI is a promising area for future investigation.

### 2.3.2. Upregulated Druggable Proteins without SCI Citations (Figure 2c,g)

In this small network the extensive druggability of PNP (purine nucleoside phosphorylase), an enzyme that converts ribonucleosides into purine bases, is striking. PNP has been implicated as an inflammatory mediator in glia as well as peripheral T and B-cells and is a good target for anti-inflammatory therapies especially with regards to T-cell activity [31–33]. PNP has not been studied in SCI and might represent an interesting drug target given its persistent upregulation, its involvement in inflammatory mechanisms and the sizeable cohort of associated drugs (Figure 2c) that can block its function (i.e. immucillins and forodesine). Interestingly, purine derivatives that associate with PNP (guanosine, inosine, hypoxanthine) are used in experimental SCI as neuroprotective/neurotrophic agents but this is independent to their biological connection to PNP [34].

Unlike cathepsins B and D (CTSB, CTSD) discussed above, the function of upregulated CTSA, CTSH and CTSZ in SCI is unknown (Figure 2c). Similarly, neither specific cathepsin blockers (PPTs: odanacatib, toluenesulfonic acid) nor other protease inhibitors (telaprevir, boceprevir), have been tested in SCI. CTSA, CTSH and CTSZ are all persistently upregulated after SCI and CTSA has high betweenness centrality (Figure 2a). Thus, the availability of cathepsin blockers (Figure 2c) and the lack of knowledge about these cathepsins make them interesting candidates for further investigation. In addition to cathepsins, the role of the proteasome protease PSMB10 (Figure 2c) in the spinal cord is not studied and not much is known about the proteasome-ubiquitin system in SCI [35]. The proteasome inhibitor carfilzomib which interacts

with PSMB10 (Figure 2c), was recently shown to exert an acute neuroprotective effect after T10 transection SCI in rats (Figure 2g) but the authors did not implicate PSMB10 to this effect [36].

### 2.3.3. Downregulated Druggable Proteins with SCI Citations (Figure 2d,h)

This dense network contains few multi-druggable entities (Figure 2d,h). The classic neuronal tubulin beta-3 (TUBB3) is associated with many cytoskeleton-regulating drugs, mainly paclitaxel (taxol) and derivatives (docetaxel, cabazitaxel, epothilone D, patupilone/epothilone B) plus other putative microtubule stabilisers like estramustine, vinblastine and vincristine (Figure 2d). Although mainly used as anti-neoplastic agents, microtubule stabilisers (notably paclitaxel and patupilone/epothilone B) are currently at the forefront of experimental SCI therapies [5,6]. Another microtubule assembly protein, MAP2 (microtubule-associated protein 2) is consistently downregulated after SCI (Figure 1d) and is also predicted to interact with these drugs (Figure 2d). MAP2 is a well-studied neuronal marker. It has been previously shown to be downregulated after SCI and its loss is associated with destabilization and depolymerization of axonal microtubules [37].

The activity of the acidic fibroblast growth factor FGF1 can be blocked by the tyrosine kinase inhibitor pazopanib (FGF1 activates tyrosine kinase signalling) and by the anti-inflammatory amlexanox (Figure 2d) both with no citations in SCI. Nevertheless, the use of drugs that block FGF1 activity is counterintuitive, as it is persistently downregulated in our analysis plus it has been shown to be neurotrophic and neurorestorative after SCI in preclinical studies [38]. Like FGF1, neuron-specific enolase (ENO2/NSE; Figure 2d) has broad neuroprotective function in the central nervous system [39]. ENO2 is a protein with high betweenness centrality (Figure 2a) and potentially high biological importance. The anti-cancer drug fenretinide has been found to interact with enolase (Figure 2d) but the exact pharmacological action is unknown. Interestingly, fenretinide was recently shown to alleviate inflammation in murine contusion SCI but the authors did not connect this effect to ENO2 [40].

Key downregulated sterol synthesis enzymes MVK and HMGCS1 interact with the chemical farnesol (Figure 2d) but potential pharmacological effects are unclear. They also interact with substrates geranyl and farnesyl diphosphate, again with unknown pharmacological benefit. The role of MVK and HMGCS1 is unclear but cholesterol metabolism and the mevalonate cascade are recently gaining attention in the field [41].

### 2.3.4. Downregulated Druggable Proteins without SCI Citations (Figure 2e,i)

In conjunction with MVK and HMGCS1 from (Figure 2d), farnesyl diphosphate/pyrophosphate synthase (FDPS) is a critical mevalonate synthesis enzyme with multiple established bisphosphonates (i.e., alendronate, etidronate, etc.) as well as experimental (NE-10575, NSC724480) inhibitors (Figure 2e) and medium betweenness centrality (Figure 2a). Yet, the enzyme has not been studied in SCI and its function in the brain and spinal cord remains elusive [42]. In contrast, clinical and experimental inhibition of FDPS by bisphosphonates is the gold-standard approach to block bone resorption by inhibiting the function of osteoclasts. As a result, bisphosphonates are currently used to regulate inactivity-induced bone resorption in SCI patients [43] and this is independent to any potential function of FDPS in the spinal cord. ACSS2 and ACLY are important lipid synthesis mediators with high betweenness centrality but unknown role in SCI (Figure 2a). They are prominent in the drug network (Figure 2e), mainly due to their interaction with adenosine phosphate (and MgATP) and lipid metabolism intermediaries palmitate, succinate and pyruvate. Potential therapeutic effects are unknown. Notably, ACLY is involved in the synthesis of the neurotransmitter acetylcholine in the brain [44]. ACLY is also associated with ME1 (malic enzyme; Figure 2e) which generates NADPH for fatty acid synthesis. The role of ME1 in the spinal cord is also unknown but it was recently shown, together with other lipid synthesis molecules, to have a possible function in white matter development in infants [45].

ATP1A3 (Figure 2e), a sodium/potassium pump ATPase is another enzyme with unknown function in SCI and high betweenness centrality (Figure 2a). The enzyme has a distinct neuronal function as it is involved in the generation of electrical impulses and in the transport of

neurotransmitters and calcium ions across the plasma membrane [46,47]. It is associated with the cardiac glycoside digoxin/digitoxin and derivatives, which have not been tested as SCI treatments and are rarely used in modern clinical practice to enhance cardiac function.

Two highly druggable, downregulated proteins with high betweenness centrality are aldehyde dehydrogenase 5A (ALDH5A1) and 4-aminobutyrate aminotransferase (ABAT) (Figure 2a,e) both involved in the catabolism of the inhibitory neurotransmitter GABA [48,49]. Interestingly, although the role of these GABA catabolic enzymes in SCI is unknown, the associated drug valproate (plus associated vigabatrin, chlormerodrin and tiagabine) are used (Figure 2i) to increase GABA and prevent the spasticity and involuntary muscle contractility that affects the majority of SCI patients [50]. Thus, it could be speculated that the persistent downregulation of ALDH5A1 and ABAT described here, might contribute to the molecular mechanisms of post-SCI spasticity which is nevertheless caused by very complex neuronal mechanisms following injury to upper or lower motor neurons.

### 2.3.5. Transcription Factor Regulation of Persistently Differentially Regulated Proteins

One approach to regulate gene and protein expression in tissues is via interference with relevant transcription factor activity. Given that our combined intersection of transcriptomics and proteomics datasets isolated a filtered list of 40 significantly upregulated and 48 significantly downregulated proteins both at the mRNA and protein level and both at 7 days and 8 weeks post-SCI (Figure 1), we sought to examine likely transcription factor promoter-binding sites for the identified proteins. To do this, we used TRANSFAC-7-based computational prediction for transcription factor promoter binding sites (MSigDB; [51]). This analysis returned 9 transcription factors as potential regulators of the 40 upregulated proteins (Figure 3a) and 5 transcription factors potentially controlling the expression of the 48 downregulated proteins (Figure 3b).

SP1 followed by TCF3 (or TFE2) are predicted to bind to the highest number of upregulated gene promoters (Figure 3a) while MAZ and SP1 are predicted for the highest number of downregulated genes (Figure 3b). These transcription factors are conserved and abundant housekeepers and regulate a plethora of genes, hence their involvement is not surprising. Nevertheless, potential specific role of either MAZ or SP1 in SCI is currently unknown.

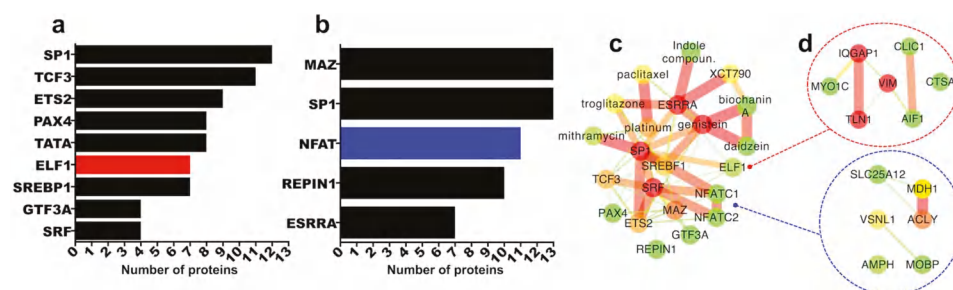


**Figure 3.** Transcription factor promoter binding site analysis for 40 and 48 persistently differentially regulated proteins: (a,b) MSigDB was used to identify transcription factors with likely promoter binding sites for the molecules that were consistently upregulated (a) or downregulated (b) in all 4 transcriptomics and proteomics datasets, at both 7 days and 8 weeks post-SCI. Graphs display the number of proteins (x axis) likely regulated by listed transcription factors. ELF1 is upregulated while NFATC1 is downregulated in both 7 days and 8 weeks transcriptomics datasets. (c) Protein-protein-drug interaction network made in StitchDB and Cytoscape depicting interacting transcription factors (from a,b) and associated drugs. Neither ELF1 nor NFATC1 have predicted drugs with either DGIdb or StitchDB. The upregulated (red) and downregulated proteins with likely promoter binding sites for ELF1 and NFATC1 are highlighted in (d).

When we examined the expression profile of these transcription factors in the transcriptomics and proteomics datasets we found that although none were differentially regulated at the protein level (proteomics datasets) ELF1 which was predicted to regulate 7 of the 40 persistently upregulated proteins (Figure 3a), was itself upregulated at the mRNA level both at 7 days and 8 weeks post-SCI (7 days SCI microarray: <https://goo.gl/XqbbgN>; 8 weeks SCI microarray: <https://goo.gl/BXYEeT>). On the other hand, NFAT transcription factor complex promoter binding sites were predicted for 11 of the 48 persistently downregulated proteins (Figure 3b) and NFATC1, one of the NFAT components, was downregulated at the mRNA level at both 7 days and 8 weeks post-SCI (7 days SCI microarray: <https://goo.gl/XqbbgN>; 8 weeks SCI microarray: <https://goo.gl/BXYEeT>). As for SP1 and MAZ (both upregulated at the mRNA level at 7 days but not 8 weeks), the potential function of either ELF1 or NFATC1 in SCI is unknown. Upregulated proteins with predicted regulation by ELF1 and downregulated proteins with predicted regulation by NFATC1 are depicted in Figure 3d. Predicted transcription factors from Figure 3a,b were also examined using DGIdb and StitchDB for potential association with drugs (Figure 3c). Neither ELF1 nor NFATC1 appear to be druggable. SP1 and ESRRA, are instead associated with anti-cancer compounds (Figure 3c) which have not been tested in SCI thus far. Interestingly, the only transcription factor found in the filtered list of the 40 upregulated molecules at the mRNA and protein level, 7 days and 8 weeks post-SCI, is STAT1 (signal transducer and activator of transcription 1), a key regulator of inflammatory mechanisms and interferon signalling in particular [52,53]. STAT1 is persistently upregulated after SCI and has a high betweenness centrality (Figure 1a–c). Although it has been involved in various inflammatory mechanisms and diseases, its function after SCI is not well-studied, albeit few recent studies have shown that blocking STAT1 activity has a positive effect post-SCI [54,55]. To the best of our knowledge, no approved drugs or inhibitors offer selective inhibition of STAT1.

### 3. Discussion

In this manuscript combination of transcriptomics, proteomics and bioinformatics provides a comprehensive overview of proteins with persistent differential expression at the mRNA and protein level and from the subacute (7 days) to the chronic (8 weeks) phase of SCI lesion development. To ensure stringent filtering, we accepted only molecules that were significantly differentially regulated in all high-throughput datasets (transcriptomics and proteomics, 7 days and 8 weeks post-SCI). The intersection of transcriptomics and proteomics is useful given that while mRNA screening provides a snapshot of the dynamic gene expression changes following SCI, proteomics confirms functional expression of proteins from regulated transcripts and underscores proteotypic changes in the injured spinal cord. To the best of our knowledge, this is the first attempt to systematically analyse the molecular druggability of SCI in high-throughput.

The intersection of transcriptomics and proteomics at 2 different injury time-points and from 2 independent labs using comparable contusion and compression SCI models in female rats, ensures unbiased validation of the high-throughput data and offers confidence in the filtering of these molecular targets. Nevertheless, it is important to note that the transcriptomics and proteomics data were based on two different SCI models as well as rat strains. More specifically, the transcriptomics analysis by Chamankhah et al. was based on a T7 aneurysm clip (35 g) compression injury (moderate to severe) in female Wistar rats [11], while our proteomics analysis was based on automated 150 kilo-dyne (1.5 Newton) spinal contusion injuries (moderate), performed on female Sprague-Dawley rats (see Section 4 for more details and [7,9,10,56]). It is important to note that different injury models might cause variable tissue pathology and sensorimotor outcomes. Differences and similarities between contusive and compressive injuries have not been studied in detail but both models are considered comparable, as they rely on blunt trauma to the spinal cord and normally involve neither penetration of the meninges, nor sharp severing of axons (as occurs in hemisections and full transections). As a result, they better simulate the biomechanical damage observed in the majority of human injuries (reviewed and summarized in [57–60]). Few studies have directly compared contusions with compressions. Pinzon et al., showed that gross lesion pathological features did not appear to differ greatly between

contusion and compression injuries [61]. More recently, Geremia and colleagues concluded that lesion volumes and gross tissue pathology were not significantly different between contusion (severe T12, 200 kilo-dyne) and clip-compression (moderate to severe T12, 35 g aneurysm clip), albeit clearly increased hematoma formation and spreading in the severe contusion group [62]. Differences in contusion/compression forces applied in different studies are clearly important in terms of defining injury severity. Comparison between strains has revealed differences in a number of studies not only between strains but even in same strains obtained from different vendors [63]. 20 years ago Popovich and colleagues focused on differences in inflammation after SCI. They found that while the basic inflammatory reaction after SCI follows similar patterns in Sprague-Dawley and Lewis rats, differences were observed in the magnitude and duration of macrophage activation and T-cell infiltration in lesions. The authors attributed these differences to strain-specific variations in corticosteroid regulation of inflammation [64]. Accordingly, using a neuronal-specific gene array, Schmitt et al., showed that the expression of several genes varies between Sprague-Dawley, Long Evans and Lewis rats after contusive SCI [65] and in a study focusing on post-SCI sensorimotor function, Mills et al., showed that strain selection significantly affects functional recovery in Sprague-Dawley and Wistar rats [57]. Thus, different strains might exhibit pathological or sensorimotor differences. Nevertheless, our focus on proteins that are differentially regulated in both models, both time-points and both at the mRNA and protein level highlights the likely importance of these differentially regulated signatures to SCI.

Our high-throughput intersection returned 40 persistently upregulated and 48 persistently downregulated proteins. To further narrow down the list of target molecules, we applied two-tier computational protein-protein-drug interaction screening combined with literature text-mining. This analysis isolated previously unappreciated druggable proteins and pharmacological substances that could be examined in future experimental and preclinical SCI studies. Notably, excluding a few proteins that have been studied extensively in SCI (i.e., vimentin, IBA1, decorin, ceruloplasmin, CTSB, CTSD, tubulin beta-3, ENO2/NSE, FGF1, MAP2 and others) many proteins and drugs identified in our comparative analysis have received little to no experimental attention and some might be excellent targets for future investigations.

While it would be very difficult within the limits of this manuscript to cover in detail the function of each protein and their potential role in SCI, we have made an effort to describe the bioactivity of multiple druggable proteins and put it in the context of SCI where applicable (see Figure 2 and associated Results). Given that the majority of drugs are antagonists, inhibitors, or function-blockers, upregulated molecules are excellent primary candidates for drug targeting. In contrast, downregulated entities might be modulated with function agonists or over-expression with more complex molecular tools such as viruses or CrispR/CAS9.

Based on biological function, druggability and crucially, lack of knowledge with regards to SCI, we could highlight few interesting proteins that are consistently upregulated or downregulated at the mRNA and protein level, at 7 days and 8 weeks individually depicted in Figure 4. From the upregulated cohort, PNP (purine nucleoside phosphorylase) is a protein with well-documented involvement in T-cell activity and function and PNP inhibitors exert potent immunomodulatory effects against T-cells, especially in diseases with dominant involvement of adaptive immunity [32,66,67]. The role of PNP in B-cell function is also under investigation. Notably, not only the potential function of PNP in SCI is unknown but in addition, the role of T-cells is still unclear, although T-cells infiltrate spinal lesions [64]. Thus, given the importance of inflammation in primary and secondary SCI pathology and the importance of T-cells in immune processes, the highly druggable PNP (Figure 2c) is a very interesting candidate.

Similarly, the role of upregulated lysosomal cathepsin A (CTSA; Figure 4) in SCI is unknown. This serine protease and carboxypeptidase is involved in the activation of sialidase and its deficiency causes the lysosomal storage disease galactosialidosis [68]. It also seems to play an important role in autophagy, which is involved in the regulation of various inflammatory mechanisms including SCI [69]. Recent work in mice showed that CTSA deficiency is associated with a severe neurological

phenotype [70]. Similarly, the role of the other consistently upregulated cathepsins CTSH and CTSZ (Figure 4) in SCI is unknown.

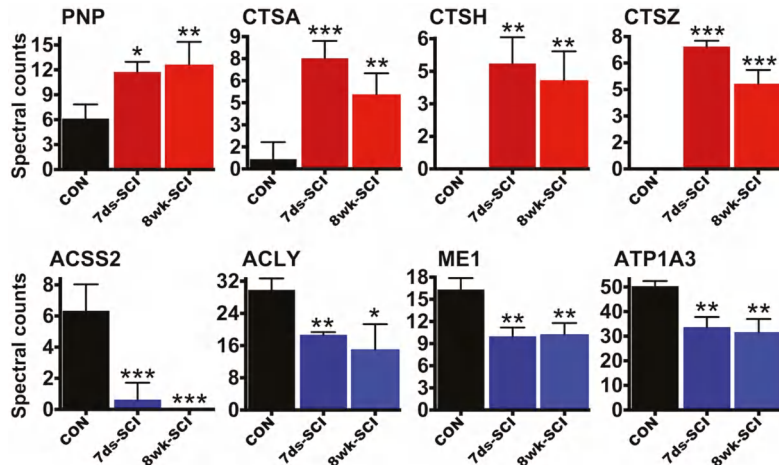


**Figure 4.** Highlighted differentially regulated proteins after SCI. Graphs depict the differential expression of upregulated purine nucleoside phosphorylase (PNP), cathepsins A, H and Z (CTSA, CTSH, CTSZ) and downregulated ACSS2 (acetyl-CoA synthetase), ATP citrate lyase (ACLY), malic enzyme (ME1) and sodium-potassium ATPase (ATP1A3) proteins using spectral counting values from shotgun liquid chromatography-tandem mass spectrometry (LC-MS/MS). These proteins are amongst the molecules that were consistently upregulated or downregulated at the mRNA and protein level and at 7 days and 8 weeks post-SCI.  $n = 3$  per group; mean  $\pm$  SD; ANOVA and Fisher post-hoc test (independent comparison); stars indicate significance versus CON (control intact T10 spinal cord segments); \*  $p \leq 0.05$ , \*\*  $p \leq 0.01$ , \*\*\*  $p \leq 0.001$ . CTSA and CTSZ spectral counts are also significantly different from 7 days to 8 weeks.

From the persistently downregulated proteins, lipid and sterol synthesis mediators including ACSS2, ACLY and ME1 (Figure 4) are attractive candidates for further research. They might be involved in lipid and energy homeostasis or in myelin synthesis post-injury. The distinctly neuronal ATP1A3 is another persistently downregulated protein (Figure 4) with very interesting properties given its involvement in neurotransmission [47]. The protein has been studied extensively for its function in the central nervous system but its role in SCI is unknown. Mutations that impair ATP1A3 activity cause rapid-onset dystonia in humans and permanent neurological dysfunction [71]. The enzyme is also downregulated after neonatal cortical injury in rats [46].

In summary, by using a combination of transcriptomics, proteomics and bioinformatics we isolated multiple proteins with drug-targeting potential and unknown function in SCI. While it might be difficult to speculate on the best possible drug target or identify a panacea for SCI, our systematic analysis might stimulate further mechanistic or therapeutic studies in the future.

#### 4. Materials and Methods

##### 4.1. Rat Transcriptomics—Microarray Analysis of Rat SCI

The rat microarray datasets analysed and integrated in this manuscript were recently performed and published by Chamankhah and colleagues. Information about the ethical use of animals in this study and in-depth information about the clinically-relevant compressive SCI model utilised in their study has been published [11]. Briefly, the authors used a clip compression SCI in female Wistar rats

using a 35 g aneurysm clip for 60 s producing a moderate to severe T7 SCI. The compression model produces comparable blunt-force gross pathology and lesion characteristics to the contusion model that we used on the thoracic spinal cord (see below). Microarray data is available online via the gene expression omnibus (GEO-NCBI). Microarray data from GEO is qualitatively and statistically curated and MIAME-compliant. Rat T7 spinal clip compression injury microarray  $n = 4$  intact versus injured T7 spinal cord samples at 7 days ( $n = 4$ ) and 8 weeks ( $n = 4$ ) post-injury. Microarray experimental information is available here (GEO-NCBI: <https://www.ncbi.nlm.nih.gov/geo/query/acc.cgi?acc=GSE45006>). Additionally, microarray expression data was downloaded and compiled to excel files (.xlsx) to enable uncomplicated examination of differential mRNA expression between control and injured spinal cord specimens at 7 days and 8 weeks post-SCI and to allow investigation of individual genes. Due to their excessive size, these excel files have been publicly deposited and are free to download from the Mendeley Data public repository. Control versus 7 days post-SCI microarray comparison can be found here: (7 days SCI microarray: <https://goo.gl/XqbbgN>; 8 weeks SCI microarray: <https://goo.gl/BXYFeT>). Expression and statistical analysis was performed by GEO-NCBI using standard *t*-test *p*-values and multiple *p*-value error adjustments. We only accepted transcripts that were significant with an adjusted *p*  $\leq 0.05$  and 2-fold change at both 7 days and 8 weeks.

#### 4.2. Spinal Cord Injury Model in Rats for Proteomics Analysis

We have previously characterised in detail spinal cord contusion in adult rats [7,9,10,56]. Briefly, adult female Sprague-Dawley rats (~200 g) were anaesthetised using breathable isofluorane. 5 mg/kg Baytril (antibiotic) and 5 mg/kg Carprofen (NSAID pain and inflammation control) were given subcutaneously at the time of surgery and the morning after surgery. Spinal laminectomies were performed at vertebral level T10, the vertebral column was stabilised using Adson forceps and the rat-specific impactor probe was positioned 2 mm above the spinal cord. An impact force of 150 kilo-dyne (mean 152.3 kilo-dyne; standard deviation 3.2;  $n = 6$  contused animals) was delivered to the exposed spinal cord through the intact dura with an Infinite Horizon impactor (Precision Systems Instrumentation) which generates a moderate severity contusion injury according to our Home Office-approved animal licence. This severity mimics more than 50% of human injuries that are “incomplete” (i.e., where some white matter tissue is spared) containing uninjured axons and the model is generally considered to be relatively clinically-relevant. After injury, all 6 animals used in the study had full bilateral hind limb paralysis and started exhibiting limited spontaneous recovery typically after the first week. After spinal contusion, the overlying muscle and skin were sutured, anaesthesia was reversed using oxygen and animals recovered in cages placed on heated blankets. Saline and Baytril (antibiotic) were given subcutaneously daily for 7 days, after injury. Bladders were manually expressed twice daily until reflexive emptying returned (typically 6–9 days after injury). The study has received approval by the institutional Animal Care and Use Committee (King’s College London; PPL 70/8032, 14/11/2016) and all surgical procedures were performed in accordance with the United Kingdom Animals (Surgical Procedures) Act 1996.

#### 4.3. Shotgun LC-MS/MS Proteomics—Proteomics Analysis of Rat SCI

We have recently described in detail and published high-resolution shotgun LC-MS/MS proteomics analysis of rat SCI [10]. Prior to proteomics spinal cord tissue from intact ( $n = 3$ ) or injured T10 spinal cord segments 7 days ( $n = 3$ ) and 8 weeks ( $n = 3$ ) post-injury were extracted using a sequential protein extraction protocol previously developed by us [10,12,13]. This approach improves separation of easily soluble cellular proteins (0.08% SDS) followed by isolation of insoluble and cross-linked, extracellular, matrix and matrix-associated extracellular proteins from tissue specimens (4 M guanidine). This method has been published multiple times and is widely used for different tissues including the spinal cord. Following protein extraction shotgun LC-MS/MS was performed as described in depth [10]. Briefly, protein samples were digested by trypsin, tryptic peptides were separated in 2–35%, 120 min acetonitrile gradient and analysed on Q Exactive orbitrap mass spectrometer. Protein identifications were performed using Mascot

Version 2.4.1 (Matrix Science). Scaffold [72] (version 4.2.1) was used to validate MS/MS based peptide and protein identifications. Peptide identifications were accepted only if they could be established at greater than 95.0% probability by the Peptide Prophet algorithm with Scaffold delta-mass correction. Protein identifications were accepted only if they could be established at greater than 95.0% probability and contained at least 2 unique identified peptides. Scaffold was also used to calculate normalised spectral counts for quantitation. All accepted protein spectra (95% probability plus 2 unique peptides minimum) were included in the analysis and no outliers were removed. Although there are multiple different approaches to achieve relative protein quantitation using LC-MS/MS, spectral counting is very simple and less prone to technical errors in comparison to protein-labelling approaches especially when combined with orthogonal validation of findings [10,14]. In this manuscript, extra confidence is obtained from the fact that we focus only on proteins that are common across 2 independent transcriptomics and proteomics datasets and across 2 different time-points. Only proteins with  $t$ -test  $p \leq 0.05$  at both 7 days and 8 weeks and concomitant significant differential regulation ( $p \leq 0.05$ ) at the transcript level (from microarrays described above) at both 7 days and 8 weeks were accepted. All proteomics identifications and spectral counting quantitation has been deposited online at Mendeley Data: 7 days proteomics: <https://goo.gl/k93LwN>; 8 weeks proteomics: <https://goo.gl/qYoTJz>.

#### 4.4. Computational and Bioinformatics Analysis of High-Throughput Data

Hierarchical clustering and heat-maps were created in the MeV TM4 platform [73]. Significantly different ( $p \leq 0.05$ ;  $t$ -test) spectral counts were z-normalised (-3; low to +3; high) to obtain a more linear colour representation of the data. Pairwise similarity in spectral counts between different proteins (rows) was computed using Pearson correlation coefficient. Protein-protein interaction networks were created using StringDB v10 (<https://string-db.org>) [74] of known and predicted protein-protein interactions and inferring protein associations from multiple databases as well as text-mining. For protein-protein interaction networks, a low threshold of association (0.15) was used to capture the largest possible interaction probability. Network parameters were visualised in Cytoscape v2.8 [75], which was also used to calculate the betweenness centrality of interacting proteins within networks. Drug candidate analysis was performed using DGIdb (<http://www.dgideb.org>) [19]. This software is searching multiple different drug databases and uses text-mining to identify drugs matching input proteins. Drug-protein interactions were then validated and filtered using StitchDB v5 (<http://stitch.embl.de>) [20]. This step resulted in significant filtering of the drug-protein interaction data. StitchDB also creates organic drug-protein and protein-protein interaction networks, the latter using the StringDB platform and generates interaction scores. For protein-drug interactions, a medium threshold of association (0.40) was used to ensure more stringent filtering of drugs and chemicals. As above, network parameters were visualised in Cytoscape v2.8, which was also used to calculate the betweenness centrality of interacting proteins and drugs within networks. Transcription factor analysis was performed using MSigDB (<http://software.broadinstitute.org/gsea/msigdb>) [51], transcription factor targets sub-collection. Mammalian transcriptional regulatory motifs were extracted from v7.4 TRANSFAC database. Each gene set consists of all human genes whose promoters contains at least one conserved instance of the TRANSFAC motif, where a promoter is defined as the non-coding sequence contained within 4-kilobases from the transcription start site.

#### 4.5. Gene and Drug Java Text-Mining Tool

The custom-made text-mining tool was constructed using Java in IntelliJ IDEA community edition. The code used has been publicly deposited in Mendeley Data for Journals and can be found here together with running instructions to operate the tool in IntelliJ for free (<https://goo.gl/vRScJ3>). Firstly, the nomenclature for the text-mined genes is retrieved using the HGNC REST web-service API (<https://www.genenames.org/help/rest-web-service-help>). The gene symbol, gene name and synonym identifiers were used in the literature queries. The gene nomenclature is enriched by a set of algorithms that are designed to permute names and omit obsolete name parts. The literature queries

are performed using the Europe PubMed Central (EPMC) REST web-service API after nomenclature retrieval. The EPMC database queries are structured into two blocks; the first block contains all gene names, abbreviations, synonyms and accepted protein names from HGNC, whereas the second block contains the keywords of interest including: “spinal cord injury” and “spinal injury” as well as with the words “trauma,” “contusion” or “transection” replacing “injury” in the query. The search clause is structured so that at least one search term belonging to each of the search blocks must be present in the abstract or title of the retrieved articles. All search terms were enclosed in quotations to ensure that the terms are searched as is and that individual words within the term are not matched mistakenly. The retrieved articles were manually verified to satisfy search requirements. Drug text-mining was performed similarly. The drugs for the differentially regulated genes were derived manually with the use of DGIdb and StitchDB. Next, EPMC was queried in the same way as for the genes, where the first block of the query contained the primary drug names instead of gene names. This article set contained no false positives. Please note that different text-mining search engines such as Google Scholar might retrieve more or different studies regarding the usage of certain drugs in SCI but in our experience PubMed is more reliable with regards to peer-reviewed research-based studies and in our experience, retrieves fewer false-positives. A deeper text-mining was then performed using all drug synonyms, chemical names and commercial names to ensure a full, in-depth retrieval of literature. Drug synonyms were retrieved using the PubChem REST web-service APIs. The risk for the retrieval of false positive articles was high in this search due to the extensive variety of drug synonyms stored in the PubChem database. To avoid the retrieval of false positives, the results of the deep text mining were overlaid with the “drug name only” results and differences in article numbers between the two datasets were inspected manually and false positives eliminated. URL addresses for all online database queries (PubChem, HGNC, EPMC, UniProt) are output in the console at runtime. The user can verify database query parameters by navigating to these URLs manually. Please note that although every effort was made to minimise retrieval of false-positive associations via text-mining, users must ensure a stringent manual search of target molecules.

**Author Contributions:** A.D. conceived this work, designed experiments, analysed data, prepared figures and wrote the manuscript; J.T. designed experiments (text-mining), analysed data, prepared figures and wrote the manuscript; E.J.B. supervised part of this work and edited the manuscript.

**Acknowledgments:** This work was funded by the RoseTrees Trust (M276 and A1384) to Athanasios Didangelos and Elizabeth J. Bradbury; EU 7th framework program (PrimeXS 0220) to Athanasios Didangelos; the Medical Research Council (MRC; SNCF G1002055) to Elizabeth J. Bradbury; MRC and EU funded MR/R005532/1 ERA-NET NEURON to Elizabeth J. Bradbury and Athanasios Didangelos. Athanasios Didangelos was funded by the London Law Trust and King’s College London.

**Conflicts of Interest:** The authors declare no conflict of interest.

## Abbreviations

SCI	Spinal cord injury
LC-MS/MS	Liquid-chromatography and tandem mass-spectrometry

## References

1. Cregg, J.M.; DePaul, M.A.; Filous, A.R.; Lang, B.T.; Tran, A.; Silver, J. Functional regeneration beyond the glial scar. *Exp. Neurol.* **2014**, *253*, 197–207. [[CrossRef](#)] [[PubMed](#)]
2. Ramer, L.M.; Ramer, M.S.; Bradbury, E.J. Restoring function after spinal cord injury: Towards clinical translation of experimental strategies. *Lancet Neurol.* **2014**, *13*, 1241–1256. [[CrossRef](#)]
3. Fitch, M.T.; Silver, J. CNS injury, glial scars and inflammation: Inhibitory extracellular matrices and regeneration failure. *Exp. Neurol.* **2008**, *209*, 294–301. [[CrossRef](#)] [[PubMed](#)]
4. Fawcett, J.W.; Schwab, M.E.; Montani, L.; Brazda, N.; Muller, H.W. Defeating inhibition of regeneration by scar and myelin components. *Handb. Clin. Neurol.* **2012**, *109*, 503–522. [[PubMed](#)]

5. Hellal, F.; Hurtado, A.; Ruschel, J.; Flynn, K.C.; Laskowski, C.J.; Umlauf, M.; Kapitein, L.C.; Strikis, D.; Lemmon, V.; Bixby, J.; et al. Microtubule stabilization reduces scarring and causes axon regeneration after spinal cord injury. *Science* **2011**, *331*, 928–931. [[CrossRef](#)] [[PubMed](#)]
6. Ruschel, J.; Hellal, F.; Flynn, K.C.; Dupraz, S.; Elliott, D.A.; Tedeschi, A.; Bates, M.; Sliwinski, C.; Brook, G.; Dobrindt, K.; et al. Axonal regeneration. Systemic administration of epothilone B promotes axon regeneration after spinal cord injury. *Science* **2015**, *348*, 347–352. [[CrossRef](#)] [[PubMed](#)]
7. Bartus, K.; James, N.D.; Didangelos, A.; Bosch, K.D.; Verhaagen, J.; Yanez-Munoz, R.J.; Rogers, J.H.; Schneider, B.L.; Muir, E.M.; Bradbury, E.J. Large-scale chondroitin sulfate proteoglycan digestion with chondroitinase gene therapy leads to reduced pathology and modulates macrophage phenotype following spinal cord contusion injury. *J. Neurosci.* **2014**, *34*, 4822–4836. [[CrossRef](#)] [[PubMed](#)]
8. Bradbury, E.J.; Moon, L.D.; Popat, R.J.; King, V.R.; Bennett, G.S.; Patel, P.N.; Fawcett, J.W.; McMahon, S.B. Chondroitinase ABC promotes functional recovery after spinal cord injury. *Nature* **2002**, *416*, 636–640. [[CrossRef](#)] [[PubMed](#)]
9. Didangelos, A.; Iberl, M.; Vinsland, E.; Bartus, K.; Bradbury, E.J. Regulation of IL-10 by chondroitinase ABC promotes a distinct immune response following spinal cord injury. *J. Neurosci.* **2014**, *34*, 16424–16432. [[CrossRef](#)] [[PubMed](#)]
10. Didangelos, A.; Puglia, M.; Iberl, M.; Sanchez-Bellot, C.; Roschitzki, B.; Bradbury, E.J. High-throughput proteomics reveal alarmins as amplifiers of tissue pathology and inflammation after spinal cord injury. *Sci. Rep.* **2016**, *6*, 21607. [[CrossRef](#)] [[PubMed](#)]
11. Chamankhah, M.; Eftekharpour, E.; Karimi-Abdolrezaee, S.; Boutros, P.C.; San-Marina, S.; Fehlings, M.G. Genome-wide gene expression profiling of stress response in a spinal cord clip compression injury model. *BMC Genom.* **2013**, *14*, 583. [[CrossRef](#)] [[PubMed](#)]
12. Didangelos, A.; Yin, X.; Mandal, K.; Baumert, M.; Jahangiri, M.; Mayr, M. Proteomics characterization of extracellular space components in the human aorta. *Mol. Cell. Proteom.* **2010**, *9*, 2048–2062. [[CrossRef](#)] [[PubMed](#)]
13. Didangelos, A.; Yin, X.; Mandal, K.; Saje, A.; Smith, A.; Xu, Q.; Jahangiri, M.; Mayr, M. Extracellular matrix composition and remodelling in human abdominal aortic aneurysms: A proteomics approach. *Mol. Cell. Proteom.* **2011**, *10*. [[CrossRef](#)] [[PubMed](#)]
14. Arike, L.; Peil, L. Spectral counting label-free proteomics. *Methods Mol. Biol.* **2014**, *1156*, 213–222. [[PubMed](#)]
15. Koschutzki, D.; Schreiber, F. Centrality analysis methods for biological networks and their application to gene regulatory networks. *Gene Regul. Syst. Biol.* **2008**, *2*, 193–201. [[CrossRef](#)]
16. Shree, T.; Olson, O.C.; Elie, B.T.; Kester, J.C.; Garfall, A.L.; Simpson, K.; Bell-McGuinn, K.M.; Zabor, E.C.; Brogi, E.; Joyce, J.A. Macrophages and cathepsin proteases blunt chemotherapeutic response in breast cancer. *Genes Dev.* **2011**, *25*, 2465–2479. [[CrossRef](#)] [[PubMed](#)]
17. Saher, G.; Brugge, B.; Lappe-Siefke, C.; Mobius, W.; Tozawa, R.; Wehr, M.C.; Wieland, F.; Ishibashi, S.; Nave, K.A. High cholesterol level is essential for myelin membrane growth. *Nat. Neurosci.* **2005**, *8*, 468–475. [[CrossRef](#)] [[PubMed](#)]
18. Goodrum, J.F. Cholesterol synthesis is down-regulated during regeneration of peripheral nerve. *J. Neurochem.* **1990**, *54*, 1709–1715. [[CrossRef](#)] [[PubMed](#)]
19. Griffith, M.; Griffith, O.L.; Coffman, A.C.; Weible, J.V.; McMichael, J.F.; Spies, N.C.; Koval, J.; Das, I.; Callaway, M.B.; Eldred, J.M.; et al. DGIdb: Mining the druggable genome. *Nat. Methods* **2013**, *10*, 1209–1210. [[CrossRef](#)] [[PubMed](#)]
20. Szklarczyk, D.; Santos, A.; von Mering, C.; Jensen, L.J.; Bork, P.; Kuhn, M. STITCH 5: Augmenting protein-chemical interaction networks with tissue and affinity data. *Nucleic Acids Res.* **2016**, *44*, D380–D384. [[CrossRef](#)] [[PubMed](#)]
21. Perretti, M.; D’Acquisto, F. Annexin A1 and glucocorticoids as effectors of the resolution of inflammation. *Nat. Rev. Immunol.* **2009**, *9*, 62–70. [[CrossRef](#)] [[PubMed](#)]
22. Nesathurai, S. Steroids and spinal cord injury: Revisiting the NASCIS 2 and NASCIS 3 trials. *J. Trauma* **1998**, *45*, 1088–1093. [[CrossRef](#)] [[PubMed](#)]
23. Sekhon, L.H.; Fehlings, M.G. Epidemiology, demographics and pathophysiology of acute spinal cord injury. *Spine* **2001**, *26*, S2–S12. [[CrossRef](#)] [[PubMed](#)]
24. Elkabes, S.; Nicot, A.B. Sex steroids and neuroprotection in spinal cord injury: A review of preclinical investigations. *Exp. Neurol.* **2014**, *259*, 28–37. [[CrossRef](#)] [[PubMed](#)]

25. Banik, N.L.; Hogan, E.L.; Powers, J.M.; Smith, K.P. Proteolytic enzymes in experimental spinal cord injury. *J. Neurol. Sci.* **1986**, *73*, 245–256. [[CrossRef](#)]
26. Guo, Y.; Liu, S.; Wang, P.; Zhang, H.; Wang, F.; Bing, L.; Gao, J.; Yang, J.; Hao, A. Granulocyte colony-stimulating factor improves neuron survival in experimental spinal cord injury by regulating nucleophosmin-1 expression. *J. Neurosci. Res.* **2014**, *92*, 751–760. [[CrossRef](#)] [[PubMed](#)]
27. Babic, I.; Nurmemmedov, E.; Yenugonda, V.M.; Juarez, T.; Nomura, N.; Pingle, S.C.; Glassy, M.C.; Kesari, S. Pritumumab, the first therapeutic antibody for glioma patients. *Hum. Antib.* **2018**, *26*, 95–101. [[CrossRef](#)] [[PubMed](#)]
28. Menet, V.; Prieto, M.; Privat, A.; Gimenez y Ribotta, M. Axonal plasticity and functional recovery after spinal cord injury in mice deficient in both glial fibrillary acidic protein and vimentin genes. *Proc. Natl. Acad. Sci. USA* **2003**, *100*, 8999–9004. [[CrossRef](#)] [[PubMed](#)]
29. Luo, Y.; Xie, X.; Luo, D.; Wang, Y.; Gao, Y. The role of halofuginone in fibrosis: More to be explored? *J. Leukoc. Biol.* **2017**, *102*, 1333–1345. [[CrossRef](#)] [[PubMed](#)]
30. Jalil, J.E.; Doering, C.W.; Janicki, J.S.; Pick, R.; Shroff, S.G.; Weber, K.T. Fibrillar collagen and myocardial stiffness in the intact hypertrophied rat left ventricle. *Circ. Res.* **1989**, *64*, 1041–1050. [[CrossRef](#)] [[PubMed](#)]
31. Ciccarelli, R.; Ballerini, P.; Sabatino, G.; Rathbone, M.P.; D’Onofrio, M.; Caciagli, F.; Di Iorio, P. Involvement of astrocytes in purine-mediated reparative processes in the brain. *Int. J. Dev. Neurosci.* **2001**, *19*, 395–414. [[CrossRef](#)]
32. Kicska, G.A.; Long, L.; Horig, H.; Fairchild, C.; Tyler, P.C.; Furneaux, R.H.; Schramm, V.L.; Kaufman, H.L. Immucillin H, a powerful transition-state analog inhibitor of purine nucleoside phosphorylase, selectively inhibits human T lymphocytes. *Proc. Natl. Acad. Sci. USA* **2001**, *98*, 4593–4598. [[CrossRef](#)] [[PubMed](#)]
33. Miles, R.W.; Tyler, P.C.; Furneaux, R.H.; Bagdassarian, C.K.; Schramm, V.L. One-third-the-sites transition-state inhibitors for purine nucleoside phosphorylase. *Biochemistry* **1998**, *37*, 8615–8621. [[CrossRef](#)] [[PubMed](#)]
34. Rathbone, M.; Pilutti, L.; Caciagli, F.; Jiang, S. Neurotrophic effects of extracellular guanosine. *Nucleosides Nucleotides Nucleic Acids* **2008**, *27*, 666–672. [[CrossRef](#)] [[PubMed](#)]
35. Gong, B.; Radulovic, M.; Figueiredo-Pereira, M.E.; Cardozo, C. The Ubiquitin-Proteasome System: Potential Therapeutic Targets for Alzheimer’s Disease and Spinal Cord Injury. *Front. Mol. Neurosci.* **2016**, *9*, 4. [[CrossRef](#)] [[PubMed](#)]
36. Sharma, H.S.; Muresanu, D.F.; Lafuente, J.V.; Sjoquist, P.O.; Patnaik, R.; Sharma, A. Nanoparticles Exacerbate Both Ubiquitin and Heat Shock Protein Expressions in Spinal Cord Injury: Neuroprotective Effects of the Proteasome Inhibitor Carfilzomib and the Antioxidant Compound H-290/51. *Mol. Neurobiol.* **2015**, *52*, 882–898. [[CrossRef](#)] [[PubMed](#)]
37. Wang, X.; Arcuino, G.; Takano, T.; Lin, J.; Peng, W.G.; Wan, P.; Li, P.; Xu, Q.; Liu, Q.S.; Goldman, S.A.; et al. P2X7 receptor inhibition improves recovery after spinal cord injury. *Nat. Med.* **2004**, *10*, 821–827. [[CrossRef](#)] [[PubMed](#)]
38. Teng, Y.D.; Moccetti, I.; Wrathall, J.R. Basic and acidic fibroblast growth factors protect spinal motor neurones in vivo after experimental spinal cord injury. *Eur. J. Neurosci.* **1998**, *10*, 798–802. [[CrossRef](#)] [[PubMed](#)]
39. Haque, A.; Ray, S.K.; Cox, A.; Banik, N.L. Neuron specific enolase: A promising therapeutic target in acute spinal cord injury. *Metab. Brain Dis.* **2015**, *31*, 487–495. [[CrossRef](#)] [[PubMed](#)]
40. Lopez-Vales, R.; Redensek, A.; Skinner, T.A.; Rathore, K.I.; Ghasemlou, N.; Wojewodka, G.; DeSanctis, J.; Radzioch, D.; David, S. Ferretinide promotes functional recovery and tissue protection after spinal cord contusion injury in mice. *J. Neurosci.* **2010**, *30*, 3220–3226. [[CrossRef](#)] [[PubMed](#)]
41. Eftekharpour, E.; Nagakannan, P.; Iqbal, M.A.; Chen, Q.M. Mevalonate Cascade and Small Rho GTPase in Spinal Cord Injury. *Curr. Mol. Pharmacol.* **2017**, *10*, 141–151. [[PubMed](#)]
42. Abate, M.; Laezza, C.; Pisanti, S.; Torelli, G.; Seneca, V.; Catapano, G.; Montella, F.; Ranieri, R.; Notarnicola, M.; Gazzero, P.; et al. Deregulated expression and activity of Farnesyl Diphosphate Synthase (FDPS) in Glioblastoma. *Sci. Rep.* **2017**, *7*, 14123. [[CrossRef](#)] [[PubMed](#)]
43. Nance, P.W.; Schryvers, O.; Leslie, W.; Ludwig, S.; Krahn, J.; Uebelhart, D. Intravenous pamidronate attenuates bone density loss after acute spinal cord injury. *Arch. Phys. Med. Rehabil.* **1999**, *80*, 243–251. [[CrossRef](#)]
44. Beignoux, A.P.; Kosinski, C.; Gavino, B.; Horton, J.D.; Skarnes, W.C.; Young, S.G. ATP-citrate lyase deficiency in the mouse. *J. Biol. Chem.* **2004**, *279*, 9557–9564. [[CrossRef](#)] [[PubMed](#)]

45. Krishnan, M.L.; Wang, Z.; Silver, M.; Boardman, J.P.; Ball, G.; Counsell, S.J.; Walley, A.J.; Montana, G.; Edwards, A.D. Possible relationship between common genetic variation and white matter development in a pilot study of preterm infants. *Brain Behav.* **2016**, *6*, e00434. [[CrossRef](#)] [[PubMed](#)]
46. Chu, Y.; Parada, I.; Prince, D.A. Temporal and topographic alterations in expression of the alpha3 isoform of Na<sup>+</sup>, K(+)-ATPase in the rat freeze lesion model of microgyria and epileptogenesis. *Neuroscience* **2009**, *162*, 339–348. [[CrossRef](#)] [[PubMed](#)]
47. de Carvalho Aguiar, P.; Sweedner, K.J.; Penniston, J.T.; Zaremba, J.; Liu, L.; Caton, M.; Linazasoro, G.; Borg, M.; Tijssen, M.A.; Bressman, S.B.; et al. Mutations in the Na<sup>+</sup>/K<sup>+</sup>-ATPase alpha3 gene ATP1A3 are associated with rapid-onset dystonia parkinsonism. *Neuron* **2004**, *43*, 169–175. [[CrossRef](#)] [[PubMed](#)]
48. Besse, A.; Wu, P.; Bruni, F.; Donti, T.; Graham, B.H.; Craigen, W.J.; McFarland, R.; Moretti, P.; Lalani, S.; Scott, K.L.; et al. The GABA transaminase, ABAT, is essential for mitochondrial nucleoside metabolism. *Cell Metab.* **2015**, *21*, 417–427. [[CrossRef](#)] [[PubMed](#)]
49. Sauer, S.W.; Kolker, S.; Hoffmann, G.F.; Ten Brink, H.J.; Jakobs, C.; Gibson, K.M.; Okun, J.G. Enzymatic and metabolic evidence for a region specific mitochondrial dysfunction in brains of murine succinic semialdehyde dehydrogenase deficiency (Aldh5a1<sup>−/−</sup> mice). *Neurochem. Int.* **2007**, *50*, 653–659. [[CrossRef](#)] [[PubMed](#)]
50. Drewes, A.M.; Andreasen, A.; Poulsen, L.H. Valproate for treatment of chronic central pain after spinal cord injury. A double-blind cross-over study. *Paraplegia* **1994**, *32*, 565–569. [[CrossRef](#)] [[PubMed](#)]
51. Liberzon, A.; Birger, C.; Thorvaldsdottir, H.; Ghandi, M.; Mesirov, J.P.; Tamayo, P. The Molecular Signatures Database (MSigDB) hallmark gene set collection. *Cell Syst.* **2016**, *1*, 417–425. [[CrossRef](#)] [[PubMed](#)]
52. Durbin, J.E.; Hackenmiller, R.; Simon, M.C.; Levy, D.E. Targeted disruption of the mouse Stat1 gene results in compromised innate immunity to viral disease. *Cell* **1996**, *84*, 443–450. [[CrossRef](#)]
53. Meraz, M.A.; White, J.M.; Sheehan, K.C.; Bach, E.A.; Rodig, S.J.; Dighe, A.S.; Kaplan, D.H.; Riley, J.K.; Greenlund, A.C.; Campbell, D.; et al. Targeted disruption of the Stat1 gene in mice reveals unexpected physiologic specificity in the JAK-STAT signaling pathway. *Cell* **1996**, *84*, 431–442. [[CrossRef](#)]
54. Profyris, C.; Cheema, S.S.; Zang, D.; Azari, M.F.; Boyle, K.; Petratos, S. Degenerative and regenerative mechanisms governing spinal cord injury. *Neurobiol. Dis.* **2004**, *15*, 415–436. [[CrossRef](#)] [[PubMed](#)]
55. Wu, Y.; Yang, L.; Mei, X.; Yu, Y. Selective inhibition of STAT1 reduces spinal cord injury in mice. *Neurosci. Lett.* **2014**, *580*, 7–11. [[CrossRef](#)] [[PubMed](#)]
56. James, N.D.; Bartus, K.; Grist, J.; Bennett, D.L.; McMahon, S.B.; Bradbury, E.J. Conduction failure following spinal cord injury: Functional and anatomical changes from acute to chronic stages. *J. Neurosci.* **2011**, *31*, 18543–18555. [[CrossRef](#)] [[PubMed](#)]
57. Mills, C.D.; Hains, B.C.; Johnson, K.M.; Hulsebosch, C.E. Strain and model differences in behavioral outcomes after spinal cord injury in rat. *J. Neurotrauma* **2001**, *18*, 743–756. [[CrossRef](#)] [[PubMed](#)]
58. Kjell, J.; Olson, L. Rat models of spinal cord injury: From pathology to potential therapies. *Dis. Model. Mech.* **2016**, *9*, 1125–1137. [[CrossRef](#)] [[PubMed](#)]
59. Cherian, T.; Ryan, D.J.; Weinreb, J.H.; Cherian, J.; Paul, J.C.; Lafage, V.; Kirsch, T.; Errico, T.J. Spinal cord injury models: A review. *Spinal Cord* **2014**, *52*, 588–595. [[CrossRef](#)] [[PubMed](#)]
60. Sharif-Alhoseini, M.; Khormali, M.; Rezaei, M.; Safdarian, M.; Hajighadery, A.; Khalatbari, M.M.; Meknatkhah, S.; Rezvan, M.; Chalangari, M.; Derakhshan, P.; et al. Animal models of spinal cord injury: A systematic review. *Spinal Cord* **2017**, *55*, 714–721. [[CrossRef](#)] [[PubMed](#)]
61. Pinzon, A.; Marcillo, A.; Pabon, D.; Bramlett, H.M.; Bunge, M.B.; Dietrich, W.D. A re-assessment of erythropoietin as a neuroprotective agent following rat spinal cord compression or contusion injury. *Exp. Neurol.* **2008**, *213*, 129–136. [[CrossRef](#)] [[PubMed](#)]
62. Geremia, N.M.; Hryciw, T.; Bao, F.; Streijger, F.; Okon, E.; Lee, J.H.T.; Weaver, L.C.; Dekaban, G.A.; Kwon, B.K.; Brown, A. The effectiveness of the anti-CD11d treatment is reduced in rat models of spinal cord injury that produce significant levels of intraspinal hemorrhage. *Exp. Neurol.* **2017**, *295*, 125–134. [[CrossRef](#)] [[PubMed](#)]
63. Kjell, J.; Sandor, K.; Josephson, A.; Svensson, C.I.; Abrams, M.B. Rat substrains differ in the magnitude of spontaneous locomotor recovery and in the development of mechanical hypersensitivity after experimental spinal cord injury. *J. Neurotrauma* **2013**, *30*, 1805–1811. [[CrossRef](#)] [[PubMed](#)]
64. Popovich, P.G.; Wei, P.; Stokes, B.T. Cellular inflammatory response after spinal cord injury in Sprague-Dawley and Lewis rats. *J. Comp. Neurol.* **1997**, *377*, 443–464. [[CrossRef](#)]
65. Schmitt, C.; Miranpuri, G.S.; Dhodda, V.K.; Isaacson, J.; Vemuganti, R.; Resnick, D.K. Changes in spinal cord injury-induced gene expression in rat are strain-dependent. *Spine J.* **2006**, *6*, 113–119. [[CrossRef](#)] [[PubMed](#)]

66. Bantia, S.; Ananth, S.L.; Parker, C.D.; Horn, L.L.; Upshaw, R. Mechanism of inhibition of T-acute lymphoblastic leukemia cells by PNP inhibitor-BCX-1777. *Int. Immunopharmacol.* **2003**, *3*, 879–887. [[CrossRef](#)]
67. Somech, R.; Lev, A.; Grisaru-Soen, G.; Shiran, S.I.; Simon, A.J.; Grunebaum, E. Purine nucleoside phosphorylase deficiency presenting as severe combined immune deficiency. *Immunol. Res.* **2013**, *56*, 150–154. [[CrossRef](#)] [[PubMed](#)]
68. Hiraiwa, M. Cathepsin A/protective protein: An unusual lysosomal multifunctional protein. *Cell. Mol. Life Sci.* **1999**, *56*, 894–907. [[CrossRef](#)] [[PubMed](#)]
69. Chen, J.; Wang, Z.; Mao, Y.; Zheng, Z.; Chen, Y.; Khor, S.; Shi, K.; He, Z.; Li, J.; Gong, F.; et al. Liraglutide activates autophagy via GLP-1R to improve functional recovery after spinal cord injury. *Oncotarget* **2017**, *8*, 85949–85968. [[CrossRef](#)] [[PubMed](#)]
70. Calhan, O.Y.; Seyrantepe, V. Mice with Catalytically Inactive Cathepsin A Display Neurobehavioral Alterations. *Behav. Neurol.* **2017**, *2017*, 4261873. [[CrossRef](#)] [[PubMed](#)]
71. Carecchio, M.; Zorzi, G.; Ragona, F.; Zibordi, F.; Nardocci, N. ATP1A3-related disorders: An update. *Eur. J. Paediatr. Neurol.* **2018**, *22*, 257–263. [[CrossRef](#)] [[PubMed](#)]
72. Searle, B.C. Scaffold: A bioinformatic tool for validating MS/MS-based proteomic studies. *Proteomics* **2010**, *10*, 1265–1269. [[CrossRef](#)] [[PubMed](#)]
73. Saeed, A.I.; Bhagabati, N.K.; Braisted, J.C.; Liang, W.; Sharov, V.; Howe, E.A.; Li, J.; Thiagarajan, M.; White, J.A.; Quackenbush, J. TM4 microarray software suite. *Methods Enzymol.* **2006**, *411*, 134–193. [[PubMed](#)]
74. Szklarczyk, D.; Franceschini, A.; Wyder, S.; Forslund, K.; Heller, D.; Huerta-Cepas, J.; Simonovic, M.; Roth, A.; Santos, A.; Tsafou, K.P.; et al. STRING v10: Protein-protein interaction networks, integrated over the tree of life. *Nucleic Acids Res.* **2015**, *43*, D447–D452. [[CrossRef](#)] [[PubMed](#)]
75. Smoot, M.E.; Ono, K.; Ruscheinski, J.; Wang, P.L.; Ideker, T. Cytoscape 2.8: New features for data integration and network visualization. *Bioinformatics* **2010**, *27*, 431–432. [[CrossRef](#)] [[PubMed](#)]



© 2018 by the authors. Licensee MDPI, Basel, Switzerland. This article is an open access article distributed under the terms and conditions of the Creative Commons Attribution (CC BY) license (<http://creativecommons.org/licenses/by/4.0/>).



Article

# Level-Specific Differences in Systemic Expression of Pro- and Anti-Inflammatory Cytokines and Chemokines after Spinal Cord Injury

James Hong <sup>1,2</sup>, Alex Chang <sup>1,2</sup>, Mohammad-Masoud Zavvarian <sup>1,2</sup>, Jian Wang <sup>1</sup>, Yang Liu <sup>1</sup> and Michael G. Fehlings <sup>1,3,\*</sup>

<sup>1</sup> Division of Genetics and Development, Toronto Western Research Institute, University Health Network, Toronto, ON M5T 2S8, Canada; james.hong@live.com (J.H.); le.chang@mail.utoronto.ca (A.C.); Mohammad.zavvarian@mail.utoronto.ca (M.-M.Z.); jianw@uhnres.utoronto.ca (J.W.); Yang.Liu@uhnresearch.ca (Y.L.)

<sup>2</sup> Institute of Medical Science, University of Toronto, Toronto, ON M5S 1A8, Canada

<sup>3</sup> Spinal Program, University Health Network, Toronto Western Hospital, Toronto, ON M5T 2S8, Canada

\* Correspondence: Michael.Fehlings@uhn.ca; Tel.: +1-416-603-5627

Received: 11 July 2018; Accepted: 23 July 2018; Published: 25 July 2018

**Abstract:** While over half of all spinal cord injuries (SCIs) occur in the cervical region, the majority of preclinical studies have focused on models of thoracic injury. However, these two levels are anatomically distinct—with the cervical region possessing a greater vascular supply, grey-white matter ratio and sympathetic outflow relative to the thoracic region. As such, there exists a significant knowledge gap in the secondary pathology at these levels following SCI. In this study, we characterized the systemic plasma markers of inflammation over time (1, 3, 7, 14, 56 days post-SCI) after moderate-severe, clip-compression cervical and thoracic SCI in a rat model. Using high-throughput ELISA panels, we observed a clear level-specific difference in plasma levels of VEGF, leptin, IP10, IL18, GCSF, and fractalkine. Overall, cervical SCI had reduced expression of both pro- and anti-inflammatory proteins relative to thoracic SCI, likely due to sympathetic dysregulation associated with higher level SCIs. However, contrary to the literature, we did not observe level-dependent splenic atrophy with our incomplete SCI model. This is the first study to compare the systemic plasma-level changes following cervical and thoracic SCI using level-matched and time-matched controls. The results of this study provide the first evidence in support of level-targeted intervention and also challenge the phenomenon of high SCI-induced splenic atrophy in incomplete SCI models.

**Keywords:** spinal cord injury; inflammation; plasma

## 1. Introduction

Traumatic spinal cord injury (SCI)—despite breakthroughs in pre-operative, surgical and post-operative care—continues to be a life-threatening injury, both acutely and chronically [1]. After primary mechanical injury, a dual-edged cascade of inflammatory and vascular events—collectively referred to as the secondary injury phase—ensues [2,3]. While it is difficult to determine the causative mechanism of secondary injury, several mechanisms including vascular disruption [4], glutamate excitotoxicity [5,6], lipid peroxidation [7–9], blood-spinal-cord-barrier disruption [10–12] and ionic imbalance [13,14] have been the focus of therapeutic targeting. The ultimate consequence of these events is apoptosis, neuronal and axonal death, and de/dys-myelination manifesting as grey and white matter loss at the injury epicenter [1].

Preclinical SCI studies thus far, driven by post-operative care requirements and ease-of-use, have most commonly employed thoracic SCI (tSCI) models despite the increased prevalence and incidence of

cervical SCI (cSCI) [15]. A central rationale for specifically investigating cSCI models is the appreciation that critical anatomical differences exist between the cervical and thoracic spinal cord resulting in different pathophysiological responses to injury and treatment [16]. For instance, the cervical spine is composed of smaller vertebrae with increased mobility, has increased central and peripheral vascular supply and flow, a higher gray-white matter ratio, and contains the neural circuitry crucial for respiration, forelimb motion, and sympathetic outflow to the heart. Pathophysiologically, the cervical gray matter vasculature has less pericyte coverage than the thoracic cord, resulting in a blood spinal cord barrier (BSCB) predisposed to increased permeability [10]. Further, in high-thoracic transection models of SCI, removal of spinal sympathetic preganglionic neurons from supraspinal control results in autonomic dysreflexia [17]. This in turn has been shown to instigate immunosuppressive effects—known as SCI-induced immune depression syndrome (SCI-IDS)—that stem directly from early splenocyte death and splenic atrophy due to acute and repeated chronic exposure to glucocorticoids and intrasplenic norepinephrine [18].

As cSCI has a direct neurological impact on cardiovascular function and peripheral immunity [19–21], we aimed to characterize the temporal profile (3–56 days) of vascular and inflammatory markers after cSCI and tSCI and elucidate any level-specific changes in their expression. Further, as robust spleen-mass changes were observed in the aforementioned transection studies on SCI-IDS, we also evaluated time and sham-normalized spleen-body weight ratios in our model.

## 2. Results

Of the 35 proteins surveyed in this study, 19 passed our initial filtering criteria, while 16 proteins that contained interpolated, extrapolated or out-of-range values were removed. All comparisons below are presented in order from thoracic to cervical.

### 2.1. Level-Specific Differences in Plasma Protein Levels after Cervical and Thoracic Laminectomy

To investigate whether there were baseline differences in the expression of any of these proteins after cervical and thoracic laminectomy, heat-mapping and statistical analyses of protein concentrations were carried out with naïve plasma shown as a reference (excluded from cluster analyses). Heat-mapping (Figure 1A) demonstrated several clusters of expression. While several proteins had trending differences (RANTES,  $p = 0.06$  at 14 days; LIX,  $p = 0.052$  at 14 days; and IL10,  $p = 0.068$ ), two proteins within cluster 5 showed significant differences in the expression of IP10 (56 days,  $131.5 \pm 11.2$  vs.  $450.3 \pm 15.8$  pg/mL,  $p = 0.003$ ) and IL18 (3 days,  $745.1 \pm 84.8$  vs.  $400.2 \pm 47.5$  pg/mL,  $p = 0.036$ ). The time-series expression of these three proteins is shown in Figure 1B.

### 2.2. Level-Specific Differences in Plasma Protein Levels after Cervical and Thoracic SCI

Of the 19 proteins analyzed (Figure 2), six showed significant differences at one or more time-points between time-matched, level-matched, laminectomy-normalized cSCI and tSCI groups (expressed as fold-change to laminectomy). The six proteins that showed level-specific differences were VEGF (day 7,  $-0.1 \pm 0.2$  vs.  $1.325 \pm 0.1$ ,  $p = 0.03$ ), leptin (day 1,  $1.2 \pm 0.4$  vs.  $-0.05 \pm 0.3$ ,  $p = 0.04$ ; day 56,  $-0.1 \pm 0.4$  vs.  $-2.0 \pm 0.4$ ,  $p = 0.0009$ ), IP10 (day 1,  $0.3 \pm 0.3$  vs.  $-0.7 \pm 0.04$ ,  $p = 0.02$ ; day 7,  $-0.891 \pm 0.3$  vs.  $0.4 \pm 0.2$ ,  $p = 0.0005$ ; day 56,  $0.9 \pm 0.2$  vs.  $-1.0 \pm 0.3$ ,  $p < 0.0001$ ), IL18 (day 56,  $-1.5 \pm 0.3$  vs.  $-0.05 \pm 0.4$ ,  $p = 0.02$ ), GCSF (day 7,  $1.010 \pm 0.187$  vs.  $3.943 \pm 1.663$ ,  $p = 0.006$ ), and fractalkine (day 1,  $0.3 \pm 0.1$  vs.  $-0.6 \pm 0.2$ ,  $p = 0.004$ ). Both of the proteins (IP10 and IL18) that showed level-specific baseline differences were significant after SCI. However, while differences in the 56-day baseline of IP10 contributed to a significant result, the 3-day baseline difference in IL18 did not.

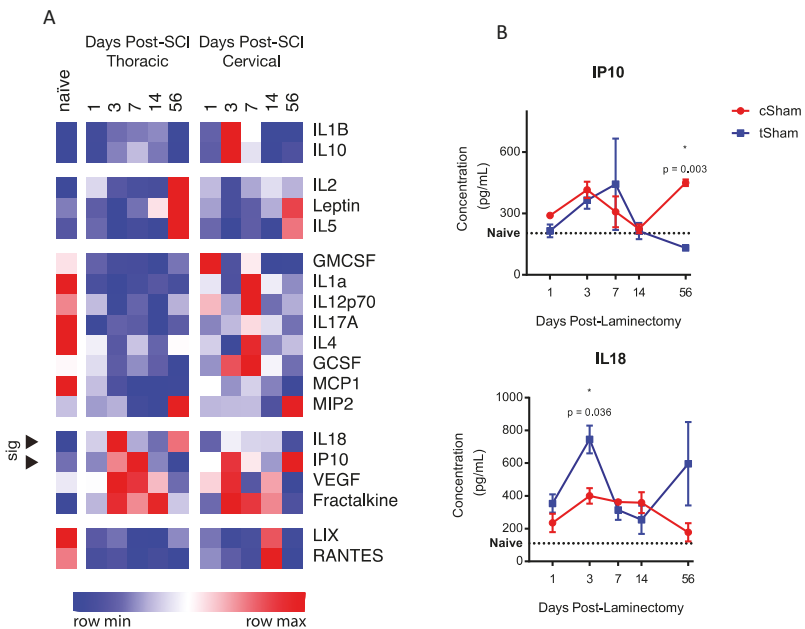


**Figure 1.** (A) Heat map and hierarchical cluster analyses reveal six clusters of temporal expression amongst cSham and tSham groups. Of the proteins analyzed, two proteins (marked with arrows) within cluster 4 reached statistical significance (IL18 and IP10). Naive data are shown as a baseline reference. Data are shown with relative color coding, with blue associated with the row minimum and red with the row maximum; all data are based on raw concentration in pg/mL; (B) Temporal expression of the two significant level-distinct proteins. Error bars represent SEM.

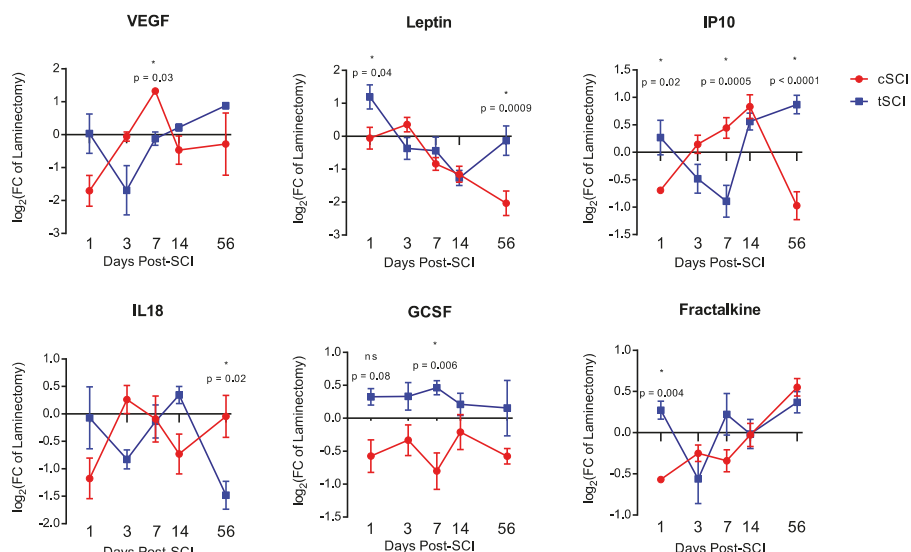


**Figure 2.** Temporal expression profile of the six significant differentially-expressed proteins: VEGF, leptin, IP10, IL18, GCSF and fractalkine. Error bars represent SEM.

### 2.3. Temporal Expression Patterns of Plasma Proteins after SCI

To dissect the various temporal expression patterns after cSCI and tSCI, heatmap and *k*-means cluster analysis were performed (Figure 3). In tSCI, three main clusters were found with cluster 1 showing acute/chronic upregulation with subacute downregulation; cluster 2 showing an acute/subacute upregulation with chronic downregulation; and cluster 3 consisting of a single member showing constitutive upregulation. Similarly, in cSCI, three major clusters were defined with cluster 1 showing constitutive downregulation with some acute upregulation; cluster 2 showing proteins with acute/subacute downregulation with chronic upregulation; and cluster 3 showing proteins that had acute/subacute upregulation followed by chronic downregulation.

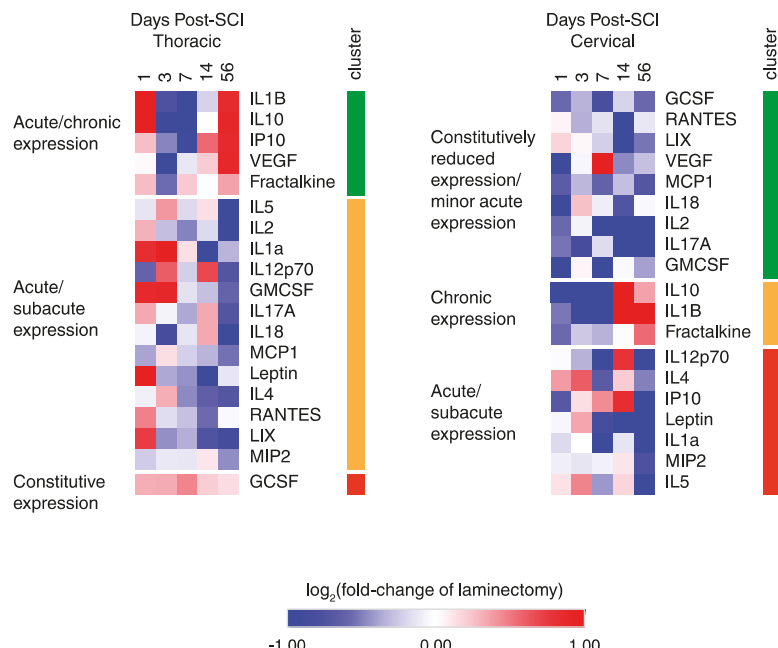


**Figure 3.** Heatmap and *k*-means clustering reveals three major clusters of temporal expression in cSCI and tSCI. Expression is displayed as  $\log_2$  (fold-change of laminectomy) with blue indicating downregulation and red indicating upregulation.

### 2.4. Functional Classification of Serum Protein after SCI

Using several reviews and meta-analyses articles [22–29], pro-inflammatory and anti-inflammatory functions were assigned to each of the 19 proteins to survey the overall inflammatory status after cSCI and tSCI (Figure 4). It is evident that overall, tSCI has increased expression of both pro- and anti-inflammatory proteins over time compared to cSCI. While most of these proteins are strikingly upregulated in the acute phase of thoracic relative to cervical SCI, a few of these differences equilibrated chronically (e.g., IL1b, fractalkine, IL10).

### 2.5. Spleen Weight

To identify whether splenic atrophy was observed in our model of incomplete SCI, mass-normalized spleen weights were measured and expressed as a fold-change of time-matched laminectomized shams (Figure 5). While a decrease in weight between injured and time-matched laminectomized shams was seen in both cSCI and tSCI, this did not reach statistical significance.

However, a significant increase in spleen weight was observed between 3 and 14 days in cSCI ( $0.862 \pm 0.078$  vs.  $1.188 \pm 0.113$ ,  $p = 0.03$ ), but only trended for tSCI ( $p = 0.06$ ).

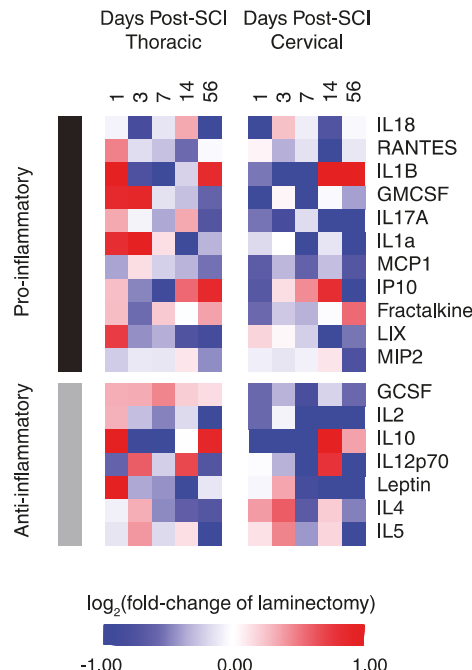


**Figure 4.** Heat map of functionally-segregated proteins after cSCI and tSCI. Expression is displayed as  $\log_2$  (fold-change of laminectomy) with blue indicating downregulation and red indicating upregulation.

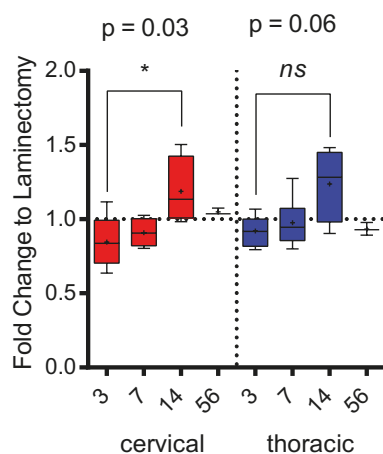


**Figure 5.** Mass: spleen ratios expressed as fold-change of time-matched laminectomized shams. Error bars represent SEM, and means are indicated by +. A significant change in spleen weight was observed in cSCI between day 3 and day 14.

### 3. Discussion

In summary, this is the first study to characterize the temporal plasma expression profile of multiple cytokines, chemokines and growth factors after SCI. It is also the first study to use clinically-relevant models of cSCI and tSCI to determine level-specific differences in the expression of these inflammation-related molecules. This study establishes three main points: (1) time and level-matched laminectomy controls are essential for accurate data interpretation after SCI; (2) there exist both acute and chronic differences in plasma protein expression between cSCI and tSCI; and (3) splenic atrophy is not a robust phenomenon after incomplete cSCI, and as there continues to be evidence of peripheral immune depression after cSCI, it is also not a conclusive diagnostic tool for assessing the state of SCI-IDS.

Inflammation after SCI is considered one of the major drivers of secondary injury and tissue loss, and is often considered a dual-edged sword [30,31]. Our current results examined a small percentage of the cytokine/chemokines/growth factors involved, however, due to the spectrum of cells that secrete these factors, we cannot accurately pinpoint the cellular mediators of the temporal and level-specific changes that we have observed. With regards to the cause of level-differences between laminectomized shams, it is likely they are due to the degree of invasiveness and its associated fibrosis above the site of laminectomy and its differential impact on the cord over time between the two levels.

Studies on five of the six level-distinct proteins have already been conducted in the rodent tSCI model, with IL18 being the only exception with no SCI-associated studies. VEGF is well-known as a potent angiogenic factor that promotes the growth and development of endothelial cells. Our lab was one of the first to study the role of VEGF as a therapeutic agent after acute tSCI [32,33]. In these studies, transcriptionally-enhancing VEGF expression resulted in increased axon preservation, reduced necrosis, and an increase in blood vessels that ultimately translated to increased functional recovery as measured by Catwalk gait analyses. Another study using a contusion tSCI model [34], found that acute intraspinal infusion of VEGF into the lesion epicentre induced autophagy and reduced inflammation in the spinal cord, ultimately resulting in functional recovery as measured by the BBB motor scale. In this study, they showed that VEGF administration reduced the expression of IL1b, IL10 and TNFa in *in vitro* cultures of LPS-treated neuro-glia co-cultures. In our study, VEGF was upregulated at day 7 relative to tSCI and this change did indeed coincide with striking systemic reductions in IL1b and IL10. Further, an upregulation of these proteins was observed at 14- and 56-days post-cSCI when VEGF expression returned to baseline. Perhaps one of the major underlying factors of this level-dependent change after cSCI is the impact of cervical injury on the systemic vasculature as autonomic dysreflexia contributes directly to frequent vascular stress. Overall, there is significant evidence to suggest that VEGF therapy would be effective in both acute cSCI and tSCI, with the potential to also reduce chronic inflammation in both models.

As a hormone produced mainly by adipose cells, leptin is crucial for energetic balance in the central nervous system. Previous studies into leptin have shown that it is often upregulated both locally and systemically after tSCI [35–37]. While these acute studies were severely limited by the lack of time-matched controls, we observed a striking upregulation of plasma leptin in tSCI, but not cSCI at 1- and 56-days post-SCI. As leptin is regulated by the sympathetic nervous system, a study has shown that patients with high level SCIs have dysfunctional leptin expression [38]—thus supporting our data. A study [39] that acutely administered purified leptin in a rodent model of tSCI showed increased expression of neuroprotective genes, reduced inflammation and improved BBB, Catwalk and von Frey metrics suggesting that acute and chronic leptin deficiency may be a potent therapeutic target in SCI.

An upregulation in systemic and local IP10 has been demonstrated in both human and rodent SCI [40–42], and while no time-matched controls were used, this upregulation persisted as long as 14 days post-SCI in the murine tSCI model. IP10, is a chemokine secreted by a wide array of immune cells, endothelial cells and fibroblasts in response to IFNg [43]. In our study, IP10 expression was inversely expressed between the two levels, with cSCI experiencing a peak of expression during the subacute phase (days 3–14), and tSCI in the acute and chronic phases (day 1 and 56). Studies that

neutralized the expression of IP10 showed markedly reduced inflammation, apoptosis, tissue loss and showed modestly improved BBB and BMS outcomes [42,44,45].

While GCSF has had no reported systemic or local expression in the SCI literature, here we find that the expression of GCSF is opposite in cSCI and tSCI. That is, while GCSF is upregulated in tSCI, it is downregulated in cSCI with time-to-time changes also in contrary motion with the exception of day 56. As purified GCSF administration alone and in combination with adipose- and bone-marrow-derived stem and neural stem cells has been shown to be highly beneficial in rodent and human tSCI—including increased tissue preservation, reduced apoptosis and scarring, and improved BBB, BMS and A [46–56]—such a paradigm may prove to be even more effective in the all stages of cSCI where a deficiency in GCSF is seen.

Receptor knockouts of the fractalkine receptor CX3CR1 have resulted in reduced iNOS<sup>+</sup>/Ly6C<sup>low</sup>/MHCII<sup>+</sup>/CD11c<sup>−</sup> macrophages and activated microglia that have reduced expression of IL6 and iNOS. In these studies, the authors observed modest improvements in the BMS score [57–59]. In our study, the systemic fractalkine ligand is significantly upregulated in tSCI at 1-day post-SCI relative to cSCI, with both tSCI and cSCI experiencing late peaks 56-days post-SCI. Fractalkine is present in both a cell-bound and soluble form, and while both forms are potent chemo-attractants for migrating monocytes, the soluble form is also known to attract T cells. As such, while fractalkine receptor antagonism may be an ideal therapeutic target for acute tSCI, it may also be a valuable target for chronic tSCI and cSCI.

Two potential mechanisms by which cSCI induces an overall decrease in circulating protein are (1) SCI-IDS [20,21] and (2) increased cellular localization (and as such cytokine/chemokines) to the site of injury [26,28,41]. SCI-IDS is a phenomenon characterized by rapid splenic atrophy due to repeated bouts of autonomic dysreflexia in higher-level injuries. Interestingly, level-dependent splenic atrophy was not observed between our two incomplete models of cSCI and tSCI (Figure 5). The latter cytokine/chemokine “sink” concept is well-supported by the literature, as recent characterizations of cytokine/chemokine profiles in the spinal cord of SCI rodents and individuals show a striking acute and chronically-persistent expression of many pro- and anti-inflammatory cytokines. This, in conjunction with the increased BSCB permeability after cSCI, may well result in the formation of an inflammatory *milieu* that can be a potent trigger for secondary injury—especially chronic inflammation. All in all, we have shown striking evidence of level-specific differences in the systemic plasma expression of various cytokines and chemokines. In light of these results, preclinical researchers should adapt time-matched laminectomized controls and consider the impact of anatomical level on the therapeutic target of interest.

#### 4. Materials and Methods

All animal experiments were approved by the Animal Care Committee of the University Health Network (Project ID Code: #2212, Date of Approval: 17 May 2017) in compliance with the Canadian Council on Animal Care.

##### 4.1. Clip-Compression SCI and Spleen Weight

Female adult Wistar rats (12-weeks old, 250–300 g,  $n = 5$ /group for injured,  $n = 3$ /group for laminectomy and naïve) were used (Charles River Laboratories, Wilmington, MA, USA, <http://www.criver.com>). Prior to surgery, 0.05 mg/kg of buprenorphine and 5 mL of saline were administered subcutaneously. 1–2% of isoflurane in a 1:1 mixture of O<sub>2</sub> and N<sub>2</sub>O was used for anesthesia, and a laminectomy was performed at C6-7 and T6-7, respectively. Following this, a moderate-severe injury was induced for 1-min at the cervical or thoracic level as described previously [15,60]. Until the endpoint (1, 3, 7, 14, 56 days post-SCI), the animals were given subcutaneous buprenorphine (0.05 mg/kg, bid), oral amoxicillin trihydrate/clavulanate potassium (Apotex Pharmaceuticals, Toronto, ON, Canada) and subcutaneous saline injections (0.9%, 5 mL sid). Animals were housed individually in cages at 27 °C, and their bladders were manually expressed thrice daily until recovery.

Prior to sacrifice and perfusion, animal mass and spleens were collected from anesthetized rats and their weight recorded and normalized to their body mass.

#### 4.2. Neurobehavioural Assessments

Starting at 7 days post-SCI, weekly forelimb and hindlimb function were assessed with the grip strength meter (SDI Grip Strength System DFM-10, San Diego Instruments, San Diego, CA, USA, <http://www.sandiegoinstruments.com>) and the BBB Locomotor Rating Scale [61] for cSCI and tSCI, respectively (Figure 6).

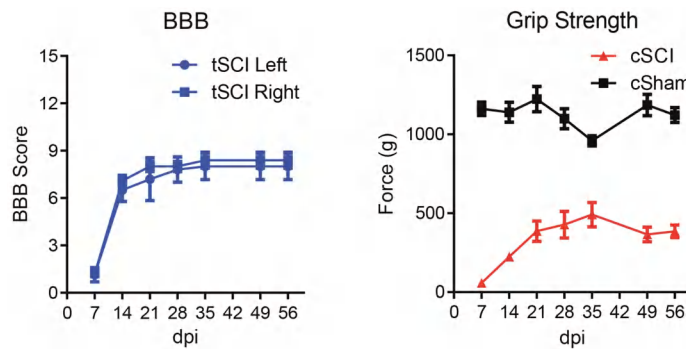


**Figure 6.** Hindlimb (BBB) and forelimb (Grip strength) assessments following tSCI and cSCI, respectively. No statistical outliers were detected using Grubb's test ( $\alpha > 0.05$ ) indicating good homogeneity of data. Error bars represent SEM.

#### 4.3. Blood Collection and High-Throughput ELISA

Blood was collected via a cardiac puncture prior to perfusion using a BD-Vacutainer® Safety-Lok™ (Franklin Lakes, New Jersey, US) blood collection set containing EDTA. The blood samples were kept on ice and immediately centrifuged at 3000 rpm (Eppendorf 5810R) for 10 min at 4 °C. The plasma (supernatant) was then carefully aspirated and transferred to a Protein Lo-Bind tube (Eppendorf, Hamburg, Germany). 100 µL of the sample was then sent to Eve Technologies (Calgary, AB, Canada, <https://www.evetechologies.com>) for high-throughput ELISA profiling using their rat Discovery Assays™ for cytokine/chemokines (RD27) and vascular injury markers (P1, P2). All proteins that contained interpolated/extrapolated/out-of-range values were removed from the study. The concentration of these proteins was calculated using a standard curve and expressed in pg/mL.

#### 4.4. Clustering and Statistical Analysis

Data are presented as mean±SEM and comparisons are presented in order from cervical to thoracic. Heatmap, *k*-means and hierarchical row clustering (1-Cosine Similarity) was performed using the Morpheus software package from the Broad Institute (Cambridge, MA, USA, <https://software.broadinstitute.org/morpheus/>). Assessment of normality was performed for each group using the Shapiro-Wilk test of the Rfit package. All protein level comparisons between cSCI and tSCI were performed in GraphPad using either the one-way ANOVA function with post-hoc Sidak's for multiple corrections (parametric, p-adjusted threshold = 0.05) or Krustal-Wallis test with post-hoc Dunn's for multiple corrections (non-parametric, p-adjusted threshold = 0.05). Spleen-body mass ratio comparisons were done in GraphPad using a one-way ANOVA with post-hoc Sidak for multiple corrections (p-adjusted threshold = 0.05).

**Author Contributions:** J.H.: conception and design, collection and/or assembly of data, data analysis and interpretation, manuscript writing, final approval of manuscript; A.C.: collection and/or assembly of data, data analysis, final approval of manuscript; M.-M.Z.: collection and/or assembly of data, final approval of manuscript; J.W.: collection and/or assembly of data, final approval of manuscript; Y.L.: collection and/or assembly of data, final approval of manuscript; M.G.F.: conception and design, data analysis and interpretation, financial support, manuscript editing, final approval of manuscript.

**Funding:** This work was supported by funds from the Unilever/Lipton Graduate Fellowship in Neuroscience (J.H.), the University of Toronto Open Fellowship (J.H.) and the Ontario Graduate Scholarship (J.H.). M.G.F. was supported by the Halbert Chair in Neural Repair and Regeneration and the DeZwirek Family Foundation.

**Acknowledgments:** We thank Paul Bradshaw and Tim Worden for project management and manuscript review.

**Conflicts of Interest:** The authors declare no conflict of interest.

## Abbreviations

BBB	Basso, Beattie and Bresnahan
BMS	Basso Mouse Scale
BSCB	Blood-spinal-cord-barrier
PBS	Phosphate buffer solution
SCI	Spinal cord injury
GMCSF	Granulocyte-macrophage colony-stimulating factor
IL1a	Interleukin 1 alpha
IL1b	Interleukin 1 beta
IL2	Interleukin-2
IL17A	Interleukin-17A
IL18	Interleukin-18
MCP1	Monocyte chemoattractant protein-1
IP10	Interferon gamma-induced protein 10
LIX	Lipopolysaccharide-induced CXC chemokine
MIP2	macrophage inflammatory protein 2
RANTES	regulated on activation, normal T cell expressed and secreted
GCSF	Granulocyte-colony stimulating factor
IL4	Interleukin-4
IL10	Interleukin-10
IL12	Interleukin-12
IL5	Interleukin-5
IFNg	Interferon gamma
VEGF	Vascular endothelial growth factor

## References

1. Ahuja, C.S.; Wilson, J.R.; Nori, S.; Kotter, M.R.N.; Druschel, C.; Curt, A.; Fehlings, M.G. Traumatic spinal cord injury. *Nat. Rev. Dis. Primers* **2017**, *3*, 17018. [[CrossRef](#)] [[PubMed](#)]
2. Tator, C.H.; Fehlings, M.G. Review of the secondary injury theory of acute spinal cord trauma with emphasis on vascular mechanisms. *J. Neurosurg.* **1991**, *75*, 15–26. [[CrossRef](#)] [[PubMed](#)]
3. Tator, C.H.; Koyanagi, I. Vascular mechanisms in the pathophysiology of human spinal cord injury. *J. Neurosurg.* **1997**, *86*, 483–492. [[CrossRef](#)] [[PubMed](#)]
4. Figley, S.A.; Khosravi, R.; Legasto, J.M.; Tseng, Y.-F.; Fehlings, M.G. Characterization of vascular disruption and blood-spinal cord barrier permeability following traumatic spinal cord injury. *J. Neurotrauma* **2014**, *31*, 541–552. [[CrossRef](#)] [[PubMed](#)]
5. Rothstein, J.D.; Dykes-Hoberg, M.; Pardo, C.A.; Kanai, Y.; Bristol, L.A.; Kuncl, R.W.; Welty, D.F.; Jin, L.; Hediger, M.A.; Wang, Y.; et al. Knockout of Glutamate Transporters Reveals a Major Role for Astroglial Transport in Excitotoxicity and Clearance of Glutamate. *Neuron* **1996**, *16*, 675–686. [[CrossRef](#)]

6. Agrawal, S.K.; Fehlings, M.G. Role of NMDA and Non-NMDA Ionotropic Glutamate Receptors in Traumatic Spinal Cord Axonal Injury. *J. Neurosci.* **1997**, *17*, 1055–1063. [[CrossRef](#)] [[PubMed](#)]
7. Braughler, J.M.; Duncan, L.A.; Chase, R.L. Interaction of lipid peroxidation and calcium in the pathogenesis of neuronal injury. *Cent. Nerv. Syst. Trauma* **1985**, *2*, 269–283. [[CrossRef](#)] [[PubMed](#)]
8. Diaz-Ruiz, A.; Rios, C.; Duarte, I.; Correa, D.; Guizar-Sahagun, G.; Grijalva, I.; Ibarra, A. Cyclosporin-A inhibits lipid peroxidation after spinal cord injury in rats. *Neurosci. Lett.* **1999**, *266*, 61–64. [[CrossRef](#)]
9. Kaptanoglu, E.; Solaroglu, I.; Okutan, O.; Surucu, H.S.; Akbiyik, F.; Beskonakli, E. Erythropoietin exerts neuroprotection after acute spinal cord injury in rats: Effect on lipid peroxidation and early ultrastructural findings. *Neurosurg. Rev.* **2004**, *27*, 113–120. [[CrossRef](#)] [[PubMed](#)]
10. Winkler, E.A.; Sengillo, J.D.; Bell, R.D.; Wang, J.; Zlokovic, B.V. Blood-spinal cord barrier pericyte reductions contribute to increased capillary permeability. *J. Cereb. Blood Flow Metab.* **2012**, *32*, 1841–1852. [[CrossRef](#)] [[PubMed](#)]
11. Whetstone, W.D.; Hsu, J.-Y.C.; Eisenberg, M.; Werb, Z.; Noble-Haeusslein, L.J. Blood-spinal cord barrier after spinal cord injury: Relation to revascularization and wound healing. *J. Neurosci. Res.* **2003**, *74*, 227–239. [[CrossRef](#)] [[PubMed](#)]
12. Noble, L.J.; Wrathall, J.R. Blood-spinal cord barrier disruption proximal to a spinal cord transection in the rat: Time course and pathways associated with protein leakage. *Exp. Neurol.* **1988**, *99*, 567–578. [[CrossRef](#)]
13. Fehlings, M.G.; Agrawal, S. Role of sodium in the pathophysiology of secondary spinal cord injury. *Spine* **1995**, *20*, 2187–2191. [[CrossRef](#)] [[PubMed](#)]
14. Schwartz, G.; Fehlings, M.G. Evaluation of the neuroprotective effects of sodium channel blockers after spinal cord injury: Improved behavioral and neuroanatomical recovery with riluzole. *J. Neurosurg. Spine* **2001**, *94*, 245–256. [[CrossRef](#)]
15. Wilcox, J.T.; Satkunendrarajah, K.; Nasirzadeh, Y.; Laliberte, A.M.; Lip, A.; Cadotte, D.W.; Foltz, W.D.; Fehlings, M.G. Generating level-dependent models of cervical and thoracic spinal cord injury: Exploring the interplay of neuroanatomy, physiology, and function. *Neurobiol. Dis.* **2017**, *105*, 194–212. [[CrossRef](#)] [[PubMed](#)]
16. Ulndreaj, A.; Badner, A.; Fehlings, M.G. Promising neuroprotective strategies for traumatic spinal cord injury with a focus on the differential effects among anatomical levels of injury. *F1000Res* **2017**, *6*, 1907. [[CrossRef](#)] [[PubMed](#)]
17. Zhang, Y.; Guan, Z.; Reader, B.; Shawler, T.; Mandrekar-Colucci, S.; Huang, K.; Weil, Z.; Bratasz, A.; Wells, J.; Powell, N.D.; et al. Autonomic Dysreflexia Causes Chronic Immune Suppression after Spinal Cord Injury. *J. Neurosci.* **2013**, *33*, 12970–12981. [[CrossRef](#)] [[PubMed](#)]
18. Lucin, K.M.; Sanders, V.M.; Popovich, P.G. Stress hormones collaborate to induce lymphocyte apoptosis after high level spinal cord injury. *J. Neurochem.* **2009**, *110*, 1409–1421. [[CrossRef](#)] [[PubMed](#)]
19. Partida, E.; Mironets, E.; Hou, S.; Tom, V.J. Cardiovascular dysfunction following spinal cord injury. *Neural Regen. Res.* **2016**, *11*, 189–194. [[PubMed](#)]
20. Brommer, B.; Engel, O.; Kopp, M.A.; Watzlawick, R.; Müller, S.; Prüss, H.; Chen, Y.; DeVivo, M.J.; Finkenstaedt, F.W.; Dirnagl, U.; et al. Spinal cord injury-induced immune deficiency syndrome enhances infection susceptibility dependent on lesion level. *Brain* **2016**, *139*, 692–707. [[CrossRef](#)] [[PubMed](#)]
21. Schwab, J.M.; Zhang, Y.; Kopp, M.A.; Brommer, B.; Popovich, P.G. The paradox of chronic neuroinflammation, systemic immune suppression, autoimmunity after traumatic chronic spinal cord injury. *Exp. Neurol.* **2014**, *258*, 121–129. [[CrossRef](#)] [[PubMed](#)]
22. Waykole, Y.P.; Doiphode, S.S.; Rakhewar, P.S.; Mhaske, M. Anticytokine therapy for periodontal diseases: Where are we now? *J. Indian Soc. Periodontol.* **2009**, *13*, 64–68. [[CrossRef](#)] [[PubMed](#)]
23. Audet, M.-C.; Anisman, H. Interplay between pro-inflammatory cytokines and growth factors in depressive illnesses. *Front. Cell. Neurosci.* **2013**, *7*, 68. [[CrossRef](#)] [[PubMed](#)]
24. Kofler, S.; Nickel, T.; Weis, M. Role of cytokines in cardiovascular diseases: A focus on endothelial responses to inflammation. *Clin. Sci.* **2005**, *108*, 205–213. [[CrossRef](#)] [[PubMed](#)]
25. Mukhamedshina, Y.O.; Akhmetzyanova, E.R.; Martynova, E.V.; Khaiboullina, S.F.; Galieva, L.R.; Rizvanov, A.A. Systemic and Local Cytokine Profile following Spinal Cord Injury in Rats: A Multiplex Analysis. *Front. Neurol.* **2017**, *8*, 581. [[CrossRef](#)] [[PubMed](#)]

26. Bartholdi, D.; Schwab, M.E. Expression of pro-inflammatory cytokine and chemokine mRNA upon experimental spinal cord injury in mouse: An in situ hybridization study. *Eur. J. Neurosci.* **1997**, *9*, 1422–1438. [CrossRef] [PubMed]
27. Klusman, I.; Schwab, M.E. Effects of pro-inflammatory cytokines in experimental spinal cord injury. *Brain Res.* **1997**, *762*, 173–184. [CrossRef]
28. Schnell, L.; Fearn, S.; Schwab, M.E.; Perry, V.H.; Anthony, D.C. Cytokine-induced acute inflammation in the brain and spinal cord. *J. Neuropathol. Exp. Neurol.* **1999**, *58*, 245–254. [CrossRef] [PubMed]
29. Francos Quijorna, I.; Santos-Nogueira, E.; Gronert, K.; Sullivan, A.B.; Kopp, M.A.; Brommer, B.; David, S.; Schwab, J.M.; Lopez Vales, R. Maresin 1 promotes inflammatory resolution, neuroprotection and functional neurological recovery after spinal cord injury. *J. Neurosci.* **2017**, *29*, 11731–11743. [CrossRef] [PubMed]
30. Anderson, A.J.; Robert, S.; Huang, W.; Young, W.; Cotman, C.W. Activation of complement pathways after contusion-induced spinal cord injury. *J. Neurotrauma* **2004**, *21*, 1831–1846. [CrossRef] [PubMed]
31. Kasinathan, N.; Vanathi, M.B.; Subrahmanyam, V.M.; Rao, J.V. A review on response of immune system in spinal cord injury and therapeutic agents useful in treatment. *Curr. Pharm. Biotechnol.* **2015**, *16*, 26–34. [CrossRef] [PubMed]
32. Figley, S.A.; Liu, Y.; Karadimas, S.K.; Satkunendrarajah, K.; Fettes, P.; Spratt, S.K.; Lee, G.; Ando, D.; Surosky, R.; Giedlin, M.; et al. Delayed administration of a bio-engineered zinc-finger VEGF-A gene therapy is neuroprotective and attenuates allodynia following traumatic spinal cord injury. *PLoS ONE* **2014**, *9*, e96137. [CrossRef] [PubMed]
33. Liu, Y.; Figley, S.; Spratt, S.K.; Lee, G.; Ando, D.; Surosky, R.; Fehlings, M.G. An engineered transcription factor which activates VEGF-A enhances recovery after spinal cord injury. *Neurobiol. Dis.* **2010**, *37*, 384–393. [CrossRef] [PubMed]
34. Wang, H.; Wang, Y.; Li, D.; Liu, Z.; Zhao, Z.; Han, D.; Yuan, Y.; Bi, J.; Mei, X. VEGF inhibits the inflammation in spinal cord injury through activation of autophagy. *Biochem. Biophys. Res. Commun.* **2015**, *464*, 453–458. [CrossRef] [PubMed]
35. Wang, L.; Tang, X.; Zhang, H.; Yuan, J.; Ding, H.; Wei, Y. Elevated leptin expression in rat model of traumatic spinal cord injury and femoral fracture. *J. Spinal Cord Med.* **2011**, *34*, 501–509. [CrossRef] [PubMed]
36. Gezici, A.R.; Ergun, R.; Karakas, A.; Gunduz, B. Serum leptin levels following acute experimental spinal cord injury. *J. Spinal Cord Med.* **2009**, *32*, 416–421. [CrossRef] [PubMed]
37. Garshick, E.; Walia, P.; Goldstein, R.L.; Teylan, M.; Lazzari, A.A.; Tun, C.G.; Hart, J.E. Plasma Leptin and Reduced FEV1 and FVC in Chronic Spinal Cord Injury. *PM R* **2017**, *10*, 276–285. [CrossRef] [PubMed]
38. Jeon, J.Y.; Steadward, R.D.; Wheeler, G.D.; Bell, G.; McCargar, L.; Harber, V. Intact sympathetic nervous system is required for leptin effects on resting metabolic rate in people with spinal cord injury. *J. Clin. Endocrinol. Metab.* **2003**, *88*, 402–407. [CrossRef] [PubMed]
39. Fernández-Martos, C.M.; González, P.; Rodriguez, F.J. Acute leptin treatment enhances functional recovery after spinal cord injury. *PLoS ONE* **2012**, *7*, e35594. [CrossRef] [PubMed]
40. Kwon, B.K.; Streijger, F.; Fallah, N.; Noonan, V.K.; Bélanger, L.M.; Ritchie, L.; Paquette, S.J.; Ailon, T.; Boyd, M.C.; Street, J.; et al. Cerebrospinal Fluid Biomarkers To Stratify Injury Severity and Predict Outcome in Human Traumatic Spinal Cord Injury. *J. Neurotrauma* **2017**, *34*, 567–580. [CrossRef] [PubMed]
41. Lee, Y.L.; Shih, K.; Bao, P.; Ghirnikar, R.S.; Eng, L.F. Cytokine chemokine expression in contused rat spinal cord. *Neurochem. Int.* **2000**, *36*, 417–425. [CrossRef]
42. Glaser, J.; Gonzalez, R.; Sadr, E.; Keirstead, H.S. Neutralization of the chemokine CXCL10 reduces apoptosis and increases axon sprouting after spinal cord injury. *J. Neurosci. Res.* **2006**, *84*, 724–734. [CrossRef] [PubMed]
43. Di Lernia, V. Targeting the IFN- $\gamma$ /CXCL10 pathway in lichen planus. *Med. Hypotheses* **2016**, *92*, 60–61. [CrossRef] [PubMed]
44. Glaser, J.; Gonzalez, R.; Perreau, V.M.; Cotman, C.W.; Keirstead, H.S. Neutralization of the chemokine CXCL10 enhances tissue sparing and angiogenesis following spinal cord injury. *J. Neurosci. Res.* **2004**, *77*, 701–708. [CrossRef] [PubMed]
45. Gonzalez, R.; Hickey, M.J.; Espinosa, J.M.; Nistor, G.; Lane, T.E.; Keirstead, H.S. Therapeutic neutralization of CXCL10 decreases secondary degeneration and functional deficit after spinal cord injury in mice. *Regen. Med.* **2007**, *2*, 771–783. [CrossRef] [PubMed]

46. Min, J.; Kim, J.H.; Choi, K.H.; Yoon, H.H.; Jeon, S.R. Is There Additive Therapeutic Effect When GCSF Combined with Adipose-Derived Stem Cell in a Rat Model of Acute Spinal Cord Injury? *J. Korean Neurosurg. Soc.* **2017**, *60*, 404–416. [[CrossRef](#)] [[PubMed](#)]
47. Nishio, Y.; Koda, M.; Kamada, T.; Someya, Y.; Kadota, R.; Mannoji, C.; Miyashita, T.; Okada, S.; Okawa, A.; Moriya, H.; et al. Granulocyte colony-stimulating factor attenuates neuronal death and promotes functional recovery after spinal cord injury in mice. *J. Neuropathol. Exp. Neurol.* **2007**, *66*, 724–731. [[CrossRef](#)] [[PubMed](#)]
48. Kato, K.; Koda, M.; Takahashi, H.; Sakuma, T.; Inada, T.; Kamiya, K.; Ota, M.; Maki, S.; Okawa, A.; Takahashi, K.; et al. Granulocyte colony-stimulating factor attenuates spinal cord injury-induced mechanical allodynia in adult rats. *J. Neural. Sci.* **2015**, *355*, 79–83. [[CrossRef](#)] [[PubMed](#)]
49. Dittgen, T.; Pitzer, C.; Plaas, C.; Kirsch, F.; Vogt, G.; Laage, R.; Schneider, A. Granulocyte-colony stimulating factor (G-CSF) improves motor recovery in the rat impactor model for spinal cord injury. *PLoS ONE* **2012**, *7*, e29880. [[CrossRef](#)] [[PubMed](#)]
50. Kadota, R.; Koda, M.; Kawabe, J.; Hashimoto, M.; Nishio, Y.; Mannoji, C.; Miyashita, T.; Furuya, T.; Okawa, A.; Takahashi, K.; et al. Granulocyte colony-stimulating factor (G-CSF) protects oligodendrocyte and promotes hindlimb functional recovery after spinal cord injury in rats. *PLoS ONE* **2012**, *7*, e50391. [[CrossRef](#)] [[PubMed](#)]
51. Guo, Y.; Liu, S.; Wang, P.; Zhang, H.; Wang, F.; Bing, L.; Gao, J.; Yang, J.; Hao, A. Granulocyte colony-stimulating factor improves neuron survival in experimental spinal cord injury by regulating nucleophosmin-1 expression. *J. Neurosci. Res.* **2014**, *92*, 751–760. [[CrossRef](#)] [[PubMed](#)]
52. Koda, M.; Nishio, Y.; Kamada, T.; Someya, Y.; Okawa, A.; Mori, C.; Yoshinaga, K.; Okada, S.; Moriya, H.; Yamazaki, M. Granulocyte colony-stimulating factor (G-CSF) mobilizes bone marrow-derived cells into injured spinal cord and promotes functional recovery after compression-induced spinal cord injury in mice. *Brain Res.* **2007**, *1149*, 223–231. [[CrossRef](#)] [[PubMed](#)]
53. Lee, J.-S.; Yang, C.-C.; Kuo, Y.-M.; Sze, C.-I.; Hsu, J.-Y.C.; Huang, Y.-H.; Tzeng, S.-F.; Tsai, C.-L.; Chen, H.-H.; Jou, I.-M. Delayed granulocyte colony-stimulating factor treatment promotes functional recovery in rats with severe contusive spinal cord injury. *Spine* **2012**, *37*, 10–17. [[CrossRef](#)] [[PubMed](#)]
54. Takahashi, H.; Yamazaki, M.; Okawa, A.; Sakuma, T.; Kato, K.; Hashimoto, M.; Hayashi, K.; Furuya, T.; Fujiyoshi, T.; Kawabe, J.; et al. Neuroprotective therapy using granulocyte colony-stimulating factor for acute spinal cord injury: A phase I/IIa clinical trial. *Eur. Spine J.* **2012**, *21*, 2580–2587. [[CrossRef](#)] [[PubMed](#)]
55. Kamiya, K.; Koda, M.; Furuya, T.; Kato, K.; Takahashi, H.; Sakuma, T.; Inada, T.; Ota, M.; Maki, S.; Okawa, A.; et al. Neuroprotective therapy with granulocyte colony-stimulating factor in acute spinal cord injury: A comparison with high-dose methylprednisolone as a historical control. *Eur. Spine J.* **2015**, *24*, 963–967. [[CrossRef](#)] [[PubMed](#)]
56. Yoon, S.H.; Shim, Y.S.; Park, Y.H.; Chung, J.K.; Nam, J.H.; Kim, M.O.; Park, H.C.; Park, S.R.; Min, B.-H.; Kim, E.Y.; et al. Complete Spinal Cord Injury Treatment Using Autologous Bone Marrow Cell Transplantation and Bone Marrow Stimulation with Granulocyte Macrophage-Colony Stimulating Factor: Phase I/II Clinical Trial. *Stem Cells* **2007**, *25*, 2066–2073. [[CrossRef](#)] [[PubMed](#)]
57. Poniatowski, L.A.; Wojdasiewicz, P.; Krawczyk, M.; Szukiewicz, D.; Gasik, R.; Kubaszewski, Ł.; Kurkowska-Jastrzębska, I. Analysis of the Role of CX3CL1 (Fractalkine) and Its Receptor CX3CR1 in Traumatic Brain and Spinal Cord Injury: Insight into Recent Advances in Actions of Neurochemokine Agents. *Mol. Neurobiol.* **2017**, *54*, 2167–2188. [[CrossRef](#)] [[PubMed](#)]
58. Donnelly, D.J.; Longbrake, E.E.; Shawler, T.M.; Kigerl, K.A.; Lai, W.; Tovar, C.A.; Ransohoff, R.M.; Popovich, P.G. Deficient CX3CR1 signaling promotes recovery after mouse spinal cord injury by limiting the recruitment and activation of Ly6Clo/iNOS+ macrophages. *J. Neurosci.* **2011**, *31*, 9910–9922. [[CrossRef](#)] [[PubMed](#)]
59. Freria, C.M.; Hall, J.C.E.; Wei, P.; Guan, Z.; McTigue, D.M.; Popovich, P.G. Deletion of the Fractalkine Receptor, CX3CR1, Improves Endogenous Repair, Axon Sprouting, and Synaptogenesis after Spinal Cord Injury in Mice. *J. Neurosci.* **2017**, *37*, 3568–3587. [[CrossRef](#)] [[PubMed](#)]

60. Wilcox, J.T.; Fehlings, M.G. Acute Clip Compression Model of SCI. In *Experimental Neurosurgery in Animal Models*; Neuromethods; Springer: New York, NY, USA, 2016; Volume 116, pp. 111–117.
61. Basso, D.M.; Beattie, M.S.; Bresnahan, J.C. A Sensitive and Reliable Locomotor Rating Scale for Open Field Testing in Rats. *J. Neurotrauma* **1995**, *12*, 1–21. [[CrossRef](#)] [[PubMed](#)]



© 2018 by the authors. Licensee MDPI, Basel, Switzerland. This article is an open access article distributed under the terms and conditions of the Creative Commons Attribution (CC BY) license (<http://creativecommons.org/licenses/by/4.0/>).



Article

# A Single Dose of Atorvastatin Applied Acutely after Spinal Cord Injury Suppresses Inflammation, Apoptosis, and Promotes Axon Outgrowth, Which Might Be Essential for Favorable Functional Outcome

Katarina Bimbova <sup>1</sup>, Maria Bacova <sup>1</sup>, Alexandra Kisucka <sup>1</sup>, Jaroslav Pavel <sup>1</sup>, Jan Galik <sup>1</sup>, Peter Zavacky <sup>2</sup>, Martin Marsala <sup>1,3</sup>, Andrea Stropkovska <sup>1</sup>, Jana Fedorova <sup>1</sup>, Stefania Papcunova <sup>1</sup>, Jana Jachova <sup>1</sup> and Nadezda Lukacova <sup>1,\*</sup>

<sup>1</sup> Institute of Neurobiology of Biomedical Research Centre of Slovak Academy of Sciences, Soltesovej 4,6, 040 01 Kosice, Slovakia; bimbova@saske.sk (K.B.); bacova@saske.sk (M.B.); kisucka@saske.sk (A.K.); pavel@saske.sk (J.P.); galik@saske.sk (J.G.); mmarsala@ucsd.edu (M.M.); stropkovska@saske.sk (A.S.); jfedorova@saske.sk (J.F.); gedrova@saske.sk (S.P.); jachova@saske.sk (J.J.)

<sup>2</sup> 1st Department of Surgery, Louis Pasteur University Hospital, Faculty of Medicine University of Pavol Jozef Safarik, Trieda SNP 1, 041 66 Kosice, Slovakia; peterzavacky963@gmail.com

<sup>3</sup> Neuroregeneration Laboratory, Department of Anesthesiology, University of California, 9500 Gilman Drive, San Diego, CA 92092-0100, USA

\* Correspondence: lukacova@saske.sk; Tel.: +421-55-72-76-225

Received: 29 January 2018; Accepted: 5 April 2018; Published: 7 April 2018

**Abstract:** The aim of our study was to limit the inflammatory response after a spinal cord injury (SCI) using Atorvastatin (ATR), a potent inhibitor of cholesterol biosynthesis. Adult Wistar rats were divided into five experimental groups: one control group, two Th9 compression (40 g/15 min) groups, and two Th9 compression + ATR (5 mg/kg, i.p.) groups. The animals survived one day and six weeks. ATR applied in a single dose immediately post-SCI strongly reduced IL-1 $\beta$  release at 4 and 24 h and considerably reduced the activation of resident cells at one day post-injury. Acute ATR treatment effectively prevented the excessive infiltration of destructive M1 macrophages cranially, at the lesion site, and caudally (by 66%, 62%, and 52%, respectively) one day post-injury, whereas the infiltration of beneficial M2 macrophages was less affected (by 27%, 41%, and 16%). In addition, at the same time point, ATR visibly decreased caspase-3 cleavage in neurons, astrocytes, and oligodendrocytes. Six weeks post-SCI, ATR increased the expression of neurofilaments in the dorsolateral columns and Gap43-positive fibers in the lateral columns around the epicenter, and from day 30 to 42, significantly improved the motor activity of the hindlimbs. We suggest that early modulation of the inflammatory response via effects on the M1/M2 macrophages and the inhibition of caspase-3 expression could be crucial for the functional outcome.

**Keywords:** spinal cord compression; inflammatory response; Atorvastatin; caspase-3; macrophages; Gap43; neurofilaments; gene expression

## 1. Introduction

Spinal cord injury (SCI) is one of the most devastating and complex clinical conditions, often leading to irreversible neurological deficits. The complex pathophysiology of a SCI, consisting of primary and secondary mechanisms, may explain the difficulty of finding a suitable therapy [1]. SCI is caused by two distinct events, which follow a somewhat overlapping temporal sequence: the acute (seconds to minutes after the injury) phase, the secondary (minutes to weeks after the injury) phase, and the chronic (months to years after the injury) phase [2,3]. In the acute phase, due to

the direct mechanical insult, the spinal tissue undergoes a cascade of events followed by secondary damage affecting intact, neighboring tissue [4]. Inflammatory response is one of the key mechanisms of secondary injury (sub-acute phase). It includes the activation of resident cells (microglia, astrocytes), the recruitment of immune cells (macrophages and neutrophils) from the bloodstream to the site of the injury, and evident up-regulation of the NADPH oxidase (NOX) enzyme. The resident and immune cells release proinflammatory cytokines, including interleukins (IL-1 $\beta$ , IL-6) and tumor necrosis factor- $\alpha$  (TNF- $\alpha$ ), all of which increase the extent of the inflammatory response. These events play an important role in secondary tissue damage and cell death [2,3,5,6]. During this period, the astrocytes begin to migrate out of the epicenter, producing molecules, such as proteoglycans and laminin, in the extracellular space. In the chronic phase of injury, there is continued necrosis, and demyelination in the white matter due to apoptotic oligodendrocytic death. Reactive astrocytes continue to invade the region surrounding the lesion center, leading to the formation of a cystic cavity surrounded by glial scar, which has been hypothesized to be a physical and biochemical barrier to axonal regeneration [7,8].

Research over the last few years has revealed numerous therapeutic approaches contributing to the modulation of the inflammation response and the reduction of the negative symptoms of a SCI [9–12]. Statins, the 3-hydroxyl-3-methylglutaryl-coenzyme A reductase inhibitors, are currently used for treatment of high cholesterol, coronary atherosclerosis, and atherosclerosis [13–15]. Atorvastatin (ATR), a drug with anti-inflammatory and immunomodulatory effects, has been widely studied in various ischemia-reperfusion and traumatic SCI models. When applied for several days before/after a SCI, it has been found to be neuroprotective [16–19]. It significantly reduced the release of pro-inflammatory cytokines and inhibited macrophage infiltration and microglial activation. In addition, this drug inhibited apoptosis and demyelination after traumatic injury and promoted the recovery of neurological functions [16,17].

Although pre- or post-long-lasting treatments with ATR have been shown to be effective in limiting pathology due to a traumatic SCI [17,18], the present study focused on treating animals in the very critical first moments after injury and on finding out whether an acute single dose of this clinically relevant drug would effectively minimize the negative impact of an acute, traumatic SCI. We found that ATR (5 mg/kg, i.p.) applied immediately after a Th9 compression favorably reduced the course of acute inflammation by decreasing the release of interleukin 1 $\beta$  4 h and 1 d after a SCI. This statin significantly reduced macrophage infiltration, resident cell activation, and caspase-3 expression one day post-SCI and promoted axon outgrowth in the whole cranio-caudal extent after six weeks of survival. The mitigation of the strong inflammatory response soon after a SCI promoted regeneration at the lesion site and cranially and caudally from the epicenter and significantly improved the neurological outcome from day 30 to 42. These results strongly support the use of ATR as one of the first-line therapeutic drugs to treat an acute, traumatic SCI.

## 2. Results

### 2.1. Short-Term Survival (24 h)

#### 2.1.1. Releasing of Pro-Inflammatory Cytokine IL-1 $\beta$ after Spinal Cord Trauma and the Atorvastatin Treatment

The activation of the inflammatory response after a spinal cord injury leads to the release of pro- and anti-inflammatory cytokines into the bloodstream [20]. We examined the effect of a single dose of ATR (5 mg/kg; i.p.) on the level of pro-inflammatory cytokine IL-1 $\beta$  in the blood serum at 4 and 24 h after a SCI. Figure 1 shows strong, up to 12-fold increase in the level of IL-1 $\beta$  ( $490.3 \pm 82$  pg/mL) at the acute (4 h) time point and rapid decrease in the cytokine level ( $84.8 \pm 11.6$  pg/mL) 24 h after the SCI. The concentration of IL-1 $\beta$  remained 2.9-fold higher after the SCI than the in naive spinal cord ( $29.3 \pm 1.2$  pg/mL). A single dose of Atorvastatin injected immediately after a Th9 compression decreased the release of IL-1 $\beta$  to  $42.8 \pm 7.3$  pg/mL after 4 h. A similar level of IL-1 $\beta$  was maintained 24 h after the SCI and the ATR treatment ( $46.3 \pm 4.6$  pg/mL).

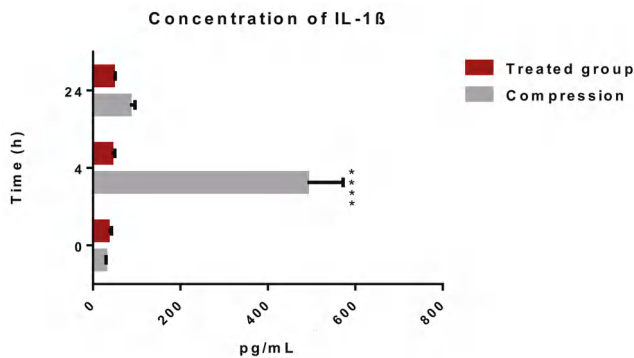
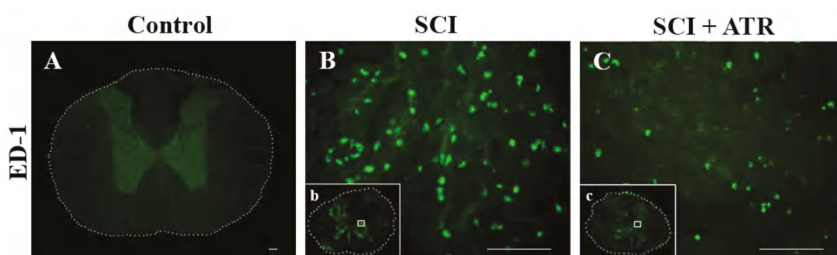


**Figure 1.** Concentration of pro-inflammatory cytokine IL-1 $\beta$  in the blood serum after a traumatic SCI and the ATR treatment. A significant elevation of IL-1 $\beta$  was noted 4 h after the SCI. ATR applied in a single dose (5 mg/kg; i.p.) immediately after the SCI reduced the release of IL-1 $\beta$  after 4 and 24 h. Data are the mean values of eight experiments  $\pm$  SD. The results were statistically evaluated using two-way analysis of variance (ANOVA) and post hoc Tukey's HSD test; \*\*\*  $p < 0.0001$ . ATR—Atorvastatin; IL-1 $\beta$ —interleukin 1 $\beta$ ; SCI—spinal cord injury.

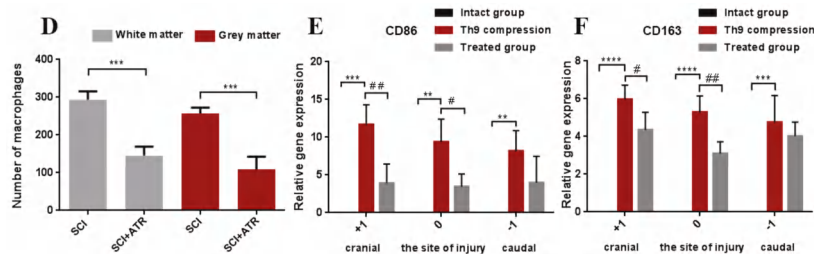
#### 2.1.2. Macrophage Response after a Spinal Cord Compression and the ATR Treatment

The ED-1 antibody, recognizing an intracellular antigen in activated macrophages, was used for identification of macrophages (ED-1) in immunostained cross-sections at the lesion site (Figure 2). No infiltrated ED-1 positive cells were detected in the intact spinal cord tissue; however, one day after the SCI, the macrophage infiltration was obvious (Figure 2B). Quantitative analysis revealed a higher number of ED-1 positive cells in the white matter ( $293 \pm 22.9$ ) than in the grey matter ( $257 \pm 20.4$ ). ATR significantly reduced the number of infiltrated macrophages in both the white ( $145 \pm 40$ ) and grey ( $109 \pm 33$ ) matter (Figure 2C,D).

Macrophages exhibit functional adaptability and can change phenotypes in response to stimuli [21]. One day after the SCI, both CD86 mRNA (M1 phenotype) and CD163 mRNA (M2 phenotype) were expressed at the lesion site and 1 cm cranially and caudally (Figure 2E,F). ATR significantly inhibited both the M1 and M2 phenotypes, but the decrease was more pronounced in the M1 phenotype, known to initiate a cascade of neurotoxic responses. Quantitative RT-PCR showed a significant decrease in CD86 mRNA expression at the lesion site ( $p < 0.05$ ) and cranially from the site of the injury ( $p < 0.01$ ) and significantly suppressed the expression of CD163 mRNA (anti-inflammatory M2 phenotype) cranially ( $p < 0.05$ ) and at the injury site ( $p < 0.01$ ) (Figure 2F).



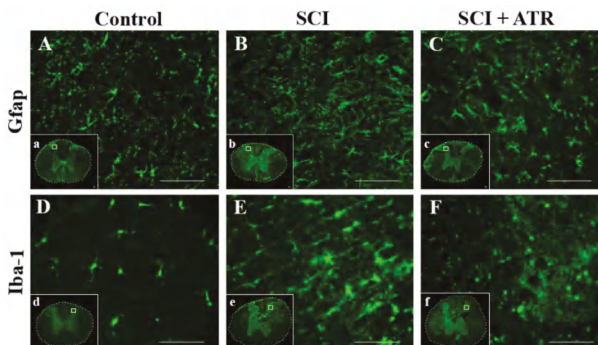
**Figure 2. Cont.**



**Figure 2.** Infiltration of the macrophages in the spinal cord 24 h after a traumatic injury and the treatment with ATR (5 mg/kg; i.p.). Figures from immunohistochemical analysis show no appearance of the macrophages in the intact spinal tissue (A), marked macrophage infiltration at the lesion site (B) and a strong decrease in macrophage influx after the ATR treatment (C). ATR significantly reduced the number of infiltrated macrophages in the grey and white matter (D). CD86 mRNA (M1 macrophages) and CD163 mRNA (M2 macrophages) were confirmed by RT-PCR in the whole cranio-caudal extent of the spinal cord (E,F). Scale bars: (A,b,c—1000  $\mu$ m; B,C—100  $\mu$ m). Data are the mean values of nine experiments (4 IHC, 5 RT-PCR)  $\pm$  SD. The results from the cell counting were statistically evaluated using a parametric T-Test and the results from the RT-PCR were evaluated with one-way ANOVA; #  $p < 0.05$ ; \*\*  $p < 0.01$ ; ##  $p < 0.01$ ; \*\*\*  $p < 0.001$ ; \*\*\*\*  $p < 0.0001$ . Atorvastatin—ATR; ED-1—macrophages; IHC—immunohistochemistry; SCI—spinal cord injury.

### 2.1.3. Changes in Glial Activation and Caspase-3 Activity

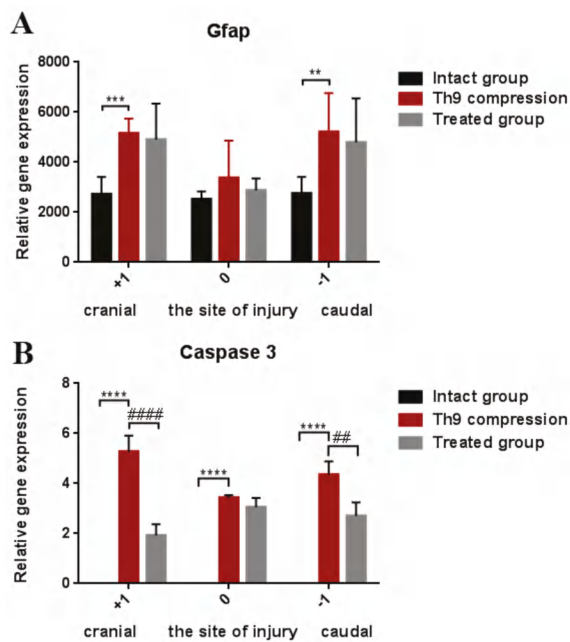
The GFAP antibody revealed a small stellate perikaryon of astrocytes, which had a few thin branched processes. Such morphology of GFAP-immunoreactive astrocytes was seen in the naive spinal cord (Figure 3A) and the in spinal tissue one day after the SCI. However, the activity of the astrocytes was more profound in the damaged regions within the impact area (Figure 3B). At the same time, the Iba-1 production, a marker for microglia, was strongly elevated (Figure 3E) at the site of the injury. The microglial cells were hypertrophied and massively distributed in the dorsal horn. Treatment with ATR (5 mg/kg; i.p.) decreased the extensive microglial activation (Figure 3F) and moderated the formation of reactive astrocytes at the lesion site (Figure 3C).



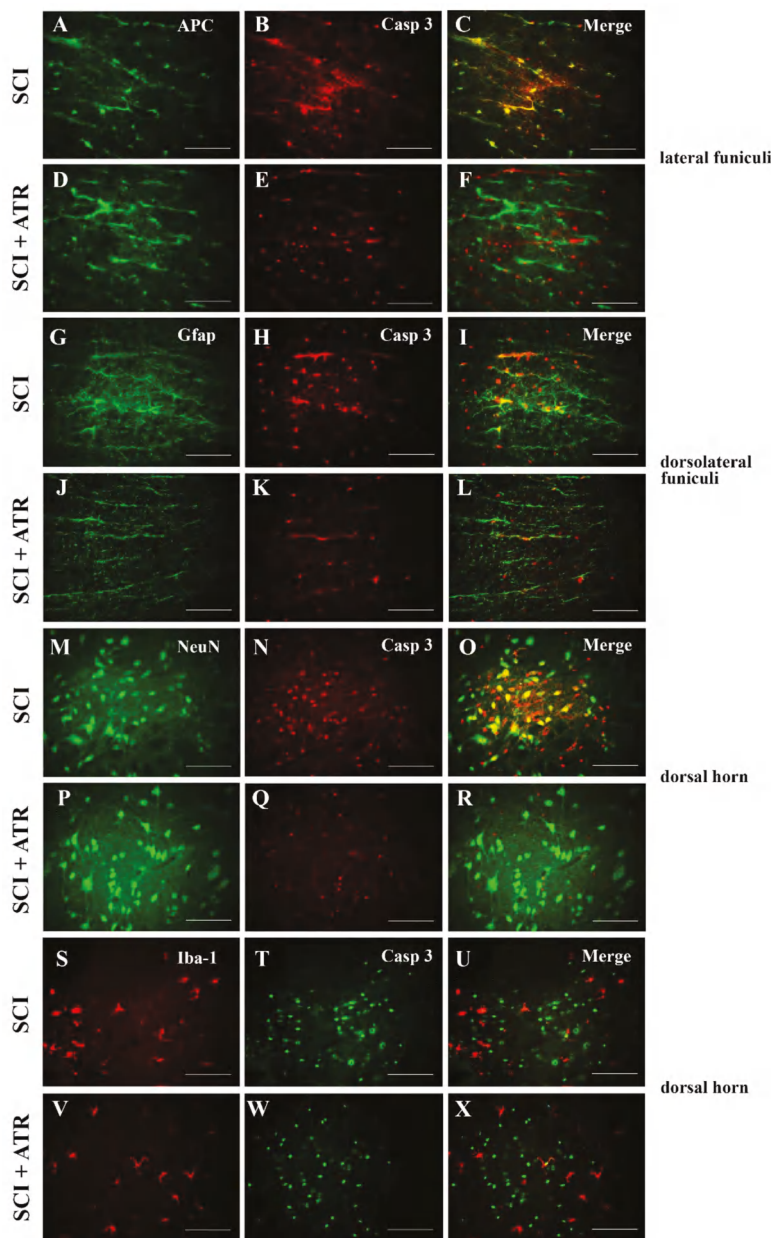
**Figure 3.** Representative images showing the activation of astrocytes and the microglia in the spinal cord after the Th9 compression and the atorvastatin treatment. Immunostaining of the astrocytes and microglial cells at the Th9 level of intact animals (A,D). Increased expression of the astrocytes (B) and the microglia (E) 24 h after the injury at the lesion site. The administration of ATR (5 mg/kg; i.p., immediately after the SCI) reduced the density of the activated astrocytes (C) and decreased the massive activation of the microglial cells (F). Scale bars: (A–F—100  $\mu$ m; a–f—1000  $\mu$ m). Atorvastatin—ATR; GFAP—astrocytes; Iba-1—microglia; SCI—spinal cord injury.

Figure 4A shows the course of astrogliosis in a 3 cm crano-caudal extent 24 h after the SCI. The GFAP gene expression was overexpressed in the cranial ( $p < 0.001$ ) and caudal ( $p < 0.01$ ) segments after the SCI, but at the site of the injury this astrocyte marker was not significantly increased. GFAP mRNA expression was not markedly changed by the ATR treatment. However, compared with the controls, a moderate improvement was visible in the caudal segment (−1).

Caspases, including caspase-3, directly and indirectly control the changes in cells during apoptosis [22]. Strong mRNA expression of caspase-3 was confirmed one day after the Th9 compression in the whole crano-caudal extent (Figure 4B). Atorvastatin (5 mg/kg; i.p.) significantly decreased the expression of caspase-3 mRNA in the cranial ( $p < 0.0001$ ) and caudal ( $p < 0.01$ ) segments. The results from the double immunostaining showed strong cleavage of caspase-3 in the oligodendrocytes, astrocytes, and neurons all around the lesion site 24 h after the Th9 compression (Figure 5). A marked reduction in apoptotic activity was noted after the ATR treatment in the oligodendrocytes and astrocytes in the dorsal and dorsolateral funiculi. Immunolabeled NeuN positive cells demonstrated a massive decrease in caspase-3 activity especially in the dorsal horns but also around the central canal. However, no cleavage of caspase-3 was observed in the microglial cells either after the SCI or after the ATR treatment at this time point.



**Figure 4.** Gene expression showing astrogliosis (GFAP) and apoptosis (caspase-3) in the spinal cord 24 h after the Th9 compression and the atorvastatin (5 mg/kg; i.p.) treatment. The graphs show the relative quantities of GFAP (A) and caspase-3 (B) in rostro-caudal manner in the controls and 24 h after the SCI and SCI + ATR treatment. Data are the mean values of five experiments  $\pm$  SD. The results were statistically evaluated using one-way ANOVA; \*\*  $p < 0.01$ ; ##  $p < 0.01$ ; \*\*\*  $p < 0.001$ ; \*\*\*\*  $p < 0.0001$ ; #####  $p < 0.0001$ . Atorvastatin—ATR; GFAP—astrocytes; SCI—spinal cord injury.



**Figure 5.** Set of microphotographs showing the immunofluorescent staining and co-localization of caspase-3 (red in B,E,H,K,N,Q; green in T,W) with APC (green), GFAP (green), NeuN (green), and Iba-1 (red) one day after the SCI and the ATR treatment. Double immunostaining demonstrates the cleavage of caspase-3 in the oligodendrocytes (A–F); astrocytes (G–L); neurons (M–R); and microglial cells (S–X) 0.5 cm caudally from the lesion site in the SCI and SCI + ATR groups. Scale bars: (A–X—100  $\mu$ m). APC—adenomatous polyposis coli positive mature oligodendrocytes; ATR—Atorvastatin; Casp 3—caspase-3; GFAP—astrocytes, Iba-1—microglia; NeuN—neurons; SCI—spinal cord injury.

## 2.2. Long-Term Survival (Six Weeks)

### 2.2.1. Regenerative Capacity of the Spinal Cord

Six weeks after the SCI, numerous Iba-1 positive cells with rounded morphology were identified predominantly in the dorsal part of the spinal cord (Figure 6B). No obvious difference was observed visually between the SCI and ATR-treated SCI rats at six weeks in the dorsal horn (Figure 6C). As shown in Figure 6F, the GFAP immunoreactivity was markedly reduced in the ATR-treated group. Although ATR effectively reduced astrogliosis in the most affected dorsal horn of the caudal segment, the gene expression of GFAP showed no significant difference between the SCI and SCI + ATR groups in the cranial, injured, and caudal segments, each taken as a whole (Figure 7A).

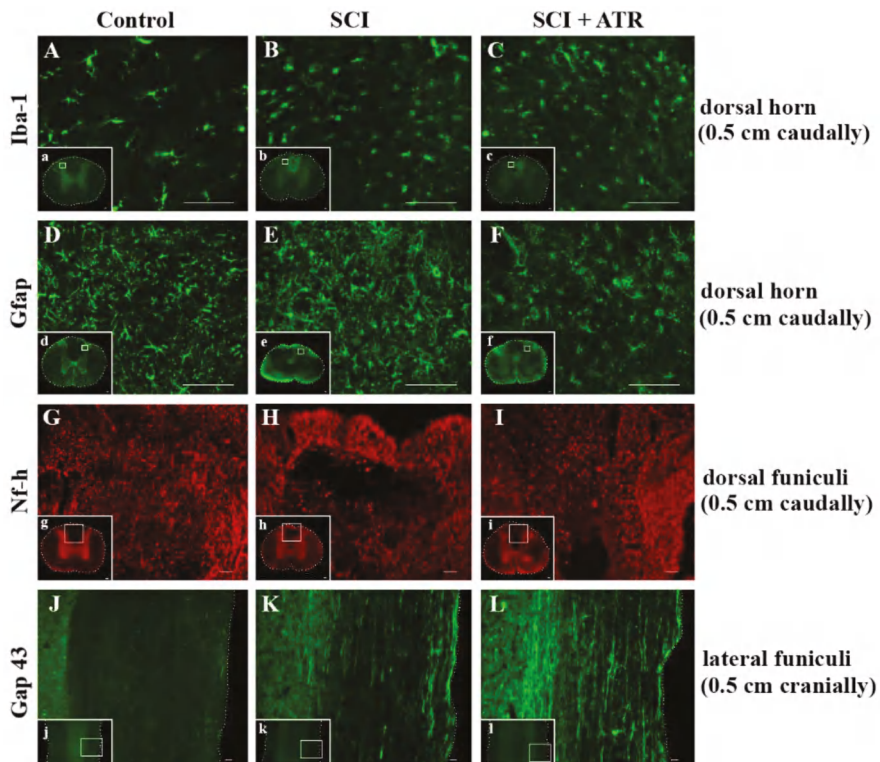


**Figure 6.** Effect of Atorvastatin on the glial cell activation and the regenerative capacity in the spinal cord six weeks after the SCI and the ATR treatment (5 mg/kg; i.p.). The microphotographs show visible changes in the activation of the microglia (green) (A–C) and astrocytes (green) (D–F) in the dorsal horn (0.5 cm caudally from the site of the injury) after the SCI and SCI + ATR. The regenerative capacity of Nf-h (red) is clearly visible in the dorsal funiculi caudally from the lesion site (G–I). Longitudinal spinal cord sections taken from the cranial segments show spontaneous axonal outgrowing (Gap43; green) after the SCI (K). More pronounced Gap43 immunoreactivity was visible in the ATR-treated group (L). Scale bars: (A–F—100  $\mu$ m; G–I—200  $\mu$ m; J–L—500  $\mu$ m; a–l—1000  $\mu$ m). ATR—Atorvastatin; Gap 43—outgrowing axons; GFAP—astrocytes; Iba-1—microglia; Nf-h—neurofilaments (heavy); SCI—spinal cord injury.

Nf-h immunoreactive axons were regularly distributed throughout the control spinal cord (Figure 6G). At six weeks, the Th9 compression resulted in massive damage to the white matter in the

dorsal and lateral columns, with their partial obliteration by a cavity (Figure 6H). The ATR treatment increased the expression of neurofilaments in the dorsolateral part of the spinal cord (Figure 6I). However, compared with the SCI group, the Nf-h mRNA measured in the segments (cranial, injured, and caudal) in toto was not increased in the ATR-treated group (Figure 7C). Similar results were observed in the gene expression of Olig2 (Figure 7D).

Axonal sprouting and outgrowing in the damaged spinal cord is one of the key factors for tissue regeneration and motor function restoration. As shown in Figure 6K, spontaneous axonal overgrowing was very low six weeks post-SCI. Immunofluorescence analysis of the longitudinal spinal cord sections revealed that the single dose of ATR (5 mg/kg, i.p.) strongly promoted the axons' outgrowth (Figure 6L). This effect was visible in the whole crano-caudal extent. The results from the RT-PCR are shown in Figure 7B. The relative gene expression of Gap43 correlated with Gap 43 immunoreactivity. The ATR-treated group confirmed a significant improvement at the site of the injury ( $p < 0.01$ ) and in the cranial segment ( $p < 0.05$ ).

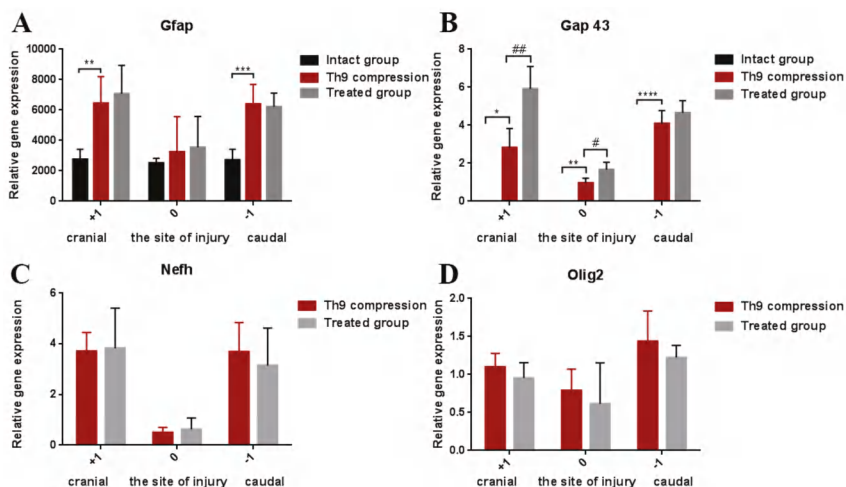


**Figure 7.** Graphs demonstrating the relative gene expression of GFAP, Gap 43, Nf-h, and Olig 2 in the spinal cord (site of the injury, cranially, and caudally) six weeks after the traumatic spinal cord injury and the ATR treatment. The lowest gene expression was observed at the lesion site. GFAP activation shows the changes in astrogliosis after the SCI and SCI + ATR (A). Markers of regenerative capacity (Gap 43, Nf-h, and Olig2) show a significant improvement in axonal outgrowing at the lesion site and in the cranial (+1) segment (B–D). The data are the mean values of five experiments  $\pm$  SD. The results were statistically evaluated using a parametric *T*-test and one-way ANOVA; \*  $p < 0.05$ ; #  $p < 0.05$ ; \*\*  $p < 0.01$ ; ##  $p < 0.01$ ; \*\*\*  $p < 0.001$ ; \*\*\*\*  $p < 0.0001$ . Atorvastatin—ATR; Gap 43—outgrowing axons; GFAP—astrocytes; Nf-h—neurofilaments (heavy); Olig2—oligodendrocytes; SCI—spinal cord injury.

## 2.2.2. Neurological Outcome

Functional outcome was evaluated using the Basso–Beattie–Bresnahan (BBB) locomotor rating score representing the recovery stages for rat hindlimb motor function. One day post-injury, all the animals suffered from complete paraplegia ( $0.25 \pm 0.39$ ) and their motor function improved spontaneously up to day 42 (six weeks) with a mean neurological score of  $9.7 \pm 0.93$  (Figure 8). Up until day 24, the development of the neurological score did not differ between the SCI and ATR-treated groups. However, the outcome was significantly different from day 30 to 42. At the end of survival, the mean score for motor outcome reached  $11.06 \pm 0.91$  in the ATR-treated group.

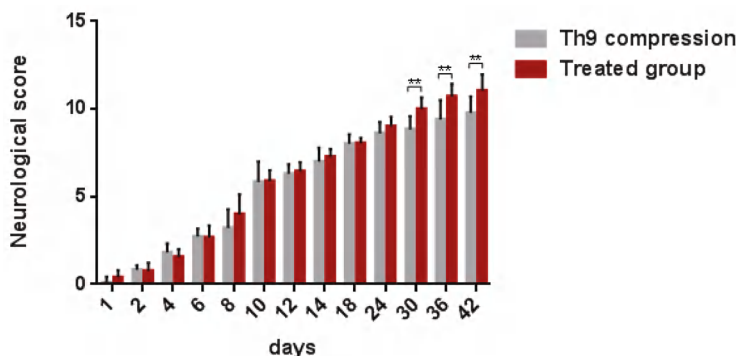


**Figure 8.** BBB scores showing the locomotor function of rats after the Th9 compression and the ATR treatment. The scoring points range from complete paraplegia (point zero) to normal hindlimb function (point 21). Data are the mean values of eighteen experiments  $\pm$  SD. The results were statistically evaluated using a parametric *T*-test. Atorvastatin—ATR; BBB score—Basso-Beattie-Bresnahan score.

### 3. Discussion

Neuroinflammation is a complex immune response, which occurs within a short time period after SCI. It includes the activation and infiltration of numerous cell populations (astrocytes, microglia, T lymphocytes, neutrophils, and monocytes) and the release of a large number of non-cell mediators (interleukins, interferons, and TNF $\alpha$ ) [23]. The first factors involved in the inflammatory response are pro- and anti- inflammatory cytokines and chemokines produced by endothelial cells and activated microglia [24]. In the CNS, the main pro-inflammatory cytokine is IL-1 $\beta$ , which is released just 2 h post-SCI [23,25]. In the present study, the levels of IL-1 $\beta$  in the blood serum were markedly (12-fold) elevated 4 h after the Th9 compression, but one day post-injury its concentration significantly decreased. Allan et al. [26] reported that this pro-inflammatory cytokine can directly affect glial cells, endothelial cells, and even neurons, as they all express interleukin 1 receptor type 1 (IL-1R1). In their rat SCI model, Nesic et al. [27] used infusions of IL1 antagonists 72 h after a SCI and reported markedly reduced injury-induced apoptosis, indicating that early expression of IL-1 $\beta$  is detrimental. It has also been shown that IL-1 $\beta$  promotes astrogliosis and triggers the astrocytic release of glutamate, nitric oxide, potassium, prostaglandins, cytokines, and chemokines [28], all of which were shown to be toxic to neurons at high concentrations [29–31]. The anti-inflammatory drug ATR applied in a single dose acutely after a Th9 compression significantly reduced the release of IL-1 $\beta$ .

Several studies have highlighted the therapeutic benefit of pre- and/or post-SCI application of ATR (long-lasting vs single and per-oral vs intraperitoneal). The present study produces new data showing the neuroprotective effect of a single dose of ATR applied immediately after a Th9 compression. First, ATR reduced the activation of the microglia within the most injured dorsolateral spinal cord and significantly reduced the infiltration of macrophages into the white and grey matter one day post-SCI. Papa et al. [9] showed that early microglial activation after spinal trauma is a key factor in the formation of a pathological environment, which supports injury progression. These authors demonstrated that early microglial inhibition induced a long-lasting recovery post-SCI (up to 63 days). As reported previously, microglia acquire pro-inflammatory phenotypes immediately after a SCI, which promote local inflammation and can lead to destructive (M1 phenotype) and beneficial (M2 phenotype) macrophage recruitment [9]. Based on their phenotype and activation status, macrophages may initiate the mechanisms of secondary injury or promote neuroregeneration of the spinal cord tissue [32]. One day after the SCI, we observed a significant increase in the expression of both the M1 and M2 phenotypes in each spinal cord region, but the presence of both macrophage phenotypes was not equal. The gene expression of the pro-inflammatory M1 macrophage marker

was substantially higher compared with the M2 marker. ATR applied soon after the Th9 compression reduced the expression of both the M1 and M2 associated genes in all the evaluated areas, but a significant decrease was noted only in the cranial segments and at the lesion site. These segments are known to host a neuroprotective and neurotrophic environment [33]. Here, we also show that in the acute phase, ATR modulated the M1 macrophage phenotype more markedly than the M2 antigenic marker. Although the neuroprotective effect of ATR on macrophage infiltration has been shown in various SCI models, the precise time point of microglia/macrophage polarization and the factors controlling their shifts are still unclear. Khayrullina et al. [34] reported that acute inhibition of NOX2 (the enzyme that is a primary source of reactive oxygen species) with the specific inhibitor, gp91ds-tat, shifted microglial/macrophage polarization toward the M2 marker at seven days post-SCI. Although single acute gp91ds-tat treatment did not induce inflammatory effects beyond seven days, functional improvement continued through at least 28 days, indicating the importance of this single acute intervention. Bermudez et al. [35] also studied the correlation between NOX expression and microglial/macrophage polarization in a mouse SCI model. These authors confirmed that the expression of two NOX isoforms (NOX2 and NOX4) was temporally and polarization related, with an M1 preference for NOX2 acutely and NOX4 chronically; the M2 polarization marker was identified at acute time points only. While both the M1 and M2 microglia/macrophages express NOX isoforms, there is an influence of NOX on polarization. These data confirmed that NOX enzyme inhibition can alter the polarization status, which plays a significant role in the functional outcome. The regulation of the polarization of the M1/M2 macrophages after a SCI may also be related to neurotrophin-3 (NT-3) [36]. Electroacupuncture at GV acupuncture points, which can be used as an adjuvant therapy for a SCI, inhibited the proportion of M1 macrophages and proinflammatory cytokines, but at the other site it upregulated the M2 marker and NT-3 expression. Although we did not study the antioxidant effect of ATR, it seems that early ATR treatment, preferentially decreasing the M1 expression in segments with neuroprotective/neurotrophic environment could be involved in the oxidative response, thus reflecting the redox state of the lesion microenvironment. Pre-ischemic administration of ATR in a spinal cord ischemia-reperfusion model of a rabbit inhibited the depletion of antioxidative enzymes, reduced lipid peroxidation, and improved the extent of locomotor recovery [37]. In addition, increased levels of myeloperoxidase (MPO) were detected in the spinal cord following ischemia/reperfusion, suggesting leukocyte infiltration into the spinal cord. The authors have shown that ATR pre-treatment prevented MPO elevation. Secondly, astrocytes play a role in the mechanical and metabolic support of neurons. After spinal cord trauma, a select population of astrocytes, known as reactive astrocytes, upregulates the expression of intermediate filament proteins, proteoglycans, and other molecules and contributes to the inhibition of axonal outgrowth and glial scar formation [38–40]. One day after Th9 compression, we detected significant upregulation of GFAP mRNA in the areas surrounding the lesion site. Over time, the GFAP mRNA was only moderately reactivated at six weeks of survival. This finding might be associated with the regulation of the ion concentration in the extracellular space, the modulation of synaptic transmission, and the repair of the spinal parenchyma through the formation of a glial scar in the later post-SCI period [41]. Pannu et al. [16,17] injected ATR (5 mg/kg) through the whole period of survival, and they demonstrated a significant reduction of astrocyte activation. A single dose of ATR (5 mg/kg; i.p.) injected immediately after the SCI modulated the acute immune response, but we did not see its significant short- or long-lasting effect. It is also evident that although inflammation plays a very important role in the development of a glial scar, paradoxically, astrocyte activation by IL-1 $\beta$  can exert neuroprotective effects by stimulating the repair of the blood-brain barrier and decreasing its permeability [25]. Recently published data show that specific parts of the astrocytic scar have a supportive function for axon regeneration following a SCI [42] and might be induced by activated microglia [43]. Thirdly, early application of ATR could be crucial for limiting the secondary injury cascade after a SCI. One day after the Th9 compression, we noticed a sharp caspase-3 mRNA expression throughout the whole injured area. Moreover, the double immunostaining of caspase-3 with NeuN, APC, or GFAP showed marked apoptotic activity of these cells around the

lesion site. Treatment with ATR, applied immediately after the Th9 compression, significantly reduced the expression of apoptotic markers. Immunohistochemical analysis showed the strong effect of the treatment on the reduction of caspase-3 cleavage in the oligodendrocytes, neurons, and astrocytes both cranially and caudally from the epicenter. Several recent studies have demonstrated the beneficial effect of ATR on the functional outcome through apoptosis inhibition. Gao et al. [18] showed that two doses of ATR (5 mg/kg; i.p.) injected one and two days after a weight-drop spinal cord injury significantly reduced caspase-3 and caspase-9 expression and activated autophagy, which was conducive to the recovery of neurological functions at seven days post-injury. Intraperitoneal injection of this drug was also effective in preventing early apoptosis at the lesion site within 2 h post-SCI administration [19]. ATR-treated rats showed a significant decrease in caspase-3 activity and a decrease in the number of TUNEL-positive cells at the injury site 4 h post-SCI, followed by an improvement in locomotion at four weeks post-SCI. While the treatment with ATR prevented excessive caspase-3 activation, it also inhibited the massive extension of the inflammatory response. Our results indicate that early inhibition of caspase-3 activity in the oligodendrocytes, neurons, and astrocytes may have a role in mitigating neurodegeneration, as well as in the remarkable functional outcome seen from day 30 to 42 after the Th9 compression. Gao et al. [44] also pointed out the positive effect of the early inhibition of programmed cell death. After Simvastatin injection (two doses, 10 mg/kg; i.p.), they observed a significant improvement in locomotor functional recovery seven weeks after a weight-drop SCI. It has been suggested that oligodendrocyte apoptosis contributes to chronic demyelination of spared axons and exacerbates the extent of the injury, eventually leading to permanent functional deficits [45]. Lee et al. [45] demonstrated that preventing oligodendrocyte cell death improved the neurological score for 35 days after a SCI in mice.

We suggest that the neuroprotective effect of ATR registered soon after a SCI could be crucial for improving tissue regeneration and the functional outcome. Markers of axonal outgrowing (Gap 43) quantified by means of the RT-PCR showed improvement in each evaluated segment. Gap-43 immunoreactive axons were distinctly visible throughout the whole crano-caudal extent, but the most extensive Gap-43 immunoreactive axons were seen in the lateral funiculi. Similarly, a very strong regenerative response was detected in the expression of the neurofilaments. Neurofilaments are particularly abundant in large myelinated axons and are essential for axon radial growth and caliber maintenance during development [46,47]. We detected a loss of neurofilament-positive axons six weeks after the Th9 compression in areas infiltrated with Iba-1 positive cells. Massive regeneration of neurofilament immunoreactive axons was detected in the injured dorsolateral funiculi after the ATR treatment, although neurofilament mRNA measured in toto did not show a significant improvement. Wang et al. [48] have reported that neurofilament gene transcriptional regulation is crucial for neurofilament expression predominantly in axonal regeneration. We have also recently pointed out the role of neurofilaments in modulating spinal microcircuits leading to a better functional outcome [49]. Although the Olig2 transcription factor, an essential regulator of oligodendrocyte development, has been seen to improve locomotor recovery and enhance myelination in a rat contusive spinal cord injury model [50], we did not see any neuroprotective effect of the ATR treatment in Olig2 mRNA.

This study underscores the protective effect of ATR applied immediately post-SCI. The results suggest that ATR, even in a single dose, has important neuroprotective potential. However, a set of research problems dealing with practical ATR application in a traumatic SCI injury currently remains unexplored.

#### 4. Materials and Methods

##### 4.1. Experimental Animals and Surgical Procedure

A total of 48 adult female Wistar rats (weighing 250–300 g) were used in the experiment. The rats were housed 5 per cage on a 12-h dark/light cycle in a temperature- and humidity-controlled environment. Female rats were used in order to relieve serious urinary tract complications after

SCI, such as hematuria (hemorrhagic cystitis). Ferrero. S.L. et al. [51] showed that after contusion injury, hematuria duration was significantly longer in males compared with females, despite similar bladder reflex onset times. All procedures were carried out in accordance with the protocols approved by the State Veterinary and Food Administration in Bratislava (decision No. 4434/16-221/3), as well as by the Animal Use Committee at the Institute of Neurobiology, Slovak Academy of Sciences, and in accordance with the EC Council Directive (2010/63/EU) regarding the use of animals in research. All efforts were made to minimize the number of rats and their suffering.

The animals were divided into five experimental groups as follows: (1) control animals ( $n = 6$ ); (2–3) rats subjected to the Th9 compression surviving for 24 h ( $n = 12$ ) and six weeks ( $n = 9$ ); and (4–5) rats after the SCI treated with post-surgical Atorvastatin administration (5 mg/kg, i.p.; Fluka by Sigma Aldrich, St. Louis, MO, USA) surviving for 24 h ( $n = 12$ ) and six weeks ( $n = 9$ ).

The surgical procedure was performed under isoflurane anesthesia (2–4%; AbbVie, BA, Slovak Republic; in 1.5–2.0 L/min oxygen), delivered by mask. After laminectomy at the Th9 segment, SCI was induced using a compression device with a weight of 40 g/15 min. The body temperature was maintained at 37 °C during the whole surgical procedure. After the Th9 compression, the rats received the antibiotic drug Amoksiklav (Sandoz Pharmaceuticals, Ljubljana, Slovenia; 30 mg/kg, i.m.) and the analgesic drug Novasul (Richterpharma, Wels, Austria; 2 mL/kg, i.m.) for three days. The Atorvastatin group of animals was treated with a single dose of Atorvastatin (5 mg/kg, i.p.), applied immediately after the SCI. The animals were housed in separated cages to recover with access to food and water ad libitum. The bladder expression of the rats after the SCI was required twice a day until the bladder reflex was restored (14–18 days).

#### 4.2. Enzyme-Linked Immunosorbent Assay (ELISA)

Blood from the rats' tail vein (250–300 µL) was taken before the SCI, 4 and 24 h after trauma (4 animals/group). Each sample was centrifuged 10 min at 10,000 rpm to obtain the blood serum. The supernatants were kept at –70 °C until the ELISA procedure was performed. The level of IL-1 $\beta$  was measured using a Rat IL-1 $\beta$  ELISA Kit (Thermo Fisher Scientific, Waltham, MA, USA) according to the manufacturer's instructions.

#### 4.3. Immunohistochemistry

At the end of the experiments, the rats ( $n = 16$ ) were deeply anesthetized with thiopental (Valeant Czech Pharma s.r.o., Prague, Czech Republic; 50 mg/kg, i.p.) and perfused transcardially with 300 mL saline followed by 300 mL 4% paraformaldehyde in 0.1 M phosphate-buffered saline (PBS; pH 7.4, Sigma-Aldrich, St. Louis, MO, USA). Spinal cord blocks (0.5 cm cranially and caudally from the epicenter of the injury and the site of the injury) were post-fixed in the same fixative overnight and subsequently cryopreserved in a solution of 30% sucrose in PBS at 4 °C for 2 days. Afterwards, each tissue block was cut into transverse serial and longitudinal sections (25 µm thick) on a cryostat (Leica CM1850, Wetzlar, Germany). The sections were washed (3 × 10 min) in PBS with 0.3% Triton X-100 (Sigma-Aldrich, St. Louis, MO, USA) and blocked for 30 min at room temperature in a PBS solution containing 5% normal goat, rabbit, or donkey serum and 0.3% Triton X-100. For the processing of macrophages, microglia, astrocytes, neurofilaments, and outgrowing axons, the sections were incubated overnight at 4 °C with the following primary antibodies: ED-1 (mouse, 1:400 Biorad, Hercules, CA, USA), IBA-1 (goat, 1:1000 abcam, Cambridge, UK), GFAP (mouse, 1:600 Burlington, MA, USA), Nf-h (mouse, 1:1000 Danvers, MA, USA), and Gap43 (mouse, 1:500 abcam, Cambridge, UK). For the identification of caspase-3-expressing cells, double immunostaining was used. Anti-caspase-3 antibody (rabbit, 1:500 abcam, Cambridge, UK) was incubated overnight at 4 °C in combination with neuronal specific NeuN (mouse, 1:1000 abcam, Cambridge, UK), APC (mouse, 1:200 Millipore, Darmstadt, Germany), IBA-1, and GFAP antibodies. After washing (3 × 10 min) in PBS with 0.3% Triton X-100, the sections were incubated in the following secondary antibodies: FITC goat anti-mouse IgG (1:200); FITC rabbit anti-goat IgG (1:125); RRX goat anti-mouse IgG (1:600) (Jackson Immunoresearch,

West Grove, PA, USA); AF donkey anti-rabbit IgG (1:500); AF donkey anti-goat IgG (1:500) (Thermo Fisher Scientific, Waltham, MA, USA) for 2 h at room temperature. Immunolabeled spinal cord sections were mounted with Prolong (Invitrogen by Thermo Fisher Scientific, Carlsbad, CA, USA). Images were captured using an Olympus BX51 (Tokyo, Japan) fluorescent microscope.

#### 4.4. Cell Counting

The ED-1 positive cells were counted using ImageJ 1.47 software (Wayne Rasband, National Institutes of Health, Bethesda, MD, USA). The number of immunostained macrophages (ED-1) was quantified at the lesion site from 25  $\mu$ m thick transverse sections. The ED-1 positive cells were counted in the grey and white matter from 20 immunofluorescently labeled sections.

#### 4.5. Tissue Processing for RT-PCR

Total RNA from the Th7-Th10 spinal cord ( $n = 20$ ) was obtained using a Trizol Reagent (Thermo Fisher Scientific, Waltham, MA, USA) according to the manufacturer's instructions. The concentration of RNA in each sample was measured using NanoDrop 2000 c (Thermo Fisher Scientific, Waltham, MA, USA). The isolated RNA (2000 ng/ $\mu$ L) was reverse transcribed into cDNA in duplicates using a High-capacity cDNA Reverse Transcription Kit (AB applied biosystems by Thermo Fisher Scientific, Waltham, MA, USA) and a T1000<sup>TM</sup> Thermal Cycler (Bio-Rad, Hercules, CA, USA). cDNA samples (20  $\mu$ L) were stored at  $-20^{\circ}$ C until real-time PCR was performed.

Immediately before the RT-PCR reaction, the cDNA samples were diluted with 80  $\mu$ L nuclease-free water (Thermo Fisher Scientific, Waltham, MA, USA). The amplification of cDNA was performed using the CFX96<sup>TM</sup> Real-Time System (Bio-Rad, Hercules, CA, USA). The reaction mixture (20  $\mu$ L) was composed of 10  $\mu$ L TaqMan<sup>®</sup> Gene Expression MasterMix (AB applied biosystems by Thermo Fisher Scientific, Waltham, MA, USA), 1  $\mu$ L TaqMan<sup>®</sup> Gene Expression Assays (AB applied biosystems by Thermo Fisher Scientific, Waltham, MA, USA)— $\beta$ -actin (Rn00667869); Gap43 (Rn01474579); Cd163 (Rn1492519); Cd86 (Rn00571654); GFAP (Rn00566603); Olig2 (Rn01767116); Casp3 (Rn00563902); Nf-h (Rn00709325), 4  $\mu$ L nuclease-free water and 5  $\mu$ L of cDNA sample. The amplifications were run under the following conditions: 10 min at  $95^{\circ}$ C followed by 50 cycles of 15 s/ $95^{\circ}$ C and 1 min/60  $^{\circ}$ C. Gene expression was normalized with  $\beta$ -actin (reference gene). As a calibration product, samples from previous reactions were used. The relative quantity of gene expression was assigned using Bio-Rad CFX Manager. For statistical analyses, GraphPad Prism version 6.01 (La Jolla, CA, USA) was used.

#### 4.6. Behavioral Assessment

The neurological outcome of animals was tested using the Basso–Beattie–Bresnahan (BBB) locomotor rating scale ranging from 0 (complete paralysis) to 21 points (normal movement with trunk stability) [52]. Each rat was scored in an open field for a period of 5 min by two examiners. The locomotor assessment was carried out one day after the SCI, every other day for the first two weeks, and then once a week until six weeks post-injury.

#### 4.7. Statistical Analysis

The data from the BBB locomotor test was analyzed using Student's parametric *T*-Test. One-way analysis of variance (ANOVA) was used to determine the statistical significance ( $p < 0.05$ ) of the differences between the compression group, ATR-treated group, and control group. All these data were analyzed using GraphPad Prism version 6.01 (La Jolla, CA, USA) and were expressed as mean values with standard deviation (SD). The data from the ELISA were analyzed using two-way ANOVA, in which the time after the spinal cord injury was the first independent variable and with or without ATR was the second independent variable. These data were analyzed using StatSoft, Inc. (2013), version 12.

## 5. Conclusions

Atorvastatin (5 mg/kg, i.p.) injected in a single dose immediately after spinal cord trauma, significantly reduced the early inflammatory response and sharply decreased the expression of caspase-3 in neurons, astrocytes, and oligodendrocytes 24 h post-SCI. Acute ATR treatment effectively prevented the excessive infiltration of destructive M1 macrophages around the lesion site, while the infiltration of beneficial M2 macrophages was less affected. This statin significantly improved the regeneration capacity of the injured tissue at six weeks, leading to the promotion of axonal outgrowth and increasing neurofilament expression. We can conclude that the early modulation of the inflammatory response via effects on the M1/M2 macrophages and the inhibition of caspase-3 expression strongly promote tissue regeneration in later periods.

**Acknowledgments:** This research was supported by APVV grant No. 15/0766, VEGA grants 2/0168/17, 2/0160/16, and the project: Formation and development of a diagnostic procedure in the treatment of trauma—Injured spinal cord (ITMS 26220220202), supported by the Research & Development Operational Programme funded by the ERDF. We are grateful to Zuzana Barkacs for her technical assistance.

**Author Contributions:** Study concept and design of experiments: Nadezda Lukacova, Katarina Bimbova. Spinal cord compression at Th9 segment: Katarina Bimbova and Peter Zavacky. Post-surgical animal care and behavioral assessment: Katarina Bimbova, Maria Bacova, Jana Fedorova and Andrea Stropkovska. Transcardial perfusion, immunohistochemical, and molecular analyses: Katarina Bimbova, Alexandra Kisucka and Jana Jachova. Data analyses: Katarina Bimbova, Maria Bacova and Stefania Papcunova. Writing of the paper: Katarina Bimbova, Jan Galik, Martin Marsala, Jaroslav Pavel and Nadezda Lukacova.

**Conflicts of Interest:** The authors declare no conflicts of interest.

## References

1. Blesch, A.; Tuszyński, M.H. Spinal cord injury: Plasticity, regeneration and the challenge of translational drug development. *Trends Neurosci.* **2009**, *32*, 41–47. [[CrossRef](#)] [[PubMed](#)]
2. Fehlings, M.G.; Nguyen, D.H. Immunoglobulin G: A Potential Treatment to Attenuate Neuroinflammation Following Spinal Cord Injury. *J. Clin. Immunol.* **2010**, *30*, S109–S112. [[CrossRef](#)] [[PubMed](#)]
3. Oyinbo, C.A. Secondary injury mechanisms in traumatic spinal cord injury: A nugget of this multiply cascade. *Acta Neurobiol. Exp.* **2011**, *71*, 281–299.
4. Tator, C.H. Update on the pathophysiology and pathology of acute spinal cord injury. *Brain Pathol.* **1995**, *5*, 407–413. [[CrossRef](#)] [[PubMed](#)]
5. Donnelly, D.J.; Popovich, P.G. Inflammation and its role in neuroprotection, axonal regeneration and functional recovery after spinal cord injury. *Exp. Neurol.* **2008**, *209*, 378–388. [[CrossRef](#)] [[PubMed](#)]
6. Silva, A.N.; Sousa, N.; Reis, R.L.; Salgado, A.J. From basics to clinical: A comprehensive review on spinal cord injury. *Prog. Neurobiol.* **2014**, *114*, 25–57. [[CrossRef](#)] [[PubMed](#)]
7. Silver, J.; Miller, J.H. Regeneration beyond the glial scar. *Nat. Rev. Neurosci.* **2004**, *5*, 146–156. [[CrossRef](#)] [[PubMed](#)]
8. Saxena, T.; Deng, B.; Stelzner, D.; Hasenwinkel, J.; Chaiken, J. Raman spectroscopic investigation of spinal cord injury in a rat model. *J. Biomed. Opt.* **2011**, *16*, 027003. [[CrossRef](#)] [[PubMed](#)]
9. Papa, S.; Caron, I.; Erba, E.; Panini, N.; De Paola, M.; Mariani, A.; Colombo, C.; Ferrari, R.; Pozzer, D.; Zanier, E.R.; et al. Early modulation of pro-inflammatory microglia by minocycline loaded nanoparticles confers long lasting protection after spinal cord injury. *Biomaterials* **2016**, *75*, 13–24. [[CrossRef](#)] [[PubMed](#)]
10. Wang, Z.; Nong, J.; Shultz, R.B.; Zhang, Z.; Kim, T.; Tom, V.J.; Ponnappan, R.K.; Zhong, Y. Local delivery of minocycline from metal ion-assisted self-assembled complexes promotes neuroprotection and functional recovery after spinal cord injury. *Biomaterials* **2017**, *112*, 62–71. [[CrossRef](#)] [[PubMed](#)]
11. Machova, U.L.; Karova, K.; Ruzicka, J.; Kloudova, A.; Shannon, C.; Dubisova, J.; Murali, R.; Kubinova, S.; Sykova, E.; Jhanwar-Uniyal, M.; et al. The Anti-inflammatory compound curcumin enhances locomotor and sensory recovery after spinal cord injury in rats by immunomodulation. *Int. J. Mol. Sci.* **2016**, *17*, 49. [[CrossRef](#)] [[PubMed](#)]
12. Wang, Y.; Zu, J.N.; Li, J.; Chen, C.; Xi, C.; Yan, J. Curcumin promotes the spinal cord repair via inhibition of glial scar formation and inflammation. *Neurosci. Lett.* **2014**, *560*, 51–56. [[CrossRef](#)] [[PubMed](#)]

13. Blauw, G.J.; Lagaay, A.M.; Smelt, A.H.; Westendorp, R.G. Stroke, statins, and cholesterol. A meta-analysis of randomized, placebo-controlled, double-blind trials with HMG-CoA reductase inhibitors. *Stroke* **1997**, *28*, 946–950. [[CrossRef](#)] [[PubMed](#)]
14. Komukai, K.; Kubo, T.; Kitabata, H.; Matsuo, Y.; Ozaki, Y.; Takarada, S.; Okumoto, Y.; Shiono, Y.; Orii, M.; Shimamura, K.; et al. Effect of atorvastatin therapy on fibrous cap thickness in coronary atherosclerotic plaque as assessed by optical coherence tomography: The EASY-FIT study. *J. Am. Coll. Cardiol.* **2014**, *64*, 2207–2217. [[CrossRef](#)] [[PubMed](#)]
15. Pordal, A.H.; Hajmiresmail, S.J.; Assadpoor-Piranfar, M.; Hedayati, M.; Ajami, M. Plasma oxysterol level in patients with coronary artery stenosis and its changes in response to the treatment with atorvastatin. *Med. J. Islam. Repub. Iran* **2015**, *29*, 192. [[PubMed](#)]
16. Pannu, R.; Barbosa, E.; Singh, A.K.; Singh, I. Attenuation of acute inflammatory response by atorvastatin after spinal cord injury in rats. *J. Neurosci. Res.* **2005**, *79*, 340–350. [[CrossRef](#)] [[PubMed](#)]
17. Pannu, R.; Christie, D.K.; Barbosa, E.; Singh, I.; Singh, A.K. Post-trauma Lipitor treatment prevents endothelial dysfunction, facilitates neuroprotection, and promotes locomotor recovery following spinal cord injury. *J. Neurochem.* **2007**, *101*, 182–200. [[CrossRef](#)] [[PubMed](#)]
18. Gao, S.; Zhang, Z.; Shen, Z.; Gao, K.; Chang, L.; Guo, Y.; Li, Z.; Wang, W.; Wang, A. Atorvastatin activates autophagy and promotes neurological function recovery after spinal cord injury. *Neural Regen. Res.* **2016**, *11*, 977–982. [[CrossRef](#)] [[PubMed](#)]
19. Déry, M.A.; Rousseau, G.; Benderdour, M.; Beaumont, E. Atorvastatin prevents early apoptosis after thoracic spinal cord contusion injury and promotes locomotion recovery. *Neurosci. Lett.* **2009**, *453*, 73–76. [[CrossRef](#)] [[PubMed](#)]
20. Alves, E.S.; Lemos, V.A.; Silva, F.R.; Lira, F.S.; Santos, R.V.T.; Rosa, J.P.P.; Caperuto, E.; Tufik, S.; Mello, M.T. Low-Grade Inflammation and Spinal Cord Injury: Exercise as Therapy? *Mediat. Inflamm.* **2013**, *2013*, 971841. [[CrossRef](#)]
21. Gensel, J.C.; Zhang, B. Macrophage activation and its role in repair and pathology after spinal cord injury. *Brain Res.* **2015**, *1619*, 1–11. [[CrossRef](#)] [[PubMed](#)]
22. Aydemir, S.; Dogan, D.; Kocak, A.; Dilsiz, N. The effect of melatonin on spinal cord after ischemia in rats. *Spinal Cord* **2016**, *54*, 360–363. [[CrossRef](#)] [[PubMed](#)]
23. Rowland, J.W.; Hawryluk, G.W.; Kwon, B.; Fehlings, M.G. Current status of acute spinal cord injury pathophysiology and emerging therapies: Promise on the horizon. *Neurosurg. Focus* **2008**, *25*, 1–17. [[CrossRef](#)] [[PubMed](#)]
24. Carlson, S.L.; Parrish, M.E.; Springer, J.E.; Doty, K.; Dosset, L. Acute Inflammatory Response in Spinal Cord Following Impact Injury. *Exp. Neurol.* **1998**, *151*, 77–88. [[CrossRef](#)] [[PubMed](#)]
25. Rust, R.; Kaiser, J. Insights into the Dual Role of Inflammation after Spinal Cord Injury. *J. Neurosci.* **2017**, *37*, 4658–4660. [[CrossRef](#)] [[PubMed](#)]
26. Allan, S.M.; Tyrrel, P.J.; Rothwell, N.J. Interleukin-1 and neuronal injury. *Nat. Rev. Immunol.* **2005**, *5*, 629–640. [[CrossRef](#)] [[PubMed](#)]
27. Nesic, O.; Xu, G.Y.; McAdoo, D.; High, K.W.; Hulsebosch, C.; Perez-Polo, R. IL-1 Receptor Antagonist Prevents Apoptosis and Caspase-3 Activation after Spinal Cord Injury. *J. Neurotrauma* **2004**, *18*, 947–956. [[CrossRef](#)] [[PubMed](#)]
28. Basu, A.; Kraday, J.K.; Levison, S.W. Interleukin-1: A master regulator of neuroinflammation. *J. Neurosci. Res.* **2004**, *78*, 151–156. [[CrossRef](#)] [[PubMed](#)]
29. David, S.; Lacroix, S. Role of the immune response in tissue damage and repair in the injured spinal cord. In *Clinical Neuroimmunology*, 3rd ed.; Antel, J., Birnbaum, G., Hartung, H.P., Vincent, A., Eds.; Oxford University Press: New York, NY, USA, 2005; pp. 53–63, ISBN 0-19-851068-3.
30. Lukacova, N.; Kolesárová, M.; Kuchárová, K.; Pavel, J.; Kolesár, D.; Radonák, J.; Marsala, M.; Chalimoníuk, M.; Langfort, J.; Marsala, J. The effect of a spinal cord hemisection on changes in nitric oxide synthase pools in the site of injury and in regions located far away from the injured site. *Cell. Mol. Neurobiol.* **2006**, *26*, 1367–1385. [[CrossRef](#)] [[PubMed](#)]
31. Lourenço, C.F.; Ferreira, N.R.; Santos, R.M.; Lukacova, N.; Barbosa, R.M.; Laranjinha, J. The pattern of glutamate-induced nitric oxide dynamics in vivo and its correlation with nNOS expression in rat hippocampus, cerebral cortex and striatum. *Brain Res.* **2014**, *1554*, 1–11. [[CrossRef](#)] [[PubMed](#)]

32. Kong, X.; Gao, J. Macrophage polarization: A key event in the secondary phase of acute spinal cord injury. *J. Cell. Mol. Med.* **2017**, *21*, 941–954. [CrossRef] [PubMed]
33. Devaux, S.; Cizkova, D.; Quanico, J.; Franck, J.; Nataf, S.; Pays, L.; Hauberg-Lotte, L.; Maass, P.; Kobarg, J.H.; Kobeissy, F.; et al. Proteomic Analysis of the Spatio-temporal Based Molecular Kinetics of Acute Spinal Cord Injury Identifies a Time- and Segment-specific Window for Effective Tissue Repair. *Mol. Cell. Proteom.* **2016**, *15*, 2641–2670. [CrossRef] [PubMed]
34. Khayrullina, G.; Bermudez, S.; Byrnes, K.R. Inhibition of NOX2 reduces locomotor impairment, inflammation, and oxidative stress after spinal cord injury. *J. Neuroinflamm.* **2015**, *12*, 172. [CrossRef] [PubMed]
35. Bermudez, S.; Khayrullina, G.; Zhao, Y.; Byrnes, K.R. NADPH oxidase isoform expression is temporally regulated and may contribute to microglial/macrophage polarization after spinal cord injury. *Mol. Cell. Neurosci.* **2016**, *77*, 53–64. [CrossRef] [PubMed]
36. Zhao, J.; Wang, L.; Li, Y. Electroacupuncture alleviates the inflammatory response via effects on M1 and M2 macrophages after spinal cord injury. *Acupunct. Med.* **2017**, *35*, 224–230. [CrossRef] [PubMed]
37. Nazli, Y.; Colak, N.; Alpay, M.F.; Uysal, S.; Uzunlar, A.K.; Cakir, O. Neuroprotective effect of atorvastatin in spinal cord ischemia-reperfusion injury. *Clinics* **2015**, *70*, 52–60. [CrossRef]
38. Raisman, G. Formation of synapses in the adult rat after injury: Similarities and differences between a peripheral and a central nervous site. *Philos. Trans. R. Soc. Lond. B Biol. Sci.* **1977**, *278*, 349–359. [CrossRef] [PubMed]
39. Codeluppi, S.; Svensson, C.I.; Hefferan, M.P.; Valencia, F.; Silldorff, M.D.; Oshiro, M.; Marsala, M.; Pasquale, E.B. The Rheb-mTOR pathway is upregulated in reactive astrocytes of the injured spinal cord. *J. Neurosci.* **2009**, *29*, 1093–1104. [CrossRef] [PubMed]
40. Lukovic, D.; Stojkovic, M.; Moreno-Manzano, V.; Jendelova, P.; Sykova, E.; Bhattacharya, S.S.; Erceg, S. Concise review: Reactive astrocytes and stem cells in spinal cord injury: Good guys or bad guys? *Stem Cells* **2015**, *33*, 1036–1041. [CrossRef] [PubMed]
41. Kucharikova, A.; Schreiberova, A.; Zavodska, M.; Gedrova, S.; Hricova, L.; Pavel, J.; Galik, J.; Marsala, M.; Lukáčová, N. Repeated Baclofen treatment ameliorates motor dysfunction, suppresses reflex activity and decreases the expression of signaling proteins in reticular nuclei and lumbar motoneurons after spinal trauma in rats. *Acta Histochem.* **2014**, *116*, 344–353. [CrossRef] [PubMed]
42. Anderson, M.A.; Burda, J.E.; Ren, Y.; Ao, Y.; O’Shea, T.M.; Kawaguchi, R.; Coppola, G.; Khakh, B.S.; Deming, T.J.; Sofroniew, M.V. Astrocyte scar formation aids central nervous system axon regeneration. *Nature* **2016**, *532*, 195–200. [CrossRef] [PubMed]
43. Liddelow, S.A.; Guttenplan, K.A.; Clarke, L.E.; Bennett, F.C.; Bohlen, C.J.; Schirmer, L.; Bennett, M.L.; Münch, A.E.; Chung, W.S.; Peterson, T.C.; et al. Neurotoxic reactive astrocytes are induced by activated microglia. *Nature* **2017**, *541*, 481–487. [CrossRef] [PubMed]
44. Gao, K.; Shen, Z.; Yuan, Y.; Han, D.; Song, C.; Guo, Y.; Mei, X. Simvastatin inhibits neural cell apoptosis and promotes locomotor recovery via activation of Wnt/β-catenin signaling pathway after spinal cord injury. *J. Neurochem.* **2016**, *138*, 139–149. [CrossRef] [PubMed]
45. Lee, J.Y.; Kang, S.R.; Yune, T.Y. Fluoxetine prevents oligodendrocyte cell death by inhibiting microglia activation after spinal cord injury. *J. Neurotrauma* **2015**, *32*, 633–644. [CrossRef] [PubMed]
46. Nishida, F.; Sisti, M.S.; Zanuzzi, C.N.; Barbeito, C.G.; Portiansky, E.L. Neurons of the rat cervical spinal cord express vimentin and neurofilament after intraparenchymal injection of kainic acid. *Neurosci. Lett.* **2017**, *643*, 103–110. [CrossRef] [PubMed]
47. Lépinoux-Chambaud, C.; Eyer, J. Review on intermediate filaments of the nervous system and their pathological alterations. *Histochem. Cell Biol.* **2013**, *140*, 13–22. [CrossRef] [PubMed]
48. Wang, H.; Wu, M.; Zhan, C.; Ma, E.; Yang, M.; Yang, X.; Li, Y. Neurofilament proteins in axonal regeneration and neurodegenerative diseases. *Neural Regen. Res.* **2012**, *7*, 620–626. [PubMed]
49. Gedrova, S.; Galik, J.; Marsala, M.; Zavodska, M.; Pavel, J.; Sulla, I.; Gajdos, M.; Lukac, I.; Kafka, J.; Ledecsky, V.; et al. Neuroprotective effect of local hypothermia in a computer-controlled compression model in minipig: Correlation of tissue sparing along the rostro-caudal axis with neurological outcome. *Exp. Ther. Med.* **2017**, *15*, 254–270. [CrossRef] [PubMed]

50. Hwang, D.H.; Kim, B.G.; Kim, E.J.; Lee, S.I.; Joo, I.S.; Suh-Kim, H.; Sohn, S.; Kim, S.U. Transplantation of human neural stem cells transduced with Olig2 transcription factor improves locomotor recovery and enhances myelination in the white matter of rat spinal cord following contusive injury. *BMC Neurosci.* **2009**, *10*, 117. [[CrossRef](#)] [[PubMed](#)]
51. Ferrero, S.L.; Brady, T.D.; Dugan, V.P.; Armstrong, J.E.; Hubscher, C.H.; Johnson, R.D. Effects of Lateral Funiculus Sparing, Spinal Lesion Level, and Gender on Recovery of Bladder Voiding Reflexes and Hematuria in Rats. *J. Neurotrauma* **2015**, *32*, 200–208. [[CrossRef](#)] [[PubMed](#)]
52. Basso, D.M.; Beattie, M.S.; Bresnahan, J.C. A sensitive and reliable locomotor rating scale for open field testing in rats. *J. Neurotrauma* **1995**, *12*, 1–21. [[CrossRef](#)] [[PubMed](#)]



© 2018 by the authors. Licensee MDPI, Basel, Switzerland. This article is an open access article distributed under the terms and conditions of the Creative Commons Attribution (CC BY) license (<http://creativecommons.org/licenses/by/4.0/>).



Article

# FM19G11 and Ependymal Progenitor/Stem Cell Combinatory Treatment Enhances Neuronal Preservation and Oligodendrogenesis after Severe Spinal Cord Injury

Ana Alastrue-Agudo <sup>1</sup>, Francisco Javier Rodriguez-Jimenez <sup>1</sup>, Eric López Mocholi <sup>1</sup>,  
Francesca De Giorgio <sup>1</sup>, Slaven Erceg <sup>2</sup> and Victoria Moreno-Manzano <sup>1,\*</sup>

<sup>1</sup> Neuronal and Tissue Regeneration Laboratory, Príncipe Felipe Research Center, 46012 Valencia, Spain;  
alastrue@cipf.es (A.A.-A.); frodriguez@cipf.es (F.J.R.-J.); elopezm@cipf.es (E.L.M.);  
f.degiorgio85@gmail.com (F.D.G.)

<sup>2</sup> Stem Cell Therapies in Neurodegenerative Diseases Laboratory, Centro de Investigación Príncipe Felipe,  
46012 Valencia, Spain; serceg@cipf.es

\* Correspondence: vmorenom@cipf.es; Tel.: +34-963-289-681 (ext. 1103)

Received: 24 September 2017; Accepted: 5 January 2018; Published: 9 January 2018

**Abstract:** Spinal cord injury (SCI) suffers from a lack of effective therapeutic strategies. We have previously shown that individual therapeutic strategies, transplantation of ependymal stem/progenitor cells of the spinal cord after injury (epSPCi) or FM19G11 pharmacological treatment, induce moderate functional recovery after SCI. Here, the combination of treatments has been assayed for functional and histological analysis. Immediately after severe SCI, one million epSPCi were intramedullary injected, and the FM19G11 compound or dimethyl sulfoxide (DMSO) (as the vehicle control) was administrated via intrathecal catheterization. The combination of treatments, epSPCi and FM19G11, improves locomotor tasks compared to the control group, but did not significantly improve the Basso, Beattie, Bresnahan (BBB) scores for locomotor analysis in comparison with the individual treatments. However, the histological analysis of the spinal cord tissues, two months after SCI and treatments, demonstrated that when we treat the animals with both epSPCi and FM19G11, an improved environment for neuronal preservation was generated by reduction of the glial scar extension. The combinatorial treatment also contributes to enhancing the oligodendrocyte precursor cells by inducing the expression of Olig1 *in vivo*. These results suggest that a combination of therapies may be an exciting new therapeutic treatment for more efficient neuronal activity recovery after severe SCI.

**Keywords:** FM19G11; spinal cord injury; ependymal progenitor stem cells; oligodendrogenesis; locomotion; neuronal regeneration; axon growth

## 1. Introduction

Traumatic spinal cord injury (SCI) is a devastating disorder with loss of neurological function immediately below the affected segment with no currently effective treatment for the subsequent paralysis. The failure to recover from SCI in adult mammals is attributed to both extrinsic and intrinsic factors [1]. The extrinsic factors include a lack of appropriate trophic support like brain-derived neurotrophic factor (BDNF), basic-fibroblast growth factor (bFGF), vascular endothelial growth factor (VEGF) [2], stromal derived factor 1 (SDF1) [3] or insulin-like growth factor 1 (IGF-1) [4], since among others, they have shown neuroprotective effects when added ectopically.

In the primary injury phase, the direct impact causes cell death at the injury site with axonal damage leading to the interruption of the ascending and descending spinal pathways. The blockade

of nerve conduction generates paralysis and temporary loss of neural functions by spinal shock. The primary injury leads to massive cell death of neurons, glial cells and endothelial cells lining the blood vessels. The surviving neurons at the lesion site respond with a barrage of action potentials that create significant local shifts in ion levels and cause also the release of excitatory neurotransmitters (i.e., glutamate), resulting in the death of more nearby neurons [5]. The inflammatory response after SCI is initiated by peripherally-derived immune cells (macrophages-monocytes, neutrophils and T-cells) and glial activation (astrocytes and microglia) [6–8]. Macrophages and microglia contribute to the inflammatory response through the release of cytokines like tumor necrosis factor  $\alpha$  (TNF- $\alpha$ ), interleukin 1 or 6 (IL1 or IL6) [9] in an initial phase; however, later, additional anti-inflammatory cytokines like IL10 are known to contribute to tissue remodeling [10,11]. The secondary phase is also marked by the massive death of oligodendrocytes. The combination of demyelination and altered ion channel function may lead to changes in surviving neurons that can produce central chronic pain. The lesion site forms a fluid-filled cavity delimited by the reactive scar acting as a containment barrier forming an impenetrable wall with extracellular matrix proteins and chondroitin sulfate limiting the axonal regrowth [12], thereby inhibiting the regenerative potential of those axons to reconnect with the distal segments [13]. SCI is a complex and multifactorial cascade of events that progressively reduces the chances of the limited endogenous regenerative capacity to rescue the lost connections. Therefore, therapeutic interventions need to rapidly interfere with this degenerative cascade via powerful neuroprotective activities, promoting in addition functional neuronal plasticity. A combination of neuroprotective and neuroregenerative treatments constitutes the current key strategies for the creation of an efficient SCI treatment. Several strategies have already shown the efficiency of the combination of cell therapy and pharmacological approaches [14]. Transplantation of neural stem/progenitor cells (NSPCs) has shown promising results in the repair and regeneration of lost neural tissues and the associated restoration of neurological deficits [14–16]. NSPCs include multipotent stem cells present in the periventricular subependymal layer and the subgranular zone of the dentate gyrus in the brain, as well as in the ependymal regions lining the central canal of the spinal cord (epSPCs) [13]. NSPCs represent an ideal candidate for stem cell-based SCI therapy based on noted functional improvements after transplantation and the absence of malignant transformation, offering a safe and relevant cell type for clinical applications. After SCI, epSPCs proliferate and migrate to the injured area and produce new oligodendrocyte progenitors [14]. We previously showed that acute transplantation of undifferentiated epSPCs from SCI donors (epSPCi) or in vitro differentiated OPCs into a rat model of severe spinal cord contusion produced significant locomotion recovery from one week after injury [15]. Moreover, we recently demonstrated the advantages of the synergistic activity of the polyacetal curcumin (PA-curcumin), a new polymeric conjugate of curcumin, with epSPCi in rats with chronic SCI. A single administration of the combinatory treatment into the intrathecal space significantly rescued the locomotor activity of the paralyzed rats, as opposed to ineffective individual treatments [17]. The PA-curcumin produced neuroprotective and anti-inflammatory capabilities, as previously reported [18–22], but also showed regenerative activity by increasing axonal elongation-related mechanisms. The epSPCi, with multipotent characteristics, lining the central canal of the spinal cord [15], after SCI, proliferate and migrate to the injured zone, giving rise to new oligodendrocyte progenitors [23]. Acute transplantation of epSPCi efficiently reversed the paralysis associated with acute SCI in rats [24,25]. The transplanted cells migrated long distances from the rostral and caudal regions to reach the neurofilament-labeled axons in and around the lesion zone, while epSPC transplanted animals always showed fewer cavities and a smaller scar area [25]. In the chronic scenario, although epSPCi improved the locomotion, only partial success was found in comparison with the acute treatment [26]. However, the combination of treatments, for instance by combining PA-curcumin and epSPCi, significantly induced both  $\beta$ -tubulin-III (neurofilament marker for neuronal projections) and GAP43 (axon growth marker) expression at the epicenter of the injury in comparison with the individually-treated groups [17].

FM19G11 was first identified as an inhibitor of HIF $\alpha$  protein expression and transcriptional activity under hypoxic conditions repressing a variety of key genes involved in stemness. Moreover, directed differentiation experiments demonstrated that FM19G11 favors oligodendrocyte differentiation blocked under hypoxia, possibly through the negative modulation of Sox2 (sex determining region Y-box 2) and Oct4 (octamer-binding transcription factor 4) expression and by allowing the epSPCs to differentiate under hypoxia [27]. However, under normoxic conditions, FM19G11 modifies the mitochondrial uncoupling process, by induction of UCP sensors, which induces glucose uptake by activation of AMPK (AMP-activated protein kinase), as well as AKT (Protein Kinase B) signaling pathways. The consequence of these molecular events is an increase of the self-renewal machinery of different stem cell populations, including the epSPCs. FM19G11 induces early glycolytic-related responses associated with PI3K/AKT/mTOR signaling induction [28,29]. Interestingly, when FM19G11 is infused during three days starting immediately after SCI, in the intrathecal space, it induces functional locomotion recovery one month after treatment, which is associated with an increase of vimentin expression and in the number of neuronal fibers in the injured area [30].

Here, we look for an enhanced effect to rescue neuronal activity for progressive motor function in severe SCI using a combination that includes cell therapy, epSPCi and the pharmacological treatment based on the local application of FM19G11.

## 2. Results

### 2.1. FM19G11 or epSPCi Improve Locomotion in Severe SCI with No Synergistic Effect

Individual treatments with FM19G11 by intrathecal administration [30] or epSPCi by intramedullary transplantation [24,25] improved locomotion when applied immediately after injury. Herein, in order to study a potential additive or synergistic effect among both treatments, a combination of both was assayed. The epSPCi, or growth medium in the control group, were transplanted by intramedullary injection at the injured area immediately after spinal cord contusion (Figure 1A, top pictures). Afterwards, the pharmacological treatment was performed by continual delivery of FM19G11 or DMSO (in the control group), using an osmotic pump, connected to a catheter, into the intrathecal space (Figure 1A, bottom pictures). All treated animals distributed into control, epSPCi, FM19G11 and FM19G11 + epSPCi groups were individually videotaped, and locomotor functional recovery was scored blind by two unbiased observers by using the 21-point Basso, Beattie, Bresnahan (BBB) scale. All three treated animals had a significant increase in the BBB scores after the fourth week, in comparison with the control group (control:  $6.3 \pm 0.26$ ; epSPCi:  $8.8 \pm 0.4$  \*; FM19G11:  $8 \pm 0.6$  \*; FM19G11 + epSPCi:  $9 \pm 0.7$  \*; \*,  $p < 0.05$  vs. control). However, no significant differences were found among the three treatments (Figure 1B). Interestingly, epSPCi transplanted animals (epSPCi and FM19G11 + epSPCi) always showed better maximum scores in the BBB test at shorter times after SCI (Figure 1B). The frame captures of representative video tape recordings in the open field test, eight weeks after surgery, showed a typical plantar placement of the paw with weight support instance, consistently found in animals treated with the combination of treatments, as well as the weight support by dorsal stepping, consistently found in the epSPCi group. Plantar placement of the paw with no weight support in the stepping was also frequently found in the FM19G11-treated group. The control animals did not show any stepping, but occasionally sweeping, without showing any weight support (Figure 1C).

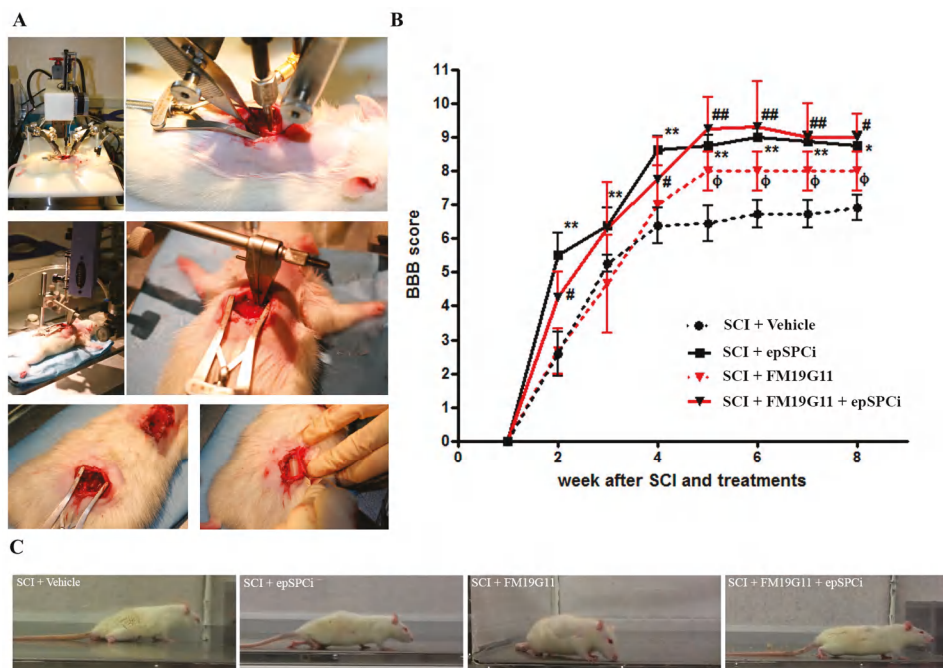


**Figure 1.** FM19G11, epSPCi or the combination of both improve locomotion in severe spinal cord injury (SCI) in comparison with the control group. (A) Surgery strategy to induce severe SCI by a 250-kdyn impact and acute transplantation by intramedullary injection of epSPCi and intrathecal catheterization for local and sustained delivery of FM19G11 using an osmotic pump; (B) functional locomotor analysis (BBB scores) over eight weeks post-treatment with vehicle, as a control, epSPCi, FM19G11 or FM19G11 + epSPCi; quantitative data are expressed as the mean  $\pm$  S.E.M.; \*, #, or  $\phi$ ,  $p < 0.05$ , \*\*,  $p < 0.01$ ; (C) representative capture images from video recordings of one animal of every group for BBB analysis at the eighth week after SCI are shown as follows: SCI + vehicle (control), SCI + epSPCi, SCI + FM19G11, SCI + FM19G11 + epSPCi.

## 2.2. FM19G11 Intrathecal Administration after SCI Preserves Spinal Cord Tissue

The lost tissue due to the destructive secondary damage including the inflammatory reaction following the SCI was evaluated. As is indicated in the illustrative model (Figure 2A, top representation of the analyzed planes in the spinal cord), the quantification of the spinal cord width (Figure 2B) at the injury area (Figure 2C) at eight consecutive points along four mm of the epicenter of the lesion was performed. The spinal cord injury area was monitored via hematoxylin-eosin (H&E) histological analysis, eight weeks post-injury (Figure 2A, bottom panels). The comparative analysis among all the groups after quantification of the spinal cord width at the injury epicenter demonstrated that since larger tissue degeneration remained in the SCI site following control treatment or epSPCi transplantation alone, FM19G11- and FM19G11 + epSPCi-treated rats presented wider cords (Figure 2B). The quantification of the total spinal cord area at the epicenter of the injury, by taking into account the elliptic shape of the cord and including the width and the length average, showed the same result. The FM19G11 and FM19G11 + epSPCi groups presented higher total areas in comparison with the control or epSPCi groups, tending to recover a closer shape to the non-injured tissue (Figure 2C).

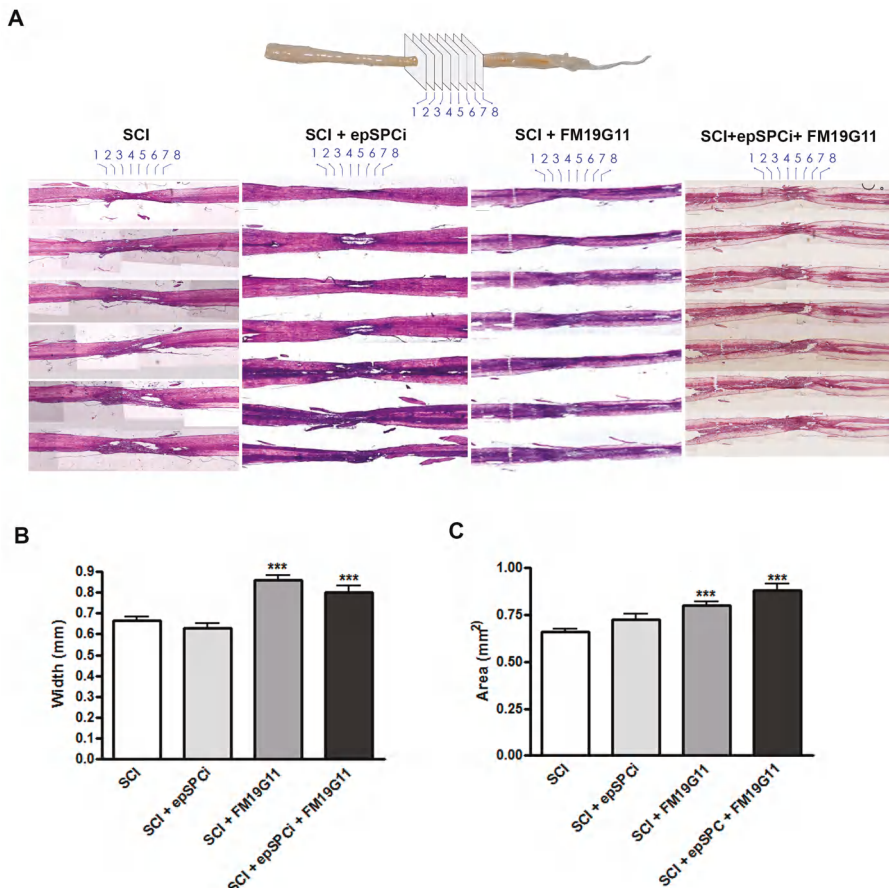


**Figure 2.** FM19G11 preserves spinal cord tissue. (A) Top panel: spinal cord model showing the eight selected points for the quantification of the width and the lesion area at the spinal cord injury epicenter; bottom panels: representative histological sections of hematoxylin/eosin staining for each experimental condition; Scale bar = 500  $\mu$ M; (B) quantification of the whole width epicenter area, including all eight selected points; (C) quantification of the lesion area considering the elliptic shape of the spinal cord, the higher and smaller radius at each section. Quantitative data are expressed as the mean  $\pm$  S.E.M; \*\*\*  $p < 0.001$  in comparison with SCI (control).

### 2.3. FM19G11 and epSPCi Combination Treatment Reduces the Scar Extension and Astrogliosis and Increases the Neuronal Fibers at the Injury Area

The glial scar has been accepted to be delimited by the astrocytes expressing glial fibrillary acidic protein (GFAP) [7]; then, as we previously reported [17,25,30], we evaluated the extension of the glial scar by measuring the negative GFAP stained area at the epicenter of the injury (Figure 3A,B). We found that only the combinatory treatment, FM19G11 and epSPCi, decreased the extension of the astrocytic negative area in comparison with the control group or the individual treatments (Figure 3B), indicating a reduction of the glial scar formation, creating a more permissive neuronal environment. However, all treatments, FM19G11 or epSPCi or their combination, reduced the astrogliosis based on a lower GFAP positive staining at the epicenter of the lesion, surrounding the scar (Figure 3A,C). Further assessment at the glial scar area was performed by measuring the  $\beta$ -tubulin-III-positive staining

for neuronal filament for those neurons crossing the glial scar. All treatments, epSPCi, FM19G11 and the combination of both, were found to always show a larger positive area for  $\beta$ -tubulin-III in comparison with the control group (Figure 3D), indicating an independent effect of the individual treatments on neuronal fiber preservation and the glial scar formation.

However, when the  $\beta$ -tubulin-III positive area was quantified at the total epicenter of the injury, including the rostral and caudal tissue surrounding the scar, only the animals that received the combination of treatments, FM19G11 + epSPCi, presented a significant result in comparison with the control group (Figure 3E).

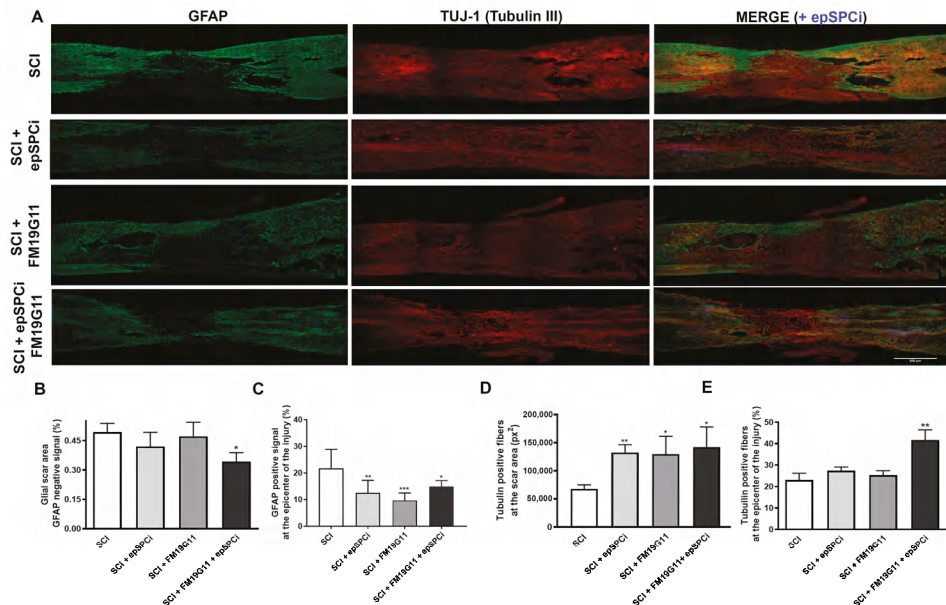


**Figure 3.** Combinatory treatment reduces the glial scar formation and preserves larger numbers of neuronal fibers. (A) Representative immunofluorescence images from glial fibrillary acidic protein (GFAP; green),  $\beta$ -tubulin-III (red) and merge including green fluorescence protein (GFP)-epSPCi in the transplanted groups (GFP, blue) with positive signals at the epicenter of the injury from spinal cord longitudinal sections in every experimental condition; Scale bar, 500  $\mu$ m; (B) quantification of the negative area or (C) the positive signal at the injury site for GFAP expressed as a percentage of the total epicenter area, equivalent in length for all tested groups; (D) quantification of the positive signal for  $\beta$ -tubulin-III (tubulin) at the negative GFAP area or (E) covering all the injury area, expressed as a percentage of the total epicenter area, equivalent in length for all tested groups. Quantitative data are expressed as the mean  $\pm$  S.E.M; \*  $p < 0.05$ , \*\*  $p < 0.01$ , \*\*\*  $p < 0.001$  in comparison with SCI (control).

#### 2.4. FM19G11 and epSPCi Induce the Expression of GAP43 Expression, an Axon Growth Marker, and RIP, a Marker for Myelinated Oligodendrocytes at the Injury

GAP43, a known marker for axonal cone growth formation [31], was assayed to analyze the capacity of each treatment to favor neuronal plasticity. Encouragingly, eight weeks after injury and treatments, a significant induction of the GAP43 positive signal was detected along the neuronal fibers at the injured site by all treated groups in comparison with the non-treated animals (Figure 4A,B). The substantial increases in  $\beta$ -tubulin-III (Figure 3D,E) and GAP43 labeling for the combinatory treatment indeed suggest a more efficient relationship between the increased preservation in the number and quality of axon fibers. Interestingly, although no significant differences in the expression

for the receptor interacting protein (RIP), a cell marker for mature oligodendrocytes by detecting 2',3'-cyclic nucleotide 3'-phosphodiesterase [32], were detected when the control group was compared to any treatment (Figure 4C), the detected signal of GAP43 maintains a significant parallel expression with the mature and myelinated axons stained with RIP in the epSPCi transplanted groups (Figure 4D), as is also shown in the representative magnified images of double staining detection of GAP43 (red) and RIP (green) for each experimental condition (Figure 4A).

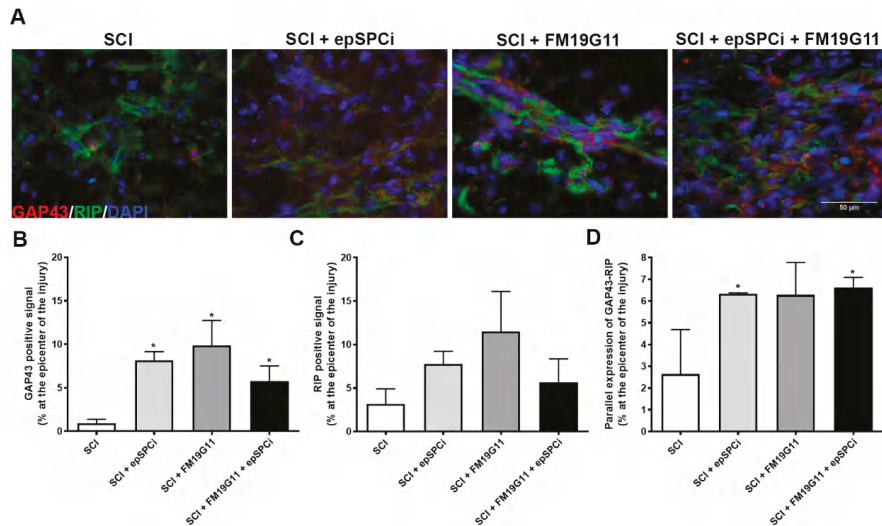


**Figure 4.** Treatment with FM19G11 plus epSPCi preserves larger numbers of neuronal fibers. (A) Representative immunofluorescence images at high magnification of receptor interacting protein (RIP, green) and GAP43 (red) expression at the epicenter of the injury are shown for every experimental condition (scale bar, 50  $\mu$ m); (B) quantification of the GAP43 (growth cone marker); (C) RIP (mature oligodendrocyte marker) or (D) the parallel detection of the GAP43 and RIP-positive signal at the epicenter of the injury expressed as a percentage of the total epicenter area, equivalent in length for all tested groups. Quantitative data are expressed as the mean  $\pm$  S.E.M. (ANOVA), \*  $p < 0.05$  in comparison with SCI (control).

## 2.5. FM19G11 Favors Oligodendrocyte Replacement

It is well established that after SCI, which causes extensive oligodendrocyte cell death [33], surviving oligodendrocyte progenitor cells (OPC) are the major source for oligodendrocyte replacement and remyelination [34]. It also has been shown that, over the first weeks post-injury, the OPCs differentiate into mature oligodendrocytes, particularly along the lesion borders, and contribute to the re-myelination process [35–37]. The detection of Olig1 expression, an early OPC marker [38], eight weeks after SCI, demonstrates a significant induction of this population by the FM19G11 treatment in combination with epSPCi transplantation (Figure 5A). However, at the time of sacrifice, no significant differences were found in the RIP population (Figure 4C), indicating a lack of maturation induction of the proliferating OPC by the treatments. FM19G11 was previously shown to allow the oligodendrocyte differentiation in vitro efficiently when it was delayed under hypoxia [27]. Here, we found that the presence of FM19G11 also improves the maturation of epSPCi into oligodendrocyte precursor cells measured as an increment of RIP expression at the protein level (Figure 5B) and NG2 expression at the protein (Figure 5C) and mRNA levels (Figure 5D) with a parallel decrease of the proliferative marker PCNA (proliferating cell nuclear antigen) or the stemness factor Sox2 (Figure 5C).

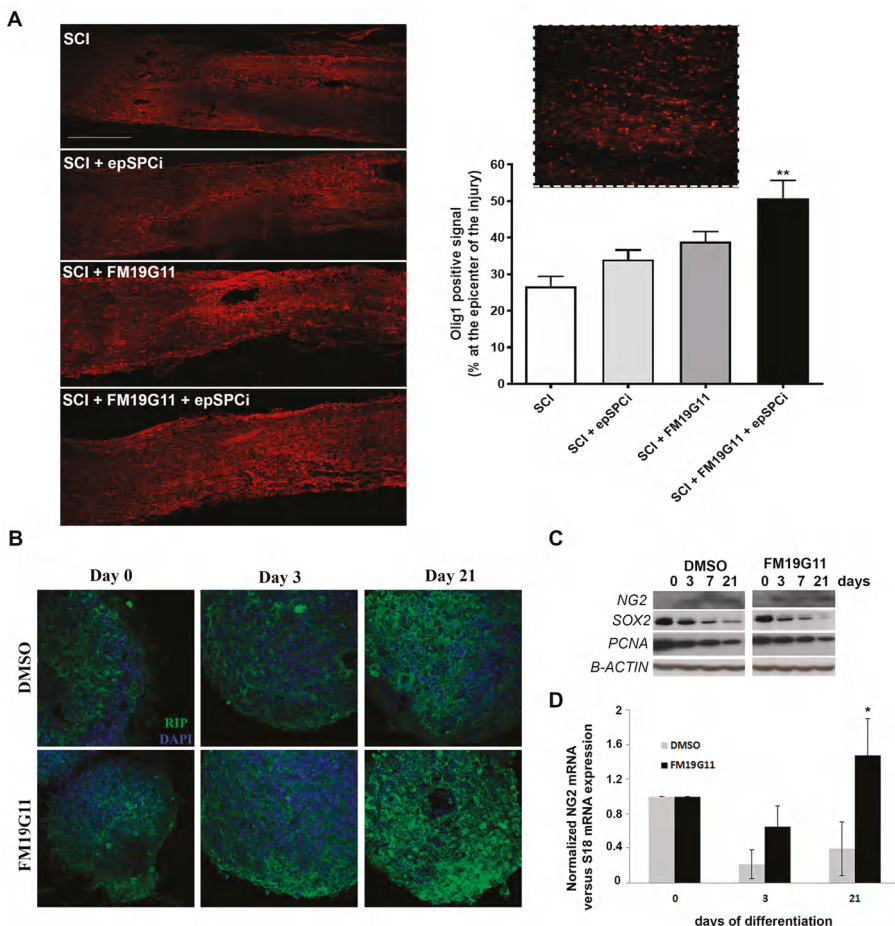


**Figure 5.** FM19G11 promotes in vivo and in vitro oligodendrocyte turnover. (A) (left panel) Representative immunofluorescent images of the Olig1-positive signal at the epicenter of the injury in every experimental condition (scale bar, 500  $\mu$ m); (right panel) quantification of the positive signal for Olig1 expressed as a percentage of the total epicenter area, equivalent in length for all tested groups. Inset: high magnification of Olig1 immunostaining. Quantitative data are expressed as the mean  $\pm$  S.E.M. \*\*  $p < 0.01$  in comparison with SCI (control); (B) representative immunofluorescent images of RIP (mature oligodendrocyte marker) at different time points through the directed induced oligodendrocyte differentiation process of epSPCi in culture in the presence of FM19G11 or vehicle (DMSO) (scale bar, 500  $\mu$ m); (C) western blotting of NG2, Sox2, PCNA and  $\beta$ -actin semi-quantitative expression and (D) quantitative RT-PCR analysis for the expression of NG2 (oligodendrocyte marker) at the different stages of the directed in vitro differentiation process into oligodendrocytes from epSPCi in the presence of FM19G11 or DMSO (vehicle), \*  $p < 0.05$  in comparison with DMSO.

### 3. Discussion

A combination of strategies with a synergistic effect of improved neuroprotection and neural plasticity may lead to significant improvements not yet achieved by unique treatments. Here, we show how the combinatory use of FM19G11 and epSPCi reduces glial scar formation, reduces astrogliosis,

increases the number of neuronal fibers at the epicenter of the lesion, increases the expression markers for neuronal plasticity and induces oligodendrocyte turnover for potential re-myelination.

Traumatic contusion injury generates a rim of spared white matter tissue, with extensive neuronal degeneration and glial scar formation generating an incomplete lesion with a variable remaining demyelinated, but initially non-interrupted axons depending on the initial severity of the trauma, which, in fact, provides a more realistic experimental setting mimicking the clinical lesions to test potential neuroprotective and additional neurorestorative strategies. Extensive proliferation of different cell types occurs at certain time points, like oligodendrocyte, neural precursor cells and also astrocytes and microglia, in a more reliable way than the transection models [39]. Here, we induced a severe contusion by applying a force of 250 kdyn (kilo dyne) in rats of ~200 g, limiting the spontaneous functional regeneration during the first weeks after injury in comparison with moderate injuries and completely impairing it at the chronic stages (one month after injury), allowing the restorative functional evaluation among the different experimental groups in a shorter period than for instance in models of a complete section [40].

We recently showed that transplantation of epSPCi, the ependymal cells that represent the latent neural stem cell population in the adult spinal cord, activated and induced to proliferate *in vivo* after spinal cord injury [33] in combination with PA-curcumin significantly improves the locomotion in a chronic and sever traumatic SCI [17]. Here, we demonstrated the beneficial contribution to the epSPCi transplantation of the addition of FM19G11 previously reported to modulate proliferation and differentiation of this cell population and to have neuroprotective properties when applied immediately after injury [30]. When all treatments were compared, the cell transplanted groups, epSPCi and FM19G11 + epSPCi, showed faster functional rescue by measuring locomotor tasks, significantly different from the locomotor recover found in the vehicle- or the FM19G11-treated group. Neither vehicle- nor FM19G11-treated animals exhibited coordinated movement, but occasional weight support or plantar steps. The NPC progeny were found to be necessary to produce several neurotrophic factors that support neuronal survival after injury [41]. A2B5-positive glial cells have been shown to promote neuroprotection and repair of the injured spinal cord, promoting axonal sprouting when induced *in vitro* to differentiate into a more astroglial fate [42]. Accumulating evidence in the last decade defends the beneficial role of the astrocytes in response to SCI, giving support to the survival cells and allowing their processes [8]. We found, eight weeks after injury, a significant decrease of the GFAP-positive reactivity for astrocyte detection at the epicenter of the injury in response to all treatments, with an increase in the neurofilament-positive fibers. However, for better interconnection of both events, additional experimentation at a shorter time of analysis or specific deletion of the astrocytic population will be required to understand a potential associated mechanism of action.

The global detection of infiltrating macrophages, positive for CD68-ED1, eight weeks after injury, did not show significant differences in any of the tested conditions; however, it has been shown by others that the focal transplantation of NPCs decreases the relative proportion of classically-activated M1-like cells among the macrophage lineage cells infiltrating the injured cord [43], favoring the shift of the balance towards tissue remodelling/repair associated also with the M2-like cells and facilitating the recovery from spinal cord injury-induced secondary damage, undetected in a global analysis [44]. The lower astrogliosis activation found in all treated groups would additionally contribute to reduce the scar extension; the combined treatment exhibited in fact the best functional outcome with reduced spared tissue, where the combination with FM19G11 with an additional neuroprotective effect could contribute to favoring environmental homeostasis. It was very interesting that GAP43, previously described as a growth cone marker for growing axons, was induced in all treated animals at the scar area showing a similar effect as TUJ-1. Moreover, the growing axon ends positive for GAP43 were mostly accompanied by myelinated oligodendrocytes when the animals were treated with FM19G11, or with epSPCi, or both, supporting more effective neuronal plasticity in comparison with non-treated animals.

At the SCI area, the vascular network is lost with edema and disruption of the BSCB, extensively justifying the local application at the subarachnoid space of the pharmacological treatment. We previously showed that FM19G11 intrathecal administration immediately after SCI accelerates locomotor recovery in the rats one month after treatment. Indeed, the sustained administration of FM19G11 during one week showed a plausible neuroprotective role, preserving more neurofilament β-tubulin III-positive fibers in the injured area surrounded by an increased number of neural precursor vimentin-positive cells [30]. Here, we found that this neuroprotective effect by FM19G11 treatment was maintained, as was determined by the histological analysis, for two months. The analysis of both the *in vitro* and *in vivo* mechanism of action of FM19G11 reveals an important influence on the mitochondrial activity by early activation of UCP proteins, and therefore, the compound modifies oxidative metabolism at least in the epSPCi population by activation of the AKT/mTOR signaling pathway, which creates an adaptive response in the cells by increasing the GLUT-4 receptors [29,30] and probably improving the exocytosis and exchange program between cells and the tissue environment, which would contribute to the neuroprotective effect.

The promotion of OPC generation would contribute and accelerate the re-myelination process after SCI. Diverse clinical trials [45,46] based on previous successful pre-clinical studies [47–50] have tried to activate oligodendrocyte replacement for inducing re-myelination. FM19G11 was shown before to accelerate the maturation of OPC when the *in vitro* differentiation process was under the control of the related self-renewal transcriptional machinery in hypoxia [30]. Here, we show that FM19G11 can accelerate the differentiation and maturation of epSPCs *in vitro* derived from adult spinal cord also under normoxic conditions, showing a relevant effect of this compound in the reprogramming of the undifferentiated progenitors into mature lineages independently in certain micro-environmental conditions. FM19G11 modulates the expression of Sox2, Oct4 and Nanog depending on the oxygen tension to which the precursor cells are exposed [27,30]. Along the oligodendrocyte-directed differentiation process, FM19G11 more quickly decreased Sox2, Oct4 and PCNA undifferentiated and proliferative markers, respectively, in parallel with the increased expression of mature oligodendrocytes like RIP. Interestingly, FM19G11 was able to significantly induce the OPC population, revealed by the increased signal of Olig1, an early oligodendrocyte marker, showing an additive effect on the combinatory treatment with epSPCi. No significant co-localization of epSPCi and Olig1 was found; however, because all samples were studied at the time of sacrifice, two months after injury, a direct influence on the differentiation of the transplanted cells by FM19G11 cannot be discarded.

#### 4. Materials and Methods

##### 4.1. Ethical Statement Regarding the Use of Animals

Female 2-month-old Sprague Dawley rats (weighing ~200 g) from Charles River and SD-Tg(GFP)2BalRrc from Rat Resource & Research Center (University of Missouri Columbia, Columbia, MO, USA) were bred at the Animal Experimentation Unit of the Research Institute Príncipe Felipe (Valencia, Spain). The experimental protocol included humanized endpoint criteria by using a score for body weight changes (>20%), body condition (lethargy, pain), autophagy or severe ulcerations and was previously approved by the Animal Care Committee of the Research Institute Príncipe Felipe (Valencia, Spain) with the protocols identified as 10-0181 and 09-0131 in accordance with the National Guide to the Care and Use of Experimental Animals (Real Decreto 1 December 2005).

##### 4.2. EpSPCi Cell Culture

EpSPCi (eGFP+/+ for cell transplantation *in vivo* or eGFP−/− for *in vitro* assays) were isolated from adult female Sprague Dawley rats and SD-Tg(GFP)2BalRrc five days after severe contusion of spinal cord (250 kdyn at T8–T9, see above) and cultured as previously described [25,51].

Oligodendrocyte precursor cell (OPC)-induced differentiation was performed as previously described [25] with slight modifications, including in the FM19G11 condition 500 nM of the compound

FM19G11 (refreshed every two days) or the corresponding amount of vehicle, DMSO in the control group. The differentiation procedure was performed until Day 21 on culture in order to induce the early oligodendrocyte precursors. Part of the OPCs was destined to immunostainings for RIP marker and the other part for total mRNA and protein isolation for quantitative PCR of NG2 and Western blotting detection of Oc4, Sox2 and PCNA. Three independent experiments were performed.

#### 4.3. Spinal Cord Contusion, epSPCi Transplantation, Intrathecal Drug Administration and Functional Locomotor Analysis

SCI by contusion was performed as previously described [25]. Briefly, severe contusion (250 kdyn, “Infinite Horizon Impactor”) at thoracic segment T8 was performed. For intramedullary transplantation,  $10^6$  in 10  $\mu\text{L}$  of total volume epSPCi were transplanted by stereotaxis distributed into rostral and caudal regions at a distance of 2 mm from the lesion at a rate of 2  $\mu\text{L}/\text{min}$  by using a 30 G Hamilton pipette filled with cell suspension and mounted on the microinjector. We waited 1 min between injections before moving the syringe to allow cell deposition into the medullar tissue. The compound FM19G11 or DMSO (as vehicle control) was administrated via intrathecal catheterization. Partial laminectomy at T13 allows introducing the catheter (Alzet Corp., Cupertino, CA, USA; previously filled with 0.9% saline solution) through a perforation in dura mater, up to the injured segments (T8). The osmotic pump, Model 1007D (Alzet Corp. Germany; previously filled with FM19G11 or DMSO and incubated overnight at 37 °C in a saline solution), delivers 0.5  $\mu\text{L}$  per hour of a 9 mM FM19G11 solution or DMSO (vehicle) during 3 days.

The rats were pre-medicated with subcutaneous morphine (2.5 mg/kg) and Baytril (enrofloxacin, 5 mg/kg, Bayer, Leverkusen, Germany) and anesthetized with 2% isoflurane in a continuous oxygen flow of 1 L/min. All animals were subjected to post-surgery care and passive and active rehabilitation protocols as previously described [25]. Open-field locomotion was evaluated by two blinded observers by using the 21-point BBB locomotion scale after blind visualization of a minimum of 5 min of free walking in an open space once a week [52]. The animals were sacrificed after 8 weeks of evaluation.

#### 4.4. Histology and Quantification of the Tissue Volume at the Injury Area

The animals were transcardially perfused with a 0.9% saline solution followed by 4% PFA in PBS and 2 days incubation time in 30% sucrose before inclusion in Tissue-Tek OCT (Sakura Finetek Barcelona, Spain). Sagittal cryosections of a 10- $\mu\text{m}$  thickness were used for immunoassays. Every fifth section was collected for eosin and hematoxylin (E&H) staining to determine the anatomical structure and tissue volume calculations in the injured area. E&H-stained sections were scanned in a Pannoramic 250 Flash II scanner (3DHISTECH Ltd.; Budapest, Hungary), and images of approximately 20  $\text{mm}^2$  of medullar tissue (including the epicenter of the lesion) were acquired with the Pannoramic viewer software. The quantification of the spinal cord width was done at eight different points within the injured area. Using Adobe Photoshop® software (version CS2, San Jose, CA, USA), the images of every section, from dorsal to ventral areas, were placed consecutively, and 8 guidelines were traced vertically separated 0.5 mm along the epicenter of the injury. Spinal cord width was measured in every eighth point of every section following the guidelines using the scale bar for absolute quantification and normalization in mm.

The total thickness of the SC at the site of the lesion was quantified by including all the consecutive slides and multiplying them by the thickness of every cryosection (10  $\mu\text{m}$ ). Considering the elliptic-shape of the SC, the area quantification was calculated as follows:

$$\text{Area } (\text{mm}^2) = \text{higher radius } (\text{higher diameter}/2) \times \text{smaller radius } (\text{smaller diameter}/2) \times \pi$$

#### 4.5. Immunocytochemistry and Immunohistochemistry

Cells or cryosectioned tissues (10  $\mu\text{m}$ ) were post-fixed with 4% paraformaldehyde at room temperature for 10 min. After permeabilization with PBS containing 0.5% Triton and 2% goat

serum (blocking solution), the primary antibodies were incubated overnight at 4 °C. Cells or tissue sections were incubated with GAP43 ( $\alpha$ -rabbit; Cat. ab128005 Abcam, Hong Kong, China),  $\beta$ -tubulin III ( $\alpha$ -mouse; Cat. MO15052 Neuromics, Edina, MN, USA), GFAP ( $\alpha$ -rabbit; Cat. Z0334 DAKO, Santa Clara, CA, USA), RIP ( $\alpha$ -mouse; Cat. MAB1580 Chemicon, Pittsburgh, PA, USA) and OLIG1 ( $\alpha$ -rabbit; Cat. AB5320 Chemicon). Primary antibodies were diluted 1:200 in blocking solution. After being rinsed three times with PBS, the cells or the tissue sections were incubated with Oregon Green-Alexa488, Alexa555 or Alexa647 dye-conjugated secondary antibodies for 1 h at room temperature. All cells and tissue sections were counterstained by incubation with DAPI for 5 min at room temperature followed by washing steps. Signals were visualized by both fluorescent microscopy (fluorescence microscope Leica DM6000B, Wetzlar, Germany) and confocal microscopy (confocal microscope Leica TCS-SP2-AOBS, Wetzlar, Germany). The quantification of immunostainings was performed using ImageJ software (Image J2, Madison, WI, USA).

#### 4.6. Western Blot

epSPCi neurosphere-like cultures at the indicated points of the OPC differentiation process were lysed in 50 mM Tris-HCl, pH 7.5, 150 mM NaCl, 0.02% NaN<sub>3</sub>, 0.1 SDS, 1% NP40, 1 mM ethylene diamine tetra acetic acid (EDTA), 2  $\mu$ g/mL leupeptin, 2  $\mu$ g/mL aprotinin, 1 mM PMSF and 1  $\times$  Protease Inhibitor Cocktail (Roche Diagnostics, San Diego, CA, USA), stored on ice for 30 min and boiled for 10 min. Twenty five  $\mu$ g of each protein extract were subjected to sodium dodecyl sulfate (SDS) polyacrylamide gel electrophoresis (PAGE; MiniProtean<sup>®</sup>, Bio-Rad, Hercules, CA, USA) and blotted with antibodies overnight at 4 °C. Signal detection was performed with an enhanced chemiluminescence kit (ECL Plus Western blotting detection reagent from GE Healthcare, Piscataway Township, NJ, USA). Primary antibodies used were Sox2 ( $\alpha$ -mouse; Cat. MAB2018. R&D System, Minneapolis, MN, USA), NG2 ( $\alpha$ -mouse; Cat. MAB5384. Chemicon), PCNA ( $\alpha$ -mouse; Cat. ab29. Abcam) and  $\beta$ -actin for the loading control ( $\alpha$ -mouse; Cat. A5441 Sigma, Saint Louis, MO, USA). At least 3 biologically independent replicates were always performed; a representative Western blot is shown.

#### 4.7. RNA Isolation and Quantitative RT-PCR

Total RNA of epSPCi at the indicated points of the OPC differentiation process was extracted by using the RNeasy Mini-kit (Qiagen, Hilden, Germany) according to the manufacturer's instructions. One microgram of total RNA was reverse-transcribed in a total reaction volume of 50  $\mu$ L at 42 °C for 30 min using random hexamer primers. For quantitative analyses, we used LightCycler SYBR<sup>®</sup> Green I technology, and the relative expression of mRNA transcripts was analyzed by the ABI PRISM 5700 Sequence Detection System (Applied Biosystems, Foster City, CA, USA). As a template, we used 40 ng of cDNA to analyze the expression of target and housekeeping genes (18S) in separate tubes for each pair of primers. The sequences from 5' to 3' of each pair of primers are: rNG2, forward primer: 5'-ATGCTTCTCAGCCCCGGACA-3'; reverse primer: 5'-GGTTGCAGGCCATTGAGAATG-3'; r18S, forward primer: ggaaggccaccaggagt; reverse primer: tgcaagccccggacatctaag. The comparative threshold cycle (C<sub>t</sub>) method was used to calculate the relative expression as follows:

$$\Delta C_t (\Delta C_t = C_t (\text{test gene}) - C_t (\text{GAPDH}))$$

$\Delta C_t$  for FM19G11-treated samples was then subtracted from the  $\Delta C_t$  for vehicle-treated samples, to generate  $\Delta\Delta C_t$  ( $\Delta\Delta C_t = \Delta C_t (\text{FM19G11}) - \Delta C_t (\text{vehicle})$ ). The mean of these  $\Delta\Delta C_t$  measurements was used to calculate the fold change in gene expression ( $2^{-\Delta\Delta C_t}$ ). Results were presented as the mean  $\pm$  standard error.

#### 4.8. Statistical Analysis

Student's *t*-test was performed for pair comparisons and one-way analysis of variance (ANOVA) for multiple value comparisons. All measurements in cell culture experiments were carried out in at least three different culture preparations, and the results were expressed as the mean  $\pm$  SEM. Statistical analysis was performed using GraphPad Prism 4 Project software (San Diego, CA, USA). In all cases,  $p < 0.05$  was considered significant.

### 5. Conclusions

Altogether, significant beneficial cellular changes at the histological level were found in the combinatory treatment with epSPCi and FM19G11 in the SCI acute rat model. The obtained results justify the combination of both strategies, cell transplantation and pharmacological treatment, as opposed to the use of the individual ones, for better success on locomotor improvements after SCI, although further investigation would be necessary to demonstrate plausible functional benefits by adjusting doses and/or treatment administrations for long-term treatment and analysis.

**Acknowledgments:** This work was supported by research grants from the Foundation Step by Step, the Spanish Ion Channel Initiative (CSD2008-00005), the Instituto Salud Carlos III (PI13/00319) and MINECO (MAT2015-66666-C3-2-R). The authors would like to thank Maravillas Mellado López for essential technical support. The authors would like to thank Richard Griffeth for manuscript editing and critical comments.

**Author Contributions:** Victoria Moreno-Manzano conceived of the idea and contribute to the materials. Slaven Erceg provided conceptual advice and contributed materials. Victoria Moreno-Manzano, Ana Alatrue-Agudo and Francisco Javier Rodriguez-Jimenez designed the research. Ana Alatrue-Agudo, Victoria Moreno-Manzano, Francisco Javier Rodriguez-Jimenez, Eric López Mocholi and Francesca De Giorgio performed the research. Victoria Moreno-Manzano, Ana Alatrue-Agudo and Francisco Javier Rodriguez-Jimenez analyzed the data. Victoria Moreno-Manzano wrote the manuscript.

**Conflicts of Interest:** The authors declare no conflict of interest.

### Abbreviations

BBB	Basso, Beattie and Bresnahan
BSCB	Blood-spinal cord barrier
DMSO	Dimethyl sulfoxide
epSPC	Ependymal stem/progenitor cells
epSPCi	Ependymal stem/progenitor cells of the spinal cord after injury
GFAP	Glial fibrillary acidic protein
GFP	Green fluorescence protein
H&E	Hematoxylin-eosin
HIF	Hypoxia inducible factor
NPC	Neural precursor cell
OPC	Oligodendrocyte precursor cell
PFA	Paraformaldehyde
PBS	Phosphate buffer solution
RT-PCR	Reverse transcription-polymerase chain reaction
SC	Spinal cord
SCI	Spinal cord injury
UCP	Uncoupling protein

### References

1. Hulsebosch, C.E. Recent advances in pathophysiology and treatment of spinal cord injury. *Adv. Physiol. Educ.* **2002**, *26*, 238–255. [[CrossRef](#)] [[PubMed](#)]
2. Robinson, J.; Lu, P. Optimization of trophic support for neural stem cell grafts in sites of spinal cord injury. *Exp. Neurol.* **2017**, *291*, 87–97. [[CrossRef](#)] [[PubMed](#)]

3. Negro, S.; Lessi, F.; Duregotti, E.; Aretini, P.; La Ferla, M.; Franceschi, S.; Menicagli, M.; Bergamin, E.; Radice, E.; Thelen, M.; et al. CXCL12alpha/SDF-1 from perisynaptic Schwann cells promotes regeneration of injured motor axon terminals. *EMBO Mol. Med.* **2017**, *9*, 1000–1010. [[CrossRef](#)] [[PubMed](#)]
4. Liu, Y.; Wang, X.; Li, W.; Zhang, Q.; Li, Y.; Zhang, Z.; Zhu, J.; Chen, B.; Williams, P.R.; Zhang, Y.; et al. A sensitized IGF1 treatment restores corticospinal axon-dependent functions. *Neuron* **2017**, *95*, 817–833. [[CrossRef](#)] [[PubMed](#)]
5. Sandler, A.N.; Tator, C.H. Review of the effect of spinal cord trauma on the vessels and blood flow in the spinal cord. *J. Neurosurg.* **1976**, *45*, 638–646. [[CrossRef](#)] [[PubMed](#)]
6. Kitayama, M.; Ueno, M.; Itakura, T.; Yamashita, T. Activated microglia inhibit axonal growth through RGMa. *PLoS ONE* **2011**, *6*, e25234. [[CrossRef](#)] [[PubMed](#)]
7. Okada, S.; Hara, M.; Kobayakawa, K.; Matsumoto, Y.; Nakashima, Y. Astrocyte reactivity and astrogliosis after spinal cord injury. *Neurosci. Res.* **2017**, *126*, 39–43. [[CrossRef](#)] [[PubMed](#)]
8. Lukovic, D.; Stojkovic, M.; Moreno-Manzano, V.; Jendelova, P.; Sykova, E.; Bhattacharya, S.S.; Erceg, S. Concise review: Reactive astrocytes and stem cells in spinal cord injury: Good guys or bad guys? *Stem Cells* **2015**, *33*, 1036–1041. [[CrossRef](#)] [[PubMed](#)]
9. David, S.; Kroner, A. Repertoire of microglial and macrophage responses after spinal cord injury. *Nat. Rev. Neurosci.* **2011**, *12*, 388–399. [[CrossRef](#)] [[PubMed](#)]
10. Donnelly, D.J.; Popovich, P.G. Inflammation and its role in neuroprotection, axonal regeneration and functional recovery after spinal cord injury. *Exp. Neurol.* **2008**, *209*, 378–388. [[CrossRef](#)] [[PubMed](#)]
11. Gensel, J.C.; Zhang, B. Macrophage activation and its role in repair and pathology after spinal cord injury. *Brain Res.* **2015**, *1619*, 1–11. [[CrossRef](#)] [[PubMed](#)]
12. Ahuja, C.S.; Nori, S.; Tetreault, L.; Wilson, J.; Kwon, B.; Harrop, J.; Choi, D.; Fehlings, M.G. Traumatic spinal cord injury-repair and regeneration. *Neurosurgery* **2017**, *80*, S9–S22. [[CrossRef](#)] [[PubMed](#)]
13. Grossman, S.D.; Rosenberg, L.J.; Wrathall, J.R. Temporal-spatial pattern of acute neuronal and glial loss after spinal cord contusion. *Exp. Neurol.* **2001**, *168*, 273–282. [[CrossRef](#)] [[PubMed](#)]
14. Ahuja, C.S.; Fehlings, M. Concise review: Bridging the gap: Novel neuroregenerative and neuroprotective strategies in spinal cord injury. *Stem Cells Transl. Med.* **2016**, *5*, 914–924. [[CrossRef](#)] [[PubMed](#)]
15. Ronaghi, M.; Erceg, S.; Moreno-Manzano, V.; Stojkovic, M. Challenges of stem cell therapy for spinal cord injury: Human embryonic stem cells, endogenous neural stem cells, or induced pluripotent stem cells? *Stem Cells* **2010**, *28*, 93–99. [[CrossRef](#)] [[PubMed](#)]
16. Gazdic, M.; Volarevic, V.; Arsenijevic, A.; Erceg, S.; Moreno-Manzano, V.; Arsenijevic, N.; Stojkovic, M. Stem cells and labeling for spinal cord injury. *Int. J. Mol. Sci.* **2016**, *18*, 6. [[CrossRef](#)] [[PubMed](#)]
17. Requejo-Aguilar, R.; Alastrue-Agudo, A.; Cases-Villar, M.; Lopez-Mocholi, E.; England, R.; Vicent, M.J.; Moreno-Manzano, V. Combined polymer-curcumin conjugate and ependymal progenitor/stem cell treatment enhances spinal cord injury functional recovery. *Biomaterials* **2017**, *113*, 18–30. [[CrossRef](#)] [[PubMed](#)]
18. Jin, W.; Wang, J.; Zhu, T.; Yuan, B.; Ni, H.; Jiang, J.; Wang, H.; Liang, W. Anti-inflammatory effects of curcumin in experimental spinal cord injury in rats. *Inflamm. Res.* **2014**, *63*, 381–387. [[CrossRef](#)] [[PubMed](#)]
19. Ormond, D.R.; Shannon, C.; Oppenheim, J.; Zeman, R.; Das, K.; Murali, R.; Jhanwar-Uniyal, M. Stem cell therapy and curcumin synergistically enhance recovery from spinal cord injury. *PLoS ONE* **2014**, *9*, e88916. [[CrossRef](#)] [[PubMed](#)]
20. Sahin Kavaklı, H.; Koca, C.; Alici, O. Antioxidant effects of curcumin in spinal cord injury in rats. *Ulus. Travma Acil Cerrahi Derg.* **2011**, *17*, 14–18. [[CrossRef](#)] [[PubMed](#)]
21. Wang, Y.F.; Zu, J.N.; Li, J.; Chen, C.; Xi, C.Y.; Yan, J.L. Curcumin promotes the spinal cord repair via inhibition of glial scar formation and inflammation. *Neurosci. Lett.* **2014**, *560*, 51–56. [[CrossRef](#)] [[PubMed](#)]
22. Yuan, J.; Zou, M.; Xiang, X.; Zhu, H.; Chu, W.; Liu, W.; Chen, F.; Lin, J. Curcumin improves neural function after spinal cord injury by the joint inhibition of the intracellular and extracellular components of glial scar. *J. Surg. Res.* **2015**, *195*, 235–245. [[CrossRef](#)] [[PubMed](#)]
23. Meletis, K.; Barnabe-Heider, F.; Carlen, M.; Evergren, E.; Tomilin, N.; Shupliakov, O.; Frisén, J. Spinal cord injury reveals multilineage differentiation of ependymal cells. *PLoS Biol.* **2008**, *6*, e182. [[CrossRef](#)] [[PubMed](#)]
24. Gomez-Villafuertes, R.; Rodriguez-Jimenez, F.J.; Alastrue-Agudo, A.; Stojkovic, M.; Miras-Portugal, M.T.; Moreno-Manzano, V. Purinergic receptors in spinal cord-derived ependymal stem/progenitor cells and their potential role in cell-based therapy for spinal cord injury. *Cell Transplant.* **2015**, *24*, 1493–1509. [[CrossRef](#)] [[PubMed](#)]

25. Moreno-Manzano, V.; Rodriguez-Jimenez, F.J.; Garcia-Rosello, M.; Lainez, S.; Erceg, S.; Calvo, M.T.; Ronaghi, M.; Lloret, M.; Planells-Cases, R.; Sánchez-Puelles, J.M. Activated spinal cord ependymal stem cells rescue neurological function. *Stem Cells* **2009**, *27*, 733–743. [[CrossRef](#)] [[PubMed](#)]
26. Thuret, S.; Moon, L.D.; Gage, F.H. Therapeutic interventions after spinal cord injury. *Nat. Rev. Neurosci.* **2006**, *7*, 628–643. [[CrossRef](#)] [[PubMed](#)]
27. Moreno-Manzano, V.; Rodriguez-Jimenez, F.J.; Acena-Bonilla, J.L.; Fustero-Lardies, S.; Erceg, S.; Dopazo, J.; Montaner, D.; Stojkovic, M.; Sánchez-Puelles, J.M. FM19G11, a new hypoxia-inducible factor (HIF) modulator, affects stem cell differentiation status. *J. Biol. Chem.* **2010**, *285*, 1333–1342. [[CrossRef](#)] [[PubMed](#)]
28. Rodriguez-Jimenez, F.J.; Moreno-Manzano, V.; Lucas-Dominguez, R.; Sanchez-Puelles, J.M. Hypoxia causes downregulation of mismatch repair system and genomic instability in stem cells. *Stem Cells* **2008**, *26*, 2052–2062. [[CrossRef](#)] [[PubMed](#)]
29. Rodriguez-Jimenez, F.J.; Moreno-Manzano, V.; Mateos-Gregorio, P.; Royo, I.; Erceg, S.; Murguia, J.R.; Sánchez-Puelles, J.M. FM19G11: A new modulator of HIF that links mTOR activation with the DNA damage checkpoint pathways. *Cell Cycle* **2010**, *9*, 2803–2813. [[CrossRef](#)] [[PubMed](#)]
30. Rodriguez-Jimenez, F.J.; Alastrue-Agudo, A.; Erceg, S.; Stojkovic, M.; Moreno-Manzano, V. FM19G11 favors spinal cord injury regeneration and stem cell self-renewal by mitochondrial uncoupling and glucose metabolism induction. *Stem Cells* **2012**, *30*, 2221–2233. [[CrossRef](#)] [[PubMed](#)]
31. Morita, S.; Miyata, S. Synaptic localization of growth-associated protein 43 in cultured hippocampal neurons during synaptogenesis. *Cell Biochem. Funct.* **2013**, *31*, 400–411. [[CrossRef](#)] [[PubMed](#)]
32. Watanabe, M.; Sakurai, Y.; Ichinose, T.; Aikawa, Y.; Kotani, M.; Itoh, K. Monoclonal antibody Rip specifically recognizes 2',3'-cyclic nucleotide 3'-phosphodiesterase in oligodendrocytes. *J. Neurosci. Res.* **2006**, *84*, 525–533. [[CrossRef](#)] [[PubMed](#)]
33. Barnabe-Heider, F.; Goritz, C.; Sabelstrom, H.; Takebayashi, H.; Pfrieger, F.W.; Meletis, K.; Frisén, J. Origin of new glial cells in intact and injured adult spinal cord. *Cell Stem Cell* **2010**, *7*, 470–482. [[CrossRef](#)] [[PubMed](#)]
34. Hesp, Z.C.; Goldstein, E.Z.; Miranda, C.J.; Kaspar, B.K.; McTigue, D.M. Chronic oligodendrogenesis and remyelination after spinal cord injury in mice and rats. *J. Neurosci.* **2015**, *35*, 1274–1290. [[CrossRef](#)] [[PubMed](#)]
35. Sellers, D.L.; Maris, D.O.; Horner, P.J. Postinjury niches induce temporal shifts in progenitor fates to direct lesion repair after spinal cord injury. *J. Neurosci.* **2009**, *29*, 6722–6733. [[CrossRef](#)] [[PubMed](#)]
36. Gledhill, R.F.; Harrison, B.M.; McDonald, W.I. Demyelination and remyelination after acute spinal cord compression. *Exp. Neurol.* **1973**, *38*, 472–487. [[CrossRef](#)]
37. Harrison, B.M.; McDonald, W.I. Remyelination after transient experimental compression of the spinal cord. *Ann. Neurol.* **1977**, *1*, 542–551. [[CrossRef](#)] [[PubMed](#)]
38. Cheng, X.; Wang, Y.; He, Q.; Qiu, M.; Whittemore, S.R.; Cao, Q. Bone morphogenetic protein signaling and olig1/2 interact to regulate the differentiation and maturation of adult oligodendrocyte precursor cells. *Stem Cells* **2007**, *25*, 3204–3214. [[CrossRef](#)] [[PubMed](#)]
39. McDonough, A.; Martinez-Cerdeno, V. Endogenous proliferation after spinal cord injury in animal models. *Stem Cells Int.* **2012**, *2012*, 387513. [[CrossRef](#)] [[PubMed](#)]
40. Lukovic, D.; Moreno-Manzano, V.; Lopez-Mocholi, E.; Rodriguez-Jimenez, F.J.; Jendelova, P.; Sykova, E.; Oria, M.; Stojkovic, M.; Erceg, S. Complete rat spinal cord transection as a faithful model of spinal cord injury for translational cell transplantation. *Sci. Rep.* **2015**, *5*, 9640. [[CrossRef](#)] [[PubMed](#)]
41. Stenudd, M.; Sabelstrom, H.; Frisen, J. Role of endogenous neural stem cells in spinal cord injury and repair. *JAMA Neurol.* **2015**, *72*, 235–237. [[CrossRef](#)] [[PubMed](#)]
42. Davies, J.E.; Proschel, C.; Zhang, N.; Noble, M.; Mayer-Proschel, M.; Davies, S.J. Transplanted astrocytes derived from BMP- or CNTF-treated glial-restricted precursors have opposite effects on recovery and allodynia after spinal cord injury. *J. Biol.* **2008**, *7*, 24. [[CrossRef](#)] [[PubMed](#)]
43. Cusimano, M.; Biziato, D.; Brambilla, E.; Donega, M.; Alfaro-Cervello, C.; Snider, S.; Salani, G.; Pucci, F.; Comi, G.; Garcia-Verdugo, J.M. Transplanted neural stem/precursor cells instruct phagocytes and reduce secondary tissue damage in the injured spinal cord. *Brain J. Neurol.* **2012**, *135 Pt 2*, 447–460. [[CrossRef](#)] [[PubMed](#)]
44. Gensel, J.C.; Kopper, T.J.; Zhang, B.; Orr, M.B.; Bailey, W.M. Predictive screening of M1 and M2 macrophages reveals the immunomodulatory effectiveness of post spinal cord injury azithromycin treatment. *Sci. Rep.* **2017**, *7*, 40144. [[CrossRef](#)] [[PubMed](#)]

45. Mekhail, M.; Almazan, G.; Tabrizian, M. Oligodendrocyte-protection and remyelination post-spinal cord injuries: A review. *Prog. Neurobiol.* **2012**, *96*, 322–339. [[CrossRef](#)] [[PubMed](#)]
46. Plemel, J.R.; Keough, M.B.; Duncan, G.J.; Sparling, J.S.; Yong, V.W.; Stys, P.K.; Tetzlaff, W. Remyelination after spinal cord injury: Is it a target for repair? *Prog. Neurobiol.* **2014**, *117*, 54–72. [[CrossRef](#)] [[PubMed](#)]
47. Karimi-Abdolrezaee, S.; Eftekharpour, E.; Wang, J.; Morshead, C.M.; Fehlings, M.G. Delayed transplantation of adult neural precursor cells promotes remyelination and functional neurological recovery after spinal cord injury. *J. Neurosci.* **2006**, *26*, 3377–3389. [[CrossRef](#)] [[PubMed](#)]
48. Cao, Q.; He, Q.; Wang, Y.; Cheng, X.; Howard, R.M.; Zhang, Y.; DeVries, W.H.; Shields, C.B.; Magnuson, D.S.; Xu, X.M. Transplantation of ciliary neurotrophic factor-expressing adult oligodendrocyte precursor cells promotes remyelination and functional recovery after spinal cord injury. *J. Neurosci.* **2010**, *30*, 2989–3001. [[CrossRef](#)] [[PubMed](#)]
49. Plemel, J.R.; Chojnacki, A.; Sparling, J.S.; Liu, J.; Plunet, W.; Duncan, G.J.; Park, S.E.; Weiss, S.; Tetzlaff, W. Platelet-derived growth factor-responsive neural precursors give rise to myelinating oligodendrocytes after transplantation into the spinal cords of contused rats and dysmyelinated mice. *Glia* **2011**, *59*, 1891–1910. [[CrossRef](#)] [[PubMed](#)]
50. Sun, Y.; Xu, C.C.; Li, J.; Guan, X.Y.; Gao, L.; Ma, L.X.; Li, R.X.; Peng, Y.W.; Zhu, G.P. Transplantation of oligodendrocyte precursor cells improves locomotion deficits in rats with spinal cord irradiation injury. *PLoS ONE* **2013**, *8*, e57534. [[CrossRef](#)] [[PubMed](#)]
51. Rodriguez-Jimenez, F.J.; Alastrue, A.; Stojkovic, M.; Erceg, S.; Moreno-Manzano, V. Connexin 50 modulates Sox2 expression in spinal-cord-derived ependymal stem/progenitor cells. *Cell Tissue Res.* **2016**, *365*, 295–307. [[CrossRef](#)] [[PubMed](#)]
52. Basso, D.M.; Beattie, M.S.; Bresnahan, J.C. A sensitive and reliable locomotor rating scale for open field testing in rats. *J. Neurotrauma* **1995**, *12*, 1–21. [[CrossRef](#)] [[PubMed](#)]



© 2018 by the authors. Licensee MDPI, Basel, Switzerland. This article is an open access article distributed under the terms and conditions of the Creative Commons Attribution (CC BY) license (<http://creativecommons.org/licenses/by/4.0/>).



Article

# The Effect of Human Mesenchymal Stem Cells Derived from Wharton's Jelly in Spinal Cord Injury Treatment Is Dose-Dependent and Can Be Facilitated by Repeated Application

Petr Krupa <sup>1,2</sup>, Irena Vackova <sup>2</sup>, Jiri Ruzicka <sup>2</sup>, Kristyna Zaviskova <sup>2,3</sup>, Jana Dubisova <sup>2,3</sup>, Zuzana Koci <sup>2,3</sup>, Karolina Turnovcova <sup>2</sup>, Lucia Machova Urdzikova <sup>2</sup>, Sarka Kubinova <sup>2</sup>, Svatopluk Rehak <sup>1</sup> and Pavla Jendelova <sup>2,3,\*</sup>

<sup>1</sup> Department of Neurosurgery, Charles University, Medical Faculty and University Hospital Hradec Králové, Sokolska 581, 50005 Hradec Kralove, Czech Republic; petr.krupa@fnhk.cz (P.K.); rehak@lfhk.cuni.cz (S.R.)

<sup>2</sup> Institute of Experimental Medicine, Czech Academy of Sciences, Vídeňská 1083, 14220 Prague 4, Czech Republic; irena.vackova@biomed.cas.cz (I.V.); j.ruzicka@biomed.cas.cz (J.R.); kristyna.zaviskova@biomed.cas.cz (K.Z.); jana.dubisova@biomed.cas.cz (J.D.); zuzana.koci@biomed.cas.cz (Z.K.); karolina.turnovcova@biomed.cas.cz (K.T.); urdzikl@biomed.cas.cz (L.M.U.); sarka.k@biomed.cas.cz (S.K.)

<sup>3</sup> Department of Neuroscience, Charles University, Second Faculty of Medicine, 15006 Prague 5, Czech Republic

\* Correspondence: jendel@biomed.cas.cz; Tel.: +420-241062828

Received: 9 April 2018; Accepted: 15 May 2018; Published: 17 May 2018

**Abstract:** Human mesenchymal stem cells derived from Wharton's jelly (WJ-MSCs) were used for the treatment of the ischemic-compression model of spinal cord injury in rats. To assess the effectiveness of the treatment, different dosages (0.5 or 1.5 million cells) and repeated applications were compared. Cells or saline were applied intrathecally by lumbar puncture for one week only, or in three consecutive weeks after injury. Rats were assessed for locomotor skills (BBB, rotarod, flat beam) for 9 weeks. Spinal cord tissue was morphometrically analyzed for axonal sprouting, sparing of gray and white matter and astrogliosis. Endogenous gene expression (*Gfap*, *Casp3*, *Irf5*, *Cd86*, *Mrc1*, *Cd163*) was studied with quantitative Real-time polymerase chain reaction (qRT PCR). Significant recovery of functional outcome was observed in all of the treated groups except for the single application of the lowest number of cells. Histochemical analyses revealed a gradually increasing effect of grafted cells, resulting in a significant increase in the number of GAP43+ fibers, a higher amount of spared gray matter and reduced astrogliosis. mRNA expression of macrophage markers and apoptosis was downregulated after the repeated application of 1.5 million cells. We conclude that the effect of hWJ-MSCs on spinal cord regeneration is dose-dependent and potentiated by repeated application.

**Keywords:** spinal cord injury; human mesenchymal stem cells; Wharton's jelly; inflammatory response; neuroregeneration; astrogliosis; axonal growth

## 1. Introduction

Spinal cord injury (SCI) is a serious mutilating injury, resulting in loss of motor, sensory, and autonomic functions, and remains a challenging medical and social problem even in the 21st century. The final neurological deficit is determined by two mechanisms—primary and secondary injury. Primary injury represents the mechanism and strength of the direct trauma. Secondary injury is characterized by the local immune reaction followed by apoptosis of the injured and vulnerable neurons, tissue atrophy with cavitation, and glial scar formation [1]. Since there is no specific

treatment for primary injury, and the endogenous potential to regenerate the spinal cord neurons is very limited [2], several treatments are focused on neuroprotection and/or reducing the impact of secondary pathological processes. Promising results in alleviation of the pathological chain of secondary damage were found in the last decade by application of mesenchymal stem cells (MSCs).

MSCs are multipotent cells with multi-differentiation and self-renewal capacity. Many types of adult and embryogenic tissue have been proven as a source of MSCs—adipose tissue, peripheral blood, lung, heart, corneal stroma, dental pulp, placenta, endometrium, amniotic membrane, and umbilical cord blood and tissue (Wharton's jelly). Under special conditions in vitro, they are capable of differentiating into various tissue cells such as osteocytes or osteoblasts, adipocytes, and chondrocytes [3–5]. However, the regenerative potential of MSCs as a therapeutic tool can be provided mainly by the paracrine effect, interacting with the environment around the injured tissue. In nervous tissue repair and regeneration, MSCs support revascularization, modulate inflammatory response [6], produce different growth factors and cytokines [7], and protect vulnerable cells from oxidative stress, causing stress-induced apoptosis [8]. Therefore, it was recently suggested by Caplan [9] that they should be renamed to medicinal signaling cells (MSCs).

In the current study, we used MSCs isolated from human Wharton's jelly (WJ-MSCs). Wharton's jelly is the primitive gelatinous connective tissue of the umbilical cord, first described by Thomas Wharton in 1656. Compared to other sources of MSCs (bone marrow, adipose tissue), WJ-MSCs are more primitive with higher proliferating potential [10], have lower immunogenicity because of a lower major histocompatibility complex class I (MHC-I) and the absence of major histocompatibility complex class II (MHC-II) expression [11], and are proven to be non-tumorigenic [12]. Furthermore, WJ-MSCs can be easily and non-invasively obtained from discarded umbilical tissue, and represent neither potential danger for the donor, nor ethical concerns [13]. They are highly proliferative and can be easily expanded.

The delivery route of stem cells is a frequently discussed issue, as the mode of delivery is an important factor in translation to clinical practice. Therefore, several studies have compared the intraspinal, intrathecal (or intracisternal), intraarterial and intravenous application of MSCs. Regardless of the delivery route, MSC treatment has improved functional recovery after SCI. Whilst the engraftment of the transplanted cells was higher in animals with intraspinal delivery [14,15], injections into the parenchyma of the spinal cord may further damage the spinal cord tissue; therefore, less invasive methods, such as intrathecal or intravenous delivery, are preferable. Indeed, the cells grafted via lumbar puncture, or intracisternally have shown the best functional recovery, even though they often remained in the intrathecal space [16,17] or accumulated around the anterior spinal artery [18]. Rats intrathecally grafted with human bone marrow MSCs (hBM-MSCs) had reduced inflammatory reactions and apoptosis, improved functional recovery, and the glial scar formation had been rearranged after SCI, though no cells were detected in the spinal cord parenchyma two months after transplantation [19,20]. Because of the relatively short survival time of MSCs in the host tissue the repetitive delivery of MSCs may prolong the beneficial effects induced by MSC application by potentiating their regenerative potential [18].

The main goal of this study was to assess the dose of the applied WJ-MSCs, and the difference between single and repetitive application on functional recovery and tissue repair after SCI in rats. WJ-MSCs were applied intrathecally by a lumbar puncture into rats with balloon-induced spinal cord compression lesion. This model simulates the compression of the human spinal cord by an unreduced dislocation or a fracture dislocation of the spine. It is assumed that both mechanical and vascular factors are involved in the pathogenesis of spinal cord injury in this model. Moreover, it is simple and reproducible and requires minimal surgical preparation of the animal (no laminectomy) [21]. The functional outcome was assessed using a set of behavioral tests (BBB, flat beam test, and rotarod). Furthermore, histological and immunohistochemical analyses were performed to evaluate the sparing of gray and white matter, axonal sprouting, and formation of glial scar. Finally, quantitative PCR analyses of selected endogenous genes were performed.

## 2. Results

### 2.1. Cell Culture

hWJ-MSCs phenotype, their multipotent differentiation potential, and high proliferation capacity was evaluated prior to transplantation (see Supplement 1, Figures S1–S3).

### 2.2. Behavioral Analysis

#### 2.2.1. BBB Test

Recovery of the hind limb locomotor function was evaluated every week starting the first week after SCI. The BBB score was calculated as a mean value from the scores of both legs (Figure 1A). One week after SCI, all tested animals had severe paraparesis or paraplegia. The average score was  $1.28 \pm 0.15$ . No differences between the groups were observed. The second week after SCI animals in all groups showed new motions in one or two joints. Among the groups, a significant difference was found between the control group ( $2.1 \pm 0.43$ ) and the group treated with a single dose of  $1.5\text{ M hWJ-MSCs}$  ( $5.28 \pm 0.59$ ) ( $p < 0.05$ ). In the third week after SCI, a rapid improvement of the locomotor functions was observed in the groups treated with a single dose of  $1.5\text{ M}$ , and the groups with repeated treatment of  $0.5$  and  $1.5\text{ M}$ , respectively. All three groups recovered significantly better than the control group ( $p < 0.05$ ,  $p < 0.001$ ). Animals treated with only  $0.5\text{ M}$  showed little improvement over the control group, which was not statistically significant. In the following weeks, improvement of movement and strength of the hind limbs continued but not so rapidly as was seen during the first three weeks. From the fourth week onward, until the end of the experiment, rats treated with  $1.5\text{ M}$  and  $3 \times 0.5\text{ M}$  and  $3 \times 1.5\text{ M}$  had comparable results, which were significantly better than the control group and animals treated by  $0.5\text{ M}$  ( $p < 0.01$ ,  $p < 0.001$ ). No significant difference between the control group and the  $0.5\text{ M}$  group was found. The final results at the end of the ninth week were  $4.29 \pm 0.57$  for the control group,  $5.19 \pm 0.36$  for  $0.5\text{ M}$ ,  $9.81 \pm 0.88$  for  $3 \times 0.5\text{ M}$ ,  $8.67 \pm 0.88$  for  $1.5\text{ M}$  and  $9.21 \pm 0.45$  for  $3 \times 1.5\text{ M}$ . Animals in the groups with repetitive treatment were mostly able to achieve effective weight support of their body when standing, or even walking. The gap between scores 8 (and lower) and 9 (and higher) is substantial when comparing the strength of the muscles of the hindlimbs.

(Two-way RM ANOVA, Treatment;  $F = 8.481$ ,  $p < 0.001$ ; for  $p$  values of post hoc pair-to-pair test, see Supplement 2).

#### 2.2.2. Rotarod Test

Coordination of the limb movements was tested by a rotarod test (Figure 1B). All animals were trained in this task before surgery at a fixed speed of 10 rpm. Testing was then performed every two weeks—2nd, 4th, 6th, and 8th week after SCI. Due to the severity of the lesion and limited recovery, no significant differences were observed between the groups.

(Two-way RM ANOVA, Treatment;  $F = 0.490$ ,  $p = 0.743$ ; for  $p$  values of post hoc pair-to-pair test, see Supplement 2).

#### 2.2.3. Beam Walk Test

Advanced locomotor skills and coordination of the hind limbs was measured by walking on the flat beam. Results were evaluated using a 0–7 scale modified from Metz and Whishaw. All animals were firstly trained in this task before surgery and then tested every week starting the second week after SCI (Figure 1C). Due to the severity of the lesion, most of the rats showed minimal ability to cross the beam and often just stayed and balanced at the starting point of the beam. The best scores (7th week after SCI  $3.1 \pm 0.33$ ) were obtained in animals treated by  $3 \times 1.5\text{ M}$ , which were significantly better, when compared to all of the other groups. For the first three weeks, animals treated with  $0.5\text{ M}$  achieved significantly better results than the control group, but in subsequent weeks they gradually

worsened and the significant difference was lost. This was most probably due to the gaining of weight, lack of motivation, and fear of falling off the beam.

(Two-way RM ANOVA, Treatment;  $F = 20.656$ ,  $p < 0.001$ ; for  $p$  values of post hoc pair-to-pair test, see Supplement 2).

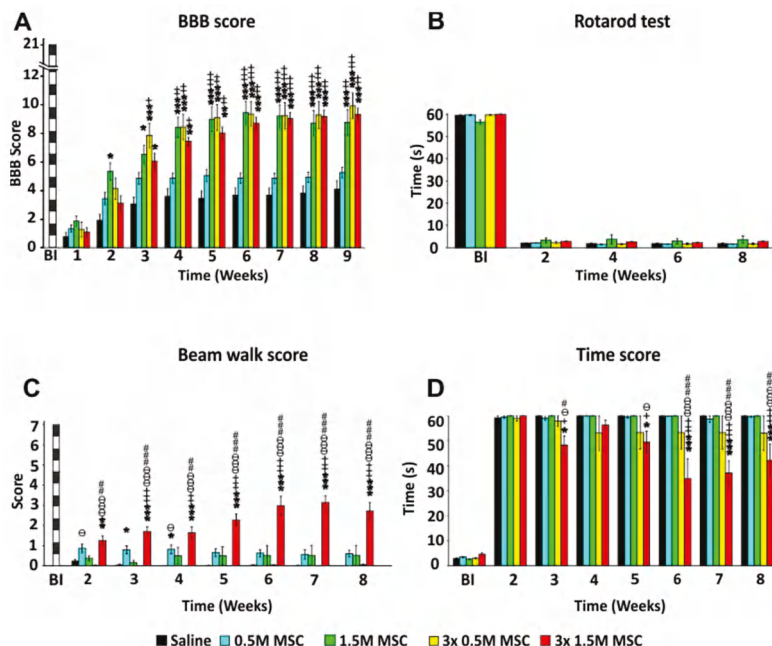


**Figure 1.** Recovery of locomotor functions following hWJ-MSCs transplantation after SCI. Treatments by a different number of administrated cells. The locomotor skills of saline- or stem cell-treated rats were measured using the BBB (A), rotarod (B), beam walk score (C), and time score (D). Animals treated with a higher single dose and by repetitive dose of hWJ-MSCs achieved significantly higher scores in the open-field BBB test when compared to saline controls and animals treated by 0.5 M hWJ-MSCs (A). Strength and limb coordination was measured by rotarod test (B), where no significant differences were found. The flat beam test (C), which is focused on advanced locomotor skills, demonstrated significantly higher scores in the group treated by 3 × 1.5 M hWJ-MSCs. Time score (D) reflects the time the rat needs to cross the beam and shows the overall stability of the rat. Animals treated by 3 × 1.5 M achieved significantly better times than the rest of the rats. \*  $p < 0.05$  versus saline; \*\*  $p < 0.01$  versus saline; \*\*\*  $p < 0.001$  versus saline; +  $p < 0.05$  versus 0.5 M MSCs; ++  $p < 0.01$  versus 0.5 M MSCs; +++  $p < 0.001$  versus 0.5 M MSCs; #  $p < 0.05$  versus 3 × 0.5 M MSCs; ##  $p < 0.01$  versus 3 × 0.5 M MSCs; ###  $p < 0.001$  versus 3 × 0.5 M MSCs; @  $p < 0.05$  versus 1.5 M MSCs; @@  $p < 0.01$  versus 1.5 M MSCs; @@@  $p < 0.001$  versus 1.5 M MSCs. BBB = Basso, Beattie, and Bresnahan test; BI = before injury; MSC = human Wharton Jelly mesenchymal stem cell; SCI = spinal cord injury.

In addition to the beam score, we measured the time needed to cross the beam (maximally for 60 s). During the pre-training, healthy rats were able to cross the beam in approximately 3.0 s (Figure 1D). The measurement was performed weekly starting the second week after SCI. Two weeks after SCI not all the rats were able to cross the beam and did not move from the starting line. In the following weeks, a significant improvement was observed between the rats treated by 3 × 1.5 M and the other groups. The best score was achieved in the sixth week in the group 3 × 1.5 M, when rats traversed the beam at an average time of  $34.9 \pm 7$  s.

(Two-way RM ANOVA, Treatment;  $F = 5.001, p = 0.002$ ; for  $p$  values of post hoc pair-to-pair test, see Supplement 2).

### 2.3. Histology and Immunohistochemistry

#### 2.3.1. Gray and White Matter Sparing

The total area of spared gray/white matter was measured on the 15 cross sections of the spinal cord 9 weeks after the SCI (7 sections cranially and caudally to the center of the lesion, which was determined as the section with the smallest area of the residual spinal cord tissue). Values were averaged and compared to the control, which was set as 100%. Concerning the gray matter preservation (Figure 2A), a significant difference was found between the group  $3 \times 1.5$  M and the control ( $p < 0.05$ ), and a strong trend was observed when compared to the group of 0.5 M ( $p = 0.051$ ). Comparison of the white matter sparing showed no significant difference between the groups as a whole (Figure 2B). Similarly to the gray matter, in the center of the lesion and in the surrounding tissue, we observed significantly more spared white matter in animals treated with  $3 \times 1.5$  M and 1.5 M when compared to the control group and rats treated with 0.5 M.

(Two-way RM ANOVA, Treatment; gray matter –  $F = 3.341, p = 0.03$ , white matter –  $F = 1.290, p = 0.307$ ; for  $p$  values of post hoc pair-to-pair test, see Supplement 3).

#### 2.3.2. Astrogliosis and Distribution of Protoplasmic Astrocytes

The total area of the glial scar formed around the central cavity was measured on 15 GFAP-CY3 stained cross sections of the spinal cord 9 weeks after the SCI (7 sections cranially and caudally to the center of the lesion, which was determined as the section with the smallest area of the residual spinal cord tissue). Values were averaged and are presented as a ratio of scar tissue to the whole section in percentages (Figure 2C). Groups treated with  $3 \times 1.5$  M as well as 0.5 M and 1.5 M had a significantly smaller GFAP positive area around the main cavity compared to the control group ( $p < 0.05$ ). The group treated by 0.5 M showed no significant difference compared to saline-treated rats.

(Two-way RM ANOVA, Treatment;  $F = 4.026, p = 0.015$ ; for  $p$  values of post hoc pair-to-pair test, see Supplement 3).

On the same slices, the number of protoplasmic astrocytes was counted (Figure 2D). Rats treated by 0.5 M and 1.5 M as well as  $3 \times 1.5$  M had a significantly lower number of protoplasmic astrocytes compared to the control group.

(Two-way RM ANOVA, Treatment;  $F = 3.997, p = 0.015$ ; for  $p$  values of post hoc pair-to-pair test, see Supplement 3).

#### 2.3.3. Axonal Sprouting

Axonal sprouting was determined as the number of GAP43<sup>+</sup> fibers, which were manually counted on the 15 cross sections of the spinal cord 9 weeks after the SCI (7 sections cranially and caudally to the center of the lesion, which was determined as the section with the smallest area of the residual spinal cord tissue). Values were averaged and compared to the control, which was set as 100%. The significant effect of the cell treatment was not only dose-dependent, but further improved after repeated application (Figure 2E). Treatment with the lowest dose—0.5 M, had no or minimal effect on axonal sprouting ( $102 \pm 4\%$ ). In the other cell-treated groups, the number of positive fibers was gradually increasing with the higher number of grafted cells (1.5 M  $140 \pm 4\%$ ), and repeated application had a significantly stronger effect than a single dose ( $3 \times 0.5$  M  $168 \pm 10\%$ ) and ( $3 \times 1.5$  M  $212 \pm 18\%$ ) ( $p < 0.05$ ).

(One-way ANOVA, Treatment;  $H_4 = 21.844, p < 0.001$ ).

## 2.4. qRT-PCR

### Expression of Intrinsic Genes after Stem Cell Transplantation, after SCI

Samples from the spinal cord for qPCR analysis were taken 4 (Figure 3A) and 9 weeks (Figure 3B) after the cell transplantation. A comparison was made against the saline-treated rats, which were set as 0. The expression of genes, which are related to the M1 (*Irf5*, *Cd86*) and M2 (*Mrc1*, *Cd163*) macrophage phenotypes, astrogliosis (*Gfap*), and apoptosis (*Casp3*), was analyzed. Pro-inflammatory genes *Irf5* and *CD86* were, 4 weeks after the transplantation of the cells, insignificantly upregulated in the groups treated by 1.5 M and 3 × 0.5 M but, 9 weeks after the transplantation, were downregulated in all groups except the 3 × 0.5 M. Statistical significance against the saline group was found only in the group 3 × 1.5 M ( $p < 0.05$ ).

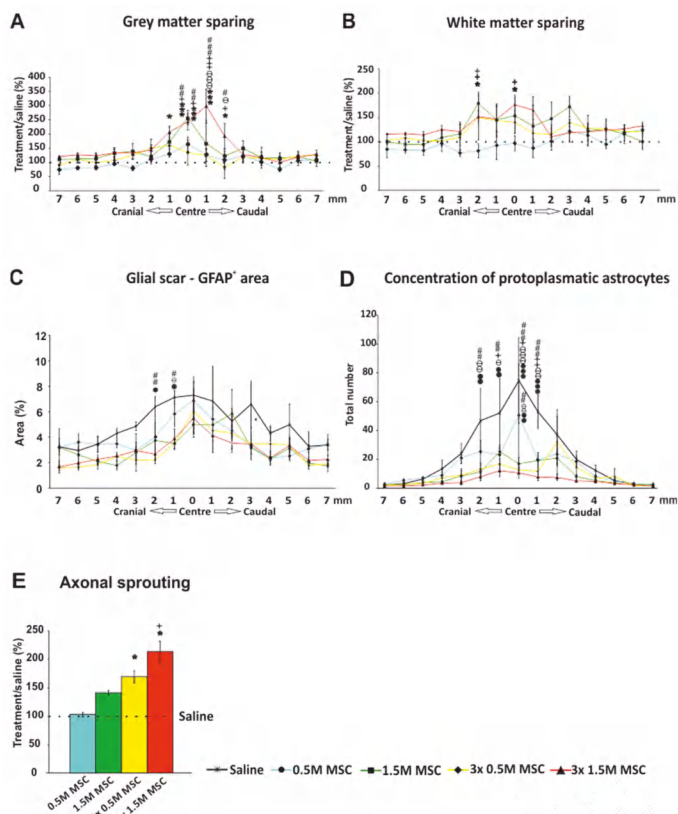


**Figure 2.** Immunohistochemical and histological analysis 9 weeks after SCI. The total area of spared gray matter was significantly higher in the group treated by 3 × 1.5 M hWJ-MSCs, mainly in the slices near the center of the lesion (A). Analysis of the white matter sparing showed similar results to the gray matter, resulting in mild yet still significant preservation in the group treated by 3 × 1.5 M hWJ-MSCs (B). The GFAP-CY3 positive area showing the glial scar formation around the central cavity was slightly smaller in all treated groups compared to the control, with a significant difference near the center of the lesion against the groups treated by repetitive doses (C). The average number of protoplasmic astrocytes near the center of the lesion was significantly higher in the control group than in the cell-treated groups (D). The average number (15 slices per rat; 5 rats) of GAP43+ fibers presented as relative when compared to the control, which is set as 100%. A gradually significant increase with the total number of applied MSCs is shown (E).

The dotted line represents the value of saline-treated rats (100%). \*  $p < 0.05$  versus saline; \*\*\*  $p < 0.001$  versus saline; +  $p < 0.05$  versus 0.5 M MSCs; ++  $p < 0.01$  versus 0.5 M MSCs; +++  $p < 0.001$  versus 0.5 M MSCs; #  $p < 0.05$  versus  $3 \times 0.5$  M MSCs; ##  $p < 0.01$  versus  $3 \times 0.5$  M MSCs; ###  $p < 0.001$  versus  $3 \times 0.5$  M MSCs; o  $p < 0.05$  versus 1.5 M MSCs; oo  $p < 0.01$  versus 1.5 M MSCs; ooo  $p < 0.001$  versus 1.5 M MSCs; •  $p < 0.05$  versus  $3 \times 1.5$  M MSCs; ••  $p < 0.01$  versus  $3 \times 1.5$  M MSCs; •••  $p < 0.001$  versus  $3 \times 1.5$  M MSCs. MSCs = human Wharton Jelly mesenchymal stem cells; SCI = spinal cord injury; GFAP-CY3 = glial fibrillary acidic protein cyanine 3; GAP43 = growth-associated protein 43.

The anti-inflammatory related genes *Mrc1* and *Cd163* were, 9 weeks after the transplantation, downregulated in all subjected groups with a significant difference in groups  $1 \times 0.5$  M ( $p < 0.05$ ) and  $3 \times 1.5$  M ( $p < 0.001$ ). However, groups treated by a total number of 1.5 M cells (1.5 M and  $3 \times 0.5$  M) were, 4 weeks after transplantation, insignificantly upregulated; thus, their dynamics changed throughout the experiment.

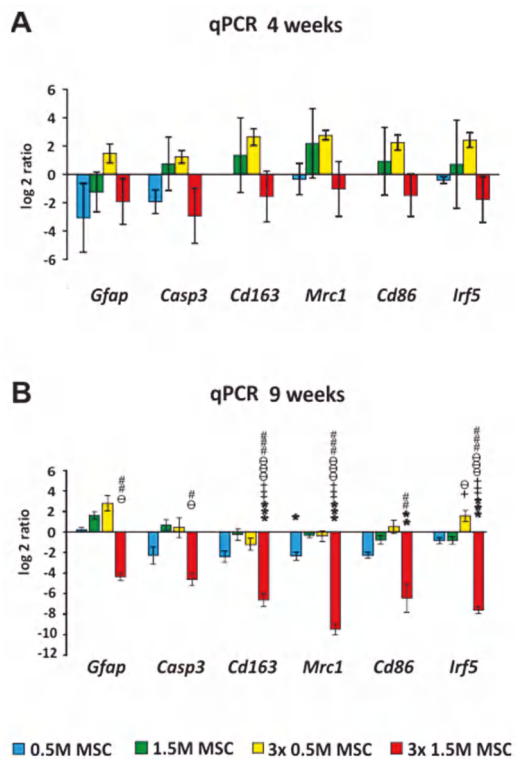


**Figure 3.** mRNA expression of selected genes 4 and 9 weeks after WJ-MSCs transplantation into the SCI. The graphs show the log<sub>2</sub>-fold changes of the  $\Delta\Delta Ct$  values of the indicated genes in comparison to the animals treated with the saline, which were set to 0 and are represented as x axis in the graphs. The expression of genes, which are related to the M1 (*Irf5*, *Cd86*) and M2 (*Mrc1*, *Cd163*) macrophage phenotypes, astrogliosis (*Gfap*), and apoptosis (*Casp3*) are shown 4 weeks after the SCI (A) and 9 weeks after the SCI (B). All of them were significantly downregulated in the group treated by  $3 \times 1.5$  M and remained stable throughout the whole experiment.

Data are expressed as mean  $\pm$  SEM. \* $p < 0.05$  versus saline; \*\* $p < 0.01$  versus saline; \*\*\* $p < 0.001$  versus saline; + $p < 0.05$  versus 0.5 M MSCs; ++ $p < 0.01$  versus 0.5 M MSCs; +++ $p < 0.001$  versus 0.5 M MSCs; # $p < 0.05$  versus  $3 \times 0.5$  M MSCs; ## $p < 0.01$  versus  $3 \times 0.5$  M MSCs; ### $p < 0.001$  versus  $3 \times 0.5$  M MSCs; ø $p < 0.05$  versus 1.5 M MSCs; øø $p < 0.01$  versus 1.5 M MSCs; øøø $p < 0.001$  versus 1.5 M MSCs. MSC: human Wharton Jelly mesenchymal stem cell; SCI: spinal cord injury; *Mrc1*: mannose receptor C type 1; *Casp3*: Caspase-3; *Gfap*: glial fibrillary acidic protein.

Four weeks after the cell implantation, *Gfap*, except in the  $3 \times 0.5$  M group, was downregulated in all groups; 9 weeks after the cell implantation, it remained downregulated only in the  $3 \times 1.5$  M group, with a significant difference that corresponds with the immunohistochemical analysis of the astrogliosis that was lowest in this group. The expression of *Casp3* insignificantly decreased in the 0.5 M and  $3 \times 1.5$  M groups and remained stable throughout the entire experiment.

(One-way ANOVA, Treatment; *Gfap* – H<sub>4</sub> = 18.454,  $p = 0.001$ , *Casp3* – H<sub>4</sub> = 15.153,  $p = 0.004$ , *Cd163* – F = 20.243,  $p < 0.001$ , *Mrc1* – F = 59.317,  $p < 0.001$ , *Cd86* – H<sub>4</sub> = 19.170,  $p < 0.001$ , *Irf5* – F = 47.495,  $p < 0.001$ ; for  $p$  values of post hoc pair-to-pair test, see Supplement 4).

## 2.5. Cell Survival

Survival of the transplanted cells (0.5 M and 1.5 M) was evaluated by staining with the antibody against HuNu, two weeks after the transplantation. Surviving cells were detected as green clusters. Most of the cells remained at the site of the implantation—caught between the folds of arachnoidea mater in the cauda equinae. There was, however, a difference in the number of cells present. While after 0.5 M application only a few cells were detected, the application of 1.5 M resulted in a greater number of trapped cells. No homing into the lesion site was observed.

## 3. Discussion

The present study aimed to determine the effect and optimal dosage of transplanted stem cells derived from Wharton's jelly into injured spinal cord. Cultured human WJ-MSCs were intrathecally implanted into spinal cord compression lesions of Wistar rats, and the impact on the recovery of the spinal cord tissue was described.

We compared single and triple repeated intrathecal delivery of hWJ-MSCs with a different number of cells (0.5 M and 1.5 M) in each application. Since cell survival in the vertebral canal is rather low [20,22,23], we hypothesized that, by repeated application, the trophic and immunomodulatory effect of the cells can be substantially increased. The route of MSC delivery varies in previous studies, and local or systemic approaches have been proposed and investigated, but the optimal method of delivery has yet to be determined.

We have chosen intrathecal delivery in our experiments. It eliminates the risk of direct surgical implantation without the need for deep analgesia and anaesthesia for the animal, and yet still guarantees a wide dissemination of cells through the subarachnoid space and around the lesion site [24]. The procedure can be done either by lumbar puncture or by suboccipital puncture of the cisterna magna. In our study, we chose lumbar puncture because it is more relevant to clinical medicine, where, especially in adult neurosurgery, it is an everyday occurrence. Additionally, repeated application via lumbar puncture is a lesser burden for animals than a suboccipital puncture of the cisterna magna. Since cell survival in the vertebral canal is rather low (approximately 14 days), repeated application substantially increased the trophic and immunomodulatory effect of the cells and could even be feasible in human patients.

Despite reports showing that intralesional transplantation provides better accumulation of the effector cells in the injury site [25], meta-analyses did not prove any statistical significant differences in locomotor improvement after delivery of MSCs using intravenous, intraparenchymal, and intrathecal administration [15,26]. Moreover, Pal et al. compared hBM-MSC injection into the spinal cord parenchyma and application via lumbar puncture. They reported that, while both i.t. and

intraspinal transplantation showed improvement in histological evaluation, only the i.t.-transplanted group performed better in all behavioral tests [27]. Recently intranasal delivery of BM-MSCs with their successful migration into the spinal cord canal was reported, but compared to direct intrathecal delivery, there was significantly lower number of cells detected and the locomotor recovery was insignificant [28].

Besides the determination of transplantation route, optimal timing of transplantation is one of the most important factors to be considered. The subacute phase, defined as the time period between 3 and 14 days post-SCI in rodents and 2 months in humans showed better cell survival as a result of the reduced aggressive host environment due to the inflammation response, and when compared to the acute phase and unlike the chronic phase, the glial scar formation has not yet been formed [18,29,30]. Therefore, we had cell application start 7 days after lesion induction. Another disputable question remains regarding the appropriate dosage of transplanted cells. The vast majority of studies proving the effect of MSCs on SCI have focused only on single transplantation of 0.2–1 M of cells [31–35]. Alternatively, repetition and higher dosage is considered to be superior to single delivery. Li et al. compared single, triple, and quintuple transplantations of 1 M BM-MSCs and concluded that triple delivery is the best [36]. Similar results were found by Cizkova et al. with the conclusion that high doses and/or repetition of the transplantation may lead to higher efficacy of cell survival, more engraftment into the host tissue, and an improvement in functional outcome.

No such experimental study with hWJ-MSCs has been conducted, so evidence of the effect of single vs. multiple deliveries, together with various amounts of cells, is in high demand.

Analysis of behavioral tests revealed that functional recovery of hind limb motion in treated rats was partially dependent on the number of applied cells, which is in agreement with findings by Himes et al., who used a similar number of hBM-MSCs [32]. Whereas the single dose of 0.5 M hWJ-MSCs showed no significant difference in BBB testing, other groups achieved similar significantly higher scores, regardless of repeated application. However, in the advanced motor function testing, such as crossing the beam, the effect was visible in animals with repeated injections. The dose-dependent effect of hBM-MSCs in more advanced motor tests (grid walk and inclined plane test) was also observed by Pal et al. who compared doses of 2 M and 5 M cells/kg body weight [27]. No effect was detected in the rotarod test, which requires a higher level of motor coordination and stepping. Our experimental setting was comparable to our previous study with the hBM-MSCs [20]. However, application of 0.5 M hBM-MSCs resulted in functional improvement similar to the one observed with single application of 1.5 M hWJ-MSCs. It is generally accepted that, due to the low ability of MSCs to survive in the donor tissue, as confirmed in our study, and their limited in vivo differentiation, the main therapeutic effect of MSCs lies in their ability to secrete trophic factors promoting local neovascularization, inhibiting cell death, and suppressing the immune response [37]. We did not perform any in vitro analysis of growth factors and bioactive molecules, which would compare the paracrine effect of hWJ-MSCs and hBM-MSCs. Though various studies include the analysis of secretory factors, results are not unified in terms of the strength of secretion of regeneration-associated neurotrophic factors. Balasubramanian et al. found that WJ-derived cells secreted higher levels of neurotrophic factors bFGF, NGF, NT3, NT4, and GDNF compared to BM and adipose tissue (AT)-derived cells [38]. Hsieh and colleagues compared MSCs derived from Wharton's jelly and bone marrow regarding their ability to regenerate infarcted myocardia; they described secretome differences that make Wharton's jelly-derived MSCs a more angiogenic, neuroprotective, and neurogenic option [39]. On the other hand, Amable et al. reported that WJ-MSCs secreted very low concentrations of VEGF-4.070 and 4.614 times lower than BM- and adipose tissue MSCs (AT-MSCs), respectively [10]. Most studies agree that hWJ-MSCs have a more effective immunosuppressive function compared to hBM-MSCs [40,41]. However, all those studies were performed in vitro, where the proliferation rate of the WJ-MSCs (cell doubling time 40 h) is much higher than the hBM-MSC doubling time of 70 h [42], resulting in more paracrine effective cells in the medium and thus higher overall secretome. Our results confirmed relatively short population doubling

time of hWJ-MSCs, which was approximately 34 h compared to 84 h of hBM-MSCs (see Supplement 1, Figure S1). Another possible explanation of the lesser effect of the same number of transplanted cells in our study is the smaller size of WJ-MSCs when compared with BM-MSCs, which can result in higher dilution in the host environment, or even leakage through the canal after the lumbar puncture. On the other hand, due to a smaller size, more cells can fit into small volumes and these cells can more easily spread through the CSF in the canal. Therefore, the dose-dependent effect can be more visible in the case of hWJ-MSCs than in hBM-MSCs.

Immunohistochemical analyses showed that transplantation of hWJ-MSCs facilitates axonal sprouting and plays a role in decreasing glial scar formation. Astrogliosis, which is closely bound up with reactive astrocytes was significantly less present in cell-treated rats. Axonal sprouting was increasingly enhanced as the total number of transplanted cells increased. This is in agreement with the findings of Li et al., who described the effect of WJ-MSCs in SCI as mainly due to the decreased expression of interleukin-1 $\beta$  (IL-1 $\beta$ ) and the increased expression of nerve growth factor (NGF), which plays an important role in axonal growth [43]. The same trend was present in the measuring of the white and gray matter preservation, which revealed a strong neuroprotective effect in gray matter, mainly in the center of the lesion and only in groups with the highest number of treated cells. A significant effect on tissue sparing was observed only in animals treated by single or triple implantation of 1.5 M hWJ-MSCs. All these finding are in contrast with behavioral analysis, where no differences between higher dosage cell-treated animal groups were found in the BBB test. It is evident that, for the simple locomotor test, such as the BBB test, a threshold of a minimum number of cells is required to trigger functional improvement. However, closer analyses of tissue microstructure have shown that an increased number of cells applied repeatedly further improve the neuroprotective and neuroregenerative properties of the hWJ-MSCs.

Overall, our results proved a substantial benefit from treatment of SCI with MSCs and are in many ways comparable to other studies that used human BM-MSCs, AT-MSCs, or UC-MSCs in rats [27,32,35,44–49] or dogs [50,51]. Meta-analysis from 2014 by Oliveri confirmed the beneficial effect of MSCs in traumatic spinal cord injury but could not detect any clear association between locomotor recovery and MSCs isolated from specific tissues [15]. Still, because of the relative easy harvesting of hWJ-MSCs from otherwise discarded tissue, we believe that hWJ-MSCs are the most suitable for potential wide use in clinics.

Most of the clinical studies with mesenchymal stromal stem cells were performed on chronic lesions with total paraplegia (Frankel A, AIS A), lasting months after the primary injury [52]. Despite some reports that note some neurological improvement after transplantation [53], the effect of WJ-MSCs in the chronic model of SCI must be elucidated. However, we suggest that this treatment should be proposed for patients with spinal trauma that causes “only” compression of the spinal cord, which is visible in the magnetic resonance imaging (MRI) of T2 and STIR sequences as a hyper intense area of the spinal cord—myelopathy. These patients usually have preserved residual motor and sensory functions (Frankel B and above) and have a good prognosis of recovery when the best medical therapy is applied. hWJ-MSCs, since they are allogenic, can be easily up-scaled, prepared in advance, cryopreserved, and made ready for use in a relatively short time. Therefore, repeated application of hWJ-MSCs could add another piece to the yet unsolvable puzzle of how to treat SCI.

#### 4. Materials and Methods

##### 4.1. Cell Culture

The collection and isolation of WJ-MSCs were performed by explant culture according to the methodology described by Koci et al. [54]. In brief, human WJ-MSCs were obtained from discarded human umbilical cords from healthy full-term neonates after spontaneous delivery, with the informed consent of the donors using the guidelines approved by the Institutional Committee at University Hospital (Pilsen, Czech Republic). About 10–15 cm per umbilical cord were aseptically

transported into sterile phosphate buffered saline (PBS; IKEM, Prague, Czech Republic) with antibiotic-antimycotic solution (Sigma, St. Louis, MO, USA) at 4 °C. After the removal of blood vessels, the remaining tissue was cut into small pieces (cca 1 mm<sup>3</sup>) and put into Nunc culture dishes (Schoeller, Thermo Fisher Scientific, Waltham, MA, USA) containing the alpha-Minimum Essential Medium (αMEM; East Port, Prague, Czech Republic), supplemented with 5% platelet lysate (IKEM, Prague, Czech Republic) and gentamicin 10 mg/mL (Sandoz, Holzkirchen, Germany), and cultivated at 37 °C in a humidified atmosphere containing 5% CO<sub>2</sub>. After 10 days, the explants were removed from the culture dishes, and the remaining adherent cells were cultured for 3 weeks or until 90% confluence and passaged using 0.05% Trypsin/EDTA (Life Technologies, Carlsbad, CA, USA). After passaging, the cells were seeded into culture flasks (Nunc; Schoeller, Thermo Fisher Scientific, Waltham, MA, USA) at a density of  $5 \times 10^3$  cells/cm<sup>2</sup>. The medium was changed twice a week. Cells of the 3rd passage were characterized by flow cytometry and their growth properties and differentiation potential was assessed (see Supplementary Material 1). For the transplantation, cells in the 3rd passage were used.

#### 4.2. Animals

As an experimental model, adult Wistar male rats were used. Animals were obtained from the breeding facility of the Academy of Sciences of the Czech Republic. All experiments were performed in accordance with the European Communities Council Directive of 22nd of September 2010 (2010/63/EU) regarding the use of animals in research and were approved 8 September 2014 by the Professional Committee for Laboratory Animal Welfare of the Institute of Experimental Medicine, Academy of Sciences of the Czech Republic in Prague as the experimental project number 53/2014. All animals were approximately 10 weeks old, with weight varying between 275–305 g ( $n = 90$ ). The first group of animals ( $n = 47$ ), surviving 9 weeks, was used for behavioral testing, histological, immunohistochemical, and qPCR analysis (9W). The second group of animals ( $n = 39$ ) was used for qPCR evaluation 4 weeks (4W) after SCI and was not included in behavioral testing. An additional four animals in the two groups ( $n = 4$ ) were used for evaluation of surviving cells two weeks after transplantation of 0.5 and 1.5 M hWJ-MSCs.

#### 4.3. Spinal Cord Injury Model

The surgical procedure was performed in an operating theatre under standard conditions. As a model of SCI, a balloon-induced ischemic-compression lesion was used [21,55]. At the beginning of the surgery, the animals were anesthetized with Isoflurane (Forane; Abbott Laboratories, Queenborough, UK), analgesia was induced by intramuscular injection of carprofen (Rimadyl, Cymedica, Horovice, Czech Republic, 4 mg/kg), and surgical prophylaxis was maintained by intramuscular injection gentamicin sulfate (Sandoz, Holzkirchen, Germany 5 mg/kg). After the skin incision, the paravertebral muscles were separated at the level of thoracic vertebra T7–T12 and laminectomy of T 10 was performed. A sterile 2-french Fogarty catheter was carefully inserted into the epidural space until the center of the balloon rested on the level of thoracic vertebra 8 (T8). The balloon was rapidly inflated with 15 µL saline and kept for 5 min. During this procedure, 3% isoflurane in air was administered at a flow rate of 0.3 L/min, and the animal's body temperature was kept at 37 °C with a heating pad. After 5 min, the catheter was rapidly deflated and removed, and separated muscles and incised skin were sutured by single non-absorbable stitches. The lesioned animals were assisted in feeding and urination until they had recovered sufficiently to perform these functions on their own. The animals received gentamicin sulfate (5 mg/kg) for 7 days to prevent postoperative infections and were allowed to feed and drink ad libitum.

#### 4.4. Transplantation

Transplantation of hWJ-MSCs was performed on the 7th, 14th, and 21st day after the SCI. Treatment was given intrathecally by a lumbar puncture between L3 and L4 or L4 and L5 through

a 25 G needle under the short-time general anaesthesia described above. Firstly, a small volume of CSF was taped as a proof of the subarachnoid space. During the injection of the saline with hWJ-MSCs there was a movement of the rats tail as a response to irritation of the nerve roots of cauda equina. After injection the needle was rested *in situ* for 30 s to prevent backflow of the content. Animals were divided into 5 groups with variable treatment. The first group (**0.5 M**) received a single transplantation of 0.5 M hWJ-MSCs in 50 µL saline on the 7th day after SCI ( $n = 12$ ). The second group (**1.5 M**) received a single transplantation of 1.5 M hWJ-MSCs in 50 µL saline on the 7th day after SCI ( $n = 9$ ). The third group (**3 × 0.5 M**) received a triple transplantation of 0.5 M hWJ-MSCs in 50 µL saline on the 7th, 14th, and 21st day after SCI ( $n = 8$ ). The fourth group (**3 × 1.5 M**) received a triple transplantation of 1.5 M hWJ-MSCs in 50 µL saline on the 7th, 14th, and 21st day after SCI ( $n = 7$ ). The control group (**saline**) received a single or triple injection of 50 µL saline on the 7th (14th and 21st) day after SCI ( $n = 11$ ). No differences between simple and repetitive transplantation of the saline were found, so the results were pooled together as a single control when compared with other types of treatment. The day before the transplantation, all animals received cyclosporine A by an intraperitoneal injection (10 mg/kg), which continued daily until the end of the experiment.

#### 4.5. Behavioral Analysis

##### 4.5.1. BBB Test

The BBB open field test, originally described by Basso, Beattie, and Bresnahan [56] was used to assess the joint movement, weight support, forelimb-hindlimb coordination, paw placement and stability of the body. The rats were placed on the floor surrounded by boundaries making a rectangular shape. Results were evaluated in the range of 0–21 points: 0 indicated complete lack of motor capability and 21 indicated the best possible score (healthy rat). Measurements were performed every week for 8 weeks starting the first week after SCI.

##### 4.5.2. Rotarod Test

A rotarod unit machine (Ugo Basile, Comerio, Italy) was used to test the advanced degree of motor coordination of the limbs according to the method first described by Dunham and Miya [57]. Ability to balance on a rotating rod was recorded. Each animal was taught this task one week before surgery. Animals were placed on a rotating rod at a fixed speed of 10 rpm before surgery and 5 rpm after surgery and were left to walk for 60 s. There were four trials per day within five consecutive days. Between trials there was always a 5 min break. The latency to fall off the rod onto the floor was measured.

##### 4.5.3. Beam Walk Test

In the flat beam test, we tested the ability to cross a 1 m long narrow beam with a flat surface. Rats were placed on one side of the beam, and on the other side an escape box was placed. The latency and the trajectory to traverse the beam were recorded by a video tracking system (TSE-Systems Inc., Bad Homburg, Germany) for a maximum of 60 s. Performance of locomotor coordination was evaluated using a 0–7 point scale modified from Metz and Whishaw [58].

#### 4.6. Histological and Immunohistochemical Analyses

At the end of the experiment (9 weeks after the SCI), all animals were anesthetized with ketamine (100 mg/kg) and xylazine (20 mg/kg) and transcardially perfused with a phosphate buffer solution (250 mL), followed by a 4% paraformaldehyde solution in a phosphate buffer (250 mL). The spinal cord was dissected and removed from the spinal column and embedded in paraffin wax. Serial cross sections (5 µm thick) were obtained by microtome within a 2-cm-long segment around the center of the lesion. Samples of five animals from each group were analyzed for the total volume of spared white and gray matter, axonal sprouting, and the extent of glial scar. Sections were stained with Luxol fast

blue and Cresyl violet to distinguish the white and gray matter, with anti-GAP43 antibody to evaluate axonal sprouting or by anti-GFAP primary antibody to visualize the glial scar and reactive astrocytes.

#### 4.6.1. Cresyl Violet-Luxol Staining

For visualizing white and gray matter of the spinal cord, Cresyl violet and Luxol fast blue staining were used. Samples from five animals from each group were obtained. Each sample of the spinal cord was cut at 1 mm intervals. A total number of 15 cross sections, including the center of the lesion, were observed with an Axioskop 2 plus microscope (Zeiss, Oberkochen, Germany). Acquired images were analyzed for the total area of spared gray and white matter by ImageJ software (NIH, Bethesda, MD, USA) (Figure 4A).

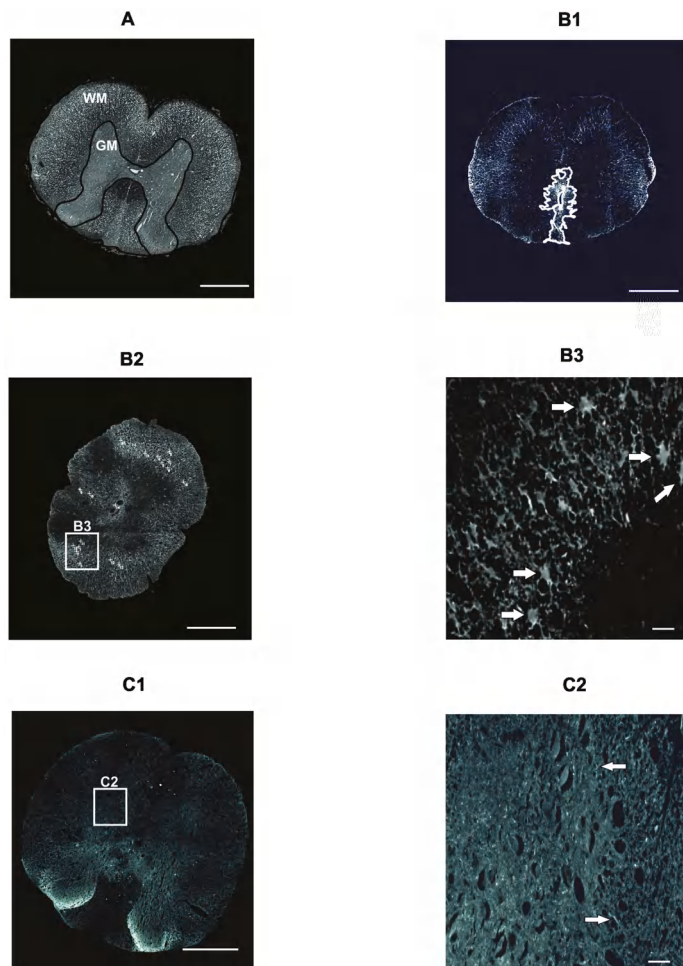


**Figure 4.** Illustrative images of morphometric and immunohistochemical analyses 9 weeks after SCI. Microscopic image of a section stained with Cresyl violet and Luxol fast blue to distinguish the white (WM) and gray (GM) matter (**A**). Scale bar: 500  $\mu$ m. The marked glial scar around the main cavity (**B1**) and the total number of protoplasmatic astrocytes (**B2**) with a detailed inset (**B3**) from slices stained with GFAP-CY3. Scale bars: 500  $\mu$ m (**B1,B2**), 10  $\mu$ m (**B3**). Illustrative image of a section labeled with a GAP43<sup>+</sup> antibody (**C1**) with a detailed inset (**C2**).

Arrows point at GAP43<sup>+</sup> fibers, which were manually counted as described in the Methods section. Scale bars: 500 µm (C1), 20 µm (C2). SCI: spinal cord injury; GM: gray matter; WM: white matter; GFAP-CY3: glial fibrillary acidic protein cyanine 3; GAP43: growth-associated protein 43.

#### 4.6.2. GFAP Staining

To determine the extent of the glial scar, immunohistochemical analysis of a CY3-conjugated primary antibody against GFAP (Sigma, St. Louis, MO, USA) was used. Samples from five animals from each group were obtained. Each sample of the spinal cord was cut at 1 mm intervals. A total number of 15 cross sections, including the center of the lesion, was observed with an Axioskop 2 plus microscope (Zeiss, Oberkochen, Germany). The acquired images were analyzed using ImageJ software (NIH, Bethesda, MD, USA). The GFAP positive area around the central cavity (Figure 4(B1)) together with the number of protoplasmic astrocytes (Figure 4(B2,B3)) was measured on each section.

#### 4.6.3. GAP43 Staining

The newly sprouted axons were visualized immunohistochemically using a primary antibody against GAP43 (Millipore, Billerica, MA, USA). Samples from five animals from each group were obtained. Each sample of the spinal cord was cut at 1 mm intervals. A total number of 15 cross sections, including the center of the lesion, were observed with an Axioskop 2 plus microscope (Zeiss, Oberkochen, Germany). The acquired images were analyzed and the number of GAP43-positive fibers per section was manually counted (Figure 4(C1,C2)).

#### 4.7. qRT-PCR

To evaluate the up- or downregulation of expression rat target genes (*Gfap*, *Mrc1*, *Irf5*, *Cd163*, *Cd86*, *Casp3*) the quantitative real-time reverse transcription polymerase chain reaction (qRT-PCR) was used. Expression was evaluated at 4 and 9 weeks after hWJ-MSC administration (five animals from each group). Studied RNA was isolated from the paraffin cross sections of injured spinal cord around the center of the lesion using the High Pure RNA Paraffin Kit (Roche, Penzberg, Germany) following the manufacturer's recommendations. The amount of RNA was measured by a spectrophotometer (NanoPhotometer™ P-Class, Munchen, Germany). cDNA was obtained from the isolated RNA by a reverse transcription using the Transcriptor Universal cDNA Master (Roche), and a thermal cycler (T100™ Thermal Cycler, Bio-Rad, Hercules, CA, USA). The qPCR chain reactions were performed using cDNA solution, FastStart Universal Probe Master (Roche, Penzberg, Germany) and the following TagMan® Gene Expression Assays (Life Technologies): *Casp3*/Rn00563902\_m1, *Gfap*/Rn00566603\_m1, *Cd86*/Rn00571654\_m1, *Irf5*/Rn01500522\_m1, *Mrc1*/Rn01487342\_m1, and *Cd163*/Rn01492519\_m1.

The final solution of 25 ng extracted RNA diluted in 10 µL of solution was amplified on a StepOnePlus™ real-time PCR cycler (StepOnePlus™, Life Technologies, Carlsbad, CA, USA). The process of amplification was repeatedly performed under the same standard conditions: 120 s at 50 °C, 300 s at 95 °C, followed by 40 cycles of 15 s at 95 °C and 60 s at 60 °C. Each array included also a negative control (water). As a reference gene, *Gapdh* was used. The ΔΔCt method was used for relative quantification of gene expression. All results were analyzed with StepOnePlus® software (StepOnePlus™, Life Technologies, Carlsbad, CA, USA). Differences between the transplanted and control (saline) groups were analyzed for statistical significance with ΔCt values level, using a one-way ANOVA test with a post hoc pair-to-pair test. Differences were considered statistically significant if  $p < 0.05$ . Data are expressed as the mean ± the standard error of mean. The values of saline-treated animals were set as zero.

#### 4.8. Statistical Analyses

Presented graphs with obtained data are shown as the mean  $\pm$  SEM. The statistical significance between the groups treated by WJ-MSCs and the saline (control) group was assessed using either one-way ANOVA, or two-way ANOVA in the case of a second factor (time). Differences between the groups in behavioral tests and in areal measuring of the gray/white matter sparing and GFAP positive area of glial scar were assessed by two-way repeated measurement (RM) ANOVA. The Student–Newman–Keuls (SNK) post hoc pair-to-pair test was used to specify for which groups and at which time points the changes were significant. Statistical evaluation of the expression of the rat target genes was performed with one-way ANOVA test with a post hoc pair-to-pair test. In case of non-parametric values Kruskal–Wallis one-way ANOVA on ranks test was used. (All in SigmaStat 3.1, Sistat Software Inc., San Jose, CA, USA). Differences were considered statistically significant if  $p < 0.05$ .

### 5. Conclusions

Implantation of human MSCs derived from Wharton’s jelly improves functional outcome, by modulating the inflammatory response, inducing axonal sprouting and remodeling the glial scar. The effect is dose-dependent, with the best result achieved by repeated delivery.

**Supplementary Materials:** Supplementary materials can be found at <http://www.mdpi.com/1422-0067/19/5/1503/s1>.

**Author Contributions:** P.K.: study conception and design, experimentation, collection and/or assembly of data, data analysis and interpretation, manuscript writing, and final approval of the manuscript; I.V.: study conception and design, and provision of study material; J.R.: study conception and design; L.M.U.: study conception and design; K.Z.: collection and/or assembly of data; J.D.: collection and/or assembly of data; Z.K.: collection and/or assembly of data, data analysis and interpretation, and manuscript writing; K.T.: collection and/or assembly of data; S.K.: qRT PCR data analysis and interpretation, manuscript writing; S.R.: study conception and design, and financial support; P.J.: study conception and design, data analysis and interpretation, manuscript writing, financial support, and final approval of the manuscript.

**Acknowledgments:** This study was supported by the Czech Science Foundation GACR P304/12/G069; GACR 17-03765S, Operational Programme Research, Development and Education in the framework of the project “Center of Reconstructive Neuroscience”, registration number CZ.02.1.01/0.0/0.0/15\_003/0000419 and from EATRIS-CZ (LM2015064). K.Z., S.K., I.V., L.M.U. and P.J. were members of the BIOCEV (CZ.1.05/1.1.00/02.0109) and their work was supported by the Ministry of Education, Youth and Sports of CR within the LQ1604 National Sustainability Program II (Project BIOCEV-FAR).

**Conflicts of Interest:** The authors declare no conflict of interest.

### References

1. Fawcett, J.W.; Asher, R.A. The glial scar and central nervous system repair. *Brain Res. Bull.* **1999**, *49*, 377–391. [[CrossRef](#)]
2. Zai, L.J.; Wrathall, J.R. Cell proliferation and replacement following contusive spinal cord injury. *Glia* **2005**, *50*, 247–257. [[CrossRef](#)] [[PubMed](#)]
3. Mbalaviele, G.; Jaiswal, N.; Meng, A.; Cheng, L.; Van Den Bos, C.; Thiede, M. Human mesenchymal stem cells promote human osteoclast differentiation from CD34+ bone marrow hematopoietic progenitors. *Endocrinology* **1999**, *140*, 3736–3743. [[CrossRef](#)] [[PubMed](#)]
4. Woodbury, D.; Schwarz, E.J.; Prockop, D.J.; Black, I.B. Adult rat and human bone marrow stromal cells differentiate into neurons. *J. Neurosci. Res.* **2000**, *61*, 364–370. [[CrossRef](#)]
5. Toma, C.; Pittenger, M.F.; Cahill, K.S.; Byrne, B.J.; Kessler, P.D. Human mesenchymal stem cells differentiate to a cardiomyocyte phenotype in the adult murine heart. *Circulation* **2002**, *105*, 93–98. [[CrossRef](#)] [[PubMed](#)]
6. Bai, L.; Lennon, D.P.; Eaton, V.; Maier, K.; Caplan, A.I.; Miller, S.D.; Miller, R.H. Human bone marrow-derived mesenchymal stem cells induce th2-polarized immune response and promote endogenous repair in animal models of multiple sclerosis. *Glia* **2009**, *57*, 1192–1203. [[CrossRef](#)] [[PubMed](#)]
7. Park, C.W.; Kim, K.S.; Bae, S.; Son, H.K.; Myung, P.K.; Hong, H.J.; Kim, H. Cytokine secretion profiling of human mesenchymal stem cells by antibody array. *Int. J. Stem Cells* **2009**, *2*, 59–68. [[CrossRef](#)] [[PubMed](#)]

8. Torres-Espin, A.; Corona-Quintanilla, D.L.; Fores, J.; Allodi, I.; Gonzalez, F.; Udina, E.; Navarro, X. Neuroprotection and axonal regeneration after lumbar ventral root avulsion by re-implantation and mesenchymal stem cells transplant combined therapy. *Neurotherapeutics* **2013**, *10*, 354–368. [CrossRef] [PubMed]
9. Caplan, A.I. Mesenchymal stem cells: Time to change the name! *Stem Cells Transl. Med.* **2017**, *6*, 1445–1451. [CrossRef] [PubMed]
10. Amable, P.R.; Teixeira, M.V.; Carias, R.B.; Granjeiro, J.M.; Borojevic, R. Protein synthesis and secretion in human mesenchymal cells derived from bone marrow, adipose tissue and wharton's jelly. *Stem Cell Res. Ther.* **2014**, *5*, 53. [CrossRef] [PubMed]
11. Zhou, C.; Yang, B.; Tian, Y.; Jiao, H.; Zheng, W.; Wang, J.; Guan, F. Immunomodulatory effect of human umbilical cord wharton's jelly-derived mesenchymal stem cells on lymphocytes. *Cell. Immunol.* **2011**, *272*, 33–38. [CrossRef] [PubMed]
12. Kim, D.W.; Staples, M.; Shinozuka, K.; Pantcheva, P.; Kang, S.D.; Borlongan, C.V. Wharton's jelly-derived mesenchymal stem cells: Phenotypic characterization and optimizing their therapeutic potential for clinical applications. *Int. J. Mol. Sci.* **2013**, *14*, 11692–11712. [CrossRef] [PubMed]
13. Zhang, J.; Li, Y.; Chen, J.; Yang, M.; Katakowski, M.; Lu, M.; Chopp, M. Expression of insulin-like growth factor 1 and receptor in ischemic rats treated with human marrow stromal cells. *Brain Res.* **2004**, *1030*, 19–27. [CrossRef] [PubMed]
14. Bao, X.; Wei, J.; Feng, M.; Lu, S.; Li, G.; Dou, W.; Ma, W.; Ma, S.; An, Y.; Qin, C.; et al. Transplantation of human bone marrow-derived mesenchymal stem cells promotes behavioral recovery and endogenous neurogenesis after cerebral ischemia in rats. *Brain Res.* **2011**, *1367*, 103–113. [CrossRef] [PubMed]
15. Oliveri, R.S.; Bello, S.; Biering-Sorensen, F. Mesenchymal stem cells improve locomotor recovery in traumatic spinal cord injury: Systematic review with meta-analyses of rat models. *Neurobiol. Dis.* **2014**, *62*, 338–353. [CrossRef] [PubMed]
16. Saito, F.; Nakatani, T.; Iwase, M.; Maeda, Y.; Murao, Y.; Suzuki, Y.; Fukushima, M.; Ide, C. Administration of cultured autologous bone marrow stromal cells into cerebrospinal fluid in spinal injury patients: A pilot study. *Restor. Neurol. Neurosci.* **2012**, *30*, 127–136. [PubMed]
17. Forostyak, S.; Jendelova, P.; Sykova, E. The role of mesenchymal stromal cells in spinal cord injury, regenerative medicine and possible clinical applications. *Biochimie* **2013**, *95*, 2257–2270. [CrossRef] [PubMed]
18. Cizkova, D.; Novotna, I.; Slovinska, L.; Vanicky, I.; Jergova, S.; Rosocha, J.; Radonak, J. Repetitive intrathecal catheter delivery of bone marrow mesenchymal stromal cells improves functional recovery in a rat model of contusive spinal cord injury. *J. Neurotrauma* **2011**, *28*, 1951–1961. [CrossRef] [PubMed]
19. Cheng, I.; Mayle, R.E.; Cox, C.A.; Park, D.Y.; Smith, R.L.; Corcoran-Schwartz, I.; Ponnusamy, K.E.; Oshtory, R.; Smuck, M.W.; Mitra, R.; et al. Functional assessment of the acute local and distal transplantation of human neural stem cells after spinal cord injury. *Spine J.* **2012**, *12*, 1040–1044. [CrossRef] [PubMed]
20. Urdzikova, L.M.; Ruzicka, J.; LaBagnara, M.; Karova, K.; Kubinova, S.; Jirakova, K.; Murali, R.; Sykova, E.; Jhanwar-Uniyal, M.; Jendelova, P. Human mesenchymal stem cells modulate inflammatory cytokines after spinal cord injury in rat. *Int. J. Mol. Sci.* **2014**, *15*, 11275–11293. [CrossRef] [PubMed]
21. Vanicky, I.; Urdzikova, L.; Saganova, K.; Cizkova, D.; Galik, J. A simple and reproducible model of spinal cord injury induced by epidural balloon inflation in the rat. *J. Neurotrauma* **2001**, *18*, 1399–1407. [CrossRef] [PubMed]
22. Antonic, A.; Sena, E.S.; Lees, J.S.; Wills, T.E.; Skeers, P.; Batchelor, P.E.; Macleod, M.R.; Howells, D.W. Stem cell transplantation in traumatic spinal cord injury: A systematic review and meta-analysis of animal studies. *PLoS Biol.* **2013**, *11*, e1001738. [CrossRef] [PubMed]
23. Ruzicka, J.; Machova-Urdzikova, L.; Gillick, J.; Amemori, T.; Romanyuk, N.; Karova, K.; Zaviskova, K.; Dubisova, J.; Kubinova, S.; Murali, R.; et al. A comparative study of three different types of stem cells for treatment of rat spinal cord injury. *Cell Transplant* **2017**, *26*, 585–603. [CrossRef] [PubMed]
24. Amemori, T.; Ruzicka, J.; Romanyuk, N.; Jhanwar-Uniyal, M.; Sykova, E.; Jendelova, P. Comparison of intraspinal and intrathecal implantation of induced pluripotent stem cell-derived neural precursors for the treatment of spinal cord injury in rats. *Stem Cell Res. Ther.* **2015**, *6*, 257. [CrossRef] [PubMed]
25. Paul, C.; Samdani, A.F.; Betz, R.R.; Fischer, I.; Neuhuber, B. Grafting of human bone marrow stromal cells into spinal cord injury: A comparison of delivery methods. *Spine* **2009**, *34*, 328–334. [CrossRef] [PubMed]

26. Sareen, D.; Gowing, G.; Sahabian, A.; Staggenborg, K.; Paradis, R.; Avalos, P.; Latter, J.; Ornelas, L.; Garcia, L.; Svendsen, C.N. Human induced pluripotent stem cells are a novel source of neural progenitor cells (iNPCs) that migrate and integrate in the rodent spinal cord. *J. Comp. Neurol.* **2014**, *522*, 2707–2728. [CrossRef] [PubMed]
27. Pal, R.; Gopinath, C.; Rao, N.M.; Banerjee, P.; Krishnamoorthy, V.; Venkataramana, N.K.; Tote, S. Functional recovery after transplantation of bone marrow-derived human mesenchymal stromal cells in a rat model of spinal cord injury. *Cytotherapy* **2010**, *12*, 792–806. [CrossRef] [PubMed]
28. Ninomiya, K.; Iwatsuki, K.; Ohnishi, Y.; Ohkawa, T.; Yoshimine, T. Intranasal delivery of bone marrow stromal cells to spinal cord lesions. *J. Neurosurg. Spine* **2015**, *23*, 111–119. [CrossRef] [PubMed]
29. Okada, S.; Ishii, K.; Yamane, J.; Iwanami, A.; Ikegami, T.; Katoh, H.; Iwamoto, Y.; Nakamura, M.; Miyoshi, H.; Okano, H.J.; et al. In vivo imaging of engrafted neural stem cells: Its application in evaluating the optimal timing of transplantation for spinal cord injury. *FASEB J.* **2005**, *19*, 1839–1841. [CrossRef] [PubMed]
30. Parr, A.M.; Kulbatski, I.; Tator, C.H. Transplantation of adult rat spinal cord stem/progenitor cells for spinal cord injury. *J. Neurotrauma* **2007**, *24*, 835–845. [CrossRef] [PubMed]
31. Chen, C.; Chen, F.; Yao, C.; Shu, S.; Feng, J.; Hu, X.; Hai, Q.; Yao, S.; Chen, X. Intrathecal injection of human umbilical cord-derived mesenchymal stem cells ameliorates neuropathic pain in rats. *Neurochem. Res.* **2016**, *41*, 3250–3260. [CrossRef] [PubMed]
32. Himes, B.T.; Neuhuber, B.; Coleman, C.; Kushner, R.; Swanger, S.A.; Kopen, G.C.; Wagner, J.; Shumsky, J.S.; Fischer, I. Recovery of function following grafting of human bone marrow-derived stromal cells into the injured spinal cord. *Neurorehabilit. Neural Repair* **2006**, *20*, 278–296. [CrossRef] [PubMed]
33. Amemori, T.; Jendelova, P.; Ruzickova, K.; Arboleda, D.; Sykova, E. Co-transplantation of olfactory ensheathing glia and mesenchymal stromal cells does not have synergistic effects after spinal cord injury in the rat. *Cytotherapy* **2010**, *12*, 212–225. [CrossRef] [PubMed]
34. Cho, S.R.; Kim, Y.R.; Kang, H.S.; Yim, S.H.; Park, C.I.; Min, Y.H.; Lee, B.H.; Shin, J.C.; Lim, J.B. Functional recovery after the transplantation of neurally differentiated mesenchymal stem cells derived from bone marrow in a rat model of spinal cord injury. *Cell Transplant.* **2009**, *18*, 1359–1368. [CrossRef] [PubMed]
35. Hu, S.L.; Luo, H.S.; Li, J.T.; Xia, Y.Z.; Li, L.; Zhang, L.J.; Meng, H.; Cui, G.Y.; Chen, Z.; Wu, N.; et al. Functional recovery in acute traumatic spinal cord injury after transplantation of human umbilical cord mesenchymal stem cells. *Crit. Care Med.* **2010**, *38*, 2181–2189. [CrossRef] [PubMed]
36. Li, H.; Wen, Y.; Luo, Y.; Lan, X.; Wang, D.; Sun, Z.; Hu, L. Transplantation of bone marrow mesenchymal stem cells into spinal cord injury: A comparison of delivery different times. *Zhongguo Xiu Fu Chong Jian Wai Ke Za Zhi* **2010**, *24*, 180–184. [PubMed]
37. Bollini, S.; Gentili, C.; Tasso, R.; Cancedda, R. The regenerative role of the fetal and adult stem cell secretome. *J. Clin. Med.* **2013**, *2*, 302–327. [CrossRef] [PubMed]
38. Balasubramanian, S.; Thej, C.; Venugopal, P.; Priya, N.; Zakaria, Z.; Sundarraj, S.; Majumdar, A.S. Higher propensity of wharton’s jelly derived mesenchymal stromal cells towards neuronal lineage in comparison to those derived from adipose and bone marrow. *Cell Biol. Int.* **2013**, *37*, 507–515. [CrossRef] [PubMed]
39. Hsieh, J.Y.; Wang, H.W.; Chang, S.J.; Liao, K.H.; Lee, I.H.; Lin, W.S.; Wu, C.H.; Lin, W.Y.; Cheng, S.M. Mesenchymal stem cells from human umbilical cord express preferentially secreted factors related to neuroprotection, neurogenesis, and angiogenesis. *PLoS ONE* **2013**, *8*, e72604. [CrossRef] [PubMed]
40. Drela, K.; Lech, W.; Figiel-Dabrowska, A.; Zychowicz, M.; Mikula, M.; Sarnowska, A.; Domanska-Janik, K. Enhanced neuro-therapeutic potential of wharton’s jelly-derived mesenchymal stem cells in comparison with bone marrow mesenchymal stem cells culture. *Cytotherapy* **2016**, *18*, 497–509. [CrossRef] [PubMed]
41. Shi, C. Recent progress toward understanding the physiological function of bone marrow mesenchymal stem cells. *Immunology* **2012**, *136*, 133–138. [CrossRef] [PubMed]
42. Li, X.; Bai, J.; Ji, X.; Li, R.; Xuan, Y.; Wang, Y. Comprehensive characterization of four different populations of human mesenchymal stem cells as regards their immune properties, proliferation and differentiation. *Int. J. Mol. Med.* **2014**, *34*, 695–704. [CrossRef] [PubMed]
43. Li, C.; Chen, X.; Qiao, S.; Liu, X.; Liu, C.; Zhu, D.; Su, J.; Wang, Z. Effects of wharton’s jelly cells of the human umbilical cord on acute spinal cord injury in rats, and expression of interleukin-1beta and nerve growth factor in spinal cord tissues. *Artif. Cells Nanomed. Biotechnol.* **2016**, *44*, 1254–1258. [CrossRef] [PubMed]

44. Lee, K.H.; Suh-Kim, H.; Choi, J.S.; Jeun, S.S.; Kim, E.J.; Kim, S.S.; Yoon, D.H.; Lee, B.H. Human mesenchymal stem cell transplantation promotes functional recovery following acute spinal cord injury in rats. *Acta Neurobiol. Exp.* **2007**, *67*, 13–22.
45. Nakajima, H.; Uchida, K.; Guerrero, A.R.; Watanabe, S.; Sugita, D.; Takeura, N.; Yoshida, A.; Long, G.; Wright, K.T.; Johnson, W.E.; et al. Transplantation of mesenchymal stem cells promotes an alternative pathway of macrophage activation and functional recovery after spinal cord injury. *J. Neurotrauma* **2012**, *29*, 1614–1625. [CrossRef] [PubMed]
46. Oh, J.S.; Park, I.S.; Kim, K.N.; Yoon, D.H.; Kim, S.H.; Ha, Y. Transplantation of an adipose stem cell cluster in a spinal cord injury. *Neuroreport* **2012**, *23*, 277–282. [CrossRef] [PubMed]
47. Park, S.I.; Lim, J.Y.; Jeong, C.H.; Kim, S.M.; Jun, J.A.; Jeun, S.S.; Oh, W.I. Human umbilical cord blood-derived mesenchymal stem cell therapy promotes functional recovery of contused rat spinal cord through enhancement of endogenous cell proliferation and oligogenesis. *J. Biomed. Biotechnol.* **2012**, *2012*, 362473. [CrossRef] [PubMed]
48. Shang, A.J.; Hong, S.Q.; Xu, Q.; Wang, H.Y.; Yang, Y.; Wang, Z.F.; Xu, B.N.; Jiang, X.D.; Xu, R.X. Nt-3-secreting human umbilical cord mesenchymal stromal cell transplantation for the treatment of acute spinal cord injury in rats. *Brain Res.* **2011**, *1391*, 102–113. [CrossRef] [PubMed]
49. Matyas, J.J.; Stewart, A.N.; Goldsmith, A.; Nan, Z.; Skeel, R.L.; Rossignol, J.; Dunbar, G.L. Effects of bone-marrow-derived msc transplantation on functional recovery in a rat model of spinal cord injury: Comparisons of transplant locations and cell concentrations. *Cell Transplant.* **2017**, *26*, 1472–1482. [CrossRef] [PubMed]
50. Gabr, H.; El-Kheir, W.A.; Farghali, H.A.; Ismail, Z.M.; Zickri, M.B.; El Maadawi, Z.M.; Kishk, N.A.; Sabaawy, H.E. Intrathecal transplantation of autologous adherent bone marrow cells induces functional neurological recovery in a canine model of spinal cord injury. *Cell Transplant.* **2015**, *24*, 1813–1827. [CrossRef] [PubMed]
51. Ryu, H.H.; Kang, B.J.; Park, S.S.; Kim, Y.; Sung, G.J.; Woo, H.M.; Kim, W.H.; Kweon, O.K. Comparison of mesenchymal stem cells derived from fat, bone marrow, wharton’s jelly, and umbilical cord blood for treating spinal cord injuries in dogs. *J. Vet. Med. Sci.* **2012**, *74*, 1617–1630. [CrossRef] [PubMed]
52. Satti, H.S.; Waheed, A.; Ahmed, P.; Ahmed, K.; Akram, Z.; Aziz, T.; Satti, T.M.; Shahbaz, N.; Khan, M.A.; Malik, S.A. Autologous mesenchymal stromal cell transplantation for spinal cord injury: A phase I pilot study. *Cytotherapy* **2016**, *18*, 518–522. [CrossRef] [PubMed]
53. Mendonca, M.V.; Larocca, T.F.; de Freitas Souza, B.S.; Villarreal, C.F.; Silva, L.F.; Matos, A.C.; Novaes, M.A.; Bahia, C.M.; de Oliveira Melo Martinez, A.C.; Kaneto, C.M.; et al. Safety and neurological assessments after autologous transplantation of bone marrow mesenchymal stem cells in subjects with chronic spinal cord injury. *Stem Cell Res. Ther.* **2014**, *5*, 126. [CrossRef] [PubMed]
54. Koci, Z.; Vyborny, K.; Dubisova, J.; Vackova, I.; Jager, A.; Lunov, O.; Jirakova, K.; Kubinova, S. Extracellular matrix hydrogel derived from human umbilical cord as a scaffold for neural tissue repair and its comparison with extracellular matrix from porcine tissues. *Tissue Eng. Part C Methods* **2017**, *23*, 333–345. [CrossRef] [PubMed]
55. Parr, A.M.; Kulbatski, I.; Zahir, T.; Wang, X.; Yue, C.; Keating, A.; Tator, C.H. Transplanted adult spinal cord-derived neural stem/progenitor cells promote early functional recovery after rat spinal cord injury. *Neuroscience* **2008**, *155*, 760–770. [CrossRef] [PubMed]
56. Yang, J.R.; Liao, C.H.; Pang, C.Y.; Huang, L.L.; Chen, Y.L.; Shiue, Y.L.; Chen, L.R. Transplantation of porcine embryonic stem cells and their derived neuronal progenitors in a spinal cord injury rat model. *Cytotherapy* **2013**, *15*, 201–208. [CrossRef] [PubMed]
57. Dunham, N.W.; Miya, T.S. A note on a simple apparatus for detecting neurological deficit in rats and mice. *J. Am. Pharm. Assoc.* **1957**, *46*, 208–209. [CrossRef]
58. Metz, G.A.; Whishaw, I.Q. The ladder rung walking task: A scoring system and its practical application. *J. Vis. Exp.* **2009**. [CrossRef] [PubMed]



© 2018 by the authors. Licensee MDPI, Basel, Switzerland. This article is an open access article distributed under the terms and conditions of the Creative Commons Attribution (CC BY) license (<http://creativecommons.org/licenses/by/4.0/>).



Article

# Localized Intrathecal Delivery of Mesenchymal Stromal Cells Conditioned Medium Improves Functional Recovery in a Rat Model of Spinal Cord Injury

Dasa Cizkova <sup>1,2,3,\*</sup>, Veronika Cubinkova <sup>1</sup>, Tomas Smolek <sup>1</sup>, Adriana-Natalia Murgoci <sup>1,2,3</sup>, Jan Danko <sup>2</sup>, Katarina Vdoviakova <sup>2</sup>, Filip Humenik <sup>2</sup>, Milan Cizek <sup>4</sup>, Jusal Quanico <sup>3</sup>, Isabelle Fournier <sup>3</sup> and Michel Salzet <sup>3</sup>

<sup>1</sup> Institute of Neuroimmunology, Slovak Academy of Sciences, Dúbravská cesta 9, 845 10 Bratislava, Slovakia; veronika.cubinkova@savba.sk (V.C.); tomas.smolek@savba.sk (T.S.); adriana.murgoci@savba.sk (A.-N.M.)

<sup>2</sup> Department of Anatomy, Histology and Physiology, University of Veterinary Medicine and Pharmacy in Košice, Komenského 73, 041 81 Košice, Slovakia; jan.danko@uvlf.sk (J.D.); katarina.vdoviakova@uvlf.sk (K.V.); filip.humenik@uvlf.sk (F.H.)

<sup>3</sup> Université de Lille, Inserm, U-1192—Laboratoire Protéomique, Réponse Inflammatoire et Spectrométrie de Masse-PRISM, F-59000 Lille, France; Jusal.Quanico@univ-lille1.fr (J.Q.); isabelle.fournier@univ-lille1.fr (I.F.); michel.salzet@univ-lille1.fr (M.S.)

<sup>4</sup> Department of Epizootiology and Parasitology, University of Veterinary Medicine and Pharmacy in Košice, Komenského 73, 041 81 Košice, Slovakia; milan.cizek@uvlf.sk

\* Correspondence: dasa.cizkova@uvlf.sk; Tel.: +421-2-5478-8100; Fax: +421-2-5477-4276

Received: 15 February 2018; Accepted: 9 March 2018; Published: 15 March 2018

**Abstract:** It was recently shown that the conditioned medium (CM) of mesenchymal stem cells can enhance viability of neural and glial cell populations. In the present study, we have investigated a cell-free approach via CM from rat bone marrow stromal cells (MScCM) applied intrathecally (IT) for spinal cord injury (SCI) recovery in adult rats. Functional in vitro test on dorsal root ganglion (DRG) primary cultures confirmed biological properties of collected MScCM for production of neurosphere-like structures and axon outgrowth. Afterwards, rats underwent SCI and were treated with IT delivery of MScCM or vehicle at postsurgical Days 1, 5, 9, and 13, and left to survive 10 weeks. Rats that received MScCM showed significantly higher motor function recovery, increase in spared spinal cord tissue, enhanced GAP-43 expression and attenuated inflammation in comparison with vehicle-treated rats. Spared tissue around the lesion site was infiltrated with GAP-43-labeled axons at four weeks that gradually decreased at 10 weeks. Finally, a cytokine array performed on spinal cord extracts after MScCM treatment revealed decreased levels of IL-2, IL-6 and TNF $\alpha$  when compared to vehicle group. In conclusion, our results suggest that molecular cocktail found in MScCM is favorable for final neuroregeneration after SCI.

**Keywords:** spinal cord injury; inflammation; regeneration; stem cells-derived conditioned media

## 1. Introduction

Spinal cord injury (SCI) is one of the major traumas of the central nervous system (CNS) leading to devastating neurological outcomes [1,2]. Unfortunately, there are few approved treatments available for stabilizing this condition and none for effective treatment [3–5]. Both animal and human studies provide evidence of multiple factors such as inflammation, reactive gliosis, axonal demyelination, neuronal death and cysts formation being the driving forces behind the secondary injury processes of SCI [6–8]. Furthermore, the regenerative capacity of the adult CNS tissue at the injury site is

significantly limited particularly due to the accumulation of inhibitory molecules and loss of trophic factors [9–11]. Therefore, the regeneration of injured nerve tissue is often a temporary process, which can occur only at a short distance and during limited period, thus representing a challenge for the development of new therapeutic strategies [12].

Indeed, in recent years, convincing immunomodulatory and neurotrophic properties have been ascribed to mesenchymal stem cells (MSc) derived from the bone marrow showing partial beneficial impact on locomotor function [13–16]. However, their true therapeutic properties rely on released secretomes comprising a soluble fraction of proteins, growth factors, cytokines and a vesicular fraction composed by microvesicles and exosomes [17]. Considering these facts, it seems that the secretomes of the MSCs appear to be of greater benefit on tissue regeneration and repair than the stem cells themselves [18]. Recently, essential attention has been paid to MSc-derived exosomes that are involved in the transmission of proteins and genetic material (e.g., mi RNA) to neighboring cells [19]. Using mass spectrometry, we have analyzed under *in vitro* conditions bioactive substances produced by rat MSc. The results confirmed that rat MScCM contains growth and migratory factors for neurons, factors for osteogenic differentiation and immunomodulatory factors [14]. Functional tests using chemotactic analysis *in vitro* confirmed that MScCM reduces migration activity in LPS-activated BV2 cells and primary microglia and stimulated nerve outgrowth in DRGs explants [14].

Furthermore, we have confirmed therapeutic efficacy of intrathecal administration of PKH67-labelled MSc by improving motor function of the hind paws after SCI [20]. Histological, morphometric and stereological analyses confirmed that transplanted MSc survived, migrated and were incorporated into the lesion site, where we have seen an increased number of growing nerve fibers [20]. Our results indicate that intrathecal administration of stem cells is a non-invasive method for local delivery of optimal dose leading to overall recovery improvement. Similarly, our previous work with systemic administration of MSc showed a therapeutic effect [21]. Furthermore, a cell-based strategy combined with bio-materials may be prospective in terms of proposing more effective approaches [22,23]. Indeed, transplanted MSc alone or seeded into smart scaffolds may fulfill the role of “pharmacies” which are providing paracrine factors mediating therapeutic benefits on demand of the host tissue [24].

As opposed to cell therapies, the local delivery of secretomes gets to the forefront of interest for possible treatment of CNS injuries. These secretomes must supply the injury site with bioactive molecules for a sufficient time to achieve optimized clinical outcomes. Therefore, frequent delivery during longer periods from about two weeks should be considered.

Supporting this concept, here we determine whether localized, intrathecal delivery of the MScCM affects tissue sparing, axonal regrowth, immune response and functional outcome after SCI. The designed CM treatment represents a promising alternative to traditional stem cell therapy for the treatment of acute spinal cord injury.

## 2. Results

### 2.1. Functionality of CM

#### 2.1.1. High-Density Plating Neurosphere-Like Structures Formation

Primary cultures of DRGs (PCDRGs) plated at a high density (800–1000 cells/mm<sup>2</sup>) continuously multiplied and formed neurosphere-like structures during one week. Immunohistochemistry using TUJ1 confirmed that these spheres were interconnected via extended neurites and formed almost confluent neuronal networks (Figure 1A,B,E). This pattern was observed when PCDRGs were cultured in medium supplemented with nerve growth factor (NGF), and MScCM (Figure 1A,B,D,E), but not when they were cultured in the basic medium (lacking trophic molecules) (Figure 1C). Quantification of neurosphere-like structures did not show differences between PCDRGs cultures with NGF and MScCM supplementation (Figure 1F).

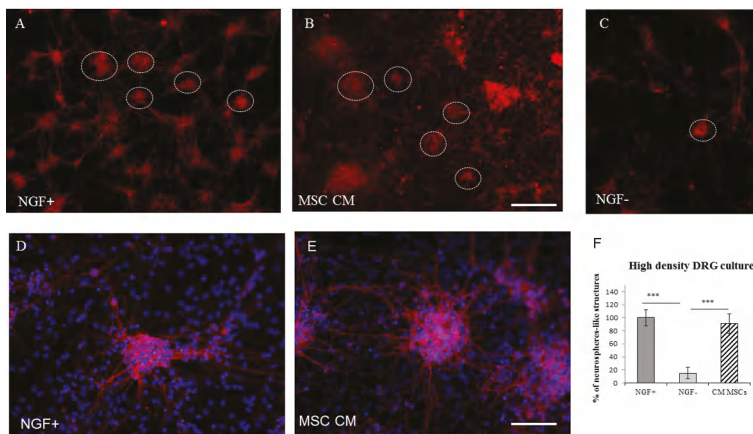


**Figure 1.** Formation of neurosphere-like structures (shown in white circles) from TUJ1 positive PCDRGs plated in high-density, supplemented: with NGF (A,D); with MScCM (B,E); and without NGF (C). Quantification of neurosphere-like structures (F). \*\*\*  $p < 0.001$  indicate significant differences between groups. Scale bars: (A–C) = 400  $\mu\text{m}$ ; and (D,E) = 100  $\mu\text{m}$ .

### 2.1.2. Low-Density Plating

For quantification of delicate neurite outgrowth, we have used low-density plating (30–50 cells/mm<sup>2</sup>). Under this condition, the surface area outside the cell body that was covered with delicate neurites was determined (Figure 2D). This showed that enhanced TUJ1 positive neurite outgrowth from cell body was stimulated with NGF+ or MScCM supplemented culture media (Figure 2A,B). Conversely, almost no outgrowth from sensory neurons occurred after incubation without NGF (Figure 2C). The mean percent of neurite outgrowth for each group was:  $100\% \pm 9.1 = \text{NGF}+$ ;  $7.07\% \pm 2.28 = \text{NGF}-$ ;  $124.97\% \pm 9.2 = \text{MScCM}$ ; \*\*\*  $p < 0.001$ .

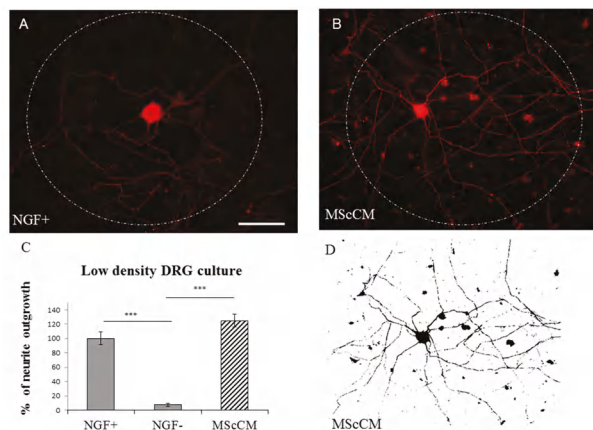


**Figure 2.** Neurite outgrowth of low-density plated PCDRGs, TUJ1 positive supplemented with: NGF (A); and MScCM (B). Quantification of neurite outgrowth. \*\*\*  $p < 0.001$  indicates significant differences between groups (C). The image indicates TUJ1 stained cell with neurites after selecting the area to be analyzed and thresholding the number of pixels covered by the extending neuritis (Image J) (D). \*\*\*  $p < 0.001$ . Scale bars: (A,B,D) 50  $\mu\text{m}$ .

## 2.2. Locomotor Function Recovery

During the initial days post-injury, contusion caused hindlimb paralysis with slight movement in one or two joints in all experimental groups. On following days, the animals in the SCI + CM treatment groups showed a gradual recovery of hindlimb locomotion up to ten weeks after SCI; greater than the recovery in the SCI + V groups, where limited recovery of motor function was noted. The significant locomotor improvement between injured groups without treatment (SCI + V) and treated group (SCI + CM) was detected at two weeks, three weeks, four weeks ( $** p < 0.01$ ), six weeks ( $* p < 0.05$ ), 8–10 weeks ( $** p < 0.01$ ) post-injury with the following BBB scores:  $9.2 \pm 1.3$ /two weeks,  $11.8 \pm 1.5$ /three weeks,  $13.3 \pm 1.4$ /four weeks,  $13.9 \pm 1.1$ /five weeks,  $14.9 \pm 1.4$ /six weeks,  $15.7 \pm 1.8$ /seven weeks,  $17.2 \pm 1.5$ /eight weeks,  $17.8 \pm 1.1$ /nine weeks,  $18.1 \pm 1.4$ /ten weeks (SCI + MScCM); and  $4.9 \pm 1.4$ /two weeks,  $6.2 \pm 1.9$ /three weeks,  $8.8 \pm 1.4$ /four weeks,  $11.2 \pm 1.2$ /five weeks,  $10.7 \pm 1.4$ /six weeks,  $11.7 \pm 1.9$ /seven weeks,  $13.1 \pm 1.3$ /eight weeks,  $13.3 \pm 1.6$ /nine weeks,  $13.1 \pm 1.2$ /ten weeks (SCI + V) (Figure 3).

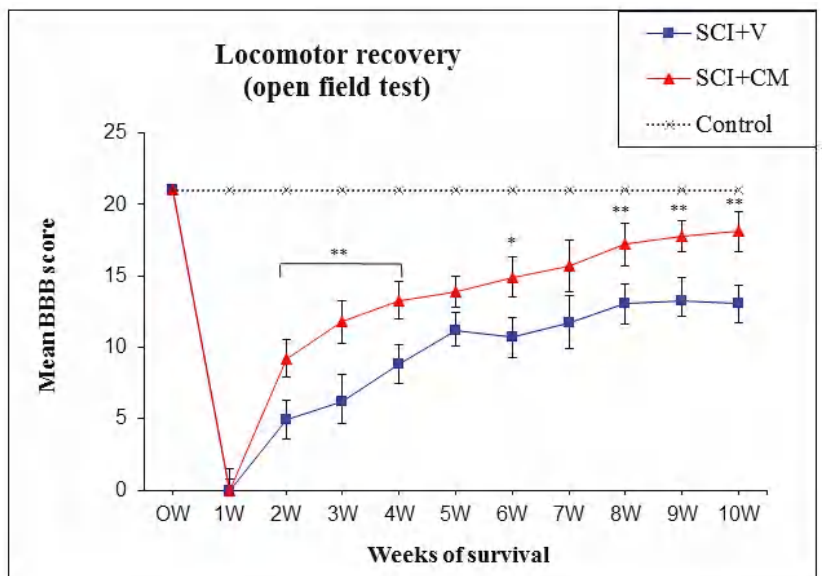


**Figure 3.** Functional recovery of hindlimb motor function following spinal cord injury (SCI) treated with MScCM (SCI + CM,  $n = 6$ ) and vehicle (SCI + V,  $n = 4$ ).  $* p < 0.05$ ,  $** p < 0.01$  indicate significant differences between groups during ten weeks, respectively.

## 2.3. Spared Spinal Cord Tissue

Histological assessment of spared tissue (gray and white matter together) was done with luxol fast blue/cresyl violet staining on coronal spinal cord sections taken from rats processed to SCI + V and SCI + CM treatment (Figure 4B,C). Staining showed an elevated amount of spared tissue in SCI + CM group (Figure 4C) compared to SCI + V (Figure 4B) at ten weeks post-surgery (Figure 4D). Quantitative stereological analyses of tissue fenestration in 1.8 cm ( $0.9+/-$ ) segment revealed significant differences among samples studied in most +cranial 9,8,7,6,5,4,3 mm ( $*** p < 0.01$ ) and -caudal sections 5,6,7,8,9 mm ( $* p < 0.05$ ); CM treated group: +cranial 9,8,7,6,5 mm = 2.6, 2.5, 2.5, 2.3,  $2.0/\pm 0.1-3$  mm; -caudal 5,6,7,8,9 mm = 1.9, 1.9, 2.1, 2.4, 2.4,  $2.1/\pm 0.2-5$  mm. Compared to the vehicle treated group; +cranial 9,8,7,6,5 mm = 1.5, 1.3, 1.1, 0.8,  $0.7/\pm 0.2-0.5$  mm; -caudal 5,6,7,8,9 mm = 0.8, 1.1, 1.3, 1.5,  $1.5/\pm 0.2-5$  mm) ( $*** p < 0.01$ ,  $* p < 0.05$ ) (Figure 4).

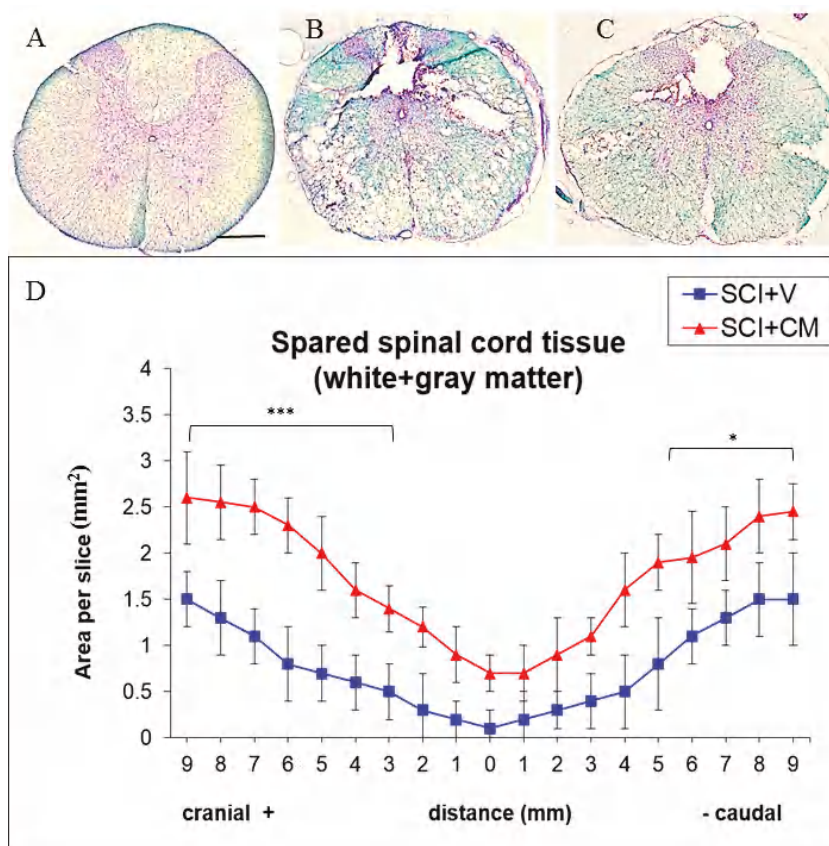


**Figure 4.** Representative cross section of spinal cord, Th8 stained with luxol fast blue of: control (A); SCI treated with vehicle (SCI + V) (B); and treated with MScCM (SCI + CM) (C). Quantitative stereological analyses of tissue fenestration in 1.8 cm (0.9+/-) segment (D). Note, there are significant differences of spared tissue (gray and white matter) between SCI + V (blue line) and SCI + CM (red line) treatment in most cranial and caudal sections (\*\*p < 0.001, \*p < 0.05). Scale bars (A–C) = 500  $\mu$ m.

#### 2.4. Neurite Sprouting

CM-mediated treatment promoted growth of GAP-43-labeled axon fibers that were infiltrating the lesion site and adjacent segments (Figure 5B,E,F). The immunohistochemistry analysis revealed the presence of GAP-43-positive axons located in the lesion (Figure 5B), the rostral (Figure 5E), as well as in the caudal segments (Figure 5F). Furthermore, the increased density of axon fibers forming a multiplicity sprouting and enhanced regrowth through the cavity showed significant differences at four weeks ( $57.2 \pm 11.2\%$  axons) and ten weeks ( $12.9 \pm 5.7\%$  axons) when compared with the vehicle group (SCI + V) at four weeks ( $2.2 \pm 0.7\%$  axons) (Figure 5C). The majority of GAP-43-labeled axons were seen in gray matter of MScCM treated group at four weeks (Figure 5B,E,F), and significantly decreased at ten weeks (Figure 5C,D). Immunocytochemical analysis of SCI + V sections revealed no or very low expression of GAP-43 fibers (Figure 5A); \*\*p < 0.01.

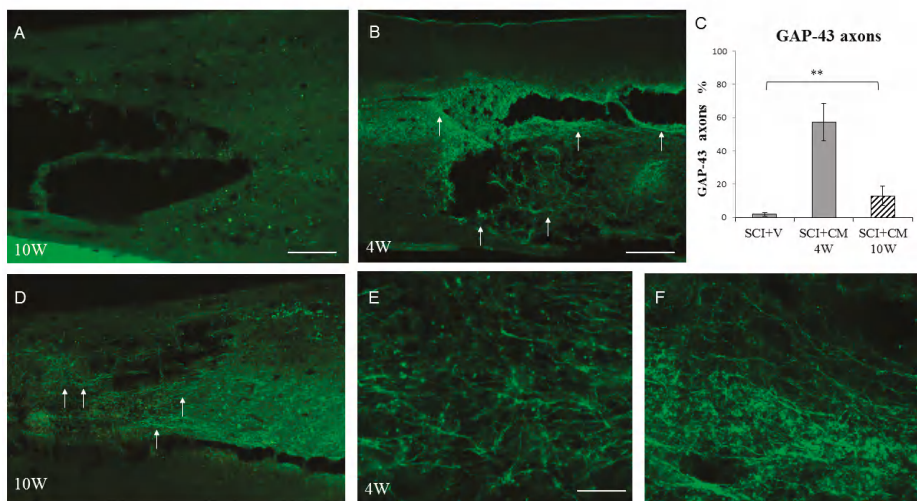


**Figure 5.** Immunohistochemistry revealing the presence of GAP-43-positive axons located in: lesion (B, arrows indicate highest positivity), the rostral (E) and caudal segments (F) in SCI + CM after four weeks. Note the significant decrease of GAP-43 fibers at ten weeks (D, arrows indicate occasional positive axons), and no expression in SCI + V group (A). Quantification of GAP-43-positive axons between groups (C) \*\*  $p < 0.01$ . Scale bars: (A,B,D) 400  $\mu$ m; and (E,F) 150  $\mu$ m.

## 2.5. Cytokines Profile

Cytokine arrays confirmed the time-dependent synthesis of chemokines and cytokines after SCI. Compared with control, CINC-2a/b, IL2, IL6, MIP-1 $\alpha$ , Rantes, CXCL3, TNF $\alpha$ , TIMP-1 and VEGF were significantly overexpressed 15 days after SCI (Figure 6A). At the same interval, treatment with CM significantly decreased IL6 and TNF $\alpha$ , while CNTF and VEGF continue to increase (Figure 6A). Cytokine and chemokine profile between SCI + V and SCI + CM has gradually evened out at ten weeks, although the levels were still higher compared to the control (Figure 6B). Taken together, these data showed that the cytokine pattern changes in time course between SCI + V and SCI + CM treatment and CM may temporarily decrease inflammatory response.

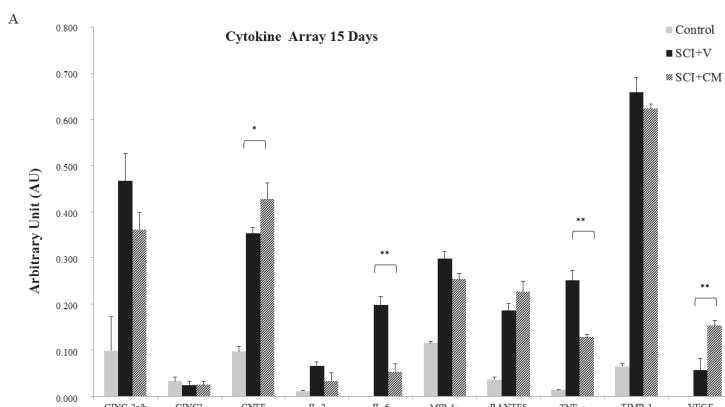


**Figure 6. Cont.**

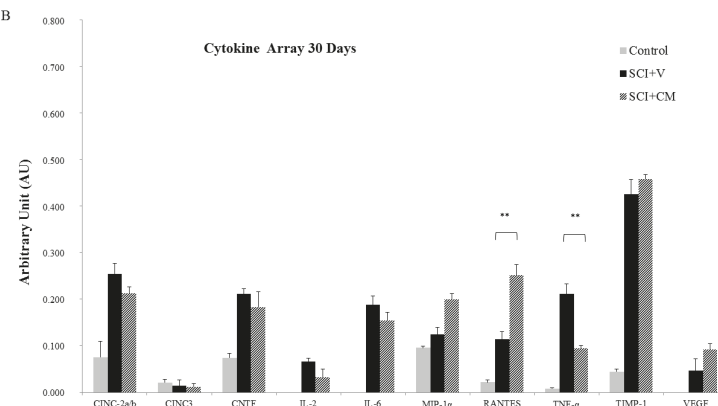


**Figure 6.** Chemokines and cytokines array after SCI in conditioned media from following groups: Control, SCI + V, SCI + CM. Comparison of cytokines and chemokines secretion at: 15 days (A); and 30 days (B) in studied groups. Bar diagrams represent the ratio of the spot mean pixel densities/reference point pixel densities. Statistical significance indicated by \*  $p < 0.05$ , \*\*  $p < 0.01$ .

### 3. Discussion

We have previously reported that IT delivered MSc migrated and incorporated into the central lesion leading to higher motor function recovery [20]. Thus, in the context of these findings, the main objective of the present study was to test whether conditioned medium derived from MSc may have similar beneficial properties for the recovery of the damaged spinal cord as cell-based treatments. First, we confirmed the functionality of MScCM biological activity in vitro on neonatal DRGs primary cultures. Supplementation of primary sensory neurons with CM stimulated formation of neurospheres and neurite outgrowth similarly as was seen after administration of NGF. These in vitro results confirm the functionality of neurotrophic and mitotic molecules released from MSc that were identified by MS/MS in our previous study [14].

Based on these results, we developed a regimen for IT CM delivery. We had to consider the optimal dose and therapeutic window to ensure a continuous supply of trophic molecules to the site of injury. Since we were delivering stem cell products that have limited biological activity, we needed to continually supply the injury site with sufficient amount of trophic molecules. Therefore, we decided to administer CM at 4-day intervals from 1 day to 13 days after injury. Four-day interval was selected due to our previous in vitro data, which showed that the supplementation of neural progenitors with trophic factors (EGF, FGF) every 3–4 days is sufficient to maintain their biological activity and to stimulate their neurogenic behavior (growth and proliferation of neurospheres). Furthermore, the pro-regenerative and inflammatory processes are initiated within the first week after SCI, which outline this period as a potential therapeutic window for treatment intervention [25,26].

In context with this strategy, our behavioral tests confirmed a progressive improvement of the motor function in the SCI + CM treated group compared to the untreated one (SCI + V). We noticed the most significant changes during the first 2–3 weeks and then from 8–10 weeks, although in the vehicle group there was small number of animals that survived up to 10 weeks. Therefore, for future studies we need to work with larger groups in order to support behavioral data. This beneficial outcome correlates with the spared white and gray matter, which was approximately 30% higher in the SCI + CM group. Furthermore, conditioned medium-induced sparing of spinal cord tissue should logically correlate with enhanced regenerative processes. For this reason, we have studied the expression of GAP-43-positive axons, which correspond to newly outgrowing axons with the capacity of re-building the neural connections after CNS damage. The regeneration in adult tissue can be

initiated only for a few days when GAP-43-positive fibers are able to grow over short distances [27,28]. However, stimulation of GAP-43-positive axons by exogenous delivery of stem cells or by limiting the inhibitory environment can significantly increase the amount of GAP-43-positive fibers over a longer period [21,28]. This fact may significantly prolong the regeneration process with overcoming the nerve fibers over the formation of a non-functional glial scar leading to improved outcome [10,29].

Another important factor influencing regeneration that needs to be considered is the severe inflammatory response after SCI. In the CM treated group, we have experienced a significant decrease in IL6 and TNF $\alpha$  and an increase in the trophic factors of CNTF and VEGF, which were gradually reduced with time to the levels observed in the untreated group. This points to the fact that MScCM is capable of temporarily modulating limited immune response as we previously demonstrated on microglia cells [25]. This is due to MSc secreted factors. In fact, MScCM is known to contain anti-inflammatory factors (TGF $\beta$  1,2,3, osteopontin) which impacts activated microglia [30] and infiltrated macrophages. However, to achieve stronger immunomodulation we need inter-cellular response, rather than their products. This was confirmed in another study showing that IT delivery of MSc reduced inflammation via suppression of a broader scope of cytokines (TNF $\alpha$ , IL-4, IL-1 $\beta$ , IL-2, IL-6 and IL-12) and increased the levels of MIP-1 $\alpha$  and RANTES [15]. Furthermore, in a recent study, the authors showed that MSc-derived exosomes specifically target M2-type macrophages at the site of SCI [31]. This supports the idea that extracellular vesicles, released by MSc, may mediate the therapeutic effects towards immune response modulation [32].

Indeed, these results positioned the MScCM treatment on the level of cell based therapy, where similar beneficial outcomes were observed [15,20]. The next step of this project will be isolation of the microvesicles (exosomes) from the MScCM as novel therapeutic agents as we recently demonstrated for microglia cells [33].

#### 4. Materials and Methods

##### 4.1. MSc Culture and Conditioned Media (MScCM) Collection

MSCs were isolated from the bone marrow of four 10-week old male Wistar rats (300 g), collected from the long bones (femur and tibia) [14,20]. The bone marrow was dissected into small pieces, gently homogenized, and filtered (70  $\mu$ m) to remove bone fragments and centrifuged. The cell pellet was re-suspended in 1 mL of alpha-Minimum essential media (MEM), the pooled cells were counted, and their viability was assessed using the trypan blue dye exclusion method. MScs were subsequently resuspended in culture medium composed of alpha-MEM supplemented with 10% of fetal calf serum (FCS; GIBCO Laboratories, Grand Island, NY, USA) and antibiotics (10,000 units/mL penicillin, 10,000 mg/mL streptomycin, and 25 mg/mL amphotericin B; Invitrogen, Carlsbad, CA, USA), and plated at a density of 30,000 cells/cm $^2$  in uncoated tissue culture flasks, as these cells readily adhere to the plastic. The cells were incubated in a humidified atmosphere with 5% CO $_2$  at 37 °C. Non-adherent cells were removed after 3–4 days by medium change and the remaining cells were fed twice per week. When the cultures reached 80% of confluence, the MScs were passaged with 0.25% trypsin/0.53 mM Ethylene diamine tetraacetic acid (EDTA; GIBCO Laboratories, Paisley, UK), centrifuged, and re-plated at a density of 5000 cells/cm $^2$ . The MScs were propagated for three passages and then characterized as previously described [14].

Cells at passage 3 cultured in Dulbecco's modification of Eagle's medium (DMEM, Sigma Aldrich, Saint Louis, MO, USA) with low glucose and without fetal bovine serum were incubated in a humidified atmosphere with 5% CO $_2$  at 37 °C for 24 h and used for MScCM collection, using a similar protocol as in the previous study [14].

##### 4.2. Primary Cultures of Dorsal Root Ganglion Neurons (PCDRGs)

Dorsal root ganglia (DRGs) located in cervical to sacral spinal levels were dissected from newborn (postnatal day 1 (P1), n = 50) Wistar rats following decapitation. Under sterile conditions and using a

stereomicroscope the DRGs were cut into smaller pieces and incubated at 37 °C in 3 mL collagenase dissolved in a dissociation solution consisting of HBSS supplemented with collagenase (concentration of 500 UI/mL; collagenase from Clostridium histolyticum C5138, Sigma Aldrich, Saint Louis, MO, USA), hyaluronidase (concentration of 150 UI/mL; hyaluronidase Type IV, Sigma Aldrich-Chemie GmbH, Buchs, Switzerland). The digestion process was stopped by adding an equal volume of HBSS, and the suspension was filtered through a stainless mesh sieve (pore size 100 µm), centrifuged for 5 min (1000 × g) and the supernatant was discarded. Cells were divided into 3 groups: (1) NGF+ group, grown in DMEM F12 medium with 1% fetal bovine serum and nerve growth factor (2.5S NGF; 50 ng/mL); (2) NGF– group, grown in DMEM F12 medium with 1% fetal bovine serum; and (3) MScCM group, grown in MScCM in DMEM F12 medium and 1% fetal bovine serum (ratio 3:1). All three groups were supplemented with 1% penicillin and streptomycin and allowed to adhere overnight onto poly-DL-ornithine (500 µg/mL) and laminin (10 ng/mL) coated glass coverslips in 12-well tissue culture plates (Costar, Corning, New York, NY, USA) at 37 °C for 7 days in vitro (7DIV). For all PCDRGs, we have used standard IHC procedures to visualize neurite outgrowth. PCDRGs were incubated in mouse anti-Neuron-specific class III beta-tubulin (TUJ1) (1:200; Merck, Darmstadt, Germany; Molecular Probes, Eugene, OR, USA) for 24 h at 4 °C. Afterwards, they were washed in 0.1 M PBS and incubated for 2 h with goat anti-mouse IgG (AlexaFlour 488, Molecular Probes, Eugene, OR, USA). For nuclear staining, we used 4,6-diamidino-2-phenylindol (DAPI, 1:200) and finally the slides were coverslipped with Vectashield mounting medium (Vector Laboratories, Inc., Burlingame, CA, USA). Digitized images of PCDRGs per treatment ( $n = 6$ ) were captured and saved with NIS-Elements Imaging Software (Nikon, Prague, Czech Republic). Neurite outgrowth was analyzed at identical sampling fields, for each CM experiment by ImageJ software according to the above-mentioned method applied for primary antibodies quantification, according to our previous study [14].

#### 4.3. Intrathecal Implant Procedure

Intrathecal (IT) catheter implantation was performed according to our previously published procedure [20]. The rats were anesthetized with 1.5–2% halothane, and following a loss of responsiveness, the head was fixed in a stereotaxic head holder. The atlanto-occipital membrane was blotted dry to visualize the entire area and a 3 to 4 mm incision was made through the dural midline using a 30-gauge needle. The PE-5 end of the IT catheter was inserted into the IT space and advancing the tip of the catheter along the spinal cord for a distance up to 3.5 cm. The opposite PE-10 catheter end was externalized on the forehead and the end was plugged with 4–5 mm of stainless steel 28-gauge wire. The overlying muscles and skin were sutured using a silk suture to fix the catheter in place. All implanted IT catheters were flushed with 15.0 µL of sterile saline for 10 min to test their transition, and in the case of an obstruction, the catheter was repositioned or exchanged. After recovery, each rat was evaluated for additional limb dysfunction, spinal asymmetry, pain or adverse surgical effects, and sacrificed immediately if any of these were observed.

#### 4.4. Spinal Cord Trauma

All experimental procedures were approved by the institutional ethical committee for animal research, and were in accordance with the Slovak Law for Animal protection (No. 39/2007, 12 December 2006). SCI was induced using the modified balloon compression technique in adult male Wistar rats ( $n = 24$ ) weighing between 300 and 320 g, according to our previous study [21]. The SCI was induced by balloon-technique in adult male rats. Surgery was performed under anesthesia with 1.5–2% halothane in air delivered through a face mask. Using a dental drill, a small hole was made at Th8–9 level and a 3-French Fogarty catheter was inserted epidurally and the balloon was inflated with 12.5 µL of saline for 5 min. SCI was also associated with damage of the autonomic nervous system, which includes regulatory functions of urinary bladder. For this reason, manual bladder expression was required (twice a day) until bladder reflex was restored. No antibiotic treatment was used.

#### 4.5. IT Delivery of MSCs Conditioned Medium (MScCM)

All SCI rats were randomly divided into the following groups: (1) MSc conditioned medium (CM) group receiving four daily injections of 30  $\mu$ L MScCM (SCI + CM) at 1, 5, 9 and 13 days; or (2) a vehicle group (SCI + V) receiving 30  $\mu$ L of DMEM per rat at the same intervals. A maximum dose of 30  $\mu$ L CM was flushed with 5  $\mu$ L of saline over 30 min through a calibrated PE10 catheter (calibrated by 5- $\mu$ L increments up to 35  $\mu$ L), which was connected to a 500- $\mu$ L Hamilton syringe attached to a mechanical mini-pump. This procedure was performed in each rat of the SCI + CM and vehicle groups. Implantation of the IT catheter was performed on the same day as IT delivery, at 1 day after SCI. Animals were intracardially perfused at 15 days and four weeks ( $n = 8$ /IT delivery CM,  $n = 6$ /IT delivery vehicle) and at ten weeks after SCI ( $n = 6$ /IT delivery CM,  $n = 4$ /IT delivery vehicle).

#### 4.6. Behavioral Testing of Motor Function (BBB Scoring)

Animals were evaluated before surgery and once a week after surgery for 10 weeks. Each rat was tested for 5 min by two blinded examiners. The motor performance was assessed using the Basso–Beattie–Bresnahan (BBB) 21-point open field locomotor scale [16]. BBB scores, which categorize combinations of rat hindlimb movements, trunk position and stability, stepping, coordination, paw placement, toe clearance and tail position, were analyzed. In this evaluation, 0 represents no locomotion and 21 represents normal motor function.

#### 4.7. Cytokines Profile

Cytokines profile of CM derived from control, SCI + V, SCI + CM after 15 days and 30 days for the segment R1 was performed by using a Rat Cytokine Array Panel A according to the manufacturer's instructions (R&D Systems, Inc., Abingdon, UK). Conditioned media from rostral segments from spinal cord tissue (all experimental groups and control) were obtained according to our previous study and afterwards processed for Cytokine profile detection [25]. We have used a similar procedure as in our previous study [26]. Briefly, the array membranes were first incubated in the blocking buffer for 1 h. Afterwards 200  $\mu$ L of CM were mixed with the detection antibody mixture and incubated for 1 h at room temperature. After removing the blocking buffer, the sample/antibody mixture was added to array membranes and incubated overnight at 4 °C. Next day, the membranes were washed with the buffer and then incubated with Streptavidin-HRP solution for 30 min at room temperature. The membranes were finally washed with buffer 4 times and the bound antibodies were detected by chemoluminescence using a chemireagent mix. The membranes were quantified by densitometry using ImageJ software. Background staining and spot size were analyzed as recommended by the manufacturer. Normalization was done with control expression.

#### 4.8. Morphometric Analysis

To analyze the amount of spared spinal cord tissue, we have performed modified luxol fast blue histological staining according to our procedure [22]. A 1.8 cm-long segment of the spinal cord was dissected between 0.9 cm cranial and 0.9 cm caudal to the injury epicenter. Spinal cords were transversally cut at 1-mm intervals along the crano-caudal axis from the lesion center and stained with cresyl violet and luxol-fast blue. Five sections were selected at 1-mm intervals and whole images of the spinal cord were taken with Leica plus microscope digital camera (Microsystems, Mannheim, Germany). We calculated the ratio between the measured injured area and the entire area of the spinal cord slice (white + gray matter) on serial transversal sections (+9 mm; 0; -9 mm) by Image J software (Wayne Rasband, National Institutes of Health, Bethesda, MD, USA). Mean number of spared tissue of evaluated groups was expressed in  $\text{mm}^2$ .

#### 4.9. Immunohistochemistry and Quantification Analysis

Experimental and control rats were deeply anesthetized with a ketamine-xylazine cocktail (15 mg/kg of xylazine and 150 mg/kg of ketamine), and transcardially perfused with 0.1 M PBS, followed by 2% paraformaldehyde in PBS. The spinal cord and externalized IT catheter was removed, post-fixed in the same fixative solution overnight at 4 °C, and embedded in the gelatin albumin substrate in 2% paraformaldehyde in PBS. Frozen spinal cord sections were cut from a 1.5-cm-long spinal cord segment positioned on the injury epicenter, embedded in embedding medium, dissected into three 0.5-cm-thick blocks (rostral, epicenter, and caudal), and stored at –20 °C. Sections 10-μm thick were then serially cut from the epicenter and mounted directly onto slides. From the rostral and caudal regions, 40-μm-thick cryostat (Leica) sections were cut and collected in 24-well plates with 0.1-M PBS containing 0.1% sodium azide. Sections were taken at 200 μm intervals and 20 sections per block were obtained. Ten sections per block were stained with hematoxylin and eosin (H&E) to assess tissue morphology and determine the injury epicenter. For immunohistochemistry, free-floating sections (40 μm) were immersed in PBS (0.1 M; pH 7.4) containing 10% normal goat serum (NGS), 0.2% Triton X-100 for 2 h at room temperature to block non-specific protein activity. This was followed by overnight incubation at 4 °C with primary antibodies: mouse anti-GAP-43 (1:1000, Sigma, Saint Louis, MO, USA) for 24 h. Afterwards sections were washed in 0.1 M PBS and incubated with secondary fluorescent antibodies goat anti-mouse conjugated fluorescein isothiocyanate (FITC) (Alexa Flour 488) at room temperature for 2 h. For general nuclear staining, DAPI (1:200) was added to the final secondary antibody solutions. Finally, sections were mounted and coverslipped with Vectashield mounting medium.

#### 4.10. Quantification Analysis

Immunochemically stained sections were analyzed using Olympus BX-50 fluorescent microscope at 10× and 20× magnifications, captured with digital camera HP Olympus and analyzed by Image J software according to the previous protocol [20,28]. Quantification of GAP-43 positivity was performed on five sagittal sections from rostral and caudal segments of each spinal cord treatment and from sham tissue. Captured digital images were transformed into monochrome 8-bit images and the mean grey level number of black and white pixels within the tissue was determined (value 0–255, when 0 = black pixels, 255 = white pixels). The result yields the mean ratio of black and white pixels expressed by the histogram. The expression of the immunofluorescence (GAP-43) within five sampling fields (perimeter of circle 300 μm) randomly placed above and below the lesion site was evaluated, and a background image of a control section of each image was digitally subtracted. Mean values were calculated as a percentage of GAP-43 axons among SCI + V, SCI + CM four weeks and SCI + CM ten weeks groups and were statistically compared using one-way ANOVA followed by Tukey's post hoc test.

#### 4.11. Data and Statistical Analysis

Obtained data from tissue analyses and behavioral testing were reported as mean ± SEM. Mean values among different experimental groups were statistically compared by one-way ANOVA and Tukey's post hoc tests using GraphPad PRISM software. Significant values were denoted with \* for  $p < 0.05$ , \*\* for  $p < 0.01$ , and \*\*\* for  $p < 0.001$ .

### 5. Conclusions

Our results confirm the pro-regenerative effects of MScCM on tissue sparing, axonal growth, immunomodulation and final functional outcome. These results suggest that multiple IT delivery of stem cell products may improve behavioral function when the dose and timing are optimized. Taken together, the molecular cocktail found in MScCM is favorable for final neuroregeneration *in vivo*.

**Acknowledgments:** This research was supported by: APVV 15-0613 (Dasa Cizkova), ERANET-AxonRepair (Dasa Cizkova), Stefanik SK-FR-2015-0018 (Dasa Cizkova, Michel Salzet), grants from Ministère de L’Education Nationale, L’Enseignement Supérieur et de la Recherche, INSERM, SIRIC ONCOLille Grant INCD a-DGOS-Inserm 6041aa (Isabelle Fournier). The study was performed with approval and in accordance to the guidelines of the Institutional Animal Care and Use Committee of the Slovak Academy of Sciences and with the European Communities Council Directive (2010/63/EU) regarding the use of animals in Research, Slovak Law for Animal Protection No. 377/2012, 436/2012, and protocol approval 739/17-221.

**Author Contributions:** Dasa Cizkova conceived and designed the experiments; Dasa Cizkova and Michel Salzet wrote the paper; Veronika Cubinkova, Tomas Smolek, Adriana-Natalia Murgoci, Milan Cizek and Filip Humenik performed in vivo experiments; Isabelle Fournier, Jan Danko, Katarina Vdoviakova, and Jusal Quanico performed in vitro experiments; and Isabelle Fournier, Jan Danko and Jusal Quanico analyzed the data.

**Conflicts of Interest:** The authors declare no conflict of interest.

## References

1. Kou, Z.; Sun, D. New era of treatment and evaluation of traumatic brain injury and spinal cord injury. *Neural Regen. Res.* **2016**, *11*, 6. [[CrossRef](#)] [[PubMed](#)]
2. Gerin, C.G.; Madueke, I.C.; Perkins, P.; Hill, S.; Smith, K.; Haley, B.; Allen, S.A.; Garcia, R.P.; Paunesku, T.; Woloschak, G. Combination strategies for repair, plasticity, and regeneration using regulation of gene expression during the chronic phase after spinal cord injury. *Synapse* **2011**, *65*, 1255–1281. [[CrossRef](#)] [[PubMed](#)]
3. Pego, A.P.; Kubinova, S.; Cizkova, D.; Vanicky, I.; Mar, F.M.; Sousa, M.M.; Sykova, R. Regenerative medicine for the treatment of spinal cord injury: More than just promises? *J. Cell. Mol. Med.* **2012**, *16*, 2564–2582. [[CrossRef](#)] [[PubMed](#)]
4. Siddiqui, A.M.; Khazaei, M.; Fehlings, M.G. Translating mechanisms of neuroprotection, regeneration, and repair to treatment of spinal cord injury. *Prog. Brain Res.* **2015**, *218*, 15–54. [[CrossRef](#)] [[PubMed](#)]
5. Nagoshi, N.; Nakashima, H.; Fehlings, M.G. Riluzole as a neuroprotective drug for spinal cord injury: From bench to bedside. *Molecules* **2015**, *20*, 7775–7789. [[CrossRef](#)] [[PubMed](#)]
6. Kakulas, B.A. Neuropathology: The foundation for new treatments in spinal cord injury. *Spinal Cord* **2004**, *42*, 549–563. [[CrossRef](#)] [[PubMed](#)]
7. Dietrich, W.D.; Atkins, C.M.; Bramlett, H.M. Protection in animal models of brain and spinal cord injury with mild to moderate hypothermia. *J. Neurotrauma* **2009**, *26*, 301–312. [[CrossRef](#)] [[PubMed](#)]
8. Nagoshi, N.; Fehlings, M.G. Investigational drugs for the treatment of spinal cord injury: Review of preclinical studies and evaluation of clinical trials from Phase I to II. *Expert Opin. Investig. Drugs* **2015**, *24*, 645–658. [[CrossRef](#)] [[PubMed](#)]
9. Fawcett, J.W. Overcoming inhibition in the damaged spinal cord. *J. Neurotrauma* **2006**, *23*, 371–383. [[CrossRef](#)] [[PubMed](#)]
10. Fawcett, J.W.; Asher, R.A. The glial scar and central nervous system repair. *Brain Res. Bull.* **1999**, *49*, 377–391. [[CrossRef](#)]
11. Garcia-Alias, G.; Barkhuysen, S.; Buckle, M.; Fawcett, J.W. Chondroitinase ABC treatment opens a window of opportunity for task-specific rehabilitation. *Nat. Neurosci.* **2009**, *12*, 1145–1151. [[CrossRef](#)] [[PubMed](#)]
12. Galtrey, C.M.; Asher, R.A.; Nothias, F.; Fawcett, J.W. Promoting plasticity in the spinal cord with chondroitinase improves functional recovery after peripheral nerve repair. *Brain* **2007**, *130 Pt 4*, 926–939. [[CrossRef](#)]
13. Jendelova, P.; Kubinova, S.; Sandvig, I.; Erceg, S.; Sandvig, A.; Sykova, E. Current developments in cell- and biomaterial-based approaches for stroke repair. *Expert Opin. Biol. Ther.* **2016**, *16*, 43–56. [[CrossRef](#)] [[PubMed](#)]
14. Cizkova, D.; Devaux, S.; Le Marrec-Croq, F.; Franck, J.; Slovinska, L.; Blasko, J.; Rosocha, R.; Spakova, T.; Lefebvre, C.; Fournier, I.; et al. Modulation properties of factors released by bone marrow stromal cells on activated microglia: An in vitro study. *Sci. Rep.* **2014**, *4*, 7514. [[CrossRef](#)] [[PubMed](#)]
15. Urdzíková, L.M.; Růžička, J.; LaBagnara, M.; Kárová, K.; Kubinová, Š.; Jiráková, K.; Murali, R.; Syková, E.; Jhanwar-Uniyal, M.; Jendelová, P. Human mesenchymal stem cells modulate inflammatory cytokines after spinal cord injury in rat. *Int. J. Mol. Sci.* **2014**, *15*, 11275–11293. [[CrossRef](#)] [[PubMed](#)]
16. Basso, D.M.; Beattie, M.S.; Bresnahan, J.C. A sensitive and reliable locomotor rating scale for open field testing in rats. *J. Neurotrauma* **1995**, *12*, 1–21. [[CrossRef](#)] [[PubMed](#)]

17. Marote, A.; Teixeira, F.B.G.; Mendes-Pinheiro, B.R.; Salgado, A.J. MSCs-derived exosomes: Cell-secreted nanovesicles with regenerative potential. *Front. Pharmacol.* **2016**, *7*, 231. [[CrossRef](#)] [[PubMed](#)]
18. Salgado, A.J.; Sousa, J.C.; Costa, B.M.; Pires, A.O.; Mateus-Pinheiro, A.; Teixeira, F.G.; Pinto, L.; Sousa, N. Mesenchymal stem cells secretome as a modulator of the neurogenic niche: Basic insights and therapeutic opportunities. *Front. Cell. Neurosci.* **2015**, *9*, 249. [[CrossRef](#)] [[PubMed](#)]
19. Teixeira, F.B.G.; Carvalho, M.M.; Neves-Carvalho, A.; Panchalingam, K.M.; Behie, L.A.; Pinto, L.; Sousa, N.; Salgado, A.J. Secretome of mesenchymal progenitors from the umbilical cord acts as modulator of neural/glial proliferation and differentiation. *Stem Cell Rev. Rep.* **2014**, *11*, 288–297. [[CrossRef](#)] [[PubMed](#)]
20. Cizkova, D.; Novotna, I.; Slovinska, L.; Vanicky, I.; Jergova, S.; Rosocha, J.; Radonak, J. Repetitive intrathecal catheter delivery of bone marrow mesenchymal stromal cells improves functional recovery in a rat model of contusive spinal cord injury. *J. Neurotrauma* **2011**, *28*, 1951–1961. [[CrossRef](#)] [[PubMed](#)]
21. Cizkova, D.; Rosocha, J.; Vanicky, I.; Jergova, S.; Cizek, M. Transplants of human mesenchymal stem cells improve functional recovery after spinal cord injury in the rat. *Cell. Mol. Neurobiol.* **2006**, *26*, 1165–1178. [[CrossRef](#)] [[PubMed](#)]
22. Grulova, I.; Slovinska, L.; Blasko, J.; Devaux, S.; Wisztorski, M.; Salzet, M.; Fournier, I.; Kryukov, O.; Cohen, S.; Cizkova, D. Delivery of alginate scaffold releasing two trophic factors for spinal cord injury repair. *Sci. Rep.* **2015**, *5*, 13702. [[CrossRef](#)] [[PubMed](#)]
23. Kubinova, S.; Horak, D.; Hejcl, A.; Plichta, Z.; Kotek, J.; Proks, V.; Forostyak, S.; Sykova, E. SIKVAV-modified highly superporous PHEMA scaffolds with oriented pores for spinal cord injury repair. *J. Tissue Eng. Regen. Med.* **2015**, *9*, 1298–1309. [[CrossRef](#)] [[PubMed](#)]
24. Ruzicka, J.; Machova-Urdzikova, L.; Gillick, J.; Amemori, T.; Romanyuk, N.; Karova, N.; Zaviskova, K.; Dubisova, J.; Kubinova, S.; Murali, R.; et al. A comparative study of three different types of stem cells for treatment of rat spinal cord injury. *Cell Transplant.* **2017**, *26*, 585–603. [[CrossRef](#)] [[PubMed](#)]
25. Cizkova, D.; Le Marrec-Croq, F.; Franck, J.; Slovinska, J.; Grulova, I.; Devaux, S.; Lefebvre, C.; Fournier, I.; Salzet, M. Alterations of protein composition along the rostro-caudal axis after spinal cord injury: Proteomic, in vitro and in vivo analyses. *Front. Cell. Neurosci.* **2014**, *8*, 105. [[CrossRef](#)] [[PubMed](#)]
26. Devaux, S.; Cizkova, D.; Quanico, J.; Franck, J.; Nataf, S.; Pays, L.; Hauberg-Lotte, L.; Maass, P.; Kobarg, J.H.; Kobeissy, F.; et al. Proteomic analysis of the spatio-temporal based molecular kinetics of acute spinal cord injury identifies a time- and segment-specific window for effective tissue repair. *Mol. Cell. Proteom.* **2016**, *15*, 2641–2670. [[CrossRef](#)] [[PubMed](#)]
27. Cizkova, D.; Racekova, E.; Vanicky, I. The expression of B-50/GAP-43 and GFAP after bilateral olfactory bulbectomy in rats. *Physiol. Res.* **1997**, *46*, 487–495. [[PubMed](#)]
28. Novotna, I.; Slovinska, L.; Vanicky, I.; Cizek, M.; Radonak, J.; Cizkova, D. IT delivery of ChABC modulates NG2 and promotes GAP-43 axonal regrowth after spinal cord injury. *Cell. Mol. Neurobiol.* **2011**, *31*, 1129–1139. [[CrossRef](#)] [[PubMed](#)]
29. Fawcett, J.W.; Curt, A.; Steeves, J.D.; Coleman, W.P.; Tuszyński, M.H.; Lammertse, D.; Bartlett, P.F.; Blight, A.R.; Dietz, V.; Ditunno, J.; et al. Guidelines for the conduct of clinical trials for spinal cord injury as developed by the ICCP panel: Spontaneous recovery after spinal cord injury and statistical power needed for therapeutic clinical trials. *Spinal Cord* **2007**, *45*, 190–205. [[CrossRef](#)] [[PubMed](#)]
30. Hofer, H.R.; Tuan, R.S. Secreted trophic factors of mesenchymal stem cells support neurovascular and musculoskeletal therapies. *Stem Cell Res. Ther.* **2016**, *7*, 131. [[CrossRef](#)] [[PubMed](#)]
31. Lankford, K.L.; Arroyo, E.J.; Nazimek, K.; Bryniarski, K.; Askenase, P.W.; Kocsis, J.D. Intravenously delivered mesenchymal stem cell-derived exosomes target M2-type macrophages in the injured spinal cord. *PLoS ONE* **2018**, *13*, e0190358. [[CrossRef](#)] [[PubMed](#)]
32. Yang, Y.; Ye, Y.; Su, X.; He, J.; Bai, W.; He, X. MSCs-derived exosomes and neuroinflammation, neurogenesis and therapy of traumatic brain injury. *Front. Cell. Neurosci.* **2017**, *11*. [[CrossRef](#)] [[PubMed](#)]
33. Murgoci, A.-N.; Cizkova, D.; Majerova, P.; Petrovova, E.; Medvecky, L.; Fournier, I.; Salzet, M. Brain cortex microglia derived exosomes: Novel nanoparticles for glioma therapy. *ChemPhysChem* **2018**. [[CrossRef](#)] [[PubMed](#)]



Article

# Modified Methacrylate Hydrogels Improve Tissue Repair after Spinal Cord Injury

Aleš Hejčl <sup>1,2,\*</sup>, Jiří Růžička <sup>1</sup>, Kristýna Kekulová <sup>1</sup>, Barbora Svobodová <sup>1</sup>, Vladimír Proks <sup>3</sup>, Hana Macková <sup>3</sup>, Kateřina Jiránková <sup>4</sup>, Kristýna Kárová <sup>1,5</sup>, Lucia Machová Urdziková <sup>1</sup>, Šárka Kubinová <sup>1</sup>, Jiří Cihlář <sup>6</sup>, Daniel Horák <sup>3</sup> and Pavla Jendelová <sup>1,5</sup>

<sup>1</sup> Institute of Experimental Medicine, Academy of Sciences of the Czech Republic, Vídeňská 1083, 142 20 Prague, Czech Republic; stoupa-ruza@seznam.cz (J.R.); kristyna.kekulova@iem.cas.cz (K.K.); barbora.svobodova@iem.cas.cz (B.S.); kristyna.karova@iem.cas.cz (K.K.); urdzikl@saske.sk (L.M.U.); sarka.kubinova@iem.cas.cz (S.K.); pavla.jendelova@iem.cas.cz (P.J.)

<sup>2</sup> Department of Neurosurgery, J. E. Purkinje University, Masaryk Hospital, Sociální Péče 12A, 401 13 Ústí nad Labem, Czech Republic

<sup>3</sup> Institute of Macromolecular Chemistry, Academy of Sciences of the Czech Republic, Heyrovského nám. 2, 162 06 Praha, Czech Republic; proks@imc.cas.cz (V.P.); mackova@imc.cas.cz (H.M.); horak@imc.cas.cz (D.H.)

<sup>4</sup> Second Faculty of Medicine, Charles University, V Úvalu 84, 150 06 Prague, Czech Republic; jirankova.katerina@seznam.cz

<sup>5</sup> Department of Neuroscience, 2nd Faculty of Medicine, Charles University, V Úvalu 84, 150 06 Prague, Czech Republic

<sup>6</sup> Department of Mathematics, Faculty of Science, J. E. Purkyně University, České Mládeže 8, 400 96 Ústí nad Labem, Czech Republic; jiri.cihlar@ujep.cz

\* Correspondence: ales.hejcl@gmail.com; Tel.: +420-241-062-230; Fax: +420-241-062-782

Received: 11 June 2018; Accepted: 17 August 2018; Published: 22 August 2018

**Abstract:** Methacrylate hydrogels have been extensively used as bridging scaffolds in experimental spinal cord injury (SCI) research. As synthetic materials, they can be modified, which leads to improved bridging of the lesion. Fibronectin, a glycoprotein of the extracellular matrix produced by reactive astrocytes after SCI, is known to promote cell adhesion. We implanted 3 methacrylate hydrogels: a scaffold based on hydroxypropylmethacrylamid (HPMA), 2-hydroxyethylmethacrylate (HEMA) and a HEMA hydrogel with an attached fibronectin (HEMA-Fn) in an experimental model of acute SCI in rats. The animals underwent functional evaluation once a week and the spinal cords were histologically assessed 3 months after hydrogel implantation. We found that both the HPMA and the HEMA-Fn hydrogel scaffolds lead to partial sensory improvement compared to control animals and animals treated with plain HEMA scaffold. The HPMA scaffold showed an increased connective tissue infiltration compared to plain HEMA hydrogels. There was a tendency towards connective tissue infiltration and higher blood vessel ingrowth in the HEMA-Fn scaffold. HPMA hydrogels showed a significantly increased axonal ingrowth compared to HEMA-Fn and plain HEMA; while there were some neurofilaments in the peripheral as well as the central region of the HEMA-Fn scaffold, no neurofilaments were found in plain HEMA hydrogels. In conclusion, HPMA hydrogel as well as the HEMA-Fn scaffold showed better bridging qualities compared to the plain HEMA hydrogel, which resulted in very limited partial sensory improvement.

**Keywords:** spinal cord injury; hydrogel; connective tissue; neurofilaments; locomotor test; plantar test

## 1. Introduction

Functional deficits of spinal cord injury (SCI) are the result of subsequent temporal events: the primary insult leads to ischemia, followed by neuronal cell death, axon damage, and demyelination. Subsequently, glial activation, the release of inflammatory factors and cytokines, and the scar formation

that prevents axons to regenerate leads to progression of the lesion. Post-traumatic syringomyelia usually develops in the chronic phase after SCI as a result of hemorrhage and tissue necrosis. The cavity is filled with tissue debris and later mostly with CSF and is surrounded by glial and mesenchymal scarring forming a barrier for tissue regeneration. Therefore, different strategies have been developed to treat SCI. One of the approaches relies on tissue engineering methods, particularly on bridging the lesion cavities. The scaffold, suitable for implantation into lesion cavity must have the appropriate chemical, physical, and mechanical properties required for cell survival and tissue formation. One of the most suitable classes of compounds for these purposes is definitely represented by hydrogels [1–3]. They are three-dimensional (3D) hydrophilic polymers held together by covalent bonds or other cohesive forces such as hydrogen or ionic bonds [3–5]. They can be either synthetic or natural in origin, or a combination of both. Synthetic polymers can be tailored in terms of composition, rate of degradation, and mechanical and chemical properties. [6]. This is much more difficult to achieve in naturally derived polymers, which, in contrast, have features supporting adhesion and cell growth.

Therefore, the presence of bioadhesive and bioactive molecules on an artificial hydrogel matrix is crucial for the successful preparation of neural biomimetic scaffolds. Synthetic materials are often coated or modified with extracellular matrix (ECM) components, e.g., laminin and fibronectin, or synthetic peptides [7–9], which can improve cell adhesion and survival by generating a permissive microenvironment within the biomaterial [10,11]. Moreover, collagen, fibronectin, and laminin are associated with wound healing and regeneration and, therefore, they can be explored for therapeutic purposes. After SCI, fibronectin is deposited within the glial scar [12]. Yet fibronectin is also known to play a role in cell differentiation, proliferation, or migration and has been used as an implant in a spinal cord lesion in some studies [13]. Fibronectin is an important glycoprotein in the developing CNS due to its involvement in cell migration [14] and it has important roles in tissue repair mainly because of its cell adhesion properties. Fibronectin was used as matrix for NSC transplants in damaged CNS and found to improve NSC survival [15]. Fibronectin can be also used in combination with other materials. For instance, poly- $\beta$ -hydroxybutyrate fibers coated with alginate hydrogel and fibronectin were used for a Schwann cell transplant in the injured rat spinal cord [13]. This combination promoted axon growth across the injury.

During the last 15 years we have implanted various biomaterials inside cavities in order to provide a scaffold for the ingrowth of new tissue, especially axons and blood vessels [16–21]. In general, we have shown that hydrogels are able to provide scaffolding for new tissue to grow inside their pores. As with other studies, we have also shown that the quantity of tissue ingrowth is influenced by various adjustments of tissue scaffold, such as in combination with adhesion molecules, modifications in chemical and physical properties, or in combination with stem cells [22–25]. Such modifications may lead to motor and sensory function improvement in experimental rats after SCI [25]. Despite some improvements, the overall results are unsatisfactory, impelling the development of new scaffolds with better proregenerating qualities. In this study we implanted methacrylate hydrogel based on poly(2-hydroxyethyl methacrylate) (HEMA) modified with attached fibronectin (HEMA-Fn) and compared it with unmodified HEMA and poly[N-(2-hydroxypropyl) methacrylamide] (HPMA) hydrogel scaffolds in terms of functional response and tissue infiltration. We utilized a spinal cord hemisection, which provides an appropriate model for evaluating scaffolds with oriented pores as the lesion is large enough for proper orientation of the scaffold within the cavity and at the same time the functional deficit is mild enough so as to avoid excessive animal loss as opposed to other more severe experimental lesions, such as spinal cord transection or balloon-induced compression lesion. In this study we wanted to assess the long-term effect of fibronectin-enriched HEMA and compare it with plain HEMA and HPMA hydrogels. Hydrogels with oriented pores were utilized as they provide an excellent scaffold for the evaluation of newly growing axons and blood vessels within the biomaterial.

## 2. Results

### 2.1. Hydrogel Scaffold

Three synthetic hydrogels, namely HEMA, HEMA-Fn, and HPMA, were obtained by free-radical copolymerization producing identical inner morphology, exemplified in Figure 1A. Longitudinally shaped pores were imprinted by needle-like ammonium oxalate crystals oriented in an axial direction (Figure 1B). The pore size corresponded to the size of the starting crystals, which were 30–90  $\mu\text{m}$  thick and approximately 0.3–10 mm long. According to published literature [26], this long pore size can be advantageous for the regeneration of peripheral axons, whereas their ingrowth and/or outgrowth needs much smaller pores (20–70  $\mu\text{m}$ ) depending on the origin of biomaterial. The pore volume calculated from an oxalate/monomer volume ratio, amounted to ~70%, which roughly corresponded to Hg porosimetry data (68.4%) [22]. The elasticity modulus of the hydrogels was ~4 and 30 kPa perpendicularly and along the pores, respectively [27].

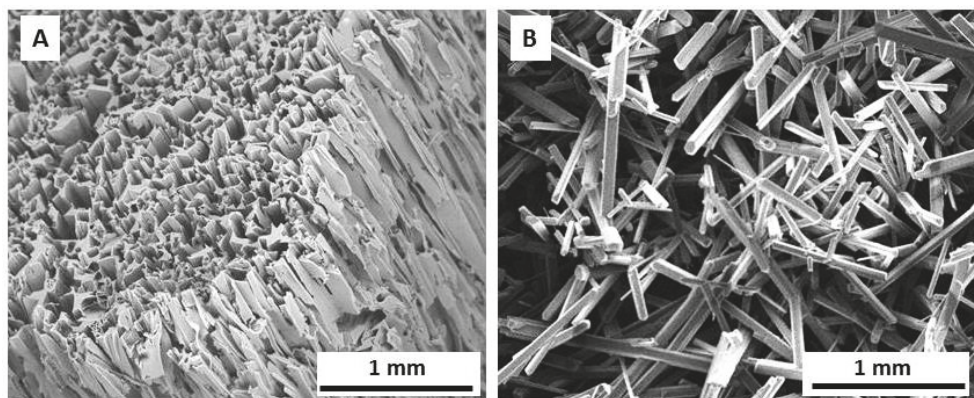


**Figure 1.** SEM micrographs of HEMA hydrogel (A) and ammonium oxalate crystals (B).

### 2.2. Functional Tests

All 34 animals underwent functional evaluation. The animals were tested for motor function and sensory function of the hindlimbs. The motor function was tested using the BBB score and sensory function using the plantar test. Considering the BBB testing, the right hindlimb was the injured one while the left hindlimb was considered the uninjured one. However, for the plantar test the left hindlimb was considered the injured one due to crossing of the spino-thalamic tract and the right hindlimb was considered uninjured.

### 2.3. BBB

All the animals in the study were pre-evaluated before surgery and then tested every week until week 12 after hydrogel implantation. The BBB scores for both legs were compared between the control group and the three groups of animals treated with hydrogels. During the 12 week period there were no statistically significant differences in the BBB scores for the left and right hindlimbs among any of the 4 groups (Figure 2).

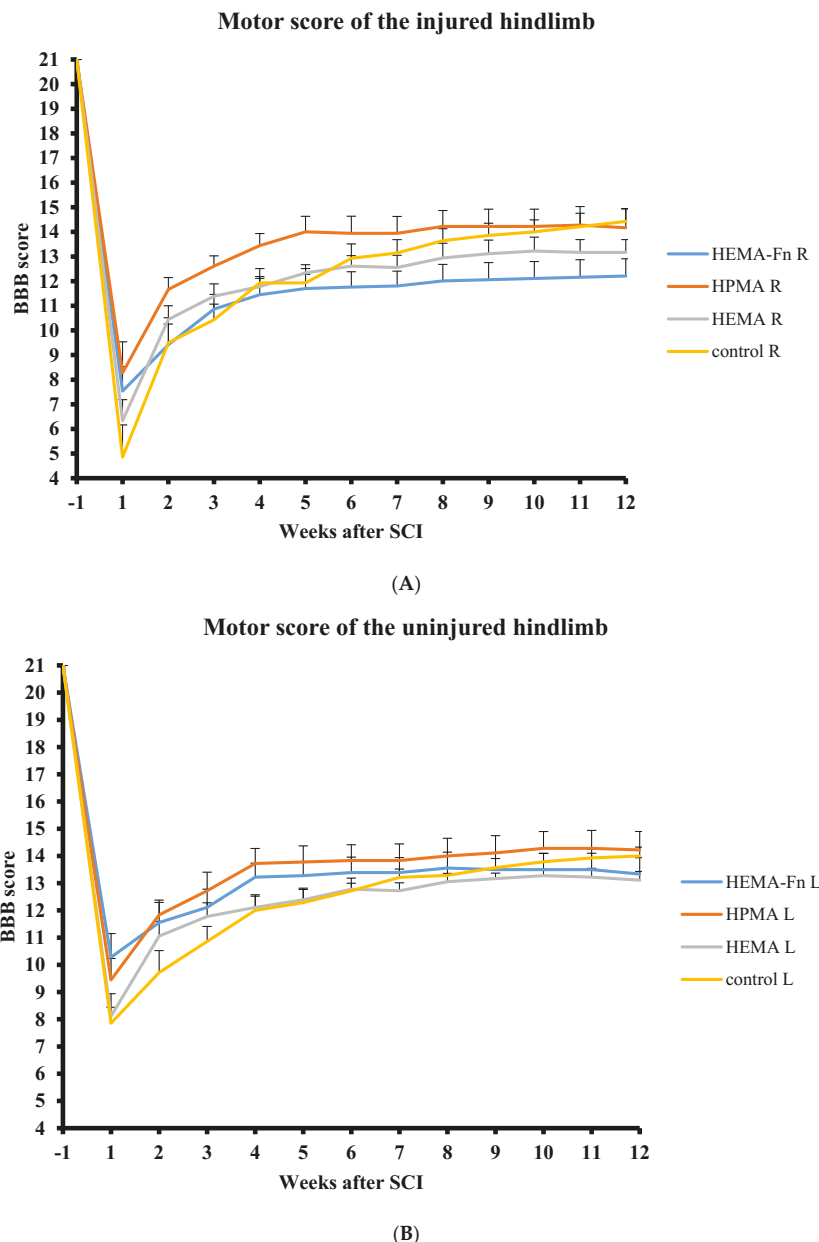


**Figure 2.** Comparison of motor function evaluation of the injured (A) and uninjured (B) side of hindlimbs using the BBB score. There were no statistically significant differences among the four groups (three treatment groups and one control group-hemisection only). Note the lower scores of the injured hindlimb on the side of the hemisection. The data represent mean values and error bars represent SEM.

#### 2.4. Plantar Test

The animals were pretreated twice before surgery and then evaluated once a week until week 12 after hydrogel implantation. The plantar test for the right leg (uninjured side, Figure 3A) was not statistically significant for any of the time period. However, for the left side (injured one, Figure 3B), we found a statistically significant difference between the HEMA-Fn and the hemisection group in week 5. Furthermore, there was a statistically significant difference between the HPMA hydrogel-treated group and the hemisection group and the HPMA-treated group and the HEMA-group in week 12.

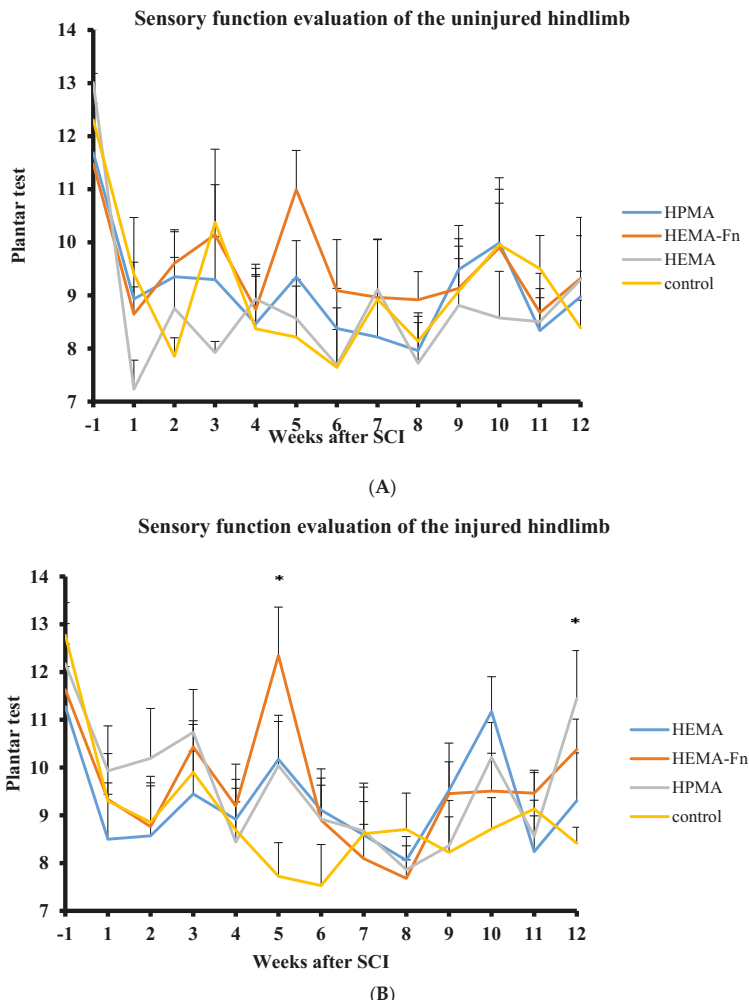


**Figure 3.** Sensory function evaluation of the uninjured (A) and injured (B) side of hindlimbs using the plantar test. There were statistically significant differences in the sensory response between rats treated with 2-hydroxyethylmethacrylate (HEMA)-Fn and the control group on week 5 and then between the HPMA and both the HEMA and the control group on week 12 (\* $p < 0.05$ ). The data represent mean values and error bars represent SEM.

## 2.5. Microscopic Evaluation of the Hydrogel Bridge

All three hydrogel scaffolds bridged the hemisection lesion providing scaffold for tissue regrowth. In some cases small residual cysts were present on the border between the hydrogel and the spinal cord (Figure 4A). There were no signs of foreign body reactions observed in or around the hydrogels 3 months after implantation. In the control group, the lesion was represented by a large cavity with no tissue inside (Figure 4B). There was a slight narrow rim of astrogliosis with small isles of astrocytes entering the border zones of all three hydrogel scaffolds (Figure 4C). We did not observe any difference despite the fact that plain HEMA resulted in upregulation of GFAP gene (see section Gene Expression). No signs of foreign body-type giant-cell granulomatous reaction were observed 3 months after hydrogel implantation. We found no statistically significant difference in the markers of immune response among any of the 3 scaffolds (see section Gene Expression).

## 2.6. Connective Tissue

All 3 types of hydrogels were filled with connective tissue, however there were obvious differences. Only a little dispersed connective tissue was present in the pores of the plain HEMA hydrogels (Figure 4D). Alternatively, in both the HPMA and the HEMA-Fn hydrogels, connective tissue elements were more abundant with a rather dense infiltration of the pores (Figure 4E,F). The HPMA hydrogel promoted connective tissue infiltration inside the scaffold, in both its peripheral as well as the central part, compared to the plain HEMA scaffold (Figure 5,  $p < 0.05$ ). The HEMA scaffold with attached fibronectin showed tendency towards higher connective tissue infiltration in both the peripheral and the central part of the hydrogel without reaching statistical significance (Figure 5,  $p < 0.05$ ).

## 2.7. Axonal Regeneration

After 3 months, HPMA hydrogels were infiltrated with axonal sprouts in the peripheral areas as well as in the central parts (Figure 6). The growth of axons was guided by the oriented pores, mostly in the cranio-caudal and caudo-cranial direction. The plain HEMA scaffold did not show any neurofilaments in its pores 3 months after implantation (Figure 4G), despite its upregulation of Gap43 (see section Gene Expression). In contrast, the HEMA-Fn hydrogels showed that some axons grew into the peripheral parts of the scaffold and a minimal amount also reached the central parts of the scaffold (Figure 4H). The amount of neurofilaments in the HPMA hydrogel was significantly higher compared to both HEMA-based scaffolds (Figure 4I). There were many new axons in the peripheral part of the HPMA scaffold which extended all the way to its central area (Figure 4J).

## 2.8. Growth of Blood Vessels in the Hydrogels

All three hydrogels showed an extensive ingrowth of blood vessels into the periphery as well as the central part of the scaffolds—both the HEMA-based hydrogels as well as the HPMA (Figure 4K,L). Despite not reaching statistical significance, the HEMA-based hydrogel modified with fibronectin supported the highest number of blood vessels compared to the plain HEMA and the HPMA scaffolds (Figure 7). There was also no difference in the VEGFA gene during molecular analysis (see section Gene Expression). As with the axons, blood vessels also grew predominantly in an oriented fashion guided by the pores

## 2.9. Gene Expression

Expression of genes related to regeneration (Vegfa, Bdnf, Gap43), glial scarring (Gfap) and infiltrating macrophage phenotype (Irf5, Cd86, Mrc1) was determined 3 months after hemisection or implantation of methacrylate scaffolds. Significant upregulation of Gfap genes was detected after treatment with HEMA when compared with controls. Implantation of HEMA resulted in a trend of upregulation of M2 associated Mrc1 when compared to both HEMA-Fn and HPMA. No other statistically significant difference in any markers within the tissue of spinal cords treated with the methacrylate hydrogels or controls were observed (Figure 8).

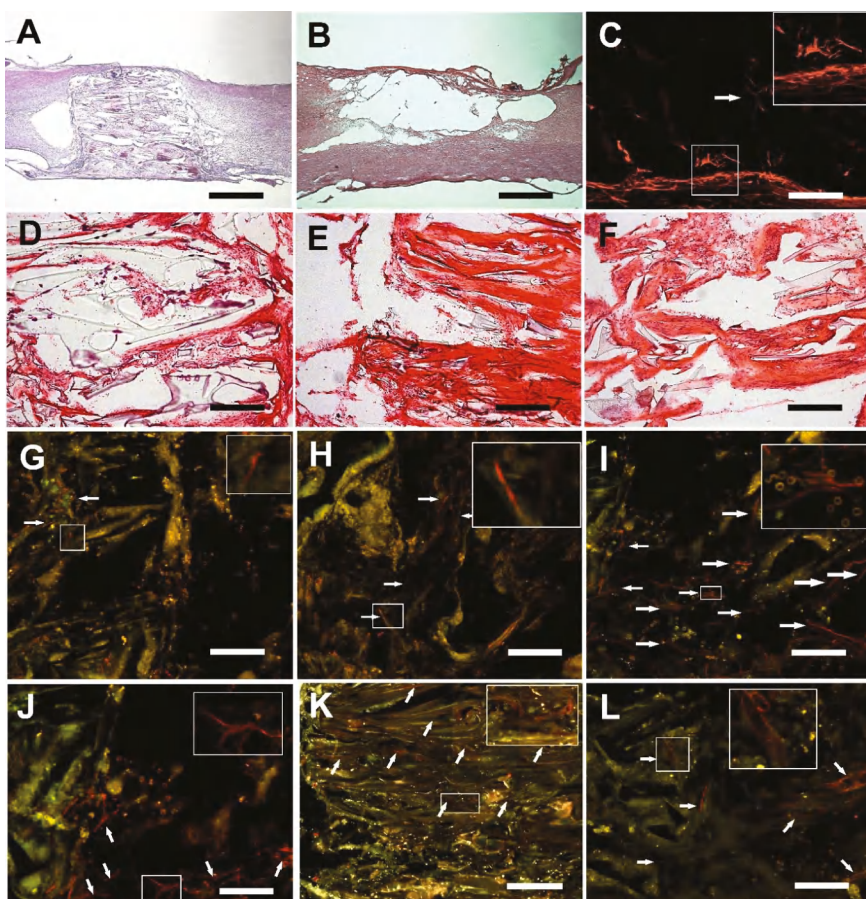


**Figure 4.** The mosaic presents various aspect of tissue ingrowth within the pores of the three methacrylate hydrogels. (A) HEMA-Fn sufficiently bridged the hemisection cavity. In some cases there were minor cavities on the border. The HEMA-Fn scaffold serves as a representative sample for all three methacrylate hydrogels (HE staining, scale bar = 1 mm). (B) The lesion resulted in a large pseudocystic cavity in the control group (HE staining, scale bar = 1 mm). (C) Subtle astrogliosis was present within the spinal cord tissue neighboring the HPMA scaffold and a few islets of astrocytes also infiltrated its peripheral part (white arrow, GFAP-Cy3 staining, scale bar = 100  $\mu$ m). (D) Sparse connective tissue elements were found in the plain HEMA scaffold; there was a more dense infiltration within the pores of the HEMA-Fn (E) and the HPMA hydrogel (F) HE staining, scale bar = 100  $\mu$ m. (G) No axonal sprouts were present in the HEMA scaffold, however, some axons (white arrows) reached the border zone of the spinal cord (NF160-g594 staining, scale bar = 25  $\mu$ m). (H) A small number of sprouts (white arrows) were present within the HEMA-Fn scaffold (NF160-g594 staining, scale bar = 25  $\mu$ m); significantly higher number of sprouts was present (white arrows) within the central parts (I) as well as the periphery (J) of the HPMA hydrogels (NF160-g594 staining, scale bar = 25  $\mu$ m). (K) Blood vessels (white arrows) grew abundantly within the pores of all three hydrogels especially the HEMA-Fn scaffold, as seen in this image (RECA-g488 staining, scale bar = 50  $\mu$ m). (L) A detailed view of the blood vessels within the HEMA-Fn scaffold (RECA-g488 staining, scale bar = 25  $\mu$ m). Insert boxes depict the typical elements described in each image of the mosaic (enlarged twice to the original size).

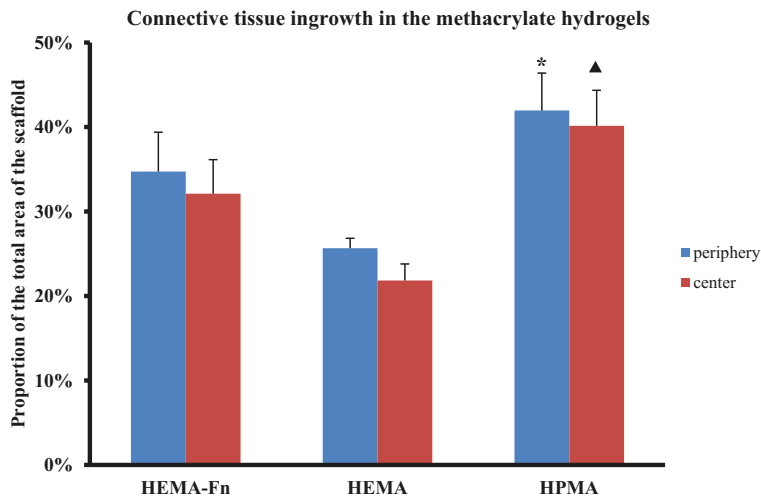


**Figure 5.** Comparison of connective tissue ingrowth within the three hydrogels. The graph presents the percentage of HE-positively stained tissue within the whole area of the peripheral (blue bars) and central (red bars) regions of the hydrogel. The HPMA scaffold showed higher connective tissue ingrowth within the periphery (\*  $p < 0.05$ ) as well as the central part (▲  $p < 0.05$ ) of the HEMA scaffold. Data shown as mean, and the error bars represent SEM. For statistical analysis, a one-way ANOVA test was used.

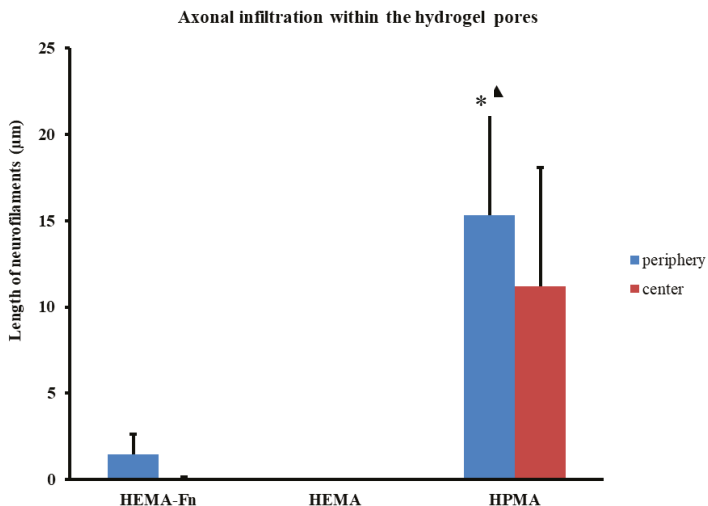


**Figure 6.** Comparison of axonal ingrowth within the three hydrogels. The total length of axons was assessed within the peripheral (blue bars) as well as the central (red bars) regions of the scaffold. The graph shows that the HPMA scaffold promoted statistically significant infiltration of axons within the pores of the scaffold compared to both HEMA hydrogels (\*  $p < 0.05$ , ▲  $p < 0.05$ ). The graph shows that there were no axons within the HEMA scaffold, while the modification of fibronectin (HEMA-Fn) showed at least some axonal infiltration with the periphery and some even grew as far as the central parts of the scaffold. Data shown as mean and the error bars represent SEM. For statistical analysis, a one-way ANOVA test was used.

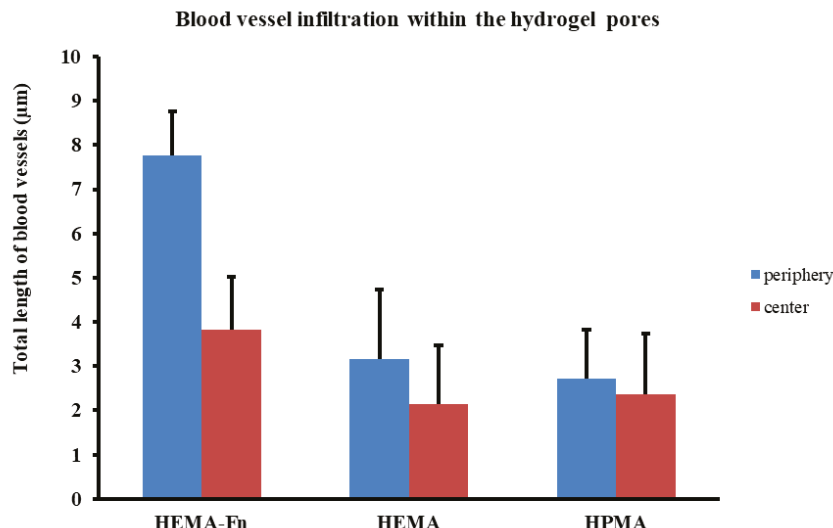


**Figure 7.** Comparison of blood vessels in growth within the three hydrogels. The total length of blood vessels was assessed within the peripheral (blue bars) as well as the central (red bars) regions of the scaffold. There was no statistically significant difference between the three groups but the HEMA-Fn scaffold showed a trend towards increased ingrowth of blood vessels within its pores, especially in the peripheral areas. Data shown as mean and the error bars represent SEM. For statistical analysis, a one-way ANOVA-test was used.

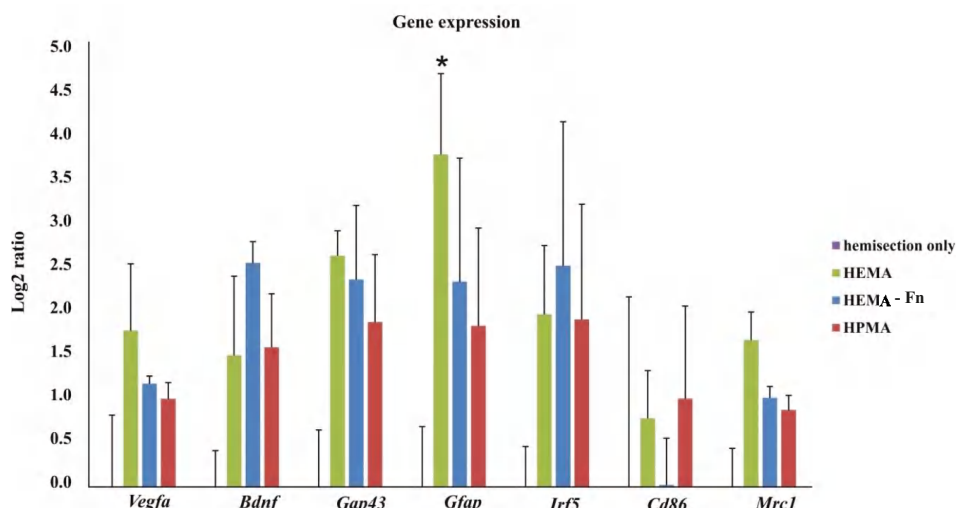


**Figure 8.** Gene expression in spinal cord tissue after treatment of hemisection with 3 different methacrylate scaffolds. Treatment with HEMA resulted in significant upregulation of *Gfap* when compared with controls (hemisection only,  $n = 3$ ). We found no other statistically significant difference in any markers within the tissue of spinal cords treated with the methacrylate hydrogels or controls. Data shown as mean and SEM relative to hemisection (injured tissue), which was set as 0 (with \*  $p < 0.05$  vs. hemisection). For statistical analysis a one-way ANOVA test was used.

### 3. Discussion

SCI, especially at its chronic stage, is characterized by glial scarring and pseudocystic cavities associated with disruption of long spinal cord tracts. Experimental studies using a variety of biomaterials, including hydrogels, have been conducted during the last 20 years [16]. In this study we evaluated two methacrylate hydrogels based on HEMA and HPMA, which are considered to be excellent synthetic biomaterials resembling living tissue, in terms of water content and mechanical properties [28,29]. Their porous properties, introduced by polymerization of the respective monomers in the presence of inorganic needle-like crystals, make them suitable for neural tissue or spinal cord reconstruction as has been shown in many studies [16,20,30,31]. The advantage of synthetic hydrogels consists not only of their biological inertness, but also in the variety of possible modifications, allowing better tissue repair promoting properties [23,32,33]. Our study showed that none of the methacrylate hydrogels caused a significant immune response, as demonstrated by no upregulation of antigen-presenting cells at 3 months. There were increased signs of tissue repair in the plain HEMA scaffold 3 months after SCI as demonstrated by an upregulation of an Mrc1 gene.

In this study, one of the HEMA scaffolds was modified with attached fibronectin. Our previous study showed better bridging qualities of the HPMA scaffold when compared to HEMA. Based on our positive results with surface modification of scaffolds, we also compared fibronectin-modified HEMA, to test whether such surface modification would balance the advantage of the HPMA scaffold. Fibronectin is known to promote cellular migration, proliferation, and differentiation [34,35]. In this study we showed better connective tissue infiltration within the HPMA scaffold compared to HEMA. There was more connective tissue within HEMA modified with fibronectin when compared to plain HEMA 3 months after SCI but without reaching statistical significance. This is an extension of the finding by other authors, which demonstrated that fibronectin enhances short-term cell adhesion [36].

Several studies have also shown that fibronectin may be neuroprotective, reducing post-traumatic apoptosis while enhancing functional outcome [37,38]. King et al. showed that fibronectin promotes the growth of axons into the implant when compared to other natural molecules such as fibrin or collagen, but with the disadvantage of having large cavities at the spinal cord lesion borderline [36]. The combination of an artificial scaffold with fibronectin thus seems to be a useful type of combined therapy that may promote the regrowth of axons while creating a positive milieu for the regrowth of new axons. The combination with a HEMA scaffold ensured good integration of the implant within the knife-cut experimental cavity while fibronectin promoted the axons to cross the hydrogel-spinal cord border and infiltrate the pores in the periphery of the implant as well as in the central area. Nonetheless, none of the three methacrylate hydrogels in our study led to motor function improvement. We did not observe any differences in BBB test, except for lower BBB score on the ipsilateral side. The results from plantar test indicate that no further hyperalgesia has developed after the hydrogel implantation. HEMA-Fn and HPMA resulted in only inconsistent sensory function difference of the left hindlimb, despite the differences in the number of axons within the three scaffolds. Spinal cord hemisection is not an ideal model for testing of functional improvement. However, it is suitable for histological evaluation and quantification of cellular ingrowth into the implant.

We did not observe any axons extending across the whole scaffold and crossing the scaffold-tissue border back and re-entering the spinal cord. A higher number of axons infiltrating the scaffold but without making connections across the bridge does not therefore necessarily result in functionally meaningful improvement.

Previous studies have also shown that fibronectin enhances axonal ingrowth after SCI but the studies were restricted to a short time evaluation period. This may not, however, reflect long-term data as we have shown in our recent paper [39]. In our study, fibronectin modification of the HEMA scaffold showed some increased but statistically insignificant difference in the ingrowth of axons into the peripheral and also central parts, while there were no axonal sprouts present in the plain HEMA 3 months after SCI. When comparing the results based on the chemical backbone of the hydrogel (HEMA vs. HPMA), the HPMA scaffold supports the regrowth of axons much better compared

to HEMA, even when the latter one is enriched with fibronectin. This is in line with our previous study, in which the HPMA scaffold showed improved axonal infiltration compared to HEMA [23]. Interestingly, molecular analysis showed a tendency towards increased sprouting in all three scaffolds. However, only HPMA hydrogel and partially HEMA-Fn create an environment which prevents the axon retraction from the hydrogel.

None of the tested scaffolds supported the ingrowth of astrocytes, though the GFAP protein was upregulated in the plain HEMA scaffold when compared with the hemisection. We observed only a slight astrogliosis around the 3 types of scaffolds.

New blood vessels grew into all three hydrogels; there were many of them throughout the periphery and growing further into the central parts. We found a tendency towards a denser blood vessel network in the HEMA-Fn hydrogel. This may be explained by the presence of the RGD (arginine–glycine–aspartate) peptide sequence within the fibronectin molecule, which has been shown to enhance vascular growth [23]. The presence of blood vessels within the lesion is vital as they promote axonal repair and enhance functional improvement [40,41].

Tissue engineering is based on creating a proregenerative environment for tissue repair within the lesion. The cells and their extensions (such as axons) should be properly guided in order to make functionally meaningful connections. The advantage of hydrogels with oriented pores is their ability to navigate the growth of new tissue along the long axis of their pores. However, solid hydrogels require a surgical opening of the spine and spinal cord during the process of implantation. Also, the hydrogels we evaluated were slightly stiffer compared to the scaffolds with randomly oriented pores used in our former studies, due to the need to properly retain the oriented inner structure [21,23,25]. This may be the cause of residual minor cavities on the border between the scaffold and the spinal cord. Injectable scaffolds, on the other hand, avoid the need for surgical incision and allow minimally-invasive implantation. They are also soft enough to adhere well to the spinal cord tissue. However, oriented pores within injectable scaffolds are more difficult to achieve, and therefore we cannot ensure targeted growth within such biomaterials [42]. Study of the synthesis of injectable scaffolds with oriented pores would be of interest in the future.

#### 4. Materials and Methods

##### 4.1. Hydrogel Scaffolds

2-Hydroxyethyl methacrylate (HEMA; Röhm, Germany) and ethylene dimethacrylate (EDMA; Ugilor S.A., France) were purified by distillation. 1-Amino-2-propanol, 1,2-diaminoethan, methacryloyl chloride, 2,2'-azobisisobutyronitrile (AIBN), 2-aminoethyl methacrylate (AEMA) hydrochloride, tris (2-carboxyethyl) phosphine hydrochloride (TCEP), and *N*- $\gamma$ -maleimidobutylsuccinimide ester (GMBS) were purchased from Sigma-Aldrich (St. Louis, USA). Ammonium oxalate (Lach-Ner; Neratovice, Czech Republic) was crystallized from water until the formation of 30–90  $\mu$ m thick and approximately 0.3–10 mm long needle-like crystals, which were used as a porogen. Fibronectin (Fn) from human plasma was obtained from Roche (Mannheim, Germany). All other chemicals were from Lach-Ner. Ultrapure Q water ultrafiltered on a Milli-Q Gradient A10 system (Millipore; Molsheim, France) was used for preparation of phosphate buffers saline (PBS) and all other experiments. *N*-(2-hydroxypropyl)methacrylamide (HPMA) and *N,N'*-ethylenebis(acrylamide) (EDMAAm) were synthetized by modification of published procedure [26]. Briefly, 1-amino-2-propanol (22.5 g), NaNO<sub>2</sub> (200 mg), and NaOH 12 g were dissolved in H<sub>2</sub>O (300 mL), cooled at 0 °C, and dry ice (40 g) and methacryloyl chloride (31.4 g) were added. The solution was slowly heated to room temperature (RT) and stirred for 4 h until formation of ethacryloyl chloride droplets. Water was evaporated and residuum was extracted by dichloromethane, the solution was dried with MgSO<sub>4</sub>, filtered through carbon black, and twice recrystallized from acetone/petroleum ether mixture. *N,N'*-ethylenebis(acrylamide) was synthetized analogously, only 1,2-diaminoethan (18 g) was used instead of 1-amino-2-propanol.

## Preparation of Superporouspoly (2-Hydroxyethyl Methacrylate) (HEMA), HEMA-Fn, and Poly [(*N*-(2-Hydroxypropyl) Methacrylamide] (HPMA) Hydrogels

Three polyethylene injection syringes (5 mL) equipped with a stainless filter were filled with needle-like ammonium oxalate crystals (~70 vol %). The monomer mixtures were prepared separately, one for each syringe: (i) HEMA (2.475 g) and EDMA (0.025 g; 1 wt %); (ii) HEMA (2.450 g), EDMA (0.025 g; 1 wt %), and AEMA (0.025 g; 1 wt %); and (iii) HPMA (2.475 g) and EDMAAm (0.025 g; 1 wt %). AIBN (40 mg) was dissolved in 1,4-dioxane (5 mL) and the solution was added to each mixture, which was transferred to the syringe containing crystals. The syringe was closed and the mixture polymerized at 60°C for 16 h. At the end of the reaction, the syringe was cut lengthwise, the hydrogel cylinder was removed and immersed in 10 wt % NH<sub>4</sub>Cl aqueous solution for 24 h, to avoid cracks and to remove 1,4-dioxane. The hydrogel was cut into 2 × 2 × 2 mm cubes, which were washed once with 0.01M HCl (100 mL) for 2 days to remove salts and finally with water. Amino groups of copolymer of HEMA and AEMA were reacted with a solution of GMBS (20 mg) in a mixture of 0.07M PBS (pH 7.4; 10.5 mL) and 1,4-dioxane (5.5 mL) at RT for 30 min to introduce maleimide (MI) groups on the surface. The product was twice washed with PBS/1,4-dioxane solution (PBS/1,4-dioxane = 10.5/5.5 v/v; 15 mL each), twice with water (15 mL each), and 0.1M PBS (pH 6.8; 15 mL). Fn (1 mg) containing glycine (1.126 mg) and sodium chloride (0.058 mg) were dissolved in PBS buffer (pH 7.4; 2 mL) for 2 h, a solution of TCEP (0.5 mg) in PBS (1 mL) was added and the mixture reacted at 23°C for 40 min. Poly HEMA-MI cubes were incubated in 0.1M PBS (pH 6.8; 20 mL), the solution of reduced Fn was added, and the reaction proceeded at RT for 1 h.

### 4.2. Animal Handling and Surgery

This study was performed in accordance with the European Communities Council Directive of 22 September 2010 (2010/63/EU) regarding the use of animals in research, and was approved by the Ethics Committee of the Institute of Experimental Medicine, Academy of Sciences of the Czech Republic.

### 4.3. Spinal Cord Injury and Hydrogel Implantation

Thirty-four male rats (Wistar, Anlab, Czech Republic) with a weight of 280–400 g, underwent a hemisection at the Th8 level. The animals were intraperitoneally injected with pentobarbital for anesthesia (0.06 g/1 kg i.p.); one dose of ATB (gentamicin 8 mg/1 kg i.m.), atropine (0.08 mg/1 kg s.c.), and mesocain to enhance local anesthesia (1 mg/1 kg s.c. + i.m.) was administered preoperatively. A linear skin incision was performed above the spinous processes of Th7-9; the paravertebral muscles were detached from the laminae Th7-9, and a Th8 laminectomy was performed. The dura was incised longitudinally in the midline and about a 2 mm-segment of spinal cord was dissected in its right half, creating a cavity within the spinal cord tissue. The hydrogel was implanted in such a way as to ensure that it would firmly adhere to the edges of the transection cavity without causing any undue pressure onto the surrounding spinal cord tissue. We implanted 9 rats with HEMA hydrogels with attached fragments of fibronectin, 9 rats with plain HEMA hydrogels, and 9 rats with HPMA hydrogels; 7 animals were left with hemisection only and served as controls. The muscles and skin were sutured again, and the animals were housed two in a cage with food and water ad libitum.

### 4.4. Behavioral Testing

#### BBB Test

The BBB open field test, originally described by Basso, Beattie, and Bresnahan [43] was used to assess basic locomotor functions (joint movement, weight support, forelimb-hindlimb coordination, paw placement, and stability of the body). All 34 rats were used for functional testing throughout the whole evaluation period. The rats were placed on the floor surrounded by boundaries making

a rectangular shape once a week. Results were evaluated in the range of 0 to 21 points (0 indicated complete lack of motor capability and 21 movements indicated a healthy rat).

#### 4.5. Plantar

The plantar test was performed using the plantar test instrument (Ugo Basile, Italy). A radiant thermal stimulus was applied to the plantar surface of the paws, and the latency of the paw withdrawal response was measured. Each paw was stimulated five times once a week. Hyperalgesia, as a response to the thermal stimulus, was defined as a significant decrease in the withdrawal latency.

#### 4.6. Tissue Processing and Histology

The animals were sacrificed 3 months after hydrogel implantation. They were then deeply anesthetized with an intraperitoneal injection of overdose pentobarbital and perfused with physiological saline, followed by 4% paraformaldehyde in 0.1M phosphate buffer. The spinal cord was left in the bone overnight, then removed and postfixed in the same fixative for at least 1 week.

A 4 cm-long segment of the spinal cord with the lesion site in the middle was dissected, and a series of 40 mm-thick longitudinal sections were collected. Hematoxylin–eosin staining was performed, using standard protocols, and the slides were specifically evaluated using an Axio Observer D1 microscope (Carl Zeiss Microimaging GmbH, Oberkochen, Germany). For immunohistochemical studies, the following primary antibodies and dilutions were used: Cy3-conjugated anti-GFAP (1:200; Sigma-Aldrich, Saint Louis, MO, USA) to identify astrocytes, anti-NF 160 (1:200; Sigma-Aldrich, Saint Louis, MO, USA) to identify neurofilaments, and RECA-1 (1:50; Abcam, Cambridge, UK) to identify endothelial cells of blood vessels. Alexa Fluor 594 goat anti–rabbit IgG (1:200; Invitrogen) and Cy3-conjugated anti-mouse IgM (1:100; Invitrogen, Carlsbad, CA, USA) were used as secondary antibodies.

#### 4.7. Tissue Quantification

The hydrogels were divided into 3 parts: the cranial end, the central part, and the caudal end. The whole surface of the scaffold per each slice was divided into 6 squares, 2 peripheral cranial and 2 peripheral caudal squares, and the central 2 squares corresponded to the hydrogel center. We calculated the number and the length of axons and blood vessels in each part of the scaffold, using the program TissueQuest Analysis Software (TissueGnostics GmbH, Vienna, Austria). Axonal fibers were manually traced within high resolution mosaic image with second channel as background. Using second channel (488 nm) as a reference channel, the combined image has shifted the background and hydrogel autofluorescence in to brown or yellow shade, whereas the specific fluorescence signal remains clear red. The mosaic was then analyzed by single squares at high magnification using a professional screen. Six spinal cords from each treatment group with 4–5 slices per spinal cord were analyzed. We then combined the data from the peripheral parts of the hydrogels (cranial and caudal ends) and evaluated them together. The central part was quantified and analyzed separately.

#### 4.8. qPCR

Expression of rat target genes *Vegfa*, *Bdnf*, *Gap43*, *Gfap*, *Irf5*, *Cd86*, and *Mrc1* at 3 months after hemisection with or without implanted hydrogel ( $n = 3\text{--}5$ ), was measured using quantitative real-time reverse transcription polymerase chain reaction (qRT-PCR). RNA was isolated from frozen spinal cord tissue sections, using the High Pure RNA Kit (Roche, Penzberg, Germany). RNA was quantified with spectrophotometer (NanoPhotometerTM P-Class, Munchen, Germany), and isolated RNA was reverse transcribed into cDNA using Transcriptor Universal cDNA Master (Roche, Penzberg, Germany) and a thermal cycler (T100™ Thermal Cycler, Bio-Rad, Hercules, CA, USA). Reactions were performed using cDNA solution, FastStart Universal Probe Master (Roche, Penzberg, Germany), and TaqMan® Gene Expression Assays (Life Technologies, Carlsbad, CA, USA): glyceraldehyde-3-phosphate dehydrogenase/Gapdh/Rn01775763\_g1,

vascular endothelial growth factor/Vegf/Rn01511602\_m1, brain-derived neurotrophic factor/Bdnf/Rn02531967\_s1, growth associated protein 43/Gap43/Rn01474579\_m1, glial fibrillary acidic protein/Gfap/Rn00566603\_m1, interferon regulatory factor 5/Irf5/Rn01500522\_m1, macrophage mannose receptor 1/Mrc1/Rn01487342\_m1, and CD86/Rn00571654\_m1. The final reaction volume was 10  $\mu$ L containing 25 ng of extracted RNA. Real-time PCR cycler (StepOnePlus<sup>TM</sup>, Life Technologies, Carlsbad, CA, USA) was used for amplification. The following cycling conditions were used, 2 min at 50 °C, 10 min at 95 °C, followed by 40 cycles of 15 s at 95 °C and 1 min at 60 °C. Relative quantification of gene expression was determined using the  $\Delta\Delta Ct$  method. Data was analyzed with StepOnePlus<sup>®</sup> software (v2.3) Life Technologies, Carlsbad, CA, USA). For normalization of gene expression levels Gapdh gene was used. A log2 scale was used to display the symmetric magnitude for up- and downregulated genes. From obtained values of control animals (hemi-section only), the arithmetical mean was calculated and this value was set as zero. The statistical analysis (*t*-test) was performed from  $\Delta Ct$  values of controls as well as treated animals.

#### 4.9. Statistical Analysis

The mean values are reported as mean  $\pm$  SEM. For behavioral tests histological analysis and gene markers intergroup differences were analyzed using one-way ANOVA (probability values <0.05).

### 5. Conclusions

The HPMA hydrogel shows better potential for SCI repair compared to HEMA hydrogel. The attachment of fibronectin improves limited connective tissue and axonal ingrowth, however without any long-term functional improvement. More sophisticated modifications of future scaffolds would be needed if we want to achieve functionally relevant long-term results.

**Author Contributions:** A.H., D.H., Š.K. and P.J. designed the study, H.M., V.P. and D.H. participated in preparing the three methacrylate hydrogel scaffolds, A.H. performed the surgical procedures (hydrogel implantation), K.K. (Kristýna Kekulová) and B.S. performed functional testing, J.R. and K.J. did tissue analysis, J.C. and A.H. participated in data analysis and statistical evaluation, A.H., Š.K. and P.J. wrote the paper and performed final revision and evaluation of the manuscript. K.K. (Kristýna Kárová) and L.M.U. did qPCR analysis.

**Funding:** The study has been supported by two grants from the Grant Agency of the Czech Republic 14-14961S, 17-11140S, the Operational Programme Research, Development and Education in the framework of the project “Centre of Reconstructive Neuroscience”, registration number CZ.02.1.01/0.0/0.0/15\_003/0000419 and by a grant from the Ministry of Education, Youth and Sports No. LO1309. K.Ke. Š.K., K.Ka., L.M.U., D.H., B.S. and P.J. were members of the BIOCEV (CZ.1.05/1.1.00/02.0109) and their work was supported by the Ministry of Education, Youth and Sports of CR within the LQ1604 National Sustainability Program II (Project BIOCEV-FAR).

**Acknowledgments:** We would like to thank Frances Zatřepálková for proofreading the manuscript.

**Conflicts of Interest:** The authors declare no conflicts of interest.

### References

1. Atala, R.; Langer, R.; Thomson, J.; Nerem, R. *Principles of Regenerative Medicine*; Academic Press: Burlington, MA, USA, 2008.
2. Hu, B.H.; Su, J.; Messersmith, P.B. Hydrogels cross-linked by native chemical ligation. *Biomacromolecules* **2009**, *10*, 2194–2200. [[CrossRef](#)] [[PubMed](#)]
3. Slaughter, B.V.; Khurshid, S.S.; Fisher, O.Z.; Khademhosseini, A.; Peppas, N.A. Hydrogels in regenerative medicine. *Adv. Mater.* **2009**, *21*, 3307–3329. [[CrossRef](#)] [[PubMed](#)]
4. Drury, J.L.; Mooney, D.J. Hydrogels for tissue engineering: Scaffold design variables and applications. *Biomaterials* **2003**, *24*, 4337–4351. [[CrossRef](#)]
5. Hoffman, A.S. Hydrogels for biomedical applications. *Adv. Drug Deliv. Rev.* **2002**, *54*, 3–12. [[CrossRef](#)]
6. Shoichet, M. Polymer scaffolds for Biomaterials Applications. *Macromolecules* **2010**, *43*, 581–591. [[CrossRef](#)]

7. Ahuja, C.S.; Fehlings, M. Concise Review: Bridging the Gap: Novel Neuroregenerative and Neuroprotective Strategies in Spinal Cord Injury. *Stem Cells Transl. Med.* **2016**, *5*, 914–924. [[CrossRef](#)] [[PubMed](#)]
8. Estrada, V.; Brazda, N.; Schmitz, C.; Heller, S.; Blazyc, H.; Martini, R.; Muller, H.W. Long-lasting significant functional improvement in chronic severe spinal cord injury following scar resection and polyethylene glycol implantation. *Neurobiol. Dis.* **2014**, *67*, 165–179. [[CrossRef](#)] [[PubMed](#)]
9. Evans, A.R.; Euteneuer, S.; Chavez, E.; Mullen, L.M.; Hui, E.E.; Bhatia, S.N.; Ryan, A.F. Laminin and fibronectin modulate inner ear spiral ganglion neurite outgrowth in an in vitro alternate choice assay. *Dev. Neurobiol.* **2007**, *67*, 1721–1730. [[CrossRef](#)] [[PubMed](#)]
10. Chen, B.K.; Knight, A.M.; de Ruiter, G.C.; Spinner, R.J.; Yaszemski, M.J.; Currier, B.L.; Windebank, A.J. Axon regeneration through scaffold into distal spinal cord after transection. *J. Neurotrauma* **2009**, *26*, 1759–1771. [[CrossRef](#)] [[PubMed](#)]
11. Miller, C.; Shanks, H.; Witt, A.; Rutkowski, G.; Mallapragada, S. Oriented Schwann cell growth on micropatterned biodegradable polymer substrates. *Biomaterials* **2001**, *22*, 1263–1269. [[CrossRef](#)]
12. Zhu, Y.; Soderblom, C.; Trojanowsky, M.; Lee, D.H.; Lee, J.K. Fibronectin Matrix Assembly after Spinal Cord Injury. *J. Neurotrauma* **2015**, *32*, 1158–1167. [[CrossRef](#)] [[PubMed](#)]
13. Novikova, L.N.; Pettersson, J.; Brohlin, M.; Wiberg, M.; Novikov, L.N. Biodegradable poly-beta-hydroxybutyrate scaffold seeded with Schwann cells to promote spinal cord repair. *Biomaterials* **2008**, *29*, 1198–1206. [[CrossRef](#)] [[PubMed](#)]
14. Venstrom, K.A.; Reichardt, L.F. Extracellular matrix. 2: Role of extracellular matrix molecules and their receptors in the nervous system. *Off. Publ. Fed. Am. Soc. Exp. Biol.* **1993**, *7*, 996–1003. [[CrossRef](#)]
15. Tysseling-Mattiace, V.M.; Sahni, V.; Niece, K.L.; Birch, D.; Czeisler, C.; Fehlings, M.G.; Stupp, S.I.; Kessler, J.A. Self-assembling nanofibers inhibit glial scar formation and promote axon elongation after spinal cord injury. *J. Neurosci.* **2008**, *28*, 3814–3823. [[CrossRef](#)] [[PubMed](#)]
16. Hejcl, A.; Lesny, P.; Pradny, M.; Michalek, J.; Jendelova, P.; Stulik, J.; Sykova, E. Biocompatible hydrogels in spinal cord injury repair. *Physiol. Res.* **2008**, *57* (Suppl. 3), S121–S132. [[PubMed](#)]
17. Pradny, M.; Michalek, J.; Lesny, P.; Hejcl, A.; Vacik, J.; Slouf, M.; Sykova, E. Macroporous hydrogels based on 2-hydroxyethyl methacrylate. Part 5: Hydrolytically degradable materials. *J. Mater. Sci. Mater. Med.* **2006**, *17*, 1357–1364. [[CrossRef](#)] [[PubMed](#)]
18. Kubinova, S.; Horak, D.; Hejcl, A.; Plichta, Z.; Kotek, J.; Sykova, E. Highly superporous cholesterol-modified poly(2-hydroxyethyl methacrylate) scaffolds for spinal cord injury repair. *J. Biomed. Mater. Res. A* **2011**, *99*, 618–629. [[CrossRef](#)] [[PubMed](#)]
19. Zaviskova, K.; Tukmachev, D.; Dubisova, J.; Vackova, I.; Hejcl, A.; Bystranova, J.; Pravda, M.; Scigalkova, I.; Sulakova, R.; Velevbny, V.; et al. Injectable hydroxyphenyl derivative of hyaluronic acid hydrogel modified with rgd as scaffold for spinal cord injury repair. *J. Biomed. Mater. Res. A* **2018**, *106*, 1129–1140. [[CrossRef](#)] [[PubMed](#)]
20. Sykova, E.; Jendelova, P.; Urdzikova, L.; Lesny, P.; Hejcl, A. Bone marrow stem cells and polymer hydrogels—Two strategies for spinal cord injury repair. *Cell Mol. Neurobiol.* **2006**, *26*, 1113–1129. [[CrossRef](#)] [[PubMed](#)]
21. Hejcl, A.; Urdzikova, L.; Sedy, J.; Lesny, P.; Pradny, M.; Michalek, J.; Burian, M.; Hajek, M.; Zamecnik, J.; Jendelova, P.; et al. Acute and delayed implantation of positively charged 2-hydroxyethyl methacrylate scaffolds in spinal cord injury in the rat. *J. Neurosurg. Spine* **2008**, *8*, 67–73. [[CrossRef](#)] [[PubMed](#)]
22. Kubinova, S.; Horak, D.; Hejcl, A.; Plichta, Z.; Kotek, J.; Proks, V.; Forostyak, S.; Sykova, E. SIKVAV-modified highly superporous PHEMA scaffolds with oriented pores for spinal cord injury repair. *J. Tissue Eng. Regen. Med.* **2015**, *9*, 1298–1309. [[CrossRef](#)] [[PubMed](#)]
23. Hejcl, A.; Ruzicka, J.; Kapcalova, M.; Turnovcova, K.; Krumbholcova, E.; Pradny, M.; Michalek, J.; Cihlar, J.; Jendelova, P.; Sykova, E. Adjusting the chemical and physical properties of hydrogels leads to improved stem cell survival and tissue ingrowth in spinal cord injury reconstruction: A comparative study of four methacrylate hydrogels. *Stem Cells Dev.* **2013**, *22*, 2794–2805. [[CrossRef](#)] [[PubMed](#)]
24. Hejcl, A.; Lesny, P.; Pradny, M.; Sedy, J.; Zamecnik, J.; Jendelova, P.; Michalek, J.; Sykova, E. Macroporous hydrogels based on 2-hydroxyethyl methacrylate. Part 6: 3D hydrogels with positive and negative surface charges and polyelectrolyte complexes in spinal cord injury repair. *J. Mater. Sci. Mater. Med.* **2009**, *20*, 1571–1577. [[CrossRef](#)] [[PubMed](#)]

25. Hejcl, A.; Sedy, J.; Kapcalova, M.; Toro, D.A.; Amemori, T.; Lesny, P.; Likavcanova-Masinova, K.; Krumbholcova, E.; Pradny, M.; Michalek, J.; et al. HPMA-RGD hydrogels seeded with mesenchymal stem cells improve functional outcome in chronic spinal cord injury. *Stem Cells Dev.* **2010**, *19*, 1535–1546. [[CrossRef](#)] [[PubMed](#)]
26. Filippov, S.; Hruby, M.; Konak, C.; Mackova, H.; Spirkova, M.; Stepanek, P. Novel pH-responsive nanoparticles. *Langmuir* **2008**, *24*, 9295–9301. [[CrossRef](#)] [[PubMed](#)]
27. Bruzauskaitė, I.; Bironaite, D.; Bagdonas, E.; Bernotiene, E. Scaffolds and cells for tissue regeneration: Different scaffold pore sizes-different cell effects. *Cytotechnology* **2016**, *68*, 355–369. [[CrossRef](#)] [[PubMed](#)]
28. Flynn, L.; Dalton, P.D.; Shoichet, M.S. Fiber templating of poly(2-hydroxyethyl methacrylate) for neural tissue engineering. *Biomaterials* **2003**, *24*, 4265–4272. [[CrossRef](#)]
29. Woerly, S.; Pinet, E.; de Robertis, L.; Van Diep, D.; Bousmina, M. Spinal cord repair with PHPMA hydrogel containing RGD peptides (NeuroGel). *Biomaterials* **2001**, *22*, 1095–1111. [[CrossRef](#)]
30. Hejcl, A.; Jendelova, P.; Sykova, E. Experimental reconstruction of the injured spinal cord. *Adv. Technol. Stand. Neurosurg.* **2011**, *37*, 65–95.
31. Loh, N.K.; Woerly, S.; Bunt, S.M.; Wilton, S.D.; Harvey, A.R. The regrowth of axons within tissue defects in the CNS is promoted by implanted hydrogel matrices that contain BDNF and CNTF producing fibroblasts. *Exp. Neurol.* **2001**, *170*, 72–84. [[CrossRef](#)] [[PubMed](#)]
32. Plant, G.W.; Woerly, S.; Harvey, A.R. Hydrogels containing peptide or aminosugar sequences implanted into the rat brain: Influence on cellular migration and axonal growth. *Exp. Neurol.* **1997**, *143*, 287–299. [[CrossRef](#)] [[PubMed](#)]
33. Kang, C.E.; Baumann, M.D.; Tator, C.H.; Shoichet, M.S. Localized and sustained delivery of fibroblast growth factor-2 from a nanoparticle-hydrogel composite for treatment of spinal cord injury. *Cells Tissues Organs* **2013**, *197*, 55–63. [[CrossRef](#)] [[PubMed](#)]
34. Danen, E.H.; Yamada, K.M. Fibronectin, integrins, and growth control. *J. Cell Physiol.* **2001**, *189*, 1–13. [[CrossRef](#)] [[PubMed](#)]
35. To, W.S.; Midwood, K.S. Plasma and cellular fibronectin: Distinct and independent functions during tissue repair. *Fibrog. Tissue Repair* **2011**, *4*, 21. [[CrossRef](#)] [[PubMed](#)]
36. King, V.R.; Alovskaya, A.; Wei, D.Y.; Brown, R.A.; Priestley, J.V. The use of injectable forms of fibrin and fibronectin to support axonal ingrowth after spinal cord injury. *Biomaterials* **2010**, *31*, 4447–4456. [[CrossRef](#)] [[PubMed](#)]
37. Sakai, T.; Johnson, K.J.; Murozono, M.; Sakai, K.; Magnuson, M.A.; Wieloch, T.; Cronberg, T.; Isshiki, A.; Erickson, H.P.; Fassler, R. Plasma fibronectin supports neuronal survival and reduces brain injury following transient focal cerebral ischemia but is not essential for skin-wound healing and hemostasis. *Nat. Med.* **2001**, *7*, 324–330. [[CrossRef](#)] [[PubMed](#)]
38. King, V.R.; Hewazy, D.; Alovskaya, A.; Phillips, J.B.; Brown, R.A.; Priestley, J.V. The neuroprotective effects of fibronectin mats and fibronectin peptides following spinal cord injury in the rat. *Neuroscience* **2010**, *168*, 523–530. [[CrossRef](#)] [[PubMed](#)]
39. Hejcl, A.; Ruzicka, J.; Proks, V.; Mackova, H.; Kubinova, S.; Tukmachev, D.; Cihlar, J.; Horak, D.; Jendelova, P. Dynamics of tissue ingrowth in SIKVAV-modified highly superporous PHEMA scaffolds with oriented pores after bridging a spinal cord transection. *J. Mater. Sci. Mater. Med.* **2018**, *29*, 89. [[CrossRef](#)] [[PubMed](#)]
40. Iida, T.; Nakagawa, M.; Asano, T.; Fukushima, C.; Tachi, K. Free vascularized lateral femoral cutaneous nerve graft with anterolateral thigh flap for reconstruction of facial nerve defects. *J. Reconstr. Microsurg.* **2006**, *22*, 343–348. [[CrossRef](#)] [[PubMed](#)]
41. Glaser, J.; Gonzalez, R.; Sadr, E.; Keirstead, H.S. Neutralization of the chemokine CXCL10 reduces apoptosis and increases axon sprouting after spinal cord injury. *J. Neurosci. Res.* **2006**, *84*, 724–734. [[CrossRef](#)] [[PubMed](#)]
42. Macaya, D.; Spector, M. Injectable hydrogel materials for spinal cord regeneration: A review. *Biomed. Mater.* **2012**, *7*, 012001. [[CrossRef](#)] [[PubMed](#)]
43. Basso, D.M.; Beattie, M.S.; Bresnahan, J.C. A sensitive and reliable locomotor rating scale for open field testing in rats. *J. Neurotrauma* **1995**, *12*, 1–21. [[CrossRef](#)] [[PubMed](#)]



© 2018 by the authors. Licensee MDPI, Basel, Switzerland. This article is an open access article distributed under the terms and conditions of the Creative Commons Attribution (CC BY) license (<http://creativecommons.org/licenses/by/4.0/>).

Article

# Perineuronal Nets in Spinal Motoneurones: Chondroitin Sulphate Proteoglycan around Alpha Motoneurones

Sian F. Irvine <sup>1</sup> and Jessica C. F. Kwok <sup>1,2,\*</sup>

<sup>1</sup> School of Biomedical Sciences, University of Leeds, Leeds LS2 9JT, UK; bs11sf@leeds.ac.uk

<sup>2</sup> Centre of Reconstructive Neurosciences, Institute of Experimental Medicine, The Czech Academy of Sciences, Prague 4, Czech Republic

\* Correspondence: J.Kwok@leeds.ac.uk; Tel.: +44-0113-343-9802

Received: 28 February 2018; Accepted: 7 April 2018; Published: 12 April 2018

**Abstract:** Perineuronal nets (PNNs) are extracellular matrix structures surrounding neuronal sub-populations throughout the central nervous system, regulating plasticity. Enzymatically removing PNNs successfully enhances plasticity and thus functional recovery, particularly in spinal cord injury models. While PNNs within various brain regions are well studied, much of the composition and associated populations in the spinal cord is yet unknown. We aim to investigate the populations of PNN neurones involved in this functional motor recovery. Immunohistochemistry for choline acetyltransferase (labelling motoneurones), PNNs using *Wisteria floribunda* agglutinin (WFA) and chondroitin sulphate proteoglycans (CSPGs), including aggrecan, was performed to characterise the molecular heterogeneity of PNNs in rat spinal motoneurones (Mns). CSPG-positive PNNs surrounded ~70–80% of Mns. Using WFA, only ~60% of the CSPG-positive PNNs co-localised with WFA in the spinal Mns, while ~15–30% of Mns showed CSPG-positive but WFA-negative PNNs. Selective labelling revealed that aggrecan encircled ~90% of alpha Mns. The results indicate that (1) aggrecan labels spinal PNNs better than WFA, and (2) there are differences in PNN composition and their associated neuronal populations between the spinal cord and cortex. Insights into the role of PNNs and their molecular heterogeneity in the spinal motor pools could aid in designing targeted strategies to enhance functional recovery post-injury.

**Keywords:** perineuronal nets; spinal cord; alpha motoneurone; gamma motoneurone; chondroitin sulphate proteoglycans

## 1. Introduction

Perineuronal nets (PNNs) are dense specialised extracellular matrix (ECM) structures that surround neuronal sub-populations throughout the central nervous system (CNS). First described by Golgi as reticular structures in the late 1800s [1], PNNs have since been implicated in pathologies of various neurological disorders, including Alzheimer's disease, epilepsy and schizophrenia [2–5], as well as in traumatic CNS injuries [6], particularly spinal cord injury (SCI) models [7,8]. A key role of PNNs is their involvement in the termination of developmental plasticity, where they form an interdigitating mesh with mature somatic and dendritic contacts to confer synaptic stabilisation [9–11].

PNNs are composed of a compact arrangement of a variety of neural ECM proteoglycans and proteins [12,13]. These components primarily consist of chondroitin sulphate proteoglycans (CSPGs) including the hyaluronan (HA) binding CSPGs called lecticans, bound upon a long HA backbone and stabilised by the HA and proteoglycan link proteins (HAPLNs) and tenascin-R [14]. Upon this basic PNN structure, the binding of other CSPGs (such as phosphacan) are thought to provide much of the heterogeneity of PNNs [15]. CSPGs are composed of chondroitin sulphate glycosaminoglycan

(CS-GAG) chains attached to a core protein that differentiates the various CSPGs from one another [15]. CS-GAGs confer a further vast degree of heterogeneity through variation of expression, chain length and sulphation patterns, even to the same core protein [16,17].

Although many studies have investigated the molecular heterogeneity of PNNs in distinct neuronal populations in regions of the brain [18–21], much of the composition and associated populations in the spinal cord is relatively unknown. Similar to the brain [22], in the spinal cord many of the known cells enwrapped by PNNs are fast-spiking inhibitory parvalbumin (PV)-positive interneurones (approximately half) [23,24], and have also been associated with calbindin-positive Renshaw cells [22]. However, in contrast to the brain, reports suggest that PNNs in the spinal cord also surround cells with large neuronal cell bodies, particularly within the ventral horn likely representing motoneurones (Mns) [22,25–27]. Mns are a heterogeneous population of neurones with the main subclasses, alpha and gamma Mns, innervating contractile extrafusal fibres and proprioceptive intrafusal fibres within the motor unit, respectively [28].

Enzymatic removal of PNNs using chondroitinase ABC (ChABC) after CNS injury has been shown in multiple models, predominately SCI, to reopen a window of plasticity to promote improvements in motor functions [7,8]. Regeneration of descending tracts can contribute to this functional recovery [29,30]; however, the extent and mechanism of changes in local spinal circuitry attributing to this recovery remains unclear. Additionally, studies also implicate exercise and rehabilitative training to activity-dependant modulation of PNNs in the ventral motor pools [31,32], suggesting a relationship between PNNs and Mns that is important for normal motor functions.

This study therefore aims to investigate the normal expression and molecular composition of PNNs in the spinal motor pools; the population of PNN-associated neurones in the spinal cord likely to be involved in functional motor recovery after SCI, and to identify the best PNN marker for this population. Immunohistochemical staining was performed using antibodies against choline acetyltransferase (ChAT), a marker of spinal Mns [33], alongside labelling for primary PNN components, including various CSPGs and the acclaimed “universal” PNN marker *Wisteria floribunda* agglutinin (WFA), to elucidate the composition of PNNs associated with spinal motor circuitry. Selective staining for the primary functional Mn subclasses was combined with PNN labelling to categorise PNN expression within the motor pool. It was found that distinct populations of Mns were surrounded by PNNs labelled by various CSPGs yet lacking WFA, indicating a difference between the composition of PNNs and associated neuronal cell types in the brain and spinal cord. PNNs were found to surround the majority of alpha Mns, suggesting that these are the main populations affected by ChABC-mediated recovery after SCI.

## 2. Results

We aim to determine the molecular heterogeneity of PNNs in the spinal cord, with a particular focus to the Mns in the ventral horn. Spinal cord sections from three different spinal levels, cervical, thoracic and lumbar, were used to compare the spatial differences of PNNs. Alongside ChAT staining, we also stained for WFA, a common PNN marker [6,7,10,34], and for CSPGs including aggrecan (ACAN), brevican (BCAN), neurocan (NCAN), versican (VCAN) and phosphacan (PTPRZ).

### 2.1. WFA-Positive PNNs Only Partially Overlap with Other CSPGs in the Ventral Motor Pools

#### 2.1.1. ACAN

ACAN is a CSPG in the lectican family and is widely considered to be a major component in PNNs [2,35,36]. Immunohistochemical staining of ACAN core protein illustrated clear expression of PNNs surrounding ventral Mns labelled with ChAT (Figure 1J–L). ACAN-positive PNNs surrounded approximately 85% of ChAT-positive Mns in all levels of the spinal cord investigated (Figure 1A–C). In comparison, WFA-positive PNNs enwrapped significantly fewer Mns (approximately 68% of the ChAT-positive Mns) than ACAN-positive PNNs (cervical  $p < 0.001$ , thoracic  $p < 0.05$  and lumbar  $p < 0.01$ ;

$n = 4$ ), illustrating that WFA does not label all PNNs in the ventral motor pools. Compounding this, the total number of ACAN-positive PNNs surrounding MnS was significantly greater than the number of ACAN+/WFA+ PNNs (cervical  $p < 0.001$ , thoracic  $p < 0.05$ , lumbar  $p < 0.01$ ;  $n = 4$ ). ACAN and WFA PNN populations appeared to overlap (Figure 1D–I). Further breakdown of PNN type revealed that, at each level, all PNNs that are positive for WFA co-localised with ACAN (n.s.;  $p = 1$ ). No investigated PNNs were WFA-positive and ACAN-negative. The results demonstrate that ACAN labels a larger population of PNN-positive MnS, and suggest that it is a better marker for PNN in the spinal cord.

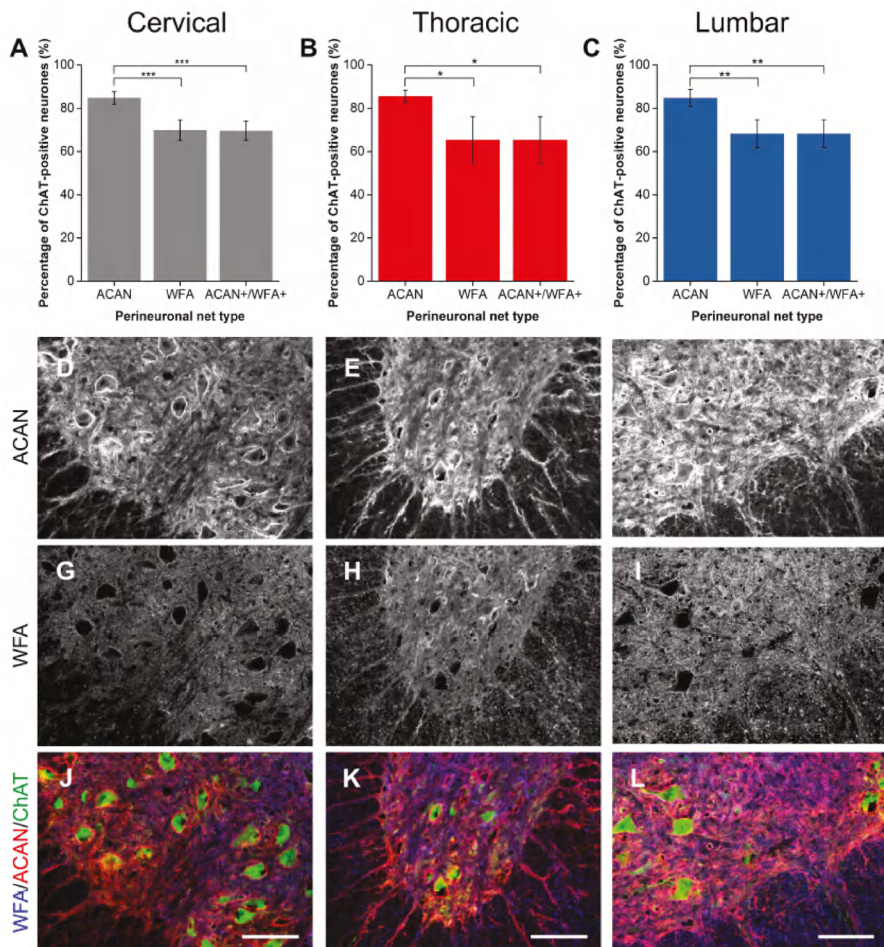


**Figure 1.** Comparison of perineuronal nets (PNNs) in the spinal ventral motor pools labelled by *Wisteria floribunda* agglutinin (WFA) and aggrecan (ACAN). (A–C) Bar graphs showing percentage of ChAT-positive motoneurones (Mns) in the ventral motor pools surrounded by ACAN-positive and WFA-positive PNNs and their co-localisation (ACAN+/WFA+) in cervical (A), thoracic (B) and lumbar (C) rat spinal cord. Error bars  $\pm$  SD;  $n = 4$ . Statistics one-way ANOVA; significance levels: \*  $p < 0.05$ , \*\*  $p < 0.01$ , \*\*\*  $p < 0.001$ . Confocal images showing ACAN-positive (D–F) and WFA-positive (G–I) PNNs surrounding ChAT-positive Mns (J–L) in the cervical, thoracic and lumbar spinal cord, respectively. Scale bars, 100  $\mu$ m.

### 2.1.2. BCAN

BCAN is a lectican CSPG found specifically in the CNS with growing evidence of its importance in regulating the plastic properties of PNNs [37]. Co-staining with ChAT-positive neurones in the ventral horn revealed a high degree of localisation, with approximately 88% of Mns encircled by BCAN-positive PNNs (Figure 2A–C). Similar to ACAN, WFA-positive PNNs appeared to denote some but not all of the BCAN-positive PNN-ensheathed Mns, labelling approximately 30% fewer Mns than BCAN (all levels  $p < 0.001$ ;  $n = 5$ ). BCAN+/WFA+ PNNs in the motor pools appeared to represent a proportion that is significantly less than the total BCAN-positive PNN population (all levels  $p < 0.001$ ;  $n = 5$ ). Additional categorisation again revealed that all WFA-positive PNNs in the motor pool co-localised with BCAN-positive PNNs.

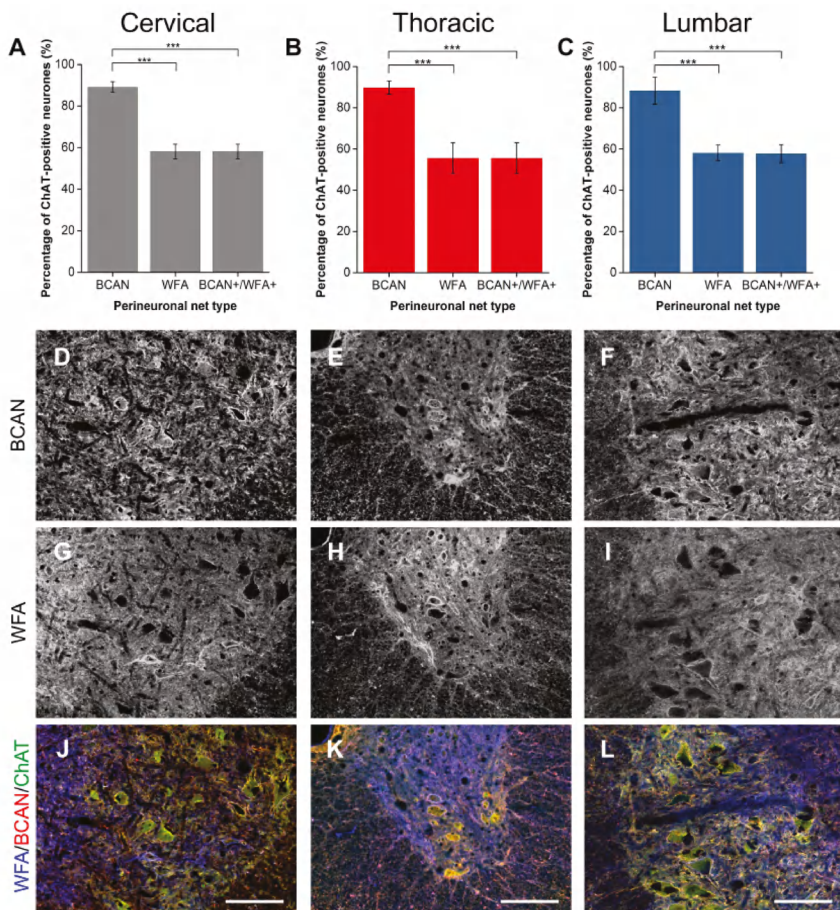


**Figure 2.** Comparison of perineuronal nets (PNNs) in the spinal ventral motor pools labelled by *Wisteria floribunda* agglutinin (WFA) and brevican (BCAN). (A–C) Bar graphs showing percentage of ChAT-positive motoneurones (Mns) in the ventral motor pools surrounded by BCAN-positive and WFA-positive PNNs and their co-localisation (BCAN+/WFA+) in cervical (A), thoracic (B) and lumbar (C) rat spinal cord. Error bars  $\pm$  SD;  $n = 5$ . Statistics one-way ANOVA; significance levels: \*\*\*  $p < 0.001$ . Confocal images showing BCAN-positive (D–F) and WFA-positive (G–I) PNNs surrounding ChAT-positive Mns (J–L) in the cervical, thoracic and lumbar spinal cord, respectively. Scale bars, 100  $\mu$ m.

### 2.1.3. NCAN

NCAN is a nervous system-specific lectican, like BCAN, known to be present in PNNs in the spinal cord [18,22,38]. In the ventral horn, NCAN staining revealed PNNs encircling approximately 87% of Mns (Figure 3A–C). Echoing the trend with ACAN and BCAN, WFA-positive PNNs enveloped 28% fewer Mns than NCAN (all levels  $p < 0.001$ ;  $n = 5$ ). Significantly, only approximately two-thirds of these NCAN-positive PNNs co-localised with WFA (all levels  $p < 0.001$ ;  $n = 5$ ). No WFA-positive PNNs lacking NCAN co-staining were observed, signifying that all WFA co-localised with NCAN.

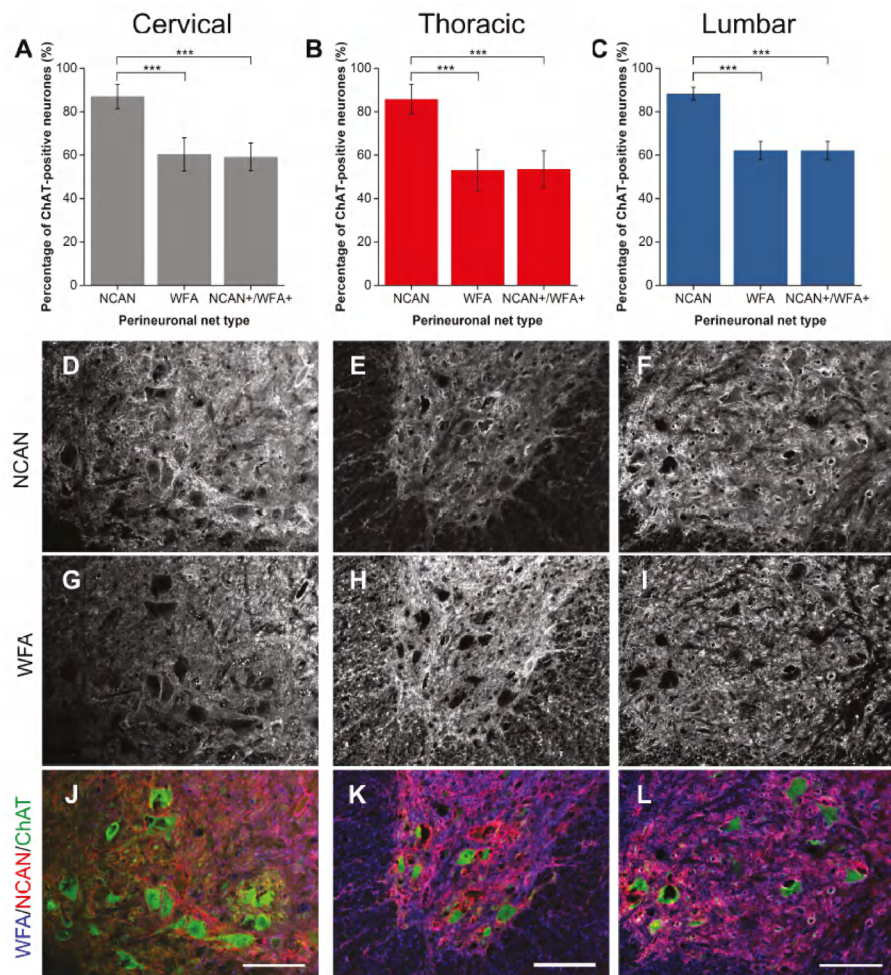


**Figure 3.** Comparison of perineuronal nets (PNNs) in the spinal ventral motor pools labelled by *Wisteria floribunda* agglutinin (WFA) and neurocan (NCAN). (A–C) Bar graphs showing percentage of ChAT-positive motoneurones (Mns) in the ventral motor pools surrounded by NCAN-positive and WFA-positive PNNs and their co-localisation (NCAN+WFA+) in cervical (A), thoracic (B) and lumbar (C) rat spinal cord. Error bars  $\pm$  SD;  $n = 5$ . Statistics: one-way ANOVA; significance levels: \*\*\*  $p < 0.001$ . Confocal images showing NCAN-positive (D–F) and WFA-positive (G–I) PNNs surrounding ChAT-positive Mns (J–L) in the cervical, thoracic and lumbar spinal cord, respectively. Scale bars, 100  $\mu$ m.

### 2.1.4. VCAN

VCAN staining revealed intense diffuse ECM expression in both the white and gray matter of the spinal cord due to its expression in the nodes of Ranvier [18,39,40]. VCAN did not show strong PNN staining in laminae other than the ventral horn. In the ventral horn, VCAN-positive PNNs surrounded approximately 82% of Mns at all spinal levels (Figure 4A–C). WFA and VCAN populations of PNNs showed a clear overlap at all spinal levels (Figure 4D–L). However, all WFA-positive PNNs co-localised with VCAN with a significant population of VCAN-positive PNNs WFA-negative (all levels  $p < 0.001$ ;  $n = 4$ ).

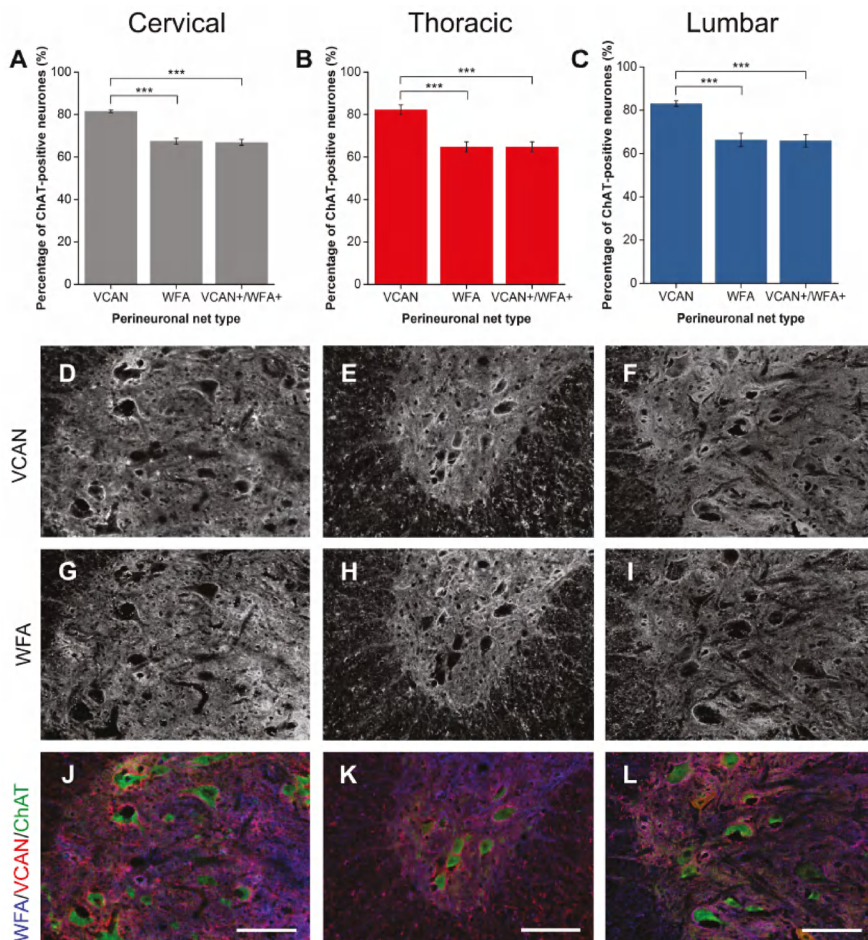


**Figure 4.** Comparison of perineuronal nets (PNNs) in the spinal ventral motor pools labelled by *Wisteria floribunda* agglutinin (WFA) and versican (VCAN). (A–C) Bar graphs showing percentage of ChAT-positive motoneurons (Mns) in the ventral motor pools surrounded by VCAN-positive and WFA-positive PNNs and their co-localisation (VCAN+/WFA+) in cervical (A), thoracic (B) and lumbar (C) rat spinal cord. Error bars  $\pm$  SD,  $n = 4$ . Statistics: one-way ANOVA; significance levels: \*  $p < 0.05$ , \*\*  $p < 0.01$ , \*\*\*  $p < 0.001$ . Confocal images showing VCAN-positive (D–F) and WFA-positive (G–I) PNNs surrounding ChAT-positive Mns (J–L) in the cervical, thoracic and lumbar spinal cord, respectively. Scale bars, 100  $\mu$ m.

## 2.1.5. PTPRZ

Phosphacan or PTPRZ is a non-HA binding CSPG that represents the extracellular domain of protein tyrosine phosphatase receptor zeta (PTPRZ) modified by glial cells [41,42] and has been found to be present in WFA-positive PNNs in the cerebral cortex [18,22,43]. Immunohistochemistry showed that PTPRZ is also found in PNNs in the ventral motor pool, surrounding approximately 76% of Mns in all levels of the cord studied (Figure 5A–C). However, in all levels of the spinal cord investigated, PTPRZ-positive PNNs surrounded 15% more Mns than WFA (all levels  $p < 0.01$ ;  $n = 4$ ), reiterating the trend shown by the lecticans above. Approximately 82% of PTPRZ-positive PNNs were also labelled by WFA, representing a significantly lower proportion of the total observed PTPRZ-positive PNNs in the motor pool (all level  $p < 0.05$ ;  $n = 4$ ).

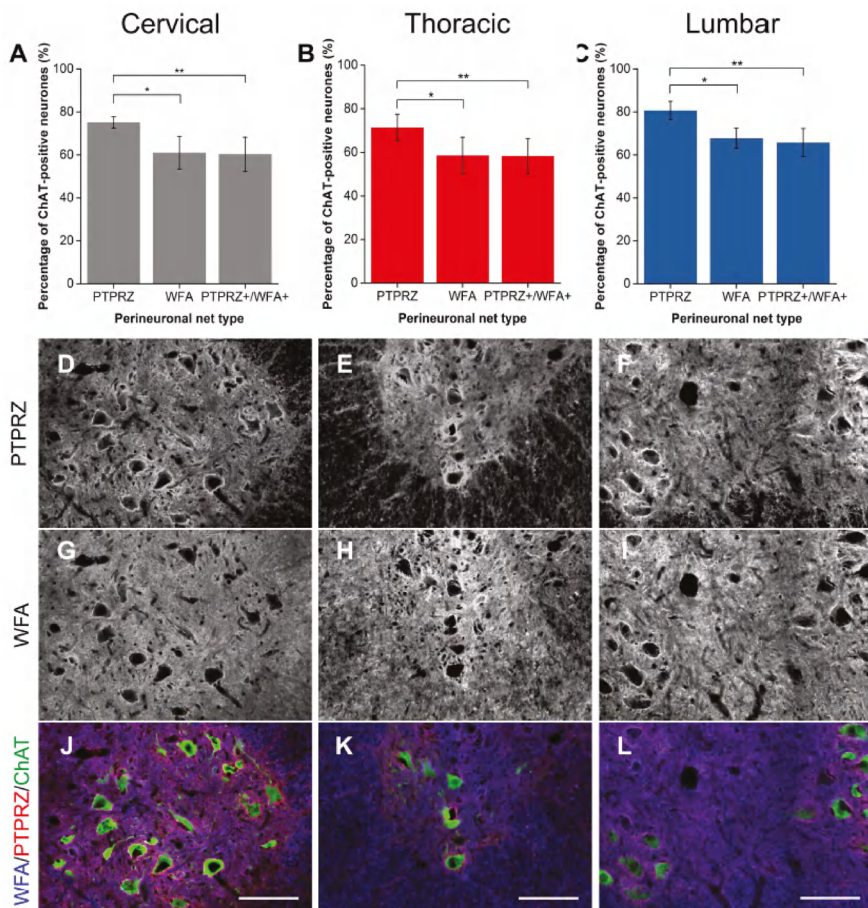


**Figure 5.** Comparison of perineuronal nets (PNNs) in the spinal ventral motor pools labelled by *Wisteria floribunda* agglutinin (WFA) and phosphacan (PTPRZ). (A–C) Bar graphs showing percentage of ChAT-positive motoneurones (Mns) in the ventral motor pools surrounded by PTPRZ-positive and WFA-positive PNNs and their co-localisation (PTPRZ+/WFA+) in cervical (A), thoracic (B) and lumbar (C) rat spinal cord. Error bars  $\pm$  SD;  $n = 4$ . Statistics: one-way ANOVA; significance levels: \*  $p < 0.05$ , \*\*  $p < 0.01$ . Confocal images showing PTPRZ-positive (D–F) and WFA-positive (G–I) PNNs surrounding ChAT-positive Mns (J–L) in the cervical, thoracic and lumbar spinal cord, respectively. Scale bars, 100  $\mu$ m.

## 2.2. Distinct Populations of CSPG-Positive yet WFA-Negative PNNs in the Motor Pools

For each CSPG investigated, a significant percentage of Mns were surrounded by PNNs that were CSPG-positive yet WFA-negative (all levels, all CSPGs  $p < 0.001$ ). The percentage of Mns with WFA-negative PNNs varied with CSPG investigated (Figure 6). While ACAN+/WFA-, VCAN+/WFA- and PTPRZ+/WFA- PNNs encircled roughly 15% of Mns (Figure 6A,D,E), a higher percentage of Mns (approximately 30%) appeared to be surrounded by BCAN+/WFA- and NCAN+/WFA- PNNs (Figure 6B,C). Overall, the results suggest that in the ventral motor pools, WFA does not denote all PNNs, and instead distinct populations of Mns with CSPG-positive, WFA-negative PNNs exist.

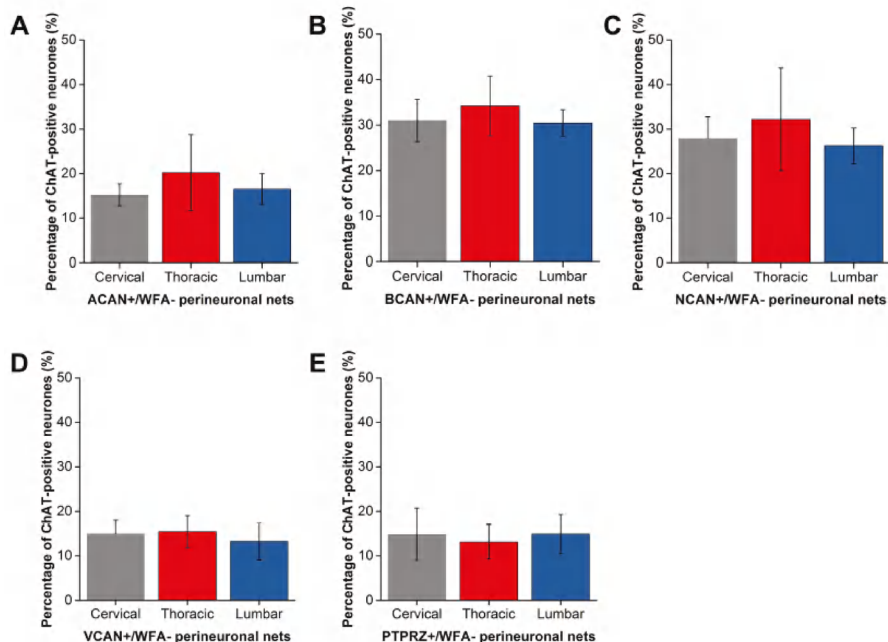


**Figure 6.** A proportion of perineuronal nets (PNNs) in the spinal motor pools were negative for *Wisteria floribunda* agglutinin (WFA). Percentage of ChAT-positive motoneurones in the ventral motor pools in the cervical, thoracic and lumbar spinal cord surrounded by CSPG-positive, WFA-negative PNNs. (A) Aggrecan (ACAN,  $n = 4$ ); (B) brevican (BCAN,  $n = 5$ ); (C) neurocan (NCAN,  $n = 5$ ); (D) versican (VCAN,  $n = 4$ ); and (E) phosphacan (PTPRZ,  $n = 4$ ). Error bars  $\pm$  SD. Statistics one-way ANOVA; n.s.

## 2.3. Alpha Mns Are Preferentially Surrounded by PNNs

Using NeuN and ChAT co-labelling, Mns in the spinal ventral motor pools were selectively labelled as either alpha (NeuN-positive) or gamma (NeuN-negative) [31,44]. It was observed that approximately 70–80% of ChAT-positive Mns were NeuN-positive (Figures 7 and 8), signifying the alpha Mn population. Firstly, as the universal marker for PNNs, WFA was used to determine the number of PNNs surrounding each Mn subtype. Similarly to the results above, WFA-positive PNNs surrounded approximately 60% of all Mns with approximately 98% of these PNNs surrounding NeuN-positive Mns (alphas; Figure 7A–C). In other words, a significant proportion of alpha Mns (~72%) were associated with WFA-positive PNNs (cervical and lumbar  $p < 0.001$ , thoracic  $p < 0.05$ ;  $n = 3$ ). As previous findings illustrated that in the ventral motor pools, WFA did not label all Mns, ACAN was also used to identify PNNs around Mn subtype. Again, most PNNs (95%) surrounded

alpha Mns (Figure 8A–C). ACAN-positive PNNS encircled roughly 90% of alpha Mns, suggesting that PNN-positive Mns and alpha Mns are the same population.

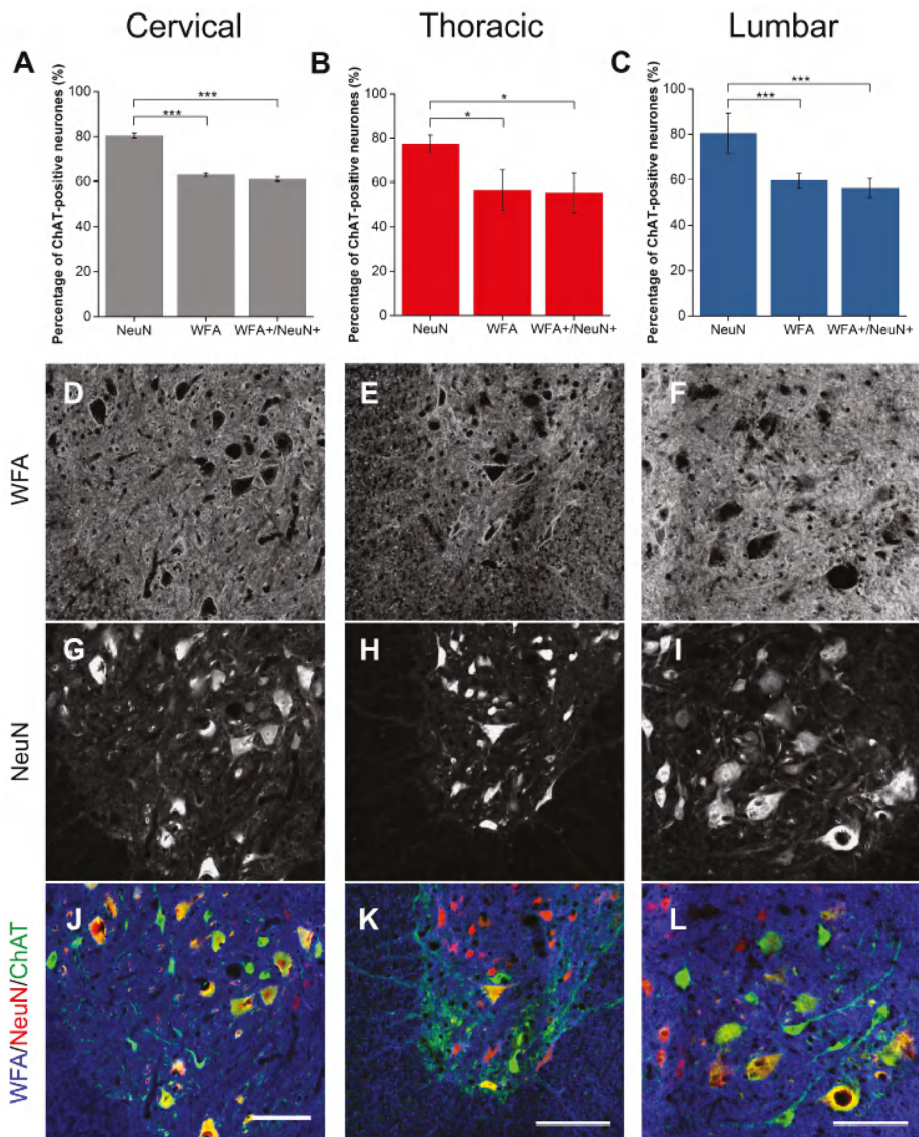


**Figure 7.** *Wisteria floribunda* agglutinin (WFA)-positive PNNS surrounded some but not all alpha motoneurones (Mns). (A–C) Bar graphs showing percentage of ChAT-positive Mns in the ventral motor pools surrounded by NeuN, WFA-positive PNNS and their co-localisation (WFA+/NeuN+) in cervical (A), thoracic (B) and lumbar (C) rat spinal cord. NeuN and ChAT co-localisation denotes alpha Mns. Error bars  $\pm$  SD;  $n = 3$ . Statistics: one-way ANOVA; significance levels: \*  $p < 0.05$ , \*\*\*  $p < 0.001$ . Confocal images showing WFA-positive PNNS (D–F) surrounding NeuN-positive (G–I) PNNS and ChAT-positive Mns (J–L) in the cervical, thoracic and lumbar spinal cord, respectively. Scale bars, 100  $\mu$ m.

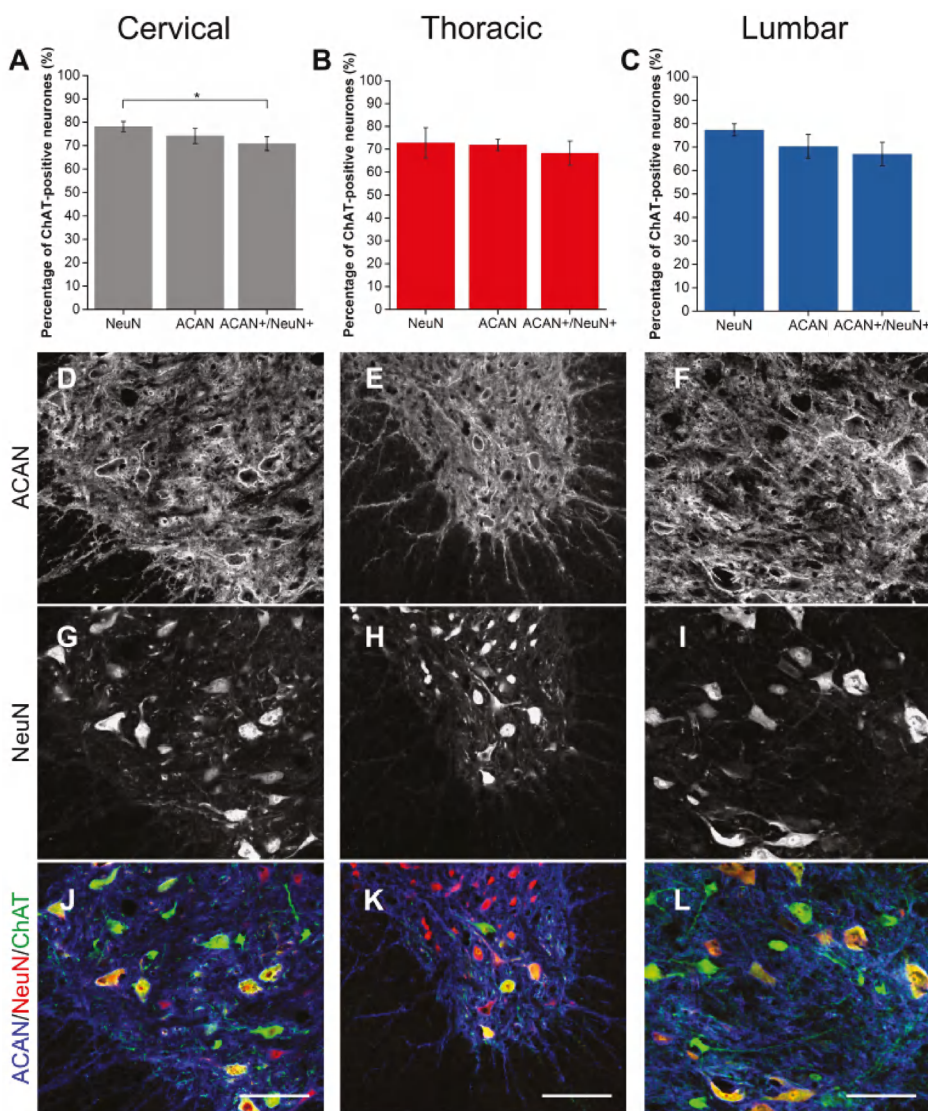


**Figure 8.** Aggrecan (ACAN)-positive PNNs surrounded most alpha motoneurones (Mns). (A–C) Bar graphs showing percentage of ChAT-positive Mns in the ventral motor pools surrounded by NeuN, ACAN-positive PNNs and their co-localisation (ACAN+/NeuN+) in cervical (A), thoracic (B) and lumbar (C) rat spinal cord. NeuN and ChAT co-localisation denotes alpha Mns. Error bars  $\pm$  SD;  $n = 3$ . Statistics: one-way ANOVA; significance levels: \*  $p < 0.05$ . Confocal images showing ACAN-positive PNNs (D–F) surrounding NeuN-positive (G–I) PNNs and ChAT-positive Mns (J–L) in the cervical, thoracic and lumbar spinal cord, respectively. Scale bars, 100  $\mu$ m.

### 3. Discussion

As removal of PNNs in the spinal cord after injury enhances motor recovery, we looked to investigate the expression of PNNs and their heterogeneity in spinal Mns; the final order neurones for

the control of voluntary movement. This is the first article to systematically and quantitatively compare the differences of CSPG- or WFA-positive PNN Ms in the ventral motor pools. Ms were identified using an antibody against ChAT to label cholinergic neurones alongside markers for PNN components and the acclaimed universal PNN marker WFA in comparison. We demonstrated that a high proportion of Ms in the ventral spinal cord were surrounded by PNNs, particularly alpha Ms. Unexpectedly, the universal marker for PNNs, WFA, did not label all of the PNNs with distinct populations of Ms surrounded by CSPG-positive yet WFA-negative PNNs. This suggests that, in contrast to the brain, WFA does not label the majority of PNN neurones in the ventral spinal cord and that studies using WFA in the spinal cord may be underestimating the number of PNNs.

### 3.1. PNNs in the Spinal Ventral Motor Pools

Previous studies have described ventral Ms as the most conspicuous neuronal population in the spinal cord to be surrounded by PNNs and this appears to be conserved across mammalian species [25,31,32,45,46]. Despite this, few studies have actually investigated the proportion of PNNs in the ventral motor pools and those that do use varying markers to determine this. Comparable to our own methods, using ChAT as a specific Mn marker, a similar proportion of ventral Ms was observed to be surrounded by PNNs to that found in our study (~80%) has been reported in non-human primates (75%), using WFA [45], and in human (71%) spinal cord, using ACAN [46]. In rats, however, this distribution has been investigated with the general neuronal marker (NeuN) using size and ventral location to identify Ms alongside WFA lectin staining to characterise PNN expression, resulting in estimates of only 30% of Ms associated with PNNs [25]. This is likely to underestimate for two reasons: (1) without a Mn-specific neuronal marker small sized Ms, including NeuN-negative gamma Ms [44,47], would have been absent from these counts, and (2) WFA does not appear to label all PNNs in the rat spinal cord. Indeed, our findings suggest that PNNs are present in almost 80% of the ChAT-positive Ms.

Although others have implicated that PNNs only surround large cell-bodied Ms in the motor pools, i.e., alpha Ms and not gamma Ms [25,31], we are the first to systematically categorise the proportion of specific Mn-subtypes associated with PNNs at different levels of the spinal cord. Despite contributing to the same goal of voluntary muscle control, alpha and gamma Ms represent distinct populations of Ms within the ventral motor pools, differing in both electrical and molecular properties [28,44,48,49]. These differences also include the innervation of different muscle targets, with alpha Ms responsible for force generation through contraction of extrafusal fibres whereas gamma Ms innervate the intrafusal fibres regulating muscle spindle sensitivity. The high proportion of enveloped alpha Ms revealed likely reflects the importance of the role of PNNs in providing synaptic stabilisation of inputs from the specific spinal circuitry and consequent contractile innervation of key muscle groups. After SCI, the stabilisation of synaptic plasticity conferred by PNNs instead becomes another mechanism inhibiting regenerative attempts and compensatory rearrangements of spared fibres. We suggest that ChABC-mediated removal of PNNs in SCI models is therefore able to induce a high degree of enhanced plasticity of synaptic connections to the abovementioned populations of alpha Ms contributing to the observed improvement of most functional motor recovery studies.

### 3.2. Differences in PNNs between the Brain and Spinal Cord

It is generally assumed that PNNs in the brain and the spinal cord are the same. While in the brain, WFA does not always co-localise with ACAN as previously discussed, other CSPG-positive PNNs always co-localise with WFA. Here, we demonstrate differences in the composition of PNNs between the brain and spinal cord, where ACAN and other CSPGs denote subclasses of Ms in the spinal cord lacking WFA. This study recommends that future staining for PNNs associated with the spinal motor pools, particularly SCI studies utilising therapies that modify PNNs such as ChABC, should seek alternatives to WFA to avoid underestimating total PNN number.

Additionally, brain PNNs are well known to target small fast-spiking inhibitory interneurones playing a modulatory role in the brain [50]. In sharp contrast, the associated neuronal populations studied here are large cell bodied neurones acting as the primary endpoint of neural control of the somatic motor system. Other neuronal cell types such as calbindin-positive Renshaw cells in the ventral spinal cord are surrounded by PNNs [22], further implicating the role of PNNs in stabilisation of connections within the spinal motor circuitry. In a recent systematic review of the CNS, motor regions, including the cerebellum and spinal cord, were more likely to have a higher proportion of neurones surrounded by PNNs than sensory structures [45]. It is possible that PNNs may have different roles in different parts of the nervous system or with different neuronal populations.

### 3.3. Composition of PNNs in the Spinal Motor Pools

Staining with the lectin WFA and antibodies for various CSPG core proteins revealed two distinct types of distributions throughout the grey matter: diffuse extracellular staining and a bright ‘halo’ of pericellular expression identifying the PNNs. The overall distributions of immunoreactivities for the CSPGs investigated and ChAT were generally similar to previous descriptions [18,22,25,33]. We showed that all of the CSPGs investigated were present in PNNs surrounding spinal MnS. These were also found to be present to varying degrees, indicating heterogeneity of PNNs in the motor pools.

ACAN in particular has been previously reported to be present in PNNs surrounding MnS [22,51,52], as well as BCAN, NCAN, VCAN and PTPRZ. It is estimated that VCAN begins to appear in PNNs around the MnS from postnatal day 8 [53]. Studies in the brain and spinal cord show that ACAN is present in all PNNs and generally co-localises with WFA expression [12,18,25]. However, consistent with all CSPGs investigated, WFA does not appear to show all PNN-associated neurones in the ventral motor pools. As WFA is supposed to bind to the CS-GAG sugar N-acetylgalactosamine (GalNAc) [50], it should bind to all CSPGs and therefore denote all PNNs. However, binding of WFA has previously been shown to be dependent on the presence of ACAN [12] and recently other studies in various regions of the brain, including the hippocampus, have reported PNNs with ACAN labelling but no WFA binding [21,54]. In the spinal cord, we observed a lack of WFA in ACAN-positive PNNs to a similar degree to that observed in the CA1 area of the hippocampus [21], appearing to denote distinct populations of MnS. As there is a vast degree of heterogeneity of CS-GAGs within CSPGs, further research is required to determine the conditions of WFA binding. It is possible that the molecular composition of CSPGs within PNNs may confer functional subclasses of MnS.

The expression of many PNN components such as ACAN, BCAN and tenascin-R show differences in expression between various brain regions [55]. In particular, BCAN is usually found at the para-nodal regions and has been shown to regulate the localisation of potassium channels and AMPA receptors [37]. The mechanism of how brevican performs these functions remains to be determined. Expression of CSPGs in PNNs across the spinal laminae has also been shown to display differential expression [22,25]. PNNs are a dynamic network of ECM components. Activity-dependant modulation has been demonstrated where the thickness of PNNs surrounding spinal MnS increases in response to exercise or rehabilitative training [31,32]. This is likely conveyed through dynamic regulation of CSPGs and/or CS-GAGs within the PNNs. There is a growing concept that the properties of the ECM have an important influence in both healthy and pathological states. Though it is beyond the scope of this study, it is hoped that further research into the heterogeneity of PNNs in CNS regions may help to unravel the functionality of these ECM components and their alterations in disease states.

### 3.4. Further Research and Conclusions

Despite the clinical relevance of PNNs targeted for CNS repair and regeneration, particularly in locomotor recovery models of SCI, the functional relationship between PNNs and the motor system is still mostly unexplored. Further research is required to look at the normal functional properties of PNNs surrounding MnS. Additionally, the molecular heterogeneity of PNNs displayed in spinal MnS

may indicate a functional role. However, understanding how the varying molecular heterogeneity of PNNs affects CNS functions is a topic still in its infancy.

Though this study begins to address a research gap surrounding the properties of PNNs in the spinal cord, much characterisation remains to be done. While ChABC has been an invaluable investigative tool for understanding the role of PNNs in promoting plasticity and functional recovery after SCI, there are clinical limitations to its therapeutic use. It is hoped that insights into the properties of PNNs and their role in the spinal cord could aid the generation of alternative and non-invasive strategies for targeted PNN removal to enhance functional recovery post-injury.

#### 4. Materials and Methods

##### 4.1. Animals

Female Lister Hooded rats (200–250 g;  $n = 5$ ) were obtained from Charles River Laboratories (Canterbury, UK) and were housed in groups in Central Biomedical Services (University of Leeds) in a temperature controlled environment ( $20 \pm 1^\circ\text{C}$ ), with a 12 h light/dark cycle (lights on at 07:00). Access to food and water was *ad libitum*. All procedures and experiments complied with the UK Animals (Scientific Procedures) Act 1986.

##### 4.2. Tissue Preparation

Animals were given an overdose of sodium pentobarbital (Pentoject; Henry Schein; 200 mg/kg; intraperitoneal injection) to deeply anaesthetise without halting cardiac function. A transcardial perfusion [56] was then performed using sodium phosphate buffer (PB; 0.12 M sodium phosphate monobasic; 0.1 M NaOH; pH 7.4) followed by 4% paraformaldehyde (PFA; in PB; pH 7.4) for tissue fixation. The spinal cord was dissected out, post-fixed in PFA (4%;  $4^\circ\text{C}$ ) overnight and cryoprotected in 30% sucrose solution (30% *v/w* sucrose in PB;  $4^\circ\text{C}$ ) until tissue saturation. The appropriate cervical (C3-T1), mid-thoracic and lumbar (L1-6) spinal cord segments were removed and frozen in optimum temperature medium (OCT; Leica FSC 22 Frozen Section Media; Leica Biosystems) before storage at  $-80^\circ\text{C}$  until sectioning. Tissue was cut using a cryostat (Leica CM1850; Leica Biosystems) into 40  $\mu\text{m}$  transverse sections. Sections were serially collected into 48-well plates containing physiological buffer solution (PBS; 0.13 M NaCl, 0.7 M sodium phosphate dibasic, 0.003 M sodium phosphate monobasic; pH 7.4) to remove the OCT before being transferred to 30% sucrose solution for storage at  $4^\circ\text{C}$ .

##### 4.3. Staining Procedures

Immunohistochemical techniques were used to label for cells in the spinal cord containing ChAT and the PNNs surrounding subsets of these cells labelled by biotinylated *Wisteria floribunda* agglutinin (bio-WFA) and CSPG components, including ACAN, BCAN and NCAN (Table 1). ChAT was used for Mn identification [57] whilst WFA is universally used as a marker for PNNs [10,12].

At room temperature (RT), free-floating sections were washed three times for 5 min each in Tris-buffered saline (TBS; 0.1 M tris base, 0.15 M NaCl; pH 7.4) to remove sucrose residue. Tissue was then blocked in 0.3% TBST (1× TBS solution and 0.3% *v/v* Triton X-100) and 3% normal donkey serum (NDS; *v/v*) for two hours. The sections were then transferred to co-incubate at  $4^\circ\text{C}$  in blocking buffer (3% NDS in 0.3% TBST; pH 7.4) containing the following primary antibodies: anti-ChAT (goat; Millipore; 1:500; 48 h), biotin-conjugated *Wisteria floribunda* agglutinin (bio-WFA; Sigma; 1:150; 24 h) and either ACAN (rabbit; Millipore; 1:250; 24 h), BCAN (mouse; DSHB; 1:500; 24 h), NCAN (mouse; DSHB; 1:100; 24 h), VCAN (mouse; DSHB; 1:100; 24 h) or PTPRZ (mouse; DSHB; 1:80; 24 h) (Table 1).

**Table 1.** Immunohistochemical detection of extracellular matrix components and neuronal markers, including concentration (conc.) of antibody used.

Detected Component	Marker	Host	Antibody Conc.	Source	Characterisation
CSPGs					
Aggrecan (mouse ACAN core protein)	Anti-ACAN	Rabbit polyclonal IgG	500 µg/mL	Millipore #AB1031	WB <sup>2</sup> (Lendvai et al., 2013 & Sutkus et al., 2014)
Brevican (BCAN; mouse cell-line derived recombinant human Brevican)	Anti-BCAN	Sheep polyclonal IgG	1 mg/mL	R&D Systems #AF4009	WB <sup>2</sup> (R&D Systems data sheet)
Neurocan (NCAN; N-terminal epitope)	Anti-NCAN	Mouse monoclonal IgG	369 µg/mL	DSHB <sup>1</sup> #1Fc6	WB <sup>2</sup> (Asher et al., 2000 & Deepa et al., 2006)
Versican (VCAN; hyaluronate-binding region)	Anti-VCAN	Mouse monoclonal IgG	169 µg/mL	DSHB <sup>1</sup> #12C5	WB <sup>2</sup> (Asher et al., 2002 & Deepa et al., 2006)
Phosphacan (PTPRZ)	Anti-PTPRZ	Mouse monoclonal IgG	165 µg/mL	DSHB <sup>1</sup> #3F8	WB <sup>2</sup> (Deepa et al., 2006 & Vitellaro-Zuccarello et al., 2006)
Lectins					
N-acetyl/galactosamine (GalNAc)	Biotinylated <i>Wistaria floribunda</i> agglutinin (WFA)	N/A	2 mg/mL	Sigma #L1766	Koppe et al., 1996
Neuronal markers					
Choline acetyltransferase (ChAT)	Anti-ChAT	Goat polyclonal IgG	—	Millipore #AB144P	
Neuron-specific nuclear protein (NeuN)	Anti-NeuN	Mouse monoclonal IgG	1 mg/mL	Millipore #MAB377	WB <sup>2</sup> (Jin et al., 2003)

<sup>1</sup> DSHB, Developmental Studies Hybridoma Bank, University of Iowa, USA. <sup>2</sup> WB, Western blotting.

Immunostaining was routinely carried out using tissue from different animals and differing spinal segments. The combinations carried out in this study used the formula: ChAT—Bio-WFA—CSPG marker using various antibodies from Table 1, including for the lecticans ACAN, BCAN, NCAN and VCAN. To differentiate between alpha and gamma Mns [31,44], ChAT was co-stained with anti-NeuN (mouse; Millipore; 1:500; 24 h). Antibodies requiring 24-h incubation were added and mixed well 48 h into a 72-h incubation with ChAT, using the protocols as above. To visualise each primary antibody staining, the tissue was then co-incubated with the appropriate species of fluorescent-conjugated secondary antibodies (1:500; 2 h; RT; Table 2).

**Table 2.** Fluorescent-conjugated secondary antibodies (2 mg/mL) used for immuno-detection of primary antibodies.

Antibody	Host	Source
Alexa fluor 488	chicken anti-goat IgG	Invitrogen #A21467
Alexa fluor 568	donkey anti-mouse IgG	Invitrogen #A31571
Alexa fluor 568	donkey anti-rabbit IgG	Invitrogen #A10042
Alexa fluor 568	donkey anti-sheep IgG	Invitrogen #A21099
Alexa fluor 647	Streptavidin-conjugated	Invitrogen #S32357

#### 4.4. Image Acquisition and Quantification Methods

The fluorophores used to label the spinal cord sections were visualised using a Zeiss LSM 880 (upright) confocal microscope and were used to generate tile scans of the entire spinal cord transverse section at 20× magnification (1.03 µs per pixel, averaging: 4). ChAT-positive cells and co-localisation with WFA-positive PNNs and other CSPG-positive PNNs were counted using the Cell Counter plugin (Kurt de Vos; <https://imagej.nih.gov/ij/plugins/cell-counter.html>) in the software FIJI [58]. Mns were identified by location within the ventral horn of ChAT-positive cellular staining. All ChAT-positive cells were individually counted and sequentially analysed for presence of PNN staining. PNNs were only counted around ChAT-positive neurones and were identified by the presence of intense staining as a bright ‘halo’ directly adjacent to the perimeter of ChAT-positive cells. Positive PNN staining was categorised into three classes: (1) only WFA-positive, (2) only positive for the appropriate CSPG stain or (3) WFA-positive and CSPG-positive. For differentiation of alpha and gamma Mns, cells co-localising both ChAT and NeuN staining were taken as alpha Mns whereas the absence of NeuN denoted gamma Mns [44,59].

#### 4.5. Experimental Design and Statistical Analysis

A minimum of three sections per spinal level (cervical, thoracic or lumbar) per animal ( $n = 5$ ) were stained and imaged, maintaining the same confocal microscopy settings per staining procedure. All counts per section were normalised by the number of ChAT-positive cells before averaging per animal. All data sets were analysed with OriginPro 2016 scientific graphing and data analysis software (OriginLab, Northampton, MA, USA), where results were statistically significant given that  $p < 0.05$ . To test the influence of spinal cord level on PNN expression and for differences between PNN types, results were pooled and analysed using one-way ANOVA, with Bonferroni correction for between-groups multiple comparison.

**Acknowledgments:** This work was financed by grants from the Wings for Life Foundation, The University of Leeds 110 Years Scholarship and the European Union—the Operational Programme Research, Development and Education in the framework of the project “Centre of Reconstructive Neuroscience”, registration number CZ.02.1.01/0.0./0.0/15\_003/0000419. The authors declare no competing financial interests.

**Author Contributions:** Jessica C. F. Kwok and Sian F. Irvine conceived and designed the experiments; Sian F. Irvine performed the experiments and analysed the data; Jessica C. F. Kwok contributed reagents/materials/analysis tools; Sian F. Irvine wrote the paper with amendments by Jessica C. F. Kwok.

**Conflicts of Interest:** The authors declare no conflict of interest. The funding sponsors had no role in the design of the study; in the collection, analyses, or interpretation of data; in the writing of the manuscript, and in the decision to publish the results.

## Abbreviations

ACAN	Aggrecan core protein
BCAN	Brevican core protein
ChAT	Choline acetyltransferase
ChABC	Chondroitinase ABC
CNS	Central nervous system
CS-GAG	Chondroitin sulphate glycosaminoglycan
CSPGs	Chondroitin sulphate proteoglycans
ECM	Extracellular matrix
GalNAc	N-acetylgalactosamine
HA	Hyaluronic acid/hyaluronan
Mn	Motoneurone
NeuN	Neuron-specific nuclear protein
NCAN	Neurocan core protein
PTPRZ	Phosphacan/protein tyrosine phosphatase receptor zeta
PNN	Perineuronal net
Mn	Motoneurone
SCI	Spinal cord injury
VCAN	Versican core protein
WFA	<i>Wisteria floribunda</i> agglutinin

## References

1. Celio, M.R.; Spreafico, R.; De Biasi, S.; Vitellaro-Zuccarello, L. Perineuronal nets: Past and present. *Trends Neurosci.* **1998**, *21*, 510–515. [[CrossRef](#)]
2. Suttkus, A.; Rohn, S.; Weigel, S.; Glöckner, P.; Arendt, T.; Morawski, M. Aggrecan, link protein and tenascin-R are essential components of the perineuronal net to protect neurons against iron-induced oxidative stress. *Cell Death Dis.* **2014**, *5*. [[CrossRef](#)] [[PubMed](#)]
3. Cabungcal, J.-H.H.; Steullet, P.; Morishita, H.; Kraftsik, R.; Cuenod, M.; Hensch, T.K.; Do, K.Q. Perineuronal nets protect fast-spiking interneurons against oxidative stress. *Proc. Natl. Acad. Sci. USA* **2013**, *110*, 9130–9135. [[CrossRef](#)] [[PubMed](#)]
4. Pantazopoulos, H.; Beretta, S. In Sickness and in Health: Perineuronal Nets and Synaptic Plasticity in Psychiatric Disorders. *Neural Plast.* **2016**, *2016*, 9847696. [[CrossRef](#)] [[PubMed](#)]
5. McRae, P.A.; Porter, B.E. The perineuronal net component of the extracellular matrix in plasticity and epilepsy. *Neurochem. Int.* **2012**, *61*, 963–972. [[CrossRef](#)] [[PubMed](#)]
6. Moon, L.D.F.; Asher, R.A.; Rhodes, K.E.; Fawcett, J.W. Regeneration of CNS axons back to their target following treatment of adult rat brain with chondroitinase ABC. *Nat. Neurosci.* **2001**, *4*, 465–466. [[CrossRef](#)] [[PubMed](#)]
7. Bradbury, E.J.; Moon, L.D.; Popat, R.J.; King, V.R.; Bennett, G.S.; Patel, P.N.; Fawcett, J.W.; McMahon, S.B. Chondroitinase ABC promotes functional recovery after spinal cord injury. *Nature* **2002**, *416*, 636–640. [[CrossRef](#)] [[PubMed](#)]
8. García-Alías, G.; Barkhuysen, S.; Buckle, M.; Fawcett, J.W. Chondroitinase ABC treatment opens a window of opportunity for task-specific rehabilitation. *Nat. Neurosci.* **2009**, *12*, 1145–1151. [[CrossRef](#)] [[PubMed](#)]
9. Carulli, D.; Pizzorusso, T.; Kwok, J.C.; Putignano, E.; Poli, A.; Forostyak, S.; Andrews, M.R.; Deepa, S.S.; Glant, T.T.; Fawcett, J.W. Animals lacking link protein have attenuated perineuronal nets and persistent plasticity. *Brain* **2010**, *133*, 2331–2347. [[CrossRef](#)] [[PubMed](#)]
10. Pizzorusso, T.; Medini, P.; Berardi, N.; Chierzi, S.; Fawcett, J.W.; Maffei, L. Reactivation of ocular dominance plasticity in the adult visual cortex. *Science* **2002**, *298*, 1248–1251. [[CrossRef](#)] [[PubMed](#)]
11. Tsien, R.Y. Very long-term memories may be stored in the pattern of holes in the perineuronal net. *Proc. Natl. Acad. Sci. USA* **2013**, *110*, 12456–12461. [[CrossRef](#)] [[PubMed](#)]

12. Giamanco, K.A.; Morawski, M.; Matthews, R.T. Perineuronal net formation and structure in aggrecan knockout mice. *Neuroscience* **2010**, *170*, 1314–1327. [[CrossRef](#)] [[PubMed](#)]
13. Kwok, J.C.; Carulli, D.; Fawcett, J.W. In vitro modeling of perineuronal nets: Hyaluronan synthase and link protein are necessary for their formation and integrity. *J. Neurochem.* **2010**, *114*, 1447–1459. [[CrossRef](#)] [[PubMed](#)]
14. Kwok, J.C.; Dick, G.; Wang, D.; Fawcett, J.W. Extracellular matrix and perineuronal nets in CNS repair. *Dev. Neurobiol.* **2011**, *71*, 1073–1089. [[CrossRef](#)] [[PubMed](#)]
15. Yamaguchi, Y. Lecticans: Organizers of the brain extracellular matrix. *Cell. Mol. Life Sci.* **2000**, *57*, 276–289. [[CrossRef](#)] [[PubMed](#)]
16. Kitagawa, H. Using sugar remodeling to study chondroitin sulfate function. *Biol. Pharm. Bull.* **2014**, *37*, 1705–1712. [[CrossRef](#)] [[PubMed](#)]
17. Gama, C.I.; Tully, S.E.; Sotogaku, N.; Clark, P.M.; Rawat, M.; Vaidehi, N.; Goddard, W.A.; Nishi, A.; Hsieh-Wilson, L.C. Sulfation patterns of glycosaminoglycans encode molecular recognition and activity. *Nat. Chem. Biol.* **2006**, *2*, 467–473. [[CrossRef](#)] [[PubMed](#)]
18. Deepa, S.S.; Carulli, D.; Galtrey, C.; Rhodes, K.; Fukuda, J.; Mikami, T.; Sugahara, K.; Fawcett, J.W. Composition of perineuronal net extracellular matrix in rat brain: A different disaccharide composition for the net-associated proteoglycans. *J. Biol. Chem.* **2006**, *281*, 17789–17800. [[CrossRef](#)] [[PubMed](#)]
19. Carulli, D.; Rhodes, K.E.; Brown, D.J.; Bonnert, T.P.; Pollack, S.J.; Oliver, K.; Strata, P.; Fawcett, J.W. Composition of perineuronal nets in the adult rat cerebellum and the cellular origin of their components. *J. Comp. Neurol.* **2006**, *494*, 559–577. [[CrossRef](#)] [[PubMed](#)]
20. Fader, S.M.; Imaizumi, K.; Yanagawa, Y.; Lee, C.C. Wisteria Floribunda Agglutinin-Labeled Perineuronal Nets in the Mouse Inferior Colliculus, Thalamic Reticular Nucleus and Auditory Cortex. *Brain Sci.* **2016**, *6*, 13. [[CrossRef](#)] [[PubMed](#)]
21. Yamada, J.; Jinno, S. Molecular heterogeneity of aggrecan-based perineuronal nets around five subclasses of parvalbumin-expressing neurons in the mouse hippocampus. *J. Comp. Neurol.* **2017**, *525*, 1234–1249. [[CrossRef](#)] [[PubMed](#)]
22. Vitellaro-Zuccarello, L.; Bosisio, P.; Mazzetti, S.; Monti, C.; De Biasi, S. Differential expression of several molecules of the extracellular matrix in functionally and developmentally distinct regions of rat spinal cord. *Cell Tissue Res.* **2007**, *327*, 433–447. [[CrossRef](#)] [[PubMed](#)]
23. Brauer, K.; Härtig, W.; Bigl, V.; Brückner, G. Distribution of parvalbumin-containing neurons and lectin-binding perineuronal nets in the rat basal forebrain. *Brain Res.* **1993**, *631*, 167–170. [[CrossRef](#)]
24. Yamada, J.; Ohgomori, T.; Jinno, S. Perineuronal nets affect parvalbumin expression in GABAergic neurons of the mouse hippocampus. *Eur. J. Neurosci.* **2015**, *41*, 368–378. [[CrossRef](#)] [[PubMed](#)]
25. Galtrey, C.M.; Kwok, J.C.; Carulli, D.; Rhodes, K.E.; Fawcett, J.W. Distribution and synthesis of extracellular matrix proteoglycans, hyaluronan, link proteins and tenascin-R in the rat spinal cord. *Eur. J. Neurosci.* **2008**, *27*, 1373–1390. [[CrossRef](#)] [[PubMed](#)]
26. Bertolotto, A.; Manzardo, E.; Guglielmino, R. Immunohistochemical mapping of perineuronal nets containing chondroitin unsulfate proteoglycan in the rat central nervous system. *Cell Tissue Res.* **1996**, *283*, 283–295. [[CrossRef](#)] [[PubMed](#)]
27. Takahashi-Iwanaga, H.; Murakami, T.; Abe, K. Three-dimensional microanatomy of perineuronal proteoglycan nets enveloping motor neurons in the rat spinal cord. *J. Neurocytol.* **1998**, *27*, 817–827. [[CrossRef](#)] [[PubMed](#)]
28. Manuel, M.; Zytnicki, D. Alpha, beta and gamma motoneurons: Functional diversity in the motor system's final pathway. *J. Integr. Neurosci.* **2011**, *10*, 243–276. [[CrossRef](#)] [[PubMed](#)]
29. Zhao, R.-R.R.; Andrews, M.R.; Wang, D.; Warren, P.; Gullo, M.; Schnell, L.; Schwab, M.E.; Fawcett, J.W. Combination treatment with anti-Nogo-A and chondroitinase ABC is more effective than single treatments at enhancing functional recovery after spinal cord injury. *Eur. J. Neurosci.* **2013**, *38*, 2946–2961. [[CrossRef](#)] [[PubMed](#)]
30. Barritt, A.W.; Davies, M.; Marchand, F.; Hartley, R.; Grist, J.; Yip, P.; McMahon, S.B.; Bradbury, E.J. Chondroitinase ABC Promotes Sprouting of Intact and Injured Spinal Systems after Spinal Cord Injury. *J. Neurosci.* **2006**, *26*, 10856–10867. [[CrossRef](#)] [[PubMed](#)]

31. Smith, C.C.; Mauricio, R.; Nobre, L.; Marsh, B.; Wüst, R.C.; Rossiter, H.B.; Ichiyama, R.M. Differential regulation of perineuronal nets in the brain and spinal cord with exercise training. *Brain Res. Bull.* **2015**, *111*, 20–26. [[CrossRef](#)] [[PubMed](#)]
32. Wang, D.; Ichiyama, R.M.; Zhao, R.; Andrews, M.R.; Fawcett, J.W. Chondroitinase combined with rehabilitation promotes recovery of forelimb function in rats with chronic spinal cord injury. *J. Neurosci.* **2011**, *31*, 9332–9344. [[CrossRef](#)] [[PubMed](#)]
33. Barber, R.P.; Phelps, P.E.; Houser, C.R.; Crawford, G.D.; Salvaterra, P.M.; Vaughn, J.E. The morphology and distribution of neurons containing choline acetyltransferase in the adult rat spinal cord: An immunocytochemical study. *J. Comp. Neurol.* **1984**, *229*, 329–346. [[CrossRef](#)] [[PubMed](#)]
34. Koppe, G.; Brückner, G.; Hartig, W.; Delpech, B.; Bigl, V. Characterization of proteoglycan-containing perineuronal nets by enzymatic treatments of rat brain sections. *Histochem. J.* **1997**, *29*, 11–20. [[CrossRef](#)] [[PubMed](#)]
35. Morawski, M.; Brückner, G.; Arendt, T.; Matthews, R.T. Aggrecan: Beyond cartilage and into the brain. *Int. J. Biochem. Cell Biol.* **2012**, *44*, 690–693. [[CrossRef](#)] [[PubMed](#)]
36. Lendvai, D.; Morawski, M.; Négyessy, L.; Gáti, G.; Jäger, C.; Baksa, G.; Glasz, T.; Attems, J.; Tanila, H.; Arendt, T.; et al. Neurochemical mapping of the human hippocampus reveals perisynaptic matrix around functional synapses in Alzheimer’s disease. *Acta Neuropathol.* **2013**, *125*, 215–229. [[CrossRef](#)] [[PubMed](#)]
37. Favuzzi, E.; Marques-Smith, A.; Deogracias, R.; Winterflood, C.M.; Sánchez-Aguilera, A.; Mantoan, L.; Maeso, P.; Fernandes, C.; Ewers, H.; Rico, B. Activity-Dependent Gating of Parvalbumin Interneuron Function by the Perineuronal Net Protein Brevican. *Neuron* **2017**, *95*. [[CrossRef](#)] [[PubMed](#)]
38. Asher, R.A.; Morgenstern, D.A.; Fidler, P.S.; Adcock, K.H.; Oohira, A.; Braisted, J.E.; Levine, J.M.; Margolis, R.U.; Rogers, J.H.; Fawcett, J.W. Neurocan is upregulated in injured brain and in cytokine-treated astrocytes. *J. Neurosci.* **2000**, *20*, 2427–2438. [[CrossRef](#)] [[PubMed](#)]
39. Dours-Zimmermann, M.T.; Maurer, K.; Rauch, U.; Stoffel, W.; Fässler, R.; Zimmermann, D.R. Versican V2 Assembles the Extracellular Matrix Surrounding the Nodes of Ranvier in the CNS. *J. Neurosci.* **2009**, *29*, 7731–7742. [[CrossRef](#)] [[PubMed](#)]
40. Asher, R.A.; Morgenstern, D.A.; Shearer, M.C.; Adcock, K.H.; Pesheva, P.; Fawcett, J.W. Versican is upregulated in CNS injury and is a product of oligodendrocyte lineage cells. *J. Neurosci.* **2002**, *22*, 2225–2236. [[PubMed](#)]
41. Maurel, P.; Rauch, U.; Flad, M.; Margolis, R.K.; Margolis, R.U. Phosphacan, a chondroitin sulfate proteoglycan of brain that interacts with neurons and neural cell-adhesion molecules, is an extracellular variant of a receptor-type protein tyrosine phosphatase. *Proc. Natl. Acad. Sci. USA* **1994**, *91*, 2512–2516. [[CrossRef](#)] [[PubMed](#)]
42. Dwyer, C.A.; Katoh, T.; Tiemeyer, M.; Matthews, R.T. Neurons and Glia Modify Receptor Protein-tyrosine Phosphatase  $\zeta$  (RPTP $\zeta$ )/Phosphacan with Cell-specific O-Mannosyl Glycans in the Developing Brain. *J. Biol. Chem.* **2015**, *290*, 10256–10273. [[CrossRef](#)] [[PubMed](#)]
43. Haunsø, A.; Celio, M.R.; Margolis, R.K.; Menoud, P.-A. Phosphacan immunoreactivity is associated with perineuronal nets around parvalbumin-expressing neurones. *Brain Res.* **1999**, *834*, 219–222. [[CrossRef](#)]
44. Friese, A.; Kutschmidt, J.A.; Ladle, D.R.; Sigrist, M.; Jessell, T.M.; Arber, S. Gamma and alpha motor neurons distinguished by expression of transcription factor Err3. *Proc. Natl. Acad. Sci. USA* **2009**, *106*, 13588–13593. [[CrossRef](#)] [[PubMed](#)]
45. Mueller, A.L.; Davis, A.; Sovich, S.; Carlson, S.S.; Robinson, F.R. Distribution of N-Acetylgalactosamine-Positive Perineuronal Nets in the Macaque Brain: Anatomy and Implications. *Neural Plast.* **2016**, *2016*. [[CrossRef](#)] [[PubMed](#)]
46. Jäger, C.; Lendvai, D.; Seeger, G.; Brückner, G.; Matthews, R.T.; Arendt, T.; Alpár, A.; Morawski, M. Perineuronal and perisynaptic extracellular matrix in the human spinal cord. *Neuroscience* **2013**, *238*, 168–184. [[CrossRef](#)] [[PubMed](#)]
47. Shneider, N.A.; Brown, M.N.; Smith, C.A.; Pickel, J.; Alvarez, F.J. Gamma motor neurons express distinct genetic markers at birth and require muscle spindle-derived GDNF for postnatal survival. *Neural Dev.* **2009**, *4*, 42. [[CrossRef](#)] [[PubMed](#)]
48. Eccles, J.C.; Eccles, R.M.; Iggo, A.; Lundberg, A. Electrophysiological studies on gamma motoneurones. *Acta Physiol. Scand.* **1960**, *50*, 32–40. [[CrossRef](#)] [[PubMed](#)]

49. Misawa, H.; Hara, M.; Tanabe, S.; Niikura, M.; Moriwaki, Y.; Okuda, T. Osteopontin is an alpha motor neuron marker in the mouse spinal cord. *J. Neurosci. Res.* **2012**, *90*, 732–742. [[CrossRef](#)] [[PubMed](#)]
50. Härtig, W.; Brauer, K.; Brückner, G. Wisteria floribunda agglutinin-labelled nets surround parvalbumin-containing neurons. *Neuroreport* **1992**, *3*, 869–872. [[CrossRef](#)] [[PubMed](#)]
51. Kalb, R.G.; Hockfield, S. Molecular evidence for early activity-dependent development of hamster motor neurons. *J. Neurosci.* **1988**, *8*, 2350–2360. [[CrossRef](#)] [[PubMed](#)]
52. Matthews, R.T.; Kelly, G.M.; Zerillo, C.A.; Gray, G.; Tiemeyer, M.; Hockfield, S. Aggrecan glycoforms contribute to the molecular heterogeneity of perineuronal nets. *J. Neurosci.* **2002**, *22*, 7536–7547. [[PubMed](#)]
53. Bignami, A.; Perides, G.; Rahemtulla, F. Versican, a hyaluronate-binding proteoglycan of embryonal precartilaginous mesenchyma, is mainly expressed postnatally in rat brain. *J. Neurosci. Res.* **1993**, *34*, 97–106. [[CrossRef](#)] [[PubMed](#)]
54. Ueno, H.; Suemitsu, S.; Okamoto, M.; Matsumoto, Y.; Ishihara, T. Sensory experience-dependent formation of perineuronal nets and expression of Cat-315 immunoreactive components in the mouse somatosensory cortex. *Neuroscience* **2017**, *355*, 161–174. [[CrossRef](#)] [[PubMed](#)]
55. Dauth, S.; Grevesse, T.; Pantazopoulos, H.; Campbell, P.H.; Maoz, B.M.; Berretta, S.; Parker, K.K. Extracellular matrix protein expression is brain region dependent. *J. Comp. Neurol.* **2016**, *524*, 1309–1336. [[CrossRef](#)] [[PubMed](#)]
56. Gage, G.J.; Kipke, D.R.; Shain, W. Whole animal perfusion fixation for rodents. *J. Vis. Exp.* **2012**. [[CrossRef](#)] [[PubMed](#)]
57. Phelps, P.E.; Barber, R.P.; Houser, C.R.; Crawford, G.D.; Salvaterra, P.M.; Vaughn, J.E. Postnatal development of neurons containing choline acetyltransferase in rat spinal cord: An immunocytochemical study. *J. Comp. Neurol.* **1984**, *229*, 347–361. [[CrossRef](#)] [[PubMed](#)]
58. Schindelin, J.; Arganda-Carreras, I.; Frise, E.; Kaynig, V.; Longair, M.; Pietzsch, T.; Preibisch, S.; Rueden, C.; Saalfeld, S.; Schmid, B.; et al. Fiji: An open-source platform for biological-image analysis. *Nat. Meth.* **2012**, *9*, 676–682. [[CrossRef](#)] [[PubMed](#)]
59. Mullen, R.J.; Buck, C.R.; Smith, A.M. NeuN, a neuronal specific nuclear protein in vertebrates. *Development* **1992**, *116*, 201–211. [[PubMed](#)]



© 2018 by the authors. Licensee MDPI, Basel, Switzerland. This article is an open access article distributed under the terms and conditions of the Creative Commons Attribution (CC BY) license (<http://creativecommons.org/licenses/by/4.0/>).

Communication

# Application of a Novel Anti-Adhesive Membrane, E8002, in a Rat Laminectomy Model

Kiyoshi Kikuchi <sup>1,2,3,4</sup>, Kentaro Setoyama <sup>5,†</sup>, Takuto Terashi <sup>6,†</sup>, Megumi Sumizono <sup>6</sup>,  
Salunya Tancharoen <sup>4</sup>, Shotaro Otsuka <sup>6</sup>, Seiya Takada <sup>6</sup>, Kazuki Nakanishi <sup>6</sup>, Koki Ueda <sup>6</sup>,  
Harutoshi Sakakima <sup>6</sup>, Ko-ichi Kawahara <sup>3,7</sup>, Ikuro Maruyama <sup>3</sup>, Gohsuke Hattori <sup>2</sup>,  
Motohiro Morioka <sup>2</sup>, Eiichiro Tanaka <sup>1,\*</sup> and Hisaaki Uchikado <sup>2,8,\*</sup>

- <sup>1</sup> Division of Brain Science, Department of Physiology, Kurume University School of Medicine, 67 Asahi-machi, Kurume, Fukuoka 830-0011, Japan; kikuchi\_kiyoshi@kurume-u.ac.jp
- <sup>2</sup> Department of Neurosurgery, Kurume University School of Medicine, 67 Asahi-machi, Kurume 830-0011, Japan; hattori\_gohsuke@kurume-u.ac.jp (G.H.); mmorioka@med.kurume-u.ac.jp (M.M.)
- <sup>3</sup> Department of Systems Biology in Thromboregulation, Kagoshima University Graduate School of Medical and Dental Sciences, 8-35-1 Sakuragaoka, Kagoshima 890-8520, Japan; koichi.kawahara@oit.ac.jp (K.K.); maruyama@m2.kufm.kagoshima-u.ac.jp (I.M.)
- <sup>4</sup> Department of Pharmacology, Faculty of Dentistry, Mahidol University, 6 Yothe Road, Rajthevee, Bangkok 10400, Thailand; salunya.tan@mahidol.edu
- <sup>5</sup> Division of Laboratory Animal Science, Natural Science Center for Research and Education, Kagoshima University, 8-35-1 Sakuragaoka, Kagoshima 890-8520, Japan; seto@m.kufm.kagoshima-u.ac.jp
- <sup>6</sup> Course of Physical Therapy, School of Health Sciences, Faculty of Medicine, Kagoshima University, 8-35-1 Sakuragaoka, Kagoshima 890-8544, Japan; k7200686@kadai.jp (T.T.); k9380225@kadai.jp (M.S.); k3360022@kadai.jp (S.O.); k5082701@kadai.jp (S.T.); k9378361@kadai.jp (K.N.); k1238698@kadai.jp (K.U.); sakaki@health.nop.kagoshima-u.ac.jp (H.S.)
- <sup>7</sup> Laboratory of Functional Foods, Department of Biomedical Engineering Osaka Institute of Technology, 5-16-1 Omiya, Asahi-ku, Osaka 535-8585, Japan
- <sup>8</sup> Uchikado Neuro-Spine Clinic, 1-2-3 Naka, Hakata-ku, Fukuoka 812-0893, Japan
- \* Correspondence: eacht@med.kurume-u.ac.jp (E.T.); uchikado@me.com (H.U.); Tel.: +81-92-477-2355 (H.U.); Fax: +81-92-477-2325 (H.U.)
- † These authors contributed equally to this work.

Received: 28 March 2018; Accepted: 16 May 2018; Published: 18 May 2018

**Abstract:** Neuropathic pain after spinal surgery, so-called failed back surgery syndrome, is a frequently observed common complication. One cause of the pain is scar tissue formation, observed as post-surgical epidural adhesions. These adhesions may compress surrounding spinal nerves, resulting in pain, even after successful spinal surgery. E8002 is an anti-adhesive membrane. In Japan, a clinical trial of E8002 is currently ongoing in patients undergoing abdominal surgery. However, animal experiments have not been performed for E8002 in spinal surgery. We assessed the anti-adhesive effect of E8002 in a rat laminectomy model. The dura matter was covered with an E8002 membrane or left uncovered as a control. Neurological evaluations and histopathological findings were compared at six weeks postoperatively. Histopathological analyses were performed by hematoxylin-eosin and aldehyde fuchsin-Masson Goldner staining. Three assessment areas were selected at the middle and margins of the laminectomy sites, and the numbers of fibroblasts and inflammatory cells were counted. Blinded histopathological evaluation revealed that adhesions and scar formation were reduced in the E8002 group compared with the control group. The E8002 group had significantly lower numbers of fibroblasts and inflammatory cells than the control group. The present results indicate that E8002 can prevent epidural scar adhesions after laminectomy.

**Keywords:** failed back surgery syndrome; anti-adhesive membrane; E8002; laminectomy

## 1. Introduction

Spinal surgery typically induces various degrees of scar tissue and adhesion formation in the epidural space, termed epidural fibrosis, and this fibrosis may cause problems if further surgery is required [1]. Epidural fibrosis can compress the intraspinal nervous tissues to induce a variety of symptoms including significant functional disability and recurrent radicular pain, and the resulting syndrome, failed back surgery syndrome (FBSS), was reported to affect 8–40% of patients undergoing lumbar disc surgery [2]. There are no effective treatments for patients with established epidural fibrosis, and the associated complications make revision surgery more complex and time-consuming, with most reoperations for FBSS being unsuccessful [3]. Prevention of epidural fibrosis formation is considered to be the best approach for FBSS [4], and various attempts have been undertaken toward such prevention.

Many biological and synthetic materials, including polymethyl methacrylate, polylactic acid, autologous leather, silastic silicone, and fat grafts, have been reported to show anti-fibrotic effects [5–9]. Pharmaceutical agents, such as mitomycin C, doxycycline, rapamycin, hydroxycamptothecine, colchicine, steroid hormone, and anti-inflammatory agents, have been used to reduce epidural fibrosis [10–14]. However, limited or variable success was achieved, and some of these medicines caused side effects such as wound infections. Therefore, it remains clinically urgent to develop new methods that can reduce epidural fibrosis.

E8002 is an anti-adhesive membrane that was previously known as nDM-14R [15]. E8002 is designed to have a three-layered structure. The central layer is composed of pullulans, which are used in foods and drugs, and are known to be innocuous and bioabsorbable. The surface layers are composed of L-lactide, glycolide, and  $\epsilon$ -caprolactone copolymers (Taki Chemical, Kakogawa, Japan) produced by ring-opening polymerization catalyzed by tin octanoate [ $\text{Sn}(\text{O}_2\text{C}_8\text{H}_{15})_2$ ]. These polymers are also used in bioabsorbable sutures. The material used for the central layer readily dissolves under moist conditions, while the materials used for the surface layers are nearly insoluble. The thickness of the central layer is set at 30  $\mu\text{m}$ , while the surface layers are approximately 100 nm. In Japan, a clinical trial on E8002 in patients undergoing abdominal surgery was initiated in 2007 and is currently ongoing [16]. However, animal experiments have not yet been performed for E8002 in spinal surgery. In the present study, we evaluated the therapeutic effect of local E8002 application on reduction of epidural fibrosis in a rat laminectomy model. If E8002 can inhibit fibroblast proliferation and reduce epidural fibrosis after laminectomy, this product may be effective for FBSS. The present results may provide a novel method for reducing epidural fibrosis, and may be applicable to future human trials on clinical use of E8002 for spinal surgery.

## 2. Results

### 2.1. E8002 Does Not Cause Neurological Adverse Effects

We evaluated neurological adverse effects in the rat laminectomy model. Preoperative and postoperative comparisons of posture, weight support, and coordination according to the Basso, Beattie, and Bresnahan (BBB) locomotion test did not show significant changes between the E8002 group and the control group (BBB score = 21) (Figure 1A). These results confirmed that the nervous tissues were not injured intraoperatively by the properties of the inserted E8002 membrane. None of the rats died intraoperatively or postoperatively, and no obvious adverse effects were observed. Therefore, E8002 did not cause neurological adverse effects.

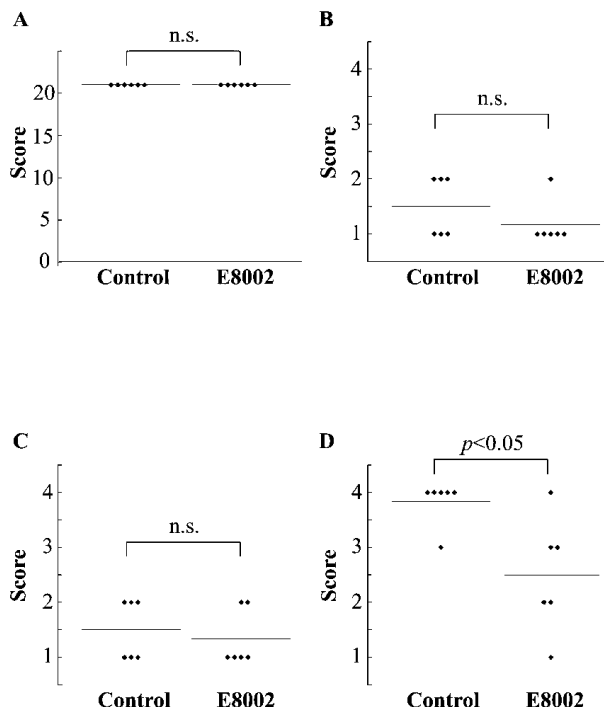


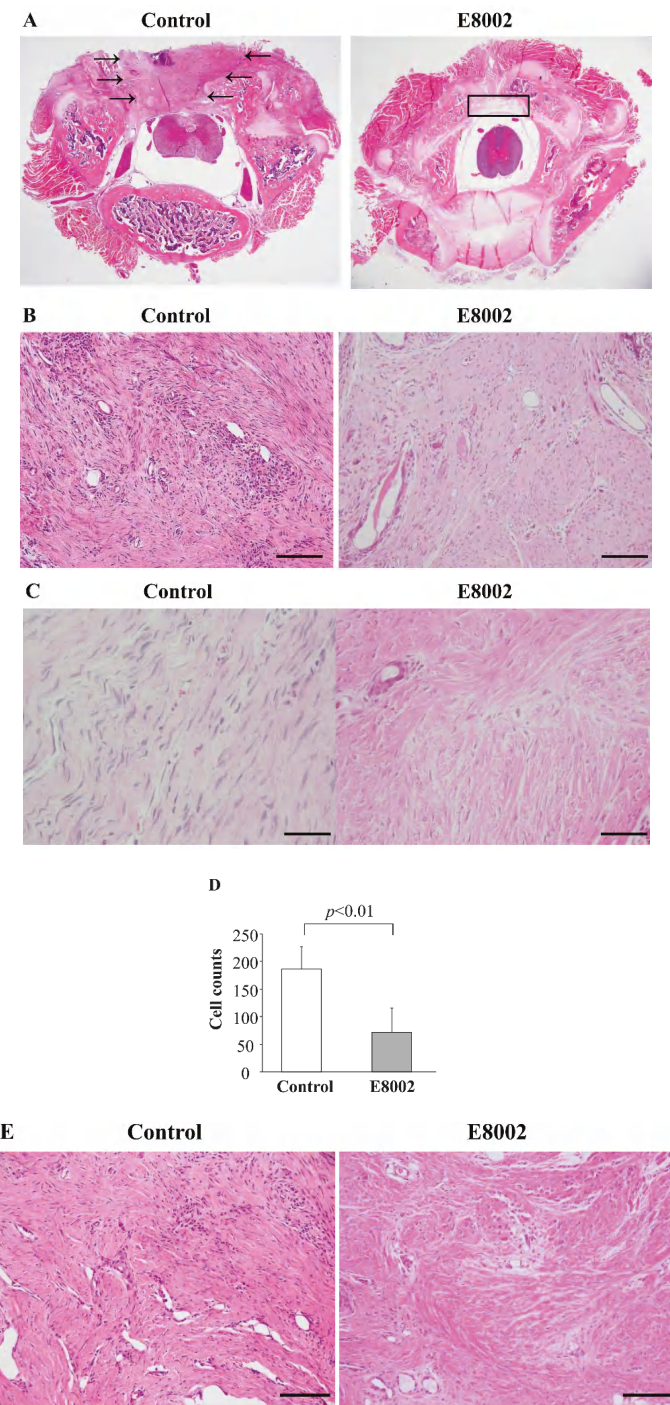
**Figure 1.** Effect of E8002 on neurological and macroscopic evaluations. (A) BBB score; (B) Macroscopic evaluation of skin; (C) Macroscopic evaluation of fascia; (D) Macroscopic evaluation of muscle. n.s., not significant.

## 2.2. E8002 Induces Muscle Healing

The data from the macroscopic evaluations are shown in Figure 1B–D. The evaluations did not show significant differences in the skin and fascia between the two groups. However, muscle healing was significantly improved in the E8002 group compared with the control group.

## 2.3. E8002 Reduce Fibroblasts and Inflammatory Cells in Epidural Scar Tissues

Typical images of hematoxylin–eosin (HE) staining of epidural scar tissues at the L1–L2 levels are shown in Figure 2A. In the control group, dense epidural scar tissue and compact collagen tissues were found at the laminectomy sites, and the scar tissue was widely adhered to the dura mater. In the E8002 group, vacuolation above the dura mater, loose scar adhesion, and less collagen tissues were observed. On histological examination, the fibroblast and inflammatory cell densities in the E8002 group were significantly lower than those in the control group (Figure 2B–F). Aldehyde fuchsin–Masson Goldner staining revealed that the E8002 group had fewer observable epidural scar adhesions compared with the control group (Figure 3).



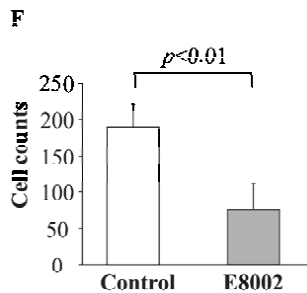


**Figure 2.** Effect of E8002 on epidural scar tissues evaluated by HE staining. (A) Photomicrographs of epidural adhesions at the laminectomy sites. Arrows indicate scar tissue. The square indicates vacuolation above the dura mater; (B) Representative images of HE staining for fibroblasts and inflammatory cells in the control group and E8002 group (original magnification,  $\times 200$ ). Scale bars, 100  $\mu\text{m}$ ; (C) Representative images of HE staining for fibroblasts in the control group and E8002 group (original magnification,  $\times 400$ ). Scale bars, 100  $\mu\text{m}$ ; (D) Counts of fibroblast density; (E) Representative images of HE staining for inflammatory cells in the control group and E8002 group (original magnification,  $\times 400$ ). Scale bars, 100  $\mu\text{m}$ ; (F) Cell counts of inflammatory cells.

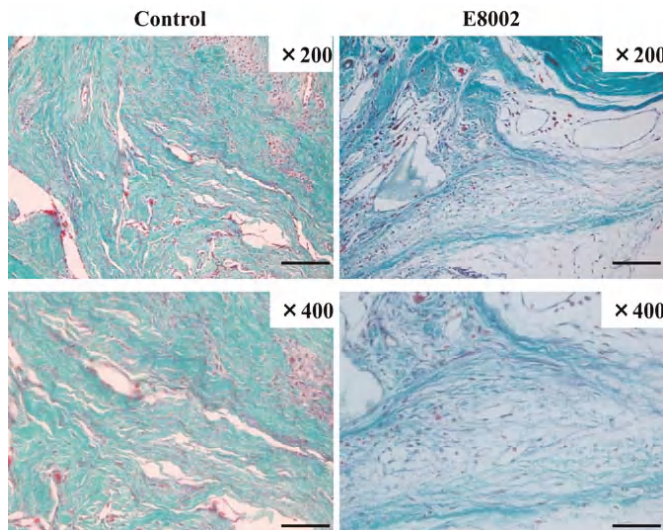


**Figure 3.** Effect of E8002 on epidural scar tissues evaluated by aldehyde fuchsin-Masson Goldner staining. Representative images of aldehyde fuchsin-Masson Goldner staining in the control group and E8002 group are shown (original magnification: upper panels  $\times 200$ , lower panels  $\times 400$ ) (scale bars: upper panels 100  $\mu\text{m}$ , lower panels 50  $\mu\text{m}$ ).

### 3. Discussion

The present findings have demonstrated reductions in scar formation and adhesions after experimental laminectomy with E8002 treatment in a rat model.

Wound healing is generally a positive physiological event that restores the anatomy and function of tissues after injury, and the ideal end result is tissue restoration to the condition before the injury [13]. An important part of the wound healing process is the formation of connective tissue or scar tissue that supports the healing tissues during regeneration [13]. However, in many cases, the newly

formed connective tissue (scar tissue) can negatively interfere with the normal function of the healing tissues [13]. Following abdominal and gynecologic surgery, it is not uncommon for the surgical procedure per se to induce adhesions that not only make subsequent surgery more difficult, but also lead to pathological conditions such as ileus or infertility [17]. Spinal surgery often results in dense scar formation termed epidural fibrosis. In some cases, this fibrosis induces significant difficulties for repeated surgery and has been reported to induce compression of the adjacent nerve tissue [1,2]. Epidural fibrosis is a major cause of FBSS. A method for controlling wound healing, particularly the formation of scar tissue and adhesions, would be of great value for post-surgical wound healing in most cases.

Many attempts have been undertaken to control scar formation. There are several methods that rely on barriers with various properties, and substantial numbers of biological and synthetic materials and pharmaceutical agents have been applied [5–14]. However, the results have not been entirely satisfactory. Because fibroblasts are responsible for producing collagen, much attention has been drawn to the regulation of fibroblasts to reduce scar formation [18–20]. In previous studies, certain compounds such as rapamycin, mitomycin C, and *all-trans* retinoic acid were shown to exert anti-adhesive effects by inhibiting fibroblast proliferation [11,12,14], similar to the case for E8002. However, there are no compounds with anti-adhesive effects that are widely used in the field of spinal surgery at clinical sites worldwide. A clinical trial using E8002 is currently ongoing in patients undergoing covering colostomy and colostomy closure. However, the spaces surrounding the intra-abdominal organs and those surrounding the spinal cord may be different. Nevertheless, even if the types of organs are different, the targets for adhesion prevention may be the same. Barriers between the two surfaces are considered the most effective method for preventing postoperative adhesions. For membrane-like anti-adhesive agents to exert an effect, two conditions are required: the damaged surface of all organs must be covered by the anti-adhesive agent until the early fibrin network is completed, and inflammatory cells must not invade the first fibrin network. The results of the above clinical trial may accelerate the start of clinical trials in patients undergoing spinal surgery.

In conclusion, the results of the present study suggest that E8002 can reduce scar formation/adhesions after spinal surgery. Although the underlying mechanisms remain to be clarified in further studies, the findings suggest the possibility for future design of potent pharmacological treatment modalities that can reduce post-surgical adhesion formation and scarring, potentially in combination with physical barriers. We should remain optimistic about the future of spinal surgery, and continue to explore new strategies to provide optimal care for patients undergoing spinal surgery.

#### 4. Materials and Methods

The experimental protocol was approved by the Institutional Animal Care and Use Committee of Kagoshima University (Kagoshima, Japan). The study protocol was approved by the local ethics committee of Kagoshima University (Ethic approval number: MD17014, Approval date: 26 May 2017).

##### 4.1. Rat Model of Laminectomy

A rat laminectomy model was used to determine the effects of E8002 on epidural fibrosis. A total of 12 male Sprague-Dawley rats aged 8 weeks and weighing 290–310 g were used in the study. Anesthesia was induced and maintained with 2.5–3.0% isoflurane inhalation and the animals were fixed in the prone position. The back hair at the L1–L2 level was shaved, and the skin was sterilized with iodophor three times. The laminectomy model was constructed as previously described [14]. All procedures were performed under sterile conditions with basic surgical tools, surgical microscopes, and an electrical drill. A median incision of the dorsal skin was made at the L1–L2 level, and the paraspinal muscles were separated. A rongeur was used to remove the spinous process and lamina, and the dura mater at the L1–L2 level was exposed. An E8002 membrane (3 × 2 mm) was applied to the surgical site. No membrane was applied in control rats. The total 12 rats were divided into two groups: control group ( $n = 6$ ) and E8002 group ( $n = 6$ ). Satisfactory hemostasis was achieved

using gauze; bone wax and cauterization after laminectomy were not needed. All procedures were performed with care to avoid injury to the neural tissues.

#### 4.2. Neurological Evaluation

At 6 weeks postoperatively, neurological evaluations were performed to confirm that the membrane did not prevent healing of the spinal cord and dura mater, or injure the nerve roots and spinal cord. All rats underwent preoperative and postoperative neurobehavioral assessments using the BBB locomotion test [21]. This test assessed posture, weight support, and coordination during open field locomotion.

#### 4.3. Macroscopic Evaluation

After 6 weeks, the rats were re-anesthetized. The skin and muscle wound healing was macroscopically graded by a person blinded to the experimental groups using a semiquantitative scale based on the Olmarker classification (healing of skin incision: 1, good healing; 2, slight diastasis; 3, pronounced diastasis; 4, infection; healing of fascia and muscle: 1, good healing; 2, slight diastasis; 3, clear diastasis; 4, hematoma or infection with loss of contact) as described [13], with small modifications.

#### 4.4. Histological Analysis

At 6 weeks postoperatively, the rats were deeply anesthetized by intraperitoneal injection of pentobarbital sodium (100 mg/kg), and perfused with heparin physiological saline, followed by 4% paraformaldehyde in 0.1 M phosphate buffer (pH 7.4) via the heart. The entire L1–L2 vertebral column, including the paraspinal muscles and epidural scar tissue, was resected en bloc. The samples were fixed in 4% paraformaldehyde at 4 °C overnight, decalcified in Kalkitox (Wako Pure Chemical Industries Ltd., Osaka, Japan) at 4 °C for 2 days and 5% sodium sulfate solution at 4 °C overnight, dehydrated in a graded ethanol series, cleared with xylene, and embedded in paraffin. The paraffin-embedded samples were cut into 4-mm transverse sections through the L1–L2 vertebrae, and stained with HE. Aldehyde fuchsin-Masson Goldner staining was also performed to identify connective tissues, such as elastic fibers and collagen fibers. Epidural scar adhesions were evaluated under a light microscope (DP21; Olympus Optical Co., Tokyo, Japan). Three areas were selected at the center and margins of the laminectomy sites. The numbers of fibroblasts and inflammatory cells were counted in these three areas, and the mean value was calculated per ×400 field as previously described [22].

#### 4.5. Statistical Analysis

Variability of data was assessed by the F-test for parametric data. Student's *t*-test for independent samples was applied to determine the statistical significance of differences between the mean values of two study groups. Values of *p* < 0.05 were considered statistically significant. If data were not normally distributed, the Mann–Whitney-*U*-test was used. Values were presented as mean ± standard deviation (SD). All statistical analyses were performed with SPSS version 24 (IBM, Chicago, IL, USA).

### 5. Study Limitations

For surgeons, the most important factor in evaluating adhesions is not the histological change of the operative field, but the feeling when actually touching the field. Using the Rydell classification (grade 0, epidural scar tissue is not adherent to the dura mater; grade 1, epidural scar tissue is adherent to the dura mater, but easily dissected; grade 2, epidural scar tissue is adherent to the dura mater and difficult to dissect without disrupting the dura mater; grade 3, epidural scar tissue is firmly adherent to the dura mater and cannot be dissected) as previously described [23], we tried to perform evaluations correctly for neurosurgeons and veterinary surgeons. However, the blinded macroscopic evaluation was unable to reveal differences in adhesions and scar formation between the two groups.

The fundamental factor for this is that the surgical field is very narrow in rats. Therefore, larger animal models may be needed to allow correct evaluations.

**Author Contributions:** K.K. and H.U. conceived and designed the experiments; K.K., K.S., T.T., M.S., S.O., Se.T., K.N. and K.U. performed the experiments; Sa.T., H.S., K-i.K., I.M., G.H. and M.M. analyzed the data; E.T. and H.U. contributed reagents, materials, and analysis tools; K.K. wrote the paper.

**Acknowledgments:** This study was supported by grants from the JSPS KAKENHI (grant No. JP16K10746 to Kiyoshi Kikuchi), General Insurance Association of Japan (to Kiyoshi Kikuchi), ZENKYOREN (National Mutual Insurance Federation of Agricultural Cooperatives) of Japan (to Kiyoshi Kikuchi), and Mitsui Sumitomo Insurance Welfare Foundation of Japan (to Kiyoshi Kikuchi). E8002 was provided by Kawasumi Laboratories Inc. (Tokyo, Japan). The authors thank Yoko Tsurusaki, Sachiko Nakashima, Rumi Ito, Tomoko Matsuo, and Akiko Katano for excellent assistance. The authors also thank Alison Sherwin from Edanz Group (<http://www.edanzediting.com>) for editing a draft of this manuscript.

**Conflicts of Interest:** The authors declare no conflict of interest.

## Abbreviations

BBB	Basso, Beattie, and Bresnahan
FBSS	failed back surgery syndrome

## References

1. North, R.B.; Ewend, M.G.; Lawton, M.T.; Kidd, D.H.; Piantadosi, S. Failed back surgery syndrome: 5-year follow-up after spinal cord stimulator implantation. *Neurosurgery* **1991**, *28*, 692–699. [[CrossRef](#)] [[PubMed](#)]
2. Xu, J.; Chen, Y.; Yue, Y.; Sun, J.; Cui, L. Reconstruction of epidural fat with engineered adipose tissue from adipose derived stem cells and PLGA in the rabbit dorsal laminectomy model. *Biomaterials* **2012**, *33*, 6965–6973. [[CrossRef](#)] [[PubMed](#)]
3. Cruccu, G.; Aziz, T.Z.; Garcia-Larrea, L.; Hansson, P.; Jensen, T.S.; Lefaucheur, J.P.; Simpson, B.A.; Taylor, R.S. EFNS guidelines on neurostimulation therapy for neuropathic pain. *Eur. J. Neurol.* **2007**, *14*, 952–970. [[CrossRef](#)] [[PubMed](#)]
4. Henderson, R.; Weir, B.; Davis, L.; Mielke, B.; Grace, M. Attempted experimental modification of the postlaminectomy membrane by local instillation of recombinant tissue-plasminogen activator gel. *Spine* **1993**, *18*, 1268–1272. [[CrossRef](#)] [[PubMed](#)]
5. Liu, S.; Boutrand, J.P.; Bitton, J.; Tadie, M. A collagen-based sealant to prevent in vivo reformation of epidural scar adhesions in an adult rat laminectomy model. *J. Neurosurg.* **2002**, *97*, 69–74. [[CrossRef](#)] [[PubMed](#)]
6. Rodgers, K.E.; Robertson, J.T.; Espinoza, T.; Oppelt, W.; Cortese, S.; diZerega, G.S.; Berg, R.A. Reduction of epidural fibrosis in lumbar surgery with Oxisplex adhesion barriers of carboxymethylcellulose and polyethylene oxide. *Spine J.* **2003**, *3*, 277–283. [[CrossRef](#)]
7. Cekinmez, M.; Sen, O.; Atalay, B.; Erdogan, B.; Baybek, M.; Caner, H.; Ozen, O.; Altinors, N. Effects of methyl prednisolone acetate, fibrin glue and combination of methyl prednisolone acetate and fibrin glue in prevention of epidural fibrosis in a rat model. *Neurol. Res.* **2010**, *32*, 700–705. [[CrossRef](#)] [[PubMed](#)]
8. Li, X.; Chen, L.; Lin, H.; Cao, L.; Cheng, J.; Dong, J.; Yu, L.; Ding, J. Efficacy of poly(D,L-lactic acid-co-glycolic acid)-poly(ethylene glycol)-poly(D,L-lactic acid-co-glycolic acid) thermogel as a barrier to prevent spinal epidural fibrosis in a postlaminectomy rat model. *Clin. Spine Surg.* **2017**, *30*, E283–E290. [[CrossRef](#)] [[PubMed](#)]
9. Tao, H.; Fan, H. Implantation of amniotic membrane to reduce postlaminectomy epidural adhesions. *Eur. Spine J.* **2009**, *18*, 1202–1212. [[CrossRef](#)] [[PubMed](#)]
10. Sun, Y.; Wang, L.X.; Wang, L.; Sun, S.X.; Cao, X.J.; Wang, P.; Feng, L. A comparison of the effectiveness of mitomycin C and 5-fluorouracil in the prevention of peridural adhesion after laminectomy. *J. Neurosurg. Spine* **2007**, *7*, 423–428. [[CrossRef](#)] [[PubMed](#)]
11. Zhang, C.; Kong, X.; Ning, G.; Liang, Z.; Qu, T.; Chen, F.; Cao, D.; Wang, T.; Sharma, H.S.; Feng, S. All-trans retinoic acid prevents epidural fibrosis through NF-κB signaling pathway in post-laminectomy rats. *Neuropharmacology* **2014**, *79*, 275–281. [[CrossRef](#)] [[PubMed](#)]

12. Sun, Y.; Ge, Y.; Fu, Y.; Yan, L.; Cai, J.; Shi, K.; Cao, X.; Lu, C. Mitomycin C induces fibroblasts apoptosis and reduces epidural fibrosis by regulating miR-200b and its targeting of RhoE. *Eur. J. Pharmacol.* **2015**, *765*, 198–208. [[CrossRef](#)] [[PubMed](#)]
13. Olmarker, K. Reduction of adhesion formation and promotion of wound healing after laminectomy by pharmacological inhibition of pro-inflammatory cytokines: An experimental study in the rat. *Eur. Spine J.* **2010**, *19*, 2117–2121. [[CrossRef](#)] [[PubMed](#)]
14. Sun, Y.; Zhao, S.; Li, X.; Yan, L.; Wang, J.; Wang, D.; Chen, H.; Dai, J.; He, J. Local application of rapamycin reduces epidural fibrosis after laminectomy via inhibiting fibroblast proliferation and prompting apoptosis. *J. Orthop. Surg. Res.* **2016**, *11*, 1–9. [[CrossRef](#)] [[PubMed](#)]
15. Mukai, T.; Kamitani, S.; Shimizu, T.; Fujino, M.; Tsutamoto, Y.; Endo, Y.; Hanasawa, K.; Tani, T. Development of a novel, nearly insoluble antiadhesive membrane. *Eur. Surg. Res.* **2011**, *47*, 248–253. [[CrossRef](#)] [[PubMed](#)]
16. UMIN CTR. Randomized Controlled Trial on Efficacy and Safety of E8002. Available online: [https://upload.umin.ac.jp/cgi-open-bin/ctr/ctr\\_view.cgi?recptno=R000032997](https://upload.umin.ac.jp/cgi-open-bin/ctr/ctr_view.cgi?recptno=R000032997) (accessed on 6 March 2018). (In Japanese)
17. Ellis, H.; Moran, B.J.; Thompson, J.N.; Parker, M.C.; Wilson, M.S.; Menzies, D.; McGuire, A.; Lower, A.M.; Hawthorn, R.J.; O'Brien, F.; et al. Adhesion-related hospital readmissions after abdominal and pelvic surgery: A retrospective cohort study. *Lancet* **1999**, *353*, 1476–1480. [[CrossRef](#)]
18. Russell, J.D.; Russell, S.B.; Trupin, K.M. Differential effects of hydrocortisone on both growth and collagen metabolism of human fibroblasts from normal and keloid tissue. *J. Cell. Physiol.* **1978**, *97*, 221–229. [[CrossRef](#)] [[PubMed](#)]
19. Elias, J.A.; Freundlich, B.; Adams, S.; Rosenbloom, J. Regulation of human lung fibroblast collagen production by recombinant interleukin-1, tumor necrosis factor, and interferon- $\gamma$ . *Ann N. Y. Acad. Sci.* **1990**, *580*, 233–244. [[CrossRef](#)] [[PubMed](#)]
20. Fukui, N.; Nakajima, K.; Tashiro, T.; Oda, H.; Nakamura, K. Neutralization of fibroblast growth factor-2 reduces intraarticular adhesions. *Clin. Orthop. Relat. Res.* **2001**, *383*, 250–258. [[CrossRef](#)]
21. Basso, D.M.; Beattie, M.S.; Bresnahan, J.C. Graded histological and locomotor outcomes after spinal cord contusion using the NYU weight-drop device versus transection. *Exp. Neurol.* **1996**, *139*, 244–256. [[CrossRef](#)] [[PubMed](#)]
22. Yildiz, K.H.; Gezen, F.; Is, M.; Cukur, S.; Dosoglu, M. Mitomycin C, 5-fluorouracil, and cyclosporin A prevent epidural fibrosis in an experimental laminectomy model. *Eur. Spine J.* **2007**, *16*, 1525–1530. [[CrossRef](#)] [[PubMed](#)]
23. Rydell, N. Decreased granulation tissue reaction after installment of hyaluronic acid. *Acta Orthop. Scand.* **1970**, *41*, 307–311. [[CrossRef](#)] [[PubMed](#)]



© 2018 by the authors. Licensee MDPI, Basel, Switzerland. This article is an open access article distributed under the terms and conditions of the Creative Commons Attribution (CC BY) license (<http://creativecommons.org/licenses/by/4.0/>).



Review

# Stress-Activated Protein Kinases in Spinal Cord Injury: Focus on Roles of p38

Yoshitoshi Kasuya <sup>1,2,\*</sup>, Hiroki Umezawa <sup>1,2,3</sup> and Masahiko Hatano <sup>1</sup>

<sup>1</sup> Department of Biomedical Science, Graduate School of Medicine, Chiba University, Chiba City, Chiba 260-8670, Japan; h-umejan@hotmail.co.jp (H.U.); hatanom@faculty.chiba-u.jp (M.H.)

<sup>2</sup> Department of Biochemistry and Molecular Pharmacology, Graduate School of Medicine, Chiba University, Chiba City, Chiba 260-8670, Japan

<sup>3</sup> Department of Respiratory, Graduate School of Medicine, Chiba University, Chiba City, Chiba 260-8670, Japan

\* Correspondence: kasuya@faculty.chiba-u.jp; Tel.: +81-43-226-2193; Fax: +81-43-226-2196

Received: 15 February 2018; Accepted: 12 March 2018; Published: 15 March 2018

**Abstract:** Spinal cord injury (SCI) consists of three phases—acute, secondary, and chronic damages—and limiting the development of secondary damage possibly improves functional recovery after SCI. A major component of the secondary phase of SCI is regarded as inflammation-triggered events: induction of cytokines, edema, microglial activation, apoptosis of cells including oligodendrocytes and neurons, demyelination, formation of the astrocytic scar, and so on. Two major stress-activated protein kinases (SAPKs)—c-Jun N-terminal kinase (JNK) and p38 mitogen-activated protein kinase (p38 MAPK)—are activated in various types of cells in response to cellular stresses such as apoptotic stimuli and inflammatory waves. In animal models of SCI, inhibition of either JNK or p38 has been shown to promote neuroprotection-associated functional recovery. Here, we provide an overview on the roles of SAPKs in SCI and, in particular, the pathological role of p38 will be discussed as a promising target for therapeutic intervention in SCI.

**Keywords:** spinal cord injury; stress-activated protein kinases; c-Jun N-terminal kinase; p38 mitogen-activated protein kinase

## 1. Introduction

Traumatic spinal cord injury (SCI) is a severe, devastating disease which often results in sensorimotor dysfunction, largely due to the poor regenerative capacity of neuronal cells in the adult mammalian central nervous system (CNS) [1]. Following the initial physical injury, the lesion proceeds to receive secondary waves of complex neuroinflammatory events that cause additional tissue destruction and functional impairments [2,3]. Under the secondary phase of SCI, however, gradual functional recovery is observed in not only several animal models but also humans to some extent, and is inversely proportional to the initial damage intensity of the SC [4]. In developing beneficial drugs for SCI, it is therefore clinically reasonable to target the secondary damages involving inflammation, blood–cerebrospinal fluid (CSF) barrier disruption, glial scar formation, cell death of neurons and oligodendrocytes, lipid peroxidation, and glutamate excitotoxicity. Indeed, many studies have recently focused on pharmacological interventions targeting the secondary damage symptoms. To strengthen the reliability of therapeutic candidates for SCI, however, the exact molecular mechanism underlying the secondary damage symptoms and the pivotal signaling pathway mediating each symptom should be evaluated precisely.

The stress-activated protein kinase (SAPK) group of mitogen-activated protein kinases (MAPKs) includes two members of the c-Jun NH<sub>2</sub>-terminal kinase (JNK) and p38 MAPK families, which are activated in response to environmental stresses such as inflammatory stimuli by cytokines and Toll-like

receptor (TLR) ligands, oxidative stress, trophic factor withdrawal, osmolarity shock, ultraviolet (UV) irradiation, chemotherapeutic drugs, and so on [5,6]. The JNK family (JNK1, JNK2, and JNK3) are encoded by three separate but closely related genes. JNK1 and JNK2 are expressed ubiquitously in adult tissues, whereas the expression of JNK3 is primarily observed in brain, heart, and testis. Ten different JNK isoforms are produced by alternative splicing of the *Jnk* transcripts: JNK1 $\alpha$ 1, JNK1 $\beta$ 1, JNK2 $\alpha$ 1, JNK2 $\beta$ 1, and JNK3 $\alpha$ 1 have a molecular weight of 46 kDa; and JNK1 $\alpha$ 2, JNK1 $\beta$ 2, JNK2 $\alpha$ 2, JNK2 $\beta$ 2, and JNK3 $\alpha$ 2 have a molecular weight of 54 kDa with an extended C-terminus [7]. Their relative contributions to the overall JNK activity remain to be elucidated. JNKs are activated by dual phosphorylation of the TGY motif within their activation loop by two upstream MAPK kinases (MAP2Ks)—MKK4 and MKK7—which are activated by various MAPKK kinases (MAP3Ks), MEKKs, Mixed-lineage kinases (MLKs), apoptosis signal-regulating kinase 1 (ASK1), thousand-and-one amino acid kinase 2 (TAO2), TNF receptor-associated factor 2- and NCK-interacting protein kinase (TNIK), and dual leucine zipper-bearing kinase (DLK) [8].

On the other hand, the p38 family consists of four isoforms ( $\alpha$ ,  $\beta$ ,  $\gamma$ , and  $\delta$ ) arising from separate genes. p38 $\alpha$  and - $\beta$  are ubiquitously expressed in adult tissues, whereas expression of p38 $\gamma$  is predominant in skeletal muscle and p38 $\delta$  shows high expression levels in the kidney and lung [9,10]. As an alternative form of p38 $\beta$  that was initially identified, p38 $\beta$ 2 with an internal deletion of 8 amino acids has been reported. p38 $\beta$ 2 showed much higher sensitivity to extracellular stimuli and p38 inhibitor than does p38 $\beta$ , which shows a level similar to that of p38 $\alpha$ . In particular, p38 $\beta$ 2 but not p38 $\beta$  phosphorylated various substrates (as p38 $\alpha$  does) in response to sorbitol [11]. Therefore, p38 $\beta$  means p38 $\beta$ 2 at present. Among p38 isoforms, the best characterized isoform is p38 $\alpha$ , the physiological and pathological roles of which have been well investigated [5,12]. In this review, we therefore mostly refer to p38 $\alpha$  as p38, unless otherwise indicated. p38 MAPKs are activated by dual phosphorylation of the TGY motif within their activation loop by two upstream MAP2K—MKK3 and MKK6—which are activated by various MAP3Ks, MEKKs, MLKs, ASK1, TAO2, TGF- $\beta$ -activated kinase 1 (TAK1), and Tumor progression locus 2 (TPL2). Consequently, JNK and p38 pathways share a number of upstream MAP3Ks although the two pathways are not redundant. In addition to this canonical activation pathway composed of three stepwise modules, specific binding of TAK1-binding protein 1 (TAB1) to p38 $\alpha$  and TCR/ $\zeta$  chain-associated protein kinase (ZAP70)-mediated phosphorylation of Tyr<sup>323</sup> in the C-terminal domain of p38 MAPKs (except p38 $\delta$ ) are described as new p38 activation pathways via upregulating autophosphorylation of p38 MAPKs [13,14].

Overview of the SAPK activation pathway is shown in Figure 1A. SAPKs activated through a typical kinase cascade promote a variety of cellular responses. In this review, we introduce increasing evidence concerning pathological functions of JNK and p38 in SCI. In particular, we will discuss the potential of targeting the p38 pathway as a disease-modifying therapy in SCI.

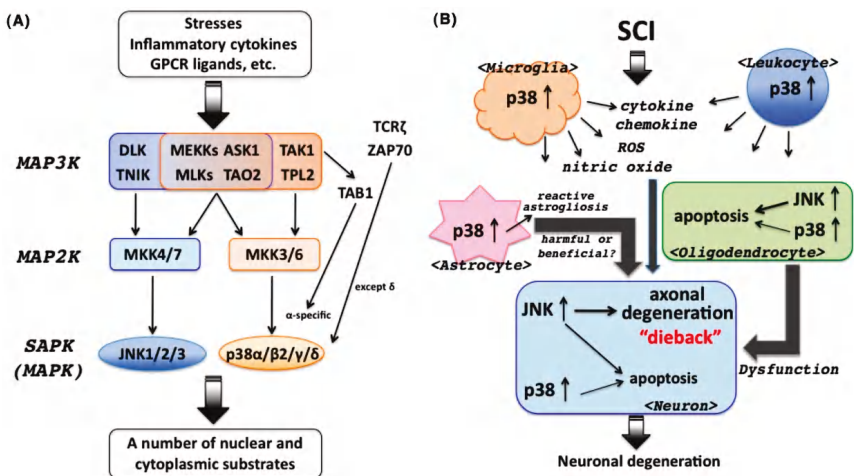


**Figure 1.** (A) Overview of the stress-activated protein kinase (SAPK) pathway. SAPKs, c-Jun N-terminal kinases (JNKs), and p38 mitogen-activated protein kinases (MAPKs) are activated in response to a variety of cellular stresses through a three-step pathway (MAP3K/MAP2K/MAPK). In addition to this canonical pathway, several pathways for p38 activation have been demonstrated. (B) Overview of the SAPK-mediated neuronal degeneration after spinal cord injury (SCI). JNK contributes to neuronal degeneration in a direct manner and also induces neuronal dysfunction in an indirect manner through oligodendrocytic cell-death-associated demyelination. p38 predominantly orchestrates SCI-triggered inflammatory responses such as activation of microglia, production of inflammatory and neurotoxic mediators from infiltrated leukocytes and activated microglia, and reactive astrogliosis. Reactive astrogliosis shows bidirectional effects on neuronal regeneration after SCI.

## 2. SAPKs in the CNS

In the CNS, JNK1 and JNK2 are expressed in various types of cells. On the other hand, the expression of JNK3 is predominantly observed in neuronal cells. The most highly expressed transcript of JNK isoform in the adult rodent brain is *Jnk3* mRNA followed by *Jnk2* mRNA and then *Jnk1* mRNA [15,16]. The cellular and behavioral phenotypes observed in JNK isoform- and compound JNK isoforms-knockout mice models clearly suggest crucial roles of JNKs in the CNS as follows: (i) *Jnk3*-knockout mice exhibit a marked reduction in kainate-induced neuronal apoptosis in the hippocampus secondary to seizure response, and in dopaminergic cell loss in the Parkinson's disease model mice using 1-methyl-4-phenyl-1,2,4,6-tetrahydropyridine (MPTP) [17–19]; (ii) *Jnk2*-knockout mice show a decrease in dopaminergic cell loss in the MPTP Parkinson's disease model [18]; (iii) *Jnk1/Jnk2*-double-knockout mice show an embryonic lethality at E11.5 because of severe dysregulation of apoptosis in the hindbrain at E9.0 [20]; (iv) *Jnk1/Jnk2/Jnk3*-triple-knockout neuronal cells (primary cultured neurons from *Jnk1*<sup>LoxP/LoxP</sup>/*Jnk2*<sup>−/−</sup>/*Jnk3*<sup>−/−</sup> mice were infected with *Ad-cre* to establish deficiency of the JNKs) exhibit marked life span extension during culture in vitro [21]. Therefore, JNK is the central player at least in neuronal apoptosis, which tempts us to consider that JNKs are able to contribute to the development of various neural diseases. Here, “knockout” represents a traditional gene knockout, unless otherwise indicated.

In contrast to the cases of JNK-knockout mice, deficiency of each p38 isoform gene does not result in defects in the CNS. *p38 $\alpha$* -knockout mice result in embryonic lethality due to dysfunction of erythropoiesis and placental organogenesis [22,23]. A deficiency of the *p38 $\beta$*  gene is functionally compensated by p38 in both activation of downstream kinases and TNF- $\alpha$ -mediated inflammatory diseases [24]. *p38 $\gamma$* -knockout mice exhibit loss of myogenic precursor cells that are primarily

responsible for skeletal muscle growth and regeneration [25]. *p38δ*-knockout mice exhibit a marked resistance to skin tumor development induced by chemical agents [26]. However, increasing evidence indicates that at least *p38α* is expressed in neurons, astrocytes, oligodendrocytes, and microglia and controls their cell fate and functions [12,27–30]. For instance, it has been proposed that amyloid β-peptide (Aβ)-induced disruption of N-cadherin-based synaptic contact results in *p38* activation, which in turn phosphorylates Tau leading to neuronal apoptosis. This phenomenon is one of the neurodegenerative processes in Alzheimer's disease (AD) [31]. Likewise, *p38* as well as JNK are activated and play roles in the innate and adaptive immune responses, and various *p38* inhibitors have been energetically developed and are in clinical trials as potential anti-inflammatory drugs [5] ([Clinicaltrials.gov](https://clinicaltrials.gov), <https://clinicaltrials.gov/>). In inflammation-associated disorders of the CNS, *p38* may therefore be a valid therapeutic target. In fact, several reports including our study have demonstrated that *p38α* contributes to the pathogenesis of experimental autoimmune encephalomyelitis (EAE, a model for multiple sclerosis) mainly via mobilizing the Th17/IL-17 axis [32–36]. Notably, *p38* inhibitors ameliorate the progression of EAE if administered even after the onset of clinical symptoms [35,36]. In AD, moreover, the intense signal of *p38* activation was observed in the brain area where neuritic β-amyloid plaques were accumulated. It has been also demonstrated that *p38* plays a crucial role in amyloid precursor protein-induced production of neurotoxic cytokines (e.g., TNF-α and IL-1β) in microglia [37]. It is noteworthy that *p38α* inhibition ameliorates the overproduction of proinflammatory cytokines associated with neuronal dysfunction and behavioral deficits in the Aβ-infused AD-relevant animal model [38].

### 3. Involvement of JNK in the Pathogenesis of SCI

Early evidence has demonstrated that contusion SCI activates the ASK1/JNK-p38 signaling axis in both neurons and oligodendrocytes proceeding to apoptosis [39]. These events were followed by further study using tiptoe-walking Yoshimura (TWY) mice that developed aging-associated spontaneous calcification in the cervical ligament, thereby causing chronic mechanical compression of the spinal cords. [40]. In those reports, the activation of ASK1-JNK and -p38 pathways was observed in apoptotic sign-bearing neurons and oligodendrocytes, suggesting that JNK and p38 contribute to neuronal and oligodendrocytic apoptosis in SCI at least phenomenologically.

The JNK-mediated apoptosis of oligodendrocytes in SCI has been precisely investigated [41]. The injury-activated JNK3 phosphorylated myeloid cell leukemia sequence-1 (Mcl-1) and facilitated the degradation of Mcl-1 by ubiquitination in oligodendrocytes, which in turn induced apoptosis-associated release of cytochrome C from mitochondria. This JNK-mediated oligodendrocytic apoptosis was canceled by a disruption of the *Jnk3* gene. Interestingly, the peak activation ratio of JNK3 was 500-fold higher than those of JNK1/2 in the SC after hemisection injury, and JNK activation monitored by phosphorylation of c-Jun was typically detected in neurons as well. Nevertheless, the number of apoptotic neuron somas (TUNEL<sup>+</sup>/NeuN<sup>+</sup>) was not significantly different between *Jnk3*-knockout mice and wild-type (WT) littermates, suggesting several possibilities as follows: (i) low activation of JNK1 or JNK2 functionally contributes to neuronal cell death after SCI; (ii) JNK3 may induce not apoptosis but another type of cell death—autophagic death—after SCI; (iii) JNK3 may not directly regulate apoptosis of neurons but may play a role in transporting the damage signal under nerve degeneration or regeneration like the case in the previous report [42]. The last notion was supported by a subsequent study.

Superior cervical ganglion 10 (SCG10), an axonal-maintenance factor, has phosphorylation sites (Ser63 and Ser73) specific for JNK and is at least partly regulated by the phosphorylation-triggered degradation program. In healthy axons, SCG10 protein may undergo rapid JNK-dependent degradation versus replenishment by axonal transport from cell bodies. Once axons were injured, loss of function of the replenishment in concert with continuous JNK-dependent degradation might result in a marked loss of SCG10 selectively in distal axon segments, which accelerates axonal fragmentation leading to anterograde axonal degeneration [43]. Hence, the JNK/SCG10 axis may

contribute to Wallerian degeneration, one of the typical pathological aspects in SCI. Furthermore, the involvement of JNK in retrograde axonal degeneration—so-called “dieback”—has been clearly demonstrated [44]. The SCI-upregulated phospho-JNK was observed in the dorsal corticospinal tract (CST) fibers labeled with biotinylated dextran amine (BDA) in the gray matter rostral to the lesion site, where amyloid- $\beta$  precursor protein, a marker for axonal degradation, was apparently accumulated. This SCI-induced axonal dieback was markedly suppressed by continuous intrathecal administration of a JNK inhibitor, SP600125, which was replicated in both *JNK1*-knockout and *JNK3*-knockout mice. Likewise, hindlimb locomotor recovery after SCI was improved in SP600125-treated WT, *JNK1*-knockout, and *JNK3*-knockout mice, suggesting that at least *JNK1* and *JNK3* positively regulate axonal dieback limiting locomotor recovery after SCI. It has been also demonstrated that the improvement of functional recovery after SCI is performed by D-JNKA1—the cell-permeable peptide inhibitor against JNK [45]. Notably, a single intraperitoneal injection of D-JNKA1 showed beneficial effects on SCI, which may be valuable as a minimally invasive strategy for clinical application of JNK inhibition.

In contrast to the axonal degeneration activity of JNK in SCI, a lot of previous reports have demonstrated that JNKs might play important roles in axonal guidance and neurite growth [8]. During the axonal regeneration process, JNK activity is necessary for neuritogenesis and sustained neurite elongation [46]. These findings strongly suggest that JNK elicits neuroregenerative function as well, tempting us to think whether the anti-JNK strategy prevents spontaneous axonal regeneration after SCI. JNK inhibition by D-JNKA1 did not reduce long-term sprouting of the serotonergic fibers in the glial scar after SCI [45]. In this case, the single administration of D-JNKA1 was performed 6 h after SCI, under the experimental condition in which D-JNKA1 might not affect the relatively late-onset sprouting. On the other hand, continuous administration with SP600125 did not interfere with axonal branches extending from the CST into the gray matter far rostral to the lesion and, more likely, preserved the axonal branches sprouting in the rostral part close to the lesion epicenter more frequently compared with vehicle-treated control mice [44]. The reason why SP600125 efficiently leads to axonal regeneration after SCI is not clear. As a plausible explanation, SCI-induced JNK activation under the axonal degeneration process may be stronger than that under the axonal regeneration process, because a significant activation of JNK in the SC is observed at 1–3 days post-injury [44]. However, further investigation as to whether JNK inhibition especially during the axonal regeneration process worsens functional recovery after SCI is informative in considering the adverse effect of JNK inhibitors.

Taken together, JNK activity (at least in neurons and oligodendrocytes) can contribute to the pathogenesis of SCI. In addition, several reports have described that JNK activity in endothelial cells and astrocytes may be involved in the breakdown of the blood-CSF barrier and neuropathic pain, respectively, after SCI [45,47]. Although JNK is closely related to innate and adaptive immunity in various pathological situations, neither activation of microglial cells nor infiltration of myeloperoxidase-positive neutrophils were affected under the condition in which JNK inhibitors improved locomotor recovery after SCI [5,45,48]. Further precise studies are required, but JNK may not primarily orchestrate inflammatory events in the secondary damage of SCI.

#### 4. Involvement of p38 in the Pathogenesis of SCI

##### 4.1. *p38 as a Central Player in Inflammatory Responses*

In the secondary phase of SCI, infiltrated leukocytes and activated glial cells exacerbate tissue damage by releasing proinflammatory cytokines/chemokines, proteases, and reactive oxygen intermediates, though they exhibit certain beneficial aspects as well in some cases. The post-traumatic inflammatory responses may contribute to axonal degeneration, neuronal and oligodendrocytic cell death, and scar formation, and finally result in the impairment of neuronal function [49]. A number of studies have described that proinflammatory cytokines such as IL-6, TNF- $\alpha$  and IL-1 $\beta$  are potent

mediators for the pathogenesis of SCI at the early stage of secondary damage [50]. Initially, p38 has been identified as a target protein for cytokine-suppressive anti-inflammatory drugs (CSAIDs) as well as a lipopolysaccharide (LPS)/TLR-activated kinase and shown to contribute to mRNA stabilization of IL-1 $\beta$  and TNF- $\alpha$  [51,52]. In addition to the function of transducing extracellular signals to the transcriptional machinery through regulating transcriptional factors (e.g., activating transcription factor 2 (ATF2), myocyte-specific enhance factor 2C/A, cAMP response element binding protein (CREB) and CEBP-homologous protein) as substrates of p38, p38 has been found to play an important role in both translation and stability of inflammatory mRNAs. For instance, AU-rich elements (AREs) found in the 3'-untranslated region of TNF- $\alpha$  mRNAs are binding sites for various factors regulating mRNA decay. The downstream kinase of p38, MAPK-activated protein kinase 2 (MK2 also known as MAPKAPK2), interferes with the interaction between AREs and the binding factors and thereby stabilizes TNF- $\alpha$  mRNA [53]. Expression of IL-6, which provokes activation and infiltration of leukocytes as one of its pleiotropic functions in SCI, is controlled by the mechanism of p38/MK2-induced mRNA stabilization as well [54]. Therefore, p38 can mobilize major SCI-related proinflammatory cytokines in the post-traumatic inflammatory process.

Using genetically manipulated mice and p38 inhibitors, it has been well documented that p38 plays important roles in various steps of inflammatory responses as follows: (i) p38 in macrophages stimulated with different TLR ligands regulates the expression of proinflammatory factors (e.g., inducible nitric oxide synthase (iNOS), cyclooxygenase 2, IL-6 and TNF- $\alpha$ ) via gene regulatory mechanisms at both transcriptional and post-transcriptional levels [5,55]; (ii) p38 is required for the LPS-, TNF-, or UV-B-induced maturation of monocyte-derived dendritic cells (DCs) [5]; (iii) p38 is involved in production of interferon (IFN)- $\gamma$  and Th1 differentiation of CD4 $^{+}$  T cells under stimulation with antigen and/or cytokines [5,56]; (iv) p38 upregulates the translational regulation of cytokine production in NKT cells through activating the MAPK-interacting serine/threonine kinase (Mnk)-eukaryotic translation initiation factor 4E (eIF4E) pathway, a downstream target of p38 [57]; (v) p38 is involved in DC-driven Th17 differentiation, Th17 proliferation, and regulation of IL-17 expression in Th17 [33,34]. As for IL-17 expression in Th17 cells, both the transcriptional regulation via ATF2/CREB activated by p38 $\alpha$  and the translational regulation via the p38 $\alpha$ /Mnk-eIF4E pathway have been proposed [35,36]. In conjunction with the fact that inhibition of p38 efficiently blocks the highly pathogenic avian influenza virus (HPAIV)-induced “cytokine storm”, the p38 pathway can regulate inflammatory responses as a central player [58].

#### 4.2. Spatial Activation of p38 after SCI

In addition to neurons and oligodendrocytes, activation of p38 was observed in activated microglia/macrophages, infiltrated neutrophils, and reactive astrocytes forming a glial scar after SCI [39,40,59,60]. Several reports have described the mechanism of p38-mediated SCI development. In a complete transection model of SCI, activation of p38 induced the expression of iNOS in activated microglia/macrophages and then caused a decrease in NeuN $^{+}$  cells. The loss of neuronal cells was effectively inhibited by either a p38 inhibitor, SB203580, or N( $\omega$ )-nitro-L-arginine methyl ester, suggesting that the p38/NO signaling axis mediates the microglial cell-induced neurotoxicity after SCI [59]. In the SC after contusion injury, induction of IL-1 $\beta$  expression and p38 phosphorylation was observed prior to neuronal apoptosis identified as the TUNEL $^{+}$ /active caspase-3 $^{+}$  somas in the gray matter. An inhibitor of the IL-1 $\beta$  pathway, IL-1Ra suppressed phosphorylation of p38, indicating that p38 functions downstream of IL-1R1. Likewise, the neuronal apoptosis was sensitive to both IL-1Ra and SB203580, suggesting that the IL-1 $\beta$ /p38 signaling axis is involved in neuronal apoptosis after SCI [61].

#### 4.3. Correlation between p38 Pathway Inhibition and Functional Recovery after SCI

##### 4.3.1. p38 Inhibitors

Initially, SB203580 was reported to prevent damage to hindlimb function after SCI [62]. In contrast, a subsequent study has shown that SB203580 could not improve functional recovery after SCI [60]. The two reports are controversial in spite of employing a similar contusion SCI model and the same administration protocol (continuous intrathecal administration). The difference in intensity of SC damage between the two cases might influence the beneficial effect of p38 inhibition on SCI. In the former report, moreover, the treatment with SB203580 did not affect inflammatory responses in the lesion area, indicating that the anti-inflammatory potential of p38 inhibition may not work as a primary therapeutic effect on SCI.

Then, we have recently validated whether p38 $\alpha$  is a potential therapeutic target in SCI. A single-copy disruption of p38 $\alpha$  gene (p38 $\alpha^{+/-}$ , p38 $\alpha^{-/-}$  is embryonic lethal as described above) reduced the tissue degenerative events (e.g., induction of various cytokines/chemokines, leukocytic infiltration, apoptosis of oligodendrocytes, loss of neuronal cells, and reactive astrogliosis) and augmented the tissue regenerative events (e.g., recruitment of oligodendrocyte progenitor cells, compaction of microglia/macrophages, and axonal regrowth), thereby causing a better functional recovery following lateral hemisection SCI. In our investigation, hence, genetic inhibition of p38 $\alpha$  markedly suppressed at least the SCI-induced inflammatory responses: an increase in infiltration of both T lymphocytes and monocytes/macrophages into the lesion epicenter, and upregulation of inflammatory-related proteins (e.g., C-X-C motif chemokine 12, macrophage inflammatory protein (MIP)-1 $\alpha$ , MIP-2, and matrix metalloproteinase 9) in the SC. These findings strongly suggest that the decrease of leukocytic infiltration associated with the suppression in expression of inflammatory-related proteins may contribute to the reduced development of SCI in p38 $\alpha^{+/-}$  mice and further that inhibition of p38 can ameliorate SCI-associated inflammatory responses. In addition, the analysis using Texas Red-BDA, an anterograde tracer, showed that axonal regeneration after SCI was accelerated or enhanced in the caudal part of the SC in p38 $\alpha^{+/-}$  mice compared with WT mice. Notably, SB239063, a p38 inhibitor that is transferable across the blood-CSF barrier, significantly improved functional recovery after SCI in WT mice if orally administered once a day at 1–3 days post-injury [63]. An overview of the SAPK-associated pathological outcome, especially the neuronal degenerative process in SCI, is shown in Figure 1B.

##### 4.3.2. Minocycline

Minocycline, known as a second-generation tetracycline, is an interesting candidate in the treatment of traumatic CNS injuries and neurodegenerative diseases because it possesses neuroprotective and anti-inflammatory properties. A number of reports have proposed that minocycline-evoked anti-inflammatory and anti-apoptotic actions could be mediated through inhibition of p38 as follows: (i) low doses of minocycline protected neurons in mixed spinal cord cultures from N-methyl-D aspartate excitotoxicity by inhibiting the p38-promoted microglial activation [64]; (ii) minocycline protected cerebellar granule neurons from NO-induced cell death via reduction of p38 activity [65]; (iii) minocycline ameliorated carrageenan-induced inflammation-associated hyperalgesia through inhibiting p38 activation in spinal microglia [66]. In fact, it has been shown that the minocycline-p38 inhibition loop improves functional recovery after SCI mainly by decreasing cell death of oligodendrocytes [67]. In that report, minocycline inhibited oligodendrocytic apoptosis via reduction of the p38 activity-dependent pro-nerve growth factor (proNGF) production in microglia, leading to the improvement of functional recovery after SCI.

NGF can promote cell death via stimulation of p75 neurotrophin receptor (p75<sup>NTR</sup>) in addition to the well-known function of neuronal differentiation/survival via tyrosine receptor kinase A (TrkA). Likewise, proNGF, the unprocessed NGF precursor, can bind p75<sup>NTR</sup> preferentially over TrkA, and the expression of p75<sup>NTR</sup> is specifically upregulated in oligodendrocytes after

SCI. Thus, the proNGF/p75<sup>NTR</sup> signaling axis-induced apoptosis may occur predominantly in oligodendrocytes after SCI [68].

In another report, gene array analysis of mRNA from the SCs of rats with SCI showed the expression of p38 $\beta$ 2 was typically and specifically downregulated by treatment with minocycline, the phenomenon of which is of interest [69]. In regards to the LPS-induced neurotoxicity secondary to the proinflammatory cytokine production in microglia, however, p38 $\beta$  but not p38 $\alpha$  is dispensable in the brain, which is similar to the case of peripheral inflammation mentioned above [24,70]. Furthermore, neuron-selective microRNAs (miRs)—miR-124 and miR-128—selectively deplete p38 $\alpha$  but not p38 $\beta$  in neurons, which results in loss of function of the p38/Mnk-eIF4E pathway in neurons. Thus, p38 $\beta$  cannot compensate p38 $\alpha$  loss at least in the translational machinery mediated by the Mnk-eIF4E pathway [71]. Further investigation is required for the pathophysiological significance of minocycline treatment-specific downregulation of p38 $\beta$ 2.

Currently, an interventional clinical trial, MASC (Minocycline in Acute Spinal Cord Injury) in phase III, is in progress with minocycline for patients with SCI ([clinicaltrials.gov](#), registration number NCT01828203). The indication expansion for minocycline is much expected [72].

#### 4.3.3. Plant-Derived Agents

Some plant-derived agents showing a beneficial effect on SCI can inhibit the p38 pathway. Curcumin, a yellow polyphenol derived from the *Curcuma longa* plant, is commonly used as a spice and also has a variety of medicinal properties including anti-inflammatory, analgesic, anti-oxidant, and antiseptic activity. It has been clearly demonstrated that curcumin enhances locomotor and sensory recovery after SCI at least partly through inhibiting the nuclear factor  $\kappa$ -light-chain-enhancer of activated B cells (NF- $\kappa$ B) pathway [73].

NF- $\kappa$ B elicits pleiotropic functions by regulating the transcription of various genes such as cytokines/chemokines, adhesion molecules, proinflammatory transcription factors, proinflammatory enzymes, and so on. In addition, it is well described that NF- $\kappa$ B is activated downstream of TLR and cytokine receptors like p38 is. In the CNS, the basal activity of NF- $\kappa$ B in glial cells is low but highly inducible in response to the change of neural environment, which may play a crucial role in brain inflammation [74]. In fact, transgenic mice with astrocyte-specific loss of function of NF- $\kappa$ B activity show a dramatic improvement of functional recovery after contusive SCI [75]. Therefore, NF- $\kappa$ B activity at least in glial cells contributes to the pathogenesis of SCI. Subsequently, it has been demonstrated that curcumin ameliorates secondary damage (e.g., production of IL-6, TNF- $\alpha$ , IL-1 $\beta$ , and nitric oxide) presumably through inhibiting both the TAK1/MKK6/p38 pathway and the NF- $\kappa$ B pathway, which may contribute to the improvement of locomotor recovery after SCI [76].

Geraniol (an acyclic monoterpene alcohol) is primarily found in rose oil, palmarosa oil, and citronella oil and commonly used in flavors and perfumes due to its rose-like scent. Geraniol has various properties including antibacterial, immune regulation, insecticidal, and antitumor activities. It has been demonstrated that Geraniol ameliorates secondary damage (e.g., edema, induction of proinflammatory cytokines, oxidative stress, and neural apoptosis) and improves locomotor recovery after SCI. As the main signaling mechanism of action, geraniol was shown to inhibit the SCI-upregulated expression of NF- $\kappa$ B and p38 [77]. Through a similar mechanism, improvement of locomotor recovery after SCI was observed in rats treated with asiaticoside, a terpenoid component extracted from *Centella asiatica* [78].

#### 4.4. p38 as a Promising Target for Therapeutic Intervention in SCI?

Accumulating evidence with animal models suggests that p38 plays a crucial role in the pathogenesis of SCI and that p38 is expected as a clinical target for the treatment of SCI. However, p38 signaling has a wide spectrum of biological activities beyond the inflammatory/stress responses in the CNS [12]. In addition, the obvious resistance of p38 $\alpha^{+/-}$  mice to various pathological inputs raises the question whether a full inhibition of p38 results in improvement of clinical symptoms [36,63,79–82].

This notion may be partly supported by the fact that highly concentrated application of SB203580 loses its beneficial effect on SCI [62]. Likewise, mitogen- and stress-activated kinases (MSKs) 1 and 2 that are activated downstream of p38 play important roles in macrophages as follows: production of the anti-inflammatory cytokine, IL-10; production of IL-1Ra; and an increase in transcription of dual-specificity protein phosphatase 1 (DUSP1 also known as MAPK phosphatase-1) leading to dephosphorylation/inactivation of p38. Thus, the p38/MSK signaling axis can function as the negative feedback loop in p38-mediated inflammatory responses [83]. Furthermore, p38 inhibitor-based therapeutic investigation is sometimes limited because of its specificity [84]. Therefore, further precise investigation is needed, focusing on the exact spatial and temporal activation of p38 which positively or negatively contributes to the functional outcome after SCI. As a result, p38 inhibition will be received as a therapeutic option without adverse effects.

## 5. Closing Remarks

Here, we gave an overview on roles of SAPKs in SCI and, in particular, discussed the potential of targeting the p38 pathway as a disease-modifying therapy in SCI. In addition to its role in the development of neuronal degeneration after SCI, p38 may contribute to SCI-associated neuropathic pain development and maintenance. After spinal nerve ligation (SNL) that is commonly used as a neuropathic pain model, p38 was markedly activated predominantly in spinal microglia, and its activity was maintained over 3 weeks [85]. The relationships between nerve-injury-induced microglial activation and pain sensitization are well characterized [86]. Therefore, p38 may represent a potent clinical target for neuropathic pain management after SCI. In fact, the therapeutic effect of SB681323, a p38 inhibitor, on neuropathic pain following nerve trauma was studied in a past clinical trial ([clinicaltrials.gov](#), registration number NCT00390845). It has been reported that nearly 80% of patients with SCI are seriously affected by pain and unpleasant sensations [87]. The development of emerging strategies for both functional recovery and neuropathic pain management after SCI is regarded as a clinically and socially urgent matter.

**Acknowledgments:** This work was supported in part by Grants-in-Aid for Scientific Research ((B), 24390137 to Yoshitoshi Kasuya) from the Ministry of Education, Science, Sports and Culture of Japan.

**Author Contributions:** Yoshitoshi Kasuya, Hiroki Umezawa and Masahiko Hatano wrote the manuscript.

**Conflicts of Interest:** The authors declare no conflict of interest.

## Abbreviations

A $\beta$	Amyloid $\beta$
AD	Alzheimer's disease
ARE	AU-rich element
ASK1	Apoptosis signal-regulating kinase 1
ATF2	Activating transcription factor 2
BDA	Biotinylated dextran amine
CNS	Central nervous system
CREB	cAMP response element binding protein
CSAID	Cytokine-suppressive anti-inflammatory drug
CSF	Cerebrospinal fluid
CST	Corticospinal tract
DCs	Dendritic cells
DLK	Dual leucine zipper-bearing kinase
EAE	Experimental autoimmune encephalomyelitis
eIF4E	Eukaryotic translation initiation factor 4E
HPAIV	Highly pathogenic avian influenza virus
IL	Interleukin

IFN- $\gamma$	Interferon- $\gamma$
iNOS	Inducible nitric oxide synthase
JNK	c-Jun N-terminal kinase
LPS	Lipopolysaccharide
MAPK	Mitogen-activated protein kinase
MAP2K	MAPK kinase
MAP3K	MAPKK kinase
Mcl-1	Myeloid cell leukemia sequence-1
miR	MicroRNA
MIP	Macrophage inflammatory protein
MK2	MAPK-activated protein kinase 2
MLK	Mixed lineage kinase
Mnk	MAPK-interacting serine/threonine kinase
MPTP	1-Methyl-4-phenyl-1,2,4,6-tetrahydropyridine
MSK	Mitogen- and stress-activated kinase
NF- $\kappa$ B	Nuclear factor $\kappa$ -light-chain-enhancer of activated B cells
NGF	Nerve growth factor
p75 <sup>NTK</sup>	p75 Neurotrophin receptor
SAPK	Stress-activated protein kinase
SCI	Spinal cord injury
SCG10	Superior cervical ganglion 10
TAB1	TAK1-binding protein 1
TAK1	TGF- $\beta$ -activated kinase 1
TAO2	Thousand-and-one amino acid kinase 2
TGF- $\beta$	Transforming growth factor- $\beta$
Th	T-helper
TNF- $\alpha$	Tumor necrosis factor- $\alpha$
TNIK	TNF receptor-associated factor 2- and NCK-interacting protein kinase
TLR	Toll-like receptor
TPL2	Tumor progression locus 2
TrkA	Tyrosine receptor kinase A
TWY	Tiptoe-walking Yoshimura
UV	Ultraviolet
ZAP70	$\zeta$ chain-associated protein kinase

## References

- Horner, P.J.; Gage, F.H. Regenerating the damaged central nervous system. *Nature* **2000**, *407*, 963–970. [[CrossRef](#)] [[PubMed](#)]
- Hilton, B.J.; Moulson, A.J.; Tetzlaff, W. Neuroprotection and secondary damage following spinal cord injury: Concepts and methods. *Neurosci. Lett.* **2017**, *652*, 3–10. [[CrossRef](#)] [[PubMed](#)]
- Zhou, X.; He, X.; Ren, Y. Function of microglia and macrophages in secondary damage after spinal cord injury. *Neural Regen. Res.* **2014**, *9*, 1787–1795. [[CrossRef](#)] [[PubMed](#)]
- Becker, D.; Sadowsky, C.L.; McDonald, J.W. Restoring function after spinal cord injury. *Neurologist* **2003**, *9*, 1–15. [[CrossRef](#)] [[PubMed](#)]
- Rincón, M.; Davis, R.J. Regulation of the immune response by stress-activated protein kinases. *Immunol. Rev.* **2009**, *228*, 212–224. [[CrossRef](#)] [[PubMed](#)]
- Le-Niculescu, H.; Bonfoco, E.; Kasuya, Y.; Claret, F.-X.; Green, D.R.; Karin, M. Withdrawal of survival factors results in activation of the JNK pathway in neuronal cells leading to Fas ligand induction and cell death. *Mol. Cell. Biol.* **1999**, *19*, 751–763. [[CrossRef](#)] [[PubMed](#)]
- Gupta, S.; Barrett, T.; Whitmarsh, A.J.; Cavanagh, J.; Sluss, H.K.; Dérijard, B.; Davis, R.J. Selective interaction of JNK protein kinase isoforms with transcription factors. *EMBO J.* **1996**, *15*, 2760–2770. [[PubMed](#)]

8. Coffey, E.T. Nuclear and cytosolic JNK signalling in neurons. *Nat. Rev. Neurosci.* **2014**, *15*, 285–299. [[CrossRef](#)] [[PubMed](#)]
9. Li, Z.; Young, J.; Ulevitch, R.J.; Han, J. The primary structure of p38γ: A new member of p38 group of MAP kinases. *Biochem. Biophys. Res. Commun.* **1996**, *228*, 334–340. [[CrossRef](#)] [[PubMed](#)]
10. Jiang, Y.; Chen, C.; Li, Z.; Guo, W.; Gegner, J.A.; Lin, S.; Han, J. Characterization of the structure and function of the fourth member of p38 group mitogen-activated protein kinases, p38δ. *J. Biol. Chem.* **1997**, *272*, 30122–30128. [[CrossRef](#)] [[PubMed](#)]
11. Kumar, S.; McDonnell, P.C.; Gum, R.J.; Hand, A.T.; Lee, J.C.; Young, P.R. Novel homologues of CSBP/p38 MAP kinase: Activation, substrate specificity and sensitivity to inhibition by pyridinyl imidazoles. *Biochem. Biophys. Res. Commun.* **1997**, *235*, 533–538. [[CrossRef](#)] [[PubMed](#)]
12. Takeda, K.; Ichijo, H. Neuronal p38 MAPK signalling: An emerging regulator of cell fate and function in the nervous system. *Genes Cells* **2002**, *7*, 1099–1111. [[CrossRef](#)] [[PubMed](#)]
13. Ge, B.; Gram, H.; Di Padova, F.; Huang, B.; New, L.; Ulevitch, R.J.; Luo, Y.; Han, J. MAPKK-Independent Activation of p38α Mediated by TAB1-Dependent Autophosphorylation of p38α. *Science* **2002**, *295*, 1291–1294. [[CrossRef](#)] [[PubMed](#)]
14. Salvador, J.M.; Mittelstadt, P.R.; Guszczynski, T.; Copeland, T.D.; Yamaguchi, H.; Appella, E.; Fornace, A.J., Jr.; Ashwell, J.D. Alternative p38 activation pathway mediated by T cell receptor-proximal tyrosine kinases. *Nat. Immunol.* **2005**, *6*, 390–395. [[CrossRef](#)] [[PubMed](#)]
15. Carboni, L.; Carletti, R.; Tacconi, S.; Corti, C.; Ferraguti, F. Differential expression of SAPK isoforms in the rat brain. An in situ hybridisation study in the adult rat brain and during post-natal development. *Mol. Brain Res.* **1998**, *60*, 57–68. [[CrossRef](#)]
16. Lein, E.S.; Hawrylycz, M.J.; Ao, N.; Ayres, M.; Bensinger, A.; Bernard, A.; Boe, A.F.; Boguski, M.S.; Brockway, K.S.; Byrnes, E.J.; et al. Genome-wide atlas of gene expression in the adult mouse brain. *Nature* **2007**, *445*, 168–176. [[CrossRef](#)] [[PubMed](#)]
17. Yang, D.D.; Kuan, C.; Whitmarsh, A.J.; Rinócn, M.; Zheng, T.S.; Davis, R.J.; Rakic, P.; Flavell, R.A. Absence of excitotoxicity-induced apoptosis in the hippocampus of mice lacking the Jnk3 gene. *Nature* **1997**, *389*, 865–870. [[CrossRef](#)] [[PubMed](#)]
18. Hunot, S.; Vila, M.; Teismann, P.; Davis, R.J.; Hirsch, E.C.; Przedborski, S.; Rakic, P.; Flavell, R.A. JNK-mediated induction of cyclooxygenase 2 is required for neurodegeneration in a mouse model of Parkinson's disease. *Proc. Natl. Acad. Sci. USA* **2004**, *101*, 665–670. [[CrossRef](#)] [[PubMed](#)]
19. Brecht, S.; Kirchhoff, R.; Chromik, A.; Willesken, M.; Nicolaus, T.; Raivich, G.; Wessig, J.; Waetzig, V.; Goetz, M.; Claussen, M.; et al. Specific pathophysiological functions of JNK isoforms in the brain. *Eur. J. Neurosci.* **2005**, *21*, 363–377. [[CrossRef](#)] [[PubMed](#)]
20. Kuan, C.Y.; Yang, D.D.; Samanta Roy, D.R.; Davis, R.J.; Rakic, P.; Flavell, R.A. The Jnk1 and Jnk2 protein kinases are required for regional specific apoptosis during early brain development. *Neuron* **1999**, *22*, 667–676. [[CrossRef](#)]
21. Xu, P.; Das, M.; Reilly, J.; Davis, R.J. JNK regulates FoxO-dependent autophagy in neurons. *Genes Dev.* **2011**, *25*, 310–322. [[CrossRef](#)] [[PubMed](#)]
22. Tamura, K.; Sudo, T.; Senftleben, U.; Dadak, A.M.; Johnson, R.; Karin, M. Requirement for p38α in erythropoietin expression: A role for stress kinases in erythropoiesis. *Cell* **2000**, *102*, 221–231. [[CrossRef](#)]
23. Adams, R.H.; Porras, A.; Alonso, G.; Jones, M.; Vintersten, K.; Panelli, S.; Valladares, A.; Perez, L.; Klein, R.; Nebreda, A.R. Essential role of p38α MAP kinase in placental but not embryonic cardiovascular development. *Mol. Cell* **2000**, *6*, 109–116. [[CrossRef](#)]
24. Beardmore, V.A.; Hinton, H.J.; Eftychi, C.; Apostolaki, M.; Armaka, M.; Darragh, J.; McIlrath, J.; Carr, J.M.; Armit, L.J.; Clacher, C.; et al. Generation and characterization of p38β (MAPK11) gene-targeted mice. *Mol. Cell. Biol.* **2005**, *25*, 10454–10464. [[CrossRef](#)] [[PubMed](#)]
25. Gillespie, M.A.; Le Grand, F.; Scimè, A.; Kuang, S.; von Maltzahn, J.; Seale, V.; Cuenda, A.; Ranish, J.A.; Rudnicki, M.A. p38-γ-dependent gene silencing restricts entry into the myogenic differentiation program. *J. Cell Biol.* **2009**, *187*, 991–1005. [[CrossRef](#)] [[PubMed](#)]
26. Schindler, E.M.; Hindes, A.; Gribben, E.L.; Burns, C.J.; Yin, Y.; Lin, M.; Owen, R.J.; Longmore, G.D.; Kissling, G.E.; Arthur, J.S.C.; et al. p38δ mitogen-activated protein kinase is essential for skin tumor development in mice. *Cancer Res.* **2004**, *69*, 4648–4655. [[CrossRef](#)] [[PubMed](#)]

27. Bu, X.; Huang, P.; Qi, Z.; Zhang, N.; Han, S.; Fang, L.; Li, J. Cell type-specific activation of p38 MAPK in the brain regions of hypoxic preconditioned mice. *Neurochem. Int.* **2007**, *51*, 459–466. [[CrossRef](#)] [[PubMed](#)]
28. Maruyama, M.; Sudo, T.; Kasuya, Y.; Siga, T.; Hu, B.; Osada, H. Immunolocalization of p38 MAPK in mouse brain. *Brain Res.* **2000**, *887*, 350–358. [[CrossRef](#)]
29. Bruchas, M.R.; Macey, T.A.; Lowe, J.D.; Chavkin, C. Kappa opioid receptor activation of p38 MAPK is GRK3- and arrestin-dependent in neurons and astrocytes. *J. Biol. Chem.* **2006**, *281*, 18081–18089. [[CrossRef](#)] [[PubMed](#)]
30. Choudhury, G.R.; Ryou, M.; Poteet, E.; Wen, Y.; He, R.; Sun, F.; Yuan, F.; Jin, K.; Yang, S. Involvement of p38 MAPK in reactive astrogliosis induced by ischemic stroke. *Brain Res.* **2014**, *1551*, 45–58. [[CrossRef](#)] [[PubMed](#)]
31. Ando, K.; Uemura, K.; Kuzuya, A.; Maesako, M.; Asada-Utsugi, M.; Kubota, M.; Aoyagi, N.; Yoshioka, K.; Okawa, K.; Inoue, H.; et al. N-cadherin regulates p38 MAPK signaling via association with JNK-associated leucine zipper protein: Implications for neurodegeneration in Alzheimer disease. *J. Biol. Chem.* **2011**, *286*, 7619–7628. [[CrossRef](#)] [[PubMed](#)]
32. Guo, X.; Harada, C.; Namekata, K.; Matsuzawa, A.; Camps, M.; Ji, H.; Swinnen, D.; Jorand-Lebrun, C.; Muzerelle, M.; Vitte, P.A.; et al. Regulation of the severity of neuroinflammation and demyelination by TLR-ASK1-p38 pathway. *EMBO Mol. Med.* **2010**, *12*, 504–515. [[CrossRef](#)] [[PubMed](#)]
33. Huang, G.; Wang, Y.; Vogel, P.; Kanneganti, T.-D.; Otsu, K.; Chi, H. Signaling via the kinase p38 $\alpha$  programs dendritic cells to drive TH17 differentiation and autoimmune inflammation. *Nat. Immunol.* **2012**, *13*, 152–161. [[CrossRef](#)] [[PubMed](#)]
34. Jirmanova, L.; Torchia, M.L.G.; Sarma, N.D.; Mittelstadt, P.R.; Ashwell, J.D. Lack of the T-cell-specific alternative p38 activation pathway reduces autoimmunity and inflammation. *Blood* **2011**, *118*, 3280–3289. [[CrossRef](#)] [[PubMed](#)]
35. Noubade, R.; Krementsov, D.N.; Rio, R.; Thornton, T.; Nagaleekar, V.; Saligrama, N.; Spitzack, A.; Spach, K.; Sabio, G.; Davis, R.J.; et al. Activation of p38 MAPK in CD4 T cells controls IL-17 production and autoimmune encephalomyelitis. *Blood* **2011**, *118*, 3290–3300. [[CrossRef](#)] [[PubMed](#)]
36. Namiki, K.; Matsunaga, H.; Yoshioka, K.; Tanaka, K.; Murata, K.; Ishida, J.; Sakairi, A.; Kim, J.; Tokuhara, N.; Shibakawa, N.; et al. Mechanism for p38 $\alpha$ -mediated experimental autoimmune encephalomyelitis. *J. Biol. Chem.* **2012**, *287*, 24228–24238. [[CrossRef](#)] [[PubMed](#)]
37. Munoz, L.; Ammit, A.J. Targeting p38 MAPK pathway for the treatment of Alzheimer’s disease. *Neuropharmacology* **2010**, *58*, 561–568. [[CrossRef](#)] [[PubMed](#)]
38. Munoz, L.; Ranaivo, H.R.; Roy, S.M.; Hu, W.; Craft, J.M.; McNamara, L.K.; Chico, L.W.; Van Eldik, L.J.; Watterson, D.M. A novel p38 $\alpha$  MAPK inhibitor suppresses brain proinflammatory cytokine up-regulation and attenuates synaptic dysfunction and behavioral deficits in an Alzheimer’s disease mouse model. *J. Neuroinflamm.* **2007**, *4*, 21. [[CrossRef](#)] [[PubMed](#)]
39. Nakahara, S.; Yone, K.; Sakou, T.; Wada, S.; Nagamine, T.; Niizyama, T.; Ichijo, H. Induction of apoptosis signal regulating kinase 1 (ASK1) after spinal cord injury in rats: Possible involvement of ASK1-JNK and -p38 pathways in neuronal apoptosis. *J. Neuropathol. Exp. Neurol.* **1999**, *58*, 442–450. [[CrossRef](#)] [[PubMed](#)]
40. Takenouchi, T.; Setoguchi, T.; Yone, K.; Komiy, S. Expression of apoptosis signal-regulating kinase 1 in mouse spinal cord under chronic mechanical compression: Possible involvement of the stress-activated mitogen-activated protein kinase pathways in spinal cord cell apoptosis. *Spine* **2008**, *33*, 1943–1950. [[CrossRef](#)] [[PubMed](#)]
41. Li, Q.M.; Tep, C.; Yune, T.Y.; Zhou, X.Z.; Uchida, T.; Lu, K.P.; Yoon, S.O. Opposite regulation of oligodendrocyte apoptosis by JNK3 and Pin1 after spinal cord injury. *J. Neurosci.* **2007**, *27*, 8395–8404. [[CrossRef](#)] [[PubMed](#)]
42. Cavalli, V.; Kujala, P.; Klumperman, J.; Goldstein, L.S.B. Sunday Driver links axonal transport to damage signaling. *J. Cell Biol.* **2005**, *168*, 775–787. [[CrossRef](#)] [[PubMed](#)]
43. Shin, J.E.; Miller, B.R.; Babetto, E.; Cho, Y.; Sasaki, Y.; Qayum, S.; Russler, E.V.; Cavalli, V.; Milbrandt, J.; DiAntonio, A. SCG10 is a JNK target in the axonal degeneration pathway. *Proc. Natl. Acad. Sci. USA* **2012**, *109*, E3696–E3705. [[CrossRef](#)] [[PubMed](#)]
44. Yoshimura, K.; Ueno, M.; Lee, S.; Nakamura, Y.; Sato, A.; Yoshimura, K.; Kishima, H.; Yoshimine, T.; Yamashita, T. C-Jun N-terminal kinase induces axonal degeneration and limits motor recovery after spinal cord injury in mice. *Neurosci. Res.* **2011**, *71*, 266–277. [[CrossRef](#)] [[PubMed](#)]

45. Repici, M.; Chen, X.; Morel, M.-P.; Doulazmi, M.; Sclip, A.; Cannaya, V.; Veglianese, P.; Kraftsik, R.; Mariani, J.; Borsello, T.; et al. Specific inhibition of the JNK pathway promotes locomotor recovery and neuroprotection after mouse spinal cord injury. *Neurobiol. Dis.* **2012**, *46*, 710–721. [CrossRef] [PubMed]
46. Barnat, M.; Enslen, H.; Propst, F.; Davis, R.J.; Soares, S.; Nothias, F. Distinct roles of c-Jun N-terminal kinase isoforms in neurite initiation and elongation during axonal regeneration. *J. Neurosci.* **2010**, *30*, 7804–7816. [CrossRef] [PubMed]
47. Lee, J.Y.; Choi, D.C.; Oh, T.H.; Yune, T.Y. Analgesic effect of acupuncture is mediated via inhibition of JNK activation in astrocytes after spinal cord injury. *PLoS ONE* **2013**, *8*, e73948. [CrossRef] [PubMed]
48. Martini, A.C.; Forner, S.; Koeppl, J.; Rae, G.A. Inhibition of spinal c-Jun-NH<sub>2</sub>-terminal kinase (JNK) improves locomotor activity of spinal cord injured rats. *Neurosci. Lett.* **2016**, *621*, 54–61. [CrossRef] [PubMed]
49. Beattie, M.S. Inflammation and apoptosis: Linked therapeutic targets in spinal cord injury. *Trends Mol. Med.* **2004**, *10*, 580–583. [CrossRef] [PubMed]
50. Okada, S. The pathophysiological role of acute inflammation after spinal cord injury. *Inflamm. Regen.* **2016**, *36*, 20. [CrossRef] [PubMed]
51. Lee, J.C.; Laydon, J.T.; McDonnell, P.C.; Gallagher, T.F.; Kumar, S.; Green, D.; McNulty, D.; Blumenthal, M.J.; Heys, J.R.; Landvatter, S.W.; et al. A protein kinase involved in the regulation of inflammatory cytokine biosynthesis. *Nature* **1994**, *372*, 739–746. [CrossRef] [PubMed]
52. Han, J.; Lee, J.D.; Bibbs, L.; Ulevitch, R.J. A MAP kinase targeted by endotoxin and hyperosmolarity in mammalian cells. *Science* **1994**, *265*, 808–811. [CrossRef] [PubMed]
53. Dean, J.L.E.; Sully, G.; Clark, A.R.; Saklatvala, J. The involvement of AU-rich element-binding proteins in p38 mitogen-activated protein kinase pathway-mediated mRNA stabilization. *Cell. Signal.* **2004**, *16*, 1113–1121. [CrossRef] [PubMed]
54. Zhao, W.; Liu, M.; Kirkwood, K.L. p38 $\alpha$  stabilizes interleukin-6 mRNA via multiple AU-rich elements. *J. Biol. Chem.* **2008**, *283*, 1778–1785. [CrossRef] [PubMed]
55. Kang, Y.J.; Chen, J.; Otsuka, M.; Mols, J.; Ren, S.; Wang, Y.; Han, J. Macrophage deletion of p38 $\alpha$  partially impairs lipopolysaccharide-induced cellular activation. *J. Immunol.* **2008**, *180*, 5075–5082. [CrossRef] [PubMed]
56. Krementsov, D.N.; Thornton, T.M.; Teuscher, C.; Rinocn, M. The emerging role of p38 mitogen-activated protein kinase in multiple sclerosis and its models. *Mol. Cell. Biol.* **2013**, *33*, 3728–3734. [CrossRef] [PubMed]
57. Nagaleekar, V.K.; Sabio, G.; Aktan, I.; Chant, A.; Howe, I.W.; Thornton, T.M.; Benoit, P.J.; Davis, R.J.; Rincon, M.; Boyson, J.E. Translational control of NKT cell cytokine production by p38 MAPK. *J. Immunol.* **2011**, *186*, 4140–4146. [CrossRef] [PubMed]
58. Börgele, Y.; Schmolke, M.; Viemann, D.; Nordhoff, C.; Roth, J.; Ludwig, S. Inhibition of p38 mitogen-activated protein kinase impairs influenza virus-induced primary and secondary host gene responses and protects mice from lethal H5N1 infection. *J. Biol. Chem.* **2014**, *289*, 13–27. [CrossRef] [PubMed]
59. Xu, Z.; Wang, B.R.; Wang, X.; Kuang, F.; Duan, X.L.; Jiao, X.Y.; Ju, G. ERK1/2 and p38 mitogen-activated protein kinase mediate iNOS-induced spinal neuron degeneration after acute traumatic spinal cord injury. *Life Sci.* **2006**, *79*, 1895–1905. [CrossRef] [PubMed]
60. Stirling, D.P.; Liu, J.; Plunet, W.; Steeves, J.D.; Tetzlaff, W. SB203580, a p38 mitogen-activated protein kinase inhibitor, fails to improve functional outcome following a moderate spinal cord injury in rat. *Neuroscience* **2008**, *155*, 128–137. [CrossRef] [PubMed]
61. Wang, X.J.; Kong, K.M.; Qi, W.L.; Ye, W.L.; Song, P.S. Interleukin-1 beta induction of neuron apoptosis depends on p38 mitogen-activated protein kinase activity after spinal cord injury. *Acta Pharmacol. Sin.* **2005**, *26*, 934–942. [CrossRef] [PubMed]
62. Horiuchi, H.; Ogata, T.; Morino, T.; Chuai, M.; Yamamoto, H. Continuous intrathecal infusion of SB203580, a selective inhibitor of p38 mitogen-activated protein kinase, reduces the damage of hind-limb function after thoracic spinal cord injury in rat. *Neurosci. Res.* **2003**, *47*, 209–217. [CrossRef]
63. Umezawa, H.; Naito, Y.; Tanaka, K.; Yoshioka, K.; Suzuki, K.; Sudo, T.; Hagihara, M.; Hatano, M.; Tatsumi, K.; Kasuya, Y. Genetic and pharmacological inhibition of p38 $\alpha$  improves locomotor recovery after spinal cord injury. *Front. Pharmacol.* **2017**, *8*, 72. [CrossRef] [PubMed]
64. Tikka, T.M.; Koistinaho, J.E. Minocycline provides neuroprotection against N-methyl-D-aspartate neurotoxicity by inhibiting microglia. *J. Immunol.* **2001**, *166*, 7527–7533. [CrossRef] [PubMed]

65. Lin, S.; Zhang, Y.; Dodel, R.; Farlow, M.R.; Paul, S.M.; Du, Y. Minocycline blocks nitric oxide-induced neurotoxicity by inhibition p38 MAP kinase in rat cerebellar granule neurons. *Neurosci. Lett.* **2011**, *315*, 61–64. [[CrossRef](#)]
66. Hua, X.; Svensson, C.I.; Matsui, T.; Fitzsimmons, B.; Yaksh, T.L.; Webb, M. Intrathecal minocycline attenuates peripheral inflammation-induced hyperalgesia by inhibiting p38 MAPK in spinal microglia. *Eur. J. Neurosci.* **2005**, *22*, 2431–2440. [[CrossRef](#)] [[PubMed](#)]
67. Yune, T.Y.; Lee, J.Y.; Jung, G.Y.; Kim, S.J.; Jiang, M.H.; Kim, Y.C.; Oh, Y.J.; Markelonis, G.J.; Oh, T.H. Minocycline alleviates death of oligodendrocytes by inhibiting pro-nerve growth factor production in microglia after spinal cord injury. *J. Neurosci.* **2007**, *27*, 7751–7761. [[CrossRef](#)] [[PubMed](#)]
68. Beattie, M.S.; Harrington, A.W.; Lee, R.; Kim, J.Y.; Boyce, S.L.; Longo, F.M.; Bresnahan, J.C.; Hempstead, B.L.; Yoon, S.O. ProNGF induces p75-mediated death of oligodendrocytes following spinal cord injury. *Neuron* **2002**, *36*, 375–386. [[CrossRef](#)]
69. Stirling, D.P.; Koochesfahani, K.M.; Steeves, J.D.; Tetzlaff, W. Minocycline as a neuroprotective agent. *Neuroscientist* **2005**, *11*, 308–322. [[CrossRef](#)] [[PubMed](#)]
70. Xing, B.; Bachstetter, A.D.; Van Eldik, L.J. Deficiency in p38 $\beta$  MAPK fails to inhibit cytokine production or protect neurons against inflammatory insult in *in vitro* and *in vivo* mouse models. *PLoS ONE* **2015**, *8*, e56852. [[CrossRef](#)] [[PubMed](#)]
71. Lawson, S.K.; Dobrikova, E.Y.; Shveygert, M.; Gromeier, M. p38 $\alpha$  mitogen-activated protein kinase depletion and repression of signal transduction to translation machinery by miR-124 and -128 in neurons. *Mol. Cell. Biol.* **2013**, *33*, 127–135. [[CrossRef](#)] [[PubMed](#)]
72. Casha, S.; Zygun, D.; McGowan, M.D.; Bains, I.; Yong, V.W.; Hurlbert, R.J. Results of a phase II placebo-controlled randomized trial of minocycline in acute spinal cord injury. *Brain* **2012**, *135*, 1224–1236. [[CrossRef](#)] [[PubMed](#)]
73. Urdzikova, L.M.; Karova, K.; Ruzicka, J.; Kloudova, A.; Shannon, C.; Dubisova, J.; Murali, R.; Kubanova, S.; Sykova, E.; Jhanwar-Uniyal, M.; et al. The anti-inflammatory compound curcumin enhances locomotor and sensory recovery after spinal cord injury in rats by immunomodulation. *Int. J. Mol. Sci.* **2016**, *17*, 49. [[CrossRef](#)] [[PubMed](#)]
74. Shih, R.; Wang, C.; Yang, C. NF- $\kappa$ B signaling pathways in neurological inflammation. *Front. Mol. Neurosci.* **2015**, *8*, 77. [[CrossRef](#)] [[PubMed](#)]
75. Brambilla, R.; Bracchi-Ricard, V.; Hu, W.; Frydel, B.; Bramwell, A.; Karmally, S.; Green, E.J.; Bethea, J.R. Inhibition of astroglial nuclear factor  $\kappa$ B reduces inflammation and improves functional recovery after spinal cord injury. *J. Exp. Med.* **2005**, *202*, 145–156. [[CrossRef](#)]
76. Zhang, N.; Wei, G.; Ye, J.; Yang, L.; Hong, Y.; Liu, G.; Zhong, H.; Cai, X. Effect of curcumin on acute spinal cord injury in mice via inhibition of inflammation and TAK1 pathway. *Pharmacol. Rep.* **2017**, *69*, 1001–1006. [[CrossRef](#)] [[PubMed](#)]
77. Wang, J.; Su, B.; Zhu, H.; Chen, C.; Zhao, G. Protective effect of geraniol inhibits inflammatory response, oxidative stress and apoptosis in traumatic injury of the spinal cord through modulation of NF- $\kappa$ B and p38 MAPK. *Exp. Ther. Med.* **2016**, *12*, 3607–3613. [[CrossRef](#)] [[PubMed](#)]
78. Luo, Y.; Fu, C.; Wang, Z.; Zhang, Z.; Wang, H.; Liu, Y. Asiaticoside attenuates the effects of spinal cord injury through antioxidant and anti-inflammatory effects, and inhibition of the p38-MAPK mechanism. *Mol. Med. Rep.* **2015**, *12*, 8294–8300. [[CrossRef](#)] [[PubMed](#)]
79. Takanami-Ohnishi, Y.; Amano, S.; Kimura, S.; Asada, S.; Utani, A.; Maruyama, M.; Osada, H.; Tsunoda, H.; Irukayama-Tomobe, Y.; Goto, K.; et al. Essential role of p38 mitogen-activated protein kinase in contact hypersensitivity. *J. Biol. Chem.* **2002**, *277*, 37896–37903. [[CrossRef](#)] [[PubMed](#)]
80. Matsuo, Y.; Amano, S.; Furuya, M.; Namiki, K.; Sakurai, K.; Nishiyama, M.; Sudo, T.; Tatsumi, K.; Kuriyama, T.; Kimura, S.; et al. Involvement of p38 $\alpha$  mitogen-activated protein kinase in lung metastasis of tumor cells. *J. Biol. Chem.* **2006**, *281*, 36767–36775. [[CrossRef](#)] [[PubMed](#)]
81. Namiki, K.; Nakamura, A.; Furuya, M.; Mizuhashi, S.; Matsuo, Y.; Tokuhara, N.; Sudo, T.; Hama, H.; Kuwaki, T.; Yano, S.; et al. Involvement of p38 $\alpha$  in kainate-induced seizure and neuronal cell damage. *J. Recept. Signal Transduct.* **2007**, *27*, 99–111. [[CrossRef](#)] [[PubMed](#)]
82. Yoshioka, K.; Namiki, K.; Sudo, T.; Kasuya, Y. p38 $\alpha$  controls self-renewal and fate decision of neurosphere-forming cells in adult hippocampus. *FEBS Open Bio* **2015**, *5*, 437–444. [[CrossRef](#)] [[PubMed](#)]

83. Bachstetter, A.D.; Van Eldik, L.J. The p38 MAP kinase family as regulators of proinflammatory cytokine production in degenerative diseases of the CNS. *Aging Dis.* **2010**, *1*, 199–211. [[PubMed](#)]
84. Godl, K.; Wissing, J.; Kurtenbach, A.; Habenberger, P.; Blencke, S.; Gutbrod, H.; Salassidis, K.; Stein-Gerlach, M.; Missio, A.; Cotton, M. An efficient proteomics method to identify the cellular targets of protein kinase inhibitors. *Proc. Natl. Acad. Sci. USA* **2003**, *100*, 15434–15439. [[CrossRef](#)] [[PubMed](#)]
85. Jin, S.X.; Zhuang, Z.Y.; Woolf, C.J.; Ji, R.R. p38 mitogen-activated protein kinase is activated after a spinal nerve ligation in spinal cord microglia and dorsal root ganglion neurons and contributes to the generation of neuropathic pain. *J. Neurosci.* **2003**, *23*, 4017–4022. [[PubMed](#)]
86. Ji, R.R.; Suter, M.R. p38 MAPK, microglial signaling, and neuropathic pain. *Mol. Pain* **2007**, *3*, 33. [[CrossRef](#)] [[PubMed](#)]
87. Finnerup, N.B.; Johannessen, I.L.; Sindrup, S.H.; Bach, F.W.; Jensen, T.S. Pain and dysesthesia in patients with spinal cord injury: A postal survey. *Spinal Cord* **2001**, *39*, 256–262. [[CrossRef](#)] [[PubMed](#)]



© 2018 by the authors. Licensee MDPI, Basel, Switzerland. This article is an open access article distributed under the terms and conditions of the Creative Commons Attribution (CC BY) license (<http://creativecommons.org/licenses/by/4.0/>).



Review

# Stem Cells Therapy for Spinal Cord Injury

Marina Gazdic <sup>1</sup>, Vladislav Volarevic <sup>2</sup>, C. Randall Harrell <sup>3</sup>, Crissy Fellabaum <sup>3</sup>,  
Nemanja Jovicic <sup>4</sup>, Nebojsa Arsenijevic <sup>2</sup> and Miodrag Stojkovic <sup>1,5,\*</sup>

- <sup>1</sup> Faculty of Medical Sciences, Department of Genetics, University of Kragujevac, 34000 Kragujevac, Serbia; marinagazdic8@gmail.com  
<sup>2</sup> Faculty of Medical Sciences, Department of Microbiology and immunology, Center for Molecular Medicine and Stem Cell Research, University of Kragujevac, 34000 Kragujevac, Serbia; drvolarevic@yahoo.com (V.V.); arne@medf.kg.ac.rs (N.A.)  
<sup>3</sup> Regenerative Processing Plant, LLC, 34176 US Highway 19 N Palm Harbor, Palm Harbor, FL 34684, USA; dr.harrell@regenerativeplant.org (C.R.H.); crissy@regenerativeplant.org (C.F.)  
<sup>4</sup> Faculty of Medical Sciences, Department of Histology and embryology, University of Kragujevac, 34000 Kragujevac, Serbia; nemanjajovicic.kg@gmail.com  
<sup>5</sup> Spebo Medical, 16 Norvezanska, 16000 Leskovac, Serbia  
\* Correspondence: mstojkovic@spebo.com; Tel.: +38-134-306-800

Received: 10 February 2018; Accepted: 5 March 2018; Published: 30 March 2018

**Abstract:** Spinal cord injury (SCI), a serious public health issue, most likely occurs in previously healthy young adults. Current therapeutic strategies for SCI includes surgical decompression and pharmacotherapy, however, there is still no gold standard for the treatment of this devastating condition. Inefficiency and adverse effects of standard therapy indicate that novel therapeutic strategies are required. Because of their neuroregenerative and neuroprotective properties, stem cells are a promising tool for the treatment of SCI. Herein, we summarize and discuss the promising therapeutic potential of human embryonic stem cells (hESC), induced pluripotent stem cells (iPSC) and ependymal stem/progenitor cells (epSPC) for SCI.

**Keywords:** spinal cord injury; stem cells; embryonic stem cells; induced pluripotent stem cells; ependymal stem/progenitor cells

## 1. Introduction

Spinal cord injury (SCI), a serious public health issue, most likely occurs in previously healthy young adults. Country-level incidence studies show that incidence of SCI ranges from 40 to 80 per million people per year [1]. The aim of modern society is to prevent traumatic SCI usually caused by road traffic accidents, falls from heights, and violence (gunshot or stab wound), as well as nontraumatic SCI resulting from cancer, spinal disk degeneration, or arthritis. Gray and white matter damage after SCI leads to partial or complete motor, sensory, or autonomic deficit in parts of the body distal to the lesion site. In accordance, the most devastating of all SCIs are injuries of the cervical spine, accompanied by high-grade dysfunction of the central nervous system (CNS). In order to determine the severity of SCI, the American Spinal Injury Association (ASIA) defined international standards for neurological classification and formulated impairment scale for neurological assessment of individuals with SCI [2]. The most severe SCI is complete, irreversible and characterized by increased mortality risk compared to the general population due to cardiovascular, respiratory and genitourinary complications, deep venous thrombosis, chronic neuropathic pain, pressure ulcers, and infections [3].

Although a detailed understanding of molecular mechanisms involved in the pathophysiology of SCI provides great promise for improving therapeutic strategies for spinal cord repair, there is still no gold standard for the treatment of this devastating condition. Because of their differentiation abilities and secretion of a variety of cytokines and growth factors, stem cells have been extensively studied

as a novel neuroregenerative and neuroprotective agents for the treatment of SCI. A large number of murine models of acute, subacute and chronic SCI, that resemble lesions that develop in the adult human spinal cord following exposure to trauma, have demonstrated not only therapeutic role of in vitro-expanded stem cell-derived progenitor, but also the cellular and molecular mechanism of spinal cord repair and neurological improvements through activation of endogenous stem cells.

In this review, we summarize the advantages and disadvantages of current surgical and pharmacological approaches and discuss promising therapeutic potential of human embryonic stem cells (hESC), induced pluripotent stem cells (iPSC) and ependymal stem/progenitor cells (epSPC) for SCI. We hope that the data highlighted in this report may be of relevance to stem cell researchers and clinicians as a backdrop to future development of stem cell-based therapy of SCI.

## 2. Pathophysiology

Neurological outcome after SCI is associated with mechanical destruction of spinal tissue and secondary injury mediated by multiple pathophysiological processes (reviewed in [4]). Displacement of the anatomical structures of the spinal cord, following the initial mechanical events underlies the onset of SCI and refers to the primary injury phase. Physical forces such as compression, contusion, laceration, and acute stretch, damage nerve cells and their axons, leading to the disruption of descending neuronal pathways [5]. During the secondary phase of SCI, the series of destructive pathological processes occur, leading to massive cellular dysfunction and death, aberrant molecular signaling and generation of harmful metabolic products. Immediately after sudden mechanical trauma, focal microhemorrhage, vasospasm and reduction in blood flow, are seen within the injured cord. Disturbance in ion homeostasis, glutamaterelease, and lipid peroxidation in the lesion site contribute to further progression of neurological dysfunction in patients with SCI by activating consequential cascade of destructive pathophysiological mechanisms [6–8]. Electrolytic imbalance in SCI is characterized by elevated extracellular concentration of potassium ( $K^+$ ) and increased intracellular concentration of sodium ( $Na^+$ ) and calcium ( $Ca^{2+}$ ) [9]. As a result of the high amount of potassium in the extracellular area, the transmission of a nerve impulse is blocked. Intracellular acidosis promotes excessive water influx into the neurons, resulting in cytotoxic edema and neuronal death (reviewed in [10,11]). Damaged cells massively release various toxic metabolites as well as excitatory amino acid glutamate, which trigger autodestructive free-radical generation and excitotoxicity [9,12]. Reactive oxygen species cause oxidative damage of DNA, and lipid peroxidation in the cellular membranes. These pathological changes observed in the lesion site lead to further progression of neurons and glia cells necrosis and apoptosis [13]. It is well known that immune response significantly contributes to pathogenesis of SCI. Interestingly, the inflammatory process has both aggressive and protective effects on damaged spinal cord. Mechanical trauma breaks the integrity and increases permeability of the blood-spinal cord barrier, thus contributing to inflammatory cell invasion, and edema generation at the lesion site. Neutrophils, macrophages, T cells and microglia infiltrate the spinal parenchyma, and produce wide range of proinflammatory cytokines tumor necrosis factor alpha (TNF- $\alpha$ ), interleukin-1 beta (IL-1 $\beta$ ), interleukin-1 alpha (IL-1 $\alpha$ ), and interleukin-6 (IL-6) [14–17]. Expression of ion channels included in the family of connexins (Cx) is augmented at early stages after traumatic SCI and contributes to secondary damage of spinal cord and neuropathic pain [18]. Neuroinflammation causes the development of a necrotic cavity surrounded by a glial scar that prevents SCI progression [19]. At the same time, activated macrophages and microglia are involved in phagocytosis of necrotic and destroyed tissue. This rapid removal of cellular debris is significant for establishing an environment beneficial for neuroregeneration [20,21].

### 3. Current Therapeutic Strategies for Spinal Cord Injury

#### 3.1. Surgical Decompression

Surgical Timing in Acute Spinal Cord Injury Study (STASCIS) showed that urgent surgical decompression within 24 h after injury significantly increased post-operative motor and sensory functions according to American Spinal Injury Association (ASIA) score [22,23]. Although early decompression reduces the risk of respiratory failure and sepsis [24], neurological surgery for the treatment of SCI is still associated with complications such as incidental durotomy or meningitis [25]. These limitations indicate that STASCIS and urgent neurological surgery in SCI as a widely adopted treatment requires further improvement.

#### 3.2. Therapeutic Hypothermia

Beneficial effects of modest (32–34 °C) systemic hypothermia induced by intravascular cooling catheter have been clearly demonstrated in SCI [26,27]. Problems related to the safety of invasive systemic treatment and relation between temperature at the spinal cord lesion and core body temperature have been successfully resolved by localized cooling of the injury site during surgical decompression [28]. Systemic hypothermia as well as local cooling attenuate main pathophysiological processes during SCI including neuronal metabolism, neuroinflammation, oxidative stress, excitotoxicity, and apoptosis [29,30]. At the same time, decreased temperature protects the spinal cord from further injury by preserving the blood-spinal cord barrier (BSCB) and reducing edema, and induces neurorepair by enhancing angiogenesis and neurogenesis [29]. However, the effects of timing and duration of hypothermia as well as the best rewarming method on endogenous mechanisms and mobilization of stem cells are still the main challenges in the use of therapeutic hypothermia for the treatment of SCI [31].

#### 3.3. Pharmacotherapy

Because of their anti-inflammatory effects and capacity to reduce oxidative stress and excitotoxicity, corticosteroids are used in many preclinical and clinical studies as therapeutic agents for the treatment of SCI [32]. Although it was expected that methylprednisolone would have the ability to suppress immune-mediated damage after SCI by decreasing the inflammatory cytokine production, several clinical studies failed to demonstrate functional repair after methylprednisolone administration [33–37]. Use of methylprednisolone in patients with SCI has become controversial, because of high rate of complications such as sepsis, pulmonary embolism, and gastrointestinal hemorrhage [33–37]. In order to improve pharmacological treatment of secondary injury phase, neuroprotective and regenerative effects of various agents were evaluated in clinical trials during the last decade. Several prospective, multicenter human studies demonstrated neurologic improvement in patients with spinal cord trauma who received riluzole [38], GM1 ganglioside [39], BA-210 [40], minocycline [41] or granulocyte-colony stimulating factor (G-CSF) [42], suggesting the potential of these agents for application in routine clinical practice.

## 4. Stem Cells—New Hope for Spinal Cord Injury

#### 4.1. Human Embryonic Stem Cells

Human embryonic stem cells (hESC) are derived from the inner cell mass of the preimplantation blastocysts, by removing the trophectoderm cells by immunosurgery [43]. hESC are positive for pluripotent stem cell surface antigens such as stage specific embryonic antigens 3 and 4 (SSEA-3 and SSEA-4), TRA-1-60, TRA-1-81, and express well-known pluripotency-associated genes octamer-binding transcription factor 3/4 (OCT3/4), sex determining region Y box-containing gene 2 (*SOX2*), and *NANOG* [44,45]. Elevated alkaline phosphatase and telomerase activity are associated with their unlimited proliferative potential [44,45]. These markers are used to verify the successful

isolation of a new hESC line and confirm the maintenance of an undifferentiated pluripotent state for established hESC.

In addition to remarkable proliferative capacity, hESC exhibit pluripotency both in vitro and in vivo. Because of their ability for differentiation into cells of ectodermal origin such as neuronal and glial cells, hESC are used in many preclinical studies (reviewed in [46]) as a new therapeutic option for SCI (Figure 1A). Several previously published papers have shown that transplantation of hESC-derived oligodendrocyte progenitor cells (OPC) to SCI models resulted in cell survival and clinically relevant recovery of neurological functions with no evidence of harmful effects [47–49].

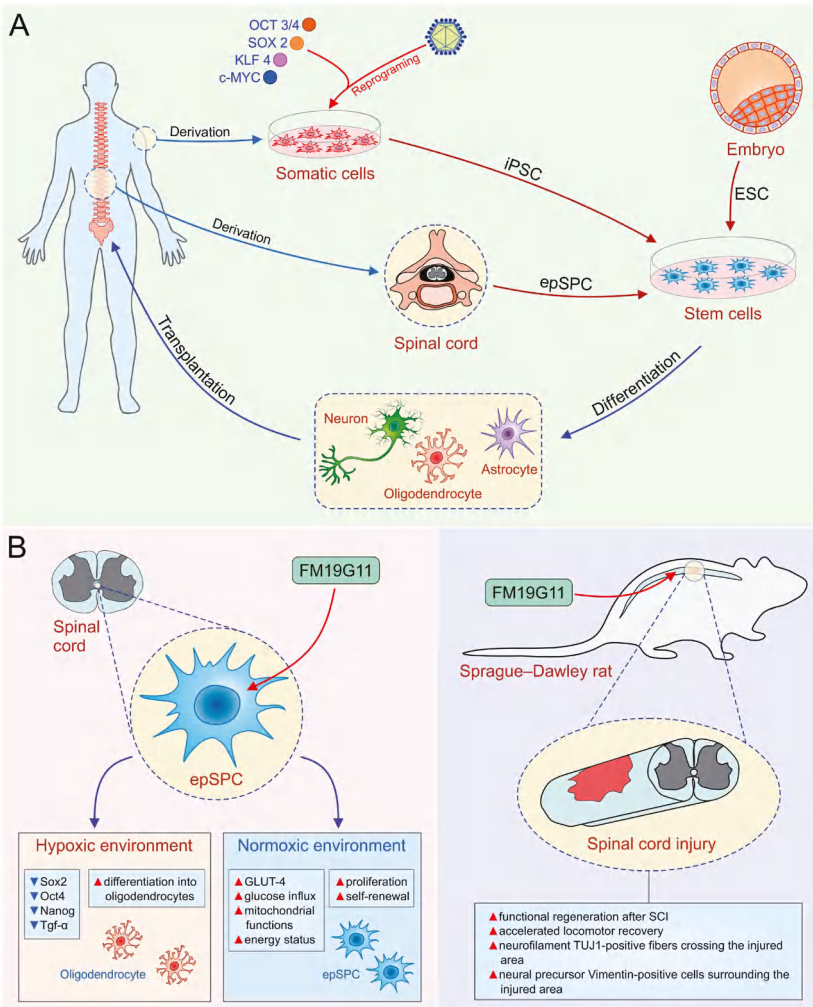


**Figure 1.** (A) Human embryonic stem cells (hESC), induced pluripotent stem cells (iPSC) and ependymal stem/progenitor cells (epSPC) as a promising tool in the therapy of SCI; (B) the role of FM19G11, an inhibitor of hypoxia inducible factor (HIF $\alpha$ ), to mobilize epSPC. OCT3/4, octamer-binding transcription factor 3/4; SOX2, sex determining region Y box-containing gene 2; KLF4, Krüppel-like factor 4; TGF- $\alpha$ , transforming growth factor-alpha; GLUT-4, glucose transporter type 4.

Keirstead and coworkers demonstrated that hESC-derived OPC transplanted seven days after SCI in rats differentiate into mature oligodendrocytes, induce myelin sheath regeneration and significantly improve locomotor function [48]. In contrast, OPC administration ten months after injury, did not manage to improve neurological outcome in injured animals compared with controls, suggesting that first week after SCI is the optimal time point for OPC transplantation [48]. Neural stem cells (NSC) clonally derived from murine embryonic stem cells (dNSCs), without embryoid bodies formation, survive and differentiate into neurons, oligodendrocytes, and astrocytes after injection into the spinal cord lesion one week after SCI in mice. Salewski et al. provided the evidence that transplanted dNSCs have broad spectrum of beneficial neuroregenerative effects associated with enhanced remyelination of damage axons [50]. In addition to differentiation into myelin-forming oligodendrocytes, hESC-derived OPC express neurotrophic factors such as neurite growth-promoting factor 2 (NEGF2), hepatocyte growth factor (HGF), activin A, transforming growth factor-beta 2 (TGF- $\beta$ 2), and brain-derived neurotrophic factor (BDNF), providing significant therapeutic effects in SCI such as neuronal survival and neurite extension [51,52].

In order to increase the yield of defined hESC-derived neural lineages, we optimized in vitro conditions for the differentiation of hESC towards motoneuron progenitors (MP) and OPC using chemically defined mediums without animal components and without feeder cells. This protocol induces conversion of hESC into rosettes and neural tube-like structures with capacity to differentiate into region specific and functional neurons, astrocytes, and oligodendrocytes [53]. For the first time, we achieved controlled differentiation of neural progenitors towards specific type of neuronal cells by stimulating the rosettes with specific signaling factors in vitro [53]. Promising results obtained under in vitro conditions suggest that neuroregenerative potential of hESC-derived OPC and MP should be investigated using an animal model of SCI. Therefore, we used a well-established rat model of complete spinal cord transection, that resemble the pathology of the most severe clinical cases of SCI in humans [54]. Our study showed that transplanted cells OPC and MP survived for at least 4 months, and migrated at least 3 mm away from the site of injury [55]. Main mechanisms of behavioral and electrophysiological improvement after OPC and MP transplantation in SCI were their differentiation into mature oligodendrocytes and neurons and their capacity to produce various neurotrophic factors [55]. Additionally, transplanted OPC and MP triggered Janus kinase/signal transducers and activators of transcription (JAK/STAT) and Notch signaling in the lesion site leading to enhanced astrogliosis [56] indicating that reactive astrocytes in synergy with transplanted cells promote survival and growth of serotonergic and dopaminergic axons [56].

Although the results of preclinical study are promising, there are important issues such as the possibility of immune rejection and the risk of tumor formation after transplantation that should be addressed to achieve successful hESC-based therapy [57].

#### 4.2. Induced Pluripotent Stem Cells

Induced pluripotent stem cells (iPSC) were originally obtained by the viral transduction of four transcription factors: SOX2, OCT3/4, tumor suppressor Krüppel-like factor 4 [*KLF4*], and proto-oncogene *c-MYC* in differentiated somatic cells [58]. The standard viral integrative reprogramming techniques are associated with many risks including insertional mutagenesis, uncontrolled expression of integrated transgenes—downregulation or silencing of the transgenes or tumor formation due to residual reactivation of transgenes, senescence-associated DNA changes, and immunogenicity of iPSC-derived cells [59]. Huge efforts have been devoted toward the development of novel protocols in order to improve quality and efficiency of reprogramming technology and to bring iPSC-derived cells closer to clinic. During the last decade, several studies suggested alternative non-integrative delivery methods for more safety iPSC generation such as use of adenovirus and Sendai virus as well as non-viral-mediated molecular strategies (*Cre-loxP*-mediated recombination, *PiggyBac*-transposition episomal DNA vectors, and direct miRNA transfection) [60–64]. All these technologies provide an opportunity to derive pluripotent cells similar to hESC in terms of morphology, karyotype, and phenotype without destruction

of human embryos. The use of patient-specific iPSC for treatment of SCI is particularly attractive, given that they avoid the ethical considerations and immunological rejection of hESC and represent a source of autologous cells that can be differentiated to neural progenitor cells (NPC), neurons, oligodendrocytes, and astrocytes at the same time underlining the integration of transplanted cells into the site of injury as an important issue of successful cell-based therapy (Figure 1A). Several research groups reported that iPSC are capable of generating mature dopaminergic neurons [65,66], motor neurons (MN) [67–69], and GABAergic interneurons [70], however, it is known that transplantation of mature neurons is characterized by poor cellular engraftment versus transplantation of neural progenitors. Consequently, transplantation of neural progenitors has been a focus, and seems to be a promising approach for the treatment of SCI. Several groups reported that autologous iPSC derived neural precursor cells (iPSC-NPC) could be efficiently derived [71,72] and used for transplantation into rodents with SCI [73,74]. Transplanted NPC predominantly gave rise to myelin-producing oligodendrocytes, leading to remyelination and improvement of nerve conduction [73]. Moreover, iPSC-NPC migrated long distances, integrated into the spinal cord and differentiated into mature neurons and glia, resulting in synaptic reconstruction and locomotor recovery [75–77]. In addition, neurotrophic factors produced by iPSC-NPC, modulate immunopathological events following SCI [78]. Hayashi and colleagues found that iPSC-derived astrocytes injected into the injured rodent spinal cord increased the sensitivity to mechanical stimulus but did not affect locomotor functions [79].

Although patient-specific iPSC are a revolutionary tool which could pave the way to personalized medicine, many issues remain to be improved including reprogramming techniques as well as protocols for targeted differentiation.

#### 4.3. Ependymal Stem/Progenitor Cells

It has been demonstrated that OPC, astrocytes, and ependymal cells are the most important dividing cells in the adult spinal cord [80–82]. Astrocytes and OPC have the capacity to self-renew, however they cannot give rise to different types of specialized cells, indicating that they are not NSC [83]. Ependymal stem/progenitor cells (epSPC) are adult multipotent stem cells characterized by the ability to differentiate into the both glial cells and neurons [18,56] and can be found around the spinal central canal [4] (Figure 1A, Table 1).

**Table 1.** The capacity of engraftment and differentiation, contribution to functional recovery and risk of tumorigenesis of transplanted hESC, iPSC and epSPC in animal model of spinal cord injury Stem cell source.

Stem Cell Source	Differentiation	Engraftment	Contribution to Functional Recovery	Tumorigenesis
hESC	differentiation into neurons and glia [53,64]	hESC-derived OPCs and MP's engraft for at least 4 months in the lesion site [55]	significant improvement of behavioral and electrophysiological, function of injured animals at early time points after SCI [55,56]	risk of teratoma formation [46,57]
iPSC	differentiation into neural progenitor cells, neurons, oligodendrocytes, and astrocytes [72–77]	integration for at least 12 weeks after transplantation into injured spinal cord tissue [74]	iPSC-derived cells promote functional recovery in an early SCI model [72–77]	more tumorigenic than hESC due to genetic and epigenetic aberrations [46]
epSPC	differentiation into glial cells (oligodendrocytes and astrocytes) and neurons [18,34]	detected 2 months after transplantation [56]	accelerates recovery of motor activity 1 week after injury [56]	low rates of tumorigenesis [4]

hESC, human embryonic stem cells; OPC, oligodendrocyte progenitor cells; MP, motoneuron progenitors; iPSC, induced pluripotent stem cells; epSPC, ependymal stem/progenitor cells; SCI, spinal cord injury.

OPC, present in the white and gray matter in the adult CNS, are the main proliferating cell types in the intact spinal cord [80]. Under homeostatic conditions, neural/glial antigen 2 (NG2)—expressing OPC proliferate and differentiate into mature oligodendrocytes maintaining tissue integrity over the lifespan. Following SCI, OPC migrate to the spinal cord lesion sites, and extensively contribute to remyelination [80,81]. The recent studies [84,85] have shown that glial growth factor 2 (GGF2) and ferritin administration promote oligodendrogenesis and improve functional recovery after SCI. Thus, enhancing the endogenous OPC response to injury could be a potential therapeutic approach to manage tissue repair and regeneration without the transplantation of exogenous cells.

It is well known that astrocyte turnover is low in healthy spinal cords, however, these cells respond to SCI by intensive dividing and forming the border of glial scar with fibromeningeal and NG2<sup>+</sup>glia cells [80,86]. Astrocytes in the scar's periphery inhibit axonal growth in the environment of SCI through secretion of inhibitory molecules such as heparan sulphate proteoglycan, dermatan sulphate proteoglycan, keratan sulphate proteoglycan and chondroitin sulphate proteoglycan (CSPG) [87]. In addition to the extracellular matrix components, semaphorin 3, ephrin-B2 and its receptor EPHB2 and the Slit proteins produced by reactive astrocytes, have largely negative effects on nerve regeneration [87]. Following these observations, several *in vivo* studies provided the evidence that application of chondroitinase ABC (ChABC) as an individual therapy or in combination with other treatments degraded CSPG in scar tissue, enhanced growth and regeneration of axons, and re-established neural pathways below the lesion (reviewed in [88]). Enzyme-based treatments may provide new opportunities to overcome detrimental effects of glial scar and may offer new hope for success in therapy of SCI.

However, as we mentioned, reactive astrocytes surrounding the spinal cord lesion prevent an excessive inflammatory cell infiltration leading to decrease in immune-mediated damage of spinal cord. Interestingly, during the last two decades, there is growing evidence suggesting novel cellular and molecular mechanisms underlying neuroprotective effect of astrogliosis after SCI. The fact that glial scar is composed of at least two phenotypically and developmentally different populations of astrocytes, may explain a dual role of scar tissue on spinal cord regeneration. Although the most extensive proliferation of epSPC occurs during embryogenesis and the early postnatal period, there are data suggesting slow proliferation rate of epSPC surrounding spinal cord in adulthood [89–91]. More importantly, endogenous epSPC are activated 72 h after SCI to migrate from spinal central canal towards the lesion site, divide extensively, and generate astrocytes, as well as a small number of oligodendrocytes [80,82,92,93]. Only small portion of epSPC differentiate toward oligodendrocytes responsible for myelin production, typically located in white matter areas of spinal cord [94]. Most of the epSPC-derived progeny express astrocytic markers [82], however, these reactive astrocytes are glial fibrillary acidic protein (GFAP) negative, invade glial scar center and promote axonal growth and regeneration [80,82,95]. In contrast to astrocytes constituting the glial scar border, epSPC-derived reactive astrocytes actively maintain extracellular homeostasis. In particular, astrocytic uptake of glutamate prevents glutamate-mediated neuronal loss, suggesting that pharmacological stimulation of astrocytes may be a promising therapeutic target for SCI as well as other pathologies involving excitotoxicity. In addition, astrocytes provide significant metabolic support to neurons, regulate extracellular potassium level, and prevent generation of free radicals [96]. The neuroprotective capacity of astrocytes is mediated by wide variety of soluble factors including brain-derived neurotrophic factor, ciliary neurotrophic factor, nerve growth factor (NGF), and basic fibroblast growth factor (FGF-2) and the extracellular matrix molecules laminin and fibronectin [97]. Thus, specific modulation of two reactive astrocyte subpopulations in the injured spinal cord, protective in the core and harmful at the periphery of glial scar, could represent a new regeneration strategy for SCI.

Although the precise mechanism for improved functional recovery after intrathecal administration of epidermal growth factor (EGF) and fibroblast growth factor 2 (FGF-2) is not known [98], these findings suggested that stimulation of resident NSC might be used as a possible new therapeutic approach for SCI treatment. Endogenous cell-based therapeutic approach avoids the risks of exogenous

cell transplantation such as risk of tumor formation after engraftment, and possible immunogenicity that requires immunosuppression. Thus, we explored a new chemical entity, FM19G11 as a new pharmacological agent for spinal cord regeneration (Figure 1B). FM19G11, by HIF2 $\alpha$ -mediated mechanisms, inhibits the transcriptional and protein expression of pluripotency markers *Sox2*, *Oct4*, *Nanog*, and *Tgf- $\alpha$*  in epSPC, leading to increased differentiation of epSPC into oligodendrocytes in a hypoxic environment [99]. However, under normoxic conditions, FM19G11 stimulates glucose intake and mitochondrial functions in epSPC, causing an increased energy status and high proliferation of epSPC (Figure 1B, left panel). Furthermore, we confirmed neuroregenerative properties of FM19G11 using an animal model of SCI [100]. In line with previous findings, paralysis of hind limbs was significantly reversed in FM19G11-treated rats with SCI compared to vehicle treated animals [100] (Figure 1B, right panel). Furthermore, we showed that epSPC isolated from rats with an SCI (epSPCi) display enhanced capability for self-renewal and differentiation toward oligodendrocyte progenitors compared to epSPC from healthy animals [56]. This is inconsistent with the fact that the inflammatory environment to which quiescent epSPCs are exposed after SCI modulates gene expression profile and induces recruitment of endogenous epSPCs to the lesion site [82,92]. In order to delineate the molecular mechanisms responsible for higher regeneration ability of epSPCi after injury, we analyzed the role of Cx50, an ion channel involved in differentiation of stem cells into glial cells within the injured area. In non-pathological conditions, epSPC show high expression levels of Cx50, however, activated epSPCi express low levels of Cx50, indicating adverse effects of Cx50 in spinal cord regeneration [18,101]. An additional molecular mechanism of increased regenerative capacities of epSPCi versus epSPC could be changes in purinergic receptors (P2Y) expression in stem cells. We showed that downregulation of P2Y1 receptor and an upregulation of P2Y4 receptor increases differentiation potential and proliferation ability of epSPCi, respectively [102]. Hence, transplantation of epSPCi or epSPCi-derived oligodendrocyte precursors [OPCi] immediately after spinal cord contusion was a more efficient therapeutic strategy for the locomotor recovery one week after treatment than epSPC or OPC transplantation [56]. Therefore, our studies revealed that transplanted epSPCi differentiated rarely and that beneficial effect of transplanted epSPCi in SCI was primarily based on their release of trophic and immunomodulatory factors that alter function of immune cells [56]. Combination of epSPCi transplantation and local application of FM19G11 reduced glial scar and enhanced generation of oligodendrocyte precursor, however, did not significantly improve the neurological outcome compared to the individual treatments [103]. Therefore, to treat SCI as complex disorder, new hope might be found in a combination of cell transplantation, pharmacotherapy, mobilization of endogenous stem cells and bioscaffolds [103,104].

## 5. Conclusions

Stem cell therapy in SCI provides a clue to solve the challenges which currently used medical procedures cannot treat. Because of their neuroregenerative, neuroprotective and immunomodulatory properties, stem cells are an innovative approach for the therapy of SCI. The presence of NSC in the adult CNS raises the possibility of the modulation of an endogenous regenerative process. Although further investigations are necessary to confirm neurological benefits by adjusting doses and drug administrations, treatments for mobilization of endogenous stem cell population have been considered as a promising therapeutic approach to enhance repair mechanisms in SCI. Additionally, results of preclinical studies indicate that application of stem cell-derived progenitors significantly reduces neurological disability in most severe SCIs. However, the main safety issue regarding pluripotent stem cell-based transplantation is still a lack of efficient protocols to obtain pure cell populations without the presence of unwanted cell types, and undifferentiated hESC/iPSC. It is important to highlight that stem cell transplantation alone is not sufficient to bridge a spinal cord lesion, therefore, a repair strategy based on combination of well-established therapeutic modalities, including surgery and medications, and stem cell-derived neural cells is an extremely attractive option for the treatment of this devastating injuries. Therefore, it is critical to develop new modalities such as directly applied pharmacology and

biomaterials that support stem cell survival and provide better tissue integration. Future studies must be focused on resolving issues such as ideal sources of stem cells and safety of stem cell-based therapy with the aim to utterly exploit the promising therapeutic potential of both exogenous and endogenous stem cells in SCI.

**Acknowledgments:** This study was supported by Serbian Ministry of Science (ON175069 and ON175103).

**Author Contributions:** Marina Gazzic, Vladislav Volarevic, C. Randall Harrell, Crissy Fellabaum, Nemanja Jovicic, Nebojsa Arsenijevic, Miodrag Stojkovic designed and wrote the manuscript.

**Conflicts of Interest:** The authors declare no conflict of interest.

## References

1. International Perspectives on Spinal Cord Injury. Available online: [http://apps.who.int/iris/bitstream/10665/94190/1/9789241564663\\_eng.pdf](http://apps.who.int/iris/bitstream/10665/94190/1/9789241564663_eng.pdf) (accessed on 15 January 2018).
2. Available online: <http://asia-spinalinjury.org> (accessed on 15 January 2018).
3. Hagen, E.M. Acute complications of spinal cord injuries. *World J. Orthop.* **2015**, *6*, 17–23. [CrossRef] [PubMed]
4. Ronaghi, M.; Erceg, S.; Moreno-Manzano, V.; Stojkovic, M. Challenges of stem cell therapy for spinal cord injury: Human embryonic stem cells, endogenous neural stem cells, or induced pluripotent stem cells? *Stem Cells* **2010**, *28*, 93–99. [CrossRef] [PubMed]
5. Ackery, A.; Tator, C.; Krassioukov, A. A global perspective on spinal cord injury epidemiology. *J. Neurotrauma* **2004**, *21*, 1355–1370. [CrossRef] [PubMed]
6. Beattie, M.S.; Li, Q.; Bresnahan, J.C. Cell death and plasticity after experimental spinal cord injury. *Prog. Brain Res.* **2000**, *128*, 9–21. [PubMed]
7. Blight, A.R. Spinal cord injury models: Neurophysiology. *J. Neurotrauma* **1992**, *9*, 147–150. [CrossRef] [PubMed]
8. Grossman, S.D.; Rosenberg, L.J.; Wrathall, J.R. Relationship of altered glutamate receptor subunit mRNA expression to acute cell loss after spinal cord contusion. *Exp. Neurol.* **2001**, *168*, 283–289. [CrossRef] [PubMed]
9. Fehlings, M.G.; Nakashima, H.; Nagoshi, N.; Chow, D.S.; Grossman, R.G.; Kopjar, B. Rationale, design and critical end points for the Riluzole in Acute Spinal Cord Injury Study (RISCIS): A randomized, double-blinded, placebo-controlled parallel multi-center trial. *Spinal Cord* **2016**, *54*, 8–15. [CrossRef] [PubMed]
10. Garcia, E.; Aguilar-Cevallos, J.; Silva-Garcia, R.; Ibarra, A. Cytokine and Growth Factor Activation In Vivo and In Vitro after Spinal Cord Injury. *Mediat. Inflamm.* **2016**, *2016*. [CrossRef] [PubMed]
11. Hayta, E.; Elden, H. Acute spinal cord injury: A review of pathophysiology and potential of non-steroidal anti-inflammatory drugs for pharmacological intervention. *J. Chem. Neuroanat.* **2017**, *87*, 25–31. [CrossRef] [PubMed]
12. Li, S.; Stys, P.K. Mechanisms of ionotropic glutamate receptor-mediated excitotoxicity in isolated spinal cord white matter. *J. Neurosci.* **2000**, *20*, 1190–1198. [PubMed]
13. Visavadiya, N.P.; Patel, S.P.; VanRooyen, J.L.; Sullivan, P.G.; Rabchevsky, A.G. Cellular and subcellular oxidative stress parameters following severe spinal cord injury. *Redox Biol.* **2016**, *8*, 59–67. [CrossRef] [PubMed]
14. Pineau, I.; Lacroix, S. Proinflammatory cytokine synthesis in the injured mouse spinal cord: Multiphasic expression pattern and identification of the cell types involved. *J. Comp. Neurol.* **2007**, *500*, 267–285. [CrossRef] [PubMed]
15. Kettenmann, H.; Hanisch, U.K.; Noda, M.; Verkhratsky, A. Physiology of microglia. *Physiol. Rev.* **2001**, *91*, 461–553. [CrossRef] [PubMed]
16. Oyinbo, C.A. Secondary injury mechanisms in traumatic spinal cord injury: A nugget of this multiply cascade. *Acta Neurobiol. Exp. (Wars)* **2011**, *71*, 281–299. [PubMed]
17. Kong, X.; Gao, J. Macrophage polarization: A key event in the secondary phase of acute spinal cord injury. *J. Cell Mol. Med.* **2017**, *21*, 941–954. [CrossRef] [PubMed]
18. Rodriguez-Jimenez, F.J.; Alastrue, A.; Stojkovic, M.; Erceg, S.; Moreno-Manzano, V. Connexin 50 modulates Sox2 expression in spinal-cord-derived ependymal stem/progenitor cells. *Cell Tissue Res.* **2016**, *365*, 295–307. [CrossRef] [PubMed]

19. Gris, P.; Tighe, A.; Levin, D.; Sharma, R.; Brown, A. Transcriptional regulation of scar gene expression in primary astrocytes. *Clia* **2007**, *55*, 1145–1155. [[CrossRef](#)] [[PubMed](#)]
20. Allison, D.J.; Ditor, D.S. Immune dysfunction and chronic inflammation following spinal cord injury. *Spinal Cord* **2015**, *53*, 14–18. [[CrossRef](#)] [[PubMed](#)]
21. David, S.; Wee Yong, V. Harmful and beneficial effects of inflammation after spinal cord injury: Potential therapeutic implications. *Handb. Clin. Neurol.* **2012**, *109*, 485–502. [[PubMed](#)]
22. Yilmaz, T.; Kaptanoğlu, E. Current and future medical therapeutic strategies for the functional repair of spinal cord injury. *World J. Orthop.* **2015**, *6*, 42–55. [[CrossRef](#)] [[PubMed](#)]
23. Wilson, J.R.; Forgione, N.; Fehlings, M.G. Emerging therapies for acute traumatic spinal cord injury. *CMAJ* **2013**, *185*, 485–492. [[CrossRef](#)] [[PubMed](#)]
24. Cengiz, S.L.; Kalkan, E.; Bayir, A.; Ilik, K.; Basefer, A. Timing of thoracolumbar spine stabilization in trauma patients: impact on neurological outcome and clinical course. A real prospective (rct) randomized controlled study. *Arch. Orthop. Trauma Surg.* **2008**, *128*, 959–966. [[CrossRef](#)] [[PubMed](#)]
25. Saxler, G.; Krämer, J.; Barden, B.; Kurt, A.; Pförtner, J.; Bernsmann, K. The long-term clinical sequelae of incidental durotomy in lumbar disc surgery. *Spine* **2005**, *30*, 2298–2302. [[CrossRef](#)] [[PubMed](#)]
26. Dididze, M.; Green, B.A.; Dietrich, W.D.; Vanni, S.; Wang, M.Y.; Levi, A.D. Systemic hypothermia in acute cervical spinal cord injury: A case-controlled study. *Spinal Cord* **2013**, *51*, 395–400. [[CrossRef](#)] [[PubMed](#)]
27. Levi, A.D.; Casella, G.; Green, B.A.; Dietrich, W.D.; Vanni, S.; Jagid, J.; Wang, M.Y. Clinical outcomes using modest intravascular hypothermia after acute cervical spinal cord injury. *Neurosurgery* **2010**, *66*, 670–677. [[CrossRef](#)] [[PubMed](#)]
28. Hansebout, R.R.; Hansebout, C.R. Local cooling for traumatic spinal cord injury: Outcomes in 20 patients and review of the literature. *J. Neurosurg. Spine* **2014**, *20*, 550–561. [[CrossRef](#)] [[PubMed](#)]
29. Wang, J.; Pearse, D.D. Therapeutic Hypothermia in Spinal Cord Injury: The Status of Its Use and Open Questions. *Int. J. Mol. Sci.* **2015**, *16*, 16848–16879. [[CrossRef](#)] [[PubMed](#)]
30. Polderman, K.H. Mechanisms of action, physiological effects, and complications of hypothermia. *Crit. Care Med.* **2009**, *37* (Suppl. 7), S186–S202. [[CrossRef](#)] [[PubMed](#)]
31. Rogers, W.K.; Todd, M. Acute spinal cord injury. *Best Pract. Res. Clin. Anaesthesiol.* **2016**, *30*, 27–39. [[CrossRef](#)] [[PubMed](#)]
32. Coutinho, A.E.; Chapman, K.E. The anti-inflammatory and immunosuppressive effects of glucocorticoids, recent developments and mechanistic insights. *Mol. Cell. Endocrinol.* **2011**, *335*, 2–13. [[CrossRef](#)] [[PubMed](#)]
33. Bracken, M.B.; Shepard, M.J.; Collins, W.F.; Holford, T.R.; Young, W.; Baskin, D.S.; Eisenberg, H.M.; Flamm, E.; Leo-Summers, L.; Maroon, J.; et al. A randomized, controlled trial of methylprednisolone or naloxone in the treatment of acute spinal-cord injury: Results of the second National Acute Spinal Cord Injury Study. *N. Engl. J. Med.* **1990**, *322*, 1405–1411. [[CrossRef](#)] [[PubMed](#)]
34. Bracken, M.B.; Shepard, M.J.; Holford, T.R.; Leo-Summers, L.; Aldrich, E.F.; Fazl, M.; Fehlings, M.; Herr, D.L.; Hitchon, P.W.; Marshall, L.F.; et al. Administration of methyl prednisolone for 24 or 48 hours or tirilazad mesylate for 48 hours in the treatment of acute spinal cord injury: Results of the third National Acute Spinal Cord Injury randomized controlled trial. *JAMA* **1997**, *277*, 1597–1604. [[CrossRef](#)] [[PubMed](#)]
35. Ito, Y.; Sugimoto, Y.; Tomioka, M.; Kai, N.; Tanaka, M. Does high dose methylprednisolone sodium succinate really improve neurological status in patient with acute cervical cord injury? A prospective study about neurological recovery and early complications. *Spine* **2009**, *34*, 2121–2124. [[CrossRef](#)] [[PubMed](#)]
36. Pointillart, V.; Petitjean, M.E.; Wiart, L.; Vital, J.M.; Lassie, P.; Thicoipé, M.; Dabadie, P. Pharmacological therapy of spinal cord injury during the acute phase. *Spinal Cord* **2000**, *38*, 71–76. [[CrossRef](#)] [[PubMed](#)]
37. Matsumoto, T.; Tamaki, T.; Kawakami, M.; Yoshida, M.; Ando, M.; Yamada, H. Early complications of high-dose methylprednisolone sodium succinate treatment in the follow-up of acute cervical spinal cord injury. *Spine* **2001**, *26*, 426–430. [[CrossRef](#)] [[PubMed](#)]
38. Grossman, R.G.; Fehlings, M.G.; Frankowski, R.F.; Burau, K.D.; Chow, D.S.; Tator, C.; Teng, A.; Toups, E.G.; Harrop, J.S.; Aarabi, B.; et al. A prospective, multicenter, phase I matched-comparison group trial of safety, pharmacokinetics, and preliminary efficacy of riluzole in patients with traumatic spinal cord injury. *J. Neurotrauma* **2014**, *31*, 239–255. [[CrossRef](#)] [[PubMed](#)]
39. Geisler, F.H.; Coleman, W.P.; Grieco, G.; Poonian, D. Sygen Study Group: The Sygen multicenter acute spinal cord injury study. *Spine* **2001**, *26* (Suppl. 24), S87–S98. [[CrossRef](#)] [[PubMed](#)]

40. Fehlings, M.G.; Theodore, N.; Harrop, J.; Maurais, G.; Kuntz, C.; Shaffrey, C.I.; Kwon, B.K.; Chapman, J.; Yee, A.; Tighe, A.; et al. A phase I/IIa clinical trial of a recombinant Rho protein antagonist in acute spinal cord injury. *J. Neurotrauma* **2011**, *28*, 787–796. [CrossRef] [PubMed]
41. Casha, S.; Zygun, D.; McGowan, M.D.; Bains, I.; Yong, V.W.; Hurlbert, R.J. Results of a phase II placebo-controlled randomized trial of minocycline in acute spinal cord injury. *Brain* **2012**, *135 Pt 4*, 1224–1236. [CrossRef] [PubMed]
42. Inada, T.; Takahashi, H.; Yamazaki, M.; Okawa, A.; Sakuma, T.; Kato, K.; Hashimoto, M.; Hayashi, K.; Furuya, T.; Fujiyoshi, T.; et al. Multicenter prospective nonrandomized controlled clinical trial to prove neurotherapeutic effects of granulocyte colony-stimulating factor for acute spinal cord injury: Analyses of follow-up cases after at least 1 year. *Spine* **2014**, *39*, 213–219. [CrossRef] [PubMed]
43. Smith, A.G. Embryo-derived stem cells: Of mice and men. *Annu. Rev. Cell Dev. Biol.* **2001**, *17*, 435–462. [CrossRef] [PubMed]
44. Thomson, J.A.; Itskovitz-Eldor, J.; Shapiro, S.S.; Waknitz, M.A.; Swiergiel, J.J.; Marshall, V.S.; Jones, J.M. Embryonic stem cell lines derived from human blastocysts. *Science* **1998**, *281*, 1145114–1145117. [CrossRef]
45. Reubinoff, B.E.; Pera, M.F.; Fong, C.Y.; Trounson, A.; Bongso, A. Embryonic stem cell lines from human blastocysts: Somatic differentiation in vitro. *Nat. Biotechnol.* **2000**, *18*, 399–404. [CrossRef] [PubMed]
46. Lukovic, D.; Moreno Manzano, V.; Stojkovic, M.; Bhattacharya, S.S.; Erceg, S. Concise review: Human pluripotent stem cells in the treatment of spinal cord injury. *Stem Cells* **2012**, *30*, 1787–1792. [CrossRef] [PubMed]
47. Nistor, G.I.; Totoiu, M.O.; Haque, N.; Carpenter, M.K.; Keirstead, H.S. Human embryonic stem cells differentiate into oligodendrocytes in high purity and myelinate after spinal cord transplantation. *Glia* **2005**, *49*, 385–396. [CrossRef] [PubMed]
48. Keirstead, H.S.; Nistor, G.; Bernal, G.; Totoiu, M.; Cloutier, F.; Sharp, K.; Steward, O. Human embryonic stem cell derived oligodendrocyte progenitor cell transplants remyelinate and restore locomotion after spinal cord injury. *J. Neurosci.* **2005**, *25*, 4694–4705. [CrossRef] [PubMed]
49. Cloutier, F.; Siegenthaler, M.M.; Nistor, G.; Keirstead, H.S. Transplantation of human embryonic stem cell-derived oligodendrocyte progenitors into rat spinal cord injuries does not cause harm. *Regen. Med.* **2006**, *1*, 469–479. [CrossRef] [PubMed]
50. Salewski, R.P.; Mitchell, R.A.; Shen, C.; Fehlings, M.G. Transplantation of neural stem cells clonally derived from embryonic stem cells promotes recovery after murine spinal cord injury. *Stem Cells Dev.* **2015**, *24*, 36–50. [CrossRef] [PubMed]
51. Faulkner, J.; Keirstead, H.S. Human embryonic stem cell-derived oligodendrocyte progenitors for the treatment of spinal cord injury. *Transpl. Immunol.* **2005**, *15*, 131–142. [CrossRef] [PubMed]
52. Zhang, Y.W.; Denham, J.; Thies, R.S. Oligodendrocyte progenitor cells derived from human embryonic stem cells express neurotrophic factors. *Stem Cells* **2006**, *15*, 943–952. [CrossRef] [PubMed]
53. Erceg, S.; Laínez, S.; Ronaghi, M.; Stojkovic, P.; Pérez-Aragó, M.A.; Moreno-Manzano, V.; Moreno-Palanques, R.; Planells-Cases, R.; Stojkovic, M. Differentiation of human embryonic stem cells to regional specific neural precursors in chemically defined medium conditions. *PLoS ONE* **2008**, *3*, e2122. [CrossRef] [PubMed]
54. Lukovic, D.; Moreno-Manzano, V.; Lopez-Mocholi, E.; Rodriguez-Jiménez, F.J.; Jendelova, P.; Sykova, E.; Oria, M.; Stojkovic, M.; Erceg, S. Complete rat spinal cord transection as a faithful model of spinal cord injury for translational cell transplantation. *Sci. Rep.* **2015**, *5*, 9640. [CrossRef] [PubMed]
55. Erceg, S.; Ronaghi, M.; Oria, M.; Roselló, M.G.; Aragó, M.A.; Lopez, M.G.; Radovic, I.; Moreno-Manzano, V.; Rodríguez-Jiménez, F.J.; Bhattacharya, S.S.; et al. Transplanted oligodendrocytes and motoneuron progenitors generated from human embryonic stem cells promote locomotor recovery after spinal cord transection. *Stem Cells* **2010**, *28*, 1541–1549. [CrossRef] [PubMed]
56. Moreno-Manzano, V.; Rodríguez-Jiménez, F.J.; García-Roselló, M.; Laínez, S.; Erceg, S.; Calvo, M.T.; Ronaghi, M.; Lloret, M.; Planells-Cases, R.; Sánchez-Puelles, J.M.; et al. Activated spinal cord ependymal stem cells rescue neurological function. *Stem Cells* **2009**, *27*, 733–743. [CrossRef] [PubMed]
57. Tetzlaff, W.; Okon, E.B.; Karimi-Abdolrezaee, S.; Hill, C.E.; Sparling, J.S.; Plemel, J.R.; Plunet, W.T.; Tsai, E.C.; Baptiste, D.; Smithson, L.J.; et al. A systematic review of cellular transplantation therapies for spinal cord injury. *J. Neurotrauma* **2011**, *28*, 1611–1682. [CrossRef] [PubMed]
58. Takahashi, K.; Yamanaka, S. Induction of pluripotent stem cells from mouse embryonic and adult fibroblast cultures by defined factors. *Cell* **2006**, *126*, 663–676. [CrossRef] [PubMed]

59. Volarevic, V.; Markovic, B.S.; Gazdic, M.; Volarevic, A.; Jovicic, N.; Arsenijevic, N.; Armstrong, L.; Djonov, V.; Lako, M.; Stojkovic, M. Ethical and Safety Issues of Stem Cell-Based Therapy. *Int. J. Med. Sci.* **2018**, *15*, 36–45. [CrossRef] [PubMed]
60. Stadtfeld, M.; Nagaya, M.; Utikal, J.; Weir, G.; Hochedlinger, K. Induced pluripotent stem cells generated without viral integration. *Science* **2008**, *322*, 945–949. [CrossRef] [PubMed]
61. Okita, K.; Nakagawa, M.; Hyenjong, H.; Ichisaka, T.; Yamanaka, S. Generation of mouse induced pluripotent stem cells without viral vectors. *Science* **2008**, *322*, 949–953. [CrossRef] [PubMed]
62. Soldner, F.; Hockemeyer, D.; Beard, C.; Gao, Q.; Bell, G.W.; Cook, E.G.; Hargas, G.; Blak, A.; Cooper, O.; Mitalipova, M.; et al. Parkinson’s disease patient-derived induced pluripotent stem cells free of viral reprogramming factors. *Cell* **2009**, *136*, 964–977. [CrossRef] [PubMed]
63. Plath, K.; Lowry, W.E. Progress in understanding reprogramming to the induced pluripotent state. *Nat. Rev. Genet.* **2011**, *12*, 253–265. [CrossRef] [PubMed]
64. Woltyen, K.; Michael, I.P.; Mohseni, P.; Desai, R.; Mileikovsky, M.; Hämaläinen, R.; Cowling, R.; Wang, W.; Liu, P.; Gertsenstein, M.; et al. piggyBac transposition reprograms fibroblasts to induced pluripotent stem cells. *Nature* **2009**, *458*, 766–770. [CrossRef] [PubMed]
65. Zhang, Y.; Pak, C.; Han, Y.; Ahlenius, H.; Zhang, Z.; Chanda, S.; Marro, S.; Patzke, C.; Acuna, C.; Covy, J.; et al. Rapid single-step induction of functional neurons from human pluripotent stem cells. *Neuron* **2013**, *78*, 785–798. [CrossRef] [PubMed]
66. Hallett, P.J.; Deleidi, M.; Astradsson, A.; Smith, G.A.; Cooper, O.; Osborn, T.M.; Sundberg, M.; Moore, M.A.; Perez-Torres, E.; Brownell, A.L.; et al. Successful function of autologous iPSC-derived dopamine neurons following transplantation in an on-human primate model of Parkinson’s Disease. *Cell Stem Cell* **2015**, *16*, 269–274. [CrossRef] [PubMed]
67. Sareen, D.; O’Rourke, J.G.; Meera, P.; Muhammad, A.K.; Grant, S.; Simpkinson, M.; Bell, S.; Carmona, S.; Ornelas, L.; Sahabian, A.; et al. Targeting RNA foci in iPSC-derived motor neurons from ALS patients with a C9ORF72 repeat expansion. *Sci. Transl. Med.* **2013**, *5*, 208ra149. [CrossRef] [PubMed]
68. Karumbayaram, S.; Novitch, B.G.; Patterson, M.; Umbach, J.A.; Richter, L.; Lindgren, A.; Conway, A.E.; Clark, A.T.; Goldman, S.A.; Plath, K.; et al. Directed differentiation of human-induced pluripotent stem cells generates active motor neurons. *Stem Cells* **2009**, *27*, 806–811. [CrossRef] [PubMed]
69. Jha, B.S.; Rao, M.; Malik, N. Motor neuron differentiation from pluripotent stem cells and other intermediate proliferative precursors that can be discriminated by lineage specific reporters. *Stem Cell Rev.* **2015**, *11*, 194–204. [CrossRef] [PubMed]
70. Nicholas, C.R.; Chen, J.; Tang, Y.; Southwell, D.G.; Chalmers, N.; Vogt, D.; Arnold, C.M.; Chen, Y.J.; Stanley, E.G.; Elefanti, A.G.; et al. Functional maturation of hPSC-derived forebrain interneurons requires an extended timeline and mimics human neural development. *Cell Stem Cell* **2013**, *12*, 573–586. [CrossRef] [PubMed]
71. Chambers, S.M.; Mica, Y.; Lee, G.; Studer, L.; Tomishima, M.J. Dual-SMAD Inhibition/WNT Activation-Based Methods to Induce Neural Crest and Derivatives from Human Pluripotent Stem Cells. *Methods Mol. Biol.* **2016**, *1307*, 329–343. [PubMed]
72. Muratore, C.R.; Srikanth, P.; Callahan, D.G.; Young-Pearse, T.L. Comparison and optimization of hiPSC forebrain cortical differentiation protocols. *PLoS ONE* **2014**, *9*, e105807. [CrossRef] [PubMed]
73. Salewski, R.P.; Mitchell, R.A.; Li, L.; Shen, C.; Milekovskaia, M.; Nagy, A.; Fehlings, M.G. Transplantation of Induced Pluripotent Stem Cell-Derived Neural Stem Cells Mediate Functional Recovery Following Thoracic Spinal Cord Injury Through Remyelination of Axons. *Stem Cells Transl. Med.* **2015**, *4*, 743–754. [CrossRef] [PubMed]
74. Nagoshi, N.; Okano, H. Applications of induced pluripotent stem cell technologies in spinal cord injury. *J. Neurochem.* **2017**, *141*, 848–860. [CrossRef] [PubMed]
75. Fujimoto, Y.; Abematsu, M.; Falk, A.; Tsujimura, K.; Sanosaka, T.; Juliandi, B.; Semi, K.; Namihira, M.; Komiya, S.; Smith, A.; et al. Treatment of a mouse model of spinal cord injury by transplantation of human induced pluripotent stem cell-derived long-term self-renewing neuroepithelial-like stem cells. *Stem Cells* **2012**, *30*, 1163–1173. [CrossRef] [PubMed]

76. Kobayashi, Y.; Okada, Y.; Itakura, G.; Iwai, H.; Nishimura, S.; Yasuda, A.; Nori, S.; Hikishima, K.; Konomi, T.; Fujiyoshi, K.; et al. Pre-evaluated safe human iPSC-derived neural stem cells promote functional recovery after spinal cord injury in common marmoset without tumorigenicity. *PLoS ONE* **2012**, *7*, e52787. [CrossRef] [PubMed]
77. Nutt, S.E.; Chang, E.A.; Suhr, S.T.; Schlosser, L.O.; Mondello, S.E.; Moritz, C.T.; Cibelli, J.B.; Horner, P.J. Caudalized human iPSC-derived neural progenitor cells produce neurons and glia but fail to restore function in an early chronic spinal cord injury model. *Exp. Neurol.* **2013**, *248*, 491–503. [CrossRef] [PubMed]
78. Amemori, T.; Ruzicka, J.; Romanyuk, N.; Jhanwar-Uniyal, M.; Sykova, E.; Jendelova, P. Comparison of intraspinal and intrathecal implantation of induced pluripotent stem cell-derived neural precursors for the treatment of spinal cord injury in rats. *Stem Cell Res. Ther.* **2015**, *6*, 257. [CrossRef] [PubMed]
79. Hayashi, K.; Hashimoto, M.; Koda, M.; Naito, A.T.; Murata, A.; Okawa, A.; Takahashi, K.; Yamazaki, M. Increase of sensitivity to mechanical stimulus after transplantation of murine induced pluripotent stem cell-derived astrocytes in a rat spinal cord injury model. *J. Neurosurg. Spine* **2011**, *15*, 582–593. [CrossRef] [PubMed]
80. Barnabé-Heider, F.; Göritz, C.; Sabelström, H.; Takebayashi, H.; Pfrieger, F.W.; Meletis, K.; Frisén, J. Origin of new glial cells in intact and injured adult spinal cord. *Cell Stem Cell* **2010**, *7*, 470–482. [CrossRef] [PubMed]
81. Horner, P.; Power, A.; Kempermann, G.; Kuhn, H.; Palmer, T.; Winkler, J.; Thal, L.; Gage, F. Proliferation and differentiation of progenitor cells throughout the intact adult rat spinal cord. *J. Neurosci.* **2000**, *20*, 2218–2228. [PubMed]
82. Meletis, K.; Barnabé-Heider, F.; Carlén, M.; Evergren, E.; Tomilin, N.; Shupliakov, O.; Frisén, J.; Abeliovich, A. Spinal cord injury reveals multilineage differentiation of ependymal cells. *PLoS Biol.* **2008**, *6*, e182. [CrossRef] [PubMed]
83. Burda, J.E.; Sofroniew, M.V. Reactive gliosis and the multicellular response to CNS damage and disease. *Neuron* **2014**, *81*, 229–248. [CrossRef] [PubMed]
84. Whittaker, M.T.; Zai, L.J.; Lee, H.J.; Pajooresh-Ganji, A.; Wu, J.; Sharp, A.; Wyse, R.; Wrathall, J.R. GGF2 (Nrg1-beta3) treatment enhances NG2+ cell response and improves functional recovery after spinal cord injury. *Glia* **2012**, *60*, 281–294. [CrossRef] [PubMed]
85. Schonberg, D.L.; Goldstein, E.Z.; Sahinkaya, F.R.; Wei, P.; Popovich, P.G.; McTigue, D.M. Ferritin stimulates oligodendrocyte genesis in the adult spinal cord and can be transferred from macrophages to NG2 cells in vivo. *J. Neurosci.* **2012**, *32*, 5374–5384. [CrossRef] [PubMed]
86. Lee-Liu, D.; Edwards-Faret, G.; Tapia, V.S.; Larraín, J. Spinal cord regeneration: Lessons for mammals from non-mammalian vertebrates. *Genesis* **2013**, *51*, 529–544. [CrossRef] [PubMed]
87. Silver, J.; Miller, J.H. Regeneration beyond the glial scar. *Nat. Rev. Neurosci.* **2004**, *5*, 146–156. [CrossRef] [PubMed]
88. Bradbury, E.J.; Carter, L.M. Manipulating the glial scar: Chondroitinase ABC as a therapy for spinal cord injury. *Brain Res. Bull.* **2011**, *84*, 306–316. [CrossRef] [PubMed]
89. Bruni, J.E. Ependymal development, proliferation, and functions: A review. *Microsc. Res. Tech.* **1998**, *41*, 2–13. [CrossRef]
90. Dromard, C.; Guillon, H.; Rigau, V.; Ripoll, C.; Sabourin, J.C.; Perrin, F.E.; Scamps, F.; Bozza, S.; Sabatier, P.; Lonjon, N.; et al. Adult human spinal cord harbors neural precursor cells that generate neurons and glial cells in vitro. *J. Neurosci. Res.* **2008**, *86*, 1916–1926. [CrossRef] [PubMed]
91. Blasko, J.; Martoncikova, M.; Lievajova, K.; Saganova, K.; Korimova, A.; Racekova, E. Regional differences of proliferation activity in the spinal cord ependyma of adult rats. *Open Life Sci.* **2012**, *7*, 397–403. [CrossRef]
92. Johansson, C.B.; Momma, S.; Clarke, D.L.; Risling, M.; Lendahl, U.; Frisén, J. Identification of a neural stem cell in the adult mammalian central nervous system. *Cell* **1999**, *96*, 25–34. [CrossRef]
93. Mothe, A.J.; Tator, C.H. Proliferation, migration, and differentiation of endogenous ependymal region stem/progenitor cells following minimal spinal cord injury in the adult rat. *Neuroscience* **2005**, *131*, 177–187. [CrossRef] [PubMed]
94. Duan, H.; Song, W.; Zhao, W.; Gao, Y.; Yang, Z.; Li, X. Endogenous neurogenesis in adult mammals after spinal cord injury. *Sci. China Life Sci.* **2016**, *59*, 1313–1318. [CrossRef] [PubMed]
95. Frisén, J.; Johansson, C.B.; Török, C.; Risling, M.; Lendahl, U. Rapid, widespread, and longlasting induction of nestin contributes to the generation of glial scar tissue after CNS injury. *J. Cell Biol.* **1995**, *131*, 453–464. [CrossRef] [PubMed]

96. Bélanger, M.; Magistretti, P.J. The role of astroglia in neuroprotection. *Dialogues Clin. Neurosci.* **2009**, *11*, 281–295. [[PubMed](#)]
97. Wiese, S.; Karus, M.; Faissner, A. Astrocytes as a source for extracellular matrix molecules and cytokines. *Front. Pharmacol.* **2012**, *3*, 120. [[CrossRef](#)] [[PubMed](#)]
98. Hamann, M.C.J.; Tator, C.H.; Shoichet, M.S. Injectable intrathecal delivery system for localized administration of EGF and FGF-2 to the injured rat spinal cord. *Exp. Neurol.* **2005**, *194*, 106–119. [[CrossRef](#)] [[PubMed](#)]
99. Moreno-Manzano, V.; Rodríguez-Jiménez, F.J.; Aceña-Bonilla, J.L.; Fustero-Lardies, S.; Erceg, S.; Dopazo, J.; Montaner, D.; Stojkovic, M.; Sánchez-Puelles, J.M. FM19G11, a new hypoxia-inducible factor (HIF) modulator, affects stem cell differentiation status. *J. Biol. Chem.* **2010**, *285*, 1333–1342. [[CrossRef](#)] [[PubMed](#)]
100. Rodríguez-Jiménez, F.J.; Alastrue-Agudo, A.; Erceg, S.; Stojkovic, M.; Moreno-Manzano, V. FM19G11 favors spinal cord injury regeneration and stem cell self-renewal by mitochondrial uncoupling and glucose metabolism induction. *Stem Cells* **2012**, *30*, 2221–2233. [[CrossRef](#)] [[PubMed](#)]
101. Rodriguez-Jimenez, F.J.; Alastrue-Agudo, A.; Stojkovic, M.; Erceg, S.; Moreno-Manzano, V. Connexin 50 Expression in Ependymal Stem Progenitor Cells after Spinal Cord Injury Activation. *Int. J. Mol. Sci.* **2015**, *16*, 26608–26618. [[CrossRef](#)] [[PubMed](#)]
102. Gómez-Villafuertes, R.; Rodríguez-Jiménez, F.J.; Alastrue-Agudo, A.; Stojkovic, M.; Miras-Portugal, M.T.; Moreno-Manzano, V. Purinergic Receptors in Spinal Cord-Derived Ependymal Stem/Progenitor Cells and Their Potential Role in Cell-Based Therapy for Spinal Cord Injury. *Cell Transpl.* **2015**, *24*, 1493–1509. [[CrossRef](#)] [[PubMed](#)]
103. Alastrue-Agudo, A.; Rodriguez-Jimenez, F.J.; Mocholi, E.L.; De Giorgio, F.; Erceg, S.; Moreno-Manzano, V. FM19G11 and Ependymal Progenitor/Stem Cell Combinatory Treatment Enhances Neuronal Preservation and Oligodendrogenesis after Severe Spinal Cord Injury. *Int. J. Mol. Sci.* **2018**, *19*, 200. [[CrossRef](#)] [[PubMed](#)]
104. Valdes-Sánchez, T.; Rodriguez-Jimenez, F.J.; García-Cruz, D.M.; Escobar-Ivirico, J.L.; Alastrue-Agudo, A.; Erceg, S.; Monleón, M.; Moreno-Manzano, V. Methacrylate-endcapped caprolactone and FM19G11 provide a proper niche for spinal cord-derived neural cells. *J. Tissue Eng. Regen. Med.* **2015**, *9*, 734–739. [[CrossRef](#)] [[PubMed](#)]



© 2018 by the authors. Licensee MDPI, Basel, Switzerland. This article is an open access article distributed under the terms and conditions of the Creative Commons Attribution (CC BY) license (<http://creativecommons.org/licenses/by/4.0/>).

Review

# Activity-Based Physical Rehabilitation with Adjuvant Testosterone to Promote Neuromuscular Recovery after Spinal Cord Injury

Dana M. Otzel <sup>1</sup>, Jimmy Lee <sup>2</sup>, Fan Ye <sup>2</sup>, Stephen E. Borst <sup>3</sup> and Joshua F. Yarrow <sup>2,4,\*</sup>

- <sup>1</sup> Brain Rehabilitation Research Center, Malcom Randall Veterans Affairs Medical Center, North Florida/South Georgia Veterans Health System, Gainesville, FL 32608, USA; dana.otzel@va.gov  
<sup>2</sup> Research Service, Malcom Randall Veterans Affairs Medical Center, North Florida/South Georgia Veterans Health System, Gainesville, FL 32608, USA; jimmylee@ufl.edu (J.L.); 2005evan@gmail.com (F.Y.)  
<sup>3</sup> Department of Applied Physiology, Kinesiology and University of Florida College of Health and Human Performance, Gainesville, FL 32603, USA; seborst@ufl.edu  
<sup>4</sup> Division of Endocrinology, Diabetes and Metabolism, University of Florida College of Medicine, Gainesville, FL 32610, USA

\* Correspondence: jfyarrow@ufl.edu; Tel.: +1-352-548-6000 (ext. 6477)

Received: 21 April 2018; Accepted: 1 June 2018; Published: 7 June 2018

**Abstract:** Neuromuscular impairment and reduced musculoskeletal integrity are hallmarks of spinal cord injury (SCI) that hinder locomotor recovery. These impairments are precipitated by the neurological insult and resulting disuse, which has stimulated interest in activity-based physical rehabilitation therapies (ABTs) that promote neuromuscular plasticity after SCI. However, ABT efficacy declines as SCI severity increases. Additionally, many men with SCI exhibit low testosterone, which may exacerbate neuromusculoskeletal impairment. Incorporating testosterone adjuvant to ABTs may improve musculoskeletal recovery and neuroplasticity because androgens attenuate muscle loss and the slow-to-fast muscle fiber-type transition after SCI, in a manner independent from mechanical strain, and promote motoneuron survival. These neuromusculoskeletal benefits are promising, although testosterone alone produces only limited functional improvement in rodent SCI models. In this review, we discuss the (1) molecular deficits underlying muscle loss after SCI; (2) independent influences of testosterone and locomotor training on neuromuscular function and musculoskeletal integrity post-SCI; (3) hormonal and molecular mechanisms underlying the therapeutic efficacy of these strategies; and (4) evidence supporting a multimodal strategy involving ABT with adjuvant testosterone, as a potential means to promote more comprehensive neuromusculoskeletal recovery than either strategy alone.

**Keywords:** neuroplasticity; bodyweight-supported treadmill training; estradiol; estrogen; muscle; PI3K; IGF-1; motor neuron; BDNF; FOXO; PGC-1 alpha; PGC-1 beta

## 1. Introduction

Spinal cord injury (SCI) results in profound sensorimotor impairment below the lesion site, which is precipitated by the insult to the spinal cord and exacerbated by a cascade of secondary cellular and molecular processes occurring in the acute and chronic post-injury phases [1–3]. Neuromuscular impairment and muscle loss are hallmarks of the SCI injury cascade that produce substantial impediments to physical therapy regimens intended to restore locomotion [3]. Activity-based physical rehabilitation therapies (ABTs) (e.g., bodyweight-supported treadmill training (BWSTT) or robotic assisted locomotor training with or without electric stimulation) have shown promise in promoting neuromuscular plasticity in humans and rodent models after motor-incomplete SCI [4,5]. However, ABTs are only partially effective in restoring function after SCI and their

neuromuscular efficacy declines as injury severity increases [6], indicating the need for adjuvant therapeutic strategies to hasten functional recovery in this population.

Low testosterone (T) is also a secondary consequence of SCI, with hypogonadism being ~ four times more prevalent in men after SCI than in non-injured populations [7]. Non-neurologically impaired men with low T exhibit low muscle mass, impaired muscle function [8], and worsened walking biomechanics [9], while T replacement therapy (TRT) improves muscle mass, neuromuscular function [10], and walking speed in older ambulatory hypogonadal men [11]. To-date, a causal relationship between low T and worsened neuromuscular function after SCI has not been elucidated, although TRT increases sublesional lean mass [12] and muscle cross-sectional area (CSA) in men with motor-complete SCI [13], in a manner completely independent from voluntary muscle contractility. Similarly, in male and female rodent SCI models, androgen treatment attenuates sublesional muscle loss and other phenotypic changes associated with impaired muscle function after SCI [14–20], and may promote slight improvement in locomotor recovery [15]. Herein, we will summarize the (1) molecular deficits underlying muscle loss after SCI; (2) independent influences of T and ABTs on neuromuscular function and musculoskeletal integrity subsequent to SCI; (3) hormonal and molecular mechanisms underlying the therapeutic efficacy of these strategies; and (4) evidence supporting a multimodal strategy involving BWSTT with adjuvant T, as a potential means to promote more comprehensive neuromusculoskeletal recovery after SCI.

## 2. Neuromuscular Adaptations after SCI

Motoneuron innervation of skeletal muscle fibers influences muscle mass and function, and fiber-type distribution [21]. After SCI, changes to the excitatory and inhibitory inputs to the motor unit (i.e., spinal motoneuron and the innervated fibers) exist [22]. For example, motor units that are dysfunctional after SCI result in a weaker and less fatigue resistant muscle [22,23], with rate of force development and motor axon conduction velocity decreasing [24,25]. These changes may exacerbate functional decline after SCI and can impair locomotor recovery, depending on the injury severity and degree of motor dysfunction [26]. The plethora of anatomical and functional consequences resulting from motor unit impairment after SCI have been detailed elsewhere [22]. Herein, we will focus on somatic motoneuron structural adaptations that influence impaired motor function after SCI [27] and how T administration [17,18] and locomotor training [28,29] may alter these adaptations and ultimately improve muscle function and/or locomotor recovery.

The muscular adaptations to SCI have been detailed previously [30], which we summarize here in brevity. Individuals with SCI exhibit an 18–46% lower sublesional muscle cross-sectional area (CSA) than those without SCI, with the degree of atrophy depending on the injury severity [31] and muscle groups involved [32–34]. Muscle loss is worsened as injury severity progresses [31], a result of more impaired motor function and extended disuse in those with motor-complete SCI. For example, muscle atrophy occurs primarily in the initial six weeks after injury in those with motor-incomplete SCI [32], while whole muscle CSA and muscle fiber (f)CSA continually decline for at least 24 weeks after motor-complete SCI [33,35]. Atrophy of both type I (slow-oxidative) and type II (fast-glycolytic) fibers occurs in humans [35,36] and rodents in response to SCI [37], preceding intramuscular fat accumulation [32] and the well-characterized slow-to-fast fiber transition [38,39]. These structural and physiologic changes impair voluntary force generation and muscle endurance [40,41], factors that are associated with locomotor recovery after SCI [42,43]. However, skeletal muscle retains the ability to reverse the molecular cascade precipitating atrophy [44,45] and to improve contractility after SCI in response to sufficient stimuli [46]. In the sections below, we discuss evidence supporting the involvement of several molecular signaling pathways that likely influence muscle deficits after SCI.

### 2.1. Ubiquitin-Proteasome Signaling after SCI

Reduced phosphorylation of the forkhead box O (FOXO) proteins FOXO1 and FOXO3a promotes the transcription of muscle atrophy F-box (MAFbx or atrogin-1) and muscle ring finger-1 (MuRF1),

muscle-specific E<sub>3</sub> ubiquitin ligases that stimulate atrophy in response to disuse and other catabolic states [47]. The influence of these ubiquitin ligases on skeletal muscle atrophy has been demonstrated by the viral overexpression of MAFbx, which reduced the myotube diameter by ~85% in vitro, and by genetic elimination of MAFbx or MuRF1, which attenuated muscle atrophy in response to sciatic nerve transection [48]. Within several days of SCI, >50 protein ubiquination pathway genes are upregulated in sublesional muscle [49], an effect that likely influences the rapid muscle atrophy in response to injury. In particular, MAFbx and MuRF1 mRNA expressions are increased five- to >40-fold within two to eight days of injury [50–54], with protein expressions elevated >two-fold prior to the initiation of muscle atrophy [55]. Interestingly, the fold inductions of MAFbx and MuRF1 were associated with the rate of skeletal muscle atrophy in response to spinal cord transection [53], suggesting that a higher expression of these genes exacerbates muscle loss after SCI. In this regard, FOXO1 mRNA was 33% higher [54] and MAFbx and MuRF1 mRNA were >two-fold higher in rodents after spinal transection than in animals receiving sciatic nerve transection [53], potentially explaining the more rapid atrophy occurring after SCI than in other disuse conditions [53,56]. However, the increased expressions of these and other ubiquitin proteasome pathway genes do not persist after experimental SCI [49], with FOXO1, MAFbx, and MuRF1 gene expressions and pFOXO1 and pFOXO3 proteins reverting to the level of uninjured controls within two to 10 weeks of spinal cord transection [53,54,57]. Similarly, in humans with motor-complete SCI, MAFbx and MuRF1 expressions are high at one-month post-injury and decline by 50–75% at three- and 12-months, resulting from reductions in pFOXO1 and/or total FOXO3 proteins [58]. Indeed, in cohorts of men with chronic SCI, MAFbx and MuRF1 gene expression appear equal to [59] or less than uninjured controls, with FOXO1, FOXO3a, and MAFbx proteins being >35% lower than controls [60]. While our discussion focused on changes in the ubiquitin-proteasome pathway, it is important to note that other catabolic pathways likely influence muscle atrophy after SCI. For example, calpain 1 mRNA expression is increased as early as day 4 after spinal cord transection, an effect that persists for at least 15 days [50], which is important given the influence of calpain signaling on myofibrillar proteolysis [61].

## 2.2. IGF-1 Signaling Pathway after SCI

IGF-1 mediated activation of the phosphatidylinositol-3 kinase (PI3K)/Akt signaling pathway promotes skeletal muscle anabolism [62]. In the immediate days after SCI, mRNA encoding IGF-1, the IGF-1 receptor (IGF-1R), and several IGF binding proteins (IGFBP) are upregulated in muscle [50,51,63], and muscle IGF-1 protein expression is increased [63]. Despite this, muscle pAkt is reduced within several days of SCI [51,55], while relatively normal total and phosphorylated 4E-BP1 and S6K1 expression persist in the first few weeks after SCI [50,51]. The inability of IGF-1 to increase pAkt and downstream targets acutely after SCI likely occurs because insulin receptor substrate-1 (IRS1) protein expression is rapidly reduced in response to SCI [51]. In this regard, IRS1 expression is required for IGF-1 mediated muscle hypertrophy, evidenced by the inability of genetic IGF-1 overexpression to promote skeletal muscle hypertrophy in IRS1 deficient animals [64]. Subsequently, the downregulation of IGF-1 signaling persists chronically after SCI, evidenced by (1) 25–40% lower circulating IGF-1 [65,66] and 50% lower IGF-1 protein expression in the muscle of individuals with chronic SCI compared with controls [60]; and (2) lower total Akt protein and lower total and phosphorylated mTOR and S6K1 in rodent muscle 10-weeks after spinal cord transection [57,67], accompanying 50% lower immunoprecipitated S6K1 activity [67]. Similarly, in humans with motor-complete SCI, total and phosphorylated mTOR and regulatory-associated protein of mTOR (RPTOR), an mTOR cofactor, were lower at three- and 12-months after injury, when compared with values obtained one-month post-SCI, likely influencing the lower p4E-BP1 and pS6 (subunit of S6K1) protein expression [58] that persists for upwards of 30 years after SCI [60]. In this regard, circulating IGF-1 has been shown to be highly correlated with increased thigh muscle CSA in men with chronic motor-complete SCI [68].

### 2.3. PGC-1 $\alpha$ and PGC-1 $\beta$ Signaling after SCI

In skeletal muscle, peroxisome proliferator-activated receptor gamma co-activator (PGC)-1 $\alpha$  regulates type I fiber expression and mitochondrial biogenesis [69], while PGC-1 $\beta$  regulates various aspects of mitochondrial structure and function [70]. As evidence, transgenic PGC-1 $\alpha$  expression results in a whole body muscular phenotype that is high in type I oxidative fibers [71] and muscle-specific PGC-1 $\alpha$  overexpression increases mitochondrial biogenesis [72]. In comparison, ablation of PGC-1 $\beta$  in skeletal muscle myofibers in adulthood reduced mitochondrial CSA and mitochondrial respiration without altering fiber-type distribution, resulting in increased oxidative stress and impaired exercise performance [70]. Baligand et al. used genome wide analysis and identified that genes associated with mitochondrial dysfunction and impaired oxidative phosphorylation were altered three to 14 days after SCI [49]. In particular, muscle PGC-1 $\alpha$  mRNA expression was suppressed to a nearly undetectable level three days after spinal cord transection [54] and within two weeks, muscle PGC-1 $\alpha$  protein was dramatically reduced, accompanying reductions in slow myosin heavy chain (MHC) protein expression [73] that is indicative of fewer oxidative fibers. Similarly, at eight-weeks post-transection, muscle PGC-1 $\alpha$  gene expression and total and nuclear PGC-1 $\alpha$  protein were >50% lower than controls, and slow MHC and slow troponin mRNA and protein were >60% lower [16]. However, at 17-weeks after spinal cord transection, muscle PGC-1 $\alpha$  mRNA expression was no longer suppressed in rodents [74]. In this regard, the hallmark slow-to-fast fiber-type shift resulting from spinal cord transection is most pronounced in the first 100 days after injury, with relatively minor changes in type I MHC expression thereafter [38]. Regardless, muscle PGC-1 $\alpha$  mRNA was 75% lower in men with chronic motor-complete SCI than in normally active men [75]. In comparison, relatively less is known about the changes in muscle PGC-1 $\beta$  after SCI. Interestingly, PGC-1 $\beta$  mRNA was reduced by 90% within three days of sciatic nerve transection [54], an effect that is mentioned because SCI typically results in relatively larger gene expression changes [76] and more rapid muscle loss than other disuse models [53,56]. Wu et al. also reported that muscle PGC-1 $\beta$  mRNA expression was 50% lower than controls at eight-weeks after spinal transection [74] and Kramer et al. reported 75% lower PGC-1 $\beta$  mRNA in men with chronic motor-complete SCI, when compared with ambulatory controls [75].

## 3. Androgenic Regulation of Muscle

Maintenance of skeletal muscle mass requires relative balance between muscle protein synthesis (i.e., anabolic processes) and protein degradation (i.e., catabolic processes), with elevated catabolic signaling and/or reduced anabolic signaling influencing muscle loss. Readers are directed to the following in-depth review of the various signaling pathways that influence skeletal muscle anabolism and catabolism in response to disuse [77]. Herein, we will discuss how androgens influence muscle mass via classical AR-mediated signaling and through interactions with other intercellular anabolic and catabolic signaling pathways (Figure 1).

### 3.1. Testosterone Synthesis and Metabolism

Testosterone is the most abundant bioactive androgen and is primarily synthesized by testicular Leydig cells in males [78] and by the ovaries in females [79], and to a lesser extent in other organs, such as the adrenal cortex [80]. The majority of T circulates are bound to protein transporters (i.e., sex-hormone binding globulin (SHBG) or albumin), with only a small fraction (~1–2%) circulating freely unbound to any protein transporter [81]. The fraction of free (i.e., unbound) T and albumin-bound T is bioavailable [82] because it can bind cell surface or cytosolic androgen receptors (ARs), in the case of free T, or cross the cell membrane and dissociate from its low affinity protein transporter, in the case of albumin, which allows subsequent cytosolic AR binding. In comparison, SHBG-bound T is biologically inactive because it cannot (1) bind cell-surface/plasma-membrane ARs; (2) cross cellular membranes and bind cytosolic ARs [83]; or (3) undergo enzymatic metabolism [84].

As such, elevated SHBG is associated with reduced androgenic action in target tissues expressing ARs, including skeletal muscle [78], bone [84], and spinal motoneurons [85–87], among others.

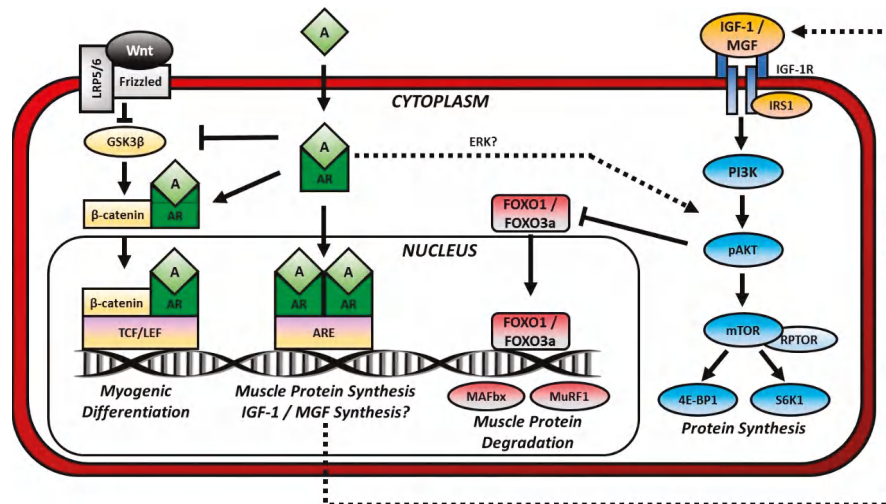


**Figure 1.** Androgen-mediated Anabolic and Anticatabolic Signaling Pathways in Muscle. Anabolic signaling: Androgens (A) pass through the plasma membrane and bind to cytosolic androgen receptors (AR). Dimerized and phosphorylated ARs pass through the nuclear membrane and bind to a region of the DNA termed the androgen response element (ARE), thereby initiating protein synthesis. Ligand-bound ARs may also enhance Wnt signaling as follows. Wnt binds to Frizzled and in turn disheveled (not shown). Disheveled inhibits the activity of glycogen synthase kinase-3β (GSK3β), which phosphorylates β-catenin and marks it for degradation. When GSK3β is inhibited, β-catenin accumulates and enters the nucleus where it binds to a region of the DNA termed the T-cell factor/lymphoid enhancer factor (TCF/LEF) that regulates genes involved in myogenic differentiation. Ligand-bound ARs enhance Wnt signaling by inhibiting GSK3β and attaching to β-catenin for nuclear shuttling. Androgens may also indirectly stimulate protein synthesis by activating the phosphatidylinositol-3 kinase (PI3K)/Akt signaling through actions of Erk or by promoting synthesis of insulin-like growth factor (IGF)-1 or mechano growth factor (MGF). IGF-1 and MGF bind cell-surface IGF-1 receptors (IGF-1R) and activate PI3K/Akt signaling. Anticatabolic signaling: Activation of PI3K/Akt signaling inhibits the transcription factor forkhead box O (FOXO). FOXO1 and FOXO3a activate muscle atrophy F-box (MAFbx or atrogin-1) and muscle ring finger-1 (MuRF1), and E<sub>3</sub> ubiquitin ligases that prepare proteins for proteasome degradation.

In addition to serving as a hormone, T is a substrate for the tissue-specific synthesis of two bioactive sex-steroid hormones, dihydrotestosterone (DHT) and estradiol (E<sub>2</sub>), via actions of the 5α-reductase and aromatase enzymes, respectively [78,84]. The localized conversion of T to DHT, via any of the three 5α-reductase isoforms [78], enhances tissue-specific androgen signaling given that DHT binds to ARs with ~three times the affinity of T [88] and that DHT maintains a longer presence in tissues because it is not aromatized to E<sub>2</sub> nor converted to androstenedione (a weaker androgen), via 17β-hydroxysteroid dehydrogenase (17β-HSD) [78]. Similarly, the aromatization of T to E<sub>2</sub> amplifies estrogen signaling in tissues expressing estrogen receptors (ERs) [89]. In males, this conversion primarily occurs in non-gonadal tissue, with >80% of circulating E<sub>2</sub> derived from localized peripheral metabolism [90]. However, in females, the peripheral aromatization of T to E<sub>2</sub> also amplifies estrogen signaling [79], an effect that is particularly evident after the menopausal transition or in other situations where ovarian estrogen synthesis declines [80].

### 3.2. Hypogonadism and Testosterone Replacement after SCI

After SCI, 45–60% of men exhibit low T (hypogonadism,  $T < 300 \text{ ng/dL}$ ) [91–93] that results, in-part, from secondary testicular dysfunction [94] and impairments in the hypothalamic-pituitary axis [95,96]. Hypogonadism is ~four times more prevalent after SCI than in able-bodied men [7], with T concentrations remaining >25% below that of age-matched healthy men for an extended duration after SCI [91,97]. Additionally, a 50% greater decline in circulating T and >10-fold higher increase in SHBG occurs throughout the age-span in response to SCI [92], indicating that assessment of total T may underestimate hypogonadism incidence after SCI, a concept that we have demonstrated in other populations that exhibit elevated SHBG [81]. A causal relationship between low T and muscle loss after SCI has yet to be identified, although it is interesting to note that Finkelstein et al. reported that healthy men receiving pharmacologic treatment to maintain circulating T in the subphysiologic range ( $191 \pm 78 \text{ ng/dL}$ ) exhibited a significant decline in whole body lean mass and thigh muscle area [98]. In this regard, the median T concentrations observed in several SCI cohort studies (i.e., 160–220 ng/dL) [93,99] were similar to that of Finkelstein et al., suggesting that the magnitude of hypogonadism after SCI is sufficient to induce muscle loss.

Our rodent severe contusion SCI model also exhibits 40–55% lower circulating T than controls for at least two months after injury [14,15,37,100] and androgen treatment attenuates muscle loss [14–16] and fCSA atrophy [17–20] in some, but not all, sublesional muscles in rodent SCI models [16,37,101]. In this regard, androgen-induced muscle preservation appears dependent upon muscle-specific AR expression, given that Phillips et al. reported muscle preservation in the sublesional levator ani/bulbocavernosus (LABC) muscle (high AR expression), but not soleus (low AR expression), in response to T treatment after SCI [37]. Importantly, neither  $E_2$  treatment [17] nor the conversion of T to DHT [14] influence muscle preservation in rodent SCI models, suggesting dispensability of aromatase and  $5\alpha$ -reductase activity in muscle. Indeed, Borst et al. [102] demonstrated that co-administration of T with finasteride (type II  $5\alpha$ -reductase inhibitor) to non-neurologically impaired men resulted in dramatically lower DHT, but did not prevent T-induced improvements in lean mass or muscle strength. Several small clinical trials have also assessed TRT in men with motor-complete SCI. For example, Cooper et al. observed ~40% lower urinary protein and creatinine excretion in SCI patients receiving TRT acutely after injury [103,104], indicating reduced whole body and muscle protein catabolism. Additionally, Bauman et al. reported that 12 months of TRT increased upper- and lower-extremity lean mass and resting energy expenditure in hypogonadal men with motor-complete SCI [12], with improvement persisting for at least 12-months after TRT discontinuation [105]. Lastly, a single case-study recently reported that TRT increased thigh muscle CSA in a man with motor-complete SCI [13].

### 3.3. Classical Androgen Signaling

Classical androgen-mediated genomic signaling is initiated by the binding of T or DHT to cytosolic ARs to form hormone-receptor complexes that translocate to the nucleus and bind androgen response elements (AREs) [106], resulting in the activation or repression of multiple gene pathways that regulate skeletal muscle [107]. Similarly,  $E_2$  stimulates classical estrogen-mediated genomic signaling that is characterized by binding cytoplasmic ER $\alpha$  or ER $\beta$ , which stimulates nuclear translocation of the hormone-receptor complex and binding to estrogen response elements (EREs). ER signaling is pronounced in bone [89], although the aromatization of T to  $E_2$  is not obligatory for skeletal muscle maintenance [98].

Androgens also exert actions that are independent of nuclear AREs [78]. For example, androgens [78] and estrogens [108] exert effects by binding non-traditional cell-surface sex-steroid hormone receptors (e.g., G-protein-coupled receptors (GPCR)) that rapidly alter several intracellular signaling pathways [106,109]. In mesenchymal multipotent C3H 10T1/2 cells, ligand-bound ARs also complex with cytosolic  $\beta$ -catenin [110]. This interaction results in the chaperoning and nuclear accumulation of the androgen-AR/ $\beta$ -catenin complex and stimulation of downstream T-cell factor (TCF)-4

genes, an effect that simultaneously promotes myogenic differentiation and suppresses adipogenic differentiation of mesenchymal pluripotent cells [110]. For further discussion on Wnt/β-catenin signaling, readers are directed to the following in-depth review [111]. Similarly, in C2C12 myotubes [112] and rodent skeletal muscle [113], androgens increase the phosphorylation of cytosolic glycogen synthase kinase-3β (GSK3β), which (1) inhibits the phosphorylation, ubiquitination, and degradation of β-catenin; and (2) promotes nuclear β-catenin accumulation and TCF activity. Ligand-bound ARs also interact with cytosolic β-catenin in motoneurons [114] and neuronal gonadotropin-releasing hormone cell lines [115] to promote nuclear shuttling of β-catenin and TCF-4 binding, which influences β-catenin-dependent transcriptional activity. To our knowledge, the functional significance of androgen-AR/β-catenin nuclear shuttling in motoneurons has not been determined. However, the loss of endogenous ARs accelerates motoneuron degeneration [116] and pharmacologically-induced stimulation of β-catenin protein expression in the spinal cord is associated with improved locomotor function after SCI [117–119], suggesting that nuclear β-catenin accumulation may promote motoneuron function.

### 3.4. Androgenic Crosstalk with IGF-1 and PI3K/Akt Signaling

Ligand-bound ARs activate PI3K/Akt signaling in muscle indirectly by stimulating the expression of (1) IGF-1 [113,120] and/or (2) other intracellular signaling molecules (e.g., Erk) that may activate or suppress components of this pathway independently of IGF-1 [121]. In support of this contention, the upstream promoter of the human *IGF-1* gene exhibits two AREs that activate IGF-1 expression [122]. In rodents, androgen administration increases IGF-1 and mechano growth factor (MGF) mRNA expression by several fold in skeletal muscle within seven days of administration [113], an effect that persists for at least one month [120]. Similarly, within one month of initiating TRT, older men exhibit a >two-fold increase in IGF-1 protein expression in muscle [123]. In cultured rodent myoblasts, T treatment stimulates protein accretion and mammalian target of rapamycin (mTOR) mRNA expression, effects that are abrogated by co-incubation with bicalutamide (competitive AR antagonist), rapamycin (mTOR inhibitor), or LY294002 (PI3K inhibitor) [121,124], indicating that T-induced protein accretion is dependent upon both AR activation and PI3K signaling. Similarly, dose-dependent phosphorylation of Akt, mTOR, S6 (subunit of S6K1), and S6K1 occurs in cultured rodent and C2C12 myotubes in response to increasing concentrations of T [125,126]. Importantly, these effects are also abolished by co-incubation with LY294002, Akt inhibitor VIII, or rapamycin [126], demonstrating dependence upon the PI3K signaling pathway. Further, complete androgen withdrawal was sufficient to reduce muscle IGF-1 mRNA and suppress Akt, mTOR, S6K1, and 4E-BP1 phosphorylation (downstream PI3K targets) by >50% in rodents, with androgen (nandrolone or DHT) treatment increasing these factors two-fold above gonadally-intact animals [125,127]. Interestingly, Serra et al. reported that orchectomy also increased RPTOR and reduced tuberous sclerosis complex protein 2 (TSC2) phosphorylation by >50%, changes associated with mTOR inhibition, while T treatment reversed these effects [128]. These findings indicate that androgens stimulate various IGF-1/PI3K/Akt signaling components in muscle and suggest that activation PI3K/Akt signaling influences androgen-mediated muscle hypertrophy. This contention is strengthened by the observation that MKR mice, which express a dominant negative IGF-1R in mature muscle fibers, exhibit attenuated hypertrophy of the highly androgen-sensitive LABC muscle in response to T treatment [128]. Regardless, IGF-1 and IGF-1R mRNA expression was not altered in animals receiving nandrolone for eight weeks after spinal cord transection, suggesting that androgens do not chronically stimulate IGF-1 expression in muscle in the absence of descending supraspinal input and/or mechanical strain [16].

### 3.5. Androgen Crosstalk with the Ubiquitin-Proteasome Pathway

Androgenic influence on FOXO expression and subsequent downstream signaling is evidenced by (1) increased total FOXO1 and FOXO3a protein and lower pFOXO3a in rodent muscle in response

to orchectomy (ORX) [125,128]; (2) 10- to 25-fold higher MAFbx and MuRF-1 mRNA expression in rodent skeletal muscle within seven days of ORX [128,129], an effect that persists for at least one month, albeit to a lesser magnitude over time [120,125]; and (3) the ability of androgen treatment to abolish these changes and prevent ORX-induced muscle atrophy [120,125,128,129]. Similarly, TRT suppresses ubiquitin-proteasome activity in the muscle of older men [130]. In C2C12 myoblasts and myotubes, androgen-induced suppression of MAFbx occurs indirectly via interactions among ligand-bound ARs and octamer binding transcription factor (Oct)-1 or Ankryin repeat domain protein 2 (Ankrd2), co-regulators of sex-steroid hormone induced transcriptional activity in target genes [131,132]. Interestingly, androgen treatment also attenuated muscle atrophy and the increases in FOXO1, MAFbx, and MuRF1 mRNA expression resulting from methylprednisolone administration after SCI [101], an effect that may be mediated by androgenic suppression of glucocorticoid receptor expression [120,133,134]. Alternatively, it is also possible that androgens indirectly influence FOXO signaling by stimulating PI3K/Akt signaling in muscle, given that FOXO1 and FOXO3a are downstream targets of pAkt signaling [62], although we are unaware of any study addressing this interesting possibility.

### 3.6. Androgenic Influence on PGC-1 $\alpha$ and PGC-1 $\beta$ Signaling after SCI

Testosterone stimulates muscle PGC-1 $\alpha$  expression via direct AR-mediated and/or ER-mediated pathways following aromatization to E<sub>2</sub>. As evidence, (1) castration lowered muscle PGC-1 $\alpha$  mRNA by 50% in male rodents and nandrolone treatment increased PGC-1 $\alpha$  mRNA >two-fold [125]; (2) ovariectomy lowered muscle PGC-1 $\alpha$  >70% in female rodents [135], while one week of E<sub>2</sub> replacement increased PGC-1 $\alpha$  mRNA and nuclear protein expression in postmenopausal women [136]; and (3) within eight days of initiating pharmacologic E<sub>2</sub> therapy, muscle PGC-1 $\alpha$  mRNA was increased by 30% in men [137]. As discussed above, PGC-1 $\alpha$  [16,54] and -1 $\beta$  expressions [74] are suppressed in response to spinal cord transection, an effect that may influence the slow-to-fast fiber transition [30] and/or mitochondrial dysfunction after SCI [138]. In this regard, chronic androgen treatment increased PGC-1 $\alpha$  mRNA >three-fold in the muscle of animals receiving spinal cord transection and prevented the SCI-induced reductions in total and nuclear PGC-1 $\alpha$  protein, changes that were accompanied by higher slow troponin mRNA and protein expression and lower fast troponin mRNA [16]. Similarly, Gregory et al. reported that androgen treatment attenuated the slow-to-fast fiber transition after spinal cord transection [20]. In addition, Wu et al. observed >two-fold higher PGC-1 $\beta$  mRNA expression in the muscle of spinal cord transected animals receiving nandrolone for eight weeks, although this change did not reach the level of statistical significance [16]. Regardless, the role of aromatase in mediating the influence of androgens on muscle PGC-1 $\alpha$  and/or PGC-1 $\beta$  expression remains to be determined after SCI.

## 4. Androgenic and Estrogenic Regulation of Motoneurons

The influence of SCI on somatic motoneuron structure depends largely upon injury characteristics and the muscle groups innervated (discussed in [27]). For example, Sengelaub et al. [17] and Byers et al. [18] reported no differences in quadriceps motoneuron counts or soma area four-weeks after mid-thoracic contusion SCI, although, dendritic length was decreased 40–50%. Similarly, four-weeks after mid-thoracic spinal transection, fewer dendrites (labeled via sciatic nerve) were present on spinal motoneuron, and dendritic arbor size and dendritic length were reduced in comparison to intact animals [28]. Reduced tibialis anterior and soleus motoneuron dendritic length was also observed four-months after mid-thoracic contusion SCI, with no difference in soma area [29]. Whereas, Bose et al. reported fewer motoneurons innervating the soleus at four-months after mid-thoracic contusion SCI, with residual motoneurons being relatively larger and having fewer total dendrites that exhibited longer dendritic lengths [27]. When taken together, these findings indicate that dendrite length is rapidly reduced after SCI, with the loss of relatively small motoneurons and short dendrites occurring thereafter.

ARs are expressed in the cytoplasm and nuclear regions of spinal motoneurons [86] in a roughly equal distribution among male and female rodents [85]. 5 $\alpha$ -reductase type II is highly expressed in several gray- and white-matter areas of the spinal cord [139], including spinal motoneurons [140]. Spinal cord homogenates and cultured NSC34 cells (immortalized motoneurons) actively convert T to DHT [141] in a manner that is ~three-times greater than that occurring in other central nervous system (CNS) regions [142] or the seminal vesicles, an androgen-sensitive tissue that highly expresses 5 $\alpha$ -reductase type II [143]. The neuronotrophic effects of androgens are evidenced by the ability of T and DHT to equally preserve motoneuron number and size in cultured rodent lumbosacral spinal cord segments [144]. Indeed, lumbosacral motoneurons innervating the quadriceps and other musculature are androgen responsive [145]. However, the androgen sensitivity of spinal motoneurons appears largely dependent upon the magnitude of AR expression in motoneurons and in the innervated skeletal muscle, given that (1) motoneurons innervating LABC (high AR expression) exhibit robust dendritic atrophy in response to ORX, which is completely prevented by T or DHT administration [146]; (2) motoneurons innervating quadriceps (relatively lower AR expression) do not exhibit dendritic atrophy in response to ORX [147]; and (3) transgenic AR overexpression in skeletal muscle increased somatic motoneuron androgenic responsiveness, evidenced by ORX-induced dendritic atrophy in normally non-androgen responsive motoneurons, which was completely prevented by T administration [147].

ER $\alpha$  and ER $\beta$  are also expressed in cytoplasmic and nuclear regions of spinal motoneurons [148,149] and cultured motoneurons actively synthesize E<sub>2</sub> in culture [149], owing to aromatase expression [148,149]. However, cultured rodent embryonic and adult spinal cord homogenates do not appear to synthesize E<sub>2</sub> when incubated with androstenedione [142] or T [141]. Regardless, E<sub>2</sub>-mediated preservation of motoneuron dendritic growth [150] is as robust as that resulting from T or DHT treatment [151] and is highly dependent upon motoneuronal ER $\alpha$  expression, at least during development [152]. In culture, E<sub>2</sub> treatment also improves spinal motoneuron cell survival during glutamate-induced toxicity, an effect that was not inhibited by ICI 182,780 (competitive ER $\alpha$ /ER $\beta$  agonist) [153], indicating that estrogen-mediated improvement in spinal motoneuron viability occurs independent of nuclear ER-signaling. In this regard, GPCR-30 (or G protein-coupled estrogen receptor-30) has been identified as a cell-surface/transmembrane ER that rapidly stimulates intracellular signaling [108] and E<sub>2</sub> has been shown to improve motoneuron viability during glucose-oxygen deprivation, an effect that was blocked by co-treatment with G15 (GPCR-30 inhibitor) [154].

#### 4.1. Influence of Androgens and Estrogens on Motoneuron Structure after SCI

As discussed above, altered dendritic length is a hallmark of SCI that has been observed in motoneurons innervating sublesional vastus lateralis [17,18], tibialis anterior [29], and soleus muscle [27]. In adult female rats, T treatment completely prevented the reduction in dendritic length of quadricep motoneurons resulting from SCI, without altering motoneuron counts, soma volume, or other motoneuron structural variables [18]. Whereas, DHT or E<sub>2</sub> treatment each attenuated the reduction in quadriceps dendritic length by 50–60% [17]. The functional consequences of preserved dendritic length after SCI remains to be determined. However, it is interesting to note that our laboratory has reported that T treatment slightly increased hindlimb locomotor recovery in male rodents subsequent to moderate-severe contusion SCI, with the largest benefit occurring in response to supraphysiologic T [15], while E<sub>2</sub> treatment is known to produce comparatively larger locomotor improvements in both male and female rodents after SCI [155].

#### 4.2. Molecular Pathways Underlying Androgen-Mediated Motoneuron Protection

Androgenic regulation of brain-derived neurotrophic factor (BDNF) and tyrosine receptor kinase (TrkB) (BDNF receptor) in spinal motoneurons appears particularly important for motoneuron anatomical preservation [156,157]. As evidence, both somatic motoneurons and the spinal nucleus of the bulbocavernosus (SNB) express BDNF and TrkB mRNA and protein [146,158], with >80% of

motoneuron dendrites identified as TrkB-positive [159]. In male rodents, ORX reduced BDNF mRNA and protein expressions in SNB [159] and in motoneurons innervating the quadriceps [158], while T treatment prevented these effects. BDNF regulates soma size independently of T, as evidenced by the ability of exogenous BDNF to maintain SNB motoneuron soma size in ORX male rats after bilateral axotomy [160]. In comparison, both BDNF and T appear necessary for the maintenance of SNB dendritic length, given that neither exogenous BDNF nor T independently prevented the reduction in SNB motoneuron dendritic length resulting from bilateral axotomy in ORX males, while co-treatment with BDNF and T increased dendritic length [161]. In females, T treatment also increased SNB motoneuron count by 50%, an effect that was prevented by the co-administration of TrkB-IgG [162]. These findings are particularly striking and suggest that androgen treatment may represent a means of stimulating BDNF/TrkB signaling, given the prevalence and severity of hypogonadism after SCI [91–93] and that the stimulation of motoneuron BDNF/TrkB signaling enhanced functional recovery in rodent SCI models [163].

In addition, estrogenic activation of GPCR-30 [108] or ER $\alpha$  [164] stimulates intercellular PI3K/Akt signaling, which promotes motoneuron survival [155]. As evidence, treatment of cultured spinal motoneurons with LY294002 (PI3K inhibitor) blocked the anti-apoptotic effects of E<sub>2</sub> treatment during glucose-oxygen deprivation, resulting in a 50% increase in apoptotic motoneurons [154]. Similarly, PC12 cell viability was reduced ~50% upon treatment with rapamycin (mTOR inhibitor), demonstrating the necessity of downstream PI3K/Akt/mTOR signaling for cell survival [165]. Interestingly, LY294002 co-administration suppressed E<sub>2</sub>-mediated voluntary locomotor recovery in male rodents after SCI [154], indicating that PI3K/Akt signaling influences locomotor recovery after SCI. Estrogens may also exert neuroprotection via other pathways that have been reviewed by others [155].

## 5. Activity-Based Physical Rehabilitation after SCI

After SCI, increasing focus has been placed on improving activity-dependent neuromuscular plasticity through the use of BWSTT, a therapy that involves robotic or manual placement of the impaired limbs into normal gait patterns on a slowly moving treadmill, or other ABTs (e.g., passive or functional electric stimulation cycling) [166]. Through intense repetitive practice, it is postulated that ABTs activate sublesional spinal networks that promote beneficial neuromuscular adaptations by retraining the CNS to recover task-specific motor activities, via stimulation of the central pattern generator (CPG) in the lumbosacral region of the spinal cord [166]. Indeed, a number of studies involving persons with motor-incomplete SCI indicate that BWSTT produces several functional benefits, including (1) improved temporal gait parameters associated with walking ability (e.g., increased number of steps, faster cadence, and improved muscle activation patterns) [167–177]; (2) improved muscle strength and rate of torque development in impaired limbs, and reduced detrimental co-activation of antagonist muscle groups [24,169,171,178–180]; and (3) reduced muscle atrophy [24,178,181–184] (Table 1). However, when data from well-controlled randomized clinical trials assessing BWSTT after SCI [179,185–188] are pooled, there appears to be only limited meaningful improvement in overground walking speed or distance [4,189–191], given that the minimal clinically important difference in walking speed is reported as 0.13 m/s in the SCI population [192]. This finding stresses the necessity of testing combinatory therapies that prime the neuromuscular system for better functional recovery when combined with BWSTT.

Preclinical studies also utilize ABTs to evaluate mechanisms underlying activity-dependent neuroplasticity after SCI and have observed locomotor and neuromuscular improvements in response to BWSTT (Table 2) [5]. However, there are considerable differences in the reported effects of BWSTT on locomotor and neuromuscular recovery in SCI rodents, in-part due to the influence of age and gender, the mechanism of producing SCI (i.e., transection, hemisection, or contusion), delay in initiating BWSTT, duration of therapy, and the methods of assessing neuromuscular recovery [5,193]. In general, better outcomes for locomotor recovery are observed in female rats with mild to moderate contusion

SCI, with training that begins seven to 14 days after injury and continues for at least eight weeks [5]. In this regard, female rodents have higher endogenous E<sub>2</sub> than males [194], which is important given that subphysiologic and physiologic E<sub>2</sub> treatment significantly improves open-field locomotor recovery in both male and female rodents after SCI, in-part, by reducing secondary apoptotic and inflammatory damage to the spinal cord [155].

### 5.1. Effects of ABTs on Muscle

In rodent SCI models, BWSTT produces relatively consistent improvements in muscle integrity, even following complete transection. As evidence, after spinal transection, the incorporation of BWSTT completely preserved the muscle mass:body mass ratio [195,196] and prevented ~55% of soleus fCSA loss [196]. Similarly, in a moderate-contusion SCI model, BWSTT produced 23% higher soleus fCSA and 38% higher soleus peak tetanic force in comparison with untrained SCI animals [197], with analogous effects reported by others [49,197–200]. Similarly, several case-report and cohort-studies have reported muscle responses in individuals with motor-incomplete SCI. For example, in persons with chronic SCI, four to six months of BWSTT increased vastus lateralis muscle fCSA [178,184]. Likewise, Jayaraman et al. reported that nine-weeks of BWSTT enhanced knee extensor and ankle plantar flexion voluntary muscle activation and increased plantar flexion peak torque by 43%, which accompanied a 15% increase in plantar flexor CSA [201], an important finding given that lower extremity strength is positively associated with walking function after SCI [42]. However, others have reported much less robust strength improvements [202,203] or no strength improvement [171] in response to BWSTT.

The structural improvements mentioned above appear to be influenced, in-part, by reduced catabolic signaling resulting from BWSTT. As evidence, in a rodent SCI model, three sessions of BWSTT suppressed >10 protein ubiquitination pathway genes, an effect accompanied by the full preservation of muscle mass [49]. Similarly, after spinal cord transection, five sessions of electrical stimulation of paralyzed muscle suppressed MAFbx and MuRF1 mRNA and myostatin mRNA in muscle [51]. Myostatin is a member of the transforming growth factor (TGF)- $\beta$  family and a muscle-derived negative regulator of muscle growth, which acts via the activin IIB receptors [204]. Additionally, muscle regeneration occurs in response to BWSTT after SCI, evidenced by the upregulation of myogenic regulatory factors and increased expression of Pax7 positive nuclei (a marker of satellite cell activation) [63,205], suggesting that BWSTT stimulates muscle anabolic signaling pathways. In this regard, IGF-1, MGF, IGF-1R, and several IGFBPs mRNA were increased 1.5 to >10-fold in rodent muscle and IGF-1 protein expression was increased >three-fold within seven days of initiating BWSTT after moderate-contusion SCI [63]. In contrast, other reports indicate that electrical stimulation of paralyzed muscle suppressed IGFBP-4 and -5 mRNA in muscle, without altering IGF-1 or MGF mRNA after spinal transection [51,206]. Similarly, no change in circulating IGF-1 was observed in persons with chronic SCI undergoing a comprehensive physical rehabilitation program involving one to two hours per week of bodyweight-supported locomotor training [207]. As such, the role of IGF-1 signaling in the muscle regenerative response to BWSTT requires further elucidation, especially given that SCI-induced downregulation of IRS1 limits IGF-1 mediated activation of PI3K/Akt signaling in muscle acutely after SCI [51].

In addition to muscle preservation, BWSTT is reported to reduce soleus fatigue and attenuate the slow-to-fast fiber transition occurring in rodent moderate-contusion SCI models [197]. Similarly, in persons with chronic SCI, four to six months of BWSTT partially reversed the slow-to-fast fiber transition, evidenced by increased oxidative fibers and fewer type IIx (glycolytic) fibers compared with the baseline [178,184]. Interestingly, lower *Mhy1*, *Mybph*, and *Myh4* gene expression (fast-twitch fiber markers) was apparent in rodent muscle within five-days of initiating BWSTT [49], indicating that reversal of the slow-to-fast fiber-type switch occurs rapidly with this physical rehabilitation modality. However, to our knowledge, changes in PGC-1 $\alpha$  or -1 $\beta$  have not been evaluated in response to BWSTT after SCI. Regardless, a five-fold increase in PGC-1 $\alpha$  mRNA in muscle was observed in men

with chronic motor-complete SCI within several hours of neuromuscular electrical stimulation of quadriceps [208] and a ~two-fold increase in PGC-1 $\alpha$  was present in men with chronic motor-complete SCI undergoing functional electric stimulation for durations of 16-weeks [209] to six-years [210], suggesting that increased PGC-1 $\alpha$  expression may underlie the slow-to-fast fiber-type reversal occurring in response to BWSTT.

### 5.2. Effects of ABTs on Motoneurons

In rodent SCI models, ABTs limit injury severity, evidenced by the preservation of myelin, axons, and collagen morphology and decreased lesion volume [198], and produce a host of anatomical and functional improvements to the motor unit [29,198,200,211–213]. For example, after spinal cord transection, BWSTT increases axonal regrowth [212], preserves motoneuron dendritic length, increases neuromuscular junction synaptic density in the lumbar motoneuron pool [29], and produces larger group Ia afferent-evoked monosynaptic excitatory postsynaptic potentials (EPSPs) in the ankle plantar flexors, an effect that is particularly prevalent in rats regaining the greatest stepping ability [213]. Similarly, after moderate-severe contusion SCI, BWSTT produced a beneficial reduction in the sprouting of small caliber afferent fibers and improved stepping patterns while on the treadmill [200], although open-field locomotor activity did not improve in this study, suggesting some limitation to functional recovery in more severe injury scenarios. Interestingly, Singh et al. induced a spinal transection at nine weeks following contusion SCI in a subgroup of rats that previously underwent BWSTT or no training and observed that kinematic improvements were maintained in BWSTT rats and worsened in untrained rats, indicating that functional improvement resulting from BWSTT occurred via neural networks originating below the lesion level [200]. Indeed, Cote et al. reported that after spinal transection, BWSTT facilitated lumbar spine motoneuron pool recruitment via improved reflex pathways resulting from afferent input [211].

In individuals with incomplete SCI, beneficial adaptations to spinal neuronal pathways have been demonstrated in response to BWSTT. For example, the soleus H-reflex phase-dependent modulation during walking normalizes homosynaptic facilitation, reverses homosynaptic depression, and improves the presynaptic inhibition of Ia afferents [214–216]. However, better functional recovery has also been associated with increased ankle dorsiflexor and knee extensor maximal motor-evoked potential, a probe of corticospinal tract excitability, in persons with motor-incomplete SCI undergoing BWSTT [180] and improved ankle dorsiflexor and plantar flexor muscle co-activation patterns accompany improved walking function in response to BWSTT [171], findings that indicate greater descending corticospinal drive. In this regard, improvements in the above-mentioned factors likely stem from the reorganization of both supraspinal and spinal cord neural circuits in response to BWSTT [214,217], with further research needed to resolve whether functional adaptations rely more heavily on improved cortical or spinal circuitry in individuals with SCI.

**Table 1.** Characteristics of Bodyweight Supported Locomotor Training in Human Spinal Cord Injury Studies.

Study	Intervention	Duration	Population	N	Outcomes
		Studies Assessing Gait			
Dobkin et al., 2007 [185]	Manual-assisted BWSTT vs. OG training	12 wk	38 ASIA B, 107 ASIA C&D	145	BWSTT increased walking speed from ~0.40 m/s at 2 weeks post-entry to 0.85 m/s for ASIA C&D. OG training increased walking speed from ~0.50 at 2 weeks post-entry to 0.84 m/s for ASIA C&D. Poor walking outcomes were observed for ASIA B participants.
Field-Fote et al., 2001 [167]	BWSTT with ES	3 days/wk, 12 wk	ASIA C	19	Walking speed increased from 0.12 to 0.21 m/s. <sup>a</sup>
Alcobendas-Maestro et al., 2012 [218]	Robotic-assisted BWSTT vs. OG training	3–6 mo	ASIA C&D	48 M/32F	Robotics-assisted BWSTT and OG training walking speed remained the same from baseline to post-training. Robotic-assisted BWSTT increased 6 min walk distance from 91 to 169 m. <sup>a</sup>
Alexeeva et al., 2011 [179]	BWS training on a fixed track vs. BWSTT vs. Comprehensive PT	3 days/wk 13 wk	ASIA C&D	30 M/5 F	BWS on a fixed track increased walking speed from 0.33 to 0.44 m/s. <sup>a</sup> BWSTT increased walking speed from 0.30 to 0.46 m/s. <sup>a</sup> PT increased walking speed from 0.41 to 0.51 m/s. <sup>a</sup>
Duffell et al., 2015 [202]	Robotic-assisted BWSTT	3 days/wk, 4 wk	ASIA C&D	19 M/7 F	Walking speed increased from ~0.25 to ~0.58 m/s. <sup>a</sup>
Esclarin-Ruzz et al., 2014 [219]	Robotic-assisted BWSTT + OG training (LKOGT) vs. Conventional OG training (OGT)	5 days/wk, 8 wk	ASIA C&D	59 M/24 F	LKOGT increased walking speed from 0.48 to 0.54 m/s and 6 min walk distance from 122 to 187 m <sup>b</sup> in participants with upper motor neuron injury. LKOGT increased walking speed from 0.4 to 0.46 m/s and 6 min walk distance from 82 to 157 m <sup>b</sup> in participants with lower motor neuron injury. OGT increased walking speed from 0.36 to 0.39 m/s and 6 min walk distance from 93 to 119 m in participants with upper motor neuron injury. OGT increased walking speed from 0.28 to 0.45 m/s and 6 min walk distance from 94 to 145 m in participants with lower motor neuron injury.
Field-Fote et al., 2005 [220]	Manual-assisted BWSTT (TM) vs. BWSTT + ES (TS) vs. BWS OG training + TS (OCS) vs. Robotic-assisted BWSTT (LR)	5 days/wk 12 wk	ASIA C&D	22 M/5 F	TM increased walking speed from ~0.07 to ~0.10. TS increased walking speed from ~0.12 to ~0.16 m/s. <sup>a</sup> OCS increased walking speed from ~0.14 to ~0.19 m/s. <sup>a</sup> LR increased walking speed from ~0.09 to ~0.11.
Field-Fote & Roach 2011 [186]	Manual-assisted BWSTT (TM) vs. BWSTT + ES (TS) vs. BWS OG training + TS (OCS) vs. Robotic-assisted BWSTT (LR)	5 days/wk, 12 wk	ASIA C&D	52 M/12 F	TM increased walk speed from 0.17 to 0.22 m/s <sup>a</sup> and 2 min distance from 22.1 to 23.0 m. TS increased walk speed from 0.18 to 0.23 m/s <sup>a</sup> and 2 min distance from 20.6 to 24.4 m. <sup>a</sup> OCS increased walk speed from 0.19 to 0.28 m/s <sup>a</sup> and 2 min distance from 24.0 to 38.3 m. <sup>ab</sup> LR increased walk speed from 0.17 to 0.18 m/s and 2 min distance from 16.8 to 17.9 m.
Gorassini et al., 2009 [169]	Manual-assisted BWSTT	5 days/wk, 14 wk	ASIA C&D	14 M/3 F	In 9 responders, walking speed increased from 0.31 to 0.35 m/s. <sup>a</sup> In 8 non-responders, there was no change in walking speed.
Harkema et al., 2012 [170]	Manual-assisted BWSTT	3 day/wk, 4 to 92 wks	ASIA C&D	148M/48 F	Walking speed increased from 0.31 to 0.51 m/s <sup>a</sup> and 6 min walk distance increased from 91 to 154 m. <sup>a</sup>

Table 1. Cont.

Study	Intervention	Duration	Population	N	Outcomes
Kapadia et al., 2014 [221]	Robotic-assisted BWSTT + ES	3 days/wk, 16 wk	ASIA C&D	13 M/3 F	Walking speed increased from 0.25 to 0.28 m/s and 6 min walk distance increased from 187.9 to 217.1 m. <sup>a</sup>
Knikou 2013 [214]	Manual-assisted BWSTT	5 days/wk, 1.5–3.5 mo	ASIA C&D	9 M/3 F	6 min walk distance increased from 36.25 to 39.05 m for ASIA C and from 252 to 279.5 m for ASIA D participants.
Krishnan et al., 2016 [171]	Robotic-assisted BWSTT	3 day/wk, 4 wk	ASIA C&D	8 M/8 F	Median walking speed increased from 0.58 to 0.66 m/s. <sup>a</sup> 6 min walking distance did not change.
Labruyere et al., 2014 [222]	Robotic-assisted BWSTT	4 days/wk, 4 wk	ASIA C&D	5 M/4 F	Walking speed increased from 0.62 to 0.66 m/s.
Lam et al., 2015 [223]	Robotic-assisted BWSTT with resistance (LR) vs. Robotic-assisted BWSTT only (LO)	3 days/wk, 12 wk	ASIA C&D	9 M/6 F	LR increased walking speed from 0.29 to 0.40 m/s. LO increased walking speed from 0.33 to 0.44 m/s.
Lucarelli et al., 2011 [187]	BWSTT vs. Conventional gait training	2 days/wk, 12 wk	ASIA C&D	20 M/10 F	BWSTT increased walking speed from 0.85 to 1.25 m/s <sup>a</sup> as well as increased cadence, distance, step length and swing phase. Conventional training did not improve gait quality or speed.
Morrison et al., 2018 [224]	Manual-assisted BWSTT	120 sessions	ASIA C&D	49 M/20 F	Median walking speed increased by 0.25 m/s. <sup>a</sup> Median 6 min walk distance increased by 66 m. <sup>a</sup>
Niu et al., 2014 [225]	Robotic-assisted BWSTT	3 days/wk, 4 wk	ASIA C&D	27 M/13 F	Walking speed increased in the low-walking capacity group from 0.12 to 0.15 m/s and in the high-walking capacity group from 0.84 to 0.97 m/s. 6 min walk distance did not change.
Nooijen et al., 2009 [172]	Manual-assisted BWSTT vs. Manual-assisted BWSTT with ES vs. OG training with ES vs. Robotic-assisted BWSTT	4 days/wk, 12 wk	ASIA C&D	40 M/11 F	All therapies led to small improvements in gait quality (increased cadence and step length) with no differences among groups.
Potsans et al., 2004 [188]	BWSTT with ES Cross-over design: treatment-control (AB); control-treatment (BA)	5 days/wk, 4 wk	ASIA C&D	12 M/2 F	In AB group, walking speed increased 0.23 m/s and 6 min walk distance increased 72.2 m. In BA group, walking speed increased 0.17 m/s and 6 min walk distance increased 63.8 m.
Thomas et al., 2005 [180]	Manual-assisted BWSTT	4 days/wk, 16 wk	ASIA C&D	8 M/2 F	Walking speed increased from 0.15 to 0.53 m/s <sup>a</sup> and 6 min walk distance increased from 34.2 to 167.6 m.
Varoqui et al., 2014 [203]	Robotic-assisted BWSTT	3 days/wk, 4 wk	ASIA C&D	14 M/ 1 F	Walking speed increased from 0.56 to 0.64 m/s <sup>a</sup> and 6 min walk distance did not change (207 to 209 m).
Winchester et al., 2005 [226]	Robotic-assisted BWSTT	3 days/wk 12 wk	ASIA C&D	4 M	Walking speed increased for 3 participants from 0.0 to 0.11, 0.0 to 0.81, 0.24 to 0.62 m/s and one remained unable to ambulate.
Wirz et al., 2005 [175]	Robotic-assisted BWSTT	4 days/wk, 8 wk	ASIA C&D	18 M/2 F	Walking speed increased from ~0.57 to ~0.48 m/s <sup>a</sup> and 6 min walk distance 120 to 160 m. <sup>a</sup>

**Table 1.** Cont.

Study	Intervention	Duration	Population	N	Outcomes
Wu et al., 2012 [227]	4 wk Robotic-assistance BWSTT + 4 wk Robotic-resistance BWSTT	3 days/wk, 8 wk	ASIA D	8 M/2 F	Walking speed increased from 0.67 to 0.76 m/s <sup>a</sup> and 6 min walk distance increased from 223 to 247 m. Step length and cadence increased. <sup>a</sup>
Studies Assessing Muscle					
Duffell et al., 2015 [202]	Robotic-assisted BWSTT	3 days/wk, 4 wk	ASIA C&D	19 M/7 F	Maximal isometric ankle dorsiflexion torque increased from 12.3 to 13.2 Nm. <sup>a</sup> but plantar flexion torque did not change (28.1 vs. 28.4 Nm).
Galen et al., 2014 [228]	Robotic-assisted BWSTT	5 days/wk, 6 wk	ASIA C&D	14 M/4 F	Percent peak torque increased 68% for hip flexion, 54% for hip extension, 93% for knee flexion and 71% for knee extension.
Gorassini et al., 2009 [169]	Manual-assisted BWSTT	5 days/wk, 14 wk	ASIA C&D	14 M/3 F	In 9 responders, peak electromyography activity increased from 67 to 135 $\mu$ V in the tibialis anterior muscle and 36 to 50 $\mu$ V in the hamstrings. In 8 non-responders, there was no change.
Jayaraman et al., 2008 [201]	Manual-assisted BWSTT	5 days/wk, 9 wk	ASIA C&D	4 M/1 F	Isometric knee extension strength increased 21%. Isometric plantar flexion strength increased 44%. Knee extension and plantar flexion voluntary muscle activation improved. Maximal CSA of the plantar flexors increased and 15%.
Krishnan et al., 2016 [171]	Robotic-assisted BWSTT	3 day/wk, 4 wk	ASIA C&D	8 M/8 F	BWSTT increased isometric ankle dorsiflexion by 20% and ankle plantar flexion by 22%.
Thomas et al., 2005 [180]	Manual-assisted BWSTT	4 days/wk, 16 wk	ASIA C&D	8 M/2 F	Peak electromyography activity averaged from four lower limb muscles increased during treadmill walking from 82.4 to 137.1 $\mu$ V.
Varoqueix et al., 2014 [203]	Robotic-assisted BWSTT	3 days/wk, 4 wk	ASIA C&D	14 M/1 F	Ankle dorsiflexion torque increased from 26.8 to 29.1 Nm <sup>a</sup> and ankle plantar flexion torque increased from 10.9 to 13.5 Nm. <sup>a</sup>

BWSTT = bodyweight supported treadmill training; CSA = cross-sectional area; ES = electrical stimulation; m = meter, min = minute; mo = month; OG = overground; PT = physical therapy; wk = week. Note: <sup>a</sup> indicates statistically different from baseline; <sup>b</sup> indicates statistically different between training groups.

**Table 2.** Characteristics of Bodyweight Supported Treadmill Training (BWSTT) in Rodent SCI Studies.

Study	Sex/Age	Injury Level	Start of Training	Training Duration	BBB wk 1	BBB End	Gait Outcome	Muscle/Electrophysiology
Studies Assessing BWSTT after Spinal Hemisection								
Maier et al., 2009 [229]	F/A	T8	1 wk	8 wk	~12	N/R	Stepping ↓	N/R
Battistuzzo et al., 2016 [230]	M/A	T10	1 wk	9 wk	N/R	N/R	Kinematics ↑	N/R
M/A	T10	1 wk	9 wk	N/R	N/R	N/R	G-CSA ↑	
Battistuzzo et al., 2017 [231]	M/A	T10	5 days	2.5 wk	N/R	N/R	Stepping ↑	N/R
Shah et al., 2013 [232]	N/R/N/R	T10	1 wk	4 wk	~3	111/6C	Kinematics ↑	G-CSA ↑
Goldsmith et al., 2008 [212]	N/R/A	T12						
Studies Assessing BWSTT after Mild Contusion SCI								
Nessler et al., 2006 [233]	F/Y	T9	1 wk	12 wk	13	14T/NoC	N/R	N/R
M/Y	T9–10	1 wk	4 wk	~4	13T/8C	N/R	N/R	
Oh et al., 2009 [234]								

Table 2. Cont.

Study	Sex/Age	Injury Level	Start of Training	Studies Assessing BWSTT after Moderate Contusion SCI	Training Duration	BBB wk 1	BBB End	Gait Outcome	Muscle/Electrophysiology
<b>Studies Assessing BWSTT after Moderate Contusion SCI</b>									
Stevens et al., 2006 [157]	F/Y	T8	1 wk	1 wk	~5	10T/6C	N/R	Sol F↑/ICSA↑	
Liu et al., 2008 [199]	F/Y	T8	8 days	12 wk	3–7	15T/11C	N/R	G-S CSA↑	
Nessler et al., 2006 [233]	F/Y	T9	1 wk	12 wk	9	11T/No C	N/R		
Shin et al., 2014 [255]	F/Y	T9	1 wk	8 wk	~6	~13T/~10C	N/R		
Wang et al., 2015 [29]	F/Y	T9	1 wk	16 wk	~7	~13T/~11C	N/R		
Singh et al., 2011 [200]	F/Y	T9–10	1 wk	8 wk	~5	~8T/~9C	N/R		
Bose et al., 2012 [198]	F/A	T8	1 wk	12 wk	~3	~15T/~11C	N/R	mass/bw↑	
Multon et al., 2003 [236]	F/A	T8	2–4 days	12 wk	~2	10T/8C	N/R		
Wu et al., 2016 [237]	F/A	T10	1 wk	4 wk	~5	~13T/~9C	N/R		
Foret et al., 2010 [238]	F/A	T10	1 day	4 wk	~2	~9T/~7C	N/R		
Ward et al., 2014 [239]	M/Y	T8	2 wk	12 wk	~7	~12T/~9C	Sol EMG↑		
Park et al., 2010 [240]	M/Y	T10	3 days	25 days	~2	11.5	N/R	N/R	
Liu et al., 2017 [241]	N/R/N/R	T9	1 wk	2 wk	N/R	N/R	Stepping↑	N/R	
<b>Studies Assessing BWSTT after Severe Contusion SCI</b>									
Hayashibe et al., 2016 [242]	F/Y	T8–9	1 wk	4 wk	<1	16T/10C	N/R		
Heng et al., 2009 [243]	F/Y	T9	42 days	8 wk	N/R	N/R	Stepping↑	N/R	
Nessler et al., 2006 [233]	F/Y	T9	1 wk	12 wk	4.5	~9T/No C	N/R		
Shirozaki et al., 2016 [244]	F/Y	T10	6 wk	8 wk	~1	4T/3C	N/R		
Robert et al., 2010 [245]	F/A	T7–8	2 wk	2 wk	~3	4T/3.5C	N/R		
Ichiyama et al., 2009 [246]	F/A	T10	30 days	8 wk	N/R	N/R	Gait not improved	N/R	
<b>Studies Assessing BWSTT after Spinal Transection</b>									
Petruska et al., 2007 [213]	F/N	T6–8	16 days	6 wk	N/R	N/R	Stepping↑	G EPSP↑	
Tillakarante et al., 2010 [247]	F/N	T7–8	26 days	8 wk	N/R	N/R	Stepping↑	N/R	
See et al., 2013 [248]	F/N	T8–9	3 wk	4 wk	N/R	N/R	Kinematics↑	N/R	
Timoszyk et al., 2005 [249]	F/N	N/R	64 days	40 days	N/R	N/R	Gait not improved	N/R	
Zhang et al., 2007 [250]	F/Y	T8	5 days	40 days	<1	~6.5T/~2C	N/R		
Lee et al., 2010 [251]	F/Y	T8	3 wk	42 wk	N/R	N/R	Gait not improved	N/R	
De Leon et al., 2006 [252]	F/Y	T9	3 wk	16 wk	N/R	N/R	Kinematics↑	N/R	
Moshonkhina et al., 2004 [253]	F/Y	T9	1 day	9 wk	N/R	N/R	Kinematics↑	N/R	
Kubasaki et al., 2008 [254]	F/N/N/R	T9	4 wk	20 wk	N/R	N/R	Gait not improved	N/R	
Fouad et al., 2000 [255]	B/A	T8	3 days	5 wk	~9	14T/14C	Kinematics↑	N/R	
Ihla et al., 2011 [196]	M/A	T8–9	6 days	9 wk	N/R	N/R	Sol ICSA↑	N/R	

Sex: B, both females and males; F, female; M, male; N/R, not reported; Age: A, adult; N, neonate; Y, young; Injury Level: T, thoracic; Start of Training: wk, week BBB end of training; T, trained; C, control SCI untrained; Other gait outcome: ↑ improvement; Muscle/Electrophysiology: bw, bodyweight EPSP evoked monosynaptic excitatory postynaptic potentials; F, force; ICSA, fiber cross-sectional area; G, gastrocnemius; G-S, gastrocnemius-soleus; ↑, increased; Sol, soleus; N/R, not reported. Note: The BBB scale ranges from 0–21 and is used to evaluate functional locomotor recovery ranging from no observable movement (0) to consistent weight-supported plantar stepping with coordinated gait (21).

While the molecular signals regulating BWSTT-induced motoneuron recovery after SCI require further elucidation, there is growing evidence that several inducible neurotrophic factors influence neuroplasticity [211]. For example, an upregulation of BDNF and TrkB (BDNF receptor) mRNA and protein has been observed in the skeletal muscle and spinal cord of healthy animals in response to voluntary wheel running or forced treadmill running, with BDNF protein levels increasing to a greater degree in the spinal cord than in the soleus [237,256,257]. In this regard, BDNF and TrkB both undergo retrograde transport from skeletal muscle to the spinal cord [258], an effect that may mediate locomotor recovery after SCI by improving synaptic transmission and plasticity, axon regeneration, and motoneuron survival [259]. Indeed, in rodent SCI models, BWSTT upregulates BDNF mRNA and protein in skeletal muscle and the spinal cord [29,196,198,211,237,260–267] and TrkB protein in the lumbar spinal cord [237,257]. Interestingly, Leech and Hornby also observed increased circulating BDNF in persons with motor-incomplete SCI undergoing treadmill training, with high-intensity treadmill exercise (performed at 100% peak gait speed) resulting in the larger BDNF increases than exercise performed at 33% or 66% peak gait speed [268]. In addition, BSWTT upregulated glial cell derived neurotrophic factor (GDNF) protein in the lumbar spinal cord, which was positively associated with the facilitation of motoneuron excitability [211].

Neurotrophin-3 (NT-3) is another endogenous neurotrophin that regulates synaptic transmission, promotes neuromuscular junction maturation, and improves the survival and function of sensory neurons via the activation of TrkC (receptor), both of which are expressed in the spinal cord [269–273]. Indeed, recent results from Fang et al. indicate that co-treatment with BDNF/TrkB and NT-3/TrkC promoted motor recovery in a rodent SCI model [274]. NT-3 is produced in the spinal cord and NT-3 mRNA and protein levels are upregulated after seven days of voluntary treadmill and wheel running in healthy rodents [256,262,265]. Similarly, following SCI, rodents exhibit increased NT-3 mRNA and protein in the spinal cord within seven days of initiating BWSTT [262,263,265,266]. Interestingly, Ying et al. reported that BWSTT did not increase spinal cord NT-3 protein expression in adult male rats after spinal cord hemisection [266], while Cote et al. observed increased NT-3 protein levels in the lumbar and thoracic spinal cord after four weeks of BWSTT in adult female rats with complete transection [211], suggesting that sex differences may exist in the NT-3 response to BWSTT. In this regard, E<sub>2</sub> treatment increases NT-3 levels in several CNS regions [275], although we are unaware of any study evaluating whether spinal cord NT-3 expression is regulated via E<sub>2</sub>-mediated mechanisms. BWSTT is also reported to upregulate genes involved in neuroplasticity (e.g., *Arc* and *Nrcam*) and angiogenesis (e.g., *Adam8* and *Tie1*), which may be important given that improved neurovascular remodeling has the potential to improve locomotor function after SCI [235].

## 6. Testosterone Adjuvant to BWSTT

We are unaware of published results from any randomized study evaluating T treatment as an adjuvant to BWSTT. However, at least one ongoing study is evaluating TRT as an adjuvant to electric stimulation-based resistance training in men with motor-complete SCI [276]. A single case-report has also indicated that a man with motor-complete SCI exhibited increased thigh muscle CSA in response to twice-weekly neuromuscular electric stimulation-based resistance training, when combined with adjuvant TRT [13]. In addition, our preliminary data indicates that the combination of testosterone-enanthate (TE), a long-acting T ester [277], and quadrupedal BWSTT (consisting of two 20-min bouts performed twice daily, five-days per week for seven-weeks) promoted more complete neuromuscular restoration than TE-alone in our rodent moderate-severe contusion SCI model [278]. Specifically, the incorporation of TE+BWSTT after SCI produced near-complete restoration of the sublesional muscle mass:body mass ratio, completely prevented the slow-to-fast fiber-type transition occurring in the soleus, attenuated the reduction in soleus fCSA by >50%, and maintained isolated soleus muscle force mechanics near the level of intact control animals. Impressively, 100% of SCI animals receiving TE+BWSTT regained the ability to perform occasional voluntary overground weight-supported hindlimb plantar stepping within seven-weeks of initiating therapy, while 0/11 SCI

animals and only 2/10 of SCI animals receiving TE-alone regained this ability. As such, our preliminary data appear to support the contention that a combinatory strategy involving BWSTT with adjuvant TE promotes musculoskeletal and neuromuscular improvement in male rodents after moderate-severe contusion SCI.

#### Potential Side-Effects of TRT

TRT is approved for the treatment of hypogonadism in adult men and has been shown to increase muscle protein synthesis in women [279]. However, given its androgenic potential, chronic TRT remains controversial for women, at least when administered in the doses necessary to produce musculoskeletal benefit in males. This should not detract from TRT research in relation to SCI because men represent ~80% of new SCI cases [280] and many of these men will develop hypogonadism of an indefinite duration [91–93]. Regardless, careful evaluation of TRT safety and efficacy is necessary prior to implementation of this therapy after SCI.

To-date, meta-analyses have confirmed that TRT produces three adverse events (AEs) in non-neurologically impaired adult men: (1) polycythemia, which occurs in ~6% of men treated with TRT; (2) a higher number of cumulative prostate-related events (discussed below); and (3) a slight decrease in HDL cholesterol, which is of unknown clinical significance [281]. The development of polycythemia in men receiving TRT has raised concerns regarding the cardiovascular safety of TRT, especially when taken in context with findings from the Testosterone in Older Men with Mobility Limitations (TOM) trial [282] and from two retrospective studies that indicated increase cardiovascular risk in hypogonadal men receiving TRT [283,284]. In this regard, the TOM trial was discontinued upon recommendation of the Data Safety Monitoring Board due to a higher prevalence of cardiovascular-related AEs in the TRT versus placebo groups [282]. However, this trial received criticism because of the relatively poor classification of cardiovascular AEs [285]. In comparison, the NIH-funded T-trials, which represent the largest randomized clinical trials to-date evaluating the safety and efficacy of TRT, reported no differences in adjudicated cardiovascular AEs in hypogonadal men receiving TRT versus placebo [11]. Similarly, heavy scientific criticism and numerous calls for retraction [286] accompanied the retrospective studies from Vigen et al. [284] and Finkel et al. [283] that reported increased cardiovascular risk in hypogonadal men receiving TRT. Indeed, the aforementioned findings remain in direct conflict with findings from the largest meta-analyses on the topic, which reported that TRT does not increase cardiovascular risk in men enrolled in well-controlled clinical trials [287,288], and with findings from the largest retrospective study ( $n = 83,010$  men with low T) that indicated TRT reduced all-cause mortality by 56% and MI and stroke risk by 24–36% in comparison with untreated hypogonadal men [289]. Of note, the potential cardiovascular responses to TRT have not been extensively evaluated in the SCI population. However, in a small clinical trial, La Fountaine et al. reported that QT<sub>a</sub> interval variability was higher in hypogonadal men with SCI than in eugonadal men with SCI, and that TRT normalized QT<sub>a</sub> interval variability, suggestive of reduced arrhythmia risk [290].

The risk for increased cumulative prostate-related events also merits mention because prostate growth and worsened urinary symptoms resulting from TRT have the potential to worsen bladder dysfunction, which is already common in the SCI population [291]. In this regard, the prostate-related AEs associated with TRT appear to be driven primarily by the 5 $\alpha$ -reduction of T to DHT [8]. As evidence, we have reported that older hypogonadal men receiving TE-alone exhibited a 43% increase in prostate volume over a period of 12-months, while men receiving TE plus finasteride exhibited no change in prostate volume [102]. In comparison, 5 $\alpha$ -reductase inhibition did not prevent the musculoskeletal or lipolytic benefits resulting from TRT in our trial [102] or others [292,293], indicating that finasteride co-treatment improves the prostate-related safety profile of TRT without inhibiting musculoskeletal efficacy in older men. The safety and efficacy of TE plus finasteride treatment in men with SCI currently remains unknown, although an ongoing clinical trial in our laboratory is evaluating this promising combinatory therapy in hypogonadal men with SCI [294].

In addition, it is important to note that a 15-yr retrospective study of 150,000 men reported that TRT was not associated with prostate cancer [295] and that no meta-analysis to-date has reported increased prostate cancer risk resulting from TRT [8].

Several less common risks are also associated with TRT, which we have previously reviewed [296], including: pain or bleeding at injection sites, skin reactions, fluid retention, breast tenderness, gynecomastia, and liver disorders. Importantly, these side-effects remain putative [8] and have not been confirmed by meta-analysis [281]. However, one potential risk that merits mention is the possibility that TRT may cause or worsen obstructive sleep apnea [297], a condition that is relatively common in tetraplegic men with SCI [298]. As such, need exists to determine TRT safety in men with SCI who display obstructive sleep apnea, especially given the higher sleep apnea prevalence in non-neurologically impaired men receiving TRT [297].

## 7. Conclusions

Upregulation of FOXO signaling occurs in the immediate days to weeks after SCI, an effect that likely influences the rapid muscle loss in this population. Similarly, muscle PGC-1 $\alpha$  and -1 $\beta$  are reduced in response to SCI, underlying the slow-to-fast fiber change and impaired mitochondrial function subsequent to SCI. In comparison, downregulation of IGF-1 and PI3K/Akt signaling occurs more chronically after SCI. These molecular changes are precipitated by the spinal injury and subsequent disuse, but may also be exacerbated by low T that occurs in many men with SCI. T promotes muscle anabolism via direct AR-mediated genomic signaling and/or via cross-talk with IGF-1 and the PI3k/Akt signaling pathway. T may also promote anticatabolic effects in muscle by directly or indirectly suppressing FOXO signaling. Further, androgen treatment increases PGC-1 $\alpha$  in muscle and attenuates the slow-to-fast muscle fiber-type transition occurring in response to spinal transection. In addition, T improves the preservation of motoneuron dendritic length after SCI directly via AR-mediated mechanisms and/or indirectly, following aromatization to E<sub>2</sub>. Regardless, these improvements appear to result in only minor improvement in locomotor recovery in rodents after moderate-severe contusion SCI, likely because only limited descending corticospinal input remains. In comparison, BWSTT improves descending corticospinal drive and/or facilitates reorganization of spinal cord neural circuitry below the lesion, which produces neuromuscular improvement and some restoration of musculoskeletal integrity. However, findings from well-controlled randomized clinical trials indicate that BWSTT only promotes limited clinically meaningful improvement in voluntary locomotor recovery in humans after SCI. Interestingly, activity-mediated neuromuscular plasticity appears to rely, in-part, upon the upregulation of BDNF/TrkB in the spinal cord. Androgen/AR signaling is required for BDNF/TrkB-mediated dendritic restoration in androgen sensitive motoneurons in the lumbosacral spinal cord, suggesting that T treatment may enhance activity-mediated neuromuscular plasticity after SCI. Indeed, our preliminary data supports this contention, given that adult male rodents receiving TE adjuvant to BWSTT exhibited profound musculoskeletal and neuromuscular improvement and recovery of voluntary weight-supported overground plantar stepping after moderate-severe contusion SCI. Elucidation of the molecular mechanisms underlying these neuromusculoskeletal and locomotor improvements will assist in validating our hypothesis and will improve the likelihood for the translation of this promising multimodal therapeutic strategy.

**Author Contributions:** Conceptualization, D.M.O., J.L., F.Y., S.E.B., and J.F.Y.; Methodology, D.M.O. and J.F.Y.; Formal Analysis, D.M.O. and J.F.Y.; Investigation, D.M.O., J.L., F.Y., S.E.B., and J.F.Y.; Resources, F.Y., S.E.B., and J.F.Y.; Data Curation, D.M.O. and J.F.Y.; Writing—Original Draft Preparation, D.M.O. and J.F.Y.; Writing—Review & Editing, J.L., F.Y., and S.E.B.; Visualization, D.M.O. and J.F.Y.; Supervision, F.Y., S.E.B., and J.F.Y.; Project Administration, D.M.O.; Funding Acquisition, F.Y. and J.F.Y.

**Funding:** This work was supported by the Office of Research and Development, Rehabilitation Research and Development Service, Department of Veterans Affairs (I101RX001449-01A1 and a Presidential Early Career Award for Scientists and Engineers (PECASE) #B9280-O to JFY and I1K1RX002327-01A1 to DMO), by a Paralyzed Veterans of America (PVA) Fellowship (#2939 to FY), and by resources provided by the North Florida/South Georgia Veterans Health System. The work reported herein does not represent the views of the US Department of Veterans Affairs or the US Government.

**Conflicts of Interest:** The authors declare no conflict of interest.

## Abbreviations

ABT	activity-based therapies
AR	androgen receptor
ARE	androgen response element
BDNF	brain-derived neurotrophic factor
BWSTT	bodyweight-supported treadmill training
CNS	central nervous system
CSA	cross-sectional area
DHT	dihydrotestosterone
E <sub>2</sub>	estradiol
EPSP	excitatory postsynaptic potential
ER	estrogen receptor
ERE	estrogen response element
fCSA	fiber cross-sectional area
FOXO	forkhead box O
GPCR	G-protein-coupled receptor
GSK3 $\beta$	glycogen synthase kinase 3 $\beta$
IGF-1	insulin-like growth factor
IGF-1R	insulin-like growth factor receptor
IGFBP	insulin-like growth factor binding protein
IRS1	insulin receptor substrate-1
LABC	levator ani/bulbocavernosus
MAFbx	muscle atrophy F-box or atrogin-1
MGF	mechano growth factor
MHC	myosin heavy chain
mTOR	mammalian target of rapamycin
MuRF1	muscle ring finger-1
NT-3	neurotrophin-3
ORX	orchectomy
PGC-1 $\alpha$	peroxisome proliferator-activated receptor gamma co-activator-1 $\alpha$
PGC-1 $\beta$	peroxisome proliferator-activated receptor gamma co-activator-1 $\beta$
PI3K	phosphatidyl inositol-3 kinase
SCI	spinal cord injury
SHBG	sex-hormone binding globulin
SNB	spinal nucleus of the bulbocavernosus
T	testosterone
TCF-4	T-cell factor-4
TE	testosterone enanthate
TrkB	tyrosine receptor kinase B
TrkC	tyrosine receptor kinase C
TRT	testosterone replacement therapy

## References

1. Beattie, M.S.; Farooqui, A.A.; Bresnahan, J.C. Review of current evidence for apoptosis after spinal cord injury. *J. Neurotrauma* **2000**, *17*, 915–925. [[CrossRef](#)] [[PubMed](#)]

2. Hilton, B.J.; Moulson, A.J.; Tetzlaff, W. Neuroprotection and secondary damage following spinal cord injury: Concepts and methods. *Neurosci. Lett.* **2017**, *652*, 3–10. [[CrossRef](#)] [[PubMed](#)]
3. Kwon, B.K.; Tetzlaff, W.; Grauer, J.N.; Beiner, J.; Vaccaro, A.R. Pathophysiology and pharmacologic treatment of acute spinal cord injury. *Spine J.* **2004**, *4*, 451–464. [[CrossRef](#)] [[PubMed](#)]
4. Morawietz, C.; Moffat, F. Effects of locomotor training after incomplete spinal cord injury: A systematic review. *Arch. Phys. Med. Rehabil.* **2013**, *94*, 2297–2308. [[CrossRef](#)] [[PubMed](#)]
5. Battistuzzo, C.R.; Callister, R.J.; Callister, R.; Galea, M.P. A systematic review of exercise training to promote locomotor recovery in animal models of spinal cord injury. *J. Neurotrauma* **2012**, *29*, 1600–1613. [[CrossRef](#)] [[PubMed](#)]
6. Behrman, A.L.; Ardolino, E.M.; Harkema, S.J. Activity-based therapy: From basic science to clinical application for recovery after spinal cord injury. *J. Neurol. Phys. Ther.* **2017**, *41* (Suppl. S3), S39–S45. [[CrossRef](#)] [[PubMed](#)]
7. Sullivan, S.D.; Nash, M.S.; Tefera, E.; Tinsley, E.; Blackman, M.R.; Groah, S. Prevalence and etiology of hypogonadism in young men with chronic spinal cord injury: A cross-sectional analysis from two university-based rehabilitation centers. *PM&R* **2017**, *9*, 751–760.
8. Borst, S.E.; Yarrow, J.F. Injection of testosterone may be safer and more effective than transdermal administration for combating loss of muscle and bone in older men. *Am. J. Physiol. Endocrinol. Metab.* **2015**, *308*, E1035–E1042. [[CrossRef](#)] [[PubMed](#)]
9. Cheung, A.S.; Gray, H.; Schache, A.G.; Hoermann, R.; Lim Joon, D.; Zajac, J.D.; Pandy, M.G.; Grossmann, M. Androgen deprivation causes selective deficits in the biomechanical leg muscle function of men during walking: A prospective case-control study. *J. Cachexia Sarcopenia Muscle* **2017**, *8*, 102–112. [[CrossRef](#)] [[PubMed](#)]
10. Skinner, J.W.; Oztel, D.M.; Bowser, A.; Nargi, D.; Agarwal, S.; Peterson, M.D.; Zou, B.; Borst, S.E.; Yarrow, J.F. Muscular responses to testosterone replacement vary by administration route: A systematic review and meta-analysis. *J. Cachexia Sarcopenia Muscle* **2018**. [[CrossRef](#)] [[PubMed](#)]
11. Snyder, P.J.; Bhasin, S.; Cunningham, G.R.; Matsumoto, A.M.; Stephens-Shields, A.J.; Cauley, J.A.; Gill, T.M.; Barrett-Connor, E.; Swerdloff, R.S.; Wang, C.; et al. Effects of testosterone treatment in older men. *N. Engl. J. Med.* **2016**, *374*, 611–624. [[CrossRef](#)] [[PubMed](#)]
12. Bauman, W.A.; Cirigliaro, C.M.; La Fountaine, M.F.; Jensen, A.M.; Wecht, J.M.; Kirshblum, S.C.; Spungen, A.M. A small-scale clinical trial to determine the safety and efficacy of testosterone replacement therapy in hypogonadal men with spinal cord injury. *Horm. Metab. Res.* **2011**, *43*, 574–579. [[CrossRef](#)] [[PubMed](#)]
13. Moore, P.D.; Georgey, A.S.; Wade, R.C.; Khalil, R.E.; Lavis, T.D.; Khan, R.; Adler, R.A. Neuromuscular electrical stimulation and testosterone did not influence heterotopic ossification size after spinal cord injury: A case series. *World J. Clin. Cases* **2016**, *4*, 172–176. [[CrossRef](#)] [[PubMed](#)]
14. Yarrow, J.F.; Phillips, E.G.; Conover, C.F.; Bassett, T.E.; Chen, C.; Teurlings, T.; Vasconez, A.; Alerte, J.; Prock, H.; Jiron, J.M.; et al. Testosterone plus finasteride prevents bone loss without prostate growth in a rodent spinal cord injury model. *J. Neurotrauma* **2017**, *34*, 2972–2981. [[CrossRef](#)] [[PubMed](#)]
15. Yarrow, J.F.; Conover, C.F.; Beggs, L.A.; Beck, D.T.; Oztel, D.M.; Balaez, A.; Combs, S.M.; Miller, J.R.; Ye, F.; Aguirre, J.I.; et al. Testosterone dose dependently prevents bone and muscle loss in rodents after spinal cord injury. *J. Neurotrauma* **2014**, *31*, 834–845. [[CrossRef](#)] [[PubMed](#)]
16. Wu, Y.; Zhao, J.; Zhao, W.; Pan, J.; Bauman, W.A.; Cardozo, C.P. Nandrolone normalizes determinants of muscle mass and fiber type after spinal cord injury. *J. Neurotrauma* **2012**, *29*, 1663–1675. [[CrossRef](#)] [[PubMed](#)]
17. Sengelaub, D.R.; Han, Q.; Liu, N.K.; Maczuga, M.A.; Szalavari, V.; Valencia, S.A.; Xu, X.M. Protective effects of estradiol and dihydrotestosterone following spinal cord injury. *J. Neurotrauma* **2018**, *35*, 825–841. [[CrossRef](#)] [[PubMed](#)]
18. Byers, J.S.; Huguenard, A.L.; Kuruppu, D.; Liu, N.K.; Xu, X.M.; Sengelaub, D.R. Neuroprotective effects of testosterone on motoneuron and muscle morphology following spinal cord injury. *J. Comp. Neurol.* **2012**, *520*, 2683–2696. [[CrossRef](#)] [[PubMed](#)]
19. Ung, R.V.; Rouleau, P.; Guertin, P.A. Effects of co-administration of clenbuterol and testosterone propionate on skeletal muscle in paraplegic mice. *J. Neurotrauma* **2010**, *27*, 1129–1142. [[CrossRef](#)] [[PubMed](#)]
20. Gregory, C.M.; Vandenoever, K.; Huang, H.F.; Ottenweller, J.E.; Dudley, G.A. Effects of testosterone replacement therapy on skeletal muscle after spinal cord injury. *Spinal Cord* **2003**, *41*, 23–28. [[CrossRef](#)] [[PubMed](#)]

21. Schiaffino, S.; Sandri, M.; Murgia, M. Activity-dependent signaling pathways controlling muscle diversity and plasticity. *Physiology* **2007**, *22*, 269–278. [[CrossRef](#)] [[PubMed](#)]
22. Thomas, C.K.; Bakels, R.; Klein, C.S.; Zijdewind, I. Human spinal cord injury: Motor unit properties and behaviour. *Acta Physiol.* **2014**, *210*, 5–19. [[CrossRef](#)] [[PubMed](#)]
23. Klein, C.S.; Hager-Ross, C.K.; Thomas, C.K. Fatigue properties of human thenar motor units paralysed by chronic spinal cord injury. *J. Physiol.* **2006**, *573*, 161–171. [[CrossRef](#)] [[PubMed](#)]
24. Jayaraman, A.; Gregory, C.M.; Bowden, M.; Stevens, J.E.; Shah, P.; Behrman, A.L.; Vandenborne, K. Lower extremity skeletal muscle function in persons with incomplete spinal cord injury. *Spinal Cord* **2006**, *44*, 680–687. [[CrossRef](#)] [[PubMed](#)]
25. Hager-Ross, C.K.; Klein, C.S.; Thomas, C.K. Twitch and tetanic properties of human thenar motor units paralyzed by chronic spinal cord injury. *J. Neurophysiol.* **2006**, *96*, 165–174. [[CrossRef](#)] [[PubMed](#)]
26. Barbeau, H.; Nadeau, S.; Garneau, C. Physical determinants, emerging concepts, and training approaches in gait of individuals with spinal cord injury. *J. Neurotrauma* **2006**, *23*, 571–585. [[CrossRef](#)] [[PubMed](#)]
27. Bose, P.; Parmer, R.; Reier, P.J.; Thompson, F.J. Morphological changes of the soleus motoneuron pool in chronic midthoracic contused rats. *Exp. Neurol.* **2005**, *191*, 13–23. [[CrossRef](#)] [[PubMed](#)]
28. Gazula, V.R.; Roberts, M.; Luzzio, C.; Jawad, A.F.; Kalb, R.G. Effects of limb exercise after spinal cord injury on motor neuron dendrite structure. *J. Comp. Neurol.* **2004**, *476*, 130–145. [[CrossRef](#)] [[PubMed](#)]
29. Wang, H.; Liu, N.K.; Zhang, Y.P.; Deng, L.; Lu, Q.B.; Shields, C.B.; Walker, M.J.; Li, J.; Xu, X.M. Treadmill training induced lumbar motoneuron dendritic plasticity and behavior recovery in adult rats after a thoracic contusive spinal cord injury. *Exp. Neurol.* **2015**, *271*, 368–378. [[CrossRef](#)] [[PubMed](#)]
30. Biering-Sorensen, B.; Kristensen, I.B.; Kjaer, M.; Biering-Sorensen, F. Muscle after spinal cord injury. *Muscle Nerve* **2009**, *40*, 499–519. [[CrossRef](#)] [[PubMed](#)]
31. Moore, C.D.; Craven, B.C.; Thabane, L.; Laing, A.C.; Frank-Wilson, A.W.; Kontulainen, S.A.; Papaioannou, A.; Adachi, J.D.; Giangregorio, L.M. Lower-extremity muscle atrophy and fat infiltration after chronic spinal cord injury. *J. Musculoskelet. Neuronal Interact.* **2015**, *15*, 32–41. [[PubMed](#)]
32. Gorgey, A.S.; Dudley, G.A. Skeletal muscle atrophy and increased intramuscular fat after incomplete spinal cord injury. *Spinal Cord* **2007**, *45*, 304–309. [[CrossRef](#)] [[PubMed](#)]
33. Castro, M.J.; Apple, D.F., Jr.; Hillegass, E.A.; Dudley, G.A. Influence of complete spinal cord injury on skeletal muscle cross-sectional area within the first 6 months of injury. *Eur. J. Appl. Physiol. Occup. Physiol.* **1999**, *80*, 373–378. [[CrossRef](#)] [[PubMed](#)]
34. Shah, P.K.; Stevens, J.E.; Gregory, C.M.; Pathare, N.C.; Jayaraman, A.; Bickel, S.C.; Bowden, M.; Behrman, A.L.; Walter, G.A.; Dudley, G.A.; et al. Lower-extremity muscle cross-sectional area after incomplete spinal cord injury. *Arch. Phys. Med. Rehabil.* **2006**, *87*, 772–778. [[CrossRef](#)] [[PubMed](#)]
35. Castro, M.J.; Apple, D.F., Jr.; Staron, R.S.; Campos, G.E.; Dudley, G.A. Influence of complete spinal cord injury on skeletal muscle within 6 mo of injury. *J. Appl. Physiol.* **1999**, *86*, 350–358. [[CrossRef](#)] [[PubMed](#)]
36. Gregory, C.M.; Vandenborne, K.; Castro, M.J.; Dudley, G.A. Human and rat skeletal muscle adaptations to spinal cord injury. *Can. J. Appl. Physiol.* **2003**, *28*, 491–500. [[CrossRef](#)] [[PubMed](#)]
37. Phillips, E.G.; Beggs, L.A.; Ye, F.; Conover, C.F.; Beck, D.T.; Oztel, D.M.; Ghosh, P.; Bassit, A.C.F.; Borst, S.E.; Yarrow, J.F. Effects of pharmacologic sclerostin inhibition or testosterone administration on soleus muscle atrophy in rodents after spinal cord injury. *PLoS ONE* **2018**, *13*, e0194440. [[CrossRef](#)] [[PubMed](#)]
38. Talmadge, R.J.; Roy, R.R.; Edgerton, V.R. Persistence of hybrid fibers in rat soleus after spinal cord transection. *Anat. Rec.* **1999**, *255*, 188–201. [[CrossRef](#)]
39. Talmadge, R.J.; Roy, R.R.; Edgerton, V.R. Prominence of myosin heavy chain hybrid fibers in soleus muscle of spinal cord-transected rats. *J. Appl. Physiol.* **1995**, *78*, 1256–1265. [[CrossRef](#)] [[PubMed](#)]
40. Thomas, C.K.; Zaidner, E.Y.; Calancie, B.; Broton, J.G.; Bigland-Ritchie, B.R. Muscle weakness, paralysis, and atrophy after human cervical spinal cord injury. *Exp. Neurol.* **1997**, *148*, 414–423. [[CrossRef](#)] [[PubMed](#)]
41. Gaviria, M.; Ohanna, F. Variability of the fatigue response of paralyzed skeletal muscle in relation to the time after spinal cord injury: Mechanical and electrophysiological characteristics. *Eur. J. Appl. Physiol. Occup. Physiol.* **1999**, *80*, 145–153. [[CrossRef](#)] [[PubMed](#)]
42. DiPiro, N.D.; Holthaus, K.D.; Morgan, P.J.; Embry, A.E.; Perry, L.A.; Bowden, M.G.; Gregory, C.M. Lower extremity strength is correlated with walking function after incomplete SCI. *Top. Spinal Cord Inj. Rehabil.* **2015**, *21*, 133–139. [[CrossRef](#)] [[PubMed](#)]

43. Gregory, C.M.; Bowden, M.G.; Jayaraman, A.; Shah, P.; Behrman, A.; Kautz, S.A.; Vandenborne, K. Resistance training and locomotor recovery after incomplete spinal cord injury: A case series. *Spinal Cord* **2007**, *45*, 522–530. [CrossRef] [PubMed]
44. Yarar-Fisher, C.; Bickel, C.S.; Windham, S.T.; McLain, A.B.; Bamman, M.M. Skeletal muscle signaling associated with impaired glucose tolerance in spinal cord-injured men and the effects of contractile activity. *J. Appl. Physiol.* **2013**, *115*, 756–764. [CrossRef] [PubMed]
45. Yarar-Fisher, C.; Bickel, C.S.; Kelly, N.A.; Windham, S.T.; McLain, A.B.; Bamman, M.M. Mechanosensitivity may be enhanced in skeletal muscles of spinal cord-injured versus able-bodied men. *Muscle Nerve* **2014**, *50*, 599–601. [CrossRef] [PubMed]
46. Panisset, M.G.; Galea, M.P.; El-Ansary, D. Does early exercise attenuate muscle atrophy or bone loss after spinal cord injury? *Spinal Cord* **2016**, *54*, 84–92. [CrossRef] [PubMed]
47. Malavaki, C.J.; Sakkas, G.K.; Mitrou, G.I.; Kalyva, A.; Stefanidis, I.; Myburgh, K.H.; Karatzafiri, C. Skeletal muscle atrophy: Disease-induced mechanisms may mask disuse atrophy. *J. Muscle Res. Cell Motil.* **2015**, *36*, 405–421. [CrossRef] [PubMed]
48. Bodine, S.C.; Latres, E.; Baumhueter, S.; Lai, V.K.; Nunez, L.; Clarke, B.A.; Poueymirou, W.T.; Panaro, F.J.; Na, E.; Dharmarajan, K.; et al. Identification of ubiquitin ligases required for skeletal muscle atrophy. *Science* **2001**, *294*, 1704–1708. [CrossRef] [PubMed]
49. Baligand, C.; Chen, Y.W.; Ye, F.; Pandey, S.N.; Lai, S.H.; Liu, M.; Vandenborne, K. Transcriptional pathways associated with skeletal muscle changes after spinal cord injury and treadmill locomotor training. *Biomed. Res. Int.* **2015**, *2015*, 387090. [CrossRef] [PubMed]
50. Haddad, F.; Roy, R.R.; Zhong, H.; Edgerton, V.R.; Baldwin, K.M. Atrophy responses to muscle inactivity. II. Molecular markers of protein deficits. *J. Appl. Physiol.* **2003**, *95*, 791–802. [CrossRef] [PubMed]
51. Kim, S.J.; Roy, R.R.; Kim, J.A.; Zhong, H.; Haddad, F.; Baldwin, K.M.; Edgerton, V.R. Gene expression during inactivity-induced muscle atrophy: Effects of brief bouts of a forceful contraction countermeasure. *J. Appl. Physiol.* **2008**, *105*, 1246–1254. [CrossRef] [PubMed]
52. Urso, M.L.; Chen, Y.W.; Scrimgeour, A.G.; Lee, P.C.; Lee, K.F.; Clarkson, P.M. Alterations in mRNA expression and protein products following spinal cord injury in humans. *J. Physiol.* **2007**, *579*, 877–892. [CrossRef] [PubMed]
53. Zeman, R.J.; Zhao, J.; Zhang, Y.; Zhao, W.; Wen, X.; Wu, Y.; Pan, J.; Bauman, W.A.; Cardozo, C. Differential skeletal muscle gene expression after upper or lower motor neuron transection. *Pflugers Arch.* **2009**, *458*, 525–535. [CrossRef] [PubMed]
54. Sacheck, J.M.; Hyatt, J.P.; Raffaello, A.; Jagoe, R.T.; Roy, R.R.; Edgerton, V.R.; Lecker, S.H.; Goldberg, A.L. Rapid disuse and denervation atrophy involve transcriptional changes similar to those of muscle wasting during systemic diseases. *FASEB J.* **2007**, *21*, 140–155. [CrossRef] [PubMed]
55. Thakore, N.P.; Samantaray, S.; Park, S.; Nozaki, K.; Smith, J.A.; Cox, A.; Krause, J.; Banik, N.L. Molecular changes in sub-lesional muscle following acute phase of spinal cord injury. *Neurochem. Res.* **2016**, *41*, 44–52. [CrossRef] [PubMed]
56. Ye, F.; Baligand, C.; Keener, J.E.; Vohra, R.; Lim, W.; Ruhella, A.; Bose, P.; Daniels, M.; Walter, G.A.; Thompson, F.; et al. Hindlimb muscle morphology and function in a new atrophy model combining spinal cord injury and cast immobilization. *J. Neurotrauma* **2013**, *30*, 227–235. [CrossRef] [PubMed]
57. Drummond, M.J.; Glynn, E.L.; Lujan, H.L.; Dicarlo, S.E.; Rasmussen, B.B. Gene and protein expression associated with protein synthesis and breakdown in paraplegic skeletal muscle. *Muscle Nerve* **2008**, *37*, 505–513. [CrossRef] [PubMed]
58. Lundell, L.S.; Savikj, M.; Kostovski, E.; Iversen, P.O.; Zierath, J.R.; Krook, A.; Chibalin, A.V.; Widegren, U. Protein translation, proteolysis and autophagy in human skeletal muscle atrophy after spinal cord injury. *Acta Physiol.* **2018**. [CrossRef] [PubMed]
59. Yarar-Fisher, C.; Bickel, C.S.; Kelly, N.A.; Stec, M.J.; Windham, S.T.; McLain, A.B.; Oster, R.A.; Bamman, M.M. Heightened tweak-nf-kappab signaling and inflammation-associated fibrosis in paralyzed muscles of men with chronic spinal cord injury. *Am. J. Physiol. Endocrinol. Metab.* **2016**, *310*, E754–761. [CrossRef] [PubMed]
60. Leger, B.; Senese, R.; Al-Khadairy, A.W.; Deriaz, O.; Gobelet, C.; Giacobino, J.P.; Russell, A.P. Atrogin-1, murf1, and foxo, as well as phosphorylated gsk-3beta and 4e-bp1 are reduced in skeletal muscle of chronic spinal cord-injured patients. *Muscle Nerve* **2009**, *40*, 69–78. [CrossRef] [PubMed]

61. Huang, J.; Zhu, X. The molecular mechanisms of calpains action on skeletal muscle atrophy. *Physiol. Res.* **2016**, *65*, 547–560. [[PubMed](#)]
62. Bikle, D.D.; Tahimic, C.; Chang, W.; Wang, Y.; Philippou, A.; Barton, E.R. Role of IGF-I signaling in muscle bone interactions. *Bone* **2015**, *80*, 79–88. [[CrossRef](#)] [[PubMed](#)]
63. Liu, M.; Stevens-Lapsley, J.E.; Jayaraman, A.; Ye, F.; Conover, C.; Walter, G.A.; Bose, P.; Thompson, F.J.; Borst, S.E.; Vandenborne, K. Impact of treadmill locomotor training on skeletal muscle IGF1 and myogenic regulatory factors in spinal cord injured rats. *Eur. J. Appl. Physiol.* **2010**, *109*, 709–720. [[CrossRef](#)] [[PubMed](#)]
64. Pete, G.; Fuller, C.R.; Oldham, J.M.; Smith, D.R.; D’Ercole, A.J.; Kahn, C.R.; Lund, P.K. Postnatal growth responses to insulin-like growth factor i in insulin receptor substrate-1-deficient mice. *Endocrinology* **1999**, *140*, 5478–5487. [[CrossRef](#)] [[PubMed](#)]
65. Tsitouras, P.D.; Zhong, Y.G.; Spungen, A.M.; Bauman, W.A. Serum testosterone and growth hormone/insulin-like growth factor-i in adults with spinal cord injury. *Horm. Metab. Res.* **1995**, *27*, 287–292. [[CrossRef](#)] [[PubMed](#)]
66. Bauman, W.A.; Spungen, A.M.; Flanagan, S.; Zhong, Y.G.; Alexander, L.R.; Tsitouras, P.D. Blunted growth hormone response to intravenous arginine in subjects with a spinal cord injury. *Horm. Metab. Res.* **1994**, *26*, 152–156. [[CrossRef](#)] [[PubMed](#)]
67. Dreyer, H.C.; Glynn, E.L.; Lujan, H.L.; Fry, C.S.; DiCarlo, S.E.; Rasmussen, B.B. Chronic paraplegia-induced muscle atrophy downregulates the mtor/s6k1 signaling pathway. *J. Appl. Physiol.* **2008**, *104*, 27–33. [[CrossRef](#)] [[PubMed](#)]
68. Gorgey, A.S.; Gater, D.R. Insulin growth factors may explain relationship between spasticity and skeletal muscle size in men with spinal cord injury. *J. Rehabil. Res. Dev.* **2012**, *49*, 373–380. [[CrossRef](#)] [[PubMed](#)]
69. Kang, C.; Ji, L.L. Role of PGC-1alpha signaling in skeletal muscle health and disease. *Ann. N. Y. Acad. Sci.* **2012**, *1271*, 110–117. [[CrossRef](#)] [[PubMed](#)]
70. Gali Ramamoorthy, T.; Laverty, G.; Schlagowski, A.I.; Zoll, J.; Messaddeq, N.; Bornert, J.M.; Panza, S.; Ferry, A.; Geny, B.; Metzger, D. The transcriptional coregulator pgc-1beta controls mitochondrial function and anti-oxidant defence in skeletal muscles. *Nat. Commun.* **2015**, *6*, 10210. [[CrossRef](#)] [[PubMed](#)]
71. Lin, J.; Wu, H.; Tarr, P.T.; Zhang, C.Y.; Wu, Z.; Boss, O.; Michael, L.F.; Puigserver, P.; Isotani, E.; Olson, E.N.; et al. Transcriptional co-activator pgc-1 alpha drives the formation of slow-twitch muscle fibres. *Nature* **2002**, *418*, 797–801. [[CrossRef](#)] [[PubMed](#)]
72. Kang, C.; Goodman, C.A.; Hornberger, T.A.; Ji, L.L. PGC-1alpha overexpression by in vivo transfection attenuates mitochondrial deterioration of skeletal muscle caused by immobilization. *FASEB J.* **2015**, *29*, 4092–4106. [[CrossRef](#)] [[PubMed](#)]
73. Higashino, K.; Matsuura, T.; Suganuma, K.; Yukata, K.; Nishisho, T.; Yasui, N. Early changes in muscle atrophy and muscle fiber type conversion after spinal cord transection and peripheral nerve transection in rats. *J. Neuroeng. Rehabil.* **2013**, *10*, 46. [[CrossRef](#)] [[PubMed](#)]
74. Wu, Y.; Collier, L.; Qin, W.; Creasey, G.; Bauman, W.A.; Jarvis, J.; Cardozo, C. Electrical stimulation modulates wnt signaling and regulates genes for the motor endplate and calcium binding in muscle of rats with spinal cord transection. *BMC Neurosci.* **2013**, *14*, 81. [[CrossRef](#)] [[PubMed](#)]
75. Kramer, D.K.; Ahlsen, M.; Norrbom, J.; Jansson, E.; Hjeltnes, N.; Gustafsson, T.; Krook, A. Human skeletal muscle fibre type variations correlate with ppar alpha, ppar delta and PGC-1 alpha mrna. *Acta Physiol.* **2006**, *188*, 207–216. [[CrossRef](#)] [[PubMed](#)]
76. Baldwin, K.M.; Haddad, F.; Pandorf, C.E.; Roy, R.R.; Edgerton, V.R. Alterations in muscle mass and contractile phenotype in response to unloading models: Role of transcriptional/pretranslational mechanisms. *Front. Physiol.* **2013**, *4*, 284. [[CrossRef](#)] [[PubMed](#)]
77. Atherton, P.J.; Greenhaff, P.L.; Phillips, S.M.; Bodine, S.C.; Adams, C.M.; Lang, C.H. Control of skeletal muscle atrophy in response to disuse: Clinical/preclinical contentions and fallacies of evidence. *Am. J. Physiol. Endocrinol. Metab.* **2016**, *311*, E594–E604. [[CrossRef](#)] [[PubMed](#)]
78. Yarrow, J.F.; McCoy, S.C.; Borst, S.E. Intracrine and myotrophic roles of 5alpha-reductase and androgens: A review. *Med. Sci. Sports Exerc.* **2012**, *44*, 818–826. [[CrossRef](#)] [[PubMed](#)]
79. Burger, H.G. Androgen production in women. *Fertil. Steril.* **2002**, *77* (Suppl. S4), S3–S5. [[CrossRef](#)]
80. Labrie, F. All sex steroids are made intracellularly in peripheral tissues by the mechanisms of introcrinology after menopause. *J. Steroid Biochem. Mol. Biol.* **2015**, *145*, 133–138. [[CrossRef](#)] [[PubMed](#)]

81. Conover, C.F.; Yarrow, J.F.; Garrett, T.J.; Ye, F.; Quinlivan, E.P.; Cannady, D.F.; Peterson, M.D.; Borst, S.E. High prevalence of low serum biologically active testosterone in older male veterans. *J. Am. Med. Dir. Assoc.* **2017**, *18*, 366.e17–366.e24. [[CrossRef](#)] [[PubMed](#)]
82. Laurent, M.R.; Helsen, C.; Antonio, L.; Schollaert, D.; Joniau, S.; Vos, M.J.; Decallonne, B.; Hammond, G.L.; Vanderschueren, D.; Claessens, F. Effects of sex hormone-binding globulin (shbg) on androgen bioactivity in vitro. *Mol. Cell. Endocrinol.* **2016**, *437*, 280–291. [[CrossRef](#)] [[PubMed](#)]
83. Thaler, M.A.; Seifert-Klauss, V.; Luppa, P.B. The biomarker sex hormone-binding globulin—From established applications to emerging trends in clinical medicine. *Best Pract. Res. Clin. Endocrinol. Metab.* **2015**, *29*, 749–760. [[CrossRef](#)] [[PubMed](#)]
84. Yarrow, J.F.; Wronski, T.J.; Borst, S.E. Testosterone and adult male bone: Actions independent of 5alpha-reductase and aromatase. *Exerc. Sport Sci. Rev.* **2015**, *43*, 222–230. [[CrossRef](#)] [[PubMed](#)]
85. Lumbroso, S.; Sandillon, F.; Georget, V.; Lobaccaro, J.M.; Brinkmann, A.O.; Privat, A.; Sultan, C. Immunohistochemical localization and immunoblotting of androgen receptor in spinal neurons of male and female rats. *Eur. J. Endocrinol.* **1996**, *134*, 626–632. [[CrossRef](#)] [[PubMed](#)]
86. Matsuura, T.; Ogata, A.; Demura, T.; Moriwaka, F.; Tashiro, K.; Koyanagi, T.; Nagashima, K. Identification of androgen receptor in the rat spinal motoneurons. Immunohistochemical and immunoblotting analyses with monoclonal antibody. *Neurosci. Lett.* **1993**, *158*, 5–8. [[CrossRef](#)]
87. Cain, M.P.; Kramer, S.A.; Tindall, D.J.; Husmann, D.A. Expression of androgen receptor protein within the lumbar spinal cord during ontologic development and following antiandrogen induced cryptorchidism. *J. Urol.* **1994**, *152*, 766–769. [[CrossRef](#)]
88. Bauer, E.R.; Daxenberger, A.; Petri, T.; Sauerwein, H.; Meyer, H.H. Characterisation of the affinity of different anabolics and synthetic hormones to the human androgen receptor, human sex hormone binding globulin and to the bovine progestin receptor. *Acta Pathol. Microbiol. Immunol. Scand.* **2000**, *108*, 838–846. [[CrossRef](#)]
89. Almeida, M.; Laurent, M.R.; Dubois, V.; Claessens, F.; O'Brien, C.A.; Bouillon, R.; Vanderschueren, D.; Manolagas, S.C. Estrogens and androgens in skeletal physiology and pathophysiology. *Physiol. Rev.* **2017**, *97*, 135–187. [[CrossRef](#)] [[PubMed](#)]
90. Gennari, L.; Nuti, R.; Bilezikian, J.P. Aromatase activity and bone homeostasis in men. *J. Clin. Endocrinol. Metab.* **2004**, *89*, 5898–5907. [[CrossRef](#)] [[PubMed](#)]
91. Durga, A.; Sepahpanah, F.; Regozzi, M.; Hastings, J.; Crane, D.A. Prevalence of testosterone deficiency after spinal cord injury. *PM&R* **2011**, *3*, 929–932.
92. Bauman, W.A.; La Fountaine, M.F.; Spungen, A.M. Age-related prevalence of low testosterone in men with spinal cord injury. *J. Spinal Cord Med.* **2014**, *37*, 32–39. [[CrossRef](#)] [[PubMed](#)]
93. Clark, M.J.; Schopp, L.H.; Mazurek, M.O.; Zaniletti, I.; Lammy, A.B.; Martin, T.A.; Thomas, F.P.; Acuff, M.E. Testosterone levels among men with spinal cord injury: Relationship between time since injury and laboratory values. *Am. J. Phys. Med. Rehabil.* **2008**, *87*, 758–767. [[CrossRef](#)] [[PubMed](#)]
94. Bauman, W.A.; La Fountaine, M.F.; Cirigliaro, C.M.; Kirshblum, S.C.; Spungen, A.M. Testicular responses to hcg stimulation at varying doses in men with spinal cord injury. *Spinal Cord* **2017**, *55*, 659–663. [[CrossRef](#)] [[PubMed](#)]
95. Bauman, W.A.; La Fountaine, M.F.; Cirigliaro, C.M.; Kirshblum, S.C.; Spungen, A.M. Provocative stimulation of the hypothalamic-pituitary-testicular axis in men with spinal cord injury. *Spinal Cord* **2016**, *54*, 961–966. [[CrossRef](#)] [[PubMed](#)]
96. Bauman, W.A.; La Fountaine, M.F.; Cirigliaro, C.M.; Kirshblum, S.C.; Spungen, A.M. Administration of increasing doses of gonadotropin-releasing hormone in men with spinal cord injury to investigate dysfunction of the hypothalamic-pituitary-gonadal axis. *Spinal Cord* **2018**, *56*, 247–258. [[CrossRef](#)] [[PubMed](#)]
97. Kostovski, E.; Iversen, P.O.; Birkeland, K.; Torjesen, P.A.; Hjeltnes, N. Decreased levels of testosterone and gonadotrophins in men with long-standing tetraplegia. *Spinal Cord* **2008**, *46*, 559–564. [[CrossRef](#)] [[PubMed](#)]
98. Finkelstein, J.S.; Lee, H.; Burnett-Bowie, S.A.; Pallais, J.C.; Yu, E.W.; Borges, L.F.; Jones, B.F.; Barry, C.V.; Wulczyn, K.E.; Thomas, B.J.; et al. Gonadal steroids and body composition, strength, and sexual function in men. *N. Engl. J. Med.* **2013**, *369*, 1011–1022. [[CrossRef](#)] [[PubMed](#)]
99. Schopp, L.H.; Clark, M.; Mazurek, M.O.; Hagglund, K.J.; Acuff, M.E.; Sherman, A.K.; Childers, M.K. Testosterone levels among men with spinal cord injury admitted to inpatient rehabilitation. *Am. J. Phys. Med. Rehabil.* **2006**, *85*, 678–684, quiz 685–677. [[CrossRef](#)] [[PubMed](#)]

100. Beggs, L.A.; Ye, F.; Ghosh, P.; Beck, D.T.; Conover, C.F.; Balaez, A.; Miller, J.R.; Phillips, E.G.; Zheng, N.; Williams, A.A.; et al. Sclerostin inhibition prevents spinal cord injury-induced cancellous bone loss. *J. Bone Miner. Res.* **2015**, *30*, 681–689. [CrossRef] [PubMed]
101. Wu, Y.; Collier, L.; Pan, J.; Qin, W.; Bauman, W.A.; Cardozo, C.P. Testosterone reduced methylprednisolone-induced muscle atrophy in spinal cord-injured rats. *Spinal Cord* **2012**, *50*, 57–62. [CrossRef] [PubMed]
102. Borst, S.E.; Yarrow, J.F.; Conover, C.F.; Nseyo, U.; Meuleman, J.R.; Lipinska, J.A.; Braith, R.W.; Beck, D.T.; Martin, J.S.; Morrow, M.; et al. Musculoskeletal and prostate effects of combined testosterone and finasteride administration in older hypogonadal men: A randomized, controlled trial. *Am. J. Physiol. Endocrinol. Metab.* **2014**, *306*, E433–E442. [CrossRef] [PubMed]
103. Cooper, I.S.; Ryneanson, E.H.; Mac, C.C.; Power, M.H. The catabolic effect of trauma of the spinal cord and its investigative treatment with testosterone propionate; preliminary report. *Proc. Staff Meet. Mayo Clin.* **1950**, *25*, 326–330. [PubMed]
104. Cooper, I.S.; Ryneanson, E.H.; Mac, C.C.; Power, M.H. Testosterone propionate as a nitrogen-sparing agent after spinal cord injury. *J. Am. Med. Assoc.* **1951**, *145*, 549–553. [CrossRef] [PubMed]
105. Bauman, W.A.; La Fountaine, M.F.; Cirigliaro, C.M.; Kirshblum, S.C.; Spungen, A.M. Lean tissue mass and energy expenditure are retained in hypogonadal men with spinal cord injury after discontinuation of testosterone replacement therapy. *J. Spinal Cord Med.* **2015**, *38*, 38–47. [CrossRef] [PubMed]
106. Bennett, N.C.; Gardiner, R.A.; Hooper, J.D.; Johnson, D.W.; Gobe, G.C. Molecular cell biology of androgen receptor signalling. *Int. J. Biochem. Cell Biol.* **2010**, *42*, 813–827. [CrossRef] [PubMed]
107. MacLean, H.E.; Chiu, W.S.; Notini, A.J.; Axell, A.M.; Davey, R.A.; McManus, J.F.; Ma, C.; Plant, D.R.; Lynch, G.S.; Zajac, J.D. Impaired skeletal muscle development and function in male, but not female, genomic androgen receptor knockout mice. *FASEB J.* **2008**, *22*, 2676–2689. [CrossRef] [PubMed]
108. Revankar, C.M.; Cimino, D.F.; Sklar, L.A.; Arterburn, J.B.; Prossnitz, E.R. A transmembrane intracellular estrogen receptor mediates rapid cell signaling. *Science* **2005**, *307*, 1625–1630. [CrossRef] [PubMed]
109. Foradori, C.D.; Weiser, M.J.; Handa, R.J. Non-genomic actions of androgens. *Front. Neuroendocrinol.* **2008**, *29*, 169–181. [CrossRef] [PubMed]
110. Singh, R.; Bhasin, S.; Braga, M.; Artaza, J.N.; Pervin, S.; Taylor, W.E.; Krishnan, V.; Sinha, S.K.; Rajavashisth, T.B.; Jasuja, R. Regulation of myogenic differentiation by androgens: Cross talk between androgen receptor/beta-catenin and follistatin/transforming growth factor-beta signaling pathways. *Endocrinology* **2009**, *150*, 1259–1268. [CrossRef] [PubMed]
111. Rudnicki, M.A.; Williams, B.O. Wnt signaling in bone and muscle. *Bone* **2015**, *80*, 60–66. [CrossRef] [PubMed]
112. Liu, X.H.; Wu, Y.; Yao, S.; Levine, A.C.; Kirschenbaum, A.; Collier, L.; Bauman, W.A.; Cardozo, C.P. Androgens up-regulate transcription of the notch inhibitor numb in c2c12 myoblasts via wnt/beta-catenin signaling to t cell factor elements in the numb promoter. *J. Biol. Chem.* **2013**, *288*, 17990–17998. [CrossRef] [PubMed]
113. Gentile, M.A.; Nantermet, P.V.; Vogel, R.L.; Phillips, R.; Holder, D.; Hodor, P.; Cheng, C.; Dai, H.; Freedman, L.P.; Ray, W.J. Androgen-mediated improvement of body composition and muscle function involves a novel early transcriptional program including igf1, mechano growth factor, and induction of {beta}-catenin. *J. Mol. Endocrinol.* **2010**, *44*, 55–73. [CrossRef] [PubMed]
114. Otto-Duessel, M.; Tew, B.Y.; Vonderfecht, S.; Moore, R.; Jones, J.O. Identification of neuron selective androgen receptor inhibitors. *World J. Biol. Chem.* **2017**, *8*, 138–150. [CrossRef] [PubMed]
115. Pawlowski, J.E.; Ertel, J.R.; Allen, M.P.; Xu, M.; Butler, C.; Wilson, E.M.; Wierman, M.E. Liganded androgen receptor interaction with beta-catenin: Nuclear co-localization and modulation of transcriptional activity in neuronal cells. *J. Biol. Chem.* **2002**, *277*, 20702–20710. [CrossRef] [PubMed]
116. Thomas, P.S., Jr.; Fraley, G.S.; Damian, V.; Woodke, L.B.; Zapata, F.; Sopher, B.L.; Plymate, S.R.; La Spada, A.R. Loss of endogenous androgen receptor protein accelerates motor neuron degeneration and accentuates androgen insensitivity in a mouse model of x-linked spinal and bulbar muscular atrophy. *Hum. Mol. Genet.* **2006**, *15*, 2225–2238. [CrossRef] [PubMed]
117. Gao, K.; Wang, Y.S.; Yuan, Y.J.; Wan, Z.H.; Yao, T.C.; Li, H.H.; Tang, P.F.; Mei, X.F. Neuroprotective effect of rapamycin on spinal cord injury via activation of the wnt/beta-catenin signaling pathway. *Neural Regen. Res.* **2015**, *10*, 951–957. [PubMed]

118. Lu, G.B.; Niu, F.W.; Zhang, Y.C.; Du, L.; Liang, Z.Y.; Gao, Y.; Yan, T.Z.; Nie, Z.K.; Gao, K. Methylprednisolone promotes recovery of neurological function after spinal cord injury: Association with wnt/beta-catenin signaling pathway activation. *Neural Regen. Res.* **2016**, *11*, 1816–1823. [PubMed]
119. Gao, K.; Shen, Z.; Yuan, Y.; Han, D.; Song, C.; Guo, Y.; Mei, X. Simvastatin inhibits neural cell apoptosis and promotes locomotor recovery via activation of wnt/beta-catenin signaling pathway after spinal cord injury. *J. Neurochem.* **2016**, *138*, 139–149. [CrossRef] [PubMed]
120. Ye, F.; McCoy, S.C.; Ross, H.H.; Bernardo, J.A.; Beharry, A.W.; Senf, S.M.; Judge, A.R.; Beck, D.T.; Conover, C.F.; Cannady, D.F.; et al. Transcriptional regulation of myotrophic actions by testosterone and trenbolone on androgen-responsive muscle. *Steroids* **2014**, *87*, 59–66. [CrossRef] [PubMed]
121. Wu, Y.; Bauman, W.A.; Blitzer, R.D.; Cardozo, C. Testosterone-induced hypertrophy of l6 myoblasts is dependent upon erk and mtor. *Biochem. Biophys. Res. Commun.* **2010**, *400*, 679–683. [CrossRef] [PubMed]
122. Wu, Y.; Zhao, W.; Zhao, J.; Pan, J.; Wu, Q.; Zhang, Y.; Bauman, W.A.; Cardozo, C.P. Identification of androgen response elements in the insulin-like growth factor i upstream promoter. *Endocrinology* **2007**, *148*, 2984–2993. [CrossRef] [PubMed]
123. Ferrando, A.A.; Sheffield-Moore, M.; Yeckel, C.W.; Gilkison, C.; Jiang, J.; Achacosa, A.; Lieberman, S.A.; Tipton, K.; Wolfe, R.R.; Urban, R.J. Testosterone administration to older men improves muscle function: Molecular and physiological mechanisms. *Am. J. Physiol. Endocrinol. Metab.* **2002**, *282*, E601–E607. [CrossRef] [PubMed]
124. Deane, C.S.; Hughes, D.C.; Sculthorpe, N.; Lewis, M.P.; Stewart, C.E.; Sharples, A.P. Impaired hypertrophy in myoblasts is improved with testosterone administration. *J. Steroid Biochem. Mol. Biol.* **2013**, *138*, 152–161. [CrossRef] [PubMed]
125. White, J.P.; Gao, S.; Puppa, M.J.; Sato, S.; Welle, S.L.; Carson, J.A. Testosterone regulation of akt/mTORC1/foxo3a signaling in skeletal muscle. *Mol. Cell. Endocrinol.* **2013**, *365*, 174–186. [CrossRef] [PubMed]
126. Basualto-Alarcon, C.; Jorqueria, G.; Altamirano, F.; Jaimovich, E.; Estrada, M. Testosterone signals through mtor and androgen receptor to induce muscle hypertrophy. *Med. Sci. Sports Exerc.* **2013**, *45*, 1712–1720. [CrossRef] [PubMed]
127. Xu, T.; Shen, Y.; Pink, H.; Triantafillou, J.; Stimpson, S.A.; Turnbull, P.; Han, B. Phosphorylation of p70s6 kinase is implicated in androgen-induced levator ani muscle anabolism in castrated rats. *J. Steroid Biochem. Mol. Biol.* **2004**, *92*, 447–454. [CrossRef] [PubMed]
128. Serra, C.; Sandor, N.L.; Jang, H.; Lee, D.; Toraldo, G.; Guarneri, T.; Wong, S.; Zhang, A.; Guo, W.; Jasuja, R.; et al. The effects of testosterone deprivation and supplementation on proteasomal and autophagy activity in the skeletal muscle of the male mouse: Differential effects on high-androgen responder and low-androgen responder muscle groups. *Endocrinology* **2013**, *154*, 4594–4606. [CrossRef] [PubMed]
129. Pires-Oliveira, M.; Maragno, A.L.; Parreira-e-Silva, L.T.; Chiavegatti, T.; Gomes, M.D.; Godinho, R.O. Testosterone represses ubiquitin ligases atrogin-1 and murf-1 expression in an androgen-sensitive rat skeletal muscle in vivo. *J. Appl. Physiol.* **2010**, *108*, 266–273. [CrossRef] [PubMed]
130. Ferrando, A.A.; Sheffield-Moore, M.; Paddon-Jones, D.; Wolfe, R.R.; Urban, R.J. Differential anabolic effects of testosterone and amino acid feeding in older men. *J. Clin. Endocrinol. Metab.* **2003**, *88*, 358–362. [CrossRef] [PubMed]
131. Zhao, W.; Pan, J.; Wang, X.; Wu, Y.; Bauman, W.A.; Cardozo, C.P. Expression of the muscle atrophy factor muscle atrophy f-box is suppressed by testosterone. *Endocrinology* **2008**, *149*, 5449–5460. [CrossRef] [PubMed]
132. Wu, Y.; Ruggiero, C.L.; Bauman, W.A.; Cardozo, C. Ankrd1 is a transcriptional repressor for the androgen receptor that is downregulated by testosterone. *Biochem. Biophys. Res. Commun.* **2013**, *437*, 355–360. [CrossRef] [PubMed]
133. MacKrell, J.G.; Yaden, B.C.; Bullock, H.; Chen, K.; Shetler, P.; Bryant, H.U.; Krishnan, V. Molecular targets of androgen signaling that characterize skeletal muscle recovery and regeneration. *Nucl. Recept. Signal.* **2015**, *13*, e005. [PubMed]
134. Zhao, J.; Bauman, W.A.; Huang, R.; Caplan, A.J.; Cardozo, C. Oxandrolone blocks glucocorticoid signaling in an androgen receptor-dependent manner. *Steroids* **2004**, *69*, 357–366. [CrossRef] [PubMed]
135. Barbosa, M.R.; Shiguemoto, G.E.; Tomaz, L.M.; Ferreira, F.C.; Rodrigues, M.F.; Domingues, M.M.; Souza Master, M.V.; Canevazzi, G.H.; Silva-Magosso, N.S.; Selistre-de-Araujo, H.S.; et al. Resistance training and ovariectomy: Antagonistic effects in mitochondrial biogenesis markers in rat skeletal muscle. *Int. J. Sports Med.* **2016**, *37*, 841–848. [CrossRef] [PubMed]

136. Park, Y.M.; Pereira, R.I.; Erickson, C.B.; Swibas, T.A.; Kang, C.; Van Pelt, R.E. Time since menopause and skeletal muscle estrogen receptors, PGC-1alpha, and ampk. *Menopause* **2017**, *24*, 815–823. [CrossRef] [PubMed]
137. Maher, A.C.; Akhtar, M.; Tarnopolsky, M.A. Men supplemented with 17beta-estradiol have increased beta-oxidation capacity in skeletal muscle. *Physiol. Genom.* **2010**, *42*, 342–347. [CrossRef] [PubMed]
138. McCully, K.K.; Mulcahy, T.K.; Ryan, T.E.; Zhao, Q. Skeletal muscle metabolism in individuals with spinal cord injury. *J. Appl. Physiol.* **2011**, *111*, 143–148. [CrossRef] [PubMed]
139. Patte-Mensah, C.; Penning, T.M.; Mensah-Nyagan, A.G. Anatomical and cellular localization of neuroactive 5 alpha/3 alpha-reduced steroid-synthesizing enzymes in the spinal cord. *J. Comp. Neurol.* **2004**, *477*, 286–299. [CrossRef] [PubMed]
140. Poletti, A.; Coscarella, A.; Negri-Cesi, P.; Colciago, A.; Celotti, F.; Martini, L. 5 alpha-reductase isozymes in the central nervous system. *Steroids* **1998**, *63*, 246–251. [CrossRef]
141. Hauser, K.F.; MacLusky, N.J.; Toran-Allerand, C.D. Androgen action in fetal mouse spinal cord cultures: Metabolic and morphologic aspects. *Brain Res.* **1987**, *406*, 62–72. [CrossRef]
142. MacLusky, N.J.; Clark, C.R.; Shanabrough, M.; Naftolin, F. Metabolism and binding of androgens in the spinal cord of the rat. *Brain Res.* **1987**, *422*, 83–91. [CrossRef]
143. Pozzi, P.; Bendotti, C.; Simeoni, S.; Piccioni, E.; Guerini, V.; Marron, T.U.; Martini, L.; Poletti, A. Androgen 5-alpha-reductase type 2 is highly expressed and active in rat spinal cord motor neurones. *J. Neuroendocrinol.* **2003**, *15*, 882–887. [CrossRef] [PubMed]
144. Hauser, K.F.; Toran-Allerand, C.D. Androgen increases the number of cells in fetal mouse spinal cord cultures: Implications for motoneuron survival. *Brain Res.* **1989**, *485*, 157–164. [CrossRef]
145. Fargo, K.N.; Foecking, E.M.; Jones, K.J.; Sengelaub, D.R. Neuroprotective actions of androgens on motoneurons. *Front. Neuroendocrinol.* **2009**, *30*, 130–141. [CrossRef] [PubMed]
146. Verhovshek, T.; Buckley, K.E.; Sergent, M.A.; Sengelaub, D.R. Testosterone metabolites differentially maintain adult morphology in a sexually dimorphic neuromuscular system. *Dev. Neurobiol.* **2010**, *70*, 206–221. [CrossRef] [PubMed]
147. Huguenard, A.L.; Fernando, S.M.; Monks, D.A.; Sengelaub, D.R. Overexpression of androgen receptors in target musculature confers androgen sensitivity to motoneuron dendrites. *Endocrinology* **2011**, *152*, 639–650. [CrossRef] [PubMed]
148. Ji, Y.X.; Zhao, M.; Liu, Y.L.; Chen, L.S.; Hao, P.L.; Sun, C. Expression of aromatase and estrogen receptors in lumbar motoneurons of mice. *Neurosci. Lett.* **2017**, *653*, 7–11. [CrossRef] [PubMed]
149. Rakotoarivelo, C.; Petite, D.; Lambard, S.; Fabre, C.; Rouleau, C.; Lumbroso, S.; de Weille, J.; Privat, A.; Carreau, S.; Mersel, M. Receptors to steroid hormones and aromatase are expressed by cultured motoneurons but not by glial cells derived from rat embryo spinal cord. *Neuroendocrinology* **2004**, *80*, 284–297. [CrossRef] [PubMed]
150. Nowacek, A.S.; Sengelaub, D.R. Estrogenic support of motoneuron dendritic growth via the neuromuscular periphery in a sexually dimorphic motor system. *J. Neurobiol.* **2006**, *66*, 962–976. [CrossRef] [PubMed]
151. Cai, Y.; Chew, C.; Munoz, F.; Sengelaub, D.R. Neuroprotective effects of testosterone metabolites and dependency on receptor action on the morphology of somatic motoneurons following the death of neighboring motoneurons. *Dev. Neurobiol.* **2017**, *77*, 691–707. [CrossRef] [PubMed]
152. Rudolph, L.M.; Sengelaub, D.R. Castration-induced upregulation of muscle eralpha supports estrogen sensitivity of motoneuron dendrites in a sexually dimorphic neuromuscular system. *Dev. Neurobiol.* **2013**, *73*, 921–935. [CrossRef] [PubMed]
153. Nakamizo, T.; Urushitani, M.; Inoue, R.; Shinohara, A.; Sawada, H.; Honda, K.; Kihara, T.; Akaike, A.; Shimohama, S. Protection of cultured spinal motor neurons by estradiol. *Neuroreport* **2000**, *11*, 3493–3497. [CrossRef] [PubMed]
154. Chen, J.; Hu, R.; Ge, H.; Duanmu, W.; Li, Y.; Xue, X.; Hu, S.; Feng, H. G-protein-coupled receptor 30-mediated antiapoptotic effect of estrogen on spinal motor neurons following injury and its underlying mechanisms. *Mol. Med. Rep.* **2015**, *12*, 1733–1740. [CrossRef] [PubMed]
155. Elkabes, S.; Nicot, A.B. Sex steroids and neuroprotection in spinal cord injury: A review of preclinical investigations. *Exp. Neurol.* **2014**, *259*, 28–37. [CrossRef] [PubMed]
156. Ottem, E.N.; Bailey, D.J.; Jordan, C.L.; Breedlove, S.M. With a little help from my friends: Androgens tap bdnf signaling pathways to alter neural circuits. *Neuroscience* **2013**, *239*, 124–138. [CrossRef] [PubMed]

157. Verhovshek, T.; Rudolph, L.M.; Sengelaub, D.R. Brain-derived neurotrophic factor and androgen interactions in spinal neuromuscular systems. *Neuroscience* **2013**, *239*, 103–114. [[CrossRef](#)] [[PubMed](#)]
158. Osborne, M.C.; Verhovshek, T.; Sengelaub, D.R. Androgen regulates trkB immunolabeling in spinal motoneurons. *J. Neurosci. Res.* **2007**, *85*, 303–309. [[CrossRef](#)] [[PubMed](#)]
159. Ottem, E.N.; Beck, L.A.; Jordan, C.L.; Breedlove, S.M. Androgen-dependent regulation of brain-derived neurotrophic factor and tyrosine kinase b in the sexually dimorphic spinal nucleus of the bulbocavernosus. *Endocrinology* **2007**, *148*, 3655–3665. [[CrossRef](#)] [[PubMed](#)]
160. Yang, L.Y.; Arnold, A.P. Interaction of bdnf and testosterone in the regulation of adult perineal motoneurons. *J. Neurobiol.* **2000**, *44*, 308–319. [[CrossRef](#)]
161. Yang, L.Y.; Verhovshek, T.; Sengelaub, D.R. Brain-derived neurotrophic factor and androgen interact in the maintenance of dendritic morphology in a sexually dimorphic rat spinal nucleus. *Endocrinology* **2004**, *145*, 161–168. [[CrossRef](#)] [[PubMed](#)]
162. Xu, J.; Gingras, K.M.; Bengston, L.; Di Marco, A.; Forger, N.G. Blockade of endogenous neurotrophic factors prevents the androgenic rescue of rat spinal motoneurons. *J. Neurosci.* **2001**, *21*, 4366–4372. [[CrossRef](#)] [[PubMed](#)]
163. Gill, L.C.; Gransee, H.M.; Sieck, G.C.; Mantilla, C.B. Functional recovery after cervical spinal cord injury: Role of neurotrophin and glutamatergic signaling in phrenic motoneurons. *Respir. Physiol. Neurobiol.* **2016**, *226*, 128–136. [[CrossRef](#)] [[PubMed](#)]
164. Cardona-Rossinyol, A.; Mir, M.; Caraballo-Miralles, V.; Llado, J.; Olmos, G. Neuroprotective effects of estradiol on motoneurons in a model of rat spinal cord embryonic explants. *Cell. Mol. Neurobiol.* **2013**, *33*, 421–432. [[CrossRef](#)] [[PubMed](#)]
165. Lin, C.W.; Chen, B.; Huang, K.L.; Dai, Y.S.; Teng, H.L. Inhibition of autophagy by estradiol promotes locomotor recovery after spinal cord injury in rats. *Neurosci. Bull.* **2016**, *32*, 137–144. [[CrossRef](#)] [[PubMed](#)]
166. Behrman, A.L.; Harkema, S.J. Physical rehabilitation as an agent for recovery after spinal cord injury. *Phys. Med. Rehabil. Clin.* **2007**, *18*, 183–202. [[CrossRef](#)] [[PubMed](#)]
167. Field-Fote, E.C. Combined use of body weight support, functional electric stimulation, and treadmill training to improve walking ability in individuals with chronic incomplete spinal cord Injury. *Arch. Phys. Med. Rehabil.* **2001**, *82*, 818–824. [[CrossRef](#)] [[PubMed](#)]
168. Forrest, G.F.; Sisto, S.A.; Barbeau, H.; Kirshblum, S.C.; Wilen, J.; Bond, Q.; Bentson, S.; Asselin, P.; Cirigliaro, C.M.; Harkema, S. Neuromotor and musculoskeletal responses to locomotor training for an individual with chronic motor complete ais-b spinal cord injury. *J. Spinal Cord Med.* **2008**, *31*, 509–521. [[CrossRef](#)] [[PubMed](#)]
169. Gorassini, M.A.; Norton, J.A.; Nevett-Duchcherer, J.; Roy, F.D.; Yang, J.F. Changes in locomotor muscle activity after treadmill training in subjects with incomplete spinal cord injury. *J. Neurophysiol.* **2009**, *101*, 969–979. [[CrossRef](#)] [[PubMed](#)]
170. Harkema, S.J.; Schmidt-Read, M.; Lorenz, D.J.; Edgerton, V.R.; Behrman, A.L. Balance and ambulation improvements in individuals with chronic incomplete spinal cord injury using locomotor training-based rehabilitation. *Arch. Phys. Med. Rehabil.* **2012**, *93*, 1508–1517. [[CrossRef](#)] [[PubMed](#)]
171. Krishnan, V.; Kindig, M.; Mirbagheri, M. Robotic-assisted locomotor training enhances ankle performance in adults with incomplete spinal cord injury. *J. Rehabil. Med.* **2016**, *48*, 781–786. [[CrossRef](#)] [[PubMed](#)]
172. Nooijen, C.F.; Ter Hoeve, N.; Field-Fote, E.C. Gait quality is improved by locomotor training in individuals with sci regardless of training approach. *J. Neuroeng. Rehabil.* **2009**, *6*, 36. [[CrossRef](#)] [[PubMed](#)]
173. Wernig, A.; Muller, S.; Nanassy, A.; Cagol, E. Laufband therapy based on ‘rules of spinal locomotion’ is effective in spinal cord injured persons. *Eur. J. Neurosci.* **1995**, *7*, 823–829. [[CrossRef](#)] [[PubMed](#)]
174. Wirz, M.; Bastiaenen, C.; de Bie, R.; Dietz, V. Effectiveness of automated locomotor training in patients with acute incomplete spinal cord injury: A randomized controlled multicenter trial. *BMC Neurol.* **2011**, *11*, 60. [[CrossRef](#)] [[PubMed](#)]
175. Wirz, M.; Zemon, D.H.; Rupp, R.; Scheel, A.; Colombo, G.; Dietz, V.; Hornby, T.G. Effectiveness of automated locomotor training in patients with chronic incomplete spinal cord injury: A multicenter trial. *Arch. Phys. Med. Rehabil.* **2005**, *86*, 672–680. [[CrossRef](#)] [[PubMed](#)]
176. Jones, M.L.; Evans, N.; Tefertiller, C.; Backus, D.; Sweatman, M.; Tansey, K.; Morrison, S. Activity-based therapy for recovery of walking in individuals with chronic spinal cord injury: Results from a randomized clinical trial. *Arch. Phys. Med. Rehabil.* **2014**, *95*, 2239–2246. [[CrossRef](#)] [[PubMed](#)]

177. Knikou, M. Plasticity of corticospinal neural control after locomotor training in human spinal cord injury. *Neural Plast.* **2012**, *2012*, 254948. [\[CrossRef\]](#) [\[PubMed\]](#)
178. Adams, M.M.; Ditor, D.S.; Tarnopolsky, M.A.; Phillips, S.M.; McCartney, N.; Hicks, A.L. The effect of body weight-supported treadmill training on muscle morphology in an individual with chronic, motor-complete spinal cord injury: A case study. *J. Spinal Cord Med.* **2006**, *29*, 167–171. [\[CrossRef\]](#) [\[PubMed\]](#)
179. Alexeeva, N.; Sames, C.; Jacobs, P.L.; Hobday, L.; Distasio, M.M.; Mitchell, S.A.; Calancie, B. Comparison of training methods to improve walking in persons with chronic spinal cord injury: A randomized clinical trial. *J. Spinal Cord Med.* **2011**, *34*, 362–379. [\[CrossRef\]](#) [\[PubMed\]](#)
180. Thomas, S.L.; Gorassini, M.A. Increases in corticospinal tract function by treadmill training after incomplete spinal cord injury. *J. Neurophysiol.* **2005**, *94*, 2844–2855. [\[CrossRef\]](#) [\[PubMed\]](#)
181. Coupaud, S.; Jack, L.P.; Hunt, K.J.; Allan, D.B. Muscle and bone adaptations after treadmill training in incomplete spinal cord injury: A case study using peripheral quantitative computed tomography. *J. Musculoskelet. Neuron. Interact.* **2009**, *9*, 288–297. [\[PubMed\]](#)
182. Giangregorio, L.; McCartney, N. Bone loss and muscle atrophy in spinal cord injury: Epidemiology, fracture prediction, and rehabilitation strategies. *J. Spinal Cord Med.* **2006**, *29*, 489–500. [\[CrossRef\]](#) [\[PubMed\]](#)
183. Giangregorio, L.M.; Hicks, A.L.; Webber, C.E.; Phillips, S.M.; Craven, B.C.; Bugaresti, J.M.; McCartney, N. Body weight supported treadmill training in acute spinal cord injury: Impact on muscle and bone. *Spinal Cord* **2005**, *43*, 649–657. [\[CrossRef\]](#) [\[PubMed\]](#)
184. Stewart, B.G.; Tarnopolsky, M.A.; Hicks, A.L.; McCartney, N.; Mahoney, D.J.; Staron, R.S.; Phillips, S.M. Treadmill training-induced adaptations in muscle phenotype in persons with incomplete spinal cord injury. *Muscle Nerve* **2004**, *30*, 61–68. [\[CrossRef\]](#) [\[PubMed\]](#)
185. Dobkin, B.; Barbeau, H.; Deforge, D.; Ditunno, J.; Elashoff, R.; Apple, D.; Basso, M.; Behrman, A.; Harkema, S.; Saulino, M.; et al. The evolution of walking-related outcomes over the first 12 weeks of rehabilitation for incomplete traumatic spinal cord injury: The multicenter randomized spinal cord injury locomotor trial. *NeuroRehabil. Neural Repair* **2007**, *21*, 25–35. [\[CrossRef\]](#) [\[PubMed\]](#)
186. Field-Fote, E.C.; Roach, K.E. Influence of a locomotor training approach on walking speed and distance in people with chronic spinal cord injury: A randomized clinical trial. *Phys. Ther.* **2011**, *91*, 48–60. [\[CrossRef\]](#) [\[PubMed\]](#)
187. Lucarelli, P.R.; Lima, M.O.; Lima, F.P.; de Almeida, J.G.; Brech, G.C.; D’Andrea Greve, J.M. Gait analysis following treadmill training with body weight support versus conventional physical therapy: A prospective randomized controlled single blind study. *Spinal Cord* **2011**, *49*, 1001–1007. [\[CrossRef\]](#) [\[PubMed\]](#)
188. Postans, N.J.; Hasler, J.P.; Granat, M.H.; Maxwell, D.J. Functional electric stimulation to augment partial weight-bearing supported treadmill training for patients with acute incomplete spinal cord injury: A pilot study. *Arch. Phys. Med. Rehabil.* **2004**, *85*, 604–610. [\[CrossRef\]](#) [\[PubMed\]](#)
189. Mehrholz, J.; Kugler, J.; Pohl, M. Locomotor training for walking after spinal cord injury. *Cochrane Database Syst. Rev.* **2012**, *11*, CD006676. [\[CrossRef\]](#) [\[PubMed\]](#)
190. Nam, K.Y.; Kim, H.J.; Kwon, B.S.; Park, J.W.; Lee, H.J.; Yoo, A. Robot-assisted gait training (lokomat) improves walking function and activity in people with spinal cord injury: A systematic review. *J. Neuroeng. Rehabil.* **2017**, *14*, 24. [\[CrossRef\]](#) [\[PubMed\]](#)
191. Wessels, M.; Lucas, C.; Eriks, I.; de Groot, S. Body weight-supported gait training for restoration of walking in people with an incomplete spinal cord injury: A systematic review. *J. Rehabil. Med.* **2010**, *42*, 513–519. [\[CrossRef\]](#) [\[PubMed\]](#)
192. Lam, T.; Noonan, V.K.; Eng, J.J. A systematic review of functional ambulation outcome measures in spinal cord injury. *Spinal Cord* **2008**, *46*, 246–254. [\[CrossRef\]](#) [\[PubMed\]](#)
193. De Leon, R.D.; Dy, C.J. What did we learn from the animal studies of body weight-supported treadmill training and where do we go from here? *J. Neurotrauma* **2017**, *34*, 1744–1750. [\[CrossRef\]](#) [\[PubMed\]](#)
194. Yarrow, J.F.; Conover, C.F.; Lipinska, J.A.; Santillana, C.A.; Wronski, T.J.; Borst, S.E. Methods to quantify sex steroid hormones in bone: Applications to the study of androgen ablation and administration. *Am. J. Physiol. Endocrinol. Metab.* **2010**, *299*, E841–E847. [\[CrossRef\]](#) [\[PubMed\]](#)
195. Nessler, J.A.; Moustafa-Bayoumi, M.; Soto, D.; Duhon, J.E.; Schmitt, R. Robot applied stance loading increases hindlimb muscle mass and stepping kinetics in a rat model of spinal cord injury. In Proceedings of the 2011 Annual International Conference of the IEEE Engineering in Medicine and Biology Society, Boston, MA, USA, 30 August–3 September 2011; Volume 2011, pp. 4145–4148.

196. Ilha, J.; da Cunha, N.B.; Jaeger, M.; de Souza, D.F.; Nascimento, P.S.; Marcuzzo, S.; Figueiro, M.; Gottfried, C.; Achaval, M. Treadmill step training-induced adaptive muscular plasticity in a chronic paraplegia model. *Neurosci. Lett.* **2011**, *492*, 170–174. [[CrossRef](#)] [[PubMed](#)]
197. Stevens, J.E.; Liu, M.; Bose, P.; O’Steen, W.A.; Thompson, F.J.; Anderson, D.K.; Vandenborne, K. Changes in soleus muscle function and fiber morphology with one week of locomotor training in spinal cord contusion injured rats. *J. Neurotrauma* **2006**, *23*, 1671–1681. [[CrossRef](#)] [[PubMed](#)]
198. Bose, P.K.; Hou, J.; Parmer, R.; Reier, P.J.; Thompson, F.J. Altered patterns of reflex excitability, balance, and locomotion following spinal cord injury and locomotor training. *Front. Physiol.* **2012**, *3*, 258. [[CrossRef](#)] [[PubMed](#)]
199. Liu, M.; Bose, P.; Walter, G.A.; Thompson, F.J.; Vandenborne, K. A longitudinal study of skeletal muscle following spinal cord injury and locomotor training. *Spinal Cord* **2008**, *46*, 488–493. [[CrossRef](#)] [[PubMed](#)]
200. Singh, A.; Balasubramanian, S.; Murray, M.; Lemay, M.; Houle, J. Role of spared pathways in locomotor recovery after body-weight-supported treadmill training in contused rats. *J. Neurotrauma* **2011**, *28*, 2405–2416. [[CrossRef](#)] [[PubMed](#)]
201. Jayaraman, A.; Shah, P.; Gregory, C.; Bowden, M.; Stevens, J.; Bishop, M.; Walter, G.; Behrman, A.; Vandenborne, K. Locomotor training and muscle function after incomplete spinal cord injury: Case series. *J. Spinal Cord Med.* **2008**, *31*, 185–193. [[CrossRef](#)] [[PubMed](#)]
202. Duffell, L.D.; Brown, G.L.; Mirbagheri, M.M. Facilitatory effects of anti-spastic medication on robotic locomotor training in people with chronic incomplete spinal cord injury. *J. Neuroeng. Rehabil.* **2015**, *12*, 29. [[CrossRef](#)] [[PubMed](#)]
203. Varoqui, D.; Niu, X.; Mirbagheri, M.M. Ankle voluntary movement enhancement following robotic-assisted locomotor training in spinal cord injury. *J. Neuroeng. Rehabil.* **2014**, *11*, 46. [[CrossRef](#)] [[PubMed](#)]
204. Cardozo, C.P.; Graham, Z.A. Muscle-bone interactions: Movement in the field of mechano-humoral coupling of muscle and bone. *Ann. N. Y. Acad. Sci.* **2017**, *1402*, 10–17. [[CrossRef](#)] [[PubMed](#)]
205. Jayaraman, A.; Liu, M.; Ye, F.; Walter, G.A.; Vandenborne, K. Regenerative responses in slow- and fast-twitch muscles following moderate contusion spinal cord injury and locomotor training. *Eur. J. Appl. Physiol.* **2013**, *113*, 191–200. [[CrossRef](#)] [[PubMed](#)]
206. Dupont-Versteegden, E.E.; Murphy, R.J.; Houle, J.D.; Gurley, C.M.; Peterson, C.A. Mechanisms leading to restoration of muscle size with exercise and transplantation after spinal cord injury. *Am. J. Physiol. Cell Physiol.* **2000**, *279*, C1677–C1684. [[CrossRef](#)] [[PubMed](#)]
207. Astorino, T.A.; Harness, E.T.; Witzke, K.A. Chronic activity-based therapy does not improve body composition, insulin-like growth factor-i, adiponectin, or myostatin in persons with spinal cord injury. *J. Spinal Cord Med.* **2015**, *38*, 615–625. [[CrossRef](#)] [[PubMed](#)]
208. Petrie, M.; Suneja, M.; Shields, R.K. Low-frequency stimulation regulates metabolic gene expression in paralyzed muscle. *J. Appl. Physiol.* **2015**, *118*, 723–731. [[CrossRef](#)] [[PubMed](#)]
209. Gorgey, A.S.; Graham, Z.A.; Bauman, W.A.; Cardozo, C.; Gater, D.R. Abundance in proteins expressed after functional electrical stimulation cycling or arm cycling ergometry training in persons with chronic spinal cord injury. *J. Spinal Cord Med.* **2017**, *40*, 439–448. [[CrossRef](#)] [[PubMed](#)]
210. Adams, C.M.; Suneja, M.; Dudley-Javoroski, S.; Shields, R.K. Altered mRNA expression after long-term soleus electrical stimulation training in humans with paralysis. *Muscle Nerve* **2011**, *43*, 65–75. [[CrossRef](#)] [[PubMed](#)]
211. Cote, M.P.; Azzam, G.A.; Lemay, M.A.; Zhukareva, V.; Houle, J.D. Activity-dependent increase in neurotrophic factors is associated with an enhanced modulation of spinal reflexes after spinal cord injury. *J. Neurotrauma* **2011**, *28*, 299–309. [[CrossRef](#)] [[PubMed](#)]
212. Goldshmit, Y.; Lythgoe, N.; Galea, M.P.; Turnley, A.M. Treadmill training after spinal cord hemisection in mice promotes axonal sprouting and synapse formation and improves motor recovery. *J. Neurotrauma* **2008**, *25*, 449–465. [[CrossRef](#)] [[PubMed](#)]
213. Petruska, J.C.; Ichiyama, R.M.; Jindrich, D.L.; Crown, E.D.; Tansey, K.E.; Roy, R.R.; Edgerton, V.R.; Mendell, L.M. Changes in motoneuron properties and synaptic inputs related to step training after spinal cord transection in rats. *J. Neurosci.* **2007**, *27*, 4460–4471. [[CrossRef](#)] [[PubMed](#)]
214. Knikou, M. Neurophysiological characteristics of human leg muscle action potentials evoked by transcutaneous magnetic stimulation of the spine. *Bioelectromagnetics* **2013**, *34*, 200–210. [[CrossRef](#)] [[PubMed](#)]
215. Knikou, M.; Mummidisetti, C.K. Locomotor training improves premotoneuronal control after chronic spinal cord injury. *J. Neurophysiol.* **2014**, *111*, 2264–2275. [[CrossRef](#)] [[PubMed](#)]

216. Smith, A.C.; Mummidisetti, C.K.; Rymer, W.Z.; Knikou, M. Locomotor training alters the behavior of flexor reflexes during walking in human spinal cord injury. *J. Neurophysiol.* **2014**, *112*, 2164–2175. [CrossRef] [PubMed]
217. Smith, A.C.; Knikou, M. A review on locomotor training after spinal cord injury: Reorganization of spinal neuronal circuits and recovery of motor function. *Neural Plast.* **2016**, *2016*, 1216258. [CrossRef] [PubMed]
218. Alcobendas-Maestro, M.; Esclarin-Ruz, A.; Casado-Lopez, R.M.; Munoz-Gonzalez, A.; Perez-Mateos, G.; Gonzalez-Valdizan, E.; Martin, J.L. Lokomat robotic-assisted versus overground training within 3 to 6 months of incomplete spinal cord lesion: Randomized controlled trial. *NeuroRehabil. Neural Repair* **2012**, *26*, 1058–1063. [CrossRef] [PubMed]
219. Esclarin-Ruz, A.; Alcobendas-Maestro, M.; Casado-Lopez, R.; Perez-Mateos, G.; Florido-Sanchez, M.A.; Gonzalez-Valdizan, E.; Martin, J.L. A comparison of robotic walking therapy and conventional walking therapy in individuals with upper versus lower motor neuron lesions: A randomized controlled trial. *Arch. Phys. Med. Rehabil.* **2014**, *95*, 1023–1031. [CrossRef] [PubMed]
220. Field-Fote, E.C.; Lindley, S.D.; Sherman, A.L. Locomotor training approaches for individuals with spinal cord injury: A preliminary report of walking-related outcomes. *J. Neurol. Phys. Ther.* **2005**, *29*, 127–137. [CrossRef] [PubMed]
221. Kapadia, N.; Masani, K.; Catharine Craven, B.; Giangregorio, L.M.; Hitzig, S.L.; Richards, K.; Popovic, M.R. A randomized trial of functional electrical stimulation for walking in incomplete spinal cord injury: Effects on walking competency. *J. Spinal Cord Med.* **2014**, *37*, 511–524. [CrossRef] [PubMed]
222. Labruyere, R.; van Hedel, H.J. Strength training versus robot-assisted gait training after incomplete spinal cord injury: A randomized pilot study in patients depending on walking assistance. *J. Neuroeng. Rehabil.* **2014**, *11*, 4. [CrossRef] [PubMed]
223. Lam, T.; Pauhl, K.; Ferguson, A.; Malik, R.N.; Krassioukov, A.; Eng, J.J. Training with robot-applied resistance in people with motor-incomplete spinal cord injury: Pilot study. *J. Rehabil. Res. Dev.* **2015**, *52*, 113–129. [CrossRef] [PubMed]
224. Morrison, S.A.; Lorenz, D.; Eskay, C.P.; Forrest, G.F.; Basso, D.M. Longitudinal recovery and reduced costs after 120 sessions of locomotor training for motor incomplete spinal cord injury. *Arch. Phys. Med. Rehabil.* **2018**, *99*, 555–562. [CrossRef] [PubMed]
225. Niu, X.; Varoqui, D.; Kindig, M.; Mirbagheri, M.M. Prediction of gait recovery in spinal cord injured individuals trained with robotic gait orthosis. *J. Neuroeng. Rehabil.* **2014**, *11*, 42. [CrossRef] [PubMed]
226. Winchester, P.; McColl, R.; Querry, R.; Foreman, N.; Mosby, J.; Tansey, K.; Williamson, J. Changes in supraspinal activation patterns following robotic locomotor therapy in motor-incomplete spinal cord injury. *NeuroRehabil. Neural Repair* **2005**, *19*, 313–324. [CrossRef] [PubMed]
227. Wu, M.; Landry, J.M.; Schmit, B.D.; Hornby, T.G.; Yen, S.C. Robotic resistance treadmill training improves locomotor function in human spinal cord injury: A pilot study. *Arch. Phys. Med. Rehabil.* **2012**, *93*, 782–789. [CrossRef] [PubMed]
228. Galen, S.S.; Clarke, C.J.; McLean, A.N.; Allan, D.B.; Conway, B.A. Isometric hip and knee torque measurements as an outcome measure in robot assisted gait training. *NeuroRehabilitation* **2014**, *34*, 287–295. [PubMed]
229. Maier, I.C.; Ichiyama, R.M.; Courtine, G.; Schnell, L.; Lavrov, I.; Edgerton, V.R.; Schwab, M.E. Differential effects of anti-nogo-a antibody treatment and treadmill training in rats with incomplete spinal cord injury. *Brain* **2009**, *132*, 1426–1440. [CrossRef] [PubMed]
230. Battistuzzo, C.R.; Rank, M.M.; Flynn, J.R.; Morgan, D.L.; Callister, R.; Callister, R.J.; Galea, M.P. Gait recovery following spinal cord injury in mice: Limited effect of treadmill training. *J. Spinal Cord Med.* **2016**, *39*, 335–343. [CrossRef] [PubMed]
231. Battistuzzo, C.R.; Rank, M.M.; Flynn, J.R.; Morgan, D.L.; Callister, R.; Callister, R.J.; Galea, M.P. Effects of treadmill training on hindlimb muscles of spinal cord-injured mice. *Muscle Nerve* **2017**, *55*, 232–242. [CrossRef] [PubMed]
232. Shah, P.K.; Garcia-Alias, G.; Choe, J.; Gad, P.; Gerasimenko, Y.; Tillakaratne, N.; Zhong, H.; Roy, R.R.; Edgerton, V.R. Use of quadrupedal step training to re-engage spinal interneuronal networks and improve locomotor function after spinal cord injury. *Brain* **2013**, *136*, 3362–3377. [CrossRef] [PubMed]

233. Nessler, J.A.; De Leon, R.D.; Sharp, K.; Kwak, E.; Minakata, K.; Reinkensmeyer, D.J. Robotic gait analysis of bipedal treadmill stepping by spinal contused rats: Characterization of intrinsic recovery and comparison with bbb. *J. Neurotrauma* **2006**, *23*, 882–896. [CrossRef] [PubMed]
234. Oh, M.J.; Seo, T.B.; Kwon, K.B.; Yoon, S.J.; Elzi, D.J.; Kim, B.G.; Namgung, U. Axonal outgrowth and erk1/2 activation by training after spinal cord injury in rats. *J. Neurotrauma* **2009**, *26*, 2071–2082. [CrossRef] [PubMed]
235. Shin, H.Y.; Kim, H.; Kwon, M.J.; Hwang, D.H.; Lee, K.; Kim, B.G. Molecular and cellular changes in the lumbar spinal cord following thoracic injury: Regulation by treadmill locomotor training. *PLoS ONE* **2014**, *9*, e88215. [CrossRef] [PubMed]
236. Multon, S.; Franzen, R.; Poirrier, A.L.; Scholtes, F.; Schoenen, J. The effect of treadmill training on motor recovery after a partial spinal cord compression-injury in the adult rat. *J. Neurotrauma* **2003**, *20*, 699–706. [CrossRef] [PubMed]
237. Wu, Q.; Cao, Y.; Dong, C.; Wang, H.; Wang, Q.; Tong, W.; Li, X.; Shan, C.; Wang, T. Neuromuscular interaction is required for neurotrophins-mediated locomotor recovery following treadmill training in rat spinal cord injury. *PeerJ* **2016**, *4*, e2025. [CrossRef] [PubMed]
238. Foret, A.; Quertainmont, R.; Botman, O.; Bouhy, D.; Amabili, P.; Brook, G.; Schoenen, J.; Franzen, R. Stem cells in the adult rat spinal cord: Plasticity after injury and treadmill training exercise. *J. Neurochem.* **2010**, *112*, 762–772. [CrossRef] [PubMed]
239. Ward, P.J.; Herrity, A.N.; Smith, R.R.; Willhite, A.; Harrison, B.J.; Petruska, J.C.; Harkema, S.J.; Hubscher, C.H. Novel multi-system functional gains via task specific training in spinal cord injured male rats. *J. Neurotrauma* **2014**, *31*, 819–833. [CrossRef] [PubMed]
240. Park, K.; Lee, Y.; Park, S.; Lee, S.; Hong, Y.; Kil Lee, S. Synergistic effect of melatonin on exercise-induced neuronal reconstruction and functional recovery in a spinal cord injury animal model. *J. Pineal Res.* **2010**, *48*, 270–281. [CrossRef] [PubMed]
241. Liu, Q.; Zhang, B.; Liu, C.; Zhao, D. Molecular mechanisms underlying the positive role of treadmill training in locomotor recovery after spinal cord injury. *Spinal Cord* **2017**, *55*, 441–446. [CrossRef] [PubMed]
242. Hayashibe, M.; Homma, T.; Fujimoto, K.; Oi, T.; Yagi, N.; Kashihara, M.; Nishikawa, N.; Ishizumi, Y.; Abe, S.; Hashimoto, H.; et al. Locomotor improvement of spinal cord-injured rats through treadmill training by forced plantar placement of hind paws. *Spinal Cord* **2016**, *54*, 521–529. [CrossRef] [PubMed]
243. Heng, C.; de Leon, R.D. Treadmill training enhances the recovery of normal stepping patterns in spinal cord contused rats. *Exp. Neurol.* **2009**, *216*, 139–147. [CrossRef] [PubMed]
244. Shinozaki, M.; Iwanami, A.; Fujiyoshi, K.; Tashiro, S.; Kitamura, K.; Shibata, S.; Fujita, H.; Nakamura, M.; Okano, H. Combined treatment with chondroitinase abc and treadmill rehabilitation for chronic severe spinal cord injury in adult rats. *Neurosci. Res.* **2016**, *113*, 37–47. [CrossRef] [PubMed]
245. Robert, A.A.; Al Jadid, M.S.; Bin Afif, S.; Al Sowyed, A.A.; Al-Mubarak, S. The effects of different rehabilitation strategies on the functional recovery of spinal cord injured rats: An experimental study. *Spine* **2010**, *35*, E1273–E1277. [CrossRef] [PubMed]
246. Ichiyama, R.; Potuzak, M.; Balak, M.; Kalderon, N.; Edgerton, V.R. Enhanced motor function by training in spinal cord contused rats following radiation therapy. *PLoS ONE* **2009**, *4*, e6862. [CrossRef] [PubMed]
247. Tillakaratne, N.J.; Guu, J.J.; de Leon, R.D.; Bigbee, A.J.; London, N.J.; Zhong, H.; Ziegler, M.D.; Joynes, R.L.; Roy, R.R.; Edgerton, V.R. Functional recovery of stepping in rats after a complete neonatal spinal cord transection is not due to regrowth across the lesion site. *Neuroscience* **2010**, *166*, 23–33. [CrossRef] [PubMed]
248. See, P.A.; de Leon, R.D. Robotic loading during treadmill training enhances locomotor recovery in rats spinally transected as neonates. *J. Neurophysiol.* **2013**, *110*, 760–767. [CrossRef] [PubMed]
249. Timoszyk, W.K.; Nessler, J.A.; Acosta, C.; Roy, R.R.; Edgerton, V.R.; Reinkensmeyer, D.J.; de Leon, R. Hindlimb loading determines stepping quantity and quality following spinal cord transection. *Brain Res.* **2005**, *1050*, 180–189. [CrossRef] [PubMed]
250. Zhang, Y.; Ji, S.R.; Wu, C.Y.; Fan, X.H.; Zhou, H.J.; Liu, G.L. Observation of locomotor functional recovery in adult complete spinal rats with bwstt using semiquantitative and qualitative methods. *Spinal Cord* **2007**, *45*, 496–501. [CrossRef] [PubMed]
251. Lee, Y.S.; Zdunowski, S.; Edgerton, V.R.; Roy, R.R.; Zhong, H.; Hsiao, I.; Lin, V.W. Improvement of gait patterns in step-trained, complete spinal cord-transected rats treated with a peripheral nerve graft and acidic fibroblast growth factor. *Exp. Neurol.* **2010**, *224*, 429–437. [CrossRef] [PubMed]

252. De Leon, R.D.; Acosta, C.N. Effect of robotic-assisted treadmill training and chronic quipazine treatment on hindlimb stepping in spinally transected rats. *J. Neurotrauma* **2006**, *23*, 1147–1163. [CrossRef] [PubMed]
253. Moshonkina, T.R.; Gilerovich, E.G.; Fedorova, E.A.; Avelev, V.D.; Gerasimenko, Y.P.; Otellin, V.A. Morphofunctional basis for recovery of locomotor movements in rats with completely crossed spinal cord. *Bull. Exp. Biol. Med.* **2004**, *138*, 198–201. [CrossRef] [PubMed]
254. Kubasak, M.D.; Jindrich, D.L.; Zhong, H.; Takeoka, A.; McFarland, K.C.; Munoz-Quiles, C.; Roy, R.R.; Edgerton, V.R.; Ramon-Cueto, A.; Phelps, P.E. Oeg implantation and step training enhance hindlimb-stepping ability in adult spinal transected rats. *Brain* **2008**, *131*, 264–276. [CrossRef] [PubMed]
255. Fouad, K.; Metz, G.A.; Merkler, D.; Dietz, V.; Schwab, M.E. Treadmill training in incomplete spinal cord injured rats. *Behav. Brain Res.* **2000**, *115*, 107–113. [CrossRef]
256. Gomez-Pinilla, F.; Ying, Z.; Roy, R.R.; Molteni, R.; Edgerton, V.R. Voluntary exercise induces a bdnf-mediated mechanism that promotes neuroplasticity. *J. Neurophysiol.* **2002**, *88*, 2187–2195. [CrossRef] [PubMed]
257. Skup, M.; Dwornik, A.; Macias, M.; Sulejczak, D.; Wiater, M.; Czarkowska-Bauch, J. Long-term locomotor training up-regulates trkB(fl) receptor-like proteins, brain-derived neurotrophic factor, and neurotrophin 4 with different topographies of expression in oligodendroglia and neurons in the spinal cord. *Exp. Neurol.* **2002**, *176*, 289–307. [CrossRef] [PubMed]
258. Koliatsos, V.E.; Clatterbuck, R.E.; Winslow, J.W.; Cayouette, M.H.; Price, D.L. Evidence that brain-derived neurotrophic factor is a trophic factor for motor neurons in vivo. *Neuron* **1993**, *10*, 359–367. [CrossRef]
259. Blum, R.; Konnerth, A. Neurotrophin-mediated rapid signaling in the central nervous system: Mechanisms and functions. *Physiology* **2005**, *20*, 70–78. [CrossRef] [PubMed]
260. De Leon, R.D.; See, P.A.; Chow, C.H. Differential effects of low versus high amounts of weight supported treadmill training in spinally transected rats. *J. Neurotrauma* **2011**, *28*, 1021–1033. [CrossRef] [PubMed]
261. Dupont-Versteegden, E.E.; Houle, J.D.; Dennis, R.A.; Zhang, J.; Knox, M.; Wagoner, G.; Peterson, C.A. Exercise-induced gene expression in soleus muscle is dependent on time after spinal cord injury in rats. *Muscle Nerve* **2004**, *29*, 73–81. [CrossRef] [PubMed]
262. Gomez-Pinilla, F.; Ying, Z.; Opazo, P.; Roy, R.R.; Edgerton, V.R. Differential regulation by exercise of bdnf and nt-3 in rat spinal cord and skeletal muscle. *Eur. J. Neurosci.* **2001**, *13*, 1078–1084. [CrossRef] [PubMed]
263. Hutchinson, K.J.; Gomez-Pinilla, F.; Crowe, M.J.; Ying, Z.; Basso, D.M. Three exercise paradigms differentially improve sensory recovery after spinal cord contusion in rats. *Brain* **2004**, *127*, 1403–1414. [CrossRef] [PubMed]
264. Macias, M.; Nowicka, D.; Czupryna, A.; Sulejczak, D.; Skup, M.; Skangiel-Kramska, J.; Czarkowska-Bauch, J. Exercise-induced motor improvement after complete spinal cord transection and its relation to expression of brain-derived neurotrophic factor and presynaptic markers. *BMC Neurosci.* **2009**, *10*, 144. [CrossRef] [PubMed]
265. Ying, Z.; Roy, R.R.; Edgerton, V.R.; Gomez-Pinilla, F. Voluntary exercise increases neurotrophin-3 and its receptor trkc in the spinal cord. *Brain Res.* **2003**, *987*, 93–99. [CrossRef]
266. Ying, Z.; Roy, R.R.; Edgerton, V.R.; Gomez-Pinilla, F. Exercise restores levels of neurotrophins and synaptic plasticity following spinal cord injury. *Exp. Neurol.* **2005**, *193*, 411–419. [CrossRef] [PubMed]
267. Ying, Z.; Roy, R.R.; Zhong, H.; Zdunowski, S.; Edgerton, V.R.; Gomez-Pinilla, F. Bdnf-exercise interactions in the recovery of symmetrical stepping after a cervical hemisection in rats. *Neuroscience* **2008**, *155*, 1070–1078. [CrossRef] [PubMed]
268. Leech, K.A.; Hornby, T.G. High-intensity locomotor exercise increases brain-derived neurotrophic factor in individuals with incomplete spinal cord injury. *J. Neurotrauma* **2017**, *34*, 1240–1248. [CrossRef] [PubMed]
269. Farinas, I.; Jones, K.R.; Backus, C.; Wang, X.Y.; Reichardt, L.F. Severe sensory and sympathetic deficits in mice lacking neurotrophin-3. *Nature* **1994**, *369*, 658–661. [CrossRef] [PubMed]
270. Frisen, J.; Arvidsson, U.; Lindholm, T.; Fried, K.; Verge, V.M.; Cullheim, S.; Hokfelt, T.; Risling, M. Trkc expression in the injured rat spinal cord. *Neuroreport* **1993**, *5*, 349–352. [CrossRef] [PubMed]
271. Lohof, A.M.; Ip, N.Y.; Poo, M.M. Potentiation of developing neuromuscular synapses by the neurotrophins nt-3 and bdnf. *Nature* **1993**, *363*, 350–353. [CrossRef] [PubMed]
272. Scarsbrick, I.A.; Isackson, P.J.; Windebank, A.J. Differential expression of brain-derived neurotrophic factor, neurotrophin-3, and neurotrophin-4/5 in the adult rat spinal cord: Regulation by the glutamate receptor agonist kainic acid. *J. Neurosci.* **1999**, *19*, 7757–7769. [CrossRef] [PubMed]

273. Wang, T.; Xie, K.; Lu, B. Neurotrophins promote maturation of developing neuromuscular synapses. *J. Neurosci.* **1995**, *15*, 4796–4805. [CrossRef] [PubMed]
274. Fang, H.; Liu, C.; Yang, M.; Li, H.; Zhang, F.; Zhang, W.; Zhang, J. Neurotrophic factor and trk signaling mechanisms underlying the promotion of motor recovery after acute spinal cord injury in rats. *Exp. Ther. Med.* **2017**, *14*, 652–656. [CrossRef] [PubMed]
275. Bimonte-Nelson, H.A.; Nelson, M.E.; Granholm, A.C. Progesterone counteracts estrogen-induced increases in neurotrophins in the aged female rat brain. *Neuroreport* **2004**, *15*, 2659–2663. [CrossRef] [PubMed]
276. Gorgey, A.S.; Khalil, R.E.; Gill, R.; O'Brien, L.C.; Lavis, T.; Castillo, T.; Cifu, D.X.; Savas, J.; Khan, R.; Cardozo, C.; et al. Effects of testosterone and evoked resistance exercise after spinal cord injury (terex-sci): Study protocol for a randomised controlled trial. *BMJ Open* **2017**, *7*, e014125. [CrossRef] [PubMed]
277. Yarrow, J.F.; Conover, C.F.; Purandare, A.V.; Bhakta, A.M.; Zheng, N.; Conrad, B.; Altman, M.K.; Franz, S.E.; Wronski, T.J.; Borst, S.E. Supraphysiological testosterone enanthate administration prevents bone loss and augments bone strength in gonadectomized male and female rats. *Am. J. Physiol. Endocrinol. Metab.* **2008**, *295*, E1213–E1222. [CrossRef] [PubMed]
278. Yarrow, J.F.; Phillips, E.G.; Kok, H.J.; Conover, C.F.; Bassett, T.E.; Vasconeza, A.; Alerte, J.; Prock, H.; Flores, M.; Borst, S.E.; et al. Locomotor training with adjuvant testosterone promotes activity-mediated neuromuscular plasticity in spinal cord injured rats. *Med. Sci. Sports Exerc.* **2017**, *49*, 1038. [CrossRef]
279. Wang, X.; Smith, G.I.; Patterson, B.W.; Reeds, D.N.; Kampelman, J.; Magkos, F.; Mittendorfer, B. Testosterone increases the muscle protein synthesis rate but does not affect very-low-density lipoprotein metabolism in obese premenopausal women. *Am. J. Physiol. Endocrinol. Metab.* **2012**, *302*, E740–746. [CrossRef] [PubMed]
280. Spinal Cord Injury (SCI) Facts and Figures at a Glance. Available online: <https://www.ncisc.uab.edu/Public/Facts%202016.pdf> (accessed on 25 May 2018).
281. Calof, O.M.; Singh, A.B.; Lee, M.L.; Kenny, A.M.; Urban, R.J.; Tenover, J.L.; Bhasin, S. Adverse events associated with testosterone replacement in middle-aged and older men: A meta-analysis of randomized, placebo-controlled trials. *J. Gerontol. A Biol. Sci. Med. Sci.* **2005**, *60*, 1451–1457. [CrossRef] [PubMed]
282. Basaria, S.; Covillejo, A.D.; Travison, T.G.; Storer, T.W.; Farwell, W.R.; Jette, A.M.; Eder, R.; Tennstedt, S.; Ulloor, J.; Zhang, A.; et al. Adverse events associated with testosterone administration. *N. Engl. J. Med.* **2010**, *363*, 109–122. [CrossRef] [PubMed]
283. Finkle, W.D.; Greenland, S.; Ridgeway, G.K.; Adams, J.L.; Frasco, M.A.; Cook, M.B.; Fraumeni, J.F., Jr.; Hoover, R.N. Increased risk of non-fatal myocardial infarction following testosterone therapy prescription in men. *PLoS ONE* **2014**, *9*, e85805. [CrossRef] [PubMed]
284. Vigen, R.; O'Donnell, C.I.; Baron, A.E.; Grunwald, G.K.; Maddox, T.M.; Bradley, S.M.; Barqawi, A.; Wonong, G.; Wierman, M.E.; Plomondon, M.E.; et al. Association of testosterone therapy with mortality, myocardial infarction, and stroke in men with low testosterone levels. *JAMA* **2013**, *310*, 1829–1836. [CrossRef] [PubMed]
285. Morgentaler, A.; Lunenfeld, B. Testosterone and cardiovascular risk: World's experts take unprecedented action to correct misinformation. *Aging Male* **2014**, *17*, 63–65. [CrossRef] [PubMed]
286. Traish, A.M.; Guay, A.T.; Morgentaler, A. Death by testosterone? We think not! *J. Sex. Med.* **2014**, *11*, 624–629. [CrossRef] [PubMed]
287. Borst, S.E.; Shuster, J.J.; Zou, B.; Ye, F.; Jia, H.; Wokhlu, A.; Yarrow, J.F. Cardiovascular risks and elevation of serum dht vary by route of testosterone administration: A systematic review and meta-analysis. *BMC Med.* **2014**, *12*, 211. [CrossRef] [PubMed]
288. Onasanya, O.; Iyer, G.; Lucas, E.; Lin, D.; Singh, S.; Alexander, G.C. Association between exogenous testosterone and cardiovascular events: An overview of systematic reviews. *Lancet Diabetes Endocrinol.* **2016**, *4*, 943–956. [CrossRef]
289. Sharma, R.; Oni, O.A.; Gupta, K.; Chen, G.; Sharma, M.; Dawn, B.; Parashara, D.; Savin, V.J.; Ambrose, J.A.; Barua, R.S. Normalization of testosterone level is associated with reduced incidence of myocardial infarction and mortality in men. *Eur. Heart J.* **2015**, *36*, 2706–2715. [CrossRef] [PubMed]
290. La Fountaine, M.F.; Wecht, J.M.; Cirigliaro, C.M.; Kirshblum, S.C.; Spungen, A.M.; Bauman, W.A. Testosterone replacement therapy improves q-tavi in hypogonadal men with spinal cord injury. *Neuroendocrinology* **2013**, *97*, 341–346. [CrossRef] [PubMed]
291. Hamid, R.; Averbeck, M.A.; Chiang, H.; Garcia, A.; Al Mousa, R.T.; Oh, S.J.; Patel, A.; Plata, M.; Del Popolo, G. Epidemiology and pathophysiology of neurogenic bladder after spinal cord injury. *World J. Urol.* **2018**. [CrossRef] [PubMed]

292. Page, S.T.; Amory, J.K.; Bowman, F.D.; Anawalt, B.D.; Matsumoto, A.M.; Bremner, W.J.; Tenover, J.L. Exogenous testosterone (T) alone or with finasteride increases physical performance, grip strength, and lean body mass in older men with low serum T. *J. Clin. Endocrinol. Metab.* **2005**, *90*, 1502–1510. [[CrossRef](#)] [[PubMed](#)]
293. Amory, J.K.; Watts, N.B.; Easley, K.A.; Sutton, P.R.; Anawalt, B.D.; Matsumoto, A.M.; Bremner, W.J.; Tenover, J.L. Exogenous testosterone or testosterone with finasteride increases bone mineral density in older men with low serum testosterone. *J. Clin. Endocrinol. Metab.* **2004**, *89*, 503–510. [[CrossRef](#)] [[PubMed](#)]
294. Clinicaltrials.Gov. Available online: <https://clinicaltrials.gov/ct2/show/NCT02248701> (accessed on 25 May 2018).
295. Kaplan, A.L.; Hu, J.C. Use of testosterone replacement therapy in the united states and its effect on subsequent prostate cancer outcomes. *Urology* **2013**, *82*, 321–326. [[CrossRef](#)] [[PubMed](#)]
296. Jia, H.; Sullivan, C.T.; McCoy, S.C.; Yarrow, J.F.; Morrow, M.; Borst, S.E. Review of health risks of low testosterone and testosterone administration. *World J. Clin. Cases* **2015**, *3*, 338–344. [[CrossRef](#)] [[PubMed](#)]
297. Cole, A.P.; Hanske, J.; Jiang, W.; Kwon, N.K.; Lipsitz, S.R.; Kathrins, M.; Learn, P.A.; Sun, M.; Haider, A.H.; Basaria, S.; et al. Impact of testosterone replacement therapy on thromboembolism, heart disease and obstructive sleep apnoea in men. *BJU Int.* **2018**, *121*, 811–818. [[CrossRef](#)] [[PubMed](#)]
298. Chiodo, A.E.; Sitrin, R.G.; Bauman, K.A. Sleep disordered breathing in spinal cord injury: A systematic review. *J. Spinal Cord Med.* **2016**, *39*, 374–382. [[CrossRef](#)] [[PubMed](#)]



© 2018 by the authors. Licensee MDPI, Basel, Switzerland. This article is an open access article distributed under the terms and conditions of the Creative Commons Attribution (CC BY) license (<http://creativecommons.org/licenses/by/4.0/>).



Review

# Translational Regenerative Therapies for Chronic Spinal Cord Injury

Kyriakos Dalamagkas <sup>1,2,†</sup>, Magdalini Tsintou <sup>2,3,†</sup>, Amelia Seifalian <sup>4</sup> and Alexander M. Seifalian <sup>5,\*</sup>

<sup>1</sup> The Institute for Rehabilitation and Research, Memorial Hermann Texas Medical Centre, Houston, TX 77030, USA; [dalakir@gmail.com](mailto:dalakir@gmail.com)

<sup>2</sup> Centre for Nanotechnology & Regenerative Medicine, Division of Surgery and Interventional Science, University College of London (UCL), London NW3 2QG, UK; [magda.tsintou@gmail.com](mailto:magda.tsintou@gmail.com)

<sup>3</sup> Center for Neural Systems Investigations, Massachusetts General Hospital/HST Athinoula A., Martinos Centre for Biomedical Imaging, Harvard Medical School, Boston, MA 02129, USA

<sup>4</sup> Faculty of Medical Sciences, UCL Medical School, London WC1E 6BT, UK; [asseifalian@yahoo.co.uk](mailto:asseifalian@yahoo.co.uk)

<sup>5</sup> NanoRegMed Ltd. (Nanotechnology & Regenerative Medicine Commercialization Centre), The London BioScience Innovation Centre, London NW1 0NH, UK

\* Correspondence: [a.seifalian@gmail.com](mailto:a.seifalian@gmail.com); Tel.: +44-20-7691-1122 or +44-7985-380-797

† These authors contributed equally to this work.

Received: 30 April 2018; Accepted: 6 June 2018; Published: 15 June 2018

**Abstract:** Spinal cord injury is a chronic and debilitating neurological condition that is currently being managed symptomatically with no real therapeutic strategies available. Even though there is no consensus on the best time to start interventions, the chronic phase is definitely the most stable target in order to determine whether a therapy can effectively restore neurological function. The advancements of nanoscience and stem cell technology, combined with the powerful, novel neuroimaging modalities that have arisen can now accelerate the path of promising novel therapeutic strategies from bench to bedside. Several types of stem cells have reached up to clinical trials phase II, including adult neural stem cells, human spinal cord stem cells, olfactory ensheathing cells, autologous Schwann cells, umbilical cord blood-derived mononuclear cells, adult mesenchymal cells, and autologous bone-marrow-derived stem cells. There also have been combinations of different molecular therapies; these have been either alone or combined with supportive scaffolds with nanostructures to facilitate favorable cell–material interactions. The results already show promise but it will take some coordinated actions in order to develop a proper step-by-step approach to solve impactful problems with neural repair.

**Keywords:** neuroregeneration; chronic spinal cord injury; central nervous system; stem cells; molecular therapies; biomaterials; nanotechnology; nanomaterial

## 1. Introduction

Regenerative medicine is an exciting and relatively new field of medicine that is still in its infancy. Several attempts have been made for new and innovative applications in clinical practice. Chronic spinal cord injury (SCI) sets an excellent example because there are currently no interventions to restore body functions after chronic SCI, so novel regenerative interventions can be tested using several already developed, clinically relevant chronic SCI models. This can not only make a significant difference in the clinic and the patient's overall functional outcome and quality of life, but also in the financial burden within society, given the enormous healthcare cost linked to chronic SCI [1]. Despite the severe and devastating nature of the condition, from a research point of view, chronic SCI could be perceived as a natural opportunity to utilize the potentials of regenerative therapies to overcome the

boundaries that such an untreatable condition set. Due to the inherent inability of the Central Nervous System (CNS) to regenerate, chronic SCI poses a great challenge for regenerative medicine to prove its utility for real-world applications, opening the pathway for further CNS applications.

SCI is a devastating disease that results in paralysis, either immediately following the injury or in a very short period of time, depending on the cause, e.g., neurotrauma, inflammatory disease, etc. The current state-of-the-art intervention for SCI is neurorehabilitation. Surgery might initially be needed in order to stabilize the bone structure. After that the patients are transferred to a rehabilitation unit in order to learn how to take care of their basic bodily functions, e.g., bowel and bladder management, as well as in order to develop important skills that will help them reintegrate into society. Although rehabilitation is the only strategy used to manage SCI for the time being, its efficacy and reproducibility depend on many factors. For example, the individual's personality and his perceptions may hinder his adaptation to the changes. In addition to that, the type of impairment plays a significant role too, for example, high versus low SCI lesions. Finally, another important factor to consider, which influences rehabilitation, is the type of environment/community where the person is to be reintegrated, e.g., developed versus developing countries, present or absent laws for people with disabilities in society and the needed infrastructure for an accessible environment in the community.

SCI can be divided into three phases: acute, subacute, and chronic (Figure 1). The most plausible and within reach target for regenerative medicine for proof of concept of translational applications seems to be the chronic phase, when inflammation has subsided and any kind of neural plasticity and spontaneous regeneration has already failed, making the interpretation of any results much clearer. Many scientists argue that regeneration is a major challenge after the lesion is well established in the chronic phase and this is why most of the studies focus on acute SCI, avoiding the formation of a glial scar, which would make any interventions harder. Nevertheless, it has been demonstrated before that bridging axonal regeneration in the adult CNS after a chronic SCI lesion is achievable as long as both the intrinsic growth state of the neuron and the nonpermissive established injury environment get modified [2,3].

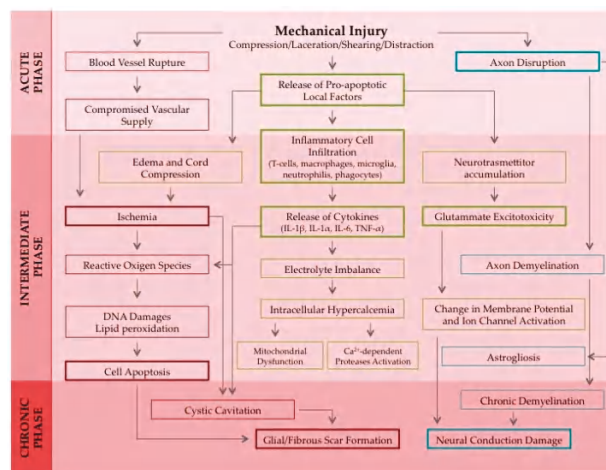


**Figure 1.** This is a schematic representation of the cascade of events that are included in the pathophysiological response to a spinal cord injury induced by a mechanical trauma. All the phases from the acute to the sub-acute and chronic SCI are being depicted until cavitation occurs in the lesion site and the glial scar forms. Abbreviations used: IL-1 $\alpha$ : Interleukin 1 $\alpha$ ; IL-1 $\beta$ : Interleukin 1 $\beta$ ; IL-6: Interleukin 6; TNF- $\alpha$ : Tumor Necrosis Factor  $\alpha$ . Figure reprinted with permission from "Nanofiber Scaffolds as Drug Delivery Systems to Bridge Spinal Cord Injury" by Faccendini et al., *Pharmaceutics* 2017, 10, 63, licensed under a Creative Commons Attribution license [4].

Currently there are several clinical trials worldwide that attempt to deliver feasibility/proof of concept for regenerative therapies. Two main approaches are currently being used and they are discussed in the “Cell therapies” and “Molecular therapies” sections below in order to bring the most promising translational research for chronic SCI to the attention of the scientific community. This is crucial, given the overwhelming number of publications, reported over 11,000 within the past five years on such a promising field, leading to the inability of research work to focus on promising therapies that are closer to clinical translation. The purpose of this article is not to include an extensive list of therapeutic strategies for chronic SCI, but to focus on the ones that are the most promising for future applications in the clinic. The key aspect affecting the success of such therapeutic strategies is the use and proper choice of biomaterials for the development of 3D scaffolds to support nerve growth within the cavity lesion, as well as providing trophic factors, biomolecules, and/or cells as delivery systems. Due to their importance, we have also included a last section with selected biomaterials that we think will be excellent candidates for future clinical applications, given their promising preclinical results.

## 2. Cell Therapies

Cell-based translational therapies have attempted using types of stem cells alone or in combination with growth factors or other molecules in order to induce nerve–axon sprouting or to neutralize the growth inhibitor factors. Stem cells have also been used in conjunction with biocompatible scaffolds, which encapsulate and gradually release the cells, guiding and tuning the process of nerve growth and repair. Several clinical trials have arisen that target chronic SCI.

### 2.1. The “Pathway Study” of Stemcell Inc. (Phase I/II Clinical Trials)

The “Pathway study” [5,6] used adult neural stem cells (NSCs) derived from fetal tissue for transplantation to chronic SCI, recruiting patients with cervical SCI lesions. Unfortunately, the study had to stop due to results that were deemed too moderate for Stemcell Inc., given the funding that the study needed for its completion. This was despite the improvement noted, especially in hand function, in a few of the recruited patients after the transplantation.

Based on the company’s reports, all state and federal guidelines were followed when obtaining the human fetal brains from Advance Bioscience Resources. The company used HuCNS-SC product in a form of “neurospheres” for transplantation. This product is comprised of a highly purified population of human neural stem cells that are grown in a suspension as clusters of cells, hence why it is called “neurospheres”. The rationale for using those cells is that they can maintain their ability to self-renew and differentiate into the three major cell types of the CNS (i.e., neurons, astrocytes, and oligodendrocytes) after being cultured and expanded for a number of generations. Even though the use of the HuCNS-SC product was found to be safe and encouraging patterns of motor and sensory improvements were noted at the 6-month mark of the study, the improvement declines over time. Even though there was still improvement compared to the baseline, the results were not considered to be adequate enough to justify the cost of the study.

### 2.2. Phase I Clinical Trial of NeuralStem Inc.

NeuralStem Inc. [7] has enrolled four American Spinal Injury Association (ASIA) Impairment Scale (AIS)-A thoracic chronic SCI subjects (1–2 years post-injury at the time of stem cell treatment) for the ongoing clinical trial phase I that they are conducting for chronic SCI. The company uses human spinal cord stem cells (NSI-566), stemming from a single 8-week-old fetus. The cells are expanded serially by epigenetic means only. NSI-566 is a novel human neural stem cell line that possesses robust growth properties and neurogenic potential. In preclinical models, when the cells were grafted into a rat spinal cord, the cells differentiated extensively into neurons and glia, secreted neurotrophic factors and formed synapses with the host neural cells, but not with muscles [8,9].

Even though there are no published data available yet, the last surgery was completed in July of 2015, so the company has already conducted a 6-month post-observation analysis of the results. The company claims that the treatment was well tolerated with no serious adverse reactions. The enrolled subjects are currently being monitored for long-term follow-up evaluations. The Food and Drug Administration (FDA) has approved the protocol amendment to treat an additional cohort of four cervical SCI patients. In April 2018, Neuralstem Inc. announced the completion of the first surgery in the cervical cohort of the Phase I clinical trial in patients with chronic SCI. At the same time, NeuralStem Inc. has already proceeded with a phase I/II clinical trial to treat motor deficits in stroke patients and to establish a treatment for Amyotrophic Lateral Sclerosis (ALS). Thus, during the next decade, there is probably a lot more to be explored in terms of clinical applications of fetal stem cells.

Recently, Rosenzweig et al. [10] published a very promising research paper about the restorative effects of NeuralStem Inc. donated cells in nonhuman primate spinal cord models. In particular, they grafted spinal cord-derived neural progenitor cells (NPCs) into sites of cervical C7 hemisection spinal cord lesions 2 weeks after the hemisections surgery took place. During a 9-month analysis, forelimb function improvement was noted several months after the grafting took place, while monkey axons were found to regenerate and form synapses, suggesting translatability of the NPCs graft therapy to humans.

### 2.3. The Chronic SCI Stem Cell Study of InVivo Therapeutics

The neurospinal scaffold made by InVivo therapeutics company in USA is composed of FDA approved poly(lactic-co-glycolic acid) (PLGA) covalently conjugated to poly(L-lysine) to facilitate favorable cell–material interactions. InVivo Therapeutics utilizes injectable combinations of biomaterials and NSCs, delivered using minimally invasive surgical instrumentation and techniques to create trails across the chronic injury site.

InVivo Therapeutics has already announced several promising results on the progress of the acute SCI study, called INSPIRE [11], which has already reached to a phase III clinical trial. The company recently reported that seven of 16 (43.8%) evaluable patients in the INSPIRE study experienced an improvement in the AIS grade from baseline at six months compared to the Objective Performance Criterion (study success definition) of 25% of patients. Of these seven patients, three of five individuals who had converted from AIS A SCI (complete) to AIS B SCI (sensory incomplete) in the first six-month period of follow-up subsequently further improved to AIS C SCI (motor incomplete) within 12 to 24 months, including a recent patient who converted from AIS B to AIS C at the 12-month exam in January 2018.

Unfortunately, three deaths were witnessed during the INSPIRE study that were considered to be unrelated to the Neuro-Spinal Scaffold used and the implantation technique. Nevertheless, the company has elected, based in part on discussions with the company's independent Data Safety Monitoring Board, to implement a temporary halt to enrolment as it engages with the FDA to determine whether any changes to patient enrolment criteria related to patients who may have a higher mortality risk or other study modifications are deemed necessary.

As a result of the temporary enrolment halt, the company anticipated completing INSPIRE enrolment in the first half of 2018 and submitting a Humanitarian Device Exemption (HDE) application in the second half of 2018. As per a recent press release of the company in March 2018, the company has received supplemental Investigational Device Exemption (IDE) approval from the US FDA for a second pivotal clinical study of the company's Neuro-Spinal Scaffold in patients with acute SCI.

In the meantime, InVivo therapeutics took the decision to focus only on the INSPIRE study for the time being, so they announced the temporary suspension of the chronic SCI stem cell study.

#### 2.4. “Walk Again Project”

Raisman and co-workers in London, who pioneered the “Walk Again Project” [12]. Unfortunately, he passed away but his work is being continued by Tabakow and co-workers in Poland, the leading neurosurgeon involved in Raisman’s project. The project focuses on the use of Olfactory Ensheathing Cells (OECs) in order to accomplish functional improvement after SCI. Even though there are many unidentified mechanisms involved, OECs have been used for years in clinical trials for CNS repair and one of their functions is thought to be helping the local propriospinal interneurons to create new circuits for bypassing the lesion. The first clinical trials of OECs have already taken place in China, Australia, and Spain in 2003, 2005, and 2006, respectively [13–15]. Ever since, significant progress has been accomplished and the safety of OECs transplantation in humans has been established through several phase I clinical trials [16]. Nevertheless, the need for robust, well-designed phase II clinical trials is still unmet in order to measure the efficacy of that technique. Through such future clinical trials, the technique can be optimized in order to accomplish the optimal harvesting methodology and maximize the viability of the cells after transplantation [17].

Despite all the current limitations regarding the OECs transplantation technique, Geoffrey Raisman’s team in UCL reported very promising results, from an injured patient, in 2014 (Figure 2). As per the report, the recipient of the transplanted OECs demonstrated significant functional recovery below the level of SCI, favoring the use of OECs as an efficient treatment of SCI [12]. It is remarkable that the patient went from complete paraplegia to incomplete (ASIA A to ASIA C) and has regained considerable functions. Nevertheless, expectations from this study have to be tempered since we are now talking about a single patient. Chronic SCI patients are still (since March 2016) being recruited for a new clinical trial taking place in Poland (Tabakow and colleagues). As far as we know, the clinical trial follows the same protocol as the one that was applied to the first patient, i.e., extraction of olfactory cells from the olfactory bulb in the patient’s brain, transplantation into the spinal cord and a peripheral nerve graft. Only patients with a transected/severed spinal cord can apply for the trial and not patients with contused spinal cord.

#### 2.5. “Miami Project” Phase I Clinical Trial

Schwan cells (SCs) are supporting cells surrounding the peripheral nerves. In the peripheral nervous system (PNS) they are thought to provide guidance to the axons for regeneration to take place [18]. The idea of using SCs after chronic SCI stems from the observation that SCs have been found around the lesion site after SCI [19,20], demonstrating beneficial effects. Nevertheless, it has been shown that apoptosis is a big obstacle, given the hostile CNS environment that does not favor the survival of those cells [21,22]. Despite the challenges, SCs are being used, for years now, in clinical trials targeting CNS lesions. Their safety has already been demonstrated in two already completed clinical trials involving SCs transplantation in human spinal cords. Currently, two more clinical trials phase I are in progress in Miami, Florida, USA, both studying sub-acute and chronic SCI subjects, in order to establish the safety of SCs before proceeding.

The “Miami Project” is a Phase I clinical trial for chronic SCI patients, it is currently recruiting patients and is expected to be completed by January 2019. Trial enrolment will target 2 cohorts. The study uses autologous Schwann cells harvested from the sural nerve of the participant, those cells are being transplanted into the epicenter of the participant’s SCI. The first cohort is announced to be thoracic (T) level 2–12 AIS grade A, B, or C ( $n =$  up to 4) and the second one to be cervical (C) level 5 through T1 AIS A, B, or C ( $n =$  up to 6).

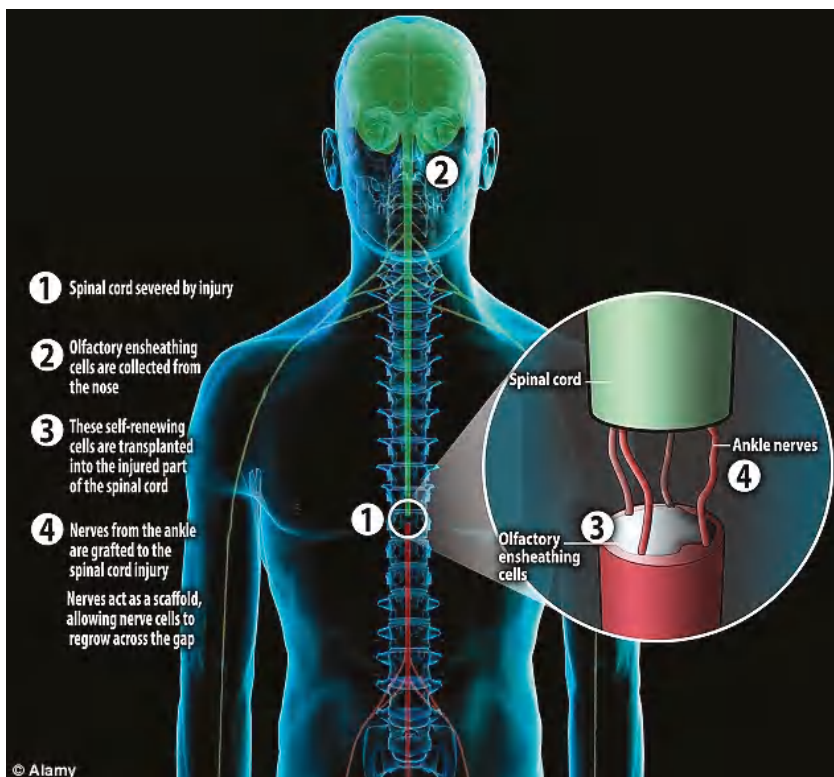


**Figure 2.** Schematic diagram shows steps of the treatment of Spinal Cord Injury (SCI) in a male patient who was paralyzed due to knife injury in 2010. He was treated with Olfactory Ensheathing Cells (OECs), a type of cell which is produced at the base of brain and through which human beings get their sense of smell. The surgeon extracted OECs from the nasal cavity and cultured those in the lab. Then nerve grafts were extracted from the ankle of the patient to support the regeneration of severed spinal cord nerve fibers to fill the spinal cavity. Both nerve grafts and stem cells were injected into the spinal cord injured site of the patient. This figure is also available online: <http://www.dailymail.co.uk/sciencetech/article-2800988/world-man-spinal-cord-severed-walks-paralysed-fireman-recovers-thanks-uk-research.html>.

## 2.6. Umbilical Cord Blood & Lithium ChinaSCINet Phase II Clinical Trial

In the fall of 2014, Wise Young, from Rutgers University and SCINetChina (available online: <http://www.chinascinet.org>), presented some preliminary information from the Umbilical Cord Blood & Lithium Phase II clinical trial that had taken place in China. In this trial [23], umbilical cord blood mononuclear cells (UCB-MNC) and lithium are used as a combinatorial therapy. The rationale for using lithium is that, apart from the low cost and availability in the clinic, it is known to stimulate UCB-MNC cells to secrete Nerve Growth Factor (NGF), Neurotrophin-3 (NT-3), and Glial cell line-derived Neurotrophic Factor (GDNF). In terms of the selection of UCB-MNCs, the aim is to improve recovery after chronic SCI. Several mechanisms have been proposed for the UCB-MNCs to improve recovery after CNS injury, involving secretion of anti-inflammatory cytokines [24–26], growth factors release [27–29], matrix metalloproteinase upregulation [25], tissue plasminogen activator downregulation [26], apoptosis prevention [24], mediation in myelination process [30,31], decreased gliosis [32], and increased angiogenesis [33].

Several groups have been known to attempt UCB-MNCs transplantation in patients with SCI with favorable outcomes. In the ChinaSCINet Phase I and II clinical trials [23], the patients were treated in Hong Kong (HK) and Kunming (KM) to assess the safety and efficacy of transplanting escalating doses of human leukocyte antigen (HLA)-matched UCB-MNCs into the spinal cords of people with chronic (1–19 years after) complete SCI. Wise Young explained in his presentation on the preliminary findings of the clinical trials that although none of the chronic ASIA A participants had improved motor scores, 15 out of the 20 patients were able to take steps with the aid of a walker whilst in rehabilitation.

Even though the motor scores of the chronic ASIA A patients did not improve, “functional recovery” was noted, which has raised some concerns. The main limitation is the absence of appropriate controls to assess the real effect of the UCB-MNCs transplantation. The fact that the intensive physiotherapy program was followed in combination with the stem cell transplant made it difficult to assess the real source of the improvements noted and would require further assessment. There is a possibility for the conduction of a phase IIb similar clinical trial in United States, aiming at proving the efficacy of the treatment. The structure of that new study is meant to be as follows: three groups of nine ASIA A, C5-T10 patients. The first group will get UCB-MNCs injections plus six weeks of oral lithium plus intensive rehabilitation. The second group will get UCB-MNCs plus intensive rehabilitation. Group three will get intensive rehabilitation only. This new study’s structure would certainly overcome the limitations of the previous study conducted in HK and KM.

## 2.7. The Puerta de Hierro Phase I/II Clinical Trial

In the Puerta de Hierro Phase I/II clinical trials [34], autologous bone marrow adult mesenchymal stem cells (MSCs) were used for the studies, establishing the safety of the technique. MSCs have already been correlated with beneficial outcomes when being transplanted in CNS lesions in small and big preclinical animal models, paving the way towards clinical translation. Even though MSCs were traditionally known to be able to self-renew and differentiate into cells of mesodermal origin, they have also been found to differentiate into tissue of nonmesoderm origin (i.e., nerve tissue) and they have the potential to modulate the inflammatory response [35,36]. In that trial, the MSCs were administered by intrathecal injection (subarachnoid and intramedullary). Improvement was noted even in the patients with the longest chronicity, while the team studied both complete and incomplete chronic SCI.

In the complete chronic SCI study, the recovery noted was considered to be a result of cytokine release by the transplanted MSCs, activating preserved but nonfunctional circuits, rather than inducing nerve regeneration. This is because the recovery of infratentorial sensitivity and vegetative functions (e.g., bladder, bowel, and sexual functions) occurred soon after surgery. In addition, a dose-dependent beneficial effect of the MSCs transplantation was suggested because the improvement noted in the scaled used (e.g., ASIA, International Association of Neurorestoratology Spinal Cord Injury Functional Rating Scale (IANR-SCI-FRS) and neurogenic bowel dysfunction (NBD)) was more significant for higher numbers of transplanted cells.

In the incomplete chronic SCI study, the repeated subarachnoid administrations of autologous MSCs supported in autologous plasma at months 1, 4, 7, and 10 of the study improved the patients’ quality of life. Nevertheless, objective neuroimaging findings that would suggest morphological changes in the lesion site after the repeated subarachnoid administration of MSCs were absent. Therefore, the improvements were considered to be a result of the release of neurotrophic factors. It is in fact thought that the potential of MSCs transplantation for CNS regeneration relies on the ability of the MSCs to modulate the environment through their secretome. Classic growth factors and cytokines packed and secreted by the MSCs [37] are now thought to play a significant role for SCI repair, possibly by decreasing the levels of proinflammatory cytokines like Interleukine-2 (IL-2), Interleukine-6 (IL-6), and Tumor Necrosis Factor  $\alpha$  (TNF $\alpha$ ), among other mechanisms. This is demonstrated in a recent paper of Cizkova et al., where the molecular cocktail found in the MSCs after the MSCs transplantation in the rat SCI model was thought to be responsible for the observed motor function recovery, the attenuated inflammatory response and for the spared spinal cord tissue [38].

The Puerta de Hierro clinical trial phase II has been completed but an announcement on future trials is still pending.

#### 2.8. "Neurocell" Pre-Clinical Study of Neuroplast (Phase I Clinical Trial in Preparation)

A preclinical study of Neuroplast, a company based in the Netherlands, showed that NEUROCELL (Neuroplast proprietary cells that are autologous bone-marrow-derived stem cells) significantly improved both locomotor functions and survival in those spinal cord-lesioned rats as compared to rats treated with a placebo. It is thought that autologous bone-marrow-derived stem cells can lead to functional improvement after CNS injuries by contributing towards the neuroplasticity and/or by exerting a paracrine effect. Neuroplast is currently preparing a Phase I clinical trial for chronic SCI patients. The trial will involve the transplantation of Neurocells and is expected to take place in Europe. The Neurocells are meant to have a positive effect, both in terms of neuroprotection and neuroplasticity, and thus contribute to a level of functional return in the case of both chronic and acute SCI. The first chronic SCI patients are expected to be recruited during 2018.

#### 2.9. Less Strictly Regulated Clinical Trials

It should be noted that further trials in SCI patients are being conducted all over the world, but they are not performed under strict regulatory environments so caution is advised when assessing the results of such studies until further work is done in order to confirm findings in a better regulated setting [39–45].

### 3. Molecular Therapies

A summary of the various molecular therapies in the nanoscale projects is included in Table 1.

**Table 1.** Summary of the various molecular therapies in the nanoscale projects that show promise for the treatment of SCI. Keys: CNS: Central Nervous System; SCI: spinal cord injury; Ch'ase: Chondroitinase.

Project Name	Mechanism	Current Progress	Future Outlook	Ref.
Nogo Trap of ReNetX Bio	A decoy receptor that binds growth inhibitors, allowing for the nerve fibers to grow naturally and directly.	Nogo Trap has demonstrated improved neurologic function following CNS damage in several animal models.	Planning phase Ib–Ila clinical trials to test safety and efficacy for patients with a chronic cervical incomplete SCI.	[46]
CHASE-IT Preclinical Initiative of the International Spinal Research Trust (ISRT)	The application of the biological enzyme Ch'ase in animal models is reported to have degraded scar tissue, promoted growth and improved activity.	Ch'ase has proven to be effective in rats, delivered to both thoracic and cervical contusion injury sites. Latest animal studies took place in 2016 and proved that longer-term application of the enzyme led to more significant motor control improvement.	Promising outcome, but one should bear in mind that data is based on rodent <i>in vivo</i> models; will this translate to humans?	[47]
Intracellular sigma peptide (ISP), Ch'ase and combinations preclinical projects	Using the biological enzyme Ch'ase in combinations with intracellular sigma peptide in order to restore breathing after long chronic C2 hemisection injury.	These projects are at a single center led by Jerry Silver. Currently these applications are at a pre-clinical stage.	Development of the product and preparation for clinical trials.	[48]

#### 3.1. Nogo Trap of ReNetX Bio (Formerly Known as Axerion Therapeutics)

Nogo Trap is a decoy receptor developed by the ReNetX Bio company. The decoy receptor is meant to modify the hostile CNS environment by binding to the growth inhibitors within the CNS. This allows new nerve fiber growth, targeting restoration across all facets of growth: axonal regeneration (long distance), axonal sprouting (medium distance), and synaptic plasticity. The main difference to the widely-known "Anti-NoGo" technology, as per the ReNetX representatives, is that the Nogo Trap is able to bind and neutralize three types of inhibitors and is not limited to the NoGo-inhibitor alone.

Nogo Trap has demonstrated improved neurologic function following CNS damage in several animal models. Based on these promising results, the company thought that Nogo Trap should be evaluated in chronic SCI patients. ReNetX Bio is planning a phase Ib–IIa clinical trial in order to test the safety and efficacy of the treatment for patients with chronic cervical incomplete SCI.

### 3.2. CHASE-IT Preclinical Initiative of the International Spinal Research Trust (ISRT)

Chondroitinase, or Ch'ase [49], is a bacterial enzyme that has attracted the attention of neuroscientists because of its ability to degrade the glial scar tissue that develops in chronic SCI. Apart from that, it has also repeatedly been proven to promote growth and to improve recovery in preclinical animal experiments. Therefore, Ch'ase is able to modify the scar tissue that develops after SCI and promote rewiring of the nervous system. This was only made possible by the molecular re-engineering of Ch'ase, developed by Muir and colleagues [50] at the University of Cambridge, who created a version of Ch'ase that could be expressed by human cells.

Gene therapy using a modified Chondroitinase ABC (ChABC) gene compatible with expression and secretion by mammalian host cells confers sustained and long-term delivery of ChABC to the injured spinal cord. It has been shown to be effective in rats to promote functional recovery in both thoracic and cervical contusion injury paradigms [51].

Several milestones have been reached since the CHASE-IT Initiative started in 2014. In particular: (1) The gene for Ch'ase can now be expressed in an active form in human cells; (2) expression of Ch'ase in the spinal cord can now be controlled, switching it on and off using an inducible switch responsive to the antibiotic doxycycline; and (3) treatment gives rise to improved walking and unprecedented upper limb function in clinically-relevant SCI models.

## 4. Selected Biomaterials That Hold Promise for Future Clinical Trials on Chronic Sci

The application of biomaterials in SCI is divided into two strategies. The first strategy involves the application of biomaterials as a scaffold for the neuronal cells or the encapsulation of certain cells for delivery. The second strategy is using biomaterials that mimic the soft tissue mechanical properties and the high conductivity required for electrical transmission in the native spinal cord for nerve tissue regeneration.

The use of biomaterials is of great importance for CNS regeneration and repair. It was soon observed that the use of potent stem cells alone could be dangerous, given the possibility of tumor formation. It has been demonstrated that the use of certain injectable hydrogels loaded with pluripotent stem cells can promote cell survival, integration, and differentiation, thereby reducing the risk of tumorigenicity that has been linked with the use of such cell lines [52,53].

The careful choice of the appropriate biomaterial for that specific application could not only guide the process with different topographical cues, but it could also provide the necessary structural support to build a temporary bridge within the cavity that is formed in chronic SCI lesions until nerve sprouting occurs.

The use of biomaterials for CNS regeneration purposes can also use nanotechnology in order to encapsulate the cells within nanoparticle-based hydrogels and develop a sustained release system that would allow a prolonged, tuned effect to accomplish the desired outcome. Trophic factors (e.g., growth factors) can also be incorporated in a scaffold made from the appropriate biomaterial in order to support the transplanted cells to live longer or even trigger endogenous regeneration through stem cell niches.

Several biomaterials have been used for supportive scaffold formation in order to accomplish CNS regeneration after chronic SCI lesions, but so far, only limited biomaterials have made it towards clinical trials as mentioned above (e.g., PLGA). There is an overwhelming amount of different combinations of biomaterials used in chronic SCI in terms of basic science experimentation, but this would be beyond the focus of the current review. Below, we will only mention a couple of selected biomaterials that we consider to be very promising in terms of future clinical applications.

Graphene Oxide (GO) 3D nano-structured scaffolds, considered “wonder biomaterials” with extraordinary potentials in the next few years based on preclinical results:

Studies have shown graphene to have great potential as a bioscaffold at the site of the lesion in chronic SCI allowing for neuronal regeneration [4,54–60]. GO nanocomposite is considered to be a favorable material for use in treatment because of its unique electro-physico-chemical properties and it is conductivity. GO has the ability to stimulate neuronal differentiation and axonal alignment at sites of SCI by providing a space for the growth, attachment, and survival of neural tissue at the lesion. Toxicity and biocompatibility of reduced graphene oxide is a debatable obstacle facing use of the material, with intravenous studies in mice showing dose-dependent toxicity and pathological damage present at lower doses [61,62]. Other routes of administration, however, such as oral [63], intravitreal [64], intraperitoneal [63], and subcutaneous [65], have proven the material to be nontoxic. The conductive properties of GO make it a viable product to use in the healing of SCI. The benefit of using GO is that the inflammatory response seen with other biomaterials is reduced and not as damaging at the site of the SCI.

GO combined with hydrogel has been used to fill the hemispinal cord transection lesion that was made in twenty rats [66]. After three months, histologic evaluation of the lesion in the spinal cords of the rats showed graphene nanoscaffolds adhering to the spinal cord tissue and an ingrowth of connective tissue elements, blood vessels, neurofilaments, and Schwann cells around the area of the graphene nanoscaffolds. A control study was carried out whereby similar rats with hemispinal cord transections had a hydrogel-only matrix injected into the lesion at site of injury. Three months later, histological evaluation showed pseudocyst cavities where the hydrogel matrix had been injected and the site of the lesion devoid of any tissue or substantial regrowth of neural cells. Even though this was a study on acute SCI, this *in vivo* preclinical study brings promise that the graphene nanoscaffolds material has potential to be used for stimulation of axonal regeneration into the lesion.

Another aspect stressing the significance and potential of Graphene, in terms of future clinical SCI repair-related applications, is the fact that Graphene has been chosen as the key biomaterial to be used as part of the project “Neurofibers” (Biofunctionalised Electroconducting Microfibers for the Treatment of Spinal Cord Injury). The project has recently started and it was selected by the European Commission in the framework of the Horizon 2020 (H2020) program in the area of emerging technologies (FET Proactive—Boosting emerging technologies) (for more information from the European Commission’s website: [https://cordis.europa.eu/project/rcn/206185\\_en.html](https://cordis.europa.eu/project/rcn/206185_en.html)).

#### 4.1. Fibrin-Based Scaffolds and Hydrogels Have Shown Impressive Results in Terms of Supporting CNS Regeneration in SCI Lesions in the Right Settings

The Fibrin glue has been approved by FDA and it is used successfully in clinically repairing cranial nerves and other tissues [67,68]. The Fibrin sealant (like the commercially available TISSEEL® (Baxter) product) has been used for years by neurosurgeons as a hemostatic agent and in order to control cerebrospinal fluid (CSF) leaks. This is of particular importance for spinal surgeries given the CSF leakage that can occur after the durotomy. In human patients, Fibrin has also been combined with FGF and the mixture was applied to the injured spinal segment of patients in order to prevent postoperative CSF leakage. The application of the FGF-containing Fibrin matrices resulted in significant motor and sensory improvements in the patients [69]. In terms of CNS repair and regenerative medicine, Fibrin could act as a carrier for therapeutic agents, such as neurotrophic factors and stem cells [70–72].

Fibrin matrices have been tested for supporting stem cells, specially embedded NSCs in fibrin matrices in order to increase the cells’ viability, when transplanted after SCI [73]. Even though the increase in NSCs viability was significant compared to the initial poor survival of the cells without the fibrin matrices, the results were even more remarkable when growth factor cocktails were added in the NSCs-containing fibrin matrices. This way the combination of NSCs with fibrin matrices and growth factors accomplished enhanced cells survival with the cells filling large lesion cavities and being differentiated into neurons and glia after spinal cord transection [2,73,74]. In a very recent

paper, Rosenzweig et al. [10] used a similar methodology in nonhuman primate models, proving for one more time that testing a promising treatment in nonhuman primates is crucial for the successful translation to humans. After several modifications to the rodent grafting technique (e.g., grafting matrix modifications, CSF drainage, more extensive immunosuppression), successful engraftment was achieved, paving the path towards clinical translation of the proposed therapy. The same group of researchers had accomplished before that the longest axonal sprouting, to the best of our knowledge, using a cocktail of growth factors and fibrin matrices. Ten growth factors were embedded in a fibrin gel to support rat or human neural stem cells grafted to the completely transected spinal cord of adult rats, accomplishing axons extending at least 25 mm in each direction in all subjects [75].

Further combinatorial approaches have been attempted using Fibrin with certain growth factors and grafts to enhance the restorative results with very promising results.

The FGF/Fibrin mixture along with human Schwann-cell grafts has been engrafted to transected rat spinal cords, stimulating fiber regeneration throughout the implant [76]. This also has been coupled with an autologous peripheral intercostal nerve segment to bridge a 5 mm gap within the transected rat spinal cords [77]. Even though this is only a small part of the literature supporting the use of Fibrin for CNS repair, it is evident that this biomaterial is also a very good candidate for future clinical applications in terms of regenerative therapeutic strategies in chronic SCI.

#### 4.2. Collagen/Heparin Sulfate Scaffolds Fabricated by a 3D Bioprinter

One promising, new approach is the use of a 3D bioprinter in producing collagen and heparin sulfate based bioscaffolds for the treatment of SCI [78]. The use of a 3D bioprinter, in order to produce the bioscaffold, is thought to have significantly amplified the mechanical properties of the mixture when compared to methods of production without the use of a 3D printer therefore methods using a 3D bioprinter will be discussed here. The current priorities when producing a bioscaffold for SCI is the biocompatibility of the scaffold, that it is made of a porous material in order to allow for neural regeneration and for it to have great strength. The team working on the 3D bioprinted collagen/heparin sulfate scaffolds believes it will be the answer to treating and stimulating neural regeneration in patients with SCI.

Locomotor recovery is the most important outcome to assess during preclinical and clinical studies and was seen in rats with SCI that had had the collagen/heparin sulfate bioscaffold implanted at the site of the lesion, during preclinical in vivo studies. The improved locomotor function after implantation and biodegradable and biocompatible properties of the collagen/heparin sulfate mixture gives promise for the use of such a bioscaffold in clinical practice to help improve the outcome of patients suffering with SCI.

#### 4.3. Peripheral Nerve Grafts Combined with Chitosan-Laminin Scaffold

Chitosan is a suitable biomaterial for use in neuronal repair due to its biocompatible and biodegradable properties [79]. It has been considered as a suitable material for many biomedical and industrial applications, such as drug delivery, due to its nontoxicity and biodegradability. Laminin is a glycoprotein that acts as a neurite outgrowth-promoting factor and so is suitable for combination in the bioscaffold. The combination of chitosan and laminin provide a promising biomaterial for use as a scaffold in promoting axonal growth and preventing neural degeneration.

Studies have shown that the use of chitosan channels containing nerve grafts promote axonal regeneration when applied to chronic SCI lesions [80]. Preclinical studies have shown that the use of chitosan-laminin scaffolds combined with peripheral nerve grafts supported axonal regeneration and positive outcomes include motor function improvement, as well as functional sensory improvement when the bioscaffolds were implanted in chronic nerve lesions [40]. Further investigation of this biomaterial would be recommended as it proves to be a promising option in the field of treatment of chronic SCI.

## 5. Conclusions and Future Perspectives

In conclusion, it is evident that more promising therapies will come up in the future regarding chronic SCI. We anticipate that the management of chronic SCI will change during the next few decades due to the fast pace of advances in the field of nanotechnology/smart materials and regenerative medicine. A combinatorial approach using cells and/or growth factors or other molecules along with biocompatible nanostructured scaffolds, that would allow fine-tuning of the release of the incorporated factors and would guide nerve growth in the CNS environment, would most probably be the key for success in such a complex tissue.

One significant component seems to be the ability to catalyze the translation of all the promising new therapies into clinical practice. This refers to imaging technology, and more specifically, Magnetic Resonance Imaging (MRI) sequences that can help assess and objectively quantify the biological response of the CNS to the tested intervention, solving a known issue of reproducibility and quantification in the application of all the new therapies. MRI could assess the biological significance, detecting tissue-related changes, while techniques like surface electromyography could assess the functional outcomes in a more objective way, leading together to the development of the much needed objective clinical scales that would take into consideration the statistical, biological and clinical significance associated with the tested therapeutic strategy or management plan. In addition, the combination of imaging technology along with the implementation of new, clinically relevant models, like the nonhuman primate model of SCI developed for evaluating pharmacologic treatments, and could open the pathway to safer and more efficient clinical application to patients in the future [81]. Nevertheless, we do anticipate that the use of bioengineered models on-a-chip and further advancements in nanomedicine might revolutionize the field and change the translational pathway in the future, accelerating the drug approval process and the implementation of new treatments in the clinic.

From the practical standpoint, there are several obstacles that need to be tackled, like the lack of published data from companies that have done significant work on SCI regeneration and repair through clinical trials. The inclusion of controls is crucial for obtaining reliable outcomes and yet certain clinical trials either fail to implement controls in their study plan or they avoid reporting the outcomes in a timely manner, hindering the progress in the field. In addition to that, researchers mainly use less clinically relevant SCI models like hemisections/transection models. There is a significant need for inclusion of contusion SCI models that are more similar to the lesions usually managed in the clinic. Last but not least, it should be stressed that acute SCI models are mainly used for research purposes aiming to address the problem soon after the injury in the clinic and to avoid complications (e.g., formation of glial scar that would hinder neuroregeneration). The inclusion of more chronic SCI models in research might seem to be a challenging task, but it is very important for the reliable assessment of the therapeutic interventions in order to solve significant questions on CNS regeneration, ensuring the safe application of future treatments to any SCI patient.

**Author Contributions:** A.M.S. proposed the review article and M.T., K.D., and A.S. worked on data gathering and drafting the review. All four authors critically analyzed and reviewed the topic and completed the review with future direction of the research.

**Acknowledgments:** M.T. was supported by Onassis Foundation during that study.

**Conflicts of Interest:** The authors declare no conflicts of interest.

## References

1. National Spinal Cord Injury Statistical Center. *Spinal Cord Injury (SCI) Facts and Figures at a Glance*; National Spinal Cord Injury Statistical Center: Birmingham, AL, USA, 2017.
2. Kadoya, K.; Tsukada, S.; Lu, P.; Coppola, G.; Geschwind, D.; Filbin, M.; Blesch, A.; Tuszyński, M.H. Combined Intrinsic and Extrinsic Neuronal Mechanisms Facilitate Bridging Axonal Regeneration One Year After Spinal Cord Injury. *Neuron* **2009**, *64*, 165–172. [[CrossRef](#)] [[PubMed](#)]

3. Gelain, F.; Panseri, S.; Antonini, S.; Cunha, C.; Donega, M.; Lowery, J.; Taraballi, F.; Cerri, G.; Montagna, M.; Baldissera, F.; et al. Transplantation of Nanostructured Composite Scaffolds Results in the Regeneration of Chronically Injured Spinal Cords. *ACS Nano* **2011**, *5*, 227–236. [[CrossRef](#)] [[PubMed](#)]
4. Faccendini, A.; Vigani, B.; Rossi, S.; Sandri, G.; Bonferoni, M.C.; Caramella, C.M.; Ferrari, F. Nanofiber Scaffolds as Drug Delivery Systems to Bridge Spinal Cord Injury. *Pharmaceutics* **2017**, *10*, 63. [[CrossRef](#)] [[PubMed](#)]
5. StemCells Inc. *Pathway Study*; StemCells Inc.: Newark, CA, USA, 2015.
6. StemCells Inc. *Phase II Trial in Cervical Spinal Cord Injury (SCI)*; StemCells Inc.: Newark, CA, USA, 2015.
7. NeuralStem Inc. *Neuralstem Reports Third Quarter 2015 Financial Results—Nov 9, 2015*; NeuralStem Inc.: Rockville, MD, USA, 2015.
8. Yan, J.; Xu, L.; Welsh, A.M.; Hatfield, G.; Hazel, T.; Johe, K.; Koliatsos, V.E. Extensive neuronal differentiation of human neural stem cell grafts in adult rat spinal cord. *PLoS Med.* **2007**, *4*, e39. [[CrossRef](#)] [[PubMed](#)]
9. Xu, L.; Yan, J.; Chen, D.; Welsh, A.M.; Hazel, T.; Johe, K.; Hatfield, G.; Koliatsos, V.E. Human neural stem cell grafts ameliorate motor neuron disease in SOD-1 transgenic rats. *Transplantation* **2006**, *82*, 865–875. [[CrossRef](#)] [[PubMed](#)]
10. Rosenzweig, E.S.; Brock, J.H.; Lu, P.; Kumamaru, H.; Salegio, E.A.; Kadoya, K.; Weber, J.L.; Liang, J.J.; Moseanko, R.; Hawbecker, S.; et al. Restorative effects of human neural stem cell grafts on the primate spinal cord. *Nat. Med.* **2018**, *24*, 484–490. [[CrossRef](#)] [[PubMed](#)]
11. Theodore, N.; Hlubek, R.; Danielson, J.; Neff, K.; Vaickus, L.; Ulich, T.R.; Ropper, A.E. First Human Implantation of a Bioresorbable Polymer Scaffold for Acute Traumatic Spinal Cord Injury: A Clinical Pilot Study for Safety and Feasibility. *Neurosurgery* **2016**, *79*, E305–E312. [[CrossRef](#)] [[PubMed](#)]
12. Tabakow, P.; Raisman, G.; Fortuna, W.; Czyz, M.; Huber, J.; Li, D.; Szewczyk, P.; Okurowski, S.; Miedzybrodzki, R.; Czapiga, B.; et al. Functional regeneration of supraspinal connections in a patient with transected spinal cord following transplantation of bulbar olfactory ensheathing cells with peripheral nerve bridging. *Cell Transpl.* **2014**, *23*, 1631–1655. [[CrossRef](#)] [[PubMed](#)]
13. Huang, H.; Chen, L.; Wang, H.; Xiu, B.; Li, B.; Wang, R.; Zhang, J.; Zhang, F.; Gu, Z.; Li, Y.; et al. Influence of patients' age on functional recovery after transplantation of olfactory ensheathing cells into injured spinal cord injury. *Chin. Med. J.* **2003**, *116*, 1488–1491. [[PubMed](#)]
14. Féron, F.; Perry, C.; Cochrane, J.; Licina, P.; Nowitzke, A.; Urquhart, S.; Geraghty, T.; Mackay-Sim, A. Autologous olfactory ensheathing cell transplantation in human spinal cord injury. *Brain* **2005**, *128*, 2951–2960. [[CrossRef](#)] [[PubMed](#)]
15. Lima, C.; Pratas-Vital, J.; Escada, P.; Hasse-Ferreira, A.; Capucho, C.; Peduzzi, J.D. Olfactory Mucosa Autografts in Human Spinal Cord Injury: A Pilot Clinical Study. *J. Spinal Cord Med.* **2006**, *29*, 191–203. [[CrossRef](#)] [[PubMed](#)]
16. Li, L.; Adnan, H.; Xu, B.; Wang, J.; Wang, C.; Li, F.; Tang, K. Effects of transplantation of olfactory ensheathing cells in chronic spinal cord injury: A systematic review and meta-analysis. *Eur. Spine J.* **2015**, *24*, 919–930. [[CrossRef](#)] [[PubMed](#)]
17. Choi, D.; Gladwin, K. Olfactory Ensheathing Cells: Part II—Source of Cells and Application to Patients. *World Neurosurg.* **2015**, *83*, 251–256. [[CrossRef](#)] [[PubMed](#)]
18. Son, Y.-J.; Thompson, W.J. Schwann cell processes guide regeneration of peripheral axons. *Neuron* **1995**, *14*, 125–132. [[CrossRef](#)]
19. Bruce, J.H.; Norenberg, M.D.; Kraydieh, S.; Puckett, W.; Marcillo, A.; Dietrich, D. Schwannosis: Role of gliosis and proteoglycan in human spinal cord injury. *J. Neurotrauma* **2000**, *17*, 781–788. [[CrossRef](#)] [[PubMed](#)]
20. Guest, J.D.; Hiester, E.D.; Bunge, R.P. Demyelination and Schwann cell responses adjacent to injury epicenter cavities following chronic human spinal cord injury. *Exp. Neurol.* **2005**, *192*, 384–393. [[CrossRef](#)] [[PubMed](#)]
21. Bunge, M.B.; Wood, P.M. Realizing the maximum potential of Schwann cells to promote recovery from spinal cord injury. *Handb. Clin. Neurol.* **2012**, *109*, 523–540. [[CrossRef](#)] [[PubMed](#)]
22. Williams, R.R.; Bunge, M.B. Schwann cell transplantation: A repair strategy for spinal cord injury? *Prog. Brain Res.* **2012**, *201*, 295–312. [[CrossRef](#)] [[PubMed](#)]
23. Zhu, H.; Poon, W.; Liu, Y.; Leung, G.K.-K.; Wong, Y.; Feng, Y.; Ng, S.C.P.; Tsang, K.S.; Sun, D.T.F.; Yeung, D.K.; et al. Phase I-II Clinical Trial Assessing Safety and Efficacy of Umbilical Cord Blood Mononuclear Cell Transplant Therapy of Chronic Complete Spinal Cord Injury. *Cell Transpl.* **2016**, *25*, 1925–1943. [[CrossRef](#)] [[PubMed](#)]

24. Dasari, V.R.; Veeravalli, K.K.; Tsung, A.J.; Gondi, C.S.; Gujrati, M.; Dinh, D.H.; Rao, J.S. Neuronal Apoptosis Is Inhibited by Cord Blood Stem Cells after Spinal Cord Injury. *J. Neurotrauma* **2009**, *26*, 2057–2069. [CrossRef] [PubMed]
25. Veeravalli, K.K.; Dasari, V.R.; Tsung, A.J.; Dinh, D.H.; Gujrati, M.; Fassett, D.; Rao, J.S. Human umbilical cord blood stem cells upregulate matrix metalloproteinase-2 in rats after spinal cord injury. *Neurobiol. Dis.* **2009**, *36*, 200–212. [CrossRef] [PubMed]
26. Veeravalli, K.K.; Dasari, V.R.; Tsung, A.J.; Dinh, D.H.; Gujrati, M.; Fassett, D.; Rao, J.S. Stem Cells Downregulate the Elevated Levels of Tissue Plasminogen Activator in Rats After Spinal Cord Injury. *Neurochem. Res.* **2009**, *34*, 1183–1194. [CrossRef] [PubMed]
27. Kao, C.-H.; Chen, S.-H.; Chio, C.-C.; Lin, M.-T. Human Umbilical Cord Blood-derived CD34+ cells may attenuate spinal cord injury by stimulating vascular endothelial and neurotrophic factors. *Shock* **2008**, *29*, 49–55. [CrossRef] [PubMed]
28. Chua, S.J.; Bielecki, R.; Yamanaka, N.; Fehlings, M.G.; Rogers, I.M.; Casper, R.F. The Effect of Umbilical Cord Blood Cells on Outcomes After Experimental Traumatic Spinal Cord Injury. *Spine* **2010**, *35*, 1520–1526. [CrossRef] [PubMed]
29. Chung, H.; Chung, W.; Lee, J.-H.; Chung, D.-J.; Yang, W.-J.; Lee, A.-J.; Choi, C.-B.; Chang, H.-S.; Kim, D.-H.; Suh, H.J.; et al. Expression of neurotrophic factors in injured spinal cord after transplantation of human-umbilical cord blood stem cells in rats. *J. Vet. Sci.* **2016**, *17*, 97–102. [CrossRef] [PubMed]
30. Dasari, V.R.; Spomar, D.G.; Gondi, C.S.; Sloffer, C.A.; Saving, K.L.; Gujrati, M.; Rao, J.S.; Dinh, D.H. Axonal Remyelination by Cord Blood Stem Cells after Spinal Cord Injury. *J. Neurotrauma* **2007**, *24*, 391–410. [CrossRef] [PubMed]
31. Cho, S.-R.; Yang, M.S.; Yim, S.H.; Park, J.H.; Lee, J.E.; Eom, Y.; Jang, I.K.; Kim, H.E.; Park, J.S.; Kim, H.O.; et al. Neurally induced umbilical cord blood cells modestly repair injured spinal cords. *NeuroReport* **2008**, *19*, 1259–1263. [CrossRef] [PubMed]
32. Ryu, H.-H.; Byeon, Y.-E.; Park, S.-S.; Kang, B.-J.; Seo, M.-S.; Park, S.-B.; Kim, W.H.; Kang, K.-S.; Kweon, O.-K. Immunohistomorphometric Analysis of Transplanted Umbilical Cord Blood-Derived Mesenchymal Stem Cells and The Resulting Anti-Inflammatory Effects on Nerve Regeneration of Injured Canine Spinal Cord. *Tissue Eng. Regen. Med.* **2011**, *8*, 173–182.
33. Ning, G.; Tang, L.; Wu, Q.; Li, Y.; Li, Y.; Zhang, C.; Feng, S. Human umbilical cord blood stem cells for spinal cord injury: Early transplantation results in better local angiogenesis. *Regen. Med.* **2013**, *8*, 271–281. [CrossRef] [PubMed]
34. Vaquero, J.; Zurita, M.; Rico, M.A.; Bonilla, C.; Aguayo, C.; Montilla, J.; Bustamante, S.; Carballido, J.; Marin, E.; Martinez, F.; et al. An approach to personalized cell therapy in chronic complete paraplegia: The Puerta de Hierro phase I/II clinical trial. *Cytotherapy* **2016**, *18*, 1025–1036. [CrossRef] [PubMed]
35. Deans, R.J.; Moseley, A.B. Mesenchymal stem cells. *Exp. Hematol.* **2000**, *28*, 875–884. [CrossRef]
36. Kopen, G.C.; Prockop, D.J.; Phinney, D.G. Marrow stromal cells migrate throughout forebrain and cerebellum, and they differentiate into astrocytes after injection into neonatal mouse brains. *Proc. Natl. Acad. Sci. USA* **1999**, *96*, 10711–10716. [CrossRef] [PubMed]
37. Hofer, H.R.; Tuan, R.S. Secreted trophic factors of mesenchymal stem cells support neurovascular and musculoskeletal therapies. *Stem Cell Res. Ther.* **2016**, *7*, 131. [CrossRef] [PubMed]
38. Cizkova, D.; Cubinkova, V.; Smolek, T.; Murgoci, A.-N.; Danko, J.; Vdoviakova, K.; Humenik, F.; Cizek, M.; Quanico, J.; Fournier, I.; et al. Localized Intrathecal Delivery of Mesenchymal Stromal Cells Conditioned Medium Improves Functional Recovery in a Rat Model of Spinal Cord Injury. *Int. J. Mol. Sci.* **2018**, *19*, 870. [CrossRef] [PubMed]
39. Bansal, H.; Verma, P.; Agrawal, A.; Leon, J.; Sundell, I.B.; Koka, P.S. Autologous Bone Marrow-Derived Stem Cells in Spinal Cord Injury. *J. Stem Cells* **2016**, *11*, 51–61. [PubMed]
40. Amr, S.M.; Gouda, A.; Koptan, W.T.; Galal, A.A.; Abdel-Fattah, D.S.; Rashed, L.A.; Atta, H.M.; Abdel-Aziz, M.T. Bridging defects in chronic spinal cord injury using peripheral nerve grafts combined with a chitosan-laminin scaffold and enhancing regeneration through them by co-transplantation with bone-marrow-derived mesenchymal stem cells: Case series of 14 patients. *J. Spinal Cord Med.* **2014**, *37*, 54–71. [CrossRef] [PubMed]

41. Frolov, A.A.; Bryukhovetskiy, A.S. Effects of hematopoietic autologous stem cell transplantation to the chronically injured human spinal cord evaluated by motor and somatosensory evoked potentials methods. *Cell Transpl.* **2012**, *21* (Suppl. 1), S49–S55. [[CrossRef](#)] [[PubMed](#)]
42. El-Kheir, W.A.; Gabr, H.; Awad, M.R.; Ghannam, O.; Barakat, Y.; Farghali, H.A.M.A.; El Maadawi, Z.M.; Ewes, I.; Sabaawy, H.E. Autologous bone marrow-derived cell therapy combined with physical therapy induces functional improvement in chronic spinal cord injury patients. *Cell Transpl.* **2014**, *23*, 729–745. [[CrossRef](#)] [[PubMed](#)]
43. Wong, Y.W.; Tam, S.; So, K.F.; Chen, J.Y.H.; Cheng, W.S.; Luk, K.D.K.; Tang, S.W.; Young, W. A three-month, open-label, single-arm trial evaluating the safety and pharmacokinetics of oral lithium in patients with chronic spinal cord injury. *Spinal Cord* **2011**, *49*, 94–98. [[CrossRef](#)] [[PubMed](#)]
44. Cristante, A.F.; Barros-Filho, T.E.P.; Tatsui, N.; Mendrone, A.; Caldas, J.G.; Camargo, A.; Alexandre, A.; Teixeira, W.G.J.; Oliveira, R.P.; Marcon, R.M. Stem cells in the treatment of chronic spinal cord injury: Evaluation of somatosensitive evoked potentials in 39 patients. *Spinal Cord* **2009**, *47*, 733–738. [[CrossRef](#)] [[PubMed](#)]
45. Moviglia, G.A.; Fernandez Viña, R.; Brizuela, J.A.; Saslavsky, J.; Vrsalovic, F.; Varela, G.; Bastos, F.; Farina, P.; Etchegaray, G.; Barbieri, M.; et al. Combined protocol of cell therapy for chronic spinal cord injury. Report on the electrical and functional recovery of two patients. *Cyotherapy* **2006**, *8*, 202–209. [[CrossRef](#)] [[PubMed](#)]
46. ReNetX. ReNetX Bio Launched to Advance Innovative Neuro-Regenerative Technology Developed at Yale University. Available online: <http://globenewswire.com/news-release/2017/07/24/1056062/0/en/ReNetX-Bio-Launched-to-Advance-Innovative-Neuro-Regenerative-Technology-Developed-at-Yale-University.html> (accessed on 20 April 2018).
47. CHASE IT. Available online: <https://www.spinal-research.org/chase-it> (accessed on 20 April 2018).
48. Tran, A.P.; Sundar, S.; Yu, M.; Lang, B.T.; Silver, J. Modulation of receptor protein tyrosine phosphatase sigma increases chondroitin sulfate proteoglycan degradation through Cathepsin B secretion to enhance axon outgrowth. *J. Neurosci.* **2018**, *32*14–3217. [[CrossRef](#)] [[PubMed](#)]
49. Bartus, K.; James, N.D.; Didangelos, A.; Bosch, K.D.; Verhaagen, J.; Yáñez-Muñoz, R.J.; Rogers, J.H.; Schneider, B.L.; Muir, E.M.; Bradbury, E.J. Large-scale chondroitin sulfate proteoglycan digestion with chondroitinase gene therapy leads to reduced pathology and modulates macrophage phenotype following spinal cord contusion injury. *J. Neurosci.* **2014**, *34*, 4822–4836. [[CrossRef](#)] [[PubMed](#)]
50. Muir, E.; Raza, M.; Ellis, C.; Burnside, E.; Love, F.; Heller, S.; Elliot, M.; Daniell, E.; Dasgupta, D.; Alves, N.; et al. Trafficking and processing of bacterial proteins by mammalian cells: Insights from chondroitinase ABC. *PLoS ONE* **2017**, *12*, e0186759. [[CrossRef](#)] [[PubMed](#)]
51. James, N.D.; Shea, J.; Muir, E.M.; Verhaagen, J.; Schneider, B.L.; Bradbury, E.J. Chondroitinase gene therapy improves upper limb function following cervical contusion injury. *Exp. Neurol.* **2015**, *271*, 131–135. [[CrossRef](#)] [[PubMed](#)]
52. Oliveira, J.M.; Carvalho, L.; Silva-Correia, J.; Vieira, S.; Majchrzak, M.; Lukomska, B.; Stanaszek, L.; Strymecka, P.; Malysz-Cymborska, I.; Golubczyk, D.; et al. Hydrogel-based scaffolds to support intrathecal stem cell transplantation as a gateway to the spinal cord: Clinical needs, biomaterials, and imaging technologies. *NPJ Regen. Med.* **2018**, *3*, 8. [[CrossRef](#)] [[PubMed](#)]
53. Führmann, T.; Tam, R.Y.; Ballarin, B.; Coles, B.; Elliott Donaghue, I.; van der Kooy, D.; Nagy, A.; Tator, C.H.; Morshead, C.M.; Shoichet, M.S. Injectable hydrogel promotes early survival of induced pluripotent stem cell-derived oligodendrocytes and attenuates longterm teratoma formation in a spinal cord injury model. *Biomaterials* **2016**, *83*, 23–36. [[CrossRef](#)] [[PubMed](#)]
54. López-Dolado, E.; González-Mayorga, A.; Gutiérrez, M.C.; Serrano, M.C. Immunomodulatory and angiogenic responses induced by graphene oxide scaffolds in chronic spinal hemisected rats. *Biomaterials* **2016**, *99*, 72–81. [[CrossRef](#)] [[PubMed](#)]
55. Mattei, T.A. How graphene is expected to impact neurotherapeutics in the near future. *Expert Rev. Neurother.* **2014**, *14*, 845–847. [[CrossRef](#)] [[PubMed](#)]
56. Domínguez-Bajo, A.; González-Mayorga, A.; López-Dolado, E.; Serrano, M.C. Graphene-Derived Materials Interfacing the Spinal Cord: Outstanding in Vitro and in Vivo Findings. *Front. Syst. Neurosci.* **2017**, *11*, 71. [[CrossRef](#)] [[PubMed](#)]

57. Zhou, K.; Motamed, S.; Thouas, G.A.; Bernard, C.C.; Li, D.; Parkington, H.C.; Coleman, H.A.; Finkelstein, D.I.; Forsythe, J.S. Graphene Functionalized Scaffolds Reduce the Inflammatory Response and Supports Endogenous Neuroblast Migration when Implanted in the Adult Brain. *PLoS ONE* **2016**, *11*, e0151589. [CrossRef] [PubMed]
58. González-Mayorga, A.; López-Dolado, E.; Gutiérrez, M.C.; Collazos-Castro, J.E.; Ferrer, M.L.; del Monte, F.; Serrano, M.C. Favorable Biological Responses of Neural Cells and Tissue Interacting with Graphene Oxide Microfibers. *ACS Omega* **2017**, *2*, 8253–8263. [CrossRef]
59. Singh, Z. Applications and Toxicity of Graphene Family Nanomaterials and Their Composites. Available online: <https://www.dovepress.com/applications-and-toxicity-of-graphene-family-nanomaterials-and-their-c-peer-reviewed-fulltext-article-NSA> (accessed on 19 April 2018).
60. Kim, C.-Y.; Sikkema, W.K.A.; Hwang, I.-K.; Oh, H.; Kim, U.J.; Lee, B.H.; Tour, J.M. Spinal cord fusion with PEG-GNRs (TexasPEG): Neurophysiological recovery in 24 hours in rats. *Surg. Neurol. Int.* **2016**, *7*, S632–S636. [CrossRef] [PubMed]
61. Mendonça, M.C.P.; Soares, E.S.; de Jesus, M.B.; Ceragioli, H.J.; Batista, Á.G.; Nyúl-Tóth, Á.; Molnár, J.; Wilhelm, I.; Maróstica, M.R.; Krizbai, I.; et al. PEGylation of Reduced Graphene Oxide Induces Toxicity in Cells of the Blood-Brain Barrier: An in Vitro and in Vivo Study. *Mol. Pharm.* **2016**, *13*, 3913–3924. [CrossRef] [PubMed]
62. Zhang, X.; Yin, J.; Peng, C.; Hu, W.; Zhu, Z.; Li, W.; Fan, C.; Huang, Q. Distribution and biocompatibility studies of graphene oxide in mice after intravenous administration. *Carbon* **2011**, *49*, 986–995. [CrossRef]
63. Yang, K.; Gong, H.; Shi, X.; Wan, J.; Zhang, Y.; Liu, Z. In vivo biodistribution and toxicology of functionalized nano-graphene oxide in mice after oral and intraperitoneal administration. *Biomaterials* **2013**, *34*, 2787–2795. [CrossRef] [PubMed]
64. Yan, L.; Wang, Y.; Xu, X.; Zeng, C.; Hou, J.; Lin, M.; Xu, J.; Sun, F.; Huang, X.; Dai, L.; et al. Can Graphene Oxide Cause Damage to Eyesight? *Chem. Res. Toxicol.* **2012**, *25*, 1265–1270. [CrossRef] [PubMed]
65. Sahu, A.; Il Choi, W.; Tae, G. A stimuli-sensitive injectable graphene oxide composite hydrogel. *Chem. Commun.* **2012**, *48*, 5820–5822. [CrossRef] [PubMed]
66. Palejwala, A.H.; Fridley, J.S.; Mata, J.A.; Samuel, E.L.G.; Luerssen, T.G.; Perlaky, L.; Kent, T.A.; Tour, J.M.; Jea, A. Biocompatibility of reduced graphene oxide nanoscaffolds following acute spinal cord injury in rats. *Surg. Neurol. Int.* **2016**, *7*, 75. [CrossRef] [PubMed]
67. Wieken, K.; Angioi-Duprez, K.; Lim, A.; Marchal, L.; Merle, M. Nerve anastomosis with glue: Comparative histologic study of fibrin and cyanoacrylate glue. *J. Reconstr. Microsurg.* **2003**, *19*, 17–20. [CrossRef] [PubMed]
68. Brodbaker, E.; Bahar, I.; Slomovic, A.R. Novel use of fibrin glue in the treatment of conjunctivochalasis. *Cornea* **2008**, *27*, 950–952. [CrossRef] [PubMed]
69. Wu, J.-C.; Huang, W.-C.; Chen, Y.-C.; Tu, T.-H.; Tsai, Y.-A.; Huang, S.-F.; Huang, H.-C.; Cheng, H. Acidic fibroblast growth factor for repair of human spinal cord injury: A clinical trial. *J. Neurosurg. Spine* **2011**, *15*, 216–227. [CrossRef] [PubMed]
70. Iwakawa, M.; Mizoi, K.; Tessler, A.; Itoh, Y. Intraspinous implants of fibrin glue containing glial cell line-derived neurotrophic factor promote dorsal root regeneration into spinal cord. *Neurorehabil. Neural Repair* **2001**, *15*, 173–182. [CrossRef] [PubMed]
71. Cheng, H.; Huang, S.S.; Lin, S.M.; Lin, M.J.; Chu, Y.C.; Chih, C.L.; Tsai, M.J.; Lin, H.C.; Huang, W.C.; Tsai, S.K. The neuroprotective effect of glial cell line-derived neurotrophic factor in fibrin glue against chronic focal cerebral ischemia in conscious rats. *Brain Res.* **2005**, *1033*, 28–33. [CrossRef] [PubMed]
72. Petter-Puchner, A.H.; Froetscher, W.; Krametter-Froetscher, R.; Lorinson, D.; Redl, H.; van Griensven, M. The long-term neurocompatibility of human fibrin sealant and equine collagen as biomatrices in experimental spinal cord injury. *Exp. Toxicol. Pathol.* **2007**, *58*, 237–245. [CrossRef] [PubMed]
73. Lu, P.; Graham, L.; Wang, Y.; Wu, D.; Tuszyński, M. Promotion of Survival and Differentiation of Neural Stem Cells with Fibrin and Growth Factor Cocktails after Severe Spinal Cord Injury. *J. Vis. Exp.* **2014**. [CrossRef] [PubMed]
74. Willerth, S.M.; Faxel, T.E.; Gottlieb, D.I.; Sakiyama-Elbert, S.E. The Effects of Soluble Growth Factors on Embryonic Stem Cell Differentiation Inside of Fibrin Scaffolds. *Stem Cells* **2007**, *25*, 2235–2244. [CrossRef] [PubMed]

75. Lu, P.; Wang, Y.; Graham, L.; McHale, K.; Gao, M.; Wu, D.; Brock, J.; Blesch, A.; Rosenzweig, E.S.; Havton, L.A.; et al. Long-Distance Growth and Connectivity of Neural Stem Cells after Severe Spinal Cord Injury. *Cell* **2012**, *150*, 1264–1273. [[CrossRef](#)] [[PubMed](#)]
76. Guest, J.D.; Hesse, D.; Schnell, L.; Schwab, M.E.; Bunge, M.B.; Bunge, R.P. Influence of IN-1 antibody and acidic FGF-fibrin glue on the response of injured corticospinal tract axons to human Schwann cell grafts. *J. Neurosci. Res.* **1997**, *30*, 888–905. [[CrossRef](#)]
77. Kuo, H.-S.; Tsai, M.-J.; Huang, M.-C.; Chiu, C.-W.; Tsai, C.-Y.; Lee, M.-J.; Huang, W.-C.; Lin, Y.-L.; Kuo, W.-C.; Cheng, H. Acid fibroblast growth factor and peripheral nerve grafts regulate Th2 cytokine expression, macrophage activation, polyamine synthesis, and neurotrophin expression in transected rat spinal cords. *J. Neurosci.* **2011**, *31*, 4137–4147. [[CrossRef](#)] [[PubMed](#)]
78. Zhang, R.; Tu, Y.; Zhao, M.; Chen, C.; Liang, H.; Wang, J.; Zhang, S.; Li, X. Preparation of Bionic Collagen-Heparin Sulfate Spinal Cord Scaffold with Three-dimentional print technology. *Zhongguo Xiufu Chong Jian Wai Ke Za Zhi* **2015**, *29*, 1022–1027. [[PubMed](#)]
79. Chen, B.; Bohnert, D.; Borgens, R.B.; Cho, Y. Pushing the science forward: Chitosan nanoparticles and functional repair of CNS tissue after spinal cord injury. *J. Biol. Eng.* **2013**, *7*, 15. [[CrossRef](#)] [[PubMed](#)]
80. Nomura, H.; Baladie, B.; Katayama, Y.; Morshead, C.M.; Shoichet, M.S.; Tator, C.H. Delayed implantation of intramedullary chitosan channels containing nerve grafts promotes extensive axonal regeneration after spinal cord injury. *Neurosurgery* **2008**, *63*, 127–141, discussion 141–143. [[CrossRef](#)] [[PubMed](#)]
81. Seth, N.; Simmons, H.A.; Masood, F.; Graham, W.A.; Rosene, D.L.; Westmoreland, S.V.; Cummings, S.M.; Gwardjan, B.; Sejdic, E.; Hoggatt, A.F.; et al. Model of Traumatic Spinal Cord Injury for Evaluating Pharmacologic Treatments in Cynomolgus Macaques (*Macaca fascicularis*). *Comp. Med.* **2018**, *68*, 63–73. [[PubMed](#)]



© 2018 by the authors. Licensee MDPI, Basel, Switzerland. This article is an open access article distributed under the terms and conditions of the Creative Commons Attribution (CC BY) license (<http://creativecommons.org/licenses/by/4.0/>).



MDPI  
St. Alban-Anlage 66  
4052 Basel  
Switzerland  
Tel. +41 61 683 77 34  
Fax +41 61 302 89 18  
[www.mdpi.com](http://www.mdpi.com)

*International Journal of Molecular Sciences* Editorial Office

E-mail: [ijms@mdpi.com](mailto:ijms@mdpi.com)  
[www.mdpi.com/journal/ijms](http://www.mdpi.com/journal/ijms)





MDPI  
St. Alban-Anlage 66  
4052 Basel  
Switzerland

Tel: +41 61 683 77 34  
Fax: +41 61 302 89 18  
[www.mdpi.com](http://www.mdpi.com)



ISBN 978-3-03897-407-9